FINITE ELEMENT ANALYSIS OF FOOTINGS

AND EMBANKMENT DAM CORES

by

MIR-MOHAMMAD DAVACHI

B.Sc.(C.Eng.), M.Sc.(C.Eng.), D.I.C.,

M.Sc.(Soil Mech.), A.M.A.S.C.E.

A Thesis submitted to the

University of London

for the degree of

Doctor of Philosophy in the Faculty of Engineering

Department of Civil Engineering

Imperial College of Science and Technology

July 1978

To SHAHNAZ and HADI

MIR-MOHAMMAD DAVACHI

FINITE ELEMENT ANALYSIS OF FOOTINGS AND

EMBANKMENT DAM CORES

ABSTRACT

Non-linear finite element techniques are used to
study the undrained behaviour of shallow foundations under
monotonic and cyclic loadings, and the cracking of embank-
ment dam cores. A main aim of the work was to examine
stress changes beneath footings for use in laboratory stress-
path testing work.

Comparisons of the finite element results with the
available closed form solutions, and with other numerical
solutions, are made to investigate the reliability and effec-
tiveness of the technique used. Good agreement was found.

In studying the undrained behaviour of shallow foun-
dations under monotonic loading, the effects of non-linea-
rity, layer thickness, side boundaries, footing rigidity,
initial state of stress, deformation properties and nonhomo-
geneity on stresses, displacements and failure loads are
examined, and failure zones and rupture figures are studied.
Some cases which have no closed form solution are analysed.
It is shown that the nonhomogeneity has a major effect on
stresses, displacements, failure loads and failure zones.

The effect of cyclic loading on displacements and
stresses is examined, and the effects of different stress-
strain models on stresses, stress changes and displacements
during cyclic loading are investigated.

In studying the cracking of an embankment dam core, stresses and stress changes in an idealised core at the end of construction and after impounding are analysed. From these analyses, investigations are made of areas of low stress and the likelihood of crack formation. It is shown that the development of seepage pressures throughout the core during impounding reduces the risk of hydraulic fracture.

During this study, it was found that some points within the core exhibit strain-softening behaviour during impounding. An iterative technique is developed and used for this strain-softening behaviour. In this technique, a modified form of the Newton-Raphson method, which enables the relevant deformation parameters for shear unloading to be assigned to every Gauss point in the domain in every iteration, was used where necessary.

TABLE OF CONTENTS

ACKNOWLEDGEMENTS

Last, but by no means least, the writer is greatly
indebted to his wife, Shahnaz, who showed extreme patience
and understanding throughout the period of this research.

CHAPTER 1

INTRODUCTION

1.1 Outline of the Research Project

In order to perform the stress analysis for a continuum, the governing equations must be solved. The enormous complexities encountered in soils can make analytical closed form approaches very difficult, and a large number of simplifying assumptions are necessary to obtain such solutions.

Fortunately, numerical techniques enable the governing equations of a complex problem to be solved approximately. The popularity and versatility of these techniques have been greatly enhanced by the availability of the large high-speed digital computers.

The most widely used numerical technique in geotechnical engineering is the finite element method. This method is essentially a process through which a continuum with infinite degrees of freedom is approximated by an assemblage of sub-regions, called finite elements, each with a specified but finite number of degrees of freedom. The fundamental property underlying the finite element method is that typical subregions can be studied for their behaviour independently of other elements. Once the behaviour of a typical element has been formulated in terms of behaviour of the nodes of the element, the complete model is then obtained by appropriate assembly of all the elements.

Generally, it is easy to obtain a reasonable solution

for a geotechnical problem using the finite element method, but it needs considerable checking to ensure that the solution is sufficiently reliable. Therefore, the effectiveness of the finite element programme must be investigated by comparing finite element results with the results obtained from closed form or approximate solutions.

In this research the finite element method is used to study the behaviour of shallow foundations, and cracking phenomenon of embankment dam cores.

The finite element programme used is designed for two dimensional plane strain and axisymmetric geotechnical problems. It uses the displacement approach to the 8-noded isoparametric element with built-in reduced Gauss integration rule for numerical integration of the element characteristics. The solution of the banded symmetric matrix is achieved by the direct Gauss elimination method. The deformation is assumed not to change the overall geometry of the problem (only small displacement and first order strain terms are considered).

The programme can handle linear and non-linear material with a shear strength cut-off. Saturated undrained shear behaviour and non-dilatent drained shear behaviour can be modelled. Non-linearity is dealt with using either incremental or iterative methods, or a combination of the two. The incremental technique can be either the tangential method or the Quasi Runge-Kutta method. For the iterative technique either the constant stiffness method or the Newton-Raphson method can be chosen.

During this research an iterative technique is developed and used in the programme for the hydraulic fracturing phenomenon which implies a strain-softening problem. A modified form of the Newton-Raphson method, which enables the relevant deformation parameters for shear unloading to be assigned to every Gauss point in the domain in every iteration, was used where necessary.

In studying the behaviour of shallow foundations, first, a comparison between finite element results and available closed form or approximate solutions is made to ensure the reliability of the method. Then, effects of layer thickness, side boundaries, footing rigidity, soil unit weight and K_o, stress-strain curve, non-homogeneity, and an increase in the applied load on displacements and stresses are investigated. Also, failure zones and rupture figures in clay are studied, and some of the geotechnical problems which have no closed form solutions, such as: inclined and eccentric loading of a finite layer whose un-drained modulus and strength vary linearly with depth, are analysed.

Furthermore, the effect of the cyclic loading on dis-placements and stresses is considered. Also, with cyclic loading, effects of different stress-strain models on stresses, stress changes, and displacements are investigated.

In studying the behaviour of crack formation in the embankment dam core, stresses and stress changes in the core at the end of construction and after impounding are analysed. From these analyses, investigations are made of areas of

low stress and the likelihood of crack formation. Also, from finite element results, it is shown that impounding tends to increase the average total stress $(\sigma_1 + \sigma_3)/2$ and so prevent cracking, as predicted by Vaughan (1976b).

1.2   Organization of the Thesis

The thesis has been divided into three parts and two Appendices. Part one consists of one chapter (Chapter 2) which considers the finite element method of analysis. The purpose of stress analysis, methods of stress analysis, and basic assumptions of the finite element method are briefly explained. Also, in Chapter 2, the two different methods for non-linear solutions (incremental and iterative) are discussed. In the final section of Chapter 2, the non-linear finite element programme used in this research is explained.

Part two, which consists of four chapters (Chapters 3, 4, 5 and 6), considers the study of the behaviour of shallow foundations. Chapters 3 and 4 consist mainly of a literature review and contain the approximate theories developed during this research. Chapter 3 deals with the stress distribution, settlement analysis, and soil-foundation interaction. Chapter 4 considers the failure and bearing capacity of footings.

In Chapter 5, the different cases for the footing studies made in this work are tabulated, including the material properties used. Chapter 6 contains the finite element results for monotonic and cyclic loading of the

footing, and discussion of these results. Also, in this chapter, comparison is made between the finite element results and available closed form solutions, in order to investigate the effectiveness of the programme.

Part three consists of two chapters (Chapters 7 and 8), and studies stresses and stress changes in an idealised embankment dam core during construction and impounding. In Chapter 7 a brief review of cracking of embankment dam cores is presented, together with the phenomena of load transfer and hydraulic fracture in the core.

Chapter 8 contains finite element results for studying stresses and stress changes in the core. The areas of low stress and the likelihood of crack formation in the core are investigated. Also, in this chapter, it is shown that impounding tends to increase the average total stresses.

In Appendix one the flow chart of the programme is given. Appendix two consists of descriptions and algorithms for the principal parts of the programme specially written for this research.

While analysing the behaviour of crack formation in the core, it was found that some points within the core exhibit strain-softening behaviour after impounding. The programme has been extended to deal with this behaviour. The algorithm for this is explained in Appendix two, and finite element results obtained after this modification are discussed in Chapter 8.

PART I

METHOD OF ANALYSIS

CHAPTER 2

THE METHOD OF ANALYSIS; FINITE ELEMENT TECHNIQUE

2.1 The Stress Analysis of a Continuum

The study of the response of a real continuous struc-
ture to a given set of loading conditions can be done by
performing an engineering stress analysis of that structure.
From this study it is possible to obtain the information
about the mechanism of behaviour; the magnitude and the
direction of displacements, stresses and/or pore water
pressure (directly or inferred) at selected points; and the
stability (or the margin of safety) of the structure. Such
analyses involve a knowledge of the applied loads; the rele-
vant material properties; and the geometry and appropriate
boundary conditions.

In the closed form solution of the stress analysis
problems three conditions should be satisfied throughout the
structure, Timoshenko and Goodier (1951). These conditions
are (i) equilibrium of forces, (ii) compatibility of dis-
placements, and (iii) the material stress-strain laws.

2.2 Methods of Stress Analysis

There are two well-tried methods for solving a continuum.
Firstly there is the model analysis, which involves the
application of scaled values of the real applied loads to
a model exhibiting all the features of the prototype structure.
The response of the model is measured and used to interpret

or predict the behaviour of the prototype. For this method a detailed knowledge of the material properties is not always necessary.

The second method is the direct solution of the structure's governing equations. The enormous complexities encountered in the natural state of the geologic media can make analytical closed form approaches very difficult. Pioneering work by Terzaghi (1943) imparted scientific and mathematical bases to many aspects of these subjects, in these developments the solutions were often obtained on the basis of differential equations that were assumed to govern the physical systems, and a large number of simplifying assumptions were necessary to obtain the closed form solutions. Although this approach has provided useful solutions for many practical situations, it cannot yield realistic solutions for problems involving such complexities as non-homogeneity, nonlinearity, in situ stress conditions, and many other factors imposed by geological characteristics.

However, numerical techniques enable the governing equations of a complex problem to be approximated by a system comprising a finite number of variables, whose solution provides an approximation to the true solution of the problem.

The most widely used methods in geotechnical engineering are the finite element and finite difference methods. Before the era of the finite element method, the finite difference method was perhaps the main numerical technique employed in geotechnical engineering. Although the finite element

method possesses certain advantages over the finite difference method, the latter can be more suitable for certain classes of problems.

The finite element method (FEM) is a particular numerical technique which can be used to approximate linear differential equations by a system of simultaneous equations, Zienkiewicz (1971). This approximation is the most important and powerful feature of the method.

2.3   Basic Assumptions of the Finite Element Method

In the FEM a structure is approximated by an assemblage of elements of the structure, interconnected at a finite number of joints or nodal points replacing infinite numbers of the element boundary points. This process is called idealisation or discretisation; it involves the evaluation of the element characteristics independently from the rest of the structure. Once the element characteristics are established, the general procedures of assembly and solution will follow a pattern for which the structural analogy provides a convenient basis. During the solution, the three conditions listed in section (2.1) are satisfied within each element and at the nodes, while in general only one of the first two conditions can be satisfied at the element interfaces depending on the approach followed. This satisfaction will allow the structure to be approximated by a finite set of primary variables inter-related by a system of simultaneous equations. These primary variables

always appear in pairs and are called the nodal variables. In the case of plane stress, plane strain, axisymmetric and three dimensional stress analysis they are the corresponding nodal components of force and displacement.

Once the primary variables have been evaluated the secondary variables, strains and stresses are uniquely defined within each element using the definition of strains and the material stress-strain laws.

As mentioned before, the finite element idealisation cannot in general satisfy fully both equilibrium and compatibility at the element interfaces. The two most common idealisations satisfy either compatibility or equilibrium across each interface of a finite element. In this research, the formulation satisfying compatibility throughout is used, it is commonly referred to as the "displacement approach". Thus the unknown primary variables are the displacements at the nodes which are inter-related to the known nodal forces by a set of equations representing the stiffness of the structure. These equations can be obtained either by the virtual work principle or by minimising the strain energy of the finite element idealisation.

The principle of virtual work or displacements does not depend on the mechanical properties of the material and is therefore valid for any state of the body such as solid, liquid, elastic or inelastic.

Generally, the displacement approach of the finite element stress analysis of a continuum involves three basic steps:-

1.   From the applied loads, the equivalent nodal
forces are calculated.   These are called the known primary
variables.

2.   From the element characteristics, the overall
structural stiffness matrix is assembled.   Inversion of
the stiffness matrix solves for the displacements at the
nodes.   These are called the unknown primary variables.

3.   From the displacements at the nodes, the strains
are calculated.   Using the material stress-strain laws,
the stresses are also calculated, thus the secondary variables
are found.

The more fundamental discussion of the steps involved
in the finite element analysis can be found in the books by
Zienkiewicz (1971), Desai and Abel (1972), and Cook (1974).

2.4   The Isoparametric Elements

The isoparametric element concept proposed by Irons
and Zienkiewicz (1968) has proven to be a simple but elegant
basis for element formulations.   Its use permits incorpora-
tion of curved boundaries and greatly facilitates   such
mathematical computations as integrations and differentia-
tions involved in an element formulation.

The term isoparametric implies common (iso-) parametric
description of the unknown displacement and geometry of the
element.   The basic idea is to express both the displacement
and the geometry of the element by using the same shape
functions.   So, if the displacement of a point in the

element is defined in terms of displacements at the nodes by using the shape functions N_i, then the coordinates of a point in the element has to be defined in terms of the coordinates of the nodal points by using the same shape functions N_i.

For Gauss quadrature, n sampling integration points are sufficient to integrate a polynomial of degree $(2n - 1)$ exactly. For example if the shape functions are quadratic in X and Y directions, the polynomial of the stiffness matrix will be quartic and 3 Gauss points are needed to integrate the stiffness matrix correctly. But in some cases in which the element type used in this research is one, it was found, Nayak (1971) and Naylor (1974), that it is possible to improve the performance by using a reduced integration rule, say 2 instead of 3 Gauss points.

The 8-noded isoparametric element with 2 integration points implies a parabolic distribution of displacements across the X or Y direction. Thus the best approximation obtainable from an element is limited by this parabolic distribution.

Strains are the first derivative of the displacements, hence, only a linear strain distribution across the element can be obtained. Therefore, if the strains are varying in a more complex distribution, the element will approximate that to a linear one.

2.5 The Stress-Strain Model used in this Research

A rigorous stress-strain law should be able to describe

analytically the state of stress and state of strain,
including the state of failure, in all three phases (solid
particles, water and air), of an element of soil under any
case of loading having satisfied all implied boundary con-
ditions.   A stress-strain law is needed together with com-
patibility conditions and equilibrium equations, in order
to solve a continuum problem.

In the geotechnical engineering, the material non-
linearities, exhibited through variable material parameters,
can be caused by a number of factors such as the state of
the stress or strain, in situ stresses, previous geological
and stress history, etc.

For many years the solutions of linear elasticity and
limit plasticity have been utilized in solving soil mechanics
and foundation engineering problems, many simplifying assump-
tions being made due to the lack of more sophisticated
solutions.   In deriving the elastic solution, the soil is
assumed to be a linear elastic body which can never fail;
in the plasticity solution the soil is assumed to be a rigid-
plastic body usually covered by the Mohr-Coulomb failure
criterion.   The former predicts deformation only, the
latter assesses stability only.   Neither approach models
the complete behaviour of a soil continuum under load.

Recent developments in numerical techniques with the
ability to predict deformations in soils (e.g. FEM) using
complicated stress-strain laws, have focussed attention on
the need to define soil stress-strain laws, the solution   .

techniques being limited by the availability of data on soil properties. Nevertheless, the literature on the subject is full of stress-strain solutions for different soil types, using mainly two categories of soil models:

1.   those utilizing only the theory of elasticity, but with attempts made to account for the nonlinearity typically observed in soil stress-strain relationships including the failure stage;

2.   those utilizing theories of plasticity, which are dependent on the type and variation of yield function and flow rule used; this category is more varied than the first.

It has to be mentioned that, at the failure stage, where an isotropic elastic model uses $E \doteq 0$, the Poisson's ratio must be equal to 0.5 or very close to it, $v = 0.499$ say, otherwise the model will produce very large volumetric strain.

Hamza (1976), in a review of the assumptions and basic principles of the elastic and plastic stress-strain models, demonstrated that a wide diversity exists in these models, and there appeared to be more fundamental differences between the various plasticity models than between the elasticity models. Also, he has mentioned that the proof of the adequacy of most of the non-linear elastic approaches has come from the successful use of these models in analysis of observed field behaviour. But no proof has been

presented for the accuracy of most of the plasticity models. Only the Roscoe and Burland (1968) plasticity model has been demonstrated to adequately simulate certain classes of soil behaviour observed in laboratory tests (Hamza, 1976). However, one fact is clear that more fundamental testing is needed to determine the most suitable model for soil behaviour.

During the course of this research a logarithmic equation is used to represent the nonlinear stress-strain curve as shown on Fig. 2.1. The explicit form of the equation for axial strain is

$$\varepsilon_r = -[\frac{1+b}{ab^2} \log(1 - ab\sigma_r) + \frac{1}{b}\sigma_r] \qquad (2.1)$$

where ε_r denotes the strain ratio $= \varepsilon/\varepsilon_e$

ε_e denotes the linear strain $= \dfrac{(\sigma_1 - \sigma_3)_f}{E_i}$

σ_r denotes the maximum shear stress mobilised $=$
$\dfrac{(\sigma_1 - \sigma_3)}{(\sigma_1 - \sigma_3)_f}$, and

a,b denote constants to be determined from the test data.

The equation is written in a dimensionless form, thus enabling a family of curves to be normalised to a single curve from which the two constants "a" and "b" can be determined. Normalisation is achieved first by normalising against the shear strength, and then against the linear strain ε_e.

The strain at failure could be written in the form:

$$\varepsilon_f = -\left(\frac{1+b}{ab^2} \log(1-ab) + \frac{1}{b}\right)\frac{2\tau_{max}}{E_i} \qquad (2.2)$$

This strain may vary with the variation of σ_3 independently of $2\tau_{max}/E_i$ by linking the constant "a" with the profile of strain at failure versus σ_3. In this case the constant "a" will be constant for single curve behaviour, but will vary for the family of curves.

The above equation is fed into the computer in the following form:

$$E_t = E_i \frac{1 - ab\,\sigma_r}{1 + a\sigma_r} \qquad (2.3)$$

which can be obtained by differentiating the original form. The latter form is more suitable for the non-linear algorithm adopted in the program used, and for any tangential stiffness method.

The initial tangent modulus E_i may be varied either:

1. Linearly with depth;

2. Exponentially with σ_3 (Janbu, 1963); or

3. Linearly with σ_3.

The shear strength is defined by the Mohr-Coulomb or Tresca failure criteria, where the latter one may be varied with depth.

2.6   Non-Linear Solution Techniques

In geotechnical engineering problems, two kinds of non-linearities exist. These are material non-linearity and geometric non-linearity. The work described in this

thesis is based on the assumption that displacements are sufficiently small for the problem geometry to be unchanged and that the theory of infinitesimal strains is valid. Thus the non-linearity is only due to material properties being dependent on the unknown required results.

The available techniques used in solving non-linear problems can be classified in two main categories:

1. Incremental Methods; and

2. Iteration Methods using the residual force concept.

The basis for classification is that the first category does not give a measure of convergence or of error (it can be inspected manually after the solution), while the second category does give a measure of convergence.

2.6.1 Incremental Methods

In these methods the result after a pre-stated number of increments or steps is considered as a solution for the non-linear problem, where the number of increments are not determined during the marching of the solution as in the iteration methods. Thus the stresses and strains of the solution are not compatible with the nominated stress-strain law, although they can be a good approximation, bearing in mind the uncertainties involved in the selection of the basic material properties used in the analyses.

2.6.1.1 The Tangential Stiffness Method

The most commonly used algorithm of the incremental method is the tangential stiffness method. Its mathematical basis is the first order Euler-Cauchy step-by-step method, which can be explained geometrically for a single equation, Fig. 2.2, as an approximation of the curve by part of a polygon whose first side is tangential to the curve at the initial point and so on.

The greater the number of increments, the closer is the approximation to the nominated stress-strain curve at the expense of more computer time.

Over-shooting above the failure surface is expected with this method since the check on stress level is carried out at the start of the increment. However, this over-shooting can be reduced by using smaller increments near the failure state of the stress. Once a point of the domain is above the failure stress, a very small value is assigned to the deformation parameter (e.g. E nearly zero).

Strain-softening cannot be modelled using this method because the overall stiffness matrix may tend to be non-positive definite.

2.6.1.2 The Quasi Runge-Kutta One-Step Method

The method is an approximation to the fourth order Runge-Kutta method which uses for each step four auxiliary quantities to arrive at the solution. In this approximation one auxiliary vector is used instead of four. It has a simple geometrical interpretation, for a single

equation, Fig. 2.3 , the curve is approximated by a straight line whose slope corresponds to the tangent of the curve at some intermediate point between the starting point and the final solution. The position of the intermediate point is arrived at by an iterative process to avoid over-shooting.

This technique has the same general limitation as the tangent method with regard to the post-peak modelling and stress-strain compatibility with the material law. This method has two main advantages:-

1. The size of the increment does not influence the results greatly because the non-linearity is dealt with during the increment, thus closer reproduction of the nominated stress-strain curve is achieved for the same computer time.

2. To avoid serious over-shooting the risk of local failure during any loading increment is examined by an iterative technique.

The more general discussion of this method has been given by Hamza (1972 & 1976).

From the comparison shown in Fig. 2.4 it is clear that the results of one step of Quasi Runge-Kutta is better than the results of two steps of the tangential stiffness method. Figures 6.52 and 6.53 (Chapter 6), show how well the technique succeeded in following to failure the nominated stress-strain curve at two different points in a problem of about 1200 degrees of freedom.

2.6.2 Iteration Methods Using the Residual Force Concept

The iterative procedure consists of successive corrections to a solution until the equilibrium under the total load is satisfied. In other words, in an iteration technique an approximation to the true solution is arrived at for each iteration using a convenient stiffness matrix (which need not be the true one). The state of the structure during this iteration is such that the displacement pattern is not in equilibrium with the external applied nodal forces because the stiffness matrix used is inappropriate.

Thus the residual forces are those forces which if added to the external loads would exactly balance the internal loads due to the incorrect state of stress in the structure. The iteration process will try to relax the structure by giving successive additional increments of displacement so that the residual force becomes zero or negligible, ending with a correct displacement vector.

In the above iterative procedure, a method has to be selected for the computation of the stiffness matrix. One choice is the Newton-Raphson method, which computes a different stiffness for each iteration, and that is the tangent stiffness at the end of the previous iterative step. The main disadvantage of this method is that in each iteration the tangential stiffness matrix for each element has to be calculated and the stiffness matrix for the whole structure has to be reassembled and inverted, which will result in a high computer cost.

The second choice is the Constant Stiffness method which, instead of computing a different stiffness for each iteration, utilizes only the initial stiffness. Obviously this method has a slower convergence than the Newton-Raphson method. The widely used initial stress and initial strain methods are variations of this concept.

Figure 2.5 shows these two methods.

2.6.3 Discussion on the Non-Linear Solution Techniques

The incremental methods are applicable to nearly all types of the non-linear behaviour, with the exception of the strain-softening materials. One other advantage of this technique is that it provides a relatively complete description of the load-deformation behaviour.

On the other hand, for the incremental method, it is difficult to know in advance what increments of loads are necessary to obtain a good approximation to the exact solution.

The iterative technique is applicable for the analysis of structures with strain-softening material properties. The principal disadvantage of the iterative method is that there is no assurance that it will converge to the exact solution.

Because the mixed method combines the advantages of both the incremental and iterative procedures and tends to minimize the disadvantages of each, incremental-iteration is being utilized increasingly.

2.7 General Description of the Programme Used in this Research

The programme is designed for two dimensional plane strain and axisymmetric geotechnical problems. It is a compact rather than a general purpose system. The programme uses the displacement approach to the 8-noded isoparametric element with built-in reduced Gauss integration rule for numerical integration of the element characteristics. The solution of the banded symmetric matrix is achieved by the direct Gauss elimination method. The deformation is assumed not to change the overall geometry of the problem (only small displacement and first order strain terms are retained).

Boundary conditions are specified in terms of displacement, in one or both of the vertical and horizontal directions, or by specifying a spring with constant stiffness. The prescribed displacement at the boundary could be prescribed to be free, a specific value of zero. (Prescribed displacement or springs could also be applied to nodes within the domain).

The programme can handle linear and non-linear material with a shear strength cut-off. Saturated undrained shear behaviour and non-dilatent drained shear behaviour can be modelled. Anisotropic linear elastic material is also available, provided that the axis of anisotropy coincides with the axis of geometry. In any problem the domain may be composed of non-linear isotropic, linear isotropic and/or linear anisotropic in terms of drained and/or undrained

deformation and shear strength parameters. In case of
undrained material properties, pore water pressure is
evaluated using the pore pressure parameters A and B. For
undrained loading if linear deformation parameters are used
pore water pressure is evaluated using water compressibility.

Types of loading include: Body forces to simulate
gravity or horizontal or inclined forces due to earthquake,
surface tangential and normal stresses, concentrated forces
and seepage forces and internal straining of the domain
(including volume change). The latter could simulate
creep and has other useful applications. Forces may be
applied in one step or in equal or non-equal increments or
in selected stages.

Non-linearity is dealt with using either incremental
or iterative methods, or a combination of the two. The
incremental technique can be either the tangential method
or the Quasi Runge-Kutta method. For the iterative tech-
nique either the constant stiffness method or the Newton-
Raphson method can be chosen.

For the tangential method the material properties are
selected at the start of each increment according to the
current state of stress. If the state of stress is near
or above the failure state, the point is given a very small
value of deformation modulus and a value very close to 0.5
for the Poisson's ratio. Obviously over-shooting is
expected and can only be controlled by repeating the runs
with more increments. The Quasi Runge-Kutta method uses

a pilot solution to determine the magnitude and direction of the stress increment. Therefore, the material properties are assigned more closely to the nominated stress-strain curve. The pilot solution enables the relevant deformation parameters for loading, unloading and reloading to be assigned to every Gauss point in the domain.

The output in terms of accumulated stresses and strains at the Gauss points and/or at the nodes and incremental displacements and residual forces of the nodes can be partly or totally printed or totally saved in a magnetic tape or permanent file for future reference. It can also be used for graphic plotting and as an input for further loading or increments.

During this research an iteration technique has been developed and used in the programme for the hydraulic fracturing phenomenon which implies a strain-softening problem. A modified form of the Newton-Raphson or Constant Stiffness method which enables the relevant deformation parameters for unloading to be assigned to every Gauss point in the domain in every iteration, was used where necessary (see Appendix 2). The root mean squares of the residual forces at the nodes are used as the measure of convergence.

A flow chart of the programme is given in Appendix 1.

2.8   Modifications and Developments in the Programme

The finite element programme used in this research is a modified form of the original programme developed by Hamza at Imperial College, 1972-74.

In the following section a list of the most important modifications has been given. Description and discussion of these modifications have been considered in Appendix 2.

1. Shear unloading and reloading;

2. Poisson's ratio varying with stress;

3. Spring as the boundary condition;

4. Applying the seepage forces;

5. Iteration modified for shear unloading; and

6. Strain-softening.

Fig. 2.1   The stress-strain curve.

F

F

F_4

F_3

F_2

F_1

Error

$F = f(\delta)$

δ

Force - displacement

σ

σ_4

σ_3

σ_2

σ_1

Error

$\sigma_i = \Phi(\sigma_{i-1})$

ε

Stress - strain

Implicit non-linear relation

$\{\delta\}_i$ $\xrightarrow{[B]}$ $\{\varepsilon\}_i$ $\xrightarrow{[D_t(\{\sigma\})]}$ $\{\sigma\}_i$ $\xrightarrow[\text{work}]{\text{Virtual}}$ $\{F\}$

Explicit non-linear law
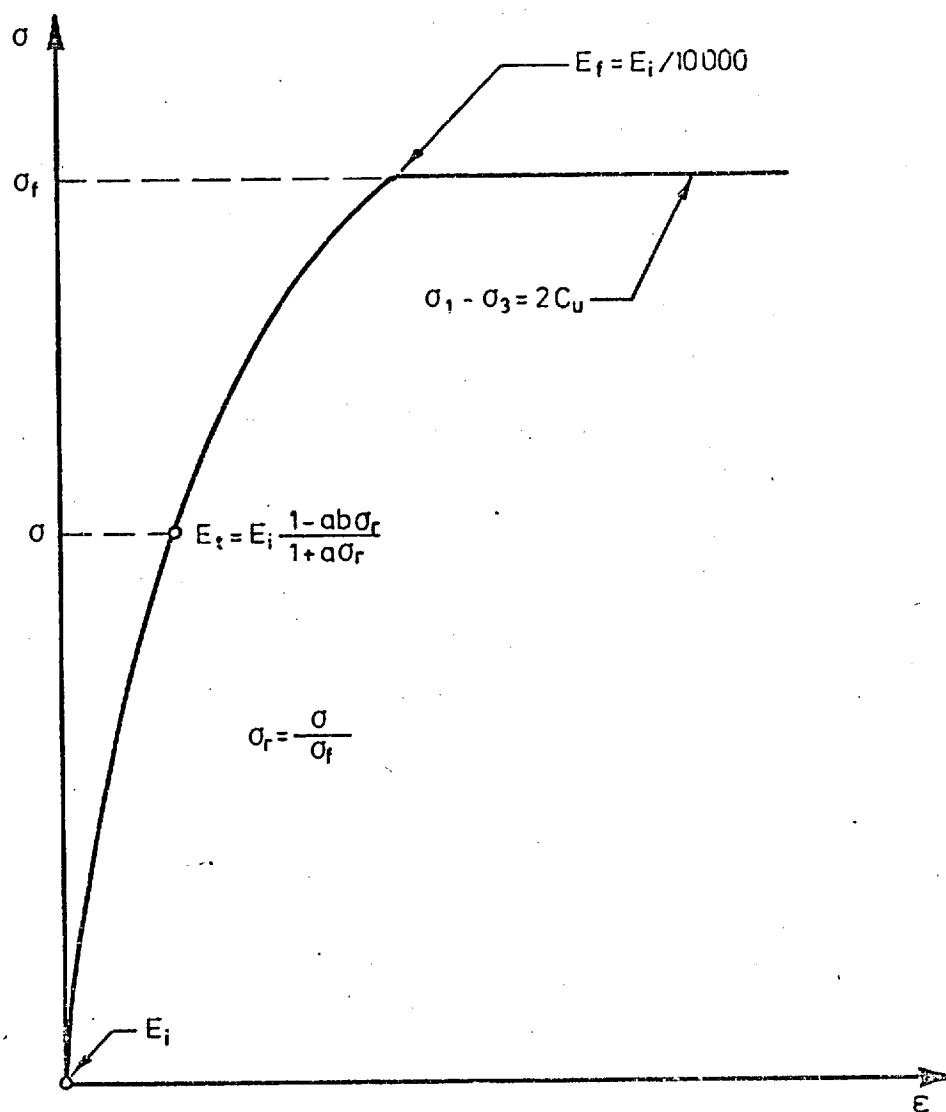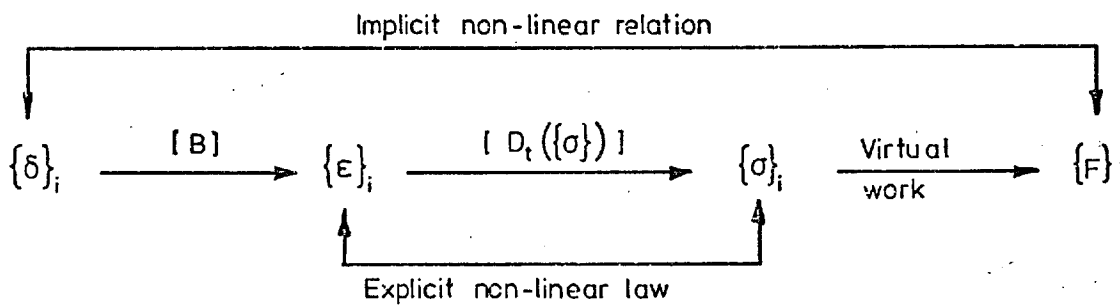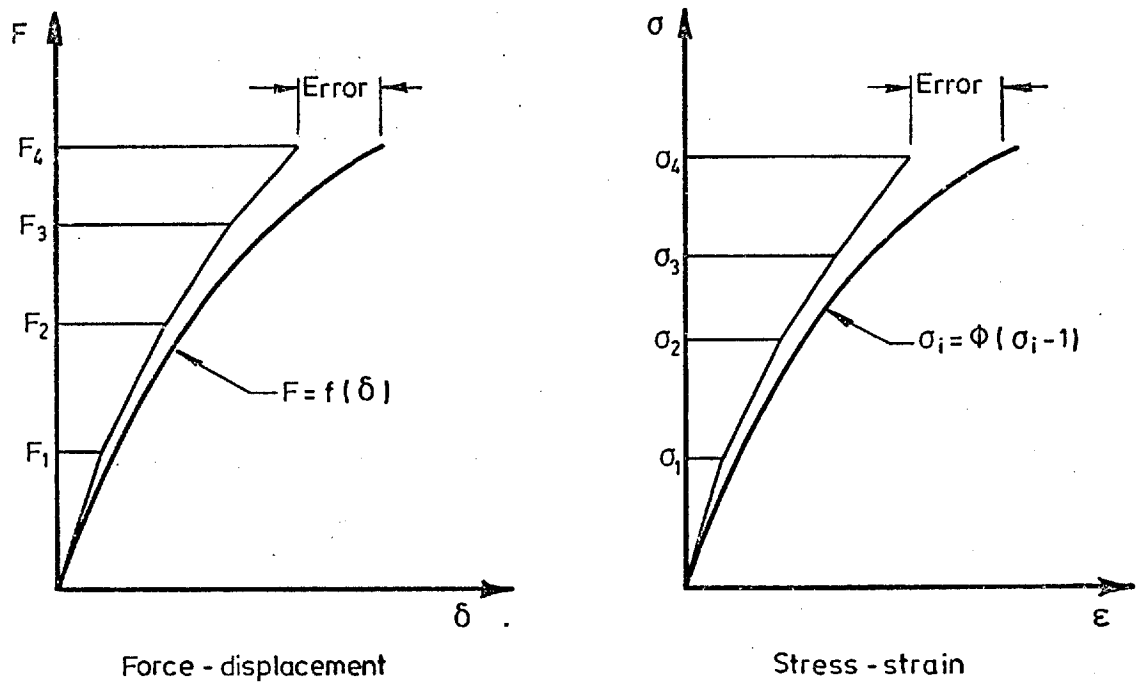
Fig. 2.2   One dimensional explanation of the Tangential
Stiffness Matrix method.
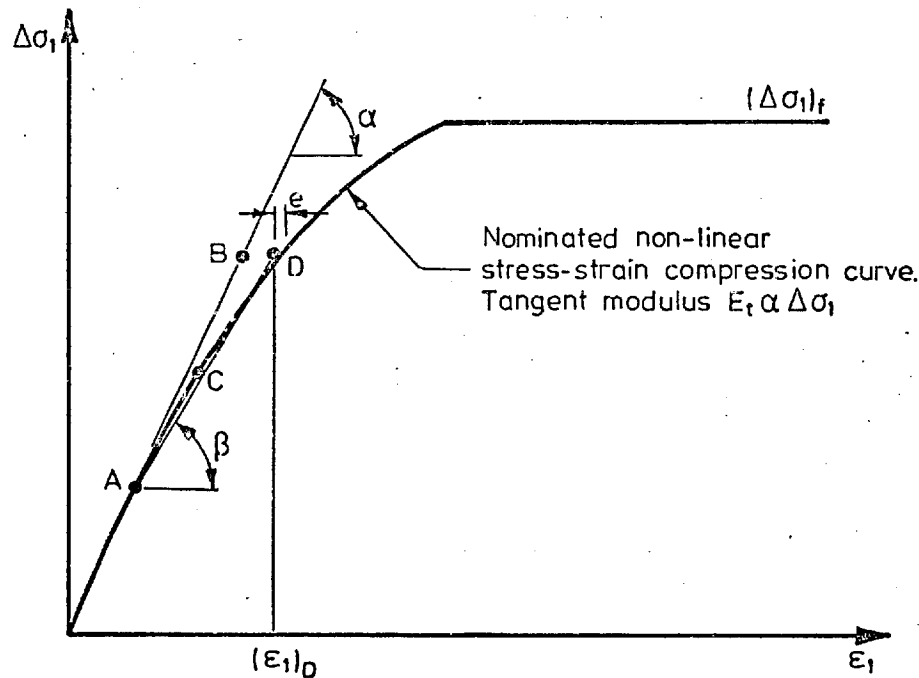
After n load increments $\quad \Delta\sigma_1 = (\Delta\sigma_1)_A$, $\quad \varepsilon_1 = (\varepsilon_1)_A$

For n+1th increment:-

    <u>First solution</u>: $E = (E_t)_A = \tan\alpha$
    gives $(\Delta\sigma_1)_B$ and $(\varepsilon_1)_B$

    <u>Second solution</u>: $E = (E_t)_C = \tan\beta$

    where $\quad (\Delta\sigma_1)_C = \dfrac{(\Delta\sigma_1)_A + (\Delta\sigma_1)_B}{2}$

    gives $(\Delta\sigma_1)_D$ and $(\varepsilon_1)_D$, curve fitting error = e

If: $(\Delta\sigma_1)_A > 0.95(\Delta\sigma_1)_f$, failure assumed and solution made with E very small.

If: $(\Delta\sigma_1)_C > (\Delta\sigma_1)_f$, try

$$(\Delta\sigma_1)'_C = (\Delta\sigma_1)_A + \frac{(\Delta\sigma_1)_B - (\Delta\sigma_1)_A}{4}$$

if $(\Delta\sigma_1)'_C < (\Delta\sigma_1)_f$ determine $(E_t)'_C$ and use in second solution.

if $(\Delta\sigma_1)'_C > (\Delta\sigma_1)_f$, try $\quad (\Delta\sigma_1)''_C = (\Delta\sigma_1)_A + \dfrac{(\Delta\sigma_1)_B - (\Delta\sigma_1)_A}{8}$

and so on.

Fig. 2.3 The Runge-Kutta algorithm for one variable problem.

BEFORE FAILURE

AT OR CLOSE TO FAILURE
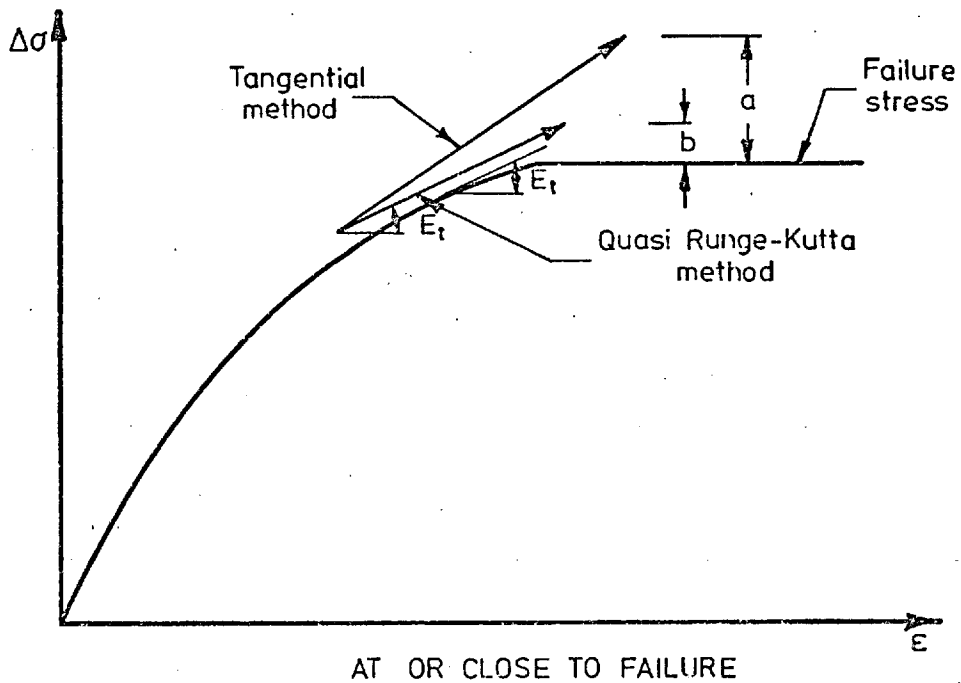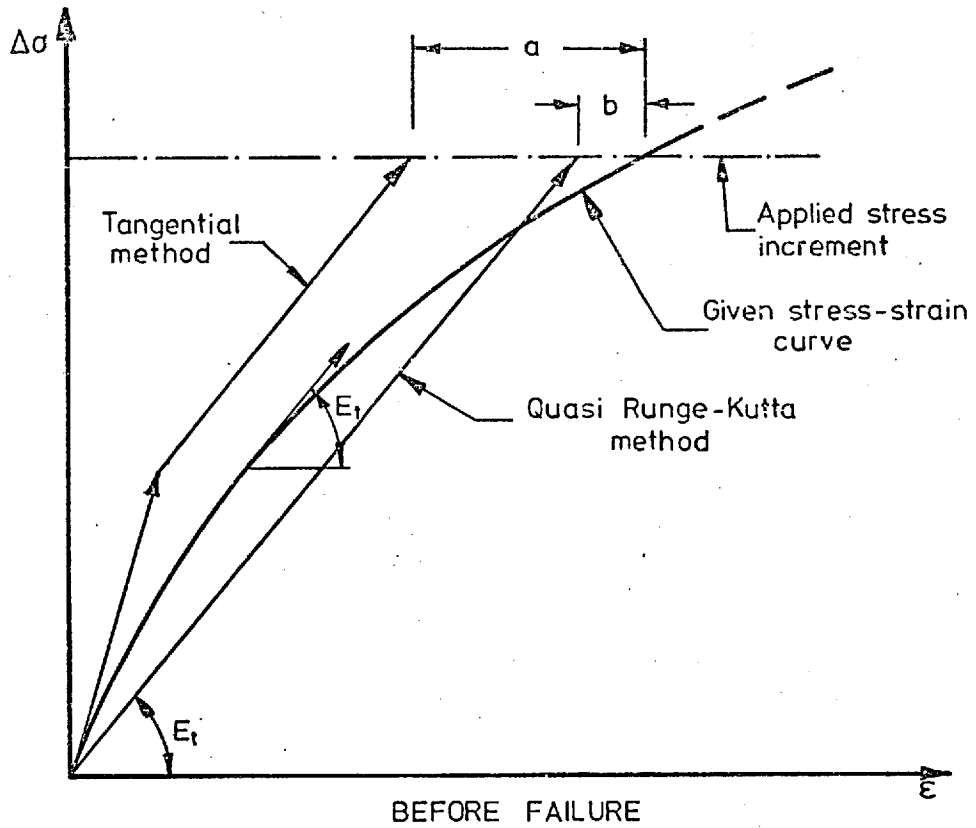
a = Error in using tangential method
b = Error in using Quasi Runge-Kutta method

Fig. 2.4   Comparison between the Tangential method and the
           Quasi Runge-Kutta method for one variable.
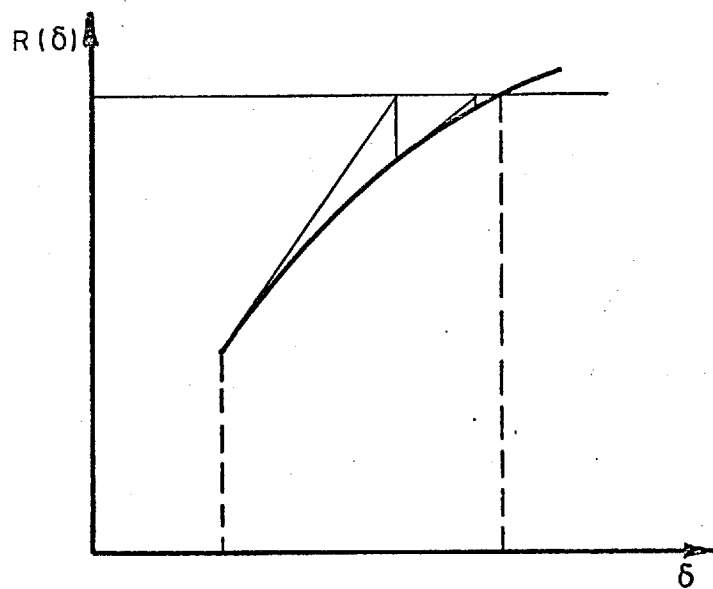
Newton-Raphson Method
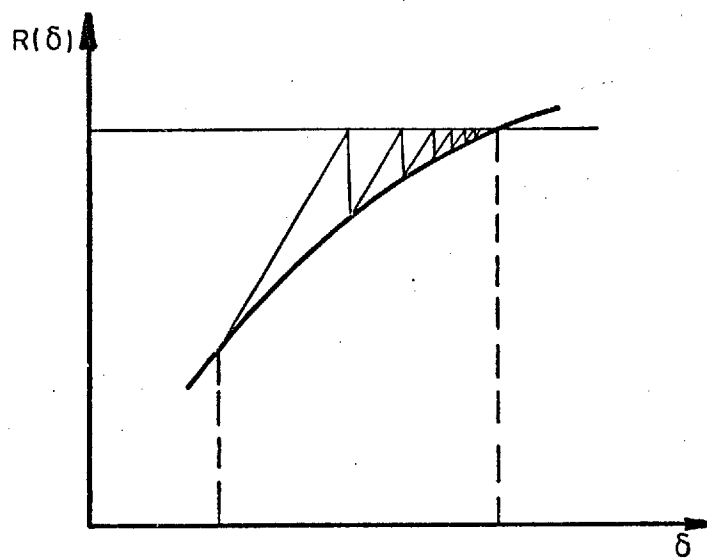
Constant Stiffness Method

Fig. 2.5   Comparison between the two iterative methods.

PART II

STABILITY ANALYSIS OF SHALLOW FOUNDATIONS

CHAPTER 3

STRESS DISTRIBUTION AND SETTLEMENT ANALYSIS

3.1 Introduction

Generally, two considerations enter into the stability

analysis of a foundation, namely, safety against failure by

excessive settlement and safety against failure by shear.

The idealised load-settlement curve for a footing on

an elasto-plastic soil can be divided into three sections,

Fig. 3.1:

(1) Linear section, AB, where the settlement is

proportional to the load;

(2) Non-linear section, BC, which represents the

region of contained failure;

(3) Section CD, which represents the failure of

the foundation at the ultimate bearing pressure.

So, analysis of a foundation requires solutions to

the three types of problems, namely, the linear phase, the

contained failure, and the ultimate load.   Elasticity,

used as linear theory, deals with stress and deformation of

the soil under the footing subjected to working load con-

ditions and mainly limited to the section AB of the curve

in Fig. 3.1, where a linear relationship between stress and

strain is assumed to exist.   The ultimate load analysis,

on the other hand, deals with the condition at the first

complete failure of the foundation.   The theory of perfect

plasticity is generally used to develop methods which are

capable of predicting the failure load. The intermediate between the elasticity and the ultimate load is the problem of contained plastic flow (D'Appolonia et al, 1971, defined this section as the region of local yielding), where the transition from the initial linear state to the final plastic state takes place in the soil around the foundation. A method of analysis which considers contained plastic flow, such as the finite element method, is required to study this region.

The point B, Fig. 3.1, is the boundary between the linear phase and the contained plastic flow region, and represents a state of stress within the soil mass, where the shear stresses induced in the soil will first reach the shear strength at some point, and local yielding will first occur (D'Appolonia et al, 1971). After this stage, a further increase in the load will cause a redistribution of the stresses within the soil to ensure that the shear stresses nowhere exceed the shear strength. Then, the deformations at a point in the soil within the zone of local failure will no longer depend solely on the stresses at that point, but will be dependent on the state of stress within the entire soil mass.

The purpose of this chapter is to summarise some of the more commonly used method of settlement prediction and to discuss the estimation of the stress distribution within the soil. This chapter is divided into three parts. The first deals with the determination of stress distribution, the second with settlement analysis, and the third with the

soil-foundation interaction. The section on settlement is subdivided into parts which deal with non-free drained and free drained soils.

The problems of the contained failure and the ultimate pressure will be considered in Chapters 4 and 6.

3.2 Stress Distribution

3.2.1 General

Determination of the stress distribution within a particular region is an important process of predicting the settlement due to the compressibility of a soil, and may also be important in certain stability problems.

The most common method for determination of the stress distribution in a homogeneous soil beneath a foundation is linear elastic theory. The justification for this lies in both laboratory and field tests which have utilized in-situ pressure cells to measure the stresses. The results of a variety of small and large scale laboratory and field tests with in-situ pressure measurements (Foster & Fergus, 1951 ; Morgan & Scala, 1968 ; and Bozozuk & Leonards, 1972) suggest that when the boundary conditions of the analytical model approximate the in-situ boundary conditions, the computed stress distribution will correspond reasonably well to that interpreted from the field measurements.

3.2.2 Calculation of Stresses Imposed by a Point Load

Boussinesq (1885) provided a solution to the distribution of stresses within an isotropic linear elastic half-space under the influence of a surface point load (Fig. 3.2). The stresses at a point can be calculated by means of the following expressions:

$$\sigma_z = \frac{3p}{2\pi} \frac{z^3}{R^5} \tag{3.1}$$

$$\sigma_r = \frac{p}{2\pi} \left[\frac{3zr^2}{R^5} - \frac{1-2\nu}{R(R+z)} \right] \tag{3.2}$$

$$\sigma_\theta = \frac{p}{2\pi}(1-2\nu) \left[\frac{1}{R(R+z)} - \frac{z}{R^3} \right] \tag{3.3}$$

$$\tau_{rz} = \frac{3p}{2\pi} \frac{rz^2}{R^5} \tag{3.4}$$

$$\tau_{\theta z} = \tau_{r\theta} = 0 \tag{3.5}$$

where ν is the Poisson's ratio and other quantities in the equations are defined in Fig. 3.2. These stresses are for a weightless medium, and pre-existing stresses due to the weight of the material must be superimposed upon these.

As the vertical normal stress σ_z is independent of ν, the Eq. 3.1 can be written:

$$\sigma_z = I_{zB} \frac{p}{z^2} \tag{3.6}$$

where I_{zB} is an influence value which depends only upon the geometry:

$$I_{zB} = \frac{3}{2\pi} \left[\frac{1}{1 + \left(\frac{r}{z}\right)^2} \right]^{5/2} \tag{3.7}$$

This influence value is plotted in Fig. 3.3.

The Boussinesq formula for the vertical stress applies only for isotropic and homogeneous soil masses. When the soil is stratified, Westergaard (1938) worked out a limiting solution on the assumption that the soil is restricted from horizontal deformation. The vertical stress according to Westergaard is:

$$\sigma_z = I_{zw} \frac{p}{z^2} \qquad (3.8)$$

$$I_{zw} = \frac{1}{\pi}[\frac{1}{1 + 2(\frac{r}{z})^2}]^{3/2} \qquad (3.9)$$

I_{zw} is the influence value for Westergaard solution, and it has been plotted in Fig. 3.3.

3.2.3 Calculation of Stresses Imposed by a Loaded Area

By the principle of superposition, the point load results can be integrated over a finite area to produce the stress distribution resulting from a uniform stress applied to the surface.

Janbu, Bjerrum and Kjaernsli (1956) have given a design chart (Fig. 3.4) for the values of the vertical stresses beneath the centre of a uniformly loaded flexible area of strip, rectangular or circular shape.

For estimating the vertical stresses beneath flexible, uniformly loaded areas of irregular shapes the chart given by Newmark (1942) and shown in Fig. 3.5 can be used.

The vertical stresses at any location under a loaded area can be calculated by using the principle of superposition and Figs. 3.4 and 3.5.

After determining the stress increments due to sur-
face loading at a variety of points within a medium, it is
useful to draw these stresses graphically in relation to
their points of action.

3.2.4 Analysis of Layered Systems

Natural soil deposits and fills are often composed
of two or more layers with different properties.   Concern
about the potential influence of a layered system on the
distribution of stresses and displacements has led to
analysis of elastic systems consisting of layers of differ-
ing elastic properties.   Burmister (1943) developed
expressions for stresses and displacements of 2- and 3-
layer flexible elastic systems subjected to a uniform stress
acting over a circular area of the surface.   Numerical
values of these results have been presented by Acum and Fox
(1951); Burmister (1958, 1967); Jones (1962) and Peattie
(1962).

If there are more than three layers in the real system,
similar layers can be grouped together and assigned average
physical properties (Peattie, 1963) in order to reduce the
number of layers to three.

Figure 3.6 represents a typical stress distribution
in which a uniformly loaded circular area is acting on the
surface of a 2-layer elastic system.   The vertical stress
distribution under the centre of the loaded area is shown
as a function of depth for various ratios of Young's moduli.

The results show that when the upper layer is much stiffer than the lower layer, the stress in the lower layer is significantly reduced. Conversely, the stress in a layer underlain by a very stiff layer is increased remarkably. Thus, the stresses in an elastic layer underlain by a stiff granular material or rock would be significantly higher than those predicted by Boussinesq theory for a homogeneous semi-infinite elastic layer. This difference is remarkable near the base of the elastic layer, where a concentration of stresses occurs.

For natural soil deposits, the superficial layers are normally softer and weaker than those beneath, and the foundation soil or soils overlying bedrock may be considered to be a single compressible layer overlying an incompressible layer. If the upper layer is thick compared to the lateral extent of the loaded area placed on its surface, it is reasonable to assume that the layer is semi-infinite.

3.2.5 Influence of a Rigid Base below the Loaded Layer

The problem of layered system has been discussed in the previous section. The simplest case of a layered system is that of an elastic layer overlying a rigid base. The interface between the layer and base can either be perfectly rough or perfectly smooth. When the interface is perfectly smooth, surface settlement is independent of the layer thickness $(V=0.5, E_o=0)$, (Awojobi, 1974). Tabulated results for the stresses and displacements in an elastic layer overlying a smooth rigid base and subjected to a uniformly

distributed load of rectangular shape have been given by Sovinc (1961).

In soil mechanics problems, rough interface is more realistic than smooth one. Poulos (1967) has considered an elastic layer underlain by a rough rigid base, and he has given tabulated results for stresses and displacements. Figures 3.7 to 3.10 represent the influence factors I_{st} for the vertical stresses σ_z, under the edge of a strip load for four values of Poisson's ratio ν (after Poulos, 1967).

From Fig. 3.6 it has been mentioned that the stresses calculated from the Boussinesq solution for a semi-infinite layer is less than the true stresses in a finite layer. . In addition, the Poisson's ratio of the material has a more significant effect on the stress distribution in a finite layer than in a semi-infinite one (Poulos, 1967).

3.2.6 <u>Effect of the Loads acting within the Medium</u>

Terzaghi (1943) has observed that the stresses induced by a point load within a semi-infinite incompressible elastic solid ($\nu = 0.5$), are one half of the values due to the same load acting at the surface of the same medium. Mindlin(1936) and Mogami (1957) have solved for the stresses due to a vertical or horizontal point load acting within the semi-infinite medium, and tabulated results have been given in the second reference.

For practical cases, stress changes required for settlement predictions for foundations at shallow depths may be computed using net foundation pressure and the

solution for surface loading (Vaughan, 1973).

3.2.7 Effect of the Non-homogeneity

For many years the formulae, charts and tables used by engineers for problems of surface loading, based on the solution of Boussinesq's problem, have assumed the semi-infinite soil medium to be isotropic and homogeneous.

It is now generally understood that within the real soil strata, strength and moduli increase with depth, reflecting the increasing overburden pressure (Gibson, 1974). The variation of E with depth may well be approximated by a line as given in the following expression:

$$E_z = E_o + \lambda z \tag{3.10}$$

where E_z is the value of modulus at depth z; E_o is the value of modulus at ground surface; λ is the rate of increase in E with depth; and z is the depth from soil surface.

The variation of shear strength with depth will be considered in Chapter 4, and here it should be mentioned that the ratio of undrained modulus to undrained shear strength (E_u/C_u) is constant.

Gibson (1967, 1968 & 1969) has given the expressions for the components of stress at any point within a non-homogeneous elastic half-space, due to loading normal to its plane boundary, for any linear variation of E with depth. He suggested that the effect of non-homogeneity on the stress components may be small, and for a special case

$(E_O = 0)$ the stress components are unaffected by the variation of E with depth. On the other hand, Carrier and Christian (1973) considered a smooth rigid circular plate at the surface of a non-homogeneous semi-infinite layer, and concluded that the ratio $E_O/\lambda D$ (D = plate diameter) has a marked effect on the stress distribution.

With the advent of digital computers, there have been a very large number of influence charts developed which cover a wide range of variables, see Scott (1963); Poulos and Davis (1974); and Perloff (1975).

3.3   Settlement

3.3.1 General

Prediction of settlement is important for different reasons. Probably the most important one is that the settlement of structures can result in structural damage or failure by causing redistribution of loads in structural members. It is known that, generally the differential settlement is more critical than the total settlement in this respect. A recent discussion of differential settlement is given by Grant et al (1974). Table 3.1 and Fig. 3.11 represent typical guidelines concerning total and allowable settlements, and structural damage due to angular distortion.

Settlement may be caused due to a number of reasons, Table 3.2 lists some of them and it may be noted that many of the causes are not amenable to quantitative analysis. The discussion described herein is restricted to consideration

of settlements resulting from change in vertical static load, although many of the principles may be applied to settlements due to other causes. It must be emphasized that settlements due to other causes, such as dynamic loads, change in moisture content, and the effect of nearby construction may often be as significant as those due to static loads.

In Chapter 6, the settlement due to cyclic loads will be considered.

From the standpoint of the change in volume due to changes in loading, soil can be divided into two classes, namely, non-free drained and free drained soil.

3.3.2 Settlement of Non-free Drained Soils

It is generally recognized that settlement of non-free drained soils due to change in vertical stress is made up of three components

$$\delta_t = \delta_i + \delta_c + \delta_s \qquad (3.11)$$

where δ_t is the total final settlement; δ_i is the immediate or undrained settlement; δ_c is the consolidation settlement; and δ_s is the creep or seconeary consolidation settlement.

Although it is convenient to separate each of these components for analysis, it is important to recognize that in nature all three components occur to some extent simultaneously.

Lambe (1973a) summarized some of the methods available for computing the above settlements (Table 3.3). Further

discussion of this problem is given by Moorhouse (1972);
Simons (1974); and Sowers (1975).

3.3.2.1 Immediate Settlement

Immediate settlement is defined as: the settlement
associated with the undrained shear deformation of the soil,
under constant volume change, due to rapid application of
the load to a deposit of saturated clay.

The immediate settlement may be a very significant
part of the total final settlement. However, immediate
settlements are reduced if horizontal displacements of the
foundation are constrained, and they become zero if there
is total constraint.

If the shearing stresses in a clay layer are small,
it is reasonable to assume that the shear strain will be
approximately proportional to them. Making this assumption
and considering the independence of time, it is possible to
compute the immediate settlement for the clay deposit from
linear elastic theory.

The linear elastic method used in computing the
immediate settlement is based on the approach described by
Davis and Poulos (1963 & 1968), and a similar approach by
Kerisel and Quatre (1968) and Egorov et al (1957).

The immediate settlement may be calculated either by
summation of vertical strains beneath the foundation or
directly by the use of elastic displacement theory:

(1) Elastic strain summation is based on a 3-dimensional strain calculation and is useful for non-homogeneous or stratified soil deposits:

$$\delta_i = \sum \frac{1}{E_u}[\sigma_z - \nu_u(\sigma_x + \sigma_y)]\delta h \qquad (3.12)$$

where E_u is the undrained Young's modulus of the soil; ν_u is the Poisson's ratio (for saturated soil, $\nu_u = 0.5$); σ_x, σ_y, σ_z are the stress increments; and δh is the thickness of each stratum or layer.

(2) Elastic displacement theory for calculating the immediate settlement based on the following general formula:

$$\delta_i = \frac{q B}{E_u} I_\delta \qquad (3.13)$$

where I_δ is the influence factor; B is the foundation width; and q is the applied stress.

Many solutions are available for the influence factor, including: the classical solution of Boussinesq (1885) for loading on the surface of an elastic half-space; Burmister (1956), Davis and Taylor (1961), and Poulos (1967) for a layer underlain by a rigid base; and Ueshita and Meyerhof (1967) for a 3-layer elastic system.

For computing the average immediate settlement of uniformly loaded, flexible areas, rectangular or circular in shape, Fig. 3.12 represents the chart given by Janbu et al (1956). The average settlement is obtained from Eq. 3.13

by putting $I_\delta = \mu_0 \mu_1$, and Poisson's ratio equal to 0.5.

Recently, Christian and Carrier (1978) have improved the Janbu et al (1956) chart. Their improved version of the chart is composed of Giroud (1972) results for the effect of depth and Burland (1970) results for the effect of embedment.

The more comprehensive solutions for the influence factor are given by Poulos and Davis (1974).

3.3.2.2 Effect of Local Yielding on Immediate Settlement

One of the most important shortcomings of the linear elastic theory in computing the immediate settlement is in the evaluating of the strains after stress redistribution due to local yielding.

Davis and Poulos (1968) have shown that the factor of safety against a bearing capacity failure at first local yield for normally consolidated clays is between 4 and 8, for slightly overconsolidated clays is 2 to 3, and for heavily overconsolidated clays is less than 2. Foundations for structures, on the other hand, may be designed with a factor of safety, against ultimate failure, of the order of 2½ to 3, thus, for normally consolidated clays the use of elastic method may well lead to underestimation of the immediate settlement.

D'Appolonia et al (1971) considered this problem, and proposed a correction factor to be used with the elastic method. Their modified elastic displacement is:

$$\delta_i = \frac{q \, B \, I_\delta}{E_u} \frac{1}{S_r} \tag{3.14}$$

where S_r is the settlement ratio, and its value depends on the ratio of applied stress to ultimate stress (q/q_u); ratio of layer thickness to foundation width (H/B); initial stresses in the deposit; and shear strength of the soil. Before local yield occurs, the value of S_r is equal to one, and elastic displacement theory gives the proper settlement. After local yield, the value of S_r becomes less than one, as the actual settlement is greater than that predicted from elastic theory. When the ultimate bearing capacity is approached, the value of S_r becomes equal to zero.

Figures 3.13 to 3.15 represent the values of S_r at the centre of a uniformly loaded strip foundation on a homogeneous isotropic layer. The factor f used in these figures is the initial shear stress ratio $= \frac{(1-K_O) \, \sigma'_{vo}}{2C_u}$, where K_O is the coefficient of lateral earth pressure at rest; σ'_{vo} is the initial vertical effective stress; and C_u is the undrained shear strength.

The results for $H/B = 1.5$ are applicable for all values of H/B greater than 1.5.

3.3.2.3 Effect of Foundation Rigidity and Roughness

The settlement of a flexible load is not uniform, and it settles more at the centre than at the edges. A rigid foundation, in order to produce a uniform settlement,

must experience a decrease in pressure at the centre and an increase at the edges (Fig. 3.24).

Since most foundations are neither truly rigid nor truly flexible, this becomes the classic soil-foundation interaction problem.

Davis and Poulos (1968) give the following expressions relating rigid foundation settlements to flexible foundation settlements for a semi-infinite uniform elastic foundation:-

For a circle:

$$\delta_{rigid} \simeq \frac{1}{2}\left(\delta_{centre} + \delta_{edge}\right)_{flexible} \qquad (3.15)$$

For a rectangle:

$$\delta_{rigid} \simeq \frac{1}{3}\left(2\delta_{centre} + \delta_{corner}\right)_{flexible} \qquad (3.16)$$

For a strip:

$$\delta_{rigid} \simeq \frac{1}{2}\left(\delta_{centre} + \delta_{edge}\right)_{flexible} \qquad (3.17)$$

Analysis of a rigid circular plate resting on a non-homogeneous elastic half-space (Carrier and Christian, 1973) showed that for most practical problems (with $\nu \geqslant 0.3$) roughness has no effect on the solution. Only when $E_0/\lambda D$ is large and $\nu < 0.3$ need the roughness be taken into account.

3.3.2.4 Effect of Non-homogeneity and Anisotropy

Generally, the use of an average value of E_u may give a reasonable estimate of the average immediate settlement, but if it is necessary to predict the initial deflected shape, non-homogeneity and anisotropy must be taken into

account (Simons, 1974). For effects of non-homogeneity and anisotropy reference can be made to Lambe (1964); Gibson (1967); Davis and Poulos (1968); Gibson and Sills (1971); Burland, Sills and Gibson (1973); Carrier and Christian (1973); and Hopper (1974).

Gibson (1967) has shown that the variation of modulus with depth has a marked effect on surface displacements which are concentrated within the loaded area for an incompressible medium.

Butler (1974) gives charts for the approximate settlement of the corner of a uniformly loaded, flexible rectangular area resting on the surface of a non-homogeneous elastic layer. It is assumed that the modulus increases linearly with depth. Butler's charts for immediate settlement are given in Figs. 3.16 and 3.17.

The effects of non-homogeneity and anisotropy can be summarized by three important points:

(1) Non-homogeneity localizes the settlement of the ground surface to the vicinity of the loaded area.

(2) Horizontal modulus E_h has a marked effect on the vertical displacement.

(3) The maximum settlement of a flexible loaded area is near the edge for $E_v = 0$ at the surface and E_v increasing with depth, for anisotropic soil.

The effect of non-homogeneity (Point No. 1) has been studied by Gibson (1967, 1968 & 1969) and Brown and Gibson

(1972). They assumed that the Young's modulus E increases linearly with depth according to Eq. 3.10. This effect has been represented for a uniformly loaded circular area and $\nu = 0.5$ in Fig. 3.18, which shows that by introducing non-homogeneity the surface settlement at the outside of the loaded area becomes smaller, and finally for "Gibson Soil" $(E_o = 0)$ the settlements are:

$$\delta(r) = \delta(o) = \frac{3q}{2\lambda} \qquad r \leqslant R \qquad (3.18)$$

$$\delta(r) = 0 \qquad r > R \qquad (3.19)$$

where R is the radius or half-width of loaded area; r is the horizontal distance from the centre line of loaded area; $\delta(o)$ is the surface settlement at the centre; and $\delta(r)$ is the surface settlement at distance r from the centre.

The effect of anisotropy (points 2 and 3) have been given by Simons and Menzies (1975), and have been shown in Fig. 3.19 (after Rodrigues, 1975) for a uniformly loaded flexible circular footing resting on a wide deep elastic solid.

3.3.2.5 Consolidation Settlement

When foundation load is transmitted to cohesive subsoil, there is a tendency for volumetric strain which in the case of a saturated material is manifested in an increase in pore water pressure. With sufficient elapsed time, the excess pore water pressure dissipates, accompanied

by volumetric strains, which results in vertical settlements. When the dimensions of the loaded area are large relative to the thickness of the compressible layer, or when the compressible material lies between two stiffer soils, whose presence tends to reduce the magnitude of horizontal strains, it is reasonable to assume that there are only vertical strains.

Based on this assumption, Terzaghi (1943) developed a method, known as "conventional one-dimensional method", which involves the numerical summation or integration of vertical strains beneath the foundation. The resulting settlement will be referred to as δ_{oed}, and is calculated as:

$$\delta_{oed} = \sum m_v \cdot \Delta\sigma_z \cdot \delta_z \qquad (3.20)$$

where m_v is the coefficient of compressibility; $\Delta\sigma_z$ is the increase in vertical stress at the centre of the layer; and δ_z is the thickness of each layer.

Alternative forms of Eq. 3.20, which is in terms of the compression index of the soil, are available (Perloff, 1975).

The 1-dimensional method assumes that:

$$\delta_t = \delta_{oed} \qquad (3.21)$$

which has been modified with the subsequent recognition of the immediate settlement to:

$$\delta_c = \delta_{oed} \qquad (3.22)$$

At any time t after the application of the foundation

load, the consolidation settlement is:

$$\delta_{ct} = U_c \cdot \delta_c \qquad (3.23)$$

where U_c is the rate of settlement; and δ_c refers to ultimate consolidation settlement.

3.3.2.6 Skempton and Bjerrum Method

To take into account the effect of the 3-dimensional nature of the settlement process, Skempton and Bjerrum (1957), developed a semiempirical method which is based upon the following two assumptions:

(1) Consolidation settlement δ_c is expressed by:

$$\delta_c = \sum m_v \cdot \Delta u \cdot \delta_z \qquad (3.24)$$

where Δu is the induced excess pore water pressure at each depth z due to an increment of stress applied at the surface, and other symbols are defined in Eq. 3.20.

(2) The excess pore water pressure Δu is given by the Skempton (1954) - Bishop (1954) equation for saturated soils:

$$\Delta u = \Delta\sigma_3 + A(\Delta\sigma_1 - \Delta\sigma_3) \qquad (3.25)$$

where A is a pore pressure parameter, and $\Delta\sigma_1$, $\Delta\sigma_3$ are the major and minor principal stress increases.

From these assumptions it is clear that even though the excess pore water pressure is from a 3-dimensional analysis, the settlement is still 1-dimensional.

The consolidation settlement, based on pore pressure

generated according to three dimensional theory, followed
by one dimensional consolidation, is given by:-

$$\delta_c = \mu \cdot \delta_{oed} \tag{3.26}$$

$$\mu = A + \alpha(1-A) \tag{3.27}$$

and

$$\alpha = \frac{\Sigma \Delta \sigma_3 \cdot \delta_z}{\Sigma \Delta \sigma_1 \cdot \delta_z} \tag{3.28}$$

where μ is the settlement coefficient, a function of A and
the geometry of the problem.   Figure 3.20 shows the values
of μ.

The effect of 3-dimensional analysis also considered
by Davis and Poulos (1968).

3.3.2.7 Rate of Settlement

The consolidation process involves expulsion of
water from the soil being compressed.   The preceding dis-
cussion has been concerned with the calculation of ultimate
consolidation settlement, where the excess pore water
pressure has dissipated completely.   At any time between
application of load and the time at which essentially.
ultimate, or 100 per cent consolidation has occurred,
the progress of settlement can be described by the rate of
settlement, or degree of consolidation (Eq. 3.23).

The rate of settlement can be determined from one-
dimensional consolidation theory (Terzaghi, 1925).   If
accurate rates of consolidation are required, the use of
3-dimensional consolidation theories is required (Davis

and Poulos, 1972).

It should be mentioned that the observed rate of settlement is usually very much faster than that calculated using 1-dimensional consolidation theory. It is generally assumed that the reasons for this are the poor knowledge of drainage boundary conditions that exist at a site (Rowe, 1968 and 1972), and variation of the coefficient of permeability and the coefficient of compressibility of the soil with depth (Schiffman and Gibson, 1964). Thin layers of drained soil (sand and silt) can be easily missed in a subsoil investigation but they have a significant effect on the overall rate of settlement.

3.3.2.8 Secondary Consolidation Settlement

The consolidation of a clay deposit may be divided into two fundamental parts: first, the compression which is controlled by the flow of the pore water from the soil, known as consolidation, and discussed in the preceding section; second, the compression because of the inter-granular viscosity effects (Zeevaert, 1972), which occurs at essentially constant effective stress, and is known as secondary consolidation.

Generally, the secondary consolidation starts simultaneously with the primary consolidation. After complete dissipation of the excess pore water pressure, the primary consolidation is completed, and the secondary consolidation continues at constant effective stress (Bjerrum, 1967).

In the majority of laboratory and field measurements it has been observed that the magnitude of secondary consolidation is approximately a linear function of the logarithmic of time, after the primary consolidation has been completed (Fig. 3.21). The linear logarithmic relationship was reported for the first time by Buisman (1936) from laboratory and field observations.

The secondary consolidation settlement may be approximately estimated by the following expression:

$$\delta_s = C_s \log(t/t_c) \tag{3.29}$$

where C_s is the slope of the straight line, and known as the coefficient of secondary consolidation; t_c is the time corresponding to the 100 per cent primary consolidation and t is the time at which the magnitude of secondary consolidation is required (see Fig. 3.21).

Although much research has been conducted on secondary consolidation, no reliable methods are available for calculating the magnitude and rate of consolidation. For a detailed discussion of secondary consolidation, reference may be made to Garlanger (1972), Zaretskii (1972), and Simons (1974).

3.3.2.9 Other Methods of Predicting Settlement

Some other methods of predicting settlement of structures are outlined below.

(1) Elastic Method. The value of total settlement

may be calaculated either by Eq. 3.12 or by

Eq. 3.13, and using the drained parameters (E',

ν') instead of undrained parameters.

(2) Finite Element Method. Settlement may also be

computed using the finite element method, which

enables the analysis of any form of loading and

boundary conditions. The finite element

technique has been considered in Chapter 2, and its

application to stress analysis and immediate settle-

ment calculation will be discussed in Chapter 6.

(3) Stress Path Method. The principles of this

method have been explained by Lambe (1964 & 1967).

This method consists of four general steps:

(a) selection of one or more points within the

soil beneath the foundation; (b) estimation of

the stress path for each of the selected points,

i.e. the initial vertical and horizontal stresses

and the stresses due to the foundation; (c) carry-

ing out laboratory tests in which the specimen

is first consolidated under the initial in-situ

stresses and then the stress increases are

imposed. The undrained and consolidation verti-

cal strains are measured; and (d) the settlement

is estimated by integration of measured strains.

There are some other methods of secondary importance,

and reference may be made to Simons and Menzies (1975).

Theoretical studies suggest that the classical method

of estimating total settlement based on the assumption of one-dimensional compression is surprisingly accurate both for normally consolidated and heavily overconsolidated clays (Burland and Wroth, 1974). Therefore, accurate estimates of settlement are much more dependent on correct measurement of parameters such as m_v and C_c than on sophisticated calculations using complex stress-strain laws.

Usually, stresses are less sensitive to soil properties than settlements, so, it is better to estimate stresses, and calculate settlements from these stresses by using the linear elastic theory.

3.3.3 Settlement of Free Drained Soils

Some of the methods for settlement prediction discussed in the preceding section are applicable for the settlement of free drained soils.

Generally, it is difficult to obtain undisturbed samples of cohesionless soils, and therefore settlement analysis based on laboratory tests are rarely performed. Instead, empirical correlations based on field tests are usually used. Table 3.4 represents some of the methods used for settlement prediction (after Lambe, 1973b).

The total settlement of footings on cohesionless soil is small, however, differential settlement can approach the total settlement, and is the important parameter in settlement analysis of cohesionless soils. Bjerrum (1963) found that differential settlement is greater than 50% of the total settlement. Terzaghi and Peck (1948, 1967) suggested

a differential settlement of 75% of the estimated total settlement.   Skempton and MacDonald (1956) have also shown from case studies that differential settlement is of the same order of magnitude as total settlement.

The simplest and most widely used procedures for estimating settlement in cohesionless soils employe soundings such as the Standard Penetration Test (SPT) and the Cone Penetration Test (CPT).

3.3.3.1 Standard Penetration Test

This technique, generally, correlates the driving resistance to observed settlement for plate load tests and actual structures.   An example of the type of empirical correlation commonly used is given in Fig. 3.22, which was first published by Terzaghi and Peck (1948).   The Terzaghi and Peck correlations were originally intended to provide a conservative basis for design, irrespective of the geological origin and environment of the cohesionless soil deposit.

Meyerhof (1965) has suggested a different relationship as follows:-

$$\Delta q = \frac{N \cdot \delta}{8} \qquad \text{for } B \leqslant 4 \text{ ft} \qquad (3.30)$$

$$\Delta q = \frac{N \cdot \delta}{12} \left(\frac{B+1}{B}\right)^2 \text{ for } B > 4 \text{ ft} \qquad (3.31)$$

where Δq is the allowable load (T/ft^2);

δ is the settlement (inches);

N is the SPT Resistance; and

B is the footing width (ft)

Other correlations have been suggested by D'Appolonia et al (1968); and Peck and Bazaraa (1969) which consider the effect of overburden pressure.

3.3.3.2 Cone Penetration Test

This technique is also used to predict settlement as an indirect method. A similar approach can be used with the Cone Penetration Test as is used with the SPT. The method is discussed in detail by De Beer (1948, 1965). Schmertmann (1970) has suggested that the elastic modulus needed in the settlement analysis by elastic theory can be approximated by the following expression:

$$E = 2q_c \tag{3.32}$$

where q_c is the Cone Penetration Resistance.

3.3.3.3 Plate Load Test

Terzaghi and Peck (1948 & 1967) have developed an empirical relationship in order to predict the settlement of the prototype footing from plate load tests. Their expression is as follows:-

$$\frac{\delta}{\delta_1} = \left(\frac{2}{1 + \frac{B_1}{B}}\right)^2 \tag{3.33}$$

where δ is the settlement of prototype footing;

δ_1 is the settlement of test plate;

B is the smallest dimension of prototype footing; and

B_1 is the smallest dimension of test plate. The test plate is usually a 1 ft × 1 ft square plate.

According to Bjerrum and Eggestad (1963), although

this relationship is approximately correct, there is a large amount of scatter (Fig. 3.23). In addition to the scale effect, correlation is also dependent upon soil density.

There are also other methods for settlement analysis, e.g. stress path method (Lambe, 1964 & 1967). Reference may also be made to D'Appolonia et al (1968), Sutherland (1974), and Simons and Menzies (1975).

3.3.4 Determination of the Soil Properties

One of the most important difficulties in settlement analysis is the determination of the values of soil properties E and v (both drained and undrained). The discrepancies between the in-situ values and those on which the design is based, may cause a large error in the proper design of a footing.

The values of soil properties are usually determined from laboratory tests, or in-situ tests. In both cases some factors influence the measured values, such as sampling, sample size, anisotropy, type of test, rate of shearing, and non-homogeneity. A comprehensive discussion of the determination of soil properties and its difficulties has been given by Davachi (1974).

3.4 Soil-Foundation Interaction

3.4.1 General

In the preceding sections the problems of stress

distribution within a soil mass, and settlement of non-free drained and free drained soils resulting from a foundation load have been considered. In this section the subgrade reaction and distribution of contact pressure will be discussed.

The most significant advantage of a soil-foundation interaction study lies in including the foundation structure in the analysis. Almost all field and analytical studies have confirmed the importance of including both soil and foundation structure in the analysis (see De Jong et al, 1971).

3.4.2 The Modulus of Subgrade Reaction

Winkler (1867) represented the soil as a type of elastic springs under the loads imposed by the foundation, and introduced a linaer relationship between vertical stresses σ_v and vertical settlement δ_v:

$$\sigma_v = k_s \cdot \delta_v \tag{3.34}$$

The factor k_s is called the "modulus of subgrade reaction".

Terzaghi (1955) defined the subgrade reaction as the load per unit of area of the surface of contact between a loaded foundation and the subgrade on which it rests and on to which it transfers the load. The modulus of subgrade reaction is the ratio between this contact pressure and the settlement due to the load at any point.

$$k_s = \frac{\sigma_v}{\delta_v} \tag{3.35}$$

The modulus of subgrade reaction can be obtained by performing a plate load test and extrapolating results to the actual foundation. Empirically, Terzaghi (1955) proposed the following formula for cohesive soils when the contact pressure is less than one-half the ultimate bearing capacity.

$$k_s = \frac{1}{B} k_{s1} \qquad (3.36)$$

where k_s and B are the value of subgrade modulus and footing width for actual foundation, and k_{s1} is the subgrade modulus using a square plate of 1 ft × 1 ft.

For cohesionless soils the formula is:

$$k_s = k_{s1} \left(\frac{B+1}{2B}\right)^2 \qquad (3.37)$$

Bond (1961) indicates that Eq. 3.37 overestimates the values of subgrade modulus for medium to dense sands.

Terzaghi (1955) pointed out that the modulus is not a fundamental property. It depends on many things, such as the size of the loaded area and the length of time it is loaded. He proposed the following formulae for obtaining the modulus of subgrade reaction k_{sr1} for a rectangular plate of dimensions 1 ft and m ft using the subgrade modulus of a square plate of 1 ft × 1 ft:

For cohesive soils

$$k_{sr1} = k_{s1} \left(\frac{m+0.5}{1.5m}\right) \qquad (3.38)$$

For cohesionless soils

$$k_{sr1} = k_{s1} \qquad (3.39)$$

Several proposals have been made to attempt to find a value of modulus of subgrade reaction using laboratory tests. Vesic (1961a & 1961b) proposed using the modulus of elasticity from laboratory triaxial tests. The value of $k_{s\,B} = k_s \cdot B$ given by Vesic is:

$$k_{sB} = 0.65 \sqrt[12]{\frac{E_s \cdot B^4}{E_f \cdot I}} \frac{E_s}{1 - \nu_s^2} \qquad (3.40)$$

where E_s and ν_s = modulus of elasticity and Poisson's ratio of soil;

E_f = modulus of elasticity of footing;

B = width of footing;

I = moment of inertia of footing cross-section.

There are several other methods of obtaining the modulus of subgrade reaction, including extrapolating from consolidation tests (Young, 1960), and extrapolating from CBR tests (Nascimento et al, 1957, Black, 1961).

All these equations are applicable only to surface or near-surface conditions. The modulus of subgrade reaction would be expected to increase as a footing is placed at a greater depth in the ground. Bowles (1975) considered a footing of width B located at a depth D in a soil mass, and he gave the expression for subgrade modulus at depth k_{sd} related to the subgrade modulus at ground surface k_{ss}.

$$k_{sd} = k_{ss}\left(1 + \frac{2D}{B}\right) \qquad (3.41)$$

Bowles (1975) mentioned that it is doubtful for k_{sd} to be much greater than $2k_{ss}$ when D/B ratios are larger than 0.5.

3.4.3 Problems Associated with Modulus of Subgrade Reaction

The conventional Winkler elastic foundation assumes that the movement of any point is independent of the others. Thus, in Fig. 3.24(a) a load over region A causes settlement only under A and nowhere else. But, in reality, the surface would deform as in Fig. 3.24(b), so the Winkler theory may be seriously wrong. However, theoretical work by Gibson (1967) has shown that when the modulus of elasticity of a finite layer of soil or of a half-space increases with depth, for a special case ($E_o = 0$), the settlement behaves similarly to those in the Winkler theory.

Brown and Gibson (1972) mentioned that the condition of compressibility of the soil is vital for obtaining a surface settlement behaviour similar to the Winkler model. They showed that the effect of the presence of a small degree of compressibility on the settlement profile is far more important than a further increase in compressibility.

Furthermore, Brown and Gibson (1972) wrote that in the homogeneous case Poisson's ratio has no effect on the settlement profile, and the effect of introducing some compressibility remains quite small unless there is a considerable degree of inhomogeneity.

Carrier and Christian (1973) examined by means of a finite element analysis the effect of a modulus increasing with depth on the settlement of a smooth rigid circular plate (diameter D) at the surface of a semi-infinite half-space. Figures 3.25 and 3.26 represent the variation of

the settlement with Poisson's ratio, for a homogeneous and non-homogeneous (according to Eq. 3.10) cases, respecitvely. The results for various combinations of E_O and λ have been given in Figures 3.27 and 3.28, where I and I' are the influence factors in the expressions for settlement. For $E_O/\lambda D$ greater than 10, the solution is essentially the same as a homogeneous one, and for $E_O/\lambda D$ less than 0.01, the result is essentially identical to the one with $E_O = 0$.

Several improvements for Winkler theory have been developed (Vlasov and Leont'ev, 1966; Harr et al, 1969;and Klein and Duraev, 1971). Such improvements give an increased complexity which may not be necessary, and in many cases the Winkler theory may be reasonably valid.

Other major problems associated with the concept of modulus of subgrade reaction are:

(1)   the soil is not elastic;

(2)   the soil stratification effect;

(3)   the depth and footing size effect;

(4)   the duplicating of in-situ conditions in the laboratory.

3.4.4 Distribution of Contact Pressure

There have been several investigations (theoretical and experimental) to evaluate the actual contact pressure of the soil against the footing, such as: Cummings(1936); Borowicka (1936 & 1938); Krynine (1938); Casagrande and Fadum (1942); Benscoter (1944); Schultze (1961); Barden (1962); Sommer (1965); Ho and Lopes (1969); amd Timoshenko and Goodier (1970).

Boussinesq (1885) and Sadowsky (1928) solved for the distribution of the contact pressure for the smooth rigid circular and strip footings on elastic half-space according to the following equations (given by Timoshenko and Goodier, 1970).

$$\sigma_{V circle} = \frac{q}{2\sqrt{1 - \left(\frac{x}{R}\right)^2}} \tag{3.42}$$

$$\sigma_{V strip} = \frac{q}{\frac{\pi}{2}\sqrt{1 - \left(\frac{x}{b}\right)^2}} \tag{3.43}$$

where σ_V is the contact pressure,

  q is the applied vertical stress,

  R is the footing radius,

  b is the footing half width $= B/2$, and

  x is the horizontal distance from centre line.

For $x = R$ (edge) the value of contact pressure is infinite, and for $x = 0$ (centre) it is $q/2$ for circle and $2q/\pi$ for strip.

Borowicka (1936, 1938) considered the effect of the footing rigidity upon the distribution of contact pressure, and expressed the rigidity in terms of soil Poisson's ratio ν_s and modulus E_s, footing Poisson's ratio ν_f, modulus E_f, thickness t_f, and radius R as the following equation:

$$K_r = \frac{1}{6} \frac{(1 - \nu_s^2)}{(1 - \nu_f^2)} \frac{E_f}{E_s} \left(\frac{t_f}{R}\right)^3 \tag{3.44}$$

where $K_r = 0$ represents the fully flexible footing with uniform contact pressure ($\sigma_v = q$), and $K_r = \infty$ represents the fully rigid footing with non-uniform contact pressure. Figure 3.29 shows the Borowicka's curves for circular and strip footings for various rigidity factors. For strip footing the values of K_r are also given by Eq. 3.44.

Theoretically, the value of contact pressure at the edge is infinite, but in practice, because of the local failure, the contact pressure will be limited by the shear strength of the soil at the edge.

As shown in Fig. 3.24, the settlement of a footing that exerts a uniform pressure on the soil is not uniform. The footing, therefore, must be flexible so that it can conform to the settlement and keep the pressure uniform. When the footing is fully rigid, the settlement will be uniform, and the pressure will be greatest at the edges of the footing on an elastic soil (e.g. saturated clay) and greatest at the centre of the footing on a cohesionless soil, for safety factor close to unity (Fig. 3.24d).

3.4.5 Distribution of Contact Pressure at Failure

As mentioned at the beginning of this chapter, the increase of load on a footing causes progressive transition of the loaded material from the state of elastic to that of plastic flow. This transition influences the distribution of contact pressure by limiting its values at the points where plastic flow has been reached. By increasing

the footing load the yielded region becomes larger, and finally, when the load is equal to the ultimate bearing capacity, the distribution of contact pressure will be uniform as shown in Fig. 3.30.

The contact pressure distribution of a shallow footing is trapezoidal with a maximum at footing centre, and consists of a uniform N_c component, two relatively small triangular N_q components, and a triangular N_γ component. By increasing the footing depth, and for $\phi > 0$ the N_q component increases more rapidly than N_c and N_γ components, and at a great footing depth, where in practice the N_c and N_γ components can be neglected compared with the N_q component, the contact pressure will be uniform because the depth of the failure surface is small compared with the depth of the footing, Fig. 3.30(a).

In Fig. 3.30(a), the distribution of the N_q component is two small triangles because Meyerhof (1951) assumed an inclined equivalent free surface on which the stress γD increases from zero or a small value at the ground surface (which affects the stress at the centre of the footing) to a maximum at the footing edge. By assuming a horizontal equivalent free surface (Terzaghi, 1943) the distribution of N_q component will be uniform, Fig. 3.30(b).

To obtain a truer distribution of contact pressure for any stage of applied load, Schultze (1961) and Smoltczyk (1967) proposed an elastic-plastic concept which considers a reasonable combination of the following two extreme cases:

(1) A load of low intensity acting on a rigid
footing, and the Boussinesq and Sadowsky elastic
solutions (Eqs. 3.42 and 3.43) give an estimate
of the pressure distribution;

(2) A load according to ultimate bearing capacity
of the footing with a rectangular and triangular
distribution (Fig. 3.30).

Figure 3.31 (after Schultze, 1961) shows the distri-
bution of contact pressure for different safety factors F_s
against ultimate load. In this figure the distribution is
a combination of elastic and plastic states, and X_1 repre-
sents the distance from centre line to the intersection
between these two states.

3.4.6 Effects of a Rigid Boundary underlying the Foundation
on Contact Pressure Distribution

The problem of distribution of contact pressure between
a rigid footing and an elastic solid underlain by a rigid
base has been treated by several investigators (Poulos,
1968; Yamaguchi, et al, 1968; Brown, 1969; Milovic et al,
1970).

The ratio of layer thickness to footing radius H/R
has a marked effect on the distribution of contact pressure
except at the edge where the effect is small. By decreas-
ing the ratio H/R the distribution becomes more uniform,
Fig. 3.32.

The results of Brown (1969 a & b) show that the

effect of the ratio H/R on contact pressure distribution decreases when the footing rigidity decreases.

For a rigid strip footing Yamaguchi et al (1968) showed that when the ratio H/B (B = footing width) reaches 1.5, the distribution becomes approximately equal to Sadowsky's distribution (Eq. 3.43). Furthermore, from their results it is possible to conclude that by using the Sadowsky's distribution for the case with ratio H/B = 1 the contact pressure will be underestimated, and the maximum error is about 12% at the centreline.

The effect of Poisson's ratio on contact pressure distribution is small and when the interface between the layer and rigid base is smooth it does not affect the distribution (Yamaguchi et al,1968). The results of more recent analysis of a circular plate on non-homogeneous half-space by Boswell and Scott (1975) indicate that the contact pressure is almost independent of Poisson's ratio.

Yamaguchi et al (1968) used the "method of division" in their analysis for contact pressure distribution, which assumes that, directly under a small section into which the width of rigid footing is divided, stress is uniformly distributed. Then by calculating the displacements at the centre of each small section, due to its own load and other section's loads, and equating them to the displacement of the rigid footing, the distribution of contact pressure can be acquired. In this method of computation, the validity of the solution depends on the accuracy of calculation in

displacement of each small flexible section of the footing.

Milovic et al (1970) studied the problem of a rough strip on a finite layer underlain by a rough rigid base, and subjected to inclined and eccentric loading, using a finite element analysis.

3.4.7 Effect of Soil Non-homogeneity on Contact Pressure Distribution

It has been mentioned previously that, for $E_o = 0$, $E = \lambda z$ and $\nu = 0.5$, the surface displacement of a uniform load of any shape or size is uniform beneath the load and is zero just outside the loaded are (Gibson, 1967, 1968 & 1969). Conversely, a rigid plate may result in a uniform contact pressure, which has been confirmed for a rigid circular plate ($E = \lambda z$ and $\nu = 0.5$) by Zaretsky and Tsytovich (1965).

Figure 3.33 (after Carrier and Christian, 1973) represents the distribution of contact pressure for a smooth rigid circular plate resting on a non-homogeneous half-space with $E_o/\lambda D = 0.1$ and 1, and indicates that the effect of heterogeneity on distribution of contact pressure is remarkable.

Figure 3.33 and results given by Boswell and Scott (1975) suggest that non-homogeneity leads to more uniform distribution of contact pressure.

3.4.8 Effects of Footing Roughness and Repeated Loading upon Contact Pressure Distribution

The effect of footing roughness on contact pressure distribution has been studied by Parkes (1956), Yamaguchi et al (1968); and Schiffman (1969) for a homogeneous half-space, and it has been shown that, for Poisson's ratio equal to 0.5, the contact pressures are the same for rough and smooth footings. For smaller values of Poisson's ratio there is a slight difference between the contact pressures for rough and smooth footings.

For the case of a non-homogeneous half-space, Carrier and Christian (1973) showed that for most practical problems (Poisson's ratio greater than or equal to 0.3) the solution for a rough plate is the same as for a smooth plate.

Ho and Lopes (1969) considered the effect of repeated loading upon the distribution of contact pressure of a rigid circular footing resting on the surface of and embedded in sand. They concluded that the effect of repeated loading, for both surface and embedded footings, is important in the first two cycles of loading, provided that the maximum load in subsequent cycles is not larger than that of the first cycle, and after two cycles of repeated loading the settlement and contact pressure distribution are stabilized.

For more general discussion of the effect of repeated loading on the contact pressure distribution, the reader is referred to Chae et al (1965); and Ho and Burwash (1968).

Table 3.1   Allowable Settlement

Type of Movement	Limiting Factor	Maximum Settlement
Total settlement	Drainage	6-12 in
	Access	12-24 in
	Probability of nonuniform settlement:	
	Masonry walled structure	1- 2 in
	Framed structure	2- 4 in
	Smokestacks, silos, mats	3-12 in
Tilting	Stability against overturning	Depends on height and width
	Tilting of smokestacks, towers	$0.004l$
	Rolling of trucks, etc.	$0.01l$
	Stacking of goods	$0.01l$
	Machine operation-cotton loom	$0.003l$
	Machine operation- turbogenerator	$0.0002l$
	Crane rails	$0.003l$
	Drainage of floors	$0.01-0.02l$
Differential movement	High continuous brick walls	$0.0005-0.001l$
	One-story brick mill building, wall cracking	$0.001-0.002l$
	Plaster cracking (gypsum)	$0.001l$
	Reinforced-concrete building frame	$0.0025-0.004l$
	Reinforced-concrete building curtain walls	$0.003l$
	Steel frame, continuous	$0.002l$
	Simple steel frame	$0.005l$

From Sowers (1962)

Note: l = distance between adjacent columns that settle
       different amounts, or between any two points that
       settle differently.   Higher values are for regular
       settlements and more tolerant structures.   Lower
       values are for irregular settlements and critical
       structures

Table 3.2   Causes of Foundation Settlement

From: Sowers (1975)

Structural Load		
Mechanism	Amount of Settlement	Rate of Settlement
Deformation (change in shape of soil mass)	Compute by Elastic Theory from modulus of elasticity of plate load test or lab test	Rapid
Consolidation: Change in void Ratio under stress — Initial	Stress-void ratio curve	Rapid - from time curve
Consolidation: Change in void Ratio under stress — Primary	Stress-void ratio curve	Compute from Terzaghi Theory
Consolidation: Change in void Ratio under stress — Secondary	Compute from log time-settlement	Compute from log time settlement

Environmental Load		
Mechanism	Amount of Settlement	Rate of Settlement
Consolidation due to fill weight	Compute from stress-void ratio and stress	Compute from Terzaghi Theory
Consolidation due to water table lowering	Compute from stress-void ratio and stress change	Compute from Terzaghi theory and water table change
Shrinkage due to drying	Estimate from stress-void ratio or moisture-void ratio and moisture loss limit-shrinkage limit	Equal to rate of drying, Seldom can be estimated

Table 3.2   Continued

Environmental-continuing process		
Mechanism	Amount of Settlement	Rate of Settlement
Biochemical Decay	Estimate susceptibility	Erratic, often decreases with time, increases with water table changes
Chemical Attack	Estimate susceptibility	Erratic, depending on chemical diffusion
Mass Distortion, Shear, creep or landslide in slope	Compute susceptibility from stability analysis	Erratic: catastrophic to slow creep
Expansion - Frost, clay expansion chemical attack (Resembles Settlement	Estimate susceptibility sometimes limiting amount	Erratic: increases with wet weather, temperature changes

Environmental-sudden settlement		
Mechanism	Amount of Settlement	Rate of Settlement
Reposition particles and densification by shock, vibration,blasting and earthquakes	Estimate limit from relative density (up to 60-70%	Erratic: depends on shock, relative density, water; can be catastrophic
Liquefaction from pore pressure increase upon densification	Shear failure - large and erratic	Catastrophic in saturated cohesionless fine sands
Structural collapse - Loss of Bonding (Saturation,thawing,etc)	Estimate susceptibility and possibly limiting amount	Begins with environment change - rate erratic but sudden changes
Revelling,Erosion into openings, cavities	Estimate susceptibility but not amount	Erratic: gradual or catastrophic, often increases with time
Mass Collapse -- collapse of sewer, mine, cave	Estimate susceptibility	Likely to be catastrophic
Tectonic Fault Displacement accompanying earthquake	Possibly estimated from accumulating strains in earthquake-prone areas	Catastrophic

Table 3.3   Methods of Predicting Settlement of Cohesive Soils
             After Lambe (1973a)

Type of Deformation	Method	Reference
Initial Settlement	Elastic Displacement Elastic Strain Summation. Modified Elastic Displacement. Finite Element	Janbu, Bjerrum and Kjaernsli (1956) and Skempton and Bjerrum (1957) Davis and Poulos (1968) D'Appolonia et al. (1971)
Total Settlement	One-dimensional Skempton-Bjerrum Elastic Displacement Elastic Strain Summation. Finite Element	Terzaghi (1943) Skempton and Bjerrum (1957) Davis and Poulos (1968) Davis and Poulos (1968)
Rate of Settlement	1-D strain and drainage, average m_v and c_v 1-D strain and drainage, distributed m_v and c_v	Terzaghi (1943) Schiffman and Gibson (1964)

Table 3.4   Methods of Predicting Settlement of Cohesionless
             Soils
             After Lambe (1973b)

Predicted	Method	Parameter	Selection of Parameter
Total settlement	Based on SPT - Terzaghi & Peck - Peck & Bazaraa - Meyerhof - D'Appolonia	Blowcount N from SPT	Must use judgement because gravel affects N values
	Based on CPT - Schmertmann - Others	Static cone penetration resistance	Difficult or impossible to apply in dense soil because exceed capacity of penetrometer
	Plate load test	Settlement of standard plate	Plate loading test is not representative for large mat because only the surface soil properties are measured
	Wave velocity measurements or other dynamic test	Shear modulus and Young's modulus	Requires correlation to adjust for strain level
Differential settlement	Empirical rule	Type of soil and building	Difficult to apply experience in judging relationship between differential settlement and foundation stiffness
	Subgrade reaction Elastic theory	Modulus of subgrade reaction Elastic moduli	Many assumptions and judgements must be made because total settlement cannot even be predicted well

Settlement

A

Linear

First Local Yield — B

Load

Contained Plastic Flow

D   Failure   C
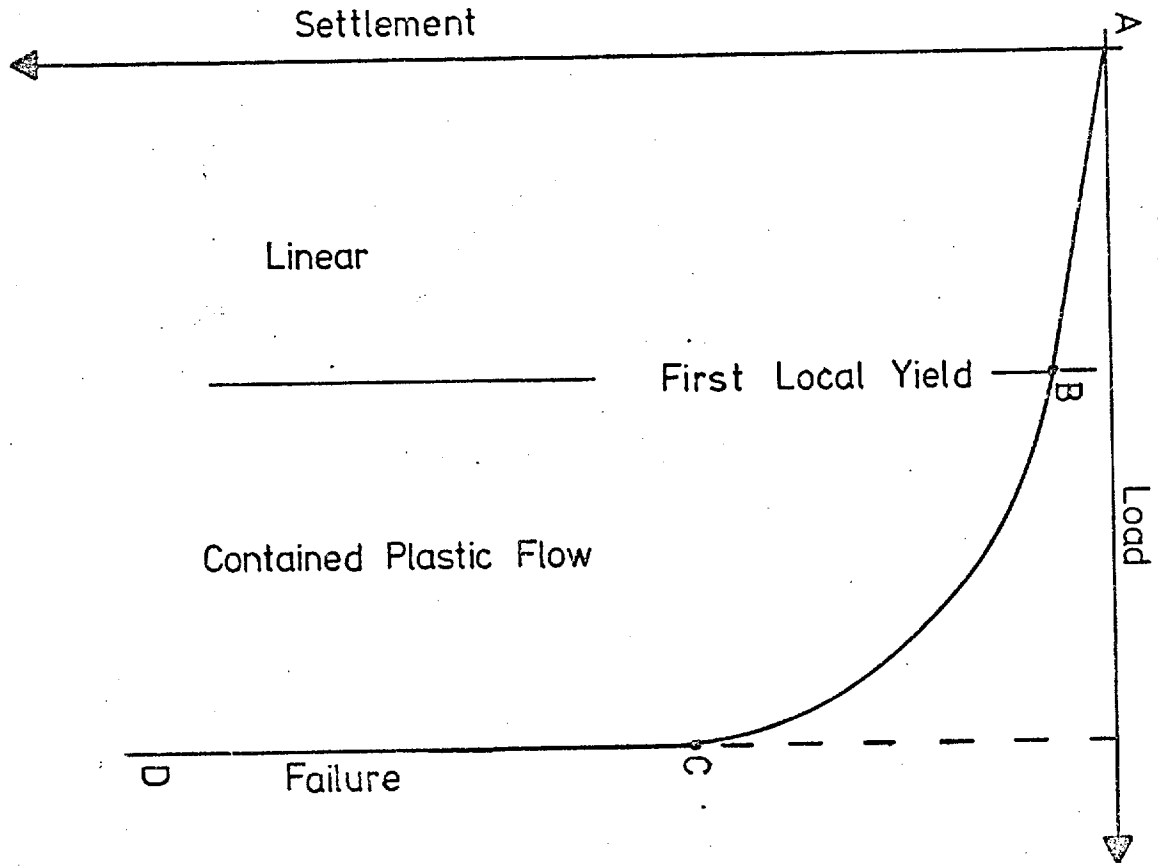
Fig. 3.1

Idealised Load-Settlement Curve

75
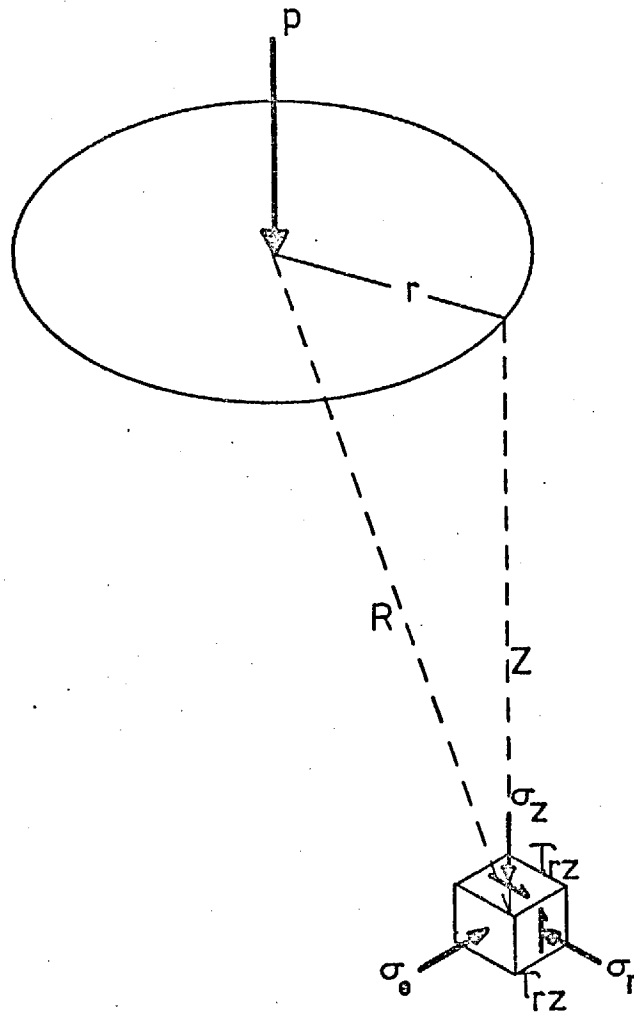
Fig. 3.2   Stresses in an elastic half-space due to
a point load at the surface.
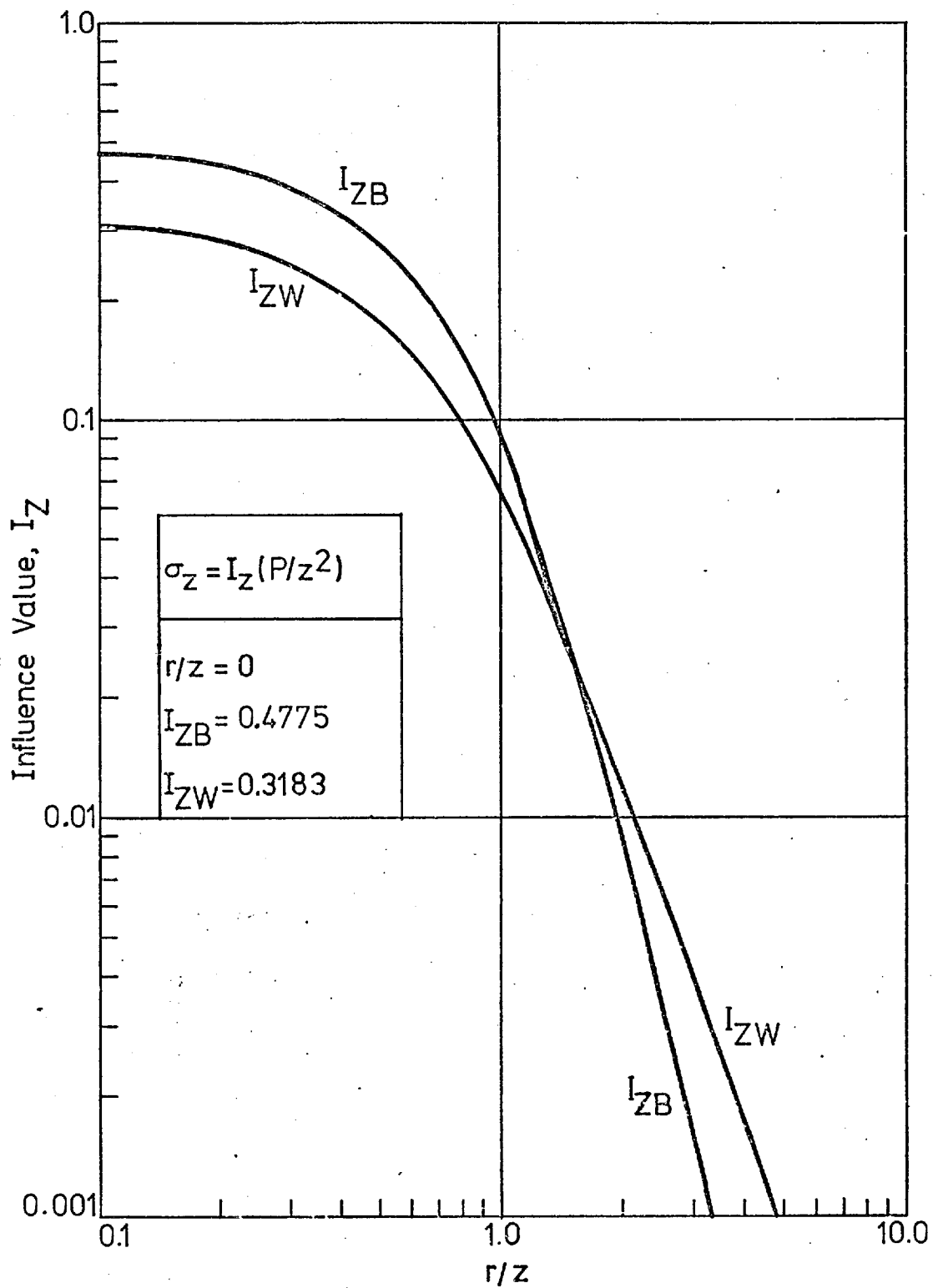
Fig. 3.3   Influence values for vertical normal stresses due to a
point load on the surface of an elastic half-space.
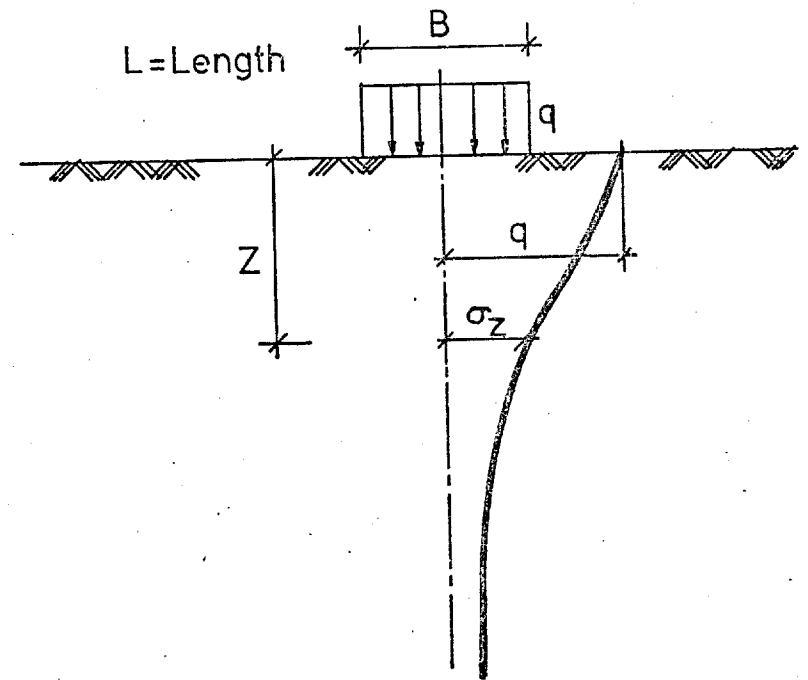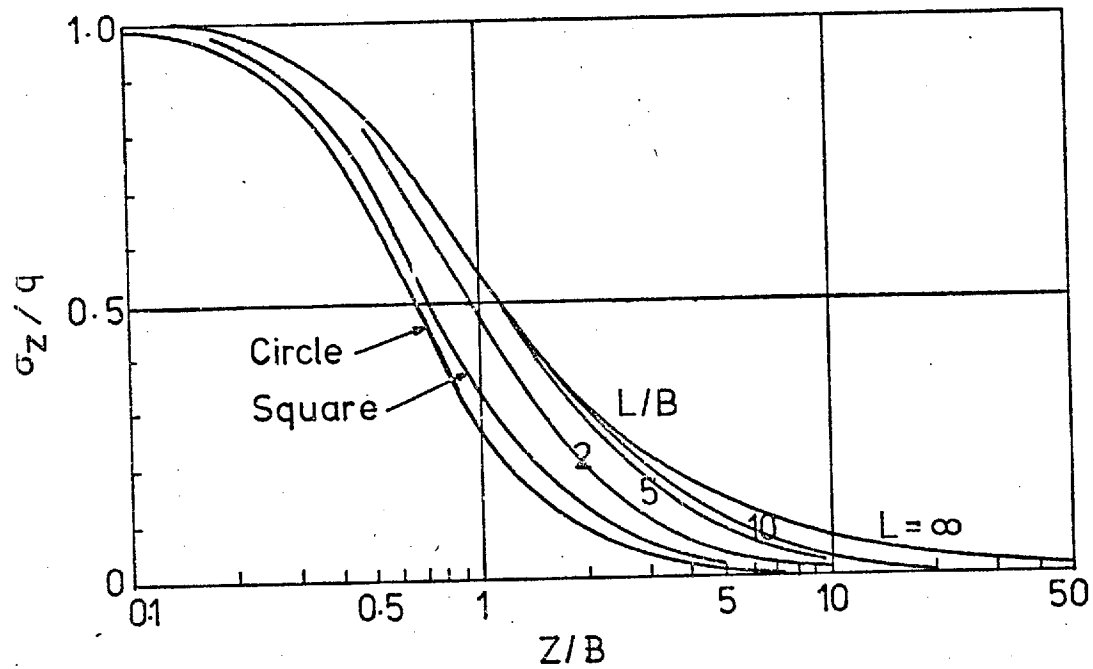
Fig. 3.4 Vertical stresses under the centre of uniformly loaded flexible footings, after Janbu, Bjerrum and Kjaernsli(1956).

Influence value 0·001
Scale
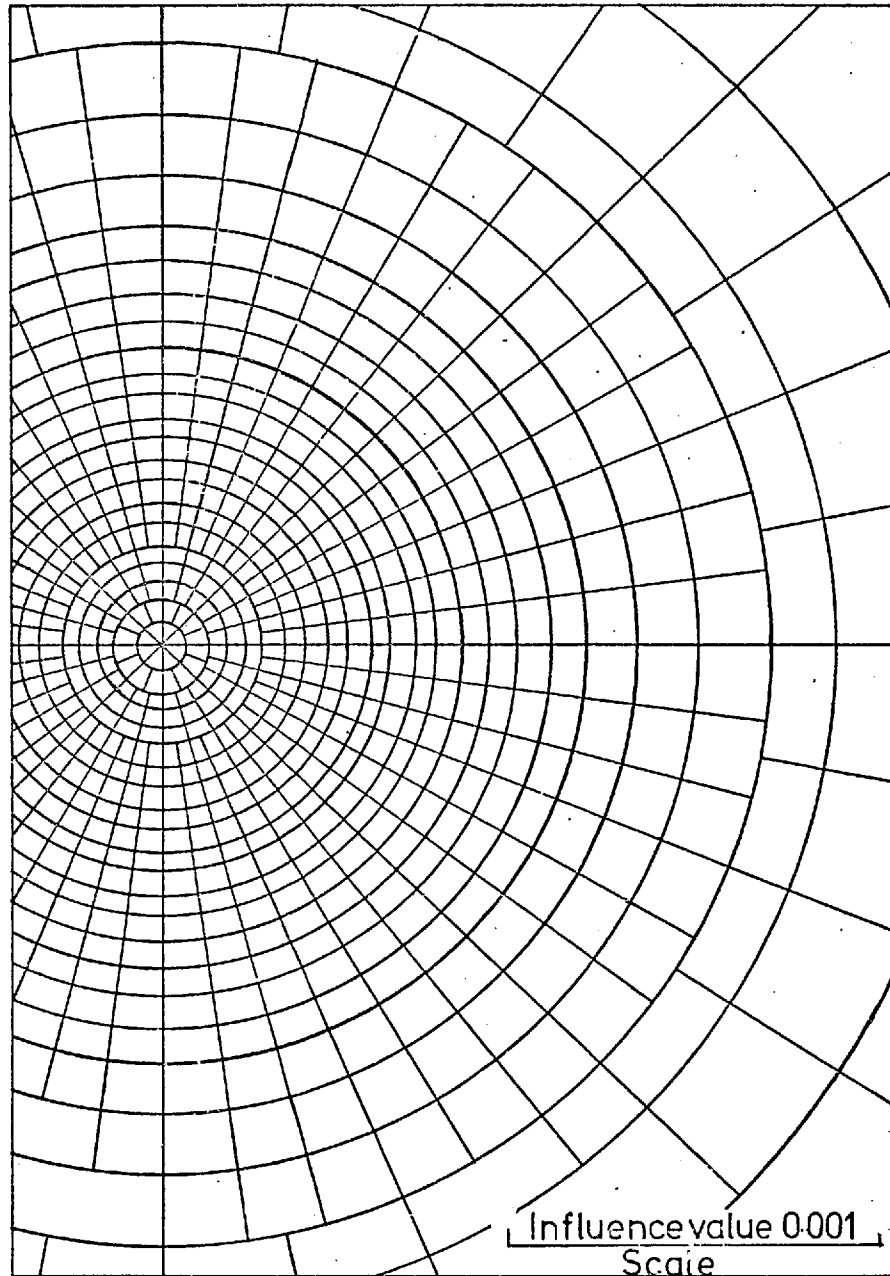
Fig. 3.5   Influence chart for the increase in vertical
stress under a uniformly loaded flexible
footing, after Newmark(1942).
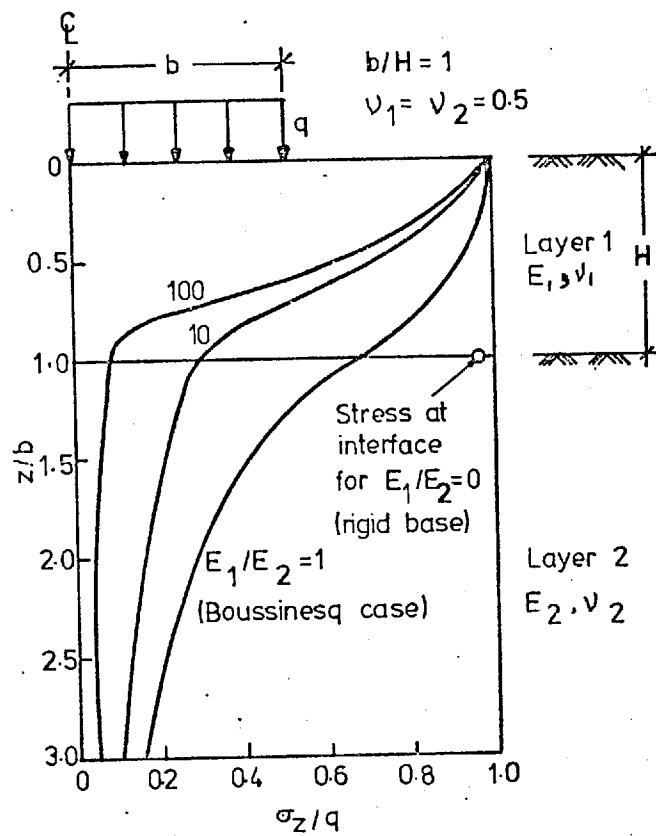
Fig. 3.6   Vertical normal stress under the centre of uniformly loaded circular area at surface of 2-layer elastic system, from Burmister(1958).
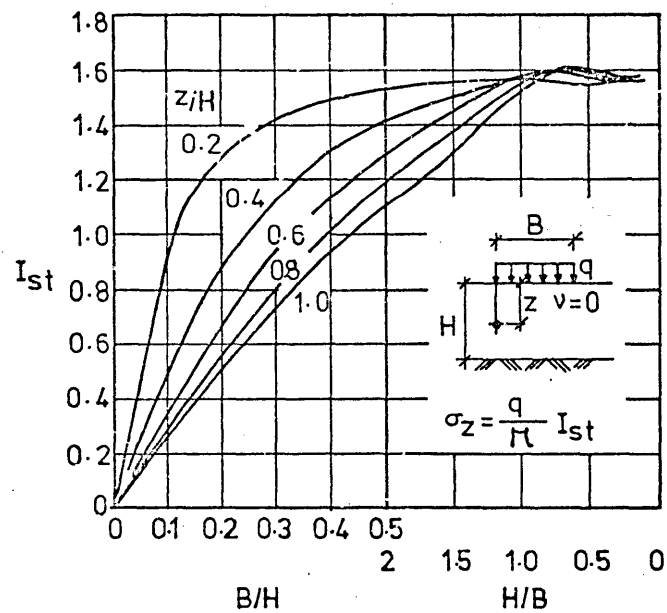
Fig. 3.7 Influence factor
for vertical stress, from
Poulos(1967).
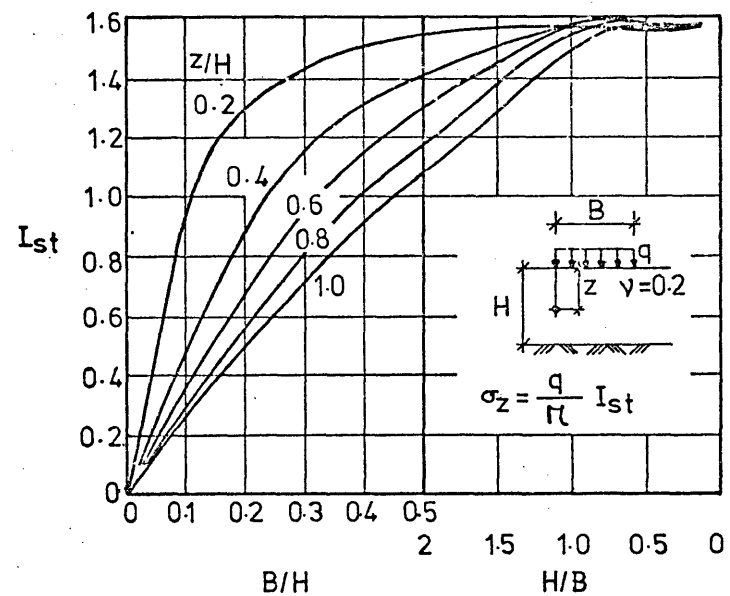
Fig. 3.8 Influence factor
for vertical stress, from
Poulos(1967).
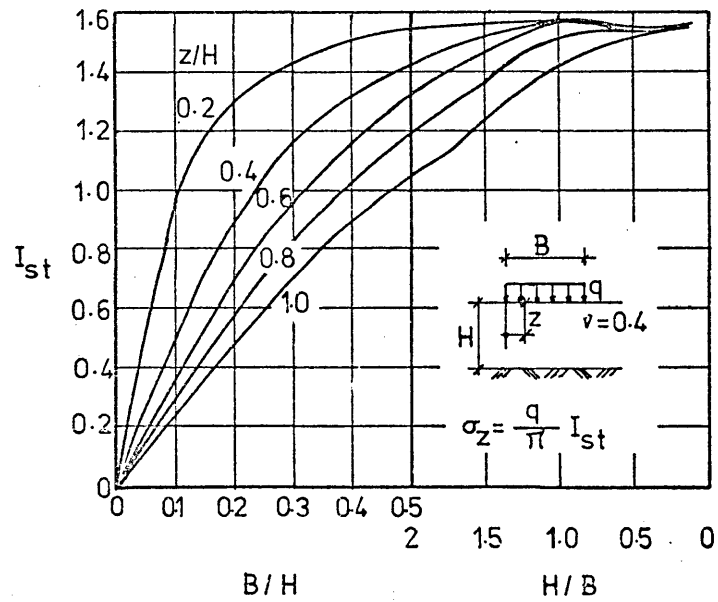
Fig. 3.9 Influence factor
for vertical stress, from
Poulos(1967).
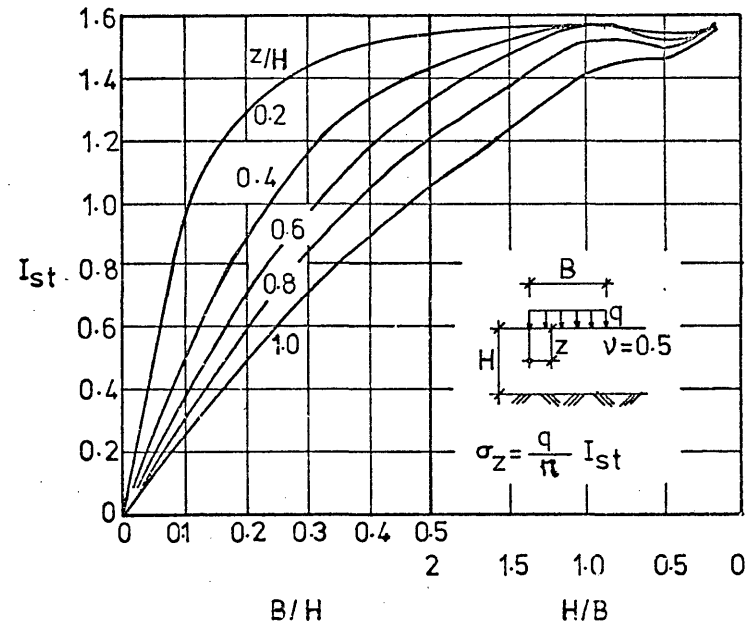
Fig. 3.10 Influence factor
for vertical stress, from
Poulos(1967).

Angular Distortion δ/l

$$\frac{1}{100} \quad \frac{1}{200} \quad \frac{1}{300} \quad \frac{1}{400} \quad \frac{1}{500} \quad \frac{1}{600} \quad \frac{1}{700} \quad \frac{1}{800} \quad \frac{1}{900} \quad \frac{1}{1000}$$

Limit where difficulties with machinery sensitive to settlements are to be feared.

Limit of danger for frames with diagonals.

Safe limit for buildings where cracking is not permissible.

Limit where first cracking in panel walls is to be expected.

Limit where difficulties with overhead cranes are to be expected.

Limit where tilting of high, rigid buildings might become visible.

Considerable cracking in panel walls and brick walls.

Safe limit for flexible brick walls, $h/l < \frac{1}{4}$.

Limit where structural damage of general buildings is to be feared.

Fig. 3.11 Limiting angular distortions, after Bjerrum(1963).

$$\delta_{\bar{c}} = \mu_1 \, \mu_0 \, \frac{q \, B}{E}$$
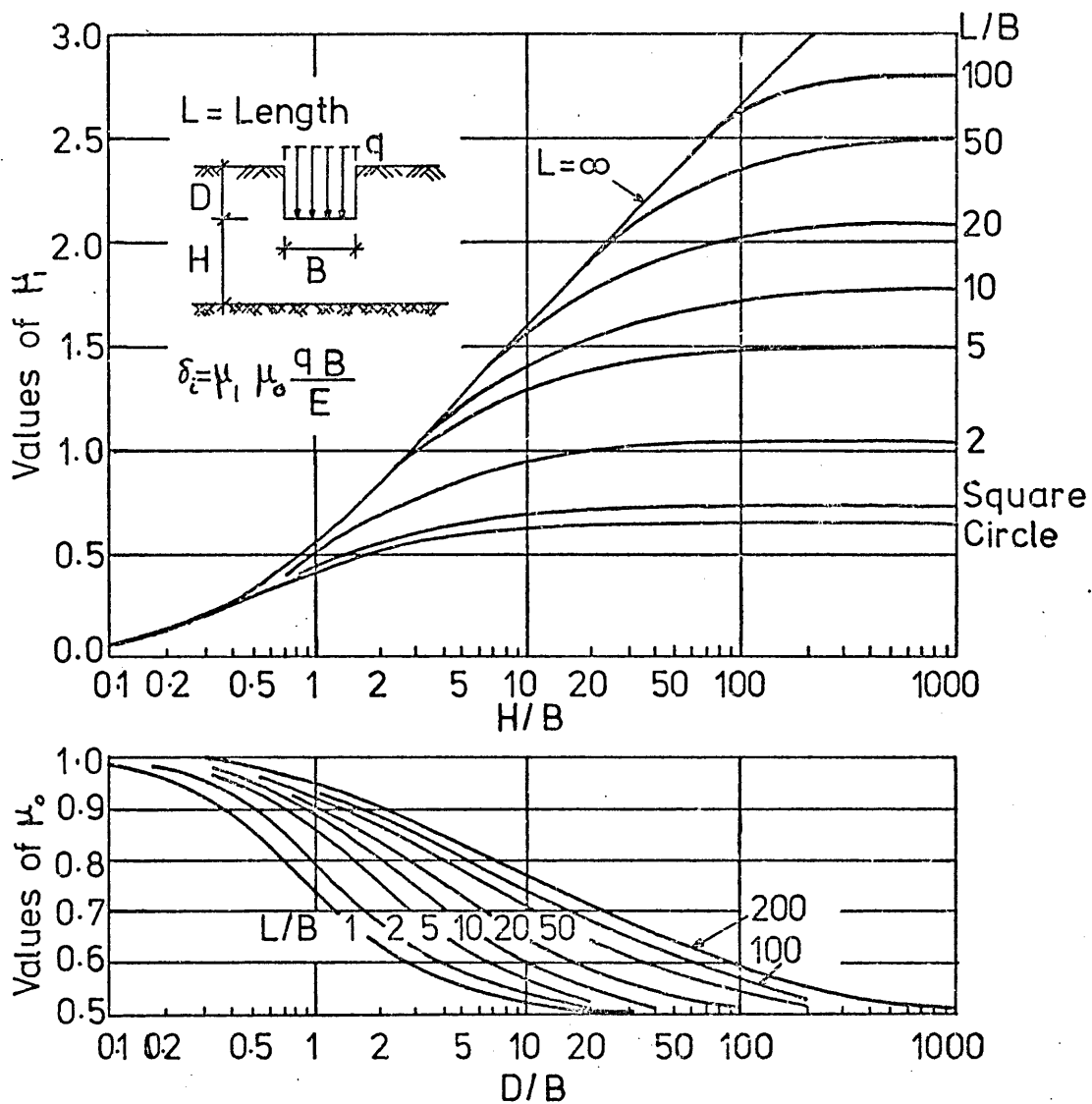
Fig. 3.12 Values of influence factors for average immediate settlement, after Janbu, Bjerrum and Kjaornsli(1956).
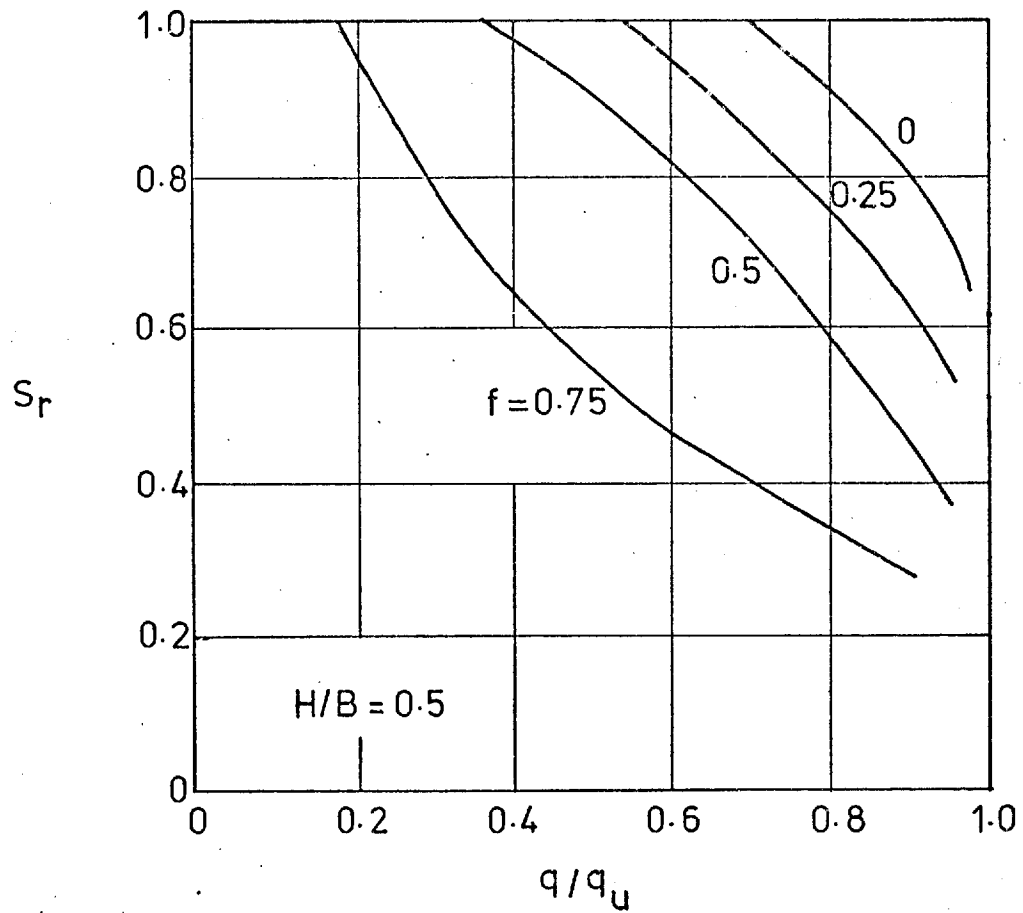
Fig. 3.13 Values of settlement ratio for H/B = 0.5, after D'Appolonia, Poulos and Ladd(1971).
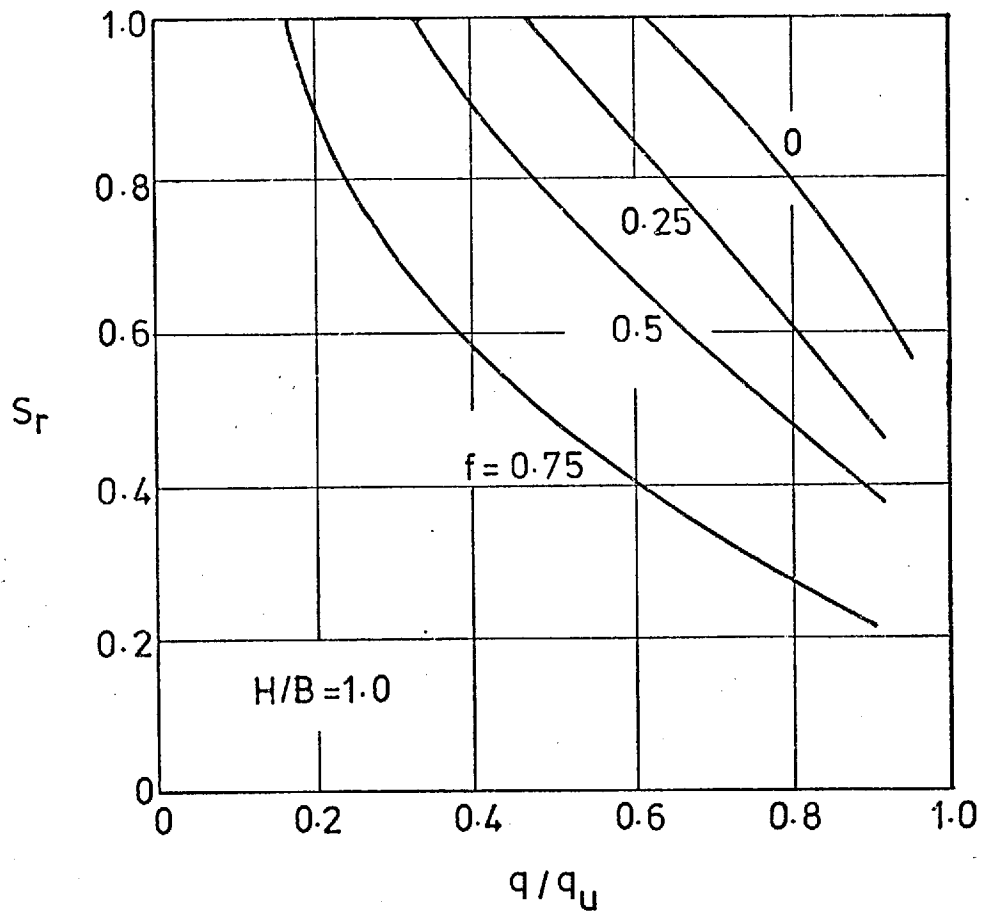
Fig. 3.14   Values of settlement ratio for H/B = 1.0,
after D'Appolonia, Poulos and Ladd(1971).
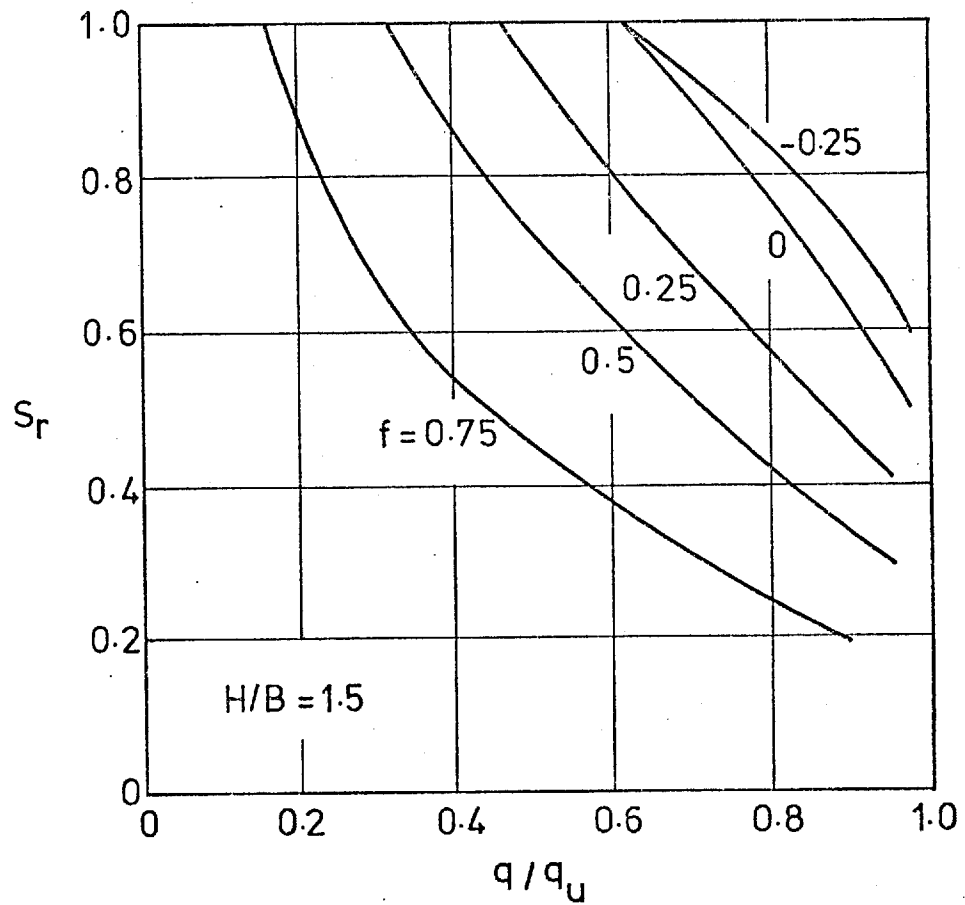
Fig. 3.15 Values of settlement ratio for H/B = 1.5 , after D'Appolonia, Poulos and Ladd(1971).
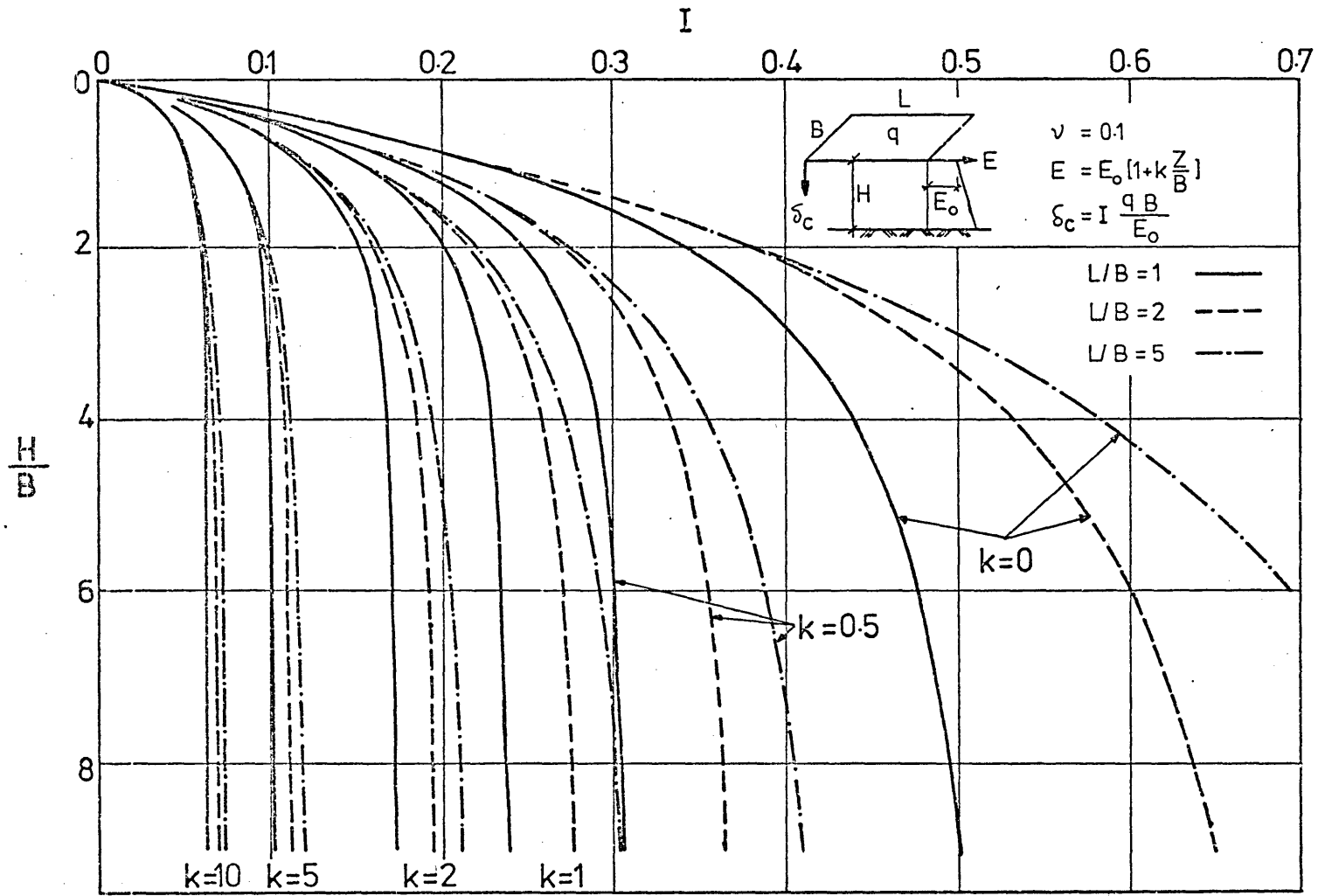
Fig. 3.16 Influence values
for immediate settlement,
after Butler(1974).
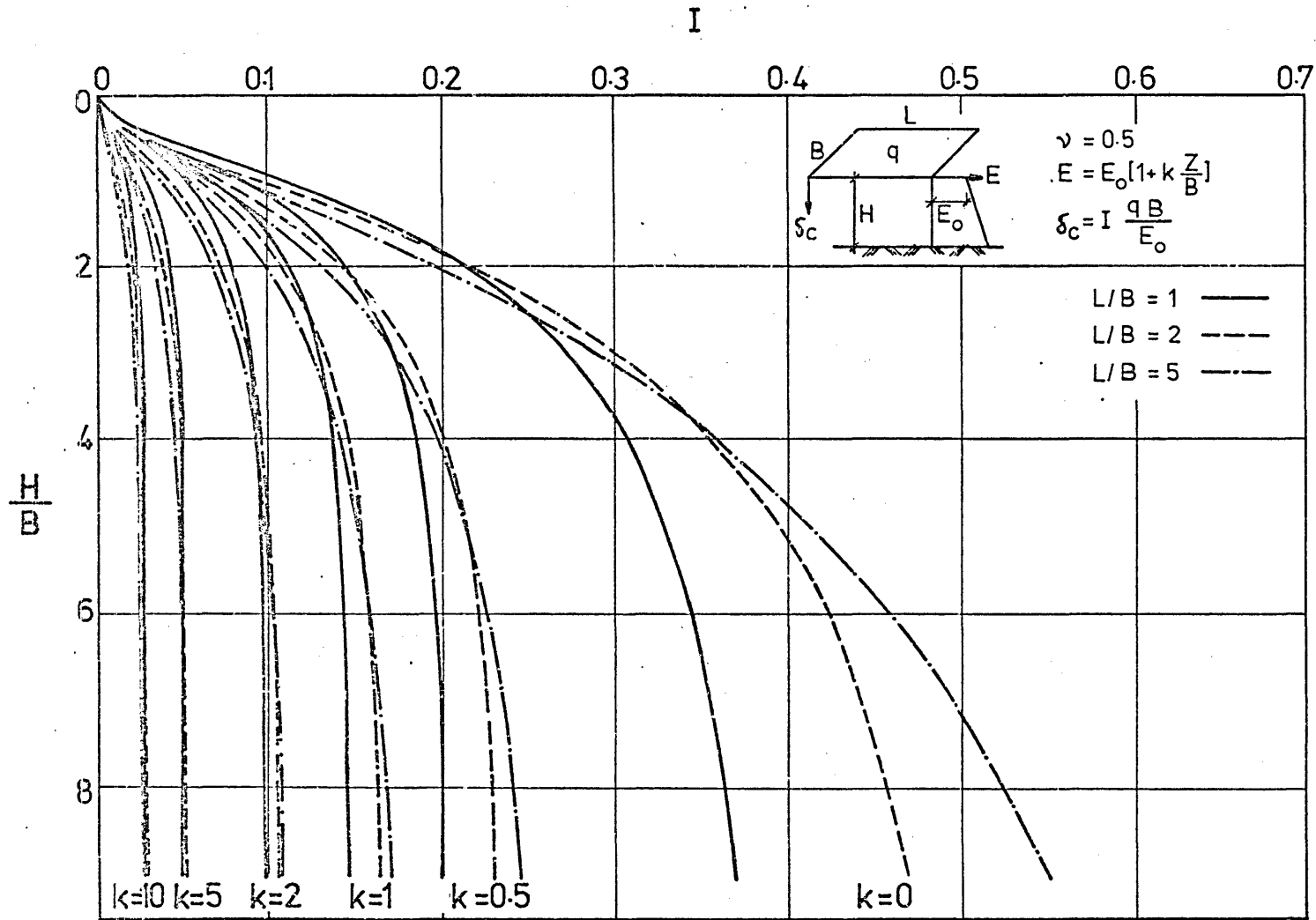
Fig. 3.17 Influence values
for immediate settlement,
after Butler(1974).
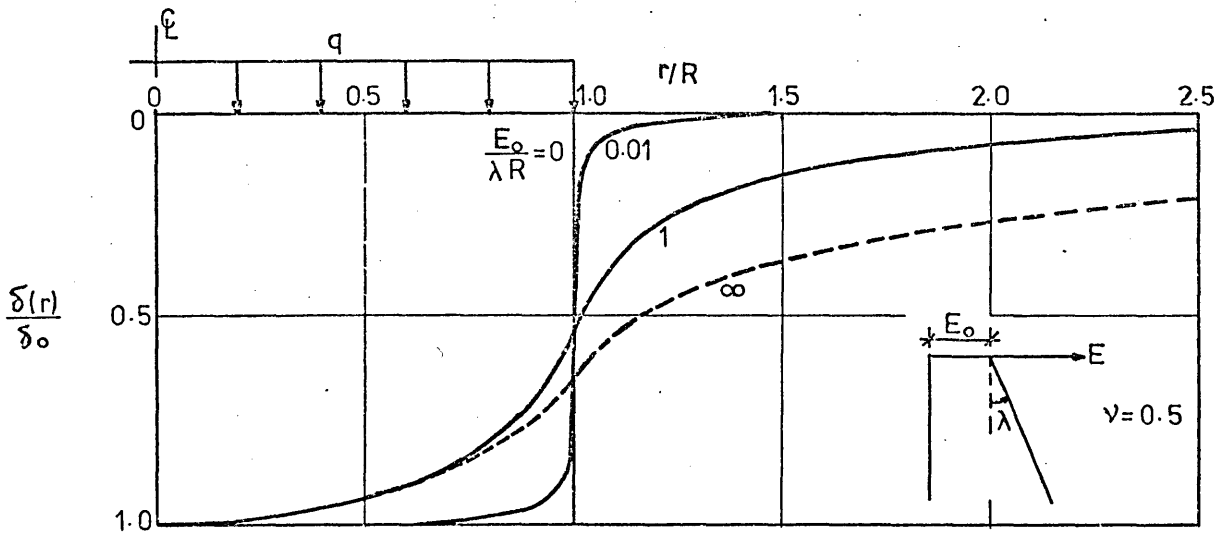
Fig. 3.18 Form of settlement profiles, after Brown & Gibson(1972).
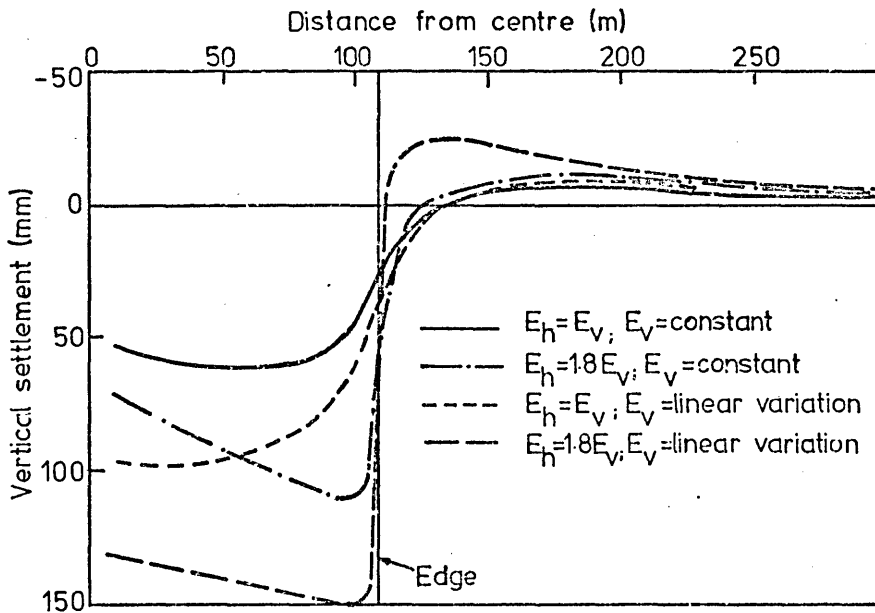
Fig. 3.19 Form of settlement profiles, after Rodrigues(1975).
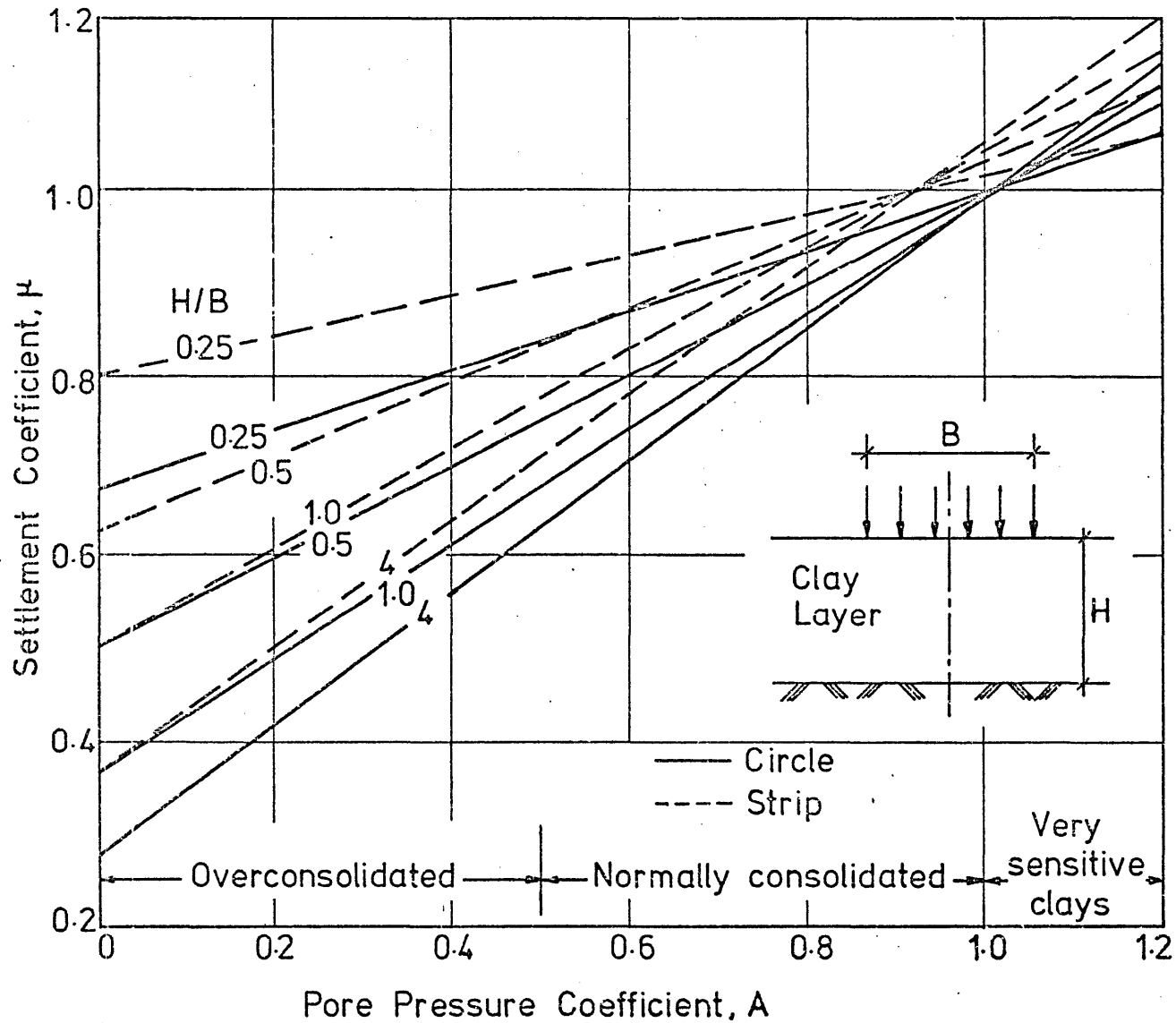
Fig. 3.20 Values of the
settlement coefficient,
(Skempton & Bjerrum, 1957)

Time (log scale)

t_c t

Primary
consolidation

δ_c

δ_s $\delta_s = C_s \log(t/t_c)$

Secondary
consolidation
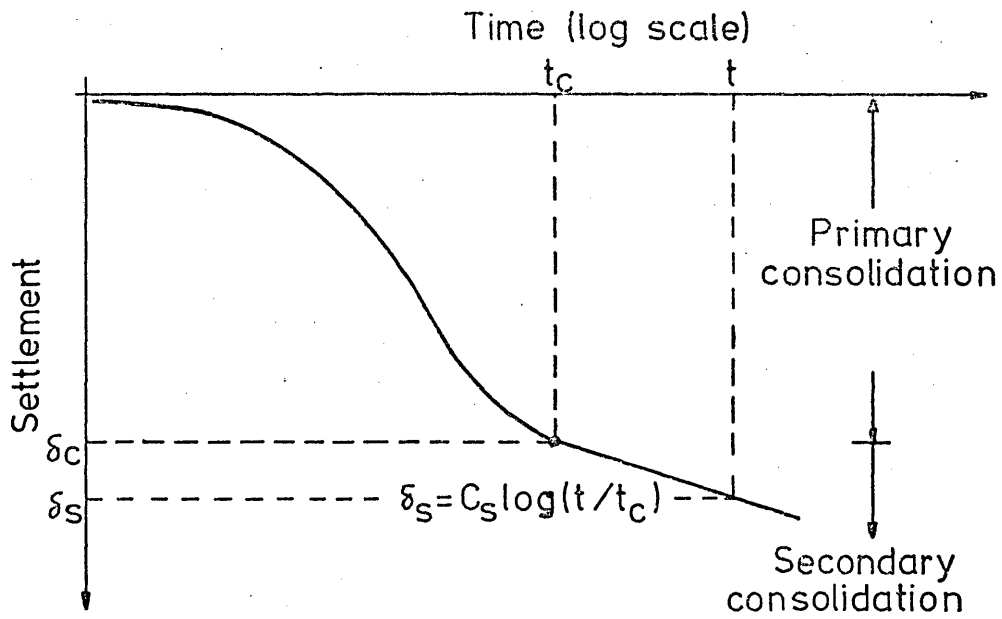
Settlement

Fig. 3.21   Typical time-settlement curve for soil.

Δq_s (Ton/ft^2) to cause 1-in. settlement

7

6

Very dense

5   N=50

4

Dense

3   N=30

2

Medium

1   N=10

Loose

0

0   5   10   15   20

Footing width (ft)
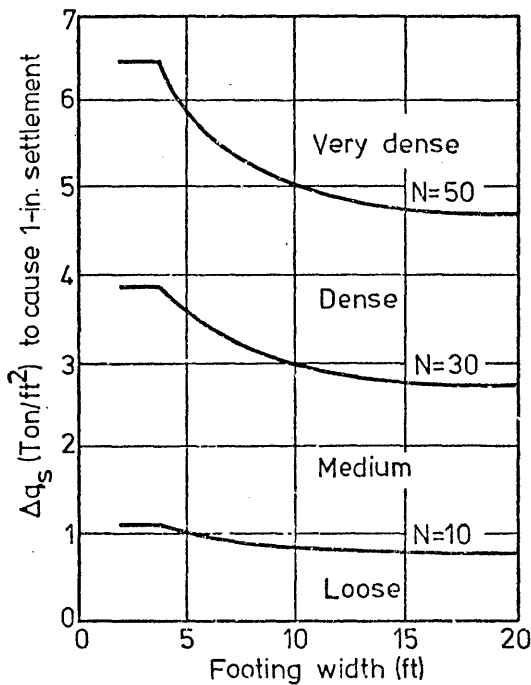
Fig. 3.22   Correlations of allowable
pressure to S.P.T. value,
after, Terzaghi and
Peck(1948).
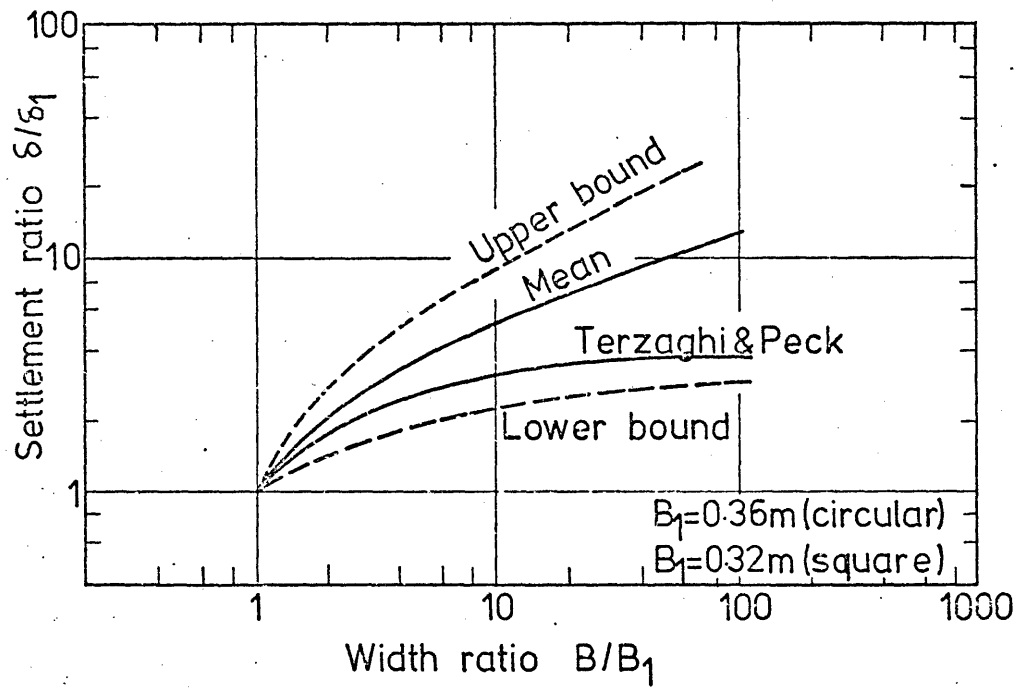
Fig. 3.23 Settlement ratio
versus breadth ratio for
footings on sand, after
Bjerrum and Eggestad(1963).

(a)

(b)

Narrow load

Wide load
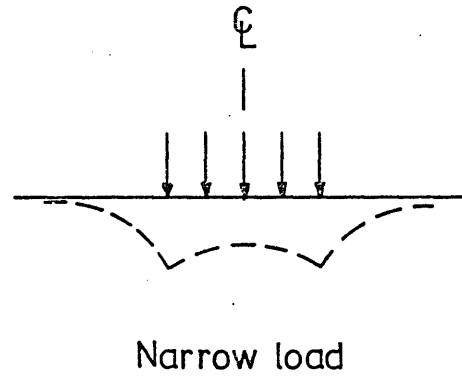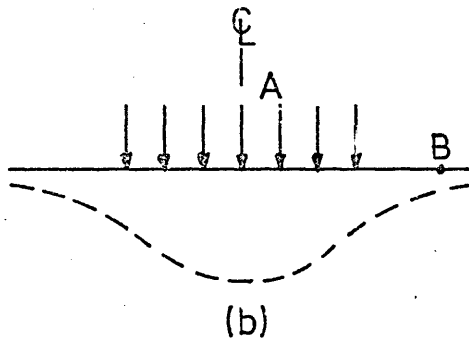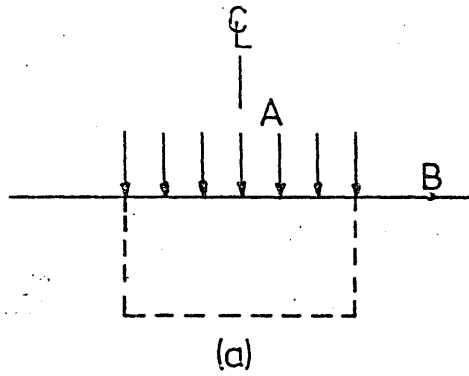
(c)
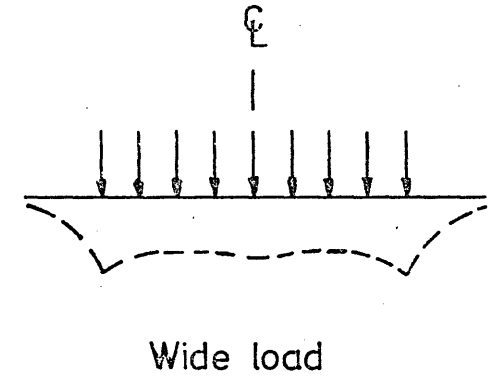
Fig. 3.24 Typical profiles of settlement and contact pressure. (a) settlement of Winkler foundation; (b) and (c) settlement of a uniformly loaded flexible footing on clay and sand respectively; (d) distribution of the contact pressure for a rigid footing on clay and sand.

Footing
on
clay

Narrow footing
on
sand

Wide footing
on
sand

(d)
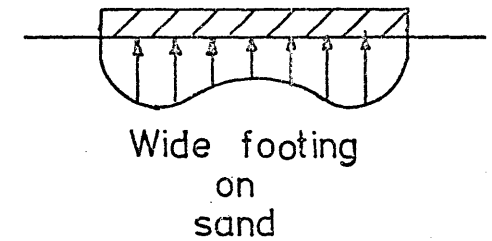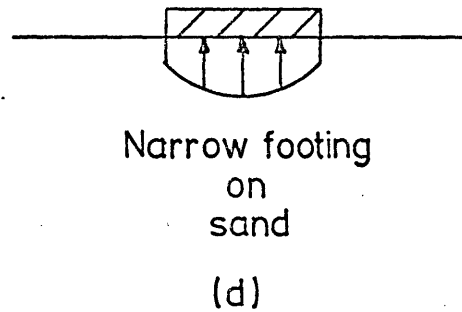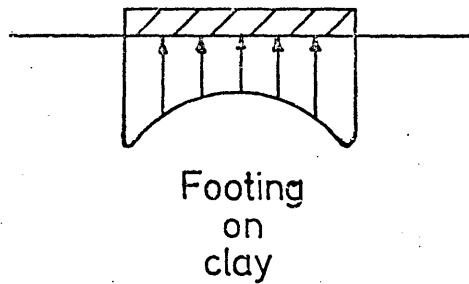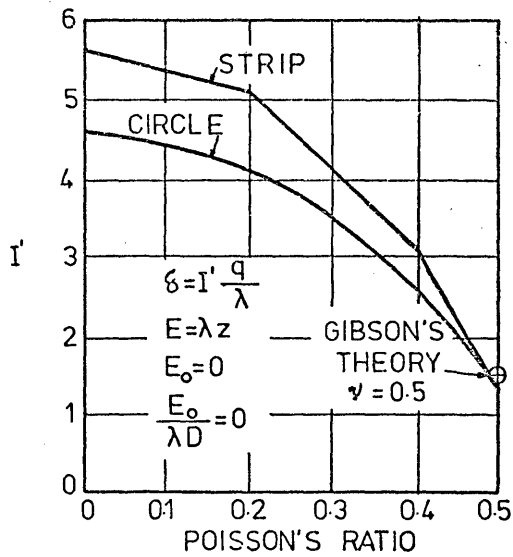
Fig. 3.26 Variation of the settlement with
Poisson's ratio for non-homogeneous
half-space, after Carrier and
Christian(1973).
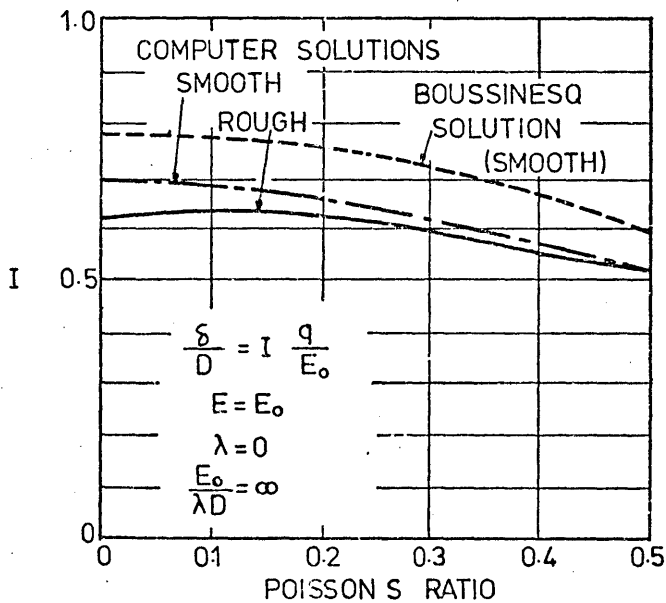
Fig. 3.25 Variation of the settlement with Poisson's ratio
for homogeneous half-space, after Carrier and
Christian(1973).
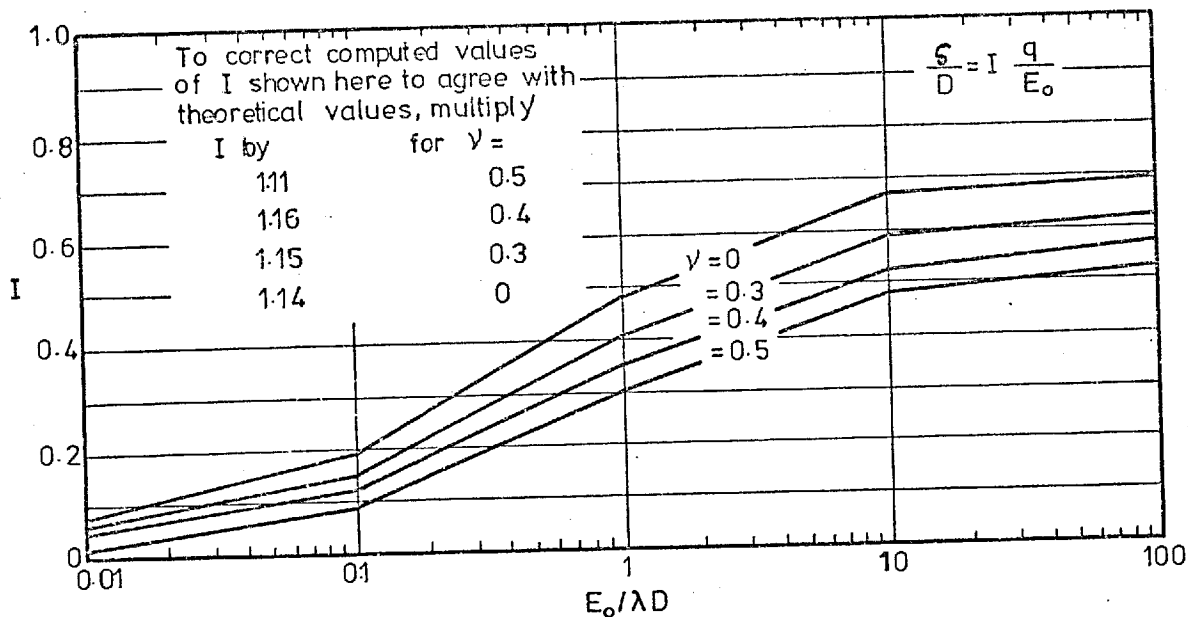
Fig. 3.27 Settlement influence factor, after Carrier and Christian(1973).
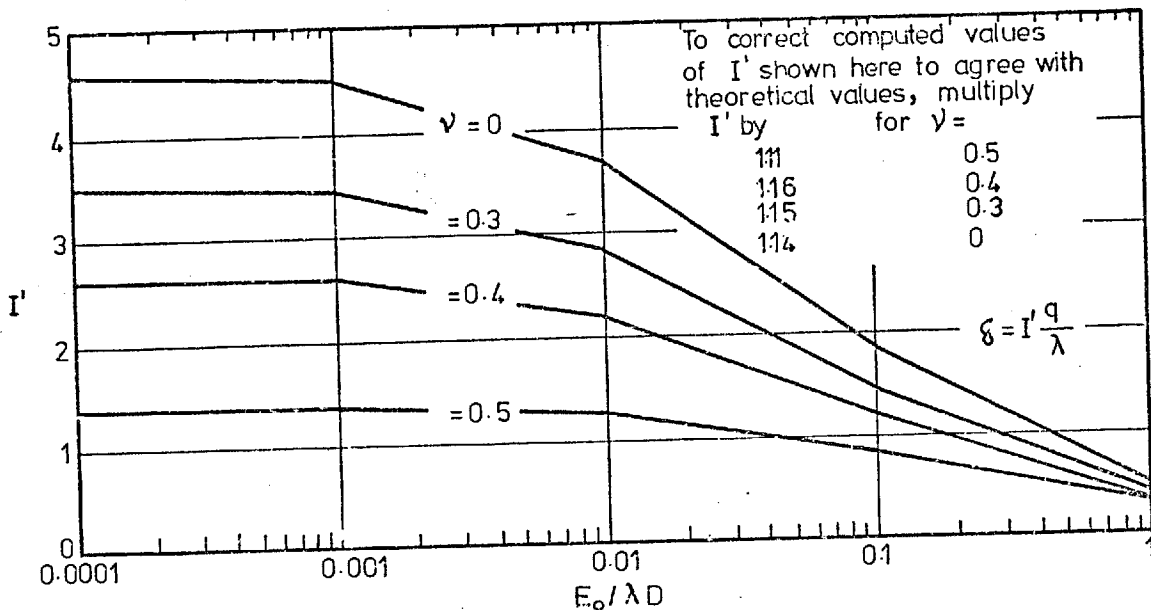
Fig. 3.28 Settlement influence factor, after Carrier and Christian(1973).
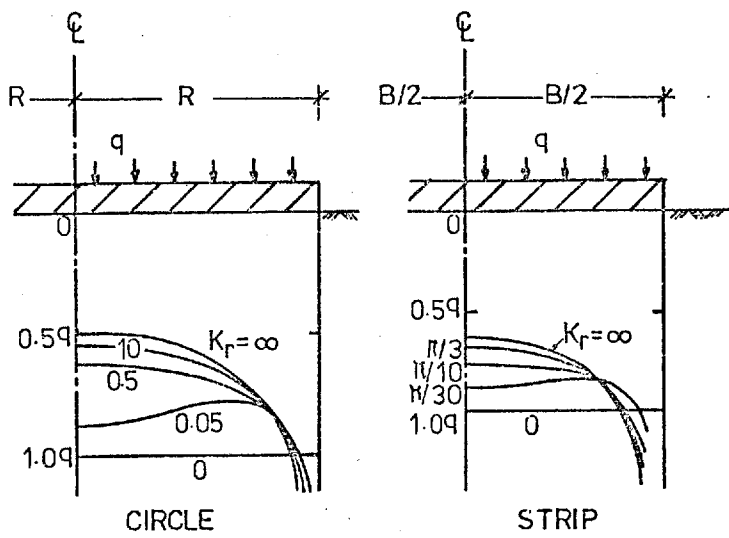
Fig. 3.29 Variation of the contact pressure with footing rigidity, after Borowicka(1936 and 1938).
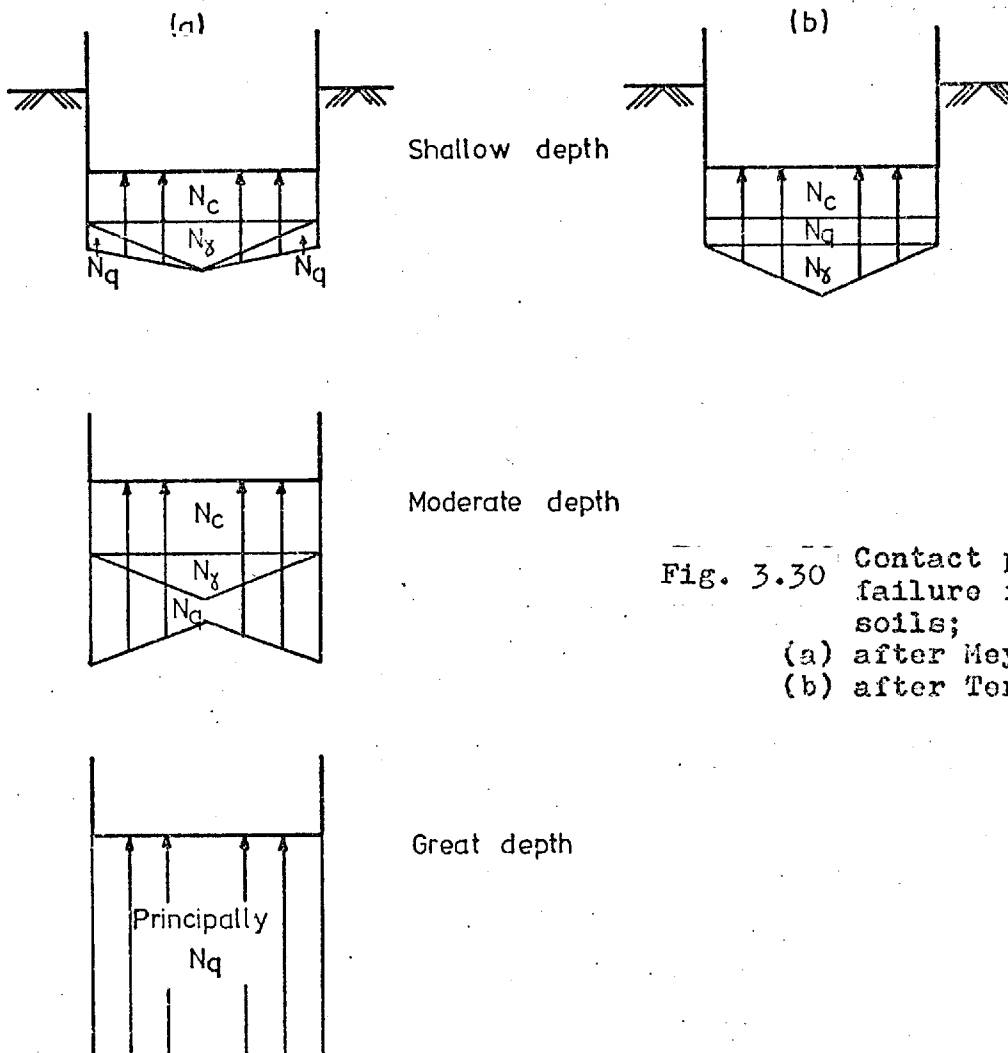
Fig. 3.30 Contact pressure at failure for cohesive soils;
(a) after Meyerhof(1951);
(b) after Terzaghi(1943).
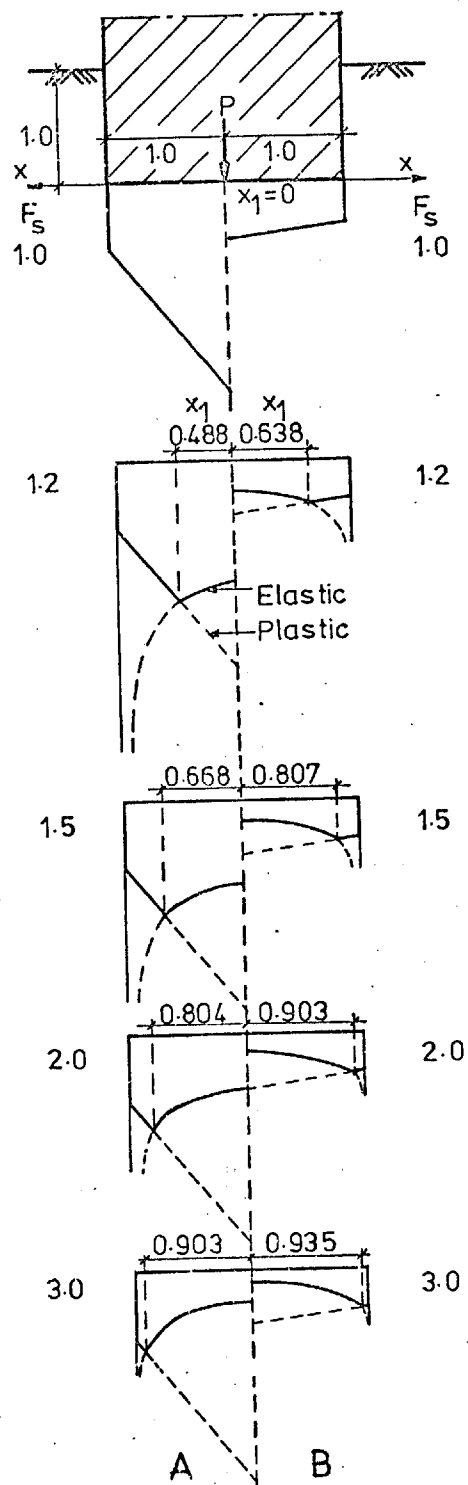
Fig. 3.31 Contact pressure distribution under a rigid strip footing, after Schultze(1961).
(A) non-cohesive soil: $\phi = 30°$; $c = 0$
(B) cohesive soil: $\phi = 15°$; $c = 1$ t/m^2.
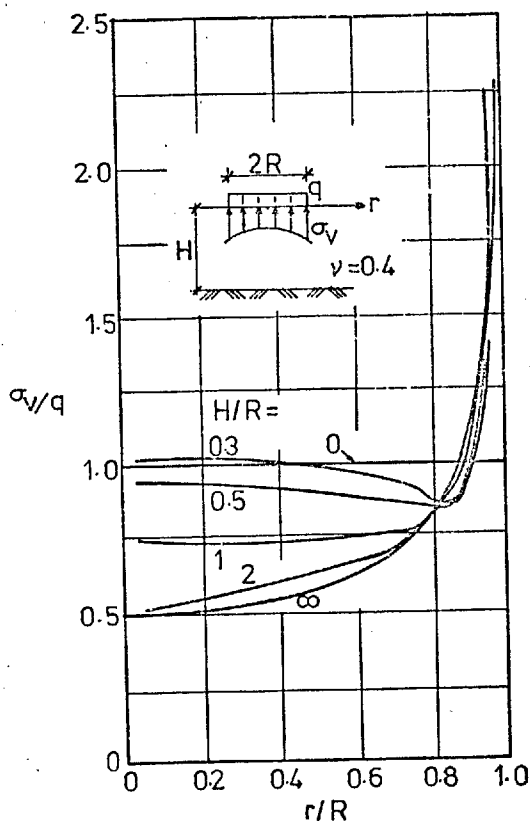
Fig. 3.32   Effect of H/R on contact pressure distribution, after Poulos(1968).
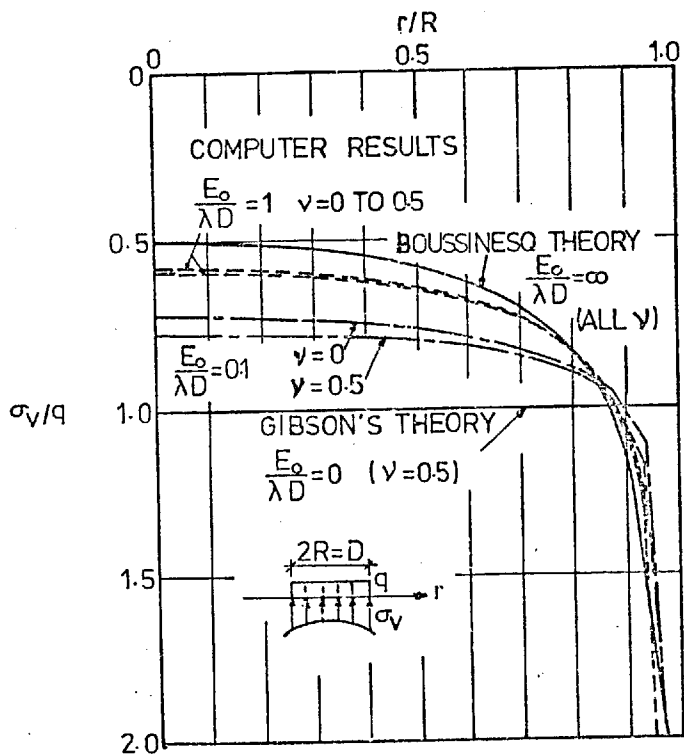
Fig. 3.33   Effect of non-homogeneity on contact pressure distribution, after Carrier and Christian(1973).

CHAPTER 4

BEARING CAPACITY OF SHALLOW FOUNDATIONS

4.1   Introduction

The purpose of this chapter is to discuss methods of

estimating the bearing capacity associated with stability

problems.   The next two chapters are concerned with the

non-linear finite element solutions which give answers

mainly to the contained plastic flow problems.

In Chapter 3, the ultimate load was defined as the

load at the first complete failure of the foundation.

This bearing capacity failure occurs usually as a shear

failure of the soil supporting the footing.   In some cases

there is not a complete rupture, and it is difficult to

recognize the exact failure load.

Before any discussion of the computation of ultimate

load, two important subjects, namely, modes of shear failure

and ultimate load definition will be considered.

4.2   Modes of Failure

It is known that rupture underneath a footing may be

produced by a general shear failure (Caquot, 1934; Buisman,

1935; and Terzaghi,1943), by local shear failure (Terzaghi,

1943; and De Beer and Vesic, 1958), or by punching shear

failure (De Beer and Vesic, 1958; and Vesic, 1963a).

Figure 4.1, after Vesic (1963a), represents these

three modes of failure.   For general shear failure there

is a well-defined failure pattern consisting of a continuous

slip surface from one edge of the footing to the ground surface. In this failure mode a tendency for bulging of adjacent soil exists on both sides of the footing, but the final soil collapse occurs only on one side.

Local shear failure has a failure pattern which is clearly defined only immediately below the foundation. The slip surfaces end somewhere in the soil mass, and they appear at the ground surface only after a large post-failure vertical displacement of the footing. There is a small, but visible, tendency of soil bulging on the sides of the footing.

In punching shear failure, there is no well-defined failure pattern, and as the load increases, the vertical movement of the footing (which is made possible by vertical shear around the footing perimeter) is accompanied by compression of the soil immediately underneath. The soil outside the loaded area has practically no movement.

The appearance of one of these failure modes depends on a number of factors, such as: relative compressibility, overburden pressure, transient or dynamic loading, layered soil and rate of the loading. Of these factors the most important is probably the relative compressibility of the soil in particular geometrical and loading conditions. For a practically incompressible soil which has a finite shear strength, failure will be a general shear. In contrast, if the soil is very compressible for its strength, it will fail in punching shear.

A footing on saturated, normally consolidated clay will fail in general shear if it is loaded so that no volume change can take place, while it may fail in punching shear if loaded slowly enough for volume change to take place in the soil under the load (Vesic, 1973).

At present, there is no general numerical criterion which can be used for prediction of the mode of shear failure of soils loaded by footings. Vesic (1963 & 1965) has given the rigidity index I_r, for evaluation of relative compressibility of the soil mass under the load, defined as:

$$I_r = \frac{G}{c + q\tan\phi} \tag{4.1}$$

where G is the shear modulus and c and ϕ are strength parameters of the soil. To take into account the average volumetric strain Δ in the plastic zone, Vesic (1965) suggested that the value given by Eq. 4.1 should be reduced to:

$$I_{rr} = \zeta_v \cdot I_r \tag{4.2}$$

and

$$\zeta_v = \frac{1}{1 + I_r \cdot \Delta} \tag{4.3}$$

The rigidity index is a function of the stress level and the character of loading, and a high value of it (> 250) represents a relatively incompressible soil mass, whereas a low value (< 10) implies a relatively compressible soil mass (Vesic, 1965).

4.3 Ultimate Bearing Capacity Criterion

From the previous comments it is apparent that in the case of the general shear failure the ultimate load corresponding to the failure is well defined and is the peak load in a load-settlement plot. In the two other failure modes, local and punching shear failure, the ultimate load is not clearly defined (Fig. 4.1).

The ultimate load criterion can be based on a settlement value or a load-settlement curve. In the first case an ultimate settlement will be defined as the settlement of the footing needed to mobilize the ultimate load. Observations in saturated clays (Skempton, 1951) indicate that these settlements may be about 3% to 7% of the footing width for surface footings.

In the second case, the ultimate load is defined as the point at which the slope of the load-settlement curve first reaches zero or a steady minimum value. This criterion has an important disadvantage; that when the failure mode is not a general shear failure, there will be a continuous increase of the load against settlement.

Brinch Hansen (1963) has defined the ultimate load as the load for which the ultimate settlement is twice the settlement at a 10% lower load.

Now, if the load per unit width and settlement are represented by q and δ respectively, then the Brinch Hansen (1963) criterion will be:

$$\frac{\Delta q}{q_f} = \frac{1}{5} \frac{\Delta \delta}{\delta_f} \qquad (4.4)$$

In general Eq. 4.4 may be written as:

$$d \ln q = C.d \ln \delta \qquad (4.5)$$

where C is a characteristic value depending on the stiffness (clay), or relative density (sand).

The criterion used in this research to predict the ultimate load (purely cohesive soil) is a dimensionless form of Eq. 4.5:

$$d \ln \frac{q}{q_f} = C_1.d \ln \frac{\delta}{B} \qquad (4.6)$$

where q is the applied pressure, q_f is the failure pressure calculated from the bearing capacity theory, B is the footing width, δ is the settlement, and C_1 is a constant.

The plot of q/q_f versus δ/B on a log/log scale consists of an upper curved part and a lower part which is a straight line (De Beer, 1970). The intersection of the curved part and the straight line that represents the smallest continuous value of C_1, will be considered as the ultimate load (Fig. 6.61 of Chapter 6).

For some clays it is impossible to distinguish a well-defined intersection point, then in such cases it is better to determine an upper and a lower limit for the ultimate load.

4.4   Calculations of the Bearing Capacity

4.4.1 General

The calculations of bearing capacity are generally

based on plasticity theory, usually combined with some simplifying assumptions. Speaking for simplicity about plane problems only, one can determine the bearing capacity when the shape and position of the critical rupture figure and the stress distribution along the different rupture lines are known.

However, the result will only be correct when the critical rupture figure is statically and kinematically admissible. Statically admissible means that all equilibrium conditions should be fulfilled throughout the soil mass, and that in all rupture zones and rupture lines the shearing stresses should be equal to those defined by the failure condition, and finally, the shear stresses outside the rupture zones and rupture lines must be smaller than those in the rupture zones and rupture lines. Kinematically admissible means that the deformation mode (or velocity field) must satisfy the velocity boundary conditions and strain and velocity compatibility conditions.

Mathematically correct solutions have been obtained in only a few very simple cases (usually for $\phi = 0$ or $\gamma = 0$), therefore most existing methods are based on different simplifying assumptions.

The most difficult part is the determination of the shape of the actual rupture figure, consequently, its general shape is usually assumed to be a straight line, a circle, a logarithmic spiral or a combination of these.

4.4.2 Methods of Analyses

The analyses of foundations can be made by employing one of the following four methods:

    (1)   Slip Line Theory;

    (2)   Limit Equilibrium;

    (3)   Limit Analysis; and

    (4)   Finite Element.

The first three methods are generally used in association with the stability problems where only the bearing capacity is sought. If a settlement of foundation and a stress distribution within the soil mass are of prime interest, then the finite element method must be used.

Studies of the bearing capacity of foundations under conditions of plane strain have been made by Terzaghi (1943); Taylor (1948); and Meyerhof (1951) using limit equilibrium methods, by Brinch Hansen (1961); and Sokolovskii (1965) using slip line methods, by Shield (1954); and Chen and Davidson (1973) using limit analysis methods, and many others. Only a brief description of each procedure is given in this thesis. More details on the first three methods can be found in Brinch Hansen (1953); Hansen (1965), Sokolovskii (1965); and Chen (1975), and on finite element methods in Chapter 2.

4.4.2.1 Slip Line Method

This method involves a construction of a family of shear or slip lines in the vicinity of the footing loads.

These slip lines which represent the directions of the

maximum shear stresses form a network known as a slip-line

field.   The plastic slip-line field is bounded by regions

which are rigid.

For solution of a problem, assumptions must be made

for:-

(1)   Failure criterion:

(2)   Equilibrium; and

(3)   Boundary conditions.

For the special case of a plane strain problem, there are

two differential equations of equilibrium and one yield

condition available for solving the three unknown stresses.

In assuming the yield criterion, recently, Bishop

(1966b)correlated all possible failure criteria with experi-

mental data and concluded that the Mohr-Coulomb yield

criterion best predicts soil failure.

4.4.2.2 Limit Equilibrium Method

This method, probably because of its simplicity and

reasonably good accuracy, is the most conventional method.

The method can be best described as an approximate approach

to the construction of a slip-line field.   For the

solution of a problem, assumptions must be made for the

shape of the failure surface and the normal stress distri-

bution along such a surfaces, which satisfies the yield

criterion and the equations of equilibrium.   By considering

different failure surfaces it is possible to find the most

critical failure surface which corresponds to the lowest failure load.

4.4.2.3 Limit Analysis Method

This method, principally, is restricted to undrained materials where no volume change can take place ($\phi = 0$).

Four basic conditions are needed in the solution, namely, equilibrium, yield criterion, stress-strain relations, and the compatibility which relates strain and displacement. In contrast to slip line and limit equilibrium methods, the limit analysis method considers the stress-strain relationship of the soil in an idealized manner (i.e. elastic-perfectly plastic). This idealization, termed normality or the flow rule, establishes the limit theorems on which limit analysis is based. The method offers an upper and a lower bound to the true solution by employing the plastic limit theorems of Drucker, Prager and Greenberg (1952).

The conditions required to establish an upper and a lower bound solution are as follows:

(1) Lower Bound Theorem

The load, determined from a stress field that satisfies the stress boundary conditions, the equilibrium equations, and nowhere violates the yield criterion (termed a statically admissible stress field), is equal to or less than the true collapse load.

It is clear that the lower bound theorem considers only
equilibrium and yield. It gives no consideration to soil
kinematics.

(2) Upper Bound Theorem

The load, determined by equating the external
rate of work to the internal rate of dissipation
in an assumed deformation field or velocity field
that satisfies the velocity boundary conditions
and strain and velocity compatibility conditions
(termed a kinematically admissible deformation
field or velocity field), is equal to or greater
than the true collapse load.

The upper bound theorem considers only velocity or failure
modes and energy dissipation. The stress distribution
need not be in equilibrium, and is only defined in the
deforming regions of the mode.

Classical plasticity theory assumes an associated
flow rule (normality) and this requires that $\psi = \phi$ (ψ is
the equivalence of the internal friction angle ϕ for the
velocity field that defines the relation between strain
rates during plastic failure, or the dilatancy behaviour),
stress and velocity characteristics then coinciding. As
mentioned by Davis (1967), only in this case do the limit
theorems hold and a solution to any problem which is both
statically and kinematically admissible is the unique
solution. Unfortunately it seems certain that all real
granular materials, even at their densest and at peak

strength, have a non-associated flow rule with values of ψ which are very much less than ϕ (Davis and Booker, 1971). Thus the theory which allows ψ to take a value less than ϕ as dictated by experimental evidence, suffers from the drawback that an exact solution to a problem is, from a mathematical point of view, not necessarily unique (because of lack of proof of the limit theorems in non-associated flow rule where the normality does not hold, Dias, 1967).

However, by suitable choice of stress and velocity fields, and the strong evidence (Booker, 1970) that the range of collapse loads in the set of possible exact non-unique solutions is likely to be insignificant in problems of practical interest, the two theorems give a lower value and an upper value for the collapse load which are close to the true collapse load.

A comprehensive treatment of the subject is given by Chen (1975).

4.4.2.4 Finite Element Method

Definition and concept of the finite element method have been considered in Chapter 2, and its application has been discussed all through this thesis.

The finite element method is the only correct and complete solution for stability analysis that makes possible the calculation of settlement and stress distribution as well as of the bearing capacity.

4.4.3 <u>Comments on the Methods of Analyses</u>

The methods described earlier are related to each other in a certain way. Most of the slip line solutions give kinematically admissible velocity fields, thus they can be considered as upper bound solutions provided that the velocity boundary conditions are satisfied. If the stress field within the plastic zone can be extended into the rigid region so that the yield criterion and equilibrium are satisfied, then slip line solutions are also lower bound solutions.

The limit equilibrium method considers the basic philosophy of the upper bound rule, where a failure surface is assumed and the least load is sought. However, it gives no consideration to soil kinematics and equilibrium conditions are satisfied only in a limited sense, thus this solution is not necessarily an upper or a lower bound. But any limit analysis upper bound solution is a limit equilibrium solution.

One other weakness of the limit equilibrium method is the neglect of the stress-strain relationship of the soil. According to the mechanics of solids, a valid solution requires satisfying the boundary conditions, equations of equilibrium, equations of compatibility, and the stress-strain relationship (Chen and Scawthorn, 1970). As the stress-strain relationship connects equilibrium to compatibility and distinguishes elasticity from plasticity or visco-elasticity theories, so a solution which neglects

considering this relationship may not be a complete one.

On the other hand, limit analysis, within the frame-
work of the idealizations, is the more efficient method and
can be extended to solve more difficult footing problems.
Its capability of providing a means for bounding the true
solution is noteworthy.

The finite element method usually gives a lower
bound value for the collapse load, as it satisfies only
a statically admissible stress field.

4.5   Bearing Capacity of a Strip Footing on a General
        c-ϕ-γ Soil

It is now generally understood that the bearing
capacity of footings depends not only on the mechanical
properties of the soil (cohesion c and internal friction
angle ϕ), but also on the physical characteristics of the
footing (width B and depth D).

The basic available solution for the bearing capacity
problem that has been solved by the methods of the theory
of plasticity (Prandtl, 1920 and Reissner, 1924) indicates
that the failure pattern for a frictionless footing should
consist of three zones (Fig. 4.2). Wedge I is an active
Rankine zone which pushes the radial Prandtl zone II side-
ways and the passive Rankine zone III in an upward
direction. The boundary ACDE is composed of two straight
lines AC and DE, and a curved section CD. The shape of
this curve depends on the angle ϕ and on the ratio γB/q.

For a frictionless soil (ϕ = 0) the curve is a circle. For frictional weightless soil ($\gamma B/q$ = 0) the curve becomes a logarithmic spiral which for ϕ = 0 degenerates into a circle. Finally, in the general case ($\gamma \neq 0$) the curve lies between a spiral and a circle, as long as $\phi \neq 0$.

For the case of a wide rough footing the lines AC and BC are not emanating from the edges. But, as mentioned by Davis and Booker (1971), a wedge of rigid materials moving with the footing may occur symmetrically about the centre for a limiting width. At the remaining segments out to the edges there is slip between soil and footing. For kinematical reasons the lines AC and BC must either pass through the edges, or must have horizontal tangents at the foundation level (Hansen, 1965). Thus AC and BC cannot be assumed to be straight lines.

Because of mathematical difficulties in the plasticity methods, the bearing capacity of the footing has been calculated by a superposition method suggested by Terzaghi (1943), which is represented by the following expression:

$$q_f = c N_c + q N_q + \frac{B\gamma}{2} N_\gamma \qquad (4.7)$$

where N_c, N_q and N_γ are dimensionless bearing capacity factors, defined by:

$$N_q = e^{\pi \tan\phi} \tan^2(\pi/4 + \phi/2) \qquad (4.8)$$

$$N_c = (N_q - 1)\cot\phi \qquad (4.9)$$

$$N_\gamma = 2(N_q + 1)\tan\phi \qquad (4.10)$$

The numerical values of these factors are given in Table 4.1 and shown graphically in Fig. 4.3.

The first stage in Eq. 4.7 is essentially based on an extension of the analytical work of Prandtl (1920) and Reissner (1924), this assumes a weightless material and gives the first part of the bearing capacity $cN_c + q N_q$ in closed form expressions. The second stage takes the weight of material (c = 0, q = 0) into account and gives the second part of the bearing capacity $\frac{B\gamma}{2} N_\gamma$.

It is generally assumed that Terzaghi's bearing capacity formula is conservative. Lundgren and Mortensen (1953), and Hansen and Christensen (1969) mentioned that the errors in this superposition are on the safe side, not exceeding 20% for $\phi = 30^\circ$ to 40°, while equal to zero for $\phi = 0^\circ$.

However, as pointed out by Ko and Scott (1973), the angle of internal friction determined from a triaxial test is several degrees less than that determined under plane strain conditions for low confining pressure (Cornforth, 1964). Therefore, if the ϕ value obtained from a triaxial test is used in calculating the N factors, then a lower bearing capacity will be predicted. But, if a plane strain angle of internal friction is used, then Terzaghi's equation will be non-conservative.

4.6   General Bearing Capacity Formula

By considering the shape and depth of the footing,

and inclination of the foundation load, the Terzaghi's formula (Eq. 4.7) can be written as follows (Brinch Hansen, 1961):

$$q_f = c\,N_c\,s_c\,d_c\,i_c + q\,N_q\,s_q\,d_q\,i_q +$$

$$+ \frac{B\gamma}{2}\,N_\gamma\,s_\gamma\,d_\gamma\,i_\gamma \qquad (4.11)$$

where s's denote the foundation shape factors;

    d's denote the foundation depth factors; and

    i's denote the load inclination factors.

The following empirical expressions, suggested by Brinch Hansen (1961), may be used to evaluate the factors.

(1) Shape Factors

$$s_c = 1 + (0.2 + \tan^6\phi)B/L \qquad (4.12)$$

$$s_q = s_c \qquad \text{for} \qquad \phi \neq 0 \qquad (4.13)$$

$$s_q = 1 \qquad \text{for} \qquad \phi = 0 \qquad (4.14)$$

$$s_\gamma = \tfrac{1}{2}(3 - s_c) \qquad (4.15)$$

where B is the footing width and L is the footing length ($\geq$ B).

(2) Depth Factors (after Brinch Hansen, 1970)

  For D/B $\leqslant$ 1:

$$d_q = 1 + 2\tan\phi(1 - \sin\phi)^2 D/B \qquad (4.16)$$

$$d_c = d_q - \frac{1 - d_q}{N_q - 1} \qquad (\phi \neq 0) \qquad (4.17)$$

$$d_c = 1 + 0.4\,D/B \qquad (\phi = 0) \qquad (4.18)$$

For D/B > 1:

$$d_q = 1 + 2\tan\phi(1 - \sin\phi)^2\tan^{-1}(D/B) \quad (4.19)$$

$$d_c = 1 + 0.4 \tan^{-1}(D/B) \quad (\phi = 0) \quad (4.20)$$

In both cases

$$d_\gamma = 1 \quad (4.21)$$

where D is the foundation depth below the ground surface.

(3)   Inclination Factors

If the foundation area (of any shape) is eccentrically loaded, the effective area (that its deduced imaginary boundaries are radially symmetric with the real outer boundaries and the resultant force acts on its centroid) will be used.

For shapes other than rectangle, the effective foundation area may be determined as that of the equivalent rectangle, constructed so that its geometric centre coincides with the load centre and that it follows as closely as possible the adjacent contour of the actual base area. A few examples (after Brinch Hansen, 1961) are shown in Fig. 4.4.

Thus the inclination factors for a general case of eccentric and inclined loading will be as follows:

$$i_q = [1 - \frac{H}{V + A'.c.\cot\phi}]^2 \quad (4.22)$$

$$i_c = i_q - \frac{1 - i_q}{N_q - 1} \quad (\phi \neq 0) \quad (4.23)$$

$$i_c = 0.5 + \frac{2\theta + \sin 2\theta}{2 + \pi} \qquad (\phi = 0) \qquad (4.24)$$

For i_γ Sokolovskii (1965) gives:

$$i_\gamma = i_q^{3/2} \qquad (4.25)$$

where V and H are the vertical and horizontal components of the load respectively, A' is the effective foundation area, and θ is defined in Fig. 4.9.

4.7   Scale and Soil Compressibility Effects

Scale effects have been known for a long time, but the understanding of the reasons for their existence has come only in recent years.   The studies of shallow foundations by De Beer (1965a and 1965b) and Kérisel (1967) indicate that the average shear strength mobilized along a slip line under the foundation decreases with foundation size.   Vesic (1973) gives three reasons for this reduction in strength, namely, the curvature of Mohr envelope, progressive rupture along the slip line, and presence of zones or seams of weakness in all soil deposits.   Thus, there will be a decrease in bearing capacity factors with size, and the decrease in N_γ values with increased size of surface footing on sand is remarkable.

As mentioned in the preceding sections, the bearing capacity analysis assumes an incompressible soil that has a general shear failure mode.   There exists a lack of rational methods for analysing bearing capacity failures in the two other modes characteristics for compressible soil.

In order to consider the influence of soil compressibility and scale effects, Vesic (1973) introduced three compressibility factors ζ_c to be used in Eq. 4.11 as other factors. These factors are:

$$\zeta_{cq} = \exp\{(-4.4 + 0.6 \frac{B}{L})\tan\phi + [\frac{(3.07\sin\phi)(\log_{10}2I_r)}{1 + \sin\phi}]\}$$

(4.26)

$$\zeta_{cc} = \zeta_{cq} - \frac{1 - \zeta_{cq}}{N_q - 1}$$

(4.27)

For $\phi = 0$

$$\zeta_{cc} = 0.32 + 0.12 \, B/L + 0.6 \, \log_{10}I_r$$

(4.28)

And for all practical purposes

$$\zeta_{c\gamma} = \zeta_{cq}$$

(4.29)

where I_r is the rigidity index (Eq. 4.1).

The use of expressions 4.26 through 4.29 makes sense, obviously, only as long as the compressibility factors remain smaller than unity.

From Eq. 4.26 it is possible to get the values of critical rigidity index for any angle ϕ and any particular foundation shape. For a particular footing, if the rigidity index (defined in Eq. 4.1) is less than the critical value, it becomes necessary to reduce the bearing capacity because of compressibility effects. This critical rigidity index, given by Vesic (1973), is:

$$(I_r)_{crit} = \frac{1}{2} \exp[(3.30 - 0.45 \frac{B}{L}) \cot(45^\circ - \frac{\phi}{2})]$$

(4.30)

Numerical values of Eq. 4.30 have been given in Table 4.2 for B/L = 0 (strip) and·B/L = 1 (square).

4.8   Effect of a Rigid Base underlying the Layer

The problem of bearing capacity of a layer of soil of limited depth H resting over a lower layer of infinite rigidity and strength has been considered for the plane strain case by Mandel and Salencon (1969). Their solution, obtained by the method of characteristics under the assumption of rigid-plastic behaviour, indicates that the presence of a rigid layer below the bearing stratum results in an increase of bearing capacity. Factors of increase R_b, analogous to other factors in Eq. 4.11, are presented in Table 4.3.

4.9   Effects of Footing Roughness and Flexibility

The bearing capacity of a smooth footing on a purely cohesive soil was first examined by Prandtl (1920). Hill (1949 & 1950) proposed an alternative failure mechanism, first reported by Hencky (1923), for smooth footing on purely cohesive soil, shown in Fig. 4.5. It has been shown that these solutions for purely cohesive soils are also valid if the footings are perfectly rough (Davis and Booker, 1971).

Ko and Davidson (1973), from their experiments, reported that the sand in footing tests with glass bottoms (smooth) failed according to the Hill mechanism, but with

sandpaper bottoms (rough) the footings failed according to the Prandtl mechanism.

On the basis of the Hill pattern, Meyerhof (1955) suggested that the bearing capacity of a smooth footing on the surface of a cohesionless soil should be only one-half of the bearing capacity of a rough footing.

Since, in almost every practical case the footing is rough, the Hill pattern may never be realized beneath an actual footing. This leads Vesic (1973) to conclude that the stress and deformation pattern under an actual footing is such that it always leads to the formation of a single wedge (Prandtl) mechanism. Thus, the footing roughness in a practical situation has little effect on bearing capacity provided that the applied external loads remain vertical.

The footing flexibility has no effect on ultimate bearing capacity, but it affects the initiation of the yield zones. For a rigid footing, yield zones start from the edges, while for a flexible footing they probably start from the centre and at a point approximately 0.5B beneath the surface (Höeg et al, 1968).

4.10 The Bearing Capacity of a Strip Footing on Purely Cohesive Soils ($\phi = 0$)

4.10.1 Prandtl Equation

The bearing capacity of a strip footing on purely cohesive soil has been given by Prandtl (1920) as:

$$q_f = (2 + \pi) C_u \qquad\qquad (4.31)$$

where C_u is the undrained shear strength of the soil.

In normally consolidated clays, usually, undrained shear strength increases with depth, and for a particular deposit, the ratio of undrained shear strength to the effective overburden stress (C_u/p) is a constant. Skempton (1948 & 1957) has given the following relationship which relates this ratio to the plasticity index I_p of the soil:-

$$\frac{C_u}{p} = 0.11 + 0.0037 \, I_p \qquad (4.32)$$

For some practical cases it is sufficiently accurate to use some average of C_u as a constant for a $\phi = 0$ bearing capcity analysis, nevertheless, the variation of C_u with depth has a significant effect on bearing capacity.

4.10.2 Effect of Increasing Strength with Depth on the Bearing Capacity

Several investigations have been carried out for the bearing capacity of a strip footing on non-homogeneous soil. Raymond (1967) and James et al (1969) treated this problem by using the limit equilibrium method (slip circle) which, when $\phi = 0$, only gives an upper limit to the correct solution.

The exact solution for a strip footing, by using the theory of plasticity, given by Davis and Booker (1973); Salencon (1974) and Salencon et al (1976).

They have assumed a linear variation of C_u with depth according to the following equation:

$$C_u = C_{u_O} + \rho z \qquad (4.33)$$

where C_{u_O} is the strength at ground surface, and ρ is the rate of increase in strength with depth.

Davis and Booker (1973) have considered the bearing capacity of both smooth and rough footings, and concluded that the roughness has a small but significant effect in increasing the bearing capacity in contrast to the homogeneous case for which roughness has no effect. Furthermore, they found that the rate of increase in strength with depth plays the same role as density plays in the bearing capacity of homogeneous cohesive-frictional soils.

For bearing capacity Davis and Booker (1973) suggested the following expression:

$$q_f = F[(2 + \pi)C_{u_O} + \rho B/4] \qquad (4.34)$$

where F is a dimensionless factor depending only on the ratio $\rho B/C_{u_O}$. Figure 4.6 shows the values of F (F_R is for a rough footing and F_S is for a smooth footing).

Figure 4.7 (after Davis and Booker, 1973) shows the stress fields for narrow and wide rough footings. As mentioned before, for a wide footing there is slip between footing and soil along some parts of the width where the shear stresses are equal to the strength.

4.10.3 Effects of Load Eccentricity and Inclination on the Bearing Capacity

In applying bearing capacity theory to cases of eccentric loading it is usual to use a reduced foundation width (Brinch Hansen, 1961). For a footing on clay of uniform strength:

$$q_f = (2 + \pi) \cdot C_u \cdot F_{ec} \qquad (4.35)$$

and

$$F_{ec} = 1 - 2e/B \qquad (4.36)$$

where e is the distance at which the load acts from the centre line. When the strength is non-homogeneous according to Eq. 4.33, the bearing capacity will be:

$$q_f = F \cdot F_{ec} [(2 + \pi) C_{u_o} + \rho \cdot B \cdot F_{ec}/4] \qquad (4.37)$$

where F (defined in Eq. 4.34) depends on $\rho(B - 2e)/C_{u_o}$.

For a central inclined load on clay of uniform strength the failure pressure is:

$$q_f = (2 + \pi) C_u i_c \qquad (4.38)$$

where i_c is defined in Eq. 4.24,

$\cos 2\theta = \tau_f/C_u = q_f \tan\alpha/C_u$, and τ_f is the average shear stress applied to the foundation surface. Horizontal sliding occurs if the angle of load inclination, $\alpha = \alpha_{crit}$, and $\tan\alpha_{crit} = \dfrac{2}{(2+\pi)}$. For $\alpha \geqslant \alpha_{crit}$, $q_f = C_u \cdot \cot\alpha$, or $i_c = \cot\alpha/(2+\pi)$.

If the clay has a linear increase in strength with

depth, approximations must be made for an inclined load, and the failure pressure may be written:

$$q_f = C_{ui} (2 + \pi) i_{cl} \qquad (4.39)$$

where C_{ul} is an average strength obtained for vertical loading from Eqs. 4.31 and 4.34.

$$C_{ul} = F[C_{uo} + \frac{\rho.B}{4(2 + \pi)}] \qquad (4.40)$$

Assuming $\cos 2\theta = \tau_h/C_{uo} = q_f \tan\alpha/C_{uo}$ and that an average strength operates which varies linearly with θ (Vaughan et al, 1976):

$$q_f = (2+\pi)C_{uo}[1 + (R-1)\frac{4\theta}{\pi}] [0.5 + \frac{2\theta+\sin 2\theta}{2 + \pi}] \qquad (4.41)$$

where $R = C_{ul}/C_{uo}$.

From Eqs. 4.29 and 4.41

$$i_{cl} = i_c[\frac{1}{R} + (1 - \frac{1}{R})\frac{4\theta}{\pi}] \qquad (4.42)$$

α_{crit} is obtained as for clay of uniform strength, and for $\alpha \geqslant \alpha_{crit}$

$$i_{cl} = \cot\alpha/[(2+\pi)R] \qquad (4.43)$$

Figure 4.8 shows the plot of inclination factor against load inclination. Finite element results will be discussed in Chapter 6.

If the loading is both eccentric and inclined and adhesive contact is still maintained over the full width of the footing, then the horizontal component of the load is distributed over the full width of the footing. Thus,

if an equivalent footing of reduced width is used to produce the effect of eccentricity in bearing capacity theory, the horizontal load carried by it must also be reduced. A modified angle of load inclination α_1 must be used, where $\tan\alpha_1 = \tan\alpha\ F_{ec}$.

4.10.4 Rupture Figure

Figure 4.9 shows the rupture figure for inclined and eccentric load on a strip footing, which consists of three zones. Zone A'BC is a rigid wedge which moves together with the footing, and pushes the radial shear zone (BCD) sideways and the passive Rankine zone (BDE) in an upward direction.

For the eccentric and inclined loading the line rupture L (Fig. 4.9) is a circle arc, and its centre is the common point of rotation for the footing and for the moving rigid wedge (Brinch Hansen, 1953; and Hansen, 1965).

As mentioned by Hansen (1965), for large eccentricities of the load (e/B ≥ 0.055) only a part of the footing, of the width (B-2e), is in contact with the clay, and for kinematical reasons the underside of the footing must be tangent to the line rupture L at the corner of the effective width. Therefore, the centre of the line rupture L will always be on the vertical line passing through this corner (Fig. 4.9). However, for small eccentricities (e/B < 0.055) the line rupture L passes through the edge of the footing.

For the central inclined loading the rupture line L is a straight line, and the shape of the wedge ABC is triangular (Sokolovskii, 1960; and Hansen, 1965). Murff and Miller (1977), in analysing the stability of the footing on the non-homogeneous clay by using the upper bound plasticity concept, mentioned that for inclined centric loads on strip footings the critical collapse loads occur as the radius of the line rupture L (Fig. 4.9) becomes infinite.

A straight line rupture L is assumed in calculating values of load inclination factors given in Fig. 4.8. The failure pressure calculated from this figure, for a uniform clay, is always lower than that given by Hansen (1965) which assumes a circular line rupture L. For a load inclination of 8 degrees, differences are approximately: 2% with no eccentricity, 4% with $e/B = 0.025$, and 7% with $e/B = 0.2$. However, the maximum difference is not greater than about 10%.

The rupture surface shown on Fig.4.9 is drawn by using the following three steps.

1. the triangle A'C'B is drawn using the value of θ calculated from Fig. 4.8;

2. the zone AA'CB is drawn by assuming that the line rupture L is a circular arc. The centre of this circular arc is defined by the intersection of the vertical line from A' (edge of the reduced width) with the perpendicular bisector of A'C'. The point C is the intersection point of the circular arc A'C' with line OB;

3. the radial shear zone BCD and the passive Rankine zone BDE are drawn.

Table 4.1   Bearing Capacity Factors

ϕ	N_c	N_q	N_γ
$0°$	5.14	1.00	0.00
1	5.38	1.09	0.07
2	5.63	1.20	0.15
3	5.90	1.31	0.24
4	6.19	1.43	0.34
5	6.49	1.57	0.45
6	6.81	1.72	0.57
7	7.16	1.88	0.71
8	7.53	2.06	0.86
9	7.92	2.25	1.03
10	8.35	2.47	1.22
11	8.80	2.71	1.44
12	9.28	2.97	1.69
13	9.81	3.26	1.97
14	10.37	3.59	2.29
15	10.98	3.94	2.65
16	11.63	4.34	3.06
17	12.34	4.77	3.53
18	13.10	5.26	4.07
19	13.93	5.80	4.68
20	14.83	6.40	5.39
21	15.82	7.07	6.20
22	16.88	7.82	7.13
23	18.05	8.66	8.20
24	19.32	9.60	9.44
25	20.72	10.66	10.88
26	22.25	11.85	12.54
27	23.94	13.20	14.47
28	25.80	14.72	16.72
29	27.86	16.44	19.34
30	30.14	18.40	22.40
31	32.67	20.63	25.99
32	35.49	23.18	30.22
33	38.64	26.09	35.19
34	42.16	29.44	41.06
35	46.12	33.30	48.03
36	50.59	37.75	56.31
37	55.63	42.92	66.19
38	61.35	48.93	78.03
39	67.87	55.96	92.25
40	75.31	64.20	109.41
41	83.86	73.90	130.22
42	93.71	85.38	155.55
43	105.11	99.02	186.54
44	118.37	115.31	224.64
45	133.88	134.88	271.76
46	152.10	158.51	330.35
47	173.64	187.21	403.67
48	199.26	222.31	496.01
49	229.93	265.51	613.16
50	266.89	319.07	762.89

Table 4.2   Values of Critical Rigidity Index
            After Vesic (1973)

Angle of Shearing Resistance ϕ	Critical Rigidity Index for:	
	Strip foundation B/L = 0	Square foundation B/L = 1
0°	13	8
5	18	11
10	25	15
15	37	20
20	55	30
25	89	44
30	152	70
35	283	120
40	592	225
45	1442	486
50	4330	1258

Table 4.3   Coefficients of Increase of Bearing Capacity
             Factors due to Presence of an Infinitely
             Stiff Layer at Depth H below the Strip
             Foundation of Width B
             After Mandel and Salencon (1969)

Coefficients R_{bc} (upper number)
                R_{bq} (lower number)

ϕ	B/H →	1	2	3	4	5	6	8	10
$0°$	$R_b = 1$ for B/H<1.41		1.02 1.00	1.11 1.00	1.21 1.00	1.30 1.00	1.40 1.00	1.59 1.00	1.78 1.00
$10°$	$R_b = 1$ for B/H<1.12		1.11 1.07	1.35 1.21	1.62 1.37	1.95 1.56	2.33 1.79	3.34 2.39	4.77 3.25
$20°$	$R_b = 1$ for B/H<0.86	1.01 1.01	1.39 1.33	2.12 1.95	3.29 2.93	5.17 4.52	8.29 7.14	22.00 18.70	61.50 51.90
$30°$	$R_b = 1$ for B/H<0.63	1.13 1.12	2.50 2.42	6.36 6.07	17.40 16.50	50.20 47.50	150.00 142.00	1444.0 1370.0	14800.0 14000.0

Coefficients $R_{b\gamma}$

ϕ	B/H →	2	3	4	5	6	8	10
$0°$	$R_{b\gamma} = 1$ for all B/H							
$10°$	$R_{b\gamma} = 1$ for B/H<4.07				1.01	1.04	1.12	1.36
$20°$	$R_{b\gamma} = 1$ for B/H<2.14		1.07	1.28	1.63	2.20	4.41	9.82
$30°$	$R_{b\gamma} = 1$ for B/H<1.30	1.20	2.07	4.23	9.90	24.8	178.0	1450

GENERAL SHEAR

LOCAL SHEAR

PUNCHING SHEAR

LOAD

SETTLEMENT

LOAD

SETTLEMENT

ULTIMATE LOAD

LOAD

SETTLEMENT

SURFACE TEST

TEST AT GREATER DEPTH
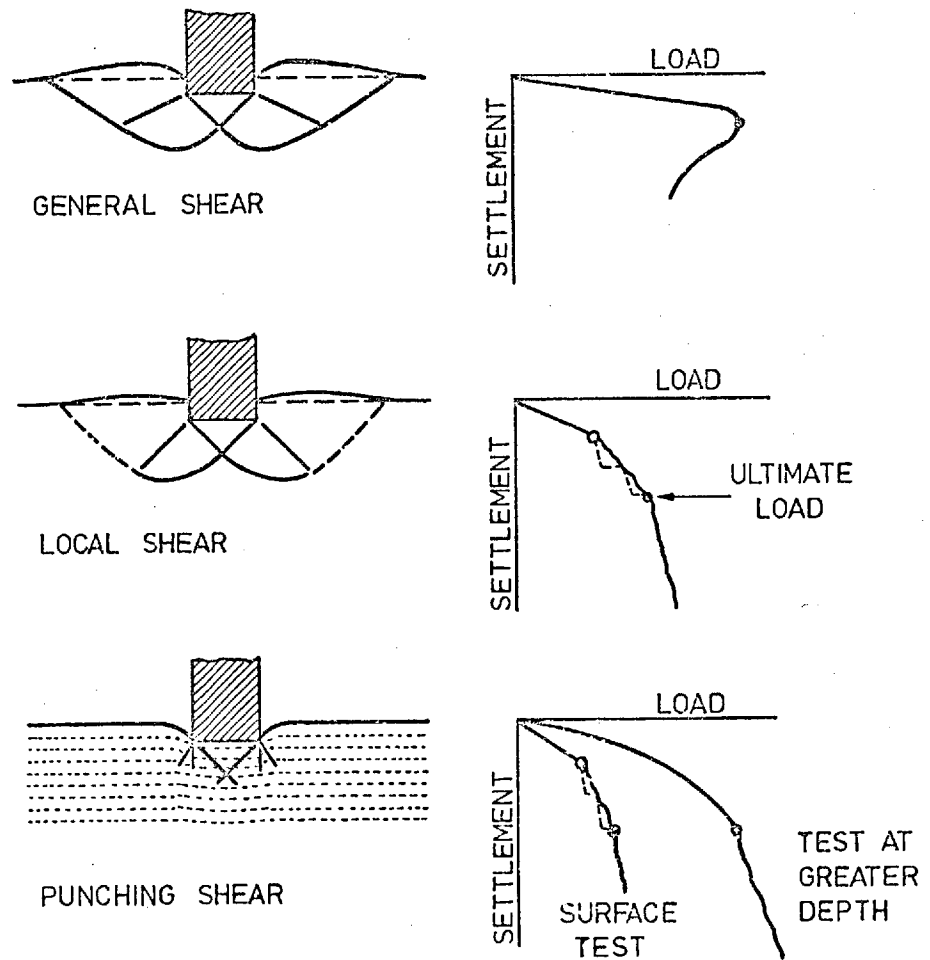
Fig. 4.1   Modes of Bearing Capacity Failure, after Vesic (1963a)
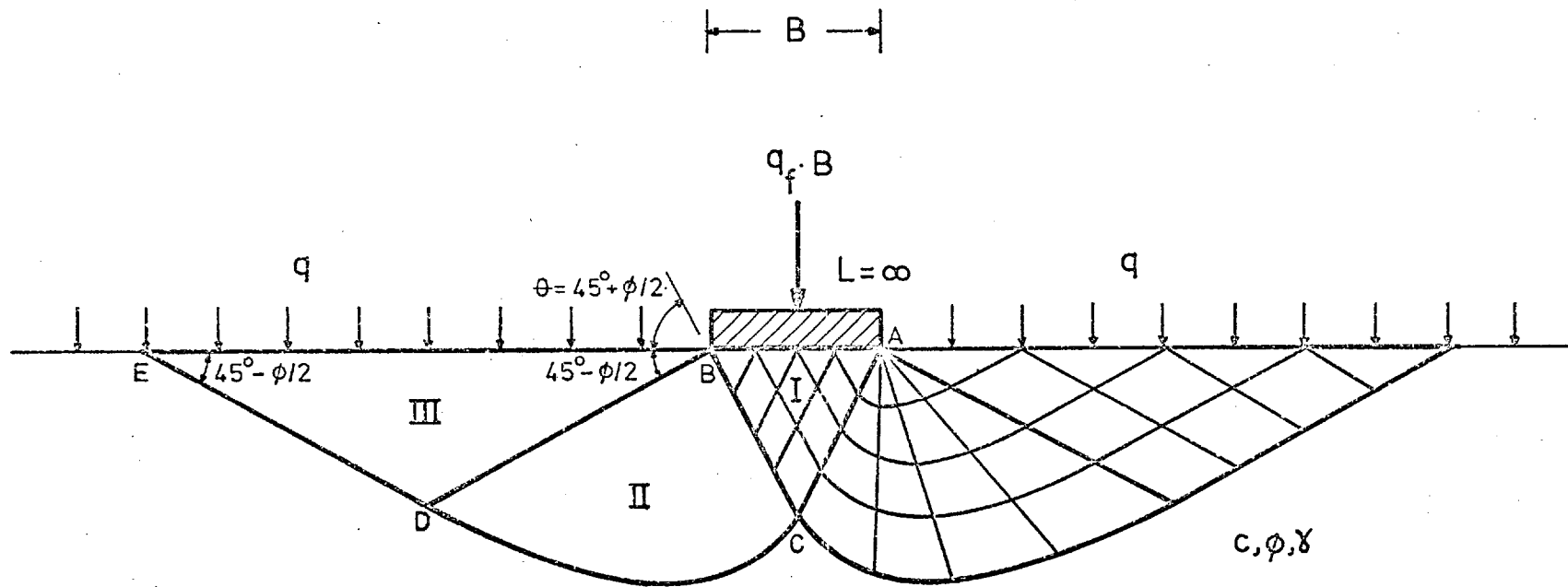
Fig. 4.2 Rupture Figure, Prandtl Mechanism.
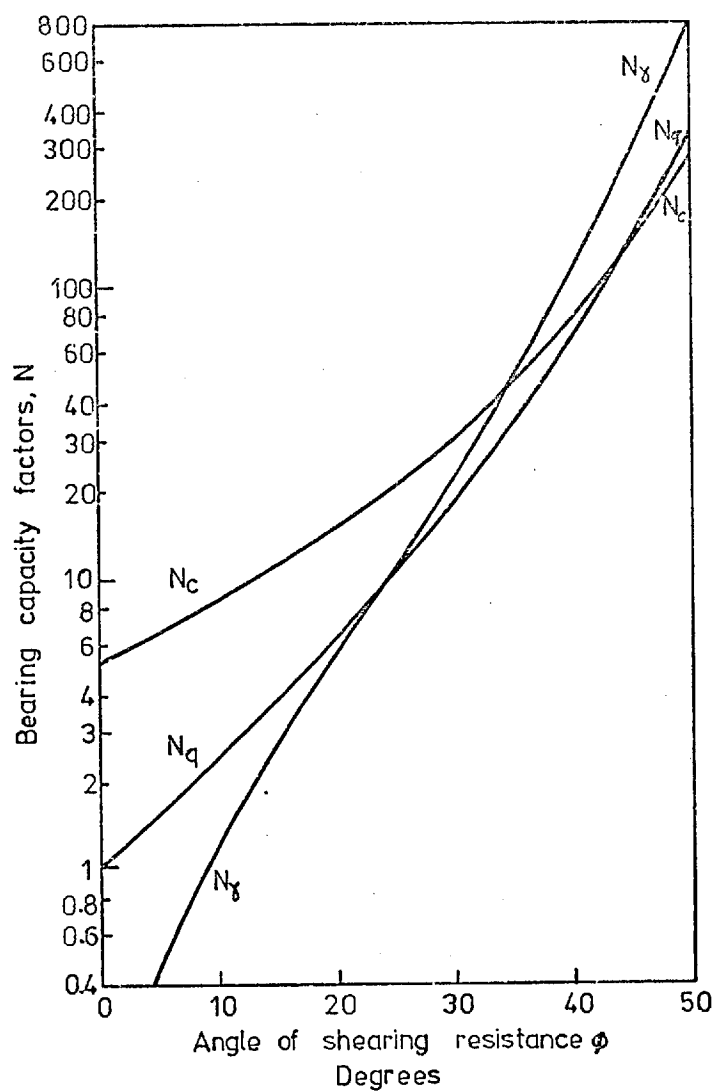
Fig. 4.3　Bearing capacity factors for shallow footings.
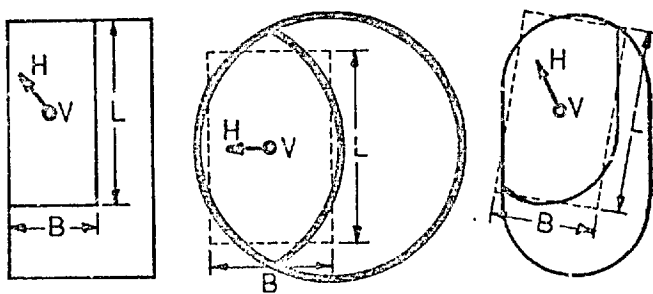
Fig. 4.4　Equivalent and effective foundation areas, after Brinch Hansen (1961).
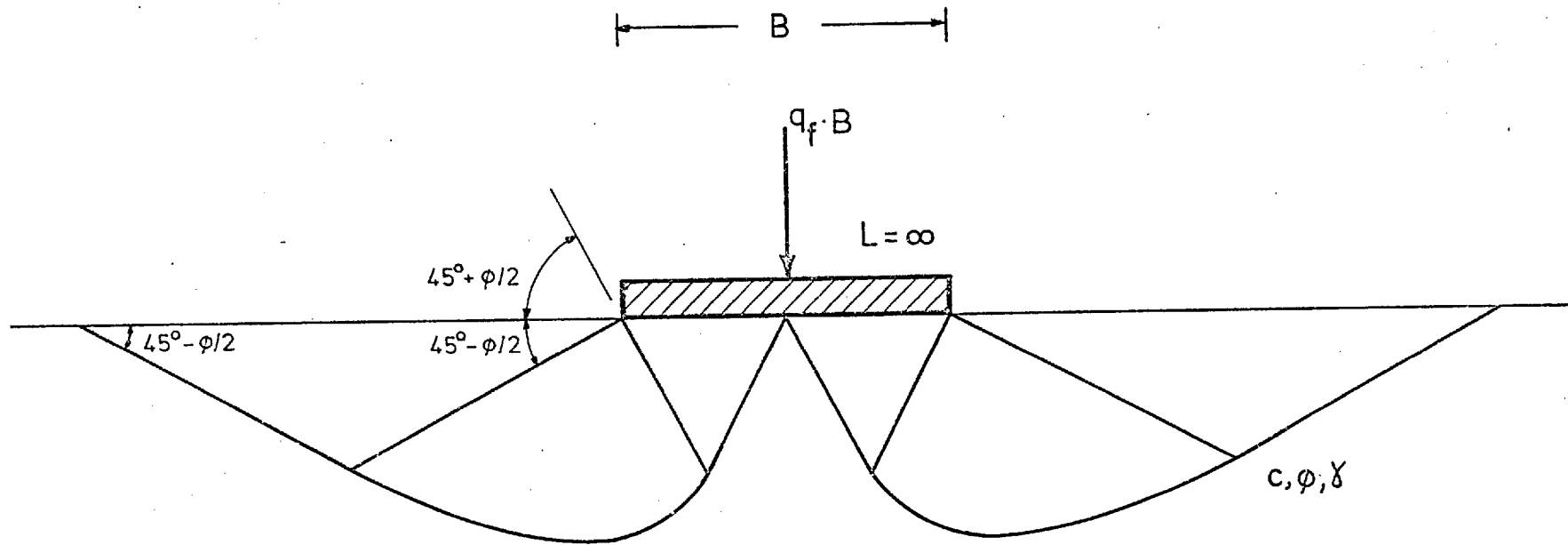
Fig. 4.5 Rupture Figure, Hill Mechanism.
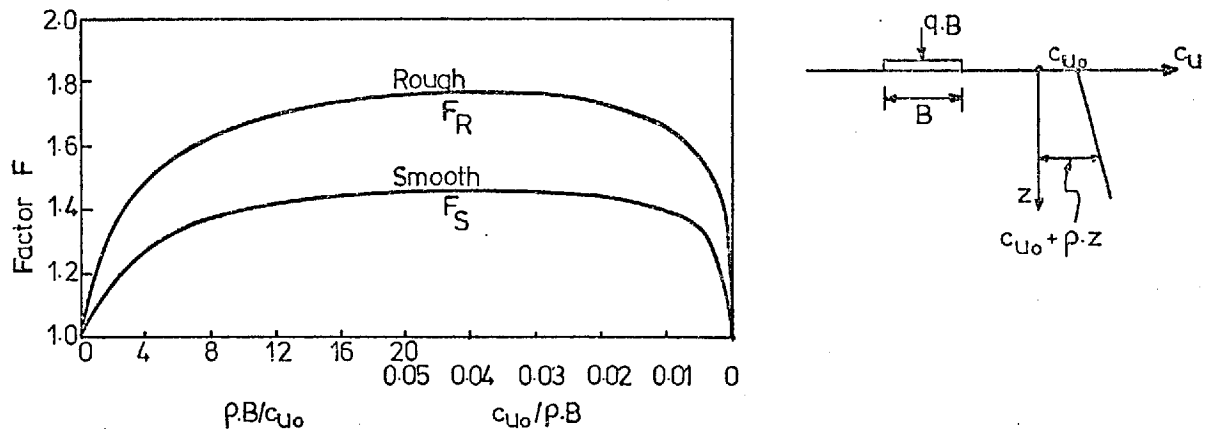
Fig. 4.6   Correction factors for rough and smooth footings,
after Davis and Booker(1973).

(A)
Narrow rough footing.

$\rho \cdot B / c_{Uo} = 1.03$

(B)
Wide rough footing.

$\rho \cdot B / c_{Uo} = 2.98$
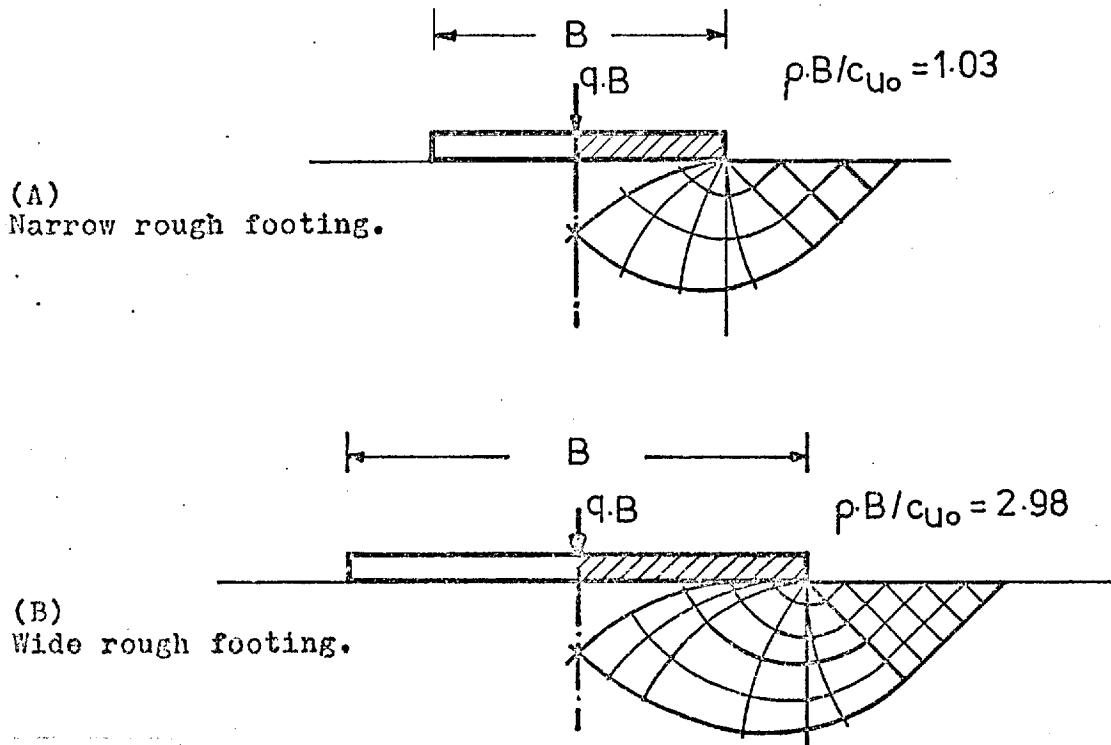
Fig. 4.7 Stress fields, after Davis and Booker(1973).
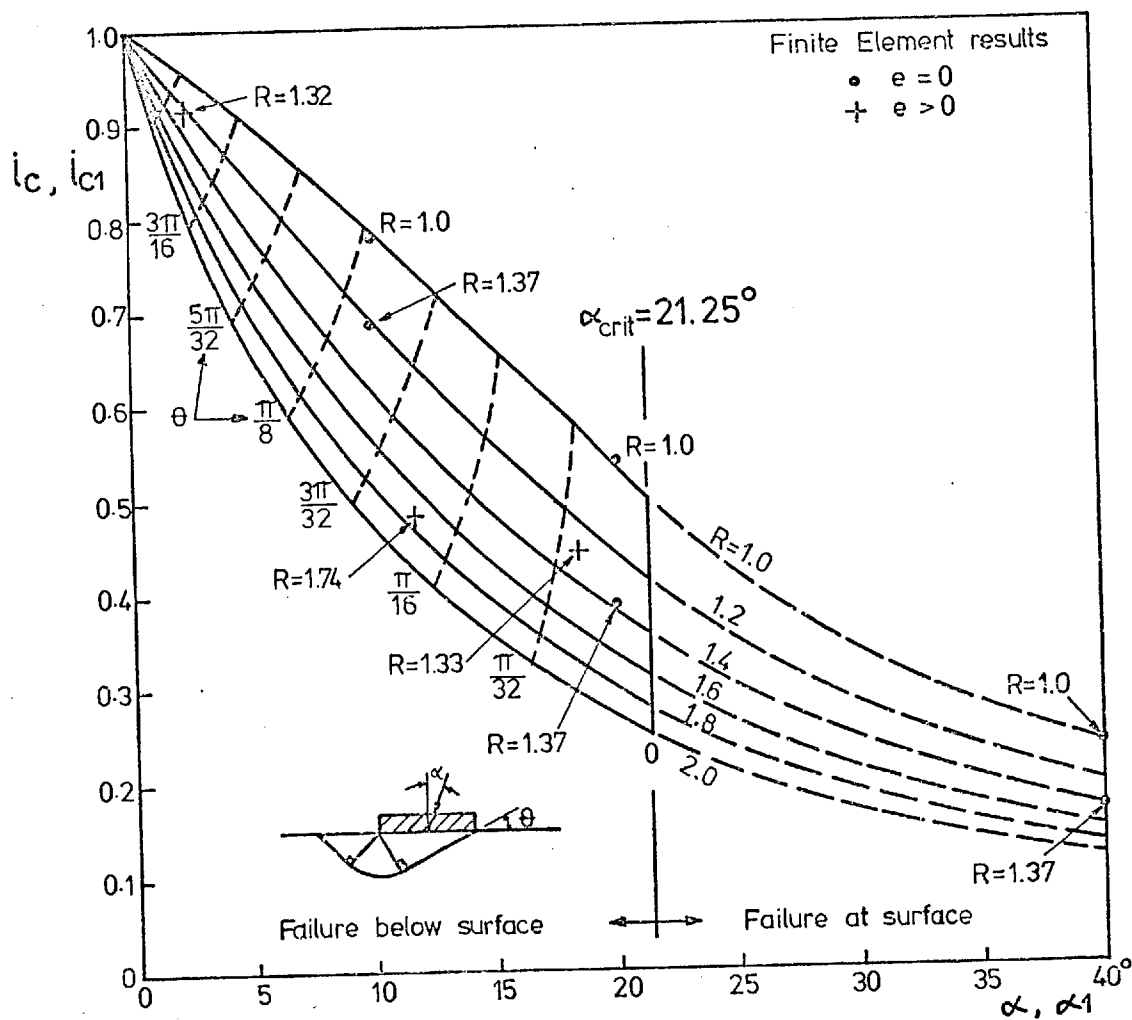
Fig. 4.8 Failure of footing with inclined and eccentric load, after Vaughan et. al.(1976).
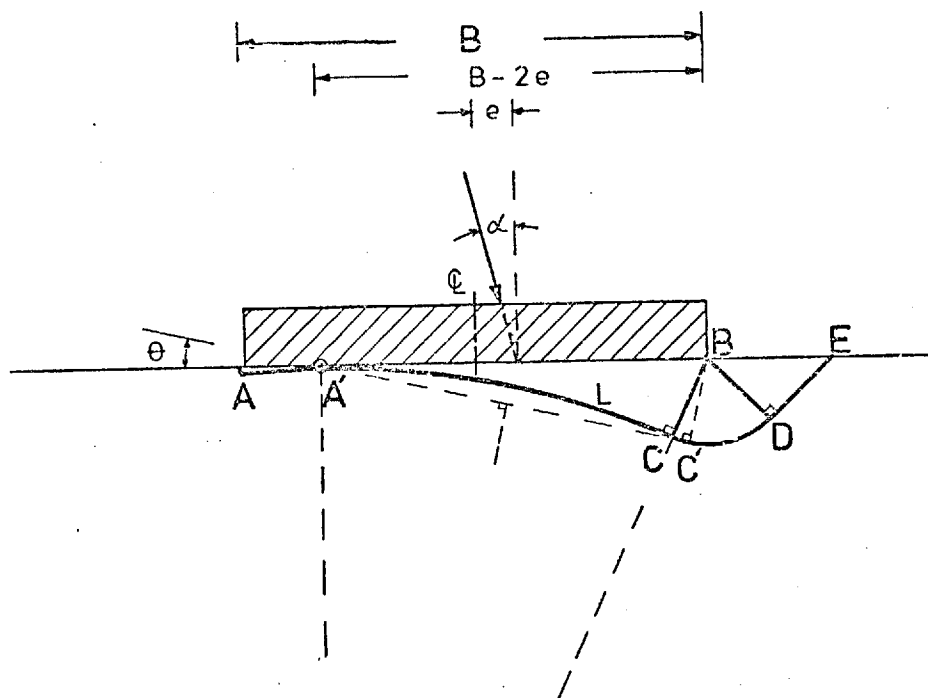
θ is calculated from Fig. 4.8.

B = 120 m.
e = 10 m.
α = 14.04°
θ = 13°

R = 1.74

Fig. 4.9   Rupture figure, inclined and eccentric load.

CHAPTER   5

COMPUTER RUNS FOR STUDYING THE FOOTING BEHAVIOUR

5.1   General

This chapter considers the computer runs for analysing
the footing behaviour.   The finite element results for the
footing will be discussed in the next chapter.

The non-linear incremental elastic technique has been
used extensively in soil mechanics for the analysis of
deformation problems.   It has the advantage of being a
well-tried technique for which efficient programmes are
available.   The programme used in these studies and
simulation of the non-linear soil properties were explained
in Chapter 2.   The shear unloading and reloading modelling,
which was discussed in Appendix 2, will be catagorised as
follows:-

Stage 1:   shear unloading and reloading according to

Fig. 5.1.a,

Stage 2:   shear unloading and reloading according to

Fig. 5.1.b,and

Stage 3:   shear unloading and reloading according to

Fig. 5.1.c.

The material non-linearity was dealt with using the
quasi Runge-Kutta incremental method.   To avoid over-
shooting the specified strength, small loading steps were
used in the analyses.   The question of how small the
increments should be was dealt with by considering the

stress-strain curve. For the initial section of the curve rather large increments were chosen, the size of the increments being reduced, with increasing shear stress. Near the failure state very small increments were used. After adding each increment the overshooting was checked to be sure that the size of the increment was small enough. Typically, overshooting did not exceed 2%, and simulation of the loading of a strip footing to failure involved about 15 loading steps, and 10 minutes computation time on a CDC 6600 machine, with 1000 degrees of freedom.

In all cases of these analyses, the footing was assumed to be strip, rough and stiff with Young's modulus equal to 4.2×10^7 KPa and Poisson's ratio equal to 0.2. Typically, the differential settlement between the centre and the edge for a footing with width equal to 120 m was about 0.3 cm for a centre settlement of 50 cm, which indicates that the footing was essentially rigid.

The ground water table was assumed at the ground surface for all the cases.

From the point of view of the use of drained or undrained parameters, the cases are divided into three major groups, namely, a sand group, a clay group, and a linear elastic group.

5.2   Cases for the Sand Group

In order to study the drained behaviour of the footing on the sand, two cases were analysed in this group. The soil properties used in these cases have been taken from

the paper by Frydman and Zeitlen (1969). Figures 5.2 and
5.3 show the shear strength, initial modulus and stress-
strain curves used in the analyses for both cases, and they
are compared with the data from Frydman and Zeitlen (1969).
The Poisson's ratio for both cases was assumed to be 0.33.

Table 5.1 summarizes the geometries and properties
used in these two cases.

For both cases, the applied load has not been increased
up to failure load. For case one, only 2% and for case
two, only 10% of failure load has been reached.

In both cases, the initial stresses had zero values
at the ground surface, and they were increased linearly
with depth according to the unit weight and K_o of the soil.

5.3 Cases for the Clay Group

In this group the analyses were carried out for
undrained conditions ($\phi' = 0$, $\nu = 0.499$). Bishop (1966a)
showed that Poisson's ratio is less than 0.5 in the undrained
state. Hamza (1976) investigated the effect of the use
of a Poisson's ratio very close to 0.5, and concluded that
by using 0.499 the error will be small and negligible.

From the point of view of the monotonic or cyclic
loading, the cases in this group are divided into two sub-
groups.

5.3.1 Monotonic Loading

In order to study the undrained behaviour of the
footing on the clay, the cases tabulated in Table 5.2 were

considered in this subgroup. In almost all the cases, the applied load was increased up to failure load. The specified initial stresses had zero values at the ground surface, and they were increased linearly with depth according to the unit weight and K_o of the soil.

5.3.2 Cyclic Loading

In this subgroup the analyses of footings under dead weight loading and cyclic wave loading were considered in order to study the behaviour of the off-shore structures. As mentioned by Vaughan et al (1976), clays, in beds of modest thickness, may remain substantially undrained during both dead weight loading and the critical design wave loading, and thus the undrained loading of clays is likely to be the critical design condition for the off-shore structures.

The dead weight and wave load have been considered as a combination of vertical load V, horizontal load H, moment M, and the weight of the wave at the ground level, P_o. The distribution of P_o may be approximated by the triangles shown in Fig. 5.19.

As the cyclic loading involves unloading and reloading of the foundation soil, the stage 3 of the shear unloading and reloading modelling (see section 5.1) was used. A problem arises during the application of the load cycles. The horizontal component of the wave load reverses approximately symmetrically. If a wave cycle equivalent to the

design wave is simulated in the analysis the difference in first loading and unloading-reloading soil behaviour results in the footing developing a permanent displacement in the direction of the first half of the loading cycle. A larger returning force is required to bring the footing back level. In contrast, real waves, building up gradually, would maintain approximate symmetry of displacement during cyclic loading. Reproduction of the gradual build up of the load in the analysis is not practical, and thus it is necessary to develop a technique to build up the cyclic loads to their maximum values in as few cycles as possible, while maintaining approximate symmetry of displacement (Vaughan et al, 1976).
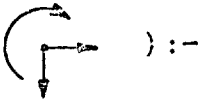
This problem can be approximately overcome by reducing the first half of the loading cycle. A reduction factor was multiplied to the loads. This load reduction factor was worked out from the theory of modulus of subrade reaction given by El-Ghamrawy (1978).

The cases considered in this subgroup are given in Table 5.3. The following assumptions are made for all the cases:

1. The mesh is given in Fig. 5.13;

2. The stress-strain relationship is according to Fig. 5.17 (except the linear case);

3. Initial stresses are:-

$$\sigma_{xo} = \sigma_{zo} = P_o + \gamma \cdot z$$

where $\gamma = 20$ KN/m^3 and $K_o = 1$.

Finally for all the cases the loading sequences are as follows (positive directions: ⟨ ⟩):-

1.   Vertical load V;

2. $(M, H, \text{ and } P_O) \times$ Load reduction factor;

3. $-M, -H, \text{ and } -P_O$;

4. $M, H, \text{ and } P_O$;

5. $-M, -H, \text{ and } -P_O$;

6. $M, H, \text{ and } P_O$;

7. $-M, -H, \text{ and } -P_O$; and

8. $M, H, \text{ and } P_O$.

Values of loads and moments are given in Table 5.3, and the value of the pressure P_O is given in Fig. 5.19.

5.4   Cases for the Linear Elastic Group

In order to investigate the effect of the variation of modulus with σ_3 on stresses, the two cases given in Table 5.4 were considered.

For these cases the following assumptions are made:-

1.   The behaviour is linear;

2.   Poisson's ratio is 1/3;

3.   The coefficient of the earth pressure at rest, K_O, is equal to $\nu/(1-\nu) = 0.5$;

4.   The mesh is given in Fig. 5.7;

5.   Initial stresses increase linearly with depth from zero values at the ground surface; and

6.   The applied load is vertical.

Table 5.1   Cases for the Sand Group

Case No.	Mesh (Fig. No.)	Angle of Shearing Resistance ϕ'°	Cohesion c' KN/m^2	Total Unit Weight γ KN/m^3	Coefficient of Earth Pressure at Rest K_o	Stage of the Shear Unloading and Reloading (see Section 5.1)	Applied Load
1	5.4	37°	0	16.3	0.41	1	Vertical
2	5.5	37°	0	16.3	0.41	1	Vertical

Table 5.2　Cases for the Clay Group, Monotonic Loading

Case No.	Mesh (Fig.No.)	Stage of** the shear unloading & reloading (see section 5.1)	Total Unit Weight γ KN/m³	Coefficient of Earth Pressure at Rest K_o	Undrained* Strength C_u KN/m²	Initial Modulus E_i KN/m²	Stress-Strain Curve (Fig.No.)	Applied[+++] Load	Applied Load Inclination $\alpha = \arctan\frac{H}{V}$	Applied Load Eccentricity e	Relative[++] Stiffness of the Footing
3	5.5	1	17.3	1	50	70000	5.14	V	0	0	Rigid
4	5.6	1	20	2	30+3.75z	$300C_u$	5.15	V	0	0	Rigid
5	5.7	1	20	2	30+3.75z	$300C_u$	5.15	V,M,H	21.8°	0.05B	Rigid
6	5.7	1	20	1	30+3.75z	$300C_u$	5.15	V,M,H	21.8°	0.05B	Rigid
7	5.7	1	20	2	30+3.75z	$300C_u$	5.15	V,M,H	2.86°	0.083B	Rigid
8	5.7	1	0	-	30+3.75z	$300C_u$	5.15	V,M,H	2.86°	0.083B	Rigid
9	5.6	2	20	2	30+3.75z	$300C_u$	5.15	V	0	0	Rigid
10	5.7	2	20	2	30+3.75z	$300C_u$	5.15	V,M,H	2.86°	0.083B	Rigid
11	5.8	2	20	2	30+3.75z	$300C_u$	5.15	V	0	0	Rigid
12	5.9	2	20	2	30+3.75z	$300C_u$	5.15	V	0	0	Rigid
13	5.10	2	20	2	30+3.75z	$300C_u$	5.15	V,M,H	2.86°	0.083B	Rigid
14	5.11	2	20	2	30+3.75z	$300C_u$	5.15	V,M,H	2.86°	0.083B	Rigid
15	5.7	2	20	1.5	30+3.75z	$300C_u$	5.16	V,M,H	2.86°	0.083B	Rigid

Table 5.2 Continued

Case No.	Mesh (Fig.No.)	Stage of** the shear unloading & reloading (see section 5.1)	Total Unit Weight γ KN/m^3	Coefficient of Earth Pressure at Rest K_o	Undrained* Strength C_u KN/m^2	Initial Modulus E_i KN/m^2	Stress-Strain Curve (Fig.No.)	Applied Load [+++]	Applied Load Inclination $\alpha = \arctan\frac{H}{V}$	Applied Load Eccentricity e	Relative Stiffness of the Footing [++]
16	5.12	2	20	1.5	30+3.75z	300C_u	5.16	V,M,H	2.86°	0.083B	Rigid
17[a]	5.7	2	20	1.5	30+3.75z	300C_u	5.16	V,M,H	2.86°	0.083B	Rigid
18	5.7	2	20	1	52.5	300C_u	5.15	V	0	0	Rigid
19	5.7	2	20	1	52.5	300C_u	5.15	V,M	0	0.042B	Rigid
20	5.7	2	20	1	52.5	300C_u	5.15	V,M	0	0.083B	Rigid
21	5.7	2	20	1	52.5	300C_u	5.15	V,M	0	0.125B	Rigid
22	5.7	2	20	1	52.5	300C_u	5.15	V,M	0	0.167B	Rigid
23	5.7	2	20	1	30+3.75z	300C_u	5.15	V	0	0	Rigid
24	5.7	2	20	1	30+3.75z	300C_u	5.15	V,M	0	0.042B	Rigid
25	5.7	2	20	1	30+3.75z	300C_u	5.15	V,M	0	0.083B	Rigid
26	5.7	2	20	1	30+3.75z	300C_u	5.15	V,M	0	0.125B	Rigid
27	5.7	2	20	1	30+3.75z	300C_u	5.15	V,M	0	0.167B	Rigid
28	5.7	2	20	1	52.5	300C_u	5.15	V,H	20°	0	Rigid

Table 5.2   Continued

Case No.	Mesh (Fig.No.)	Stage of** the shear unloading & reloading (see section 5.1)	Total Unit Weight γ KN/m^3	Coefficient of Earth Pressure at Rest K_o	Undrained* Strength C_u KN/m^2	Initial Modulus E_i KN/m^2	Stress-Strain Curve (Fig.No.)	Applied[+++] Load	Applied Load Inclination $\alpha = \arctan\frac{H}{V}$	Applied Load Eccentricity e	Relative[++] Stiffness of the Footing
29	5.7	2	20	1	52.5	$300C_u$	5.15	V,H	$40°$	0	Rigid
30	5.7	2	20	1	52.5	$300C_u$	5.15	V,H	$60°$	0	Rigid
31	5.7	2	20	1	52.5	$300C_u$	5.15	V,H	$80°$	0	Rigid
32	5.7	2	20	1	30+3.75z	$300C_u$	5.15	V,H	$20°$	0	Rigid
33	5.7	2	20	1	30+3.75z	$300C_u$	5.15	V,H	$40°$	0	Rigid
34	5.7	2	20	1	30+3.75z	$300C_u$	5.15	V,H	$60°$	0	Rigid
35	5.7	2	20	1	30+3.75z	$300C_u$	5.15	V,H	$80°$	0	Rigid
36	5.7	2	20	1	52.5	$300C_u$	5.15	V,H	$10°$	0	Rigid
37	5.7	2	20	1	30+3.75z	$300C_u$	5.15	V,H	$10°$	0	Rigid
39[+]	5.13	2	20	1.5	100+3z	$300C_u$	5.17	V,M,H	$14.04°$	0.083B	2.1
40	5.13	2	20	1.5	100+3z	$300C_u$	5.17	V,M,H	$14.04°$	0.083B	16.8
43[+]	5.13	2	20	1	100+3z	$300C_u$	5.17	V	0	0	Rigid
44	5.13	2	20	1	100	$300C_u$	5.17	V	0	0	Rigid

Table 5.2   Continued

Case No.	Mesh (Fig.No.)	Stage of** the shear unloading & reloading (see section 5.1)	Total Unit Weight γ KN/m^3	Coefficient of Earth Pressure at Rest K_o	Undrained* Strength C_u KN/m^2	Initial Modulus E_i KN/m^2	Stress-Strain Curve (Fig.No.)	Applied[+++] Load	Applied Load Inclination $\alpha = \arctan\frac{H}{V}$	Applied Load Eccentricity e	Relative[++] Stiffness of the Footing
45	5.13	2	20	1	100+3z	1000C$_u$	5.18	V	0	0	Rigid
46	5.13	2	20	1	100+3z	300C$_u$	5.18	V	0	0	Rigid

Notes:-
+   Cases 38 and 41 do not exist, and case 42 is included in cyclic loading subgroup.
++   Relative stiffness of the footing (after Boswell and Scott, 1975):

$$k_r = \frac{E_f}{E_s}\frac{1-\nu_s^2}{1-\nu_f^2}\left(\frac{t}{B/2}\right)^3 \quad , \quad k_r < 10 \text{ flexible and } k_r > 10 \text{ rigid}$$

Where E is the Young's modulus, ν is the Poisson's ratio, subscript f denotes the footing, subscript s denotes the soil, t is the footing thickness, and B is the footing width.

+++ V = Vertical, H = Horizontal and M = Movement.
*   z is the depth from ground surface.
**   For stage 2: E(Unloading) = E(Initial).
a   In case 17, vertical load has been applied first, and then moment and horizontal load have been applied.

Table 5.3 Cases for the Clay Group, Cyclic Loading

Case No.	Modulus for Unloading E_u	Modulus[+] for Reloading E_r	Undrained Strength C_u KN/m²	Initial Modulus E_i KN/m²	Load Inclination α	Load Eccentricity e	Load Reduction Factor (see section 5.3.2)	Overall[++] Factor of Safety against Failure
42	$3.5E_i$	$3.5E_i$	100+3z	$300C_u$	16.7°	0.083B	4.5/11	1.57
47	E_t	E_t	100+3z	$300C_u$	16.7°	0.083B	4.5/11	1.57
47,1	E_t	E_t	100+3z	$300C_u$	16.7°	0.083B	0.5	1.57
48	$3.5E_i$	$3.5E_i$	Linear	30000	16.7°	0.083B	4.5/11	-
49	$3.5E_i$	$3.5E_i$	100+3z	$300C_u$	10.2°	0.083B	4.5/11	2.57

Notes:-

+ E_t is the tangential modulus.

++   Applied loads: $V = 2.40 \times 10^4$KN/mrun, $M = 24 \times 10^4$mKN/mrun   and $H = 0.72 \times 10^4$KN/mrun
       (except Case 49 where $H = 0.432 \times 10^4$KN/mrun).

Table 5.4 Cases for the Linear Elastic Group

Case No.	Total Unit Weight γ KN/m^3	Modulus E$^+$ KN/m^2
51A	20	100000
51B	20	$100000 + 100\sigma_3$

Note: σ_3 is the minor principal stress
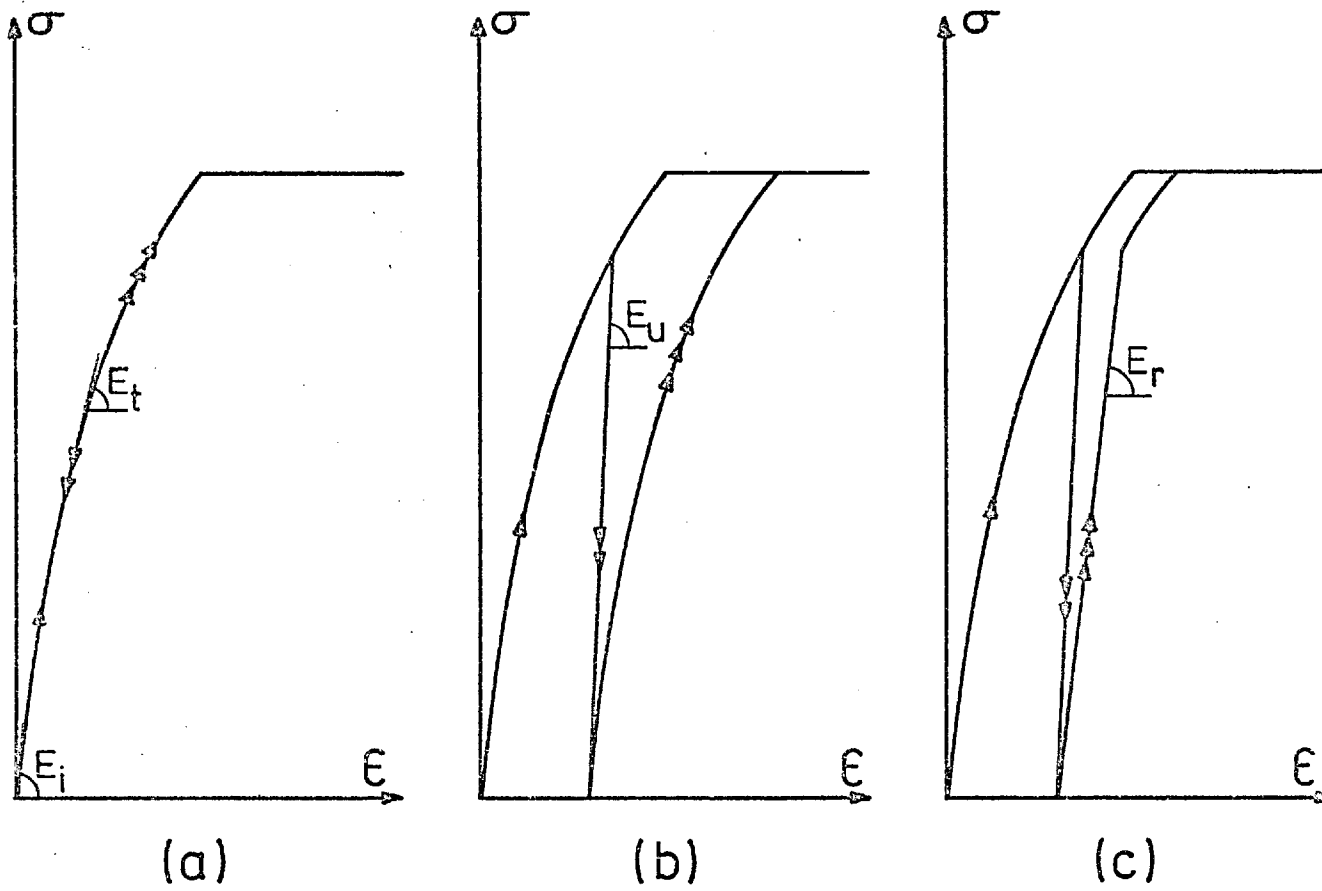
Fig.5.1 Stress-strain models.
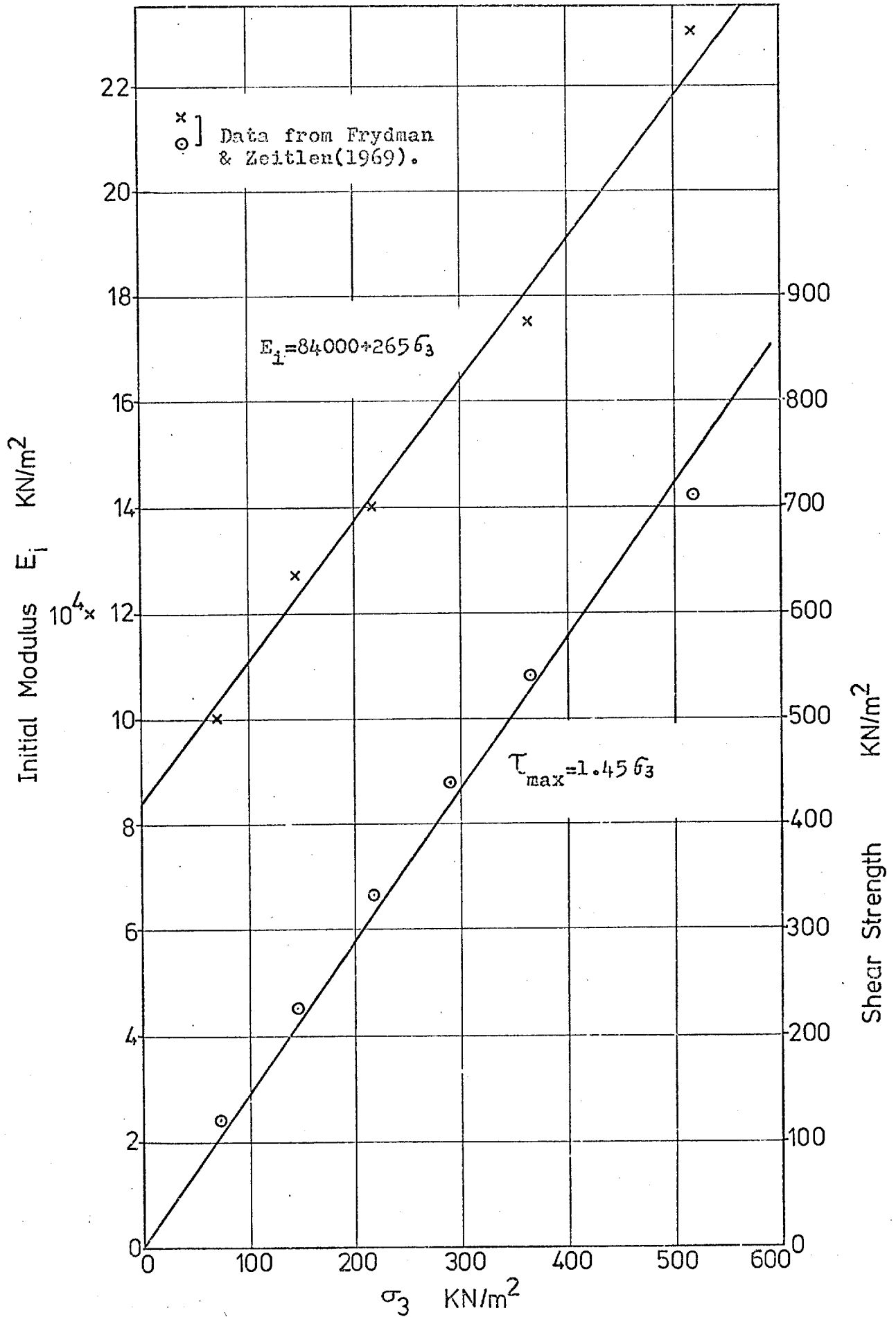
Fig. 5.2 Initial Modulus and Shear Strength versus σ_3
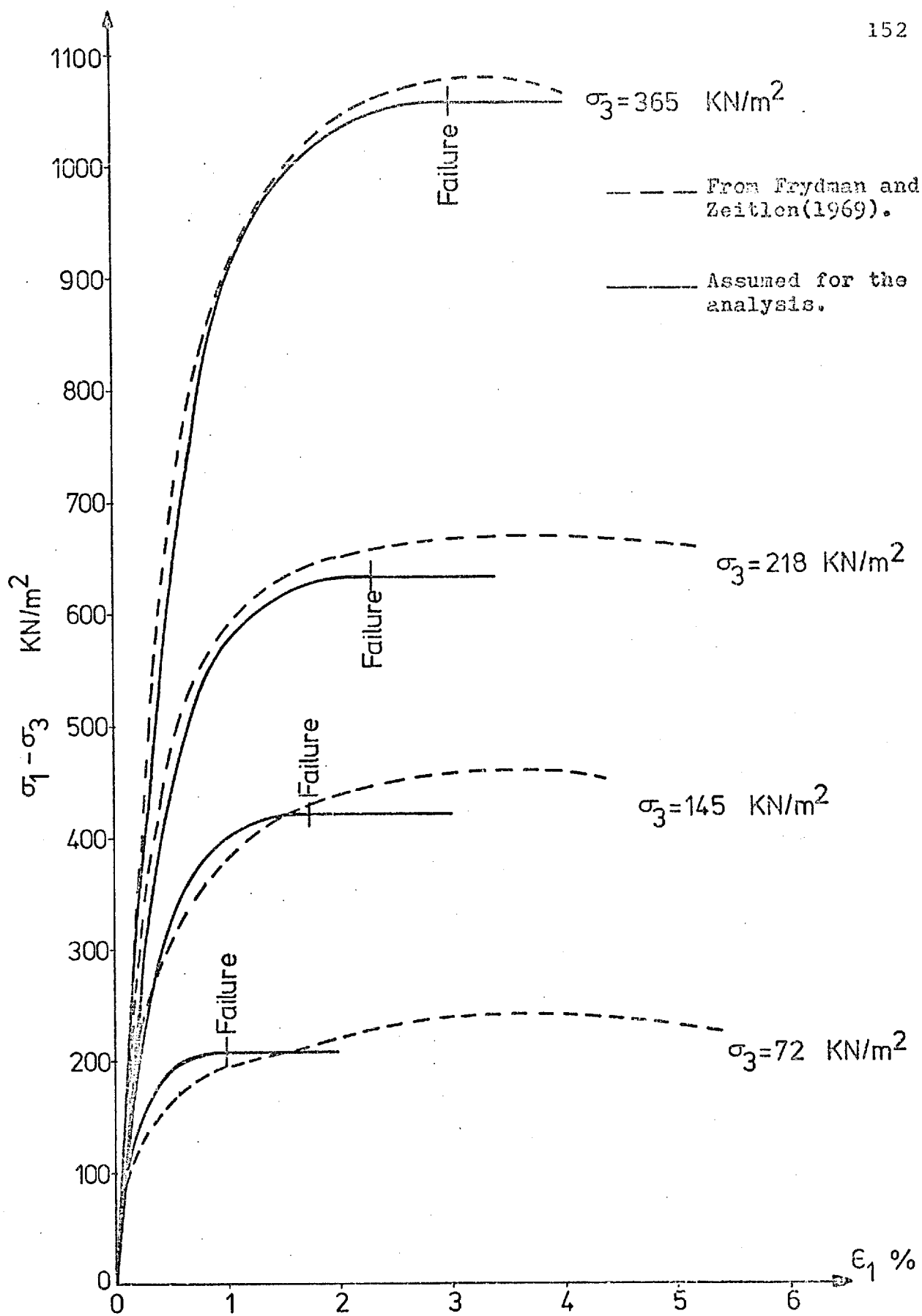
Fig. 5.3 Stress-Strain Curves, (Triaxial).

The figure shows stress-strain curves with the y-axis labeled $\sigma_1 - \sigma_3$ KN/m^2 ranging from 0 to 1100, and the x-axis labeled ϵ_1 % ranging from 0 to 6.

Curves shown:
- $\sigma_3 = 365$ KN/m^2
- $\sigma_3 = 218$ KN/m^2
- $\sigma_3 = 145$ KN/m^2
- $\sigma_3 = 72$ KN/m^2

Legend:
- − − − From Frydman and Zeitlen (1969).
- ———— Assumed for the analysis.

Failure points marked on each curve.
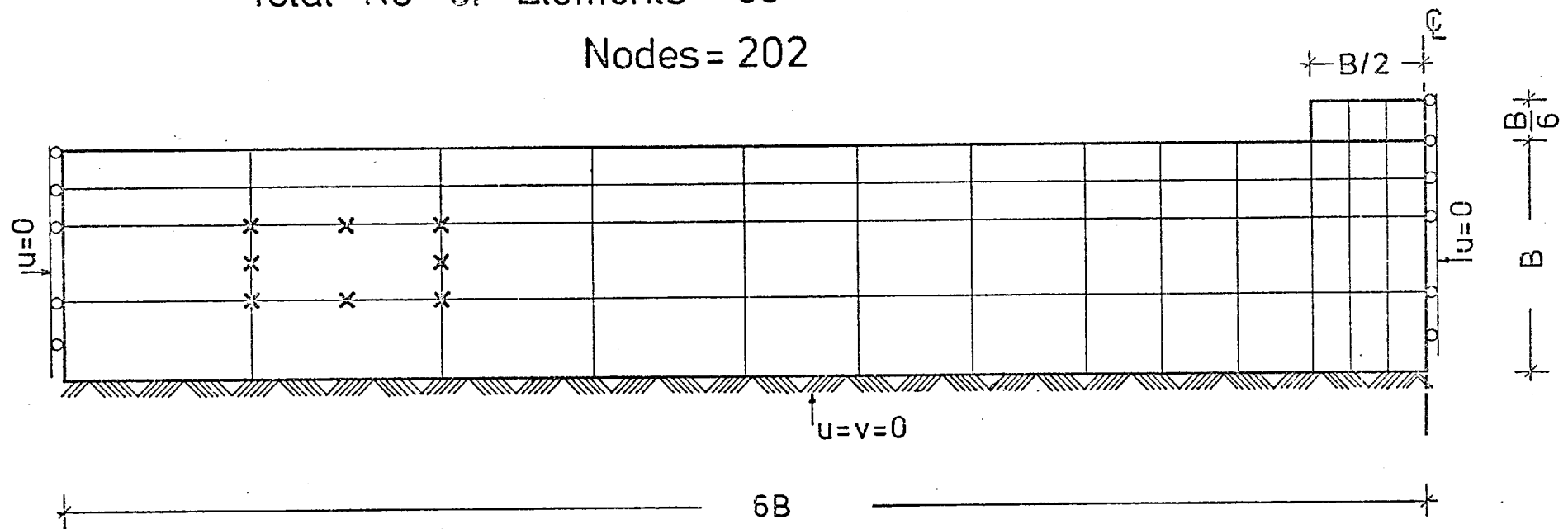
Fig. 5.4   Mesh No. 1

B = 12m.

Total No. of Elements = 120

Nodes = 413
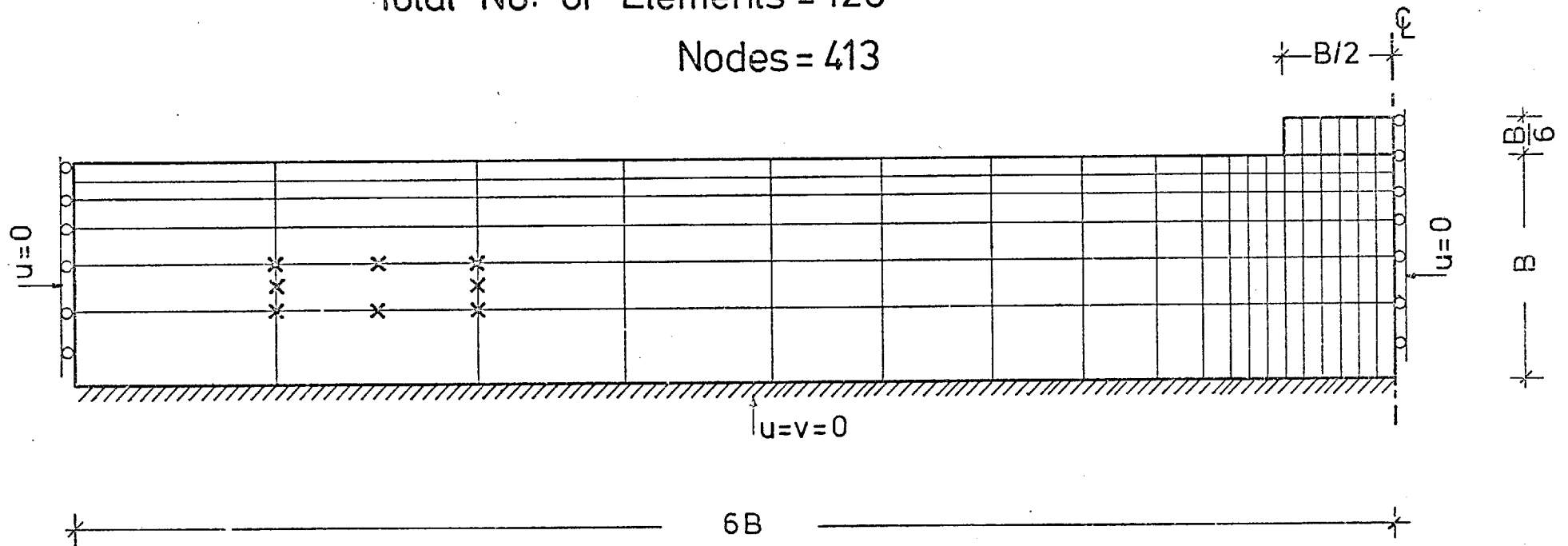
Fig. 5.5 Mesh No. 2

B = 12 m.

Total No. of Elements = 140
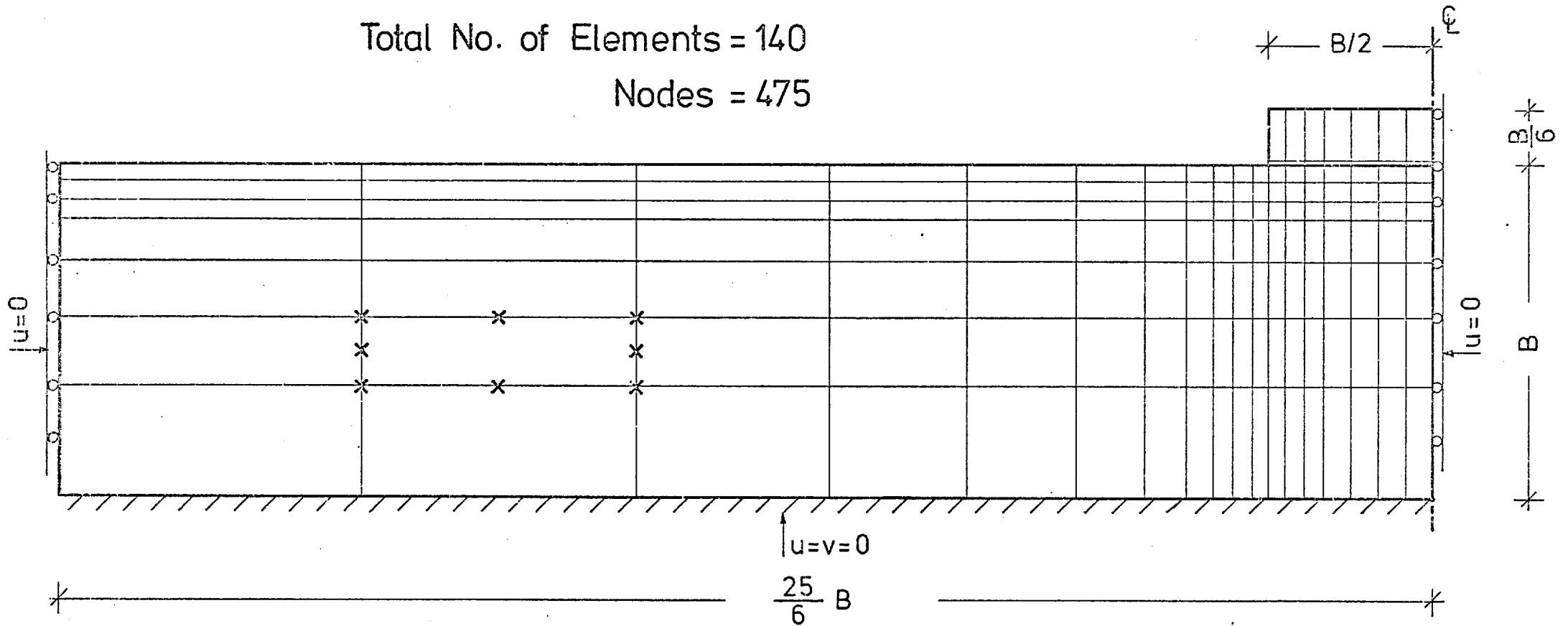
Nodes = 475

Fig. 5.6 Mesh No. 3
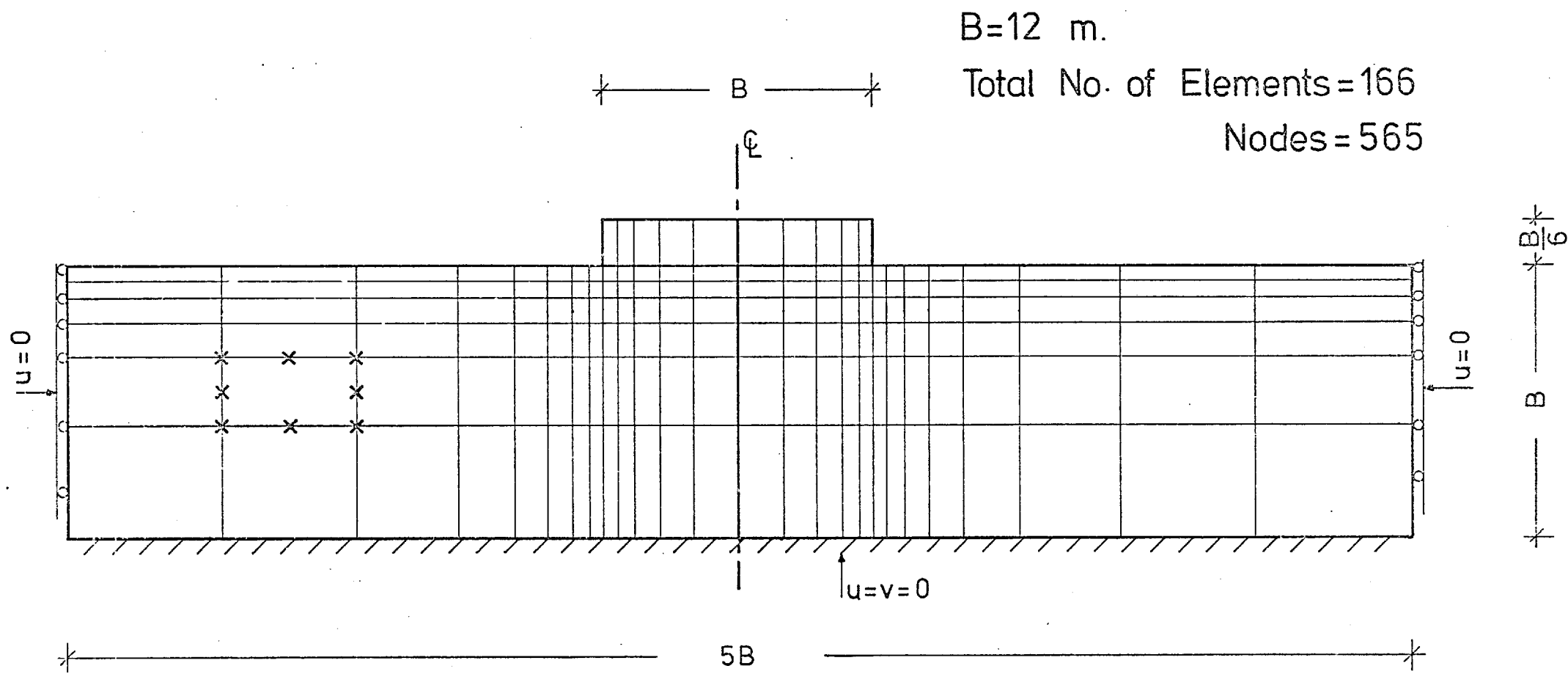
Fig. 5.7   Mesh No. 4

B = 12 m.

Total No. of Elements = 140
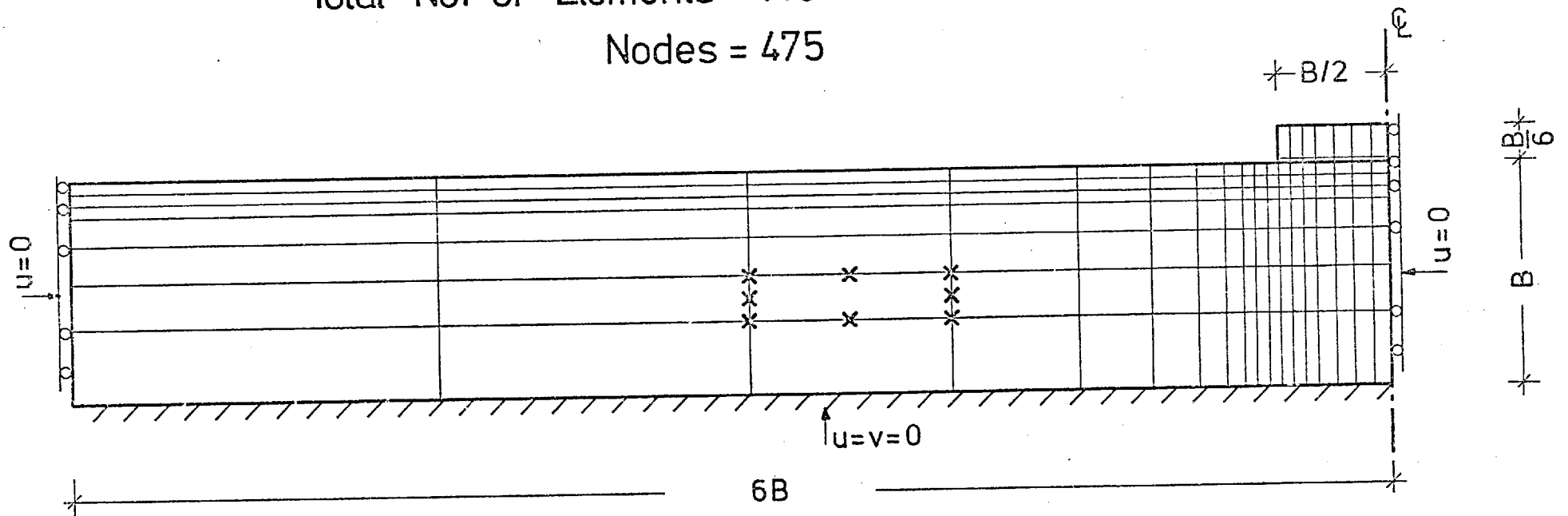
Nodes = 475

Fig. 5.8   Mesh   No. 3A

Total No. of Elements = 140
Nodes = 475

B = 12 m.

Fig. 5.9 Mesh No. 3B

158
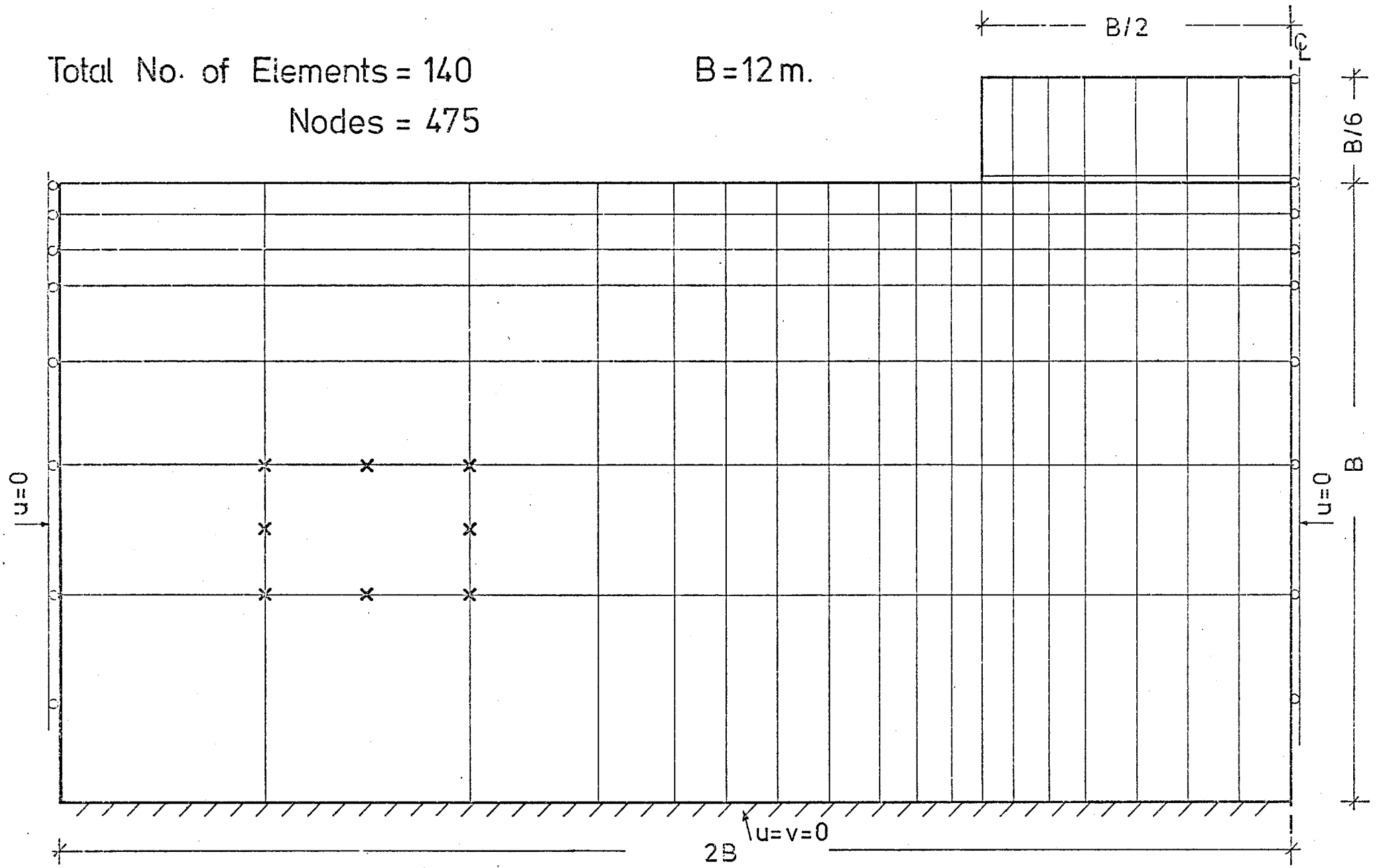
Total No. of Elements = 166

Nodes = 565

B = 12 m.
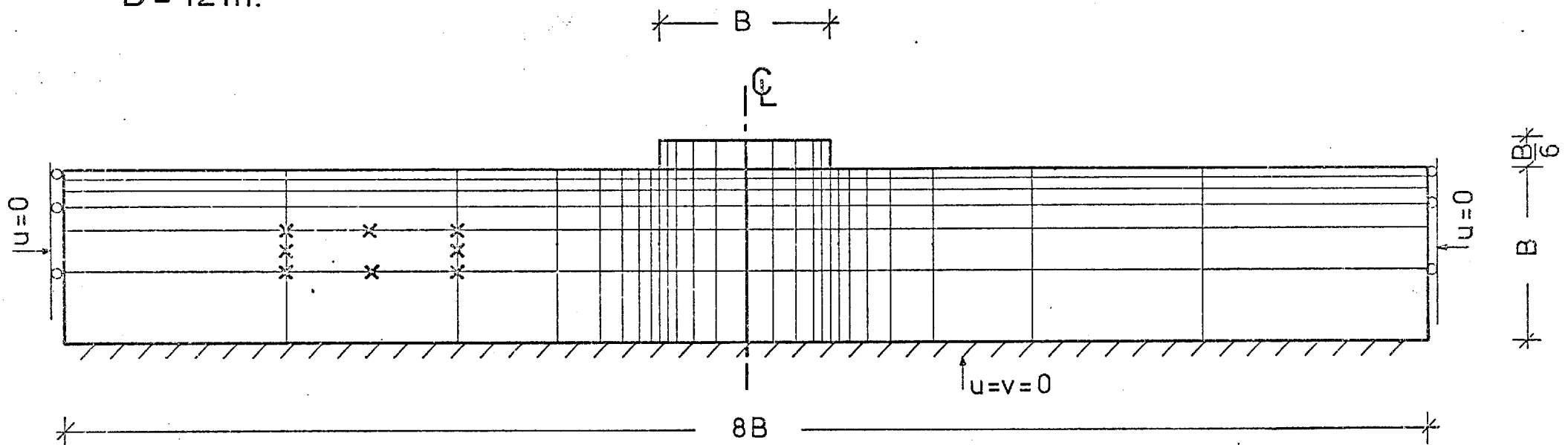
Fig. 5.10 Mesh No. 4A

B = 12 m.

Total No. of Elements = 166
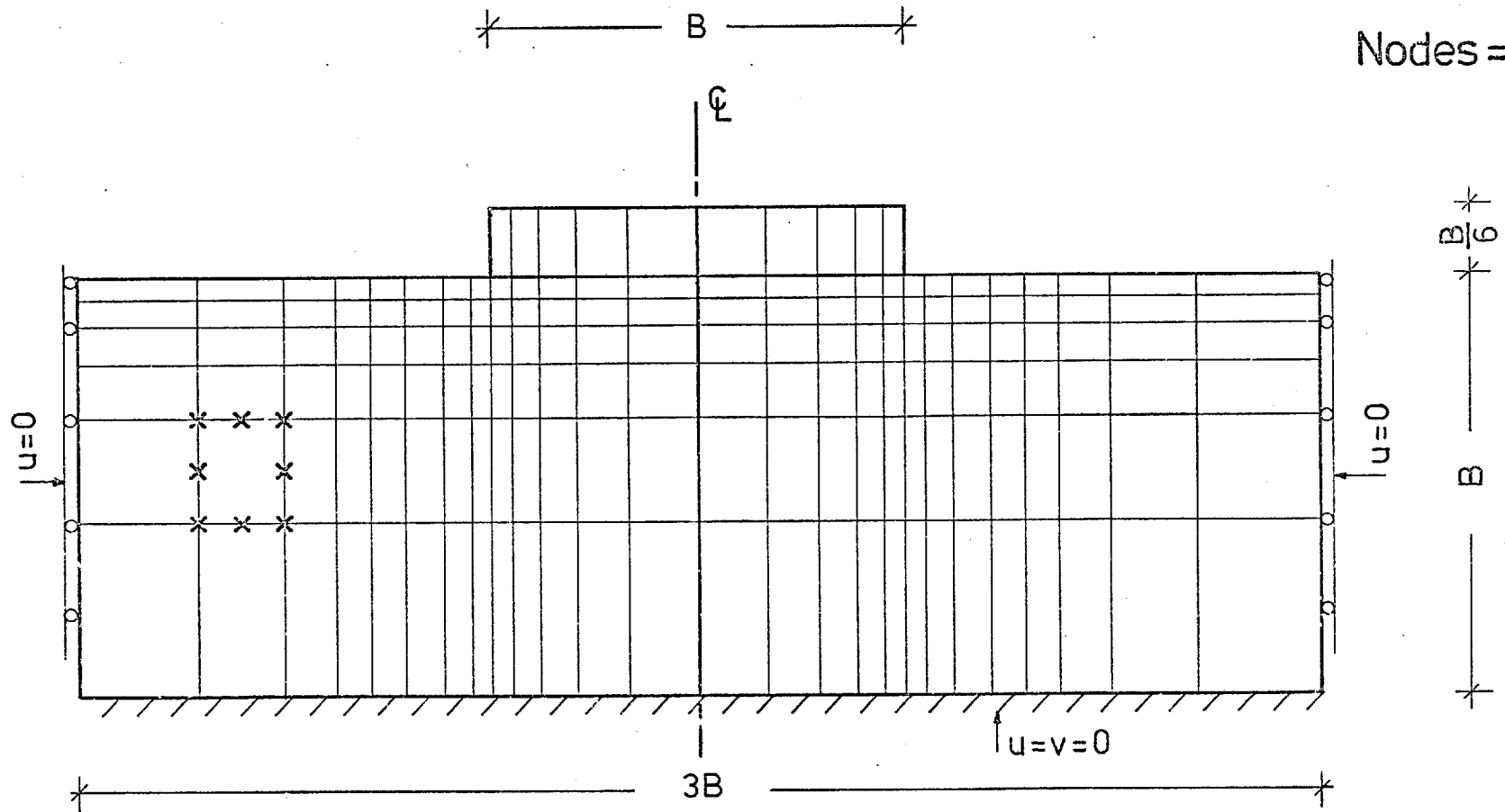
Nodes = 565

Fig. 5.11   Mesh   No. 4B

B = 12 m.

Total No. of Elements = 218

Nodes = 725

B

$\frac{B}{6}$

2B

u = 0

u = 0

u = v = 0

5B
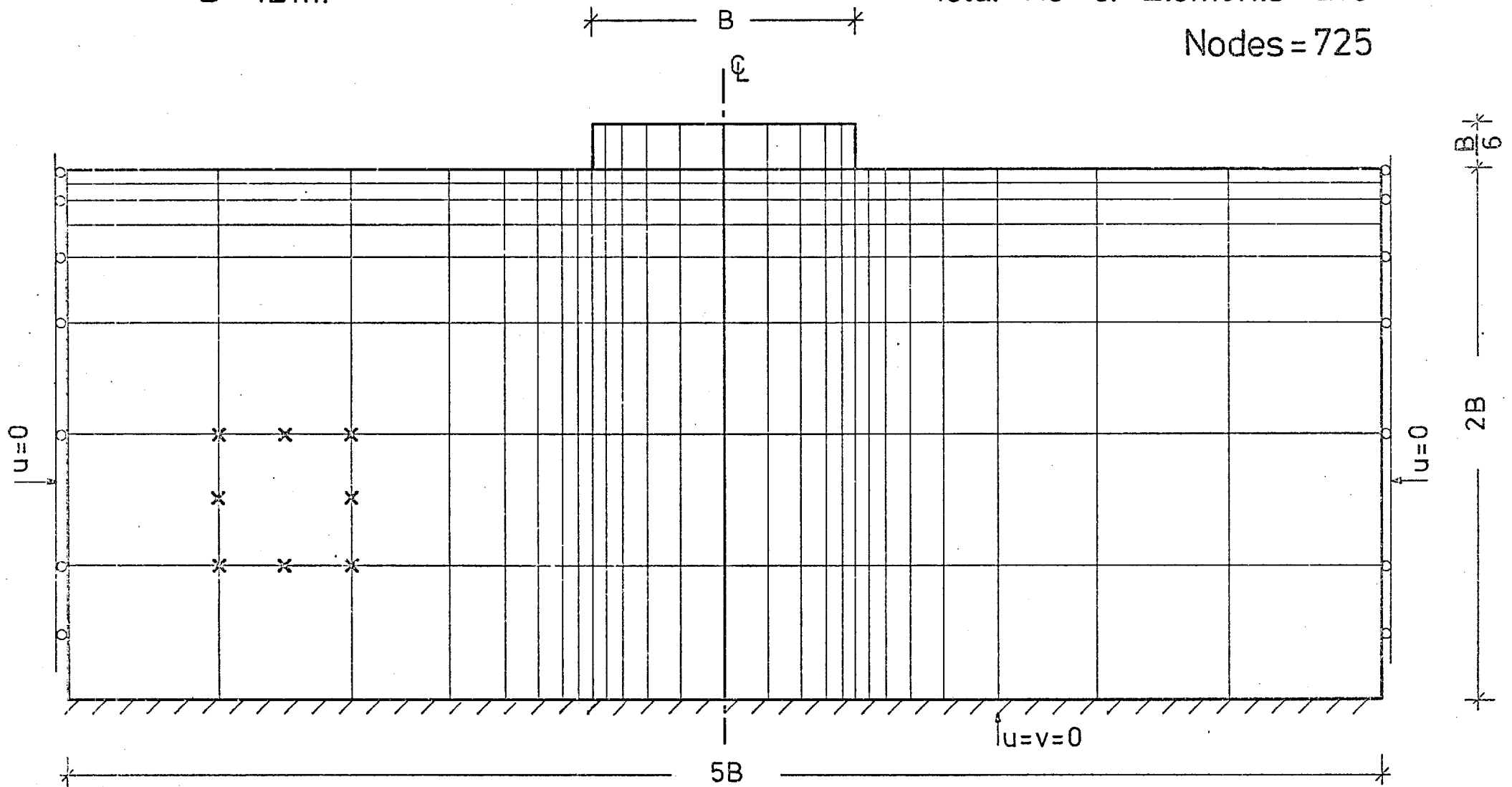
Fig. 5.12   Mesh No. 5

B=120 m.

Total No. of Elements=166

Nodes=565
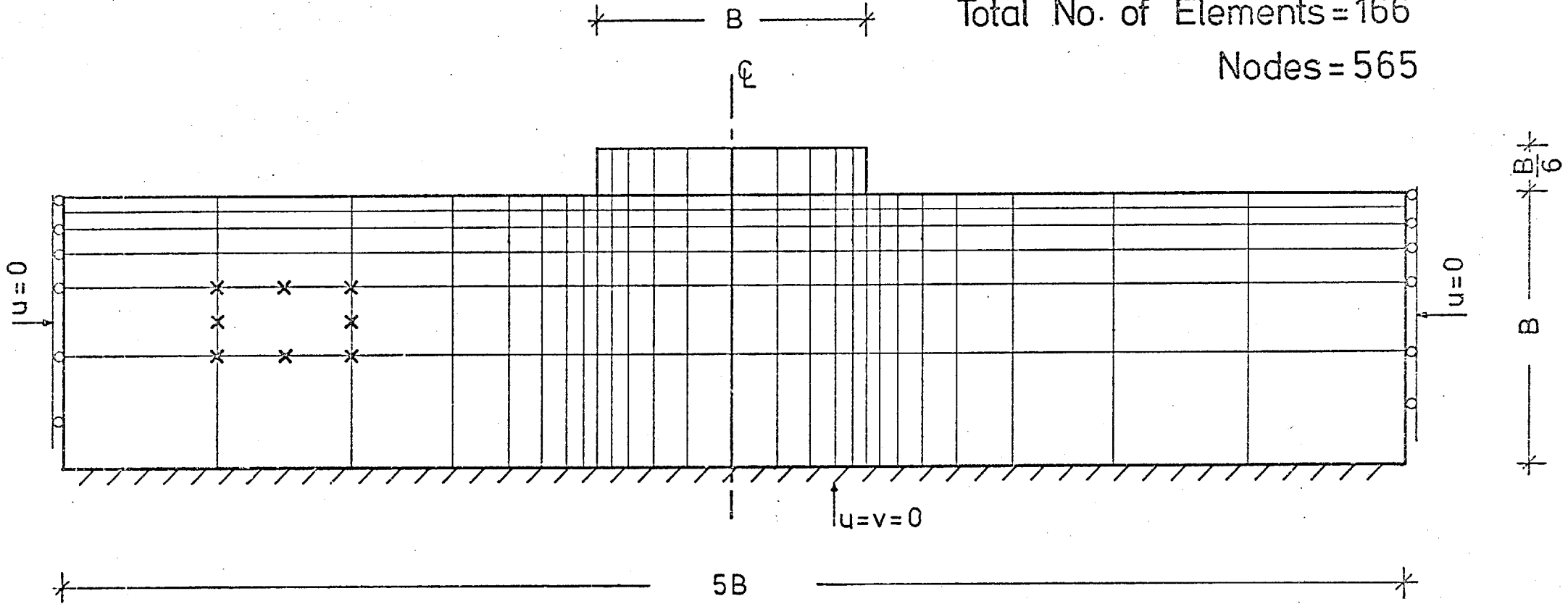
Fig.5.13   Mesh No. 4
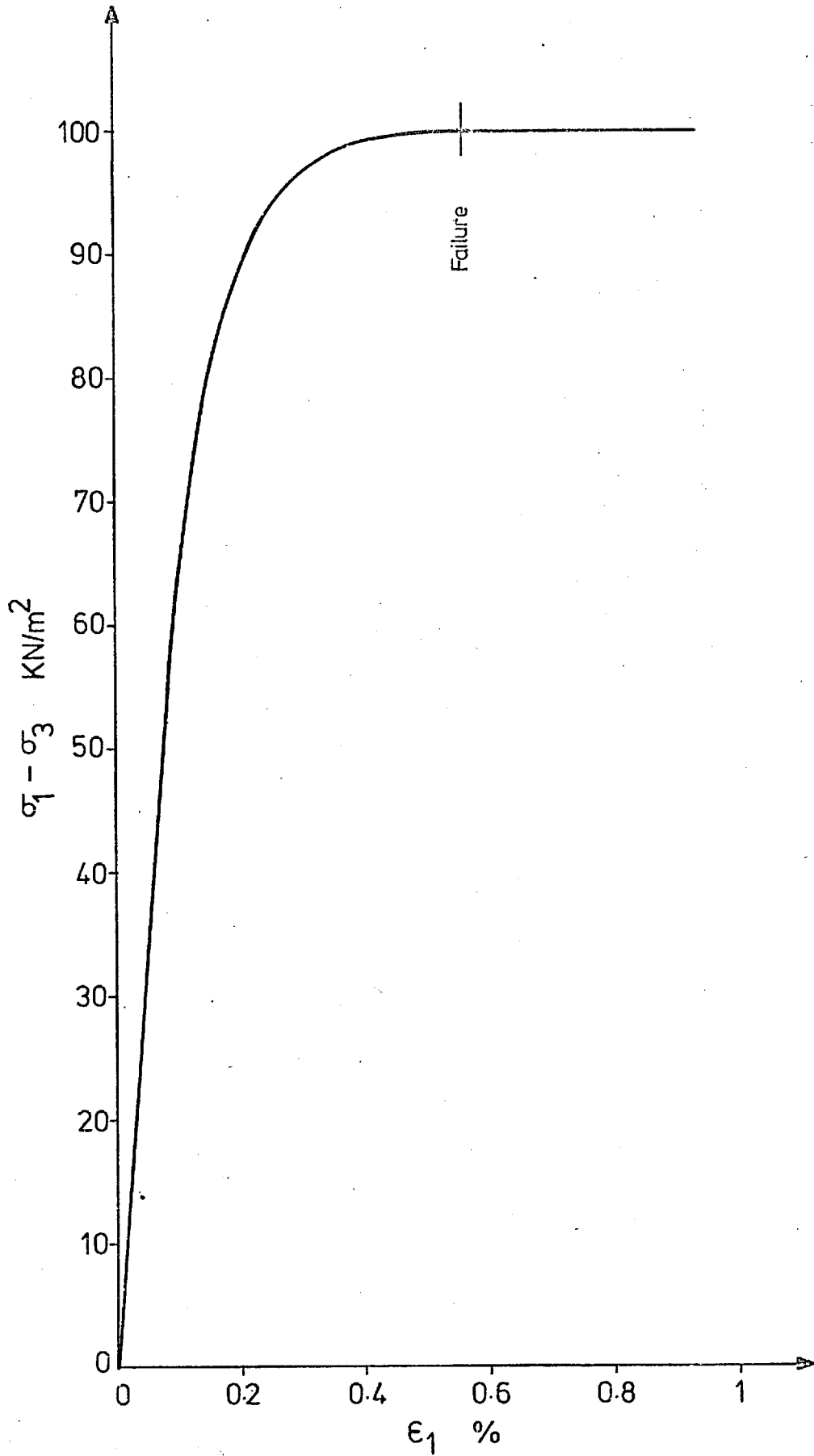
Fig. 5.14   Stress-Strain Curve, (Plane Strain).
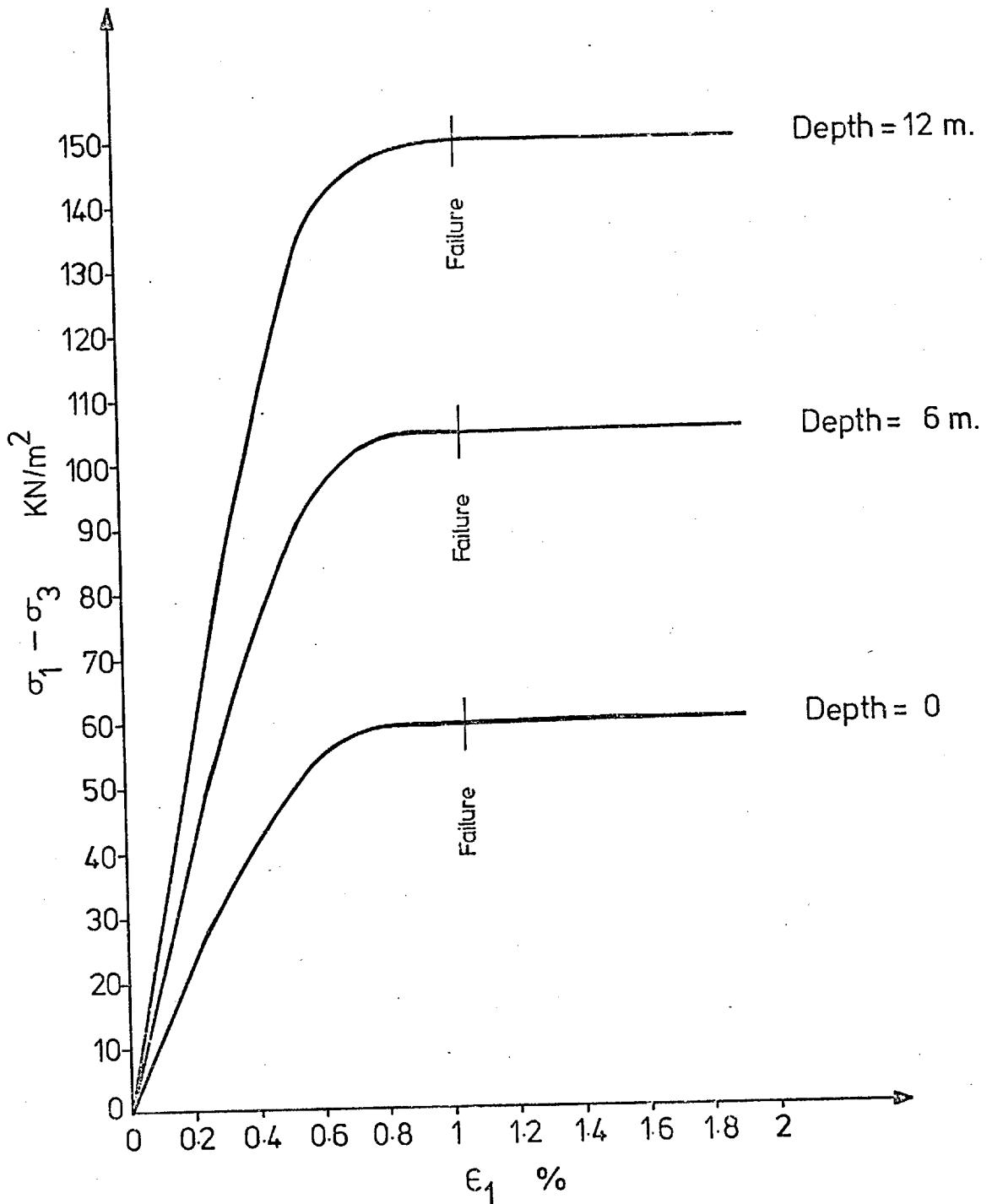
Fig. 5.15 Stress-Strain Curves, (Plane Strain).
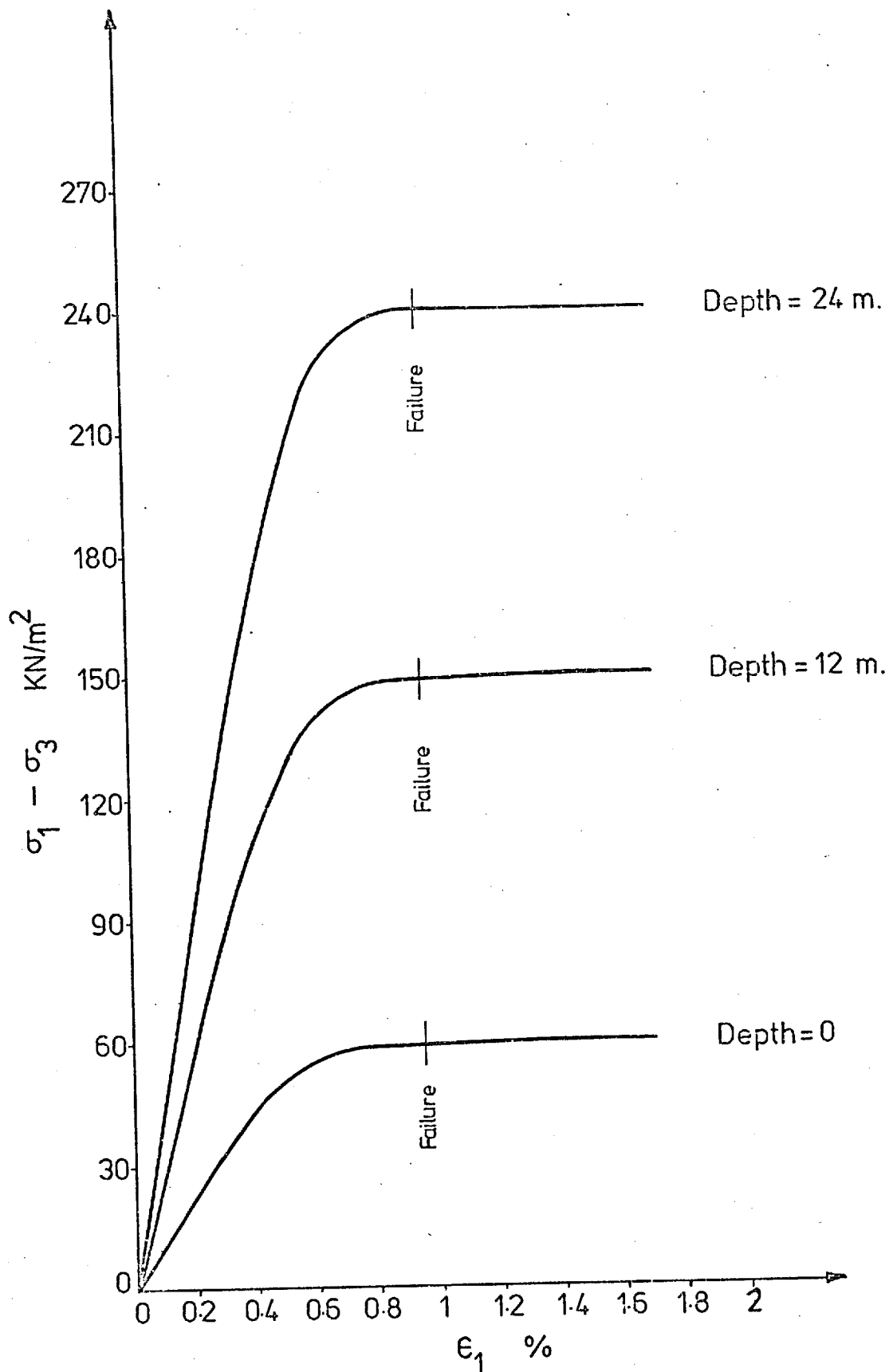
Fig. 5.16 Stress-Strain Curves, (Plane Strain).
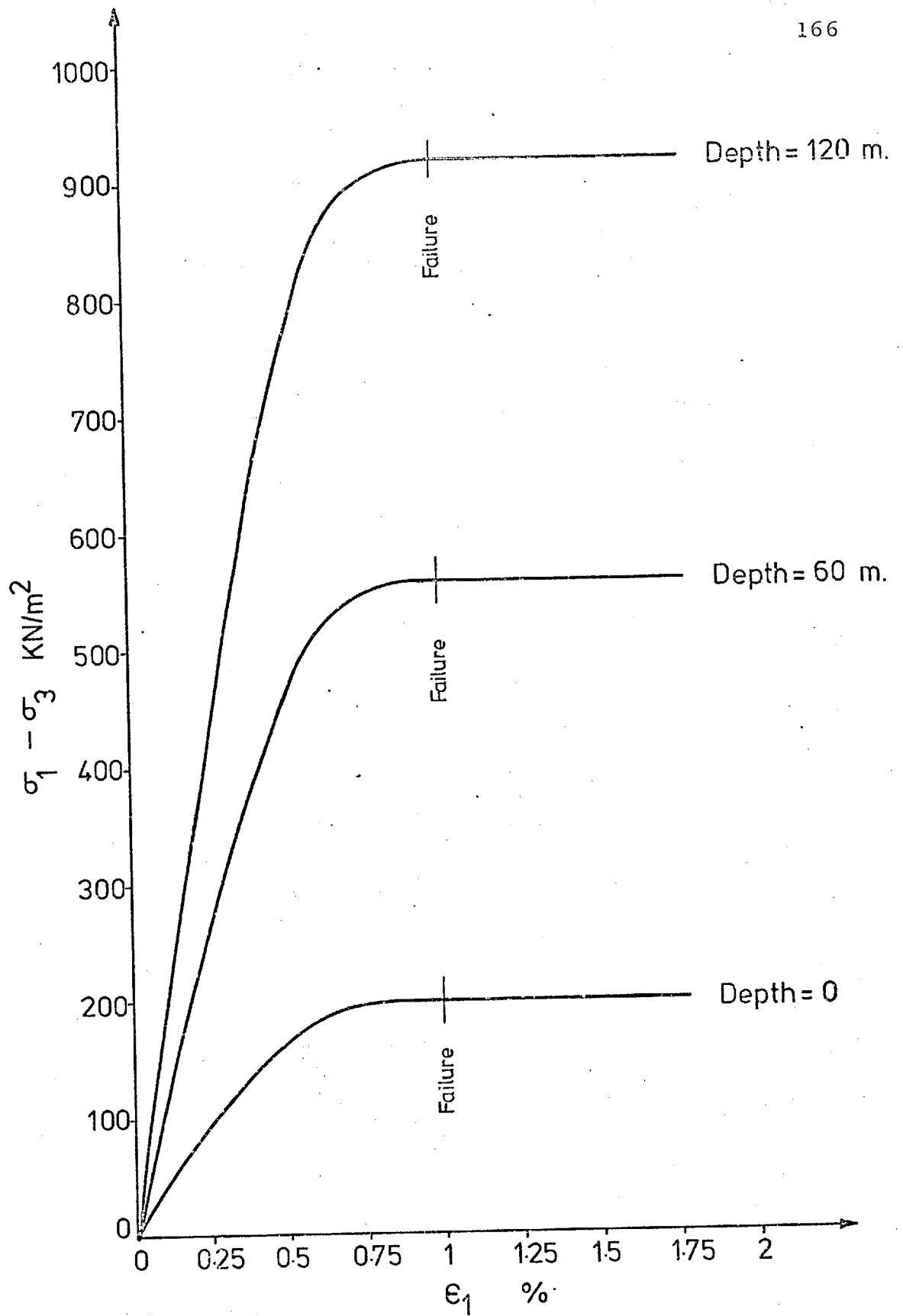
Fig. 5.17 Stress-Strain Curves, (Plane Strain).
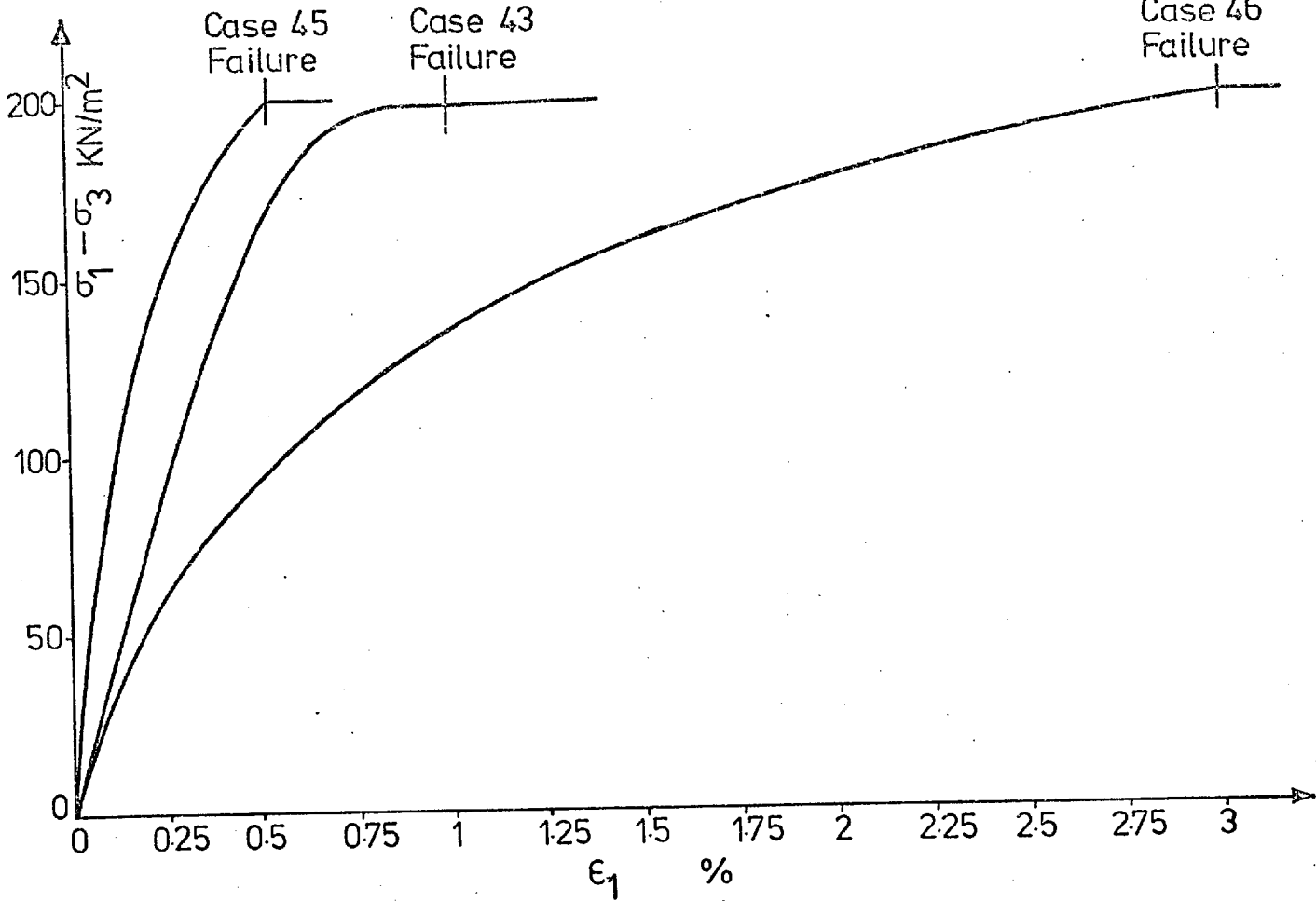
Fig. 5.18 Stress-Strain Curves, (Plane Strain).
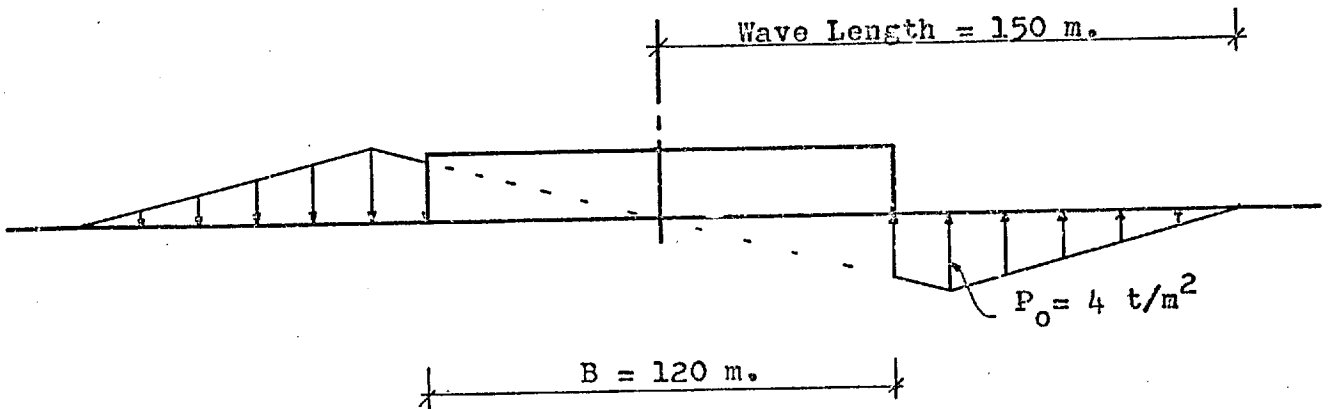
Fig. 5.19 Sea bed pressure due to the weight of the wave.

CHAPTER 6

STRESS ANALYSIS FOR SHALLOW FOUNDATIONS WITH

EMPHASIS ON UNDRAINED BEHAVIOUR

6.1   Introduction

The non-linear finite element programme, explained

in Chapter 2, was used to study the behaviour of shallow

foundations under monotonic and cyclic loadings.   A main

aim of the work was to examine stress changes beneath

footings for use in laboratory stress-path testing work.

The different cases considered in this work, plus the

material properties and geometries used, were discussed in

Chapter 5.   In this chapter, the finite element results

are presented together with the discussion of these results.

Generally, it is easy to obtain a reasonable solution

for a geotechnical problem using the finite element method,

but it needs considerable checking to ensure that the solu-

tion is sufficiently reliable.   It is therefore important

to investigate the effectiveness of any finite element

method by carrying out the calculation for a range of prob-

lems for which a reliable answer from other sources, such

as closed form solutions, is known.

Therefore, in this chapter, the comparison of the

finite element results (both drained and undrained) is made

with the available closed form, or numerical, solutions,

to ensure the reliability of the technique.

In studying the undrained behaviour of shallow

foundations under monotonic loading, the effects of two different forms of parameters, namely, the parameters which affect the validity of the solution (such as: the layer thickness, and the side boundaries), and parameters which affect the solution itself (such as: the correct modelling of shear unloading), on stresses and displacements were considered. Also, failure zones and rupture figures were studied, and some of the geotechnical problems which have no closed form solutions (such as: the inclined and eccentric loading of a finite layer whose undrained modulus and strength vary linearly with depth) were analysed.

Furthermore, the effect of the cyclic loading on displacements and stresses was considered. Also, with cyclic loading, effects of different stress-strain models on stresses, stress changes and displacements were investigated.

For drained behaviour of shallow foundations the effect of stress level on displacements and stresses, and also the effect of variation of Young's modulus with the minor principal stress on stresses were studied.

The factor of safety used throughout this chapter, is defined as the ratio between the failure load, calculated from the bearing capacity theories given in Chapter 4, and the applied load. Table 6.1 gives the calculated failure pressures q_f for different cases, analysed and discussed in this chapter (see also Chapter 5).

In all cases, the soil is assumed to be isotropic.

The interface between the layer and the underlying rigid base is perfectly rough.

The presentation and discussion of the finite element results are divided into two groups, namely, monotonic loading and cyclic loading.

6.2   Finite Element Results, Monotonic Loading

6.2.1 Stresses

6.2.1.1 Contact Pressure Distribution

The pressure acting on the interface of a foundation and the soil is the contact pressure.   It is important in the design of the foundation structure because it determines shear and moment distribution.   Also, the contact pressure is important in studying local failure, and may also be used in settlement calculations.

Figures 6.1 to 6.12 show the contact pressures distributions for different cases.   The stresses considered in these analyses are those given at the Gauss points.   The contact pressure is assumed to be equal to the stress corresponding to the average of four Gauss points stresses at the elements just underneath the footing, minus the initial vertical stresses at the same level.

The equilibrium of stresses is approximately satisfied for all cases, and the maximum error in the equilibrium of stresses is less than 8%.   For case 3 (Table 5.2, Chapter 5), when the average of four Gauss points stresses is assumed to be the contact pressure, the satisfaction of

the stress equilibrium is poor,especially for higher safety
factors (Fig. 6.3a). By assuming the average of two top
Gauss points stresses as the contact pressure (Fig. 6.3b),
the stress equilibrium is achieved, but the distribution
of contact pressure is scattered, as local failure has
started (for case 3, the first local failure occurred at a
safety factor equal to 1.66, Fig. 6.45b). However, by
considering that, in Fig. 6.3a, the maximum error in the
equilibrium of stresses is less than 8%, the contact
pressure distribution is smooth, and there is some small
amount of vertical stress which is distributed outside of
the loaded area, the average of four Gauss points stresses
is assumed to be the contact pressure.

Discussion on the contact pressure results will be
conducted from the following points of view (note that,
not all cases were considered for each result):-

1. comparison with available solutions (drained
   and undrained);

2. stress level (drained and undrained);

3. layer thickness (undrained);

4. side boundaries (undrained);

5. footing rigidity (undrained);

6. soil unit weight (undrained);

7. K_O (undrained);

8. shear unloading modelling (undrained);

9. variation of E with σ_3 (drained);

10. stress-strain relationship (undrained); and

11. nonhomogeneity (undrained).

Comparison with available solutions   Generally, the con-
tact pressures distributions given by the finite element
analyses are in reasonably good agreement with those given
by other elastic solutions, prior to local failure (Fig.
6.1).   In Fig. 6.1, the contact pressures from one drained
case (case 2, Table 5.1, Chapter 5) and one undrained case
(case 3, Table 5.2, Chapter 5) at high values of the safety
factors (for case 2, 230; and for case 3, 8.57) are com-
pared with the contact pressures given by Sadowsky (1928),
Milovic et al (1970) and the "Method of division" using
12 strips (this method is explained in section 3.4.6 of
Chapter 3).

In comparing the result of the drained case 2 with
the elastic solutions (Fig. 6.1), it is clear that the
Sadowsky method gives smaller stresses (except near the
edge) than the result for case 2, as a semi-infinite layer
is assumed in the Sadowsky method.   The contact pressure
from the Sadowsky method is 16% less than the contact
pressure for case 2, at the centre line.   This difference
decreases toward the edge, and near the edge, the contact
pressure from the Sadowsky method is 25% greater than that
for case 2.

The method of division (using 12 strips) gives
stresses which are greater (5% on the centre line and 20%
near the edge of the footing) than those for case 2.
However, as discussed in section (3.4.6) of Chapter 3, the
validity of the method of division depends on the accuracy

of calculation of displacement for each assumed small
flexible section of the footing and the number of divisions.

The contact pressures given by Milovic et al (1970)
for $\nu = 0.33$, are greater than those for case 2. The maxi-
mum difference in stresses is 20% at a distance equal to
B/4 from the centre line. Toward the footing edge and
centre line the difference decreases, and near the edge,
the contact pressure given by Milovic et al (1970) is equal
to the contact pressure for case 2.

The results of undrained case 3 (Table 5.2, Chapter
5) are in good agreement with those given by Milovic et al
(1970) for $\nu = 0.5$, except near the edge, due to material
non-linearity, the contact pressure for case 3 is about
70% of the contact pressure given by Milovic et al (1970).

Stress level   As discussed in section 3.4.5 of Chapter 3,
the increase in applied load causes progressive transition
of the loaded material from the state of elastic to the
state of failure. This transition influences the distri-
bution of contact pressure by limiting its value at the
point where local failure has occurred.

Figures 6.2 and 6.3 show the variation of contact
pressure distribution with the stress level. In Fig. 6.2,
the results for drained case 2 (Table 5:1, Chapter 5) are
considered. At a safety factor equal to 230, the local
failure has not yet started, and the contact pressure distri-
bution is similar to that given by the elastic solutions
(e.g. the Sadowsky method). For case 2, the local failure

starts at a safety factor equal to 46 (see also Figs. 6.45a and 6.55a). After the first local failure, the contact pressure is limited by the shear strength at the edges. By increasing the applied load, the local failure region becomes larger, and the amount of increase in contact pressure near the edges gets smaller than that at the central section of the footing (where failure has not yet occurred). In Fig. 6.2, the ultimate failure load has not been reached. However, at the safety factor equal to 9.2, the contact pressure distribution is similar to a triangular shape (the contact pressure distribution for N_γ term, Fig. 3.30 of Chapter 3), which it should have become as the ultimate failure was reached.

Figure 6.3 shows the contact pressure distribution for undrained case 3 (Table 5.2, Chapter 5). As discussed before, the average of four Gauss points stresses, minus the initial vertical stress at the same level, as shown on Fig. 6.3a, is assumed to be the contact pressure.

For case 3, the local failure starts at a safety factor equal to 1.66 (see also Figs. 6.45b and 6.56a), which is in good agreement with the value of $(\pi+2)/\pi = 1.64$ given by Davis and Poulos (1968) for K_o equal to unity. In Fig. 6.3a, before the start of local failure (safety factors equal to 8.57 and 2.57) the shape of contact pressure distribution curve is similar to that given by the elastic solutions (e.g. Milovic et al, 1970). However, near the edge the contact pressure from the finite element analysis

is smaller than that given by the elastic solutions (see Fig. 6.1). This is due to the effect of material non-linearity. As the state of stress near the footing edge gets closer to the state of failure (the more severe non-linear section of the stress-strain curve), the modulus decreases and the amount of increase in contact pressure near the edge becomes smaller than that at the central section of the footing. This increase in the contact pressure decreases very rapidly, and becomes equal to zero, as the first local failure occurs (safety factor equal to 1.285, Fig. 6.3a). When the ultimate failure is approached, the shape of contact pressure distribution is similar to a rectangular shape (the contact pressure distribution for N_c term, Fig. 3.30 of Chapter 3), see Fig. 6.3a, safety factor equal to 0.988.

Layer thickness   Figure 6.4 shows the effect of layer thickness on the contact pressure distribution for an inclined and eccentric load on undrained clay, whose strength and modulus increase linearly with depth (cases 15 and 16, Table 5.2 of Chapter 5).

At the safety factor equal to two, the contact pressure for case 15 (D = B) is greater than that for case 16 (D = 2B) at the central section of the footing, and it is smaller for case 15 than that for case 16 near the edges. This effect is reversed for the safety factor equal to unity. In other words, by decreasing the layer thickness, the contact pressure distribution becomes more uniform.

Side boundaries   Three   undrained cases 9, 11 and 12

(Table 5.2, Chapter 5) were considered to investigate the

effect of the side boundaries on the contact pressure.

For all cases, undrained strength and modulus increase

linearly with depth.   The horizontal distances from the

centre line to the side boundaries are 2B for case 12,

4.17B for case 9, and 6B for case 11 (B is footing width).

Figure 6.5 shows the effect of the side boundaries on

the contact pressure.   At the safety factor equal to 4.3,

the side boundaries have no effect on the contact pressure.

However, near the state of failure (safety factor = 1.08),

the contact pressure increases, by reducing the side

boundaries.   The maximum value of the difference in con-

tact pressures from case 11 and case 12 is small and equal

to 4%.

Footing rigidity   Two undrained cases 39 and 40   (Table

5.2, Chapter 5) were considered to study the effect of

footing rigidity on the contact pressure.   For both cases,

undrained strength and modulus increase linearly with

depth, and the applied load is inclined and eccentric.

Equation 6.1 (after Boswell and Scott, 1975) defines

the relative stiffness of the footing:-

$$k_r = \frac{E_f}{E_s} \frac{1 - \nu_s^2}{1 - \nu_f^2} \left(\frac{2t}{B}\right)^3 \qquad (6.1)$$

where E is the Young's modulus, ν is the Poisson's ratio,

subscript f denotes the footing, subscript s denotes the

soil, t and B are footing thickness and width.   If k_r

is greater than 10, then the footing is assumed to be rigid, and if k_r is less than 10, then the footing is assumed to be flexible. The relative stiffness is 2.1 for case 39, and it is 16.8 for case 40.

Figure 6.6 shows the contact pressures distributions for these two cases at different values of safety factor. Obviously, the contact pressure distribution for case 39 (flexible footing) is more uniform than that for case 40 (rigid footing). Near the right hand side edge of the footing, due to local failure, the contact pressure distribution is scattered for both cases at the safety factors equal to 0.95 and 0.88.

It has to be mentioned that for these two cases, local failure occurs at both edges (see Fig. 6.60), however, the local failure region must be rather deep, in order to influence effectively the contact pressure.

<u>Soil unit weight</u> Two undrained cases 7 and 8 (Table 5.2, Chapter 5) were studied in order to investigate the effect of soil unit weight on the contact pressure. For both cases, the shear strength and modulus increase linearly with depth, and the applied load is inclined and eccentric. It is obvious that the soil unit weight will affect the undrained behaviour, only, if K_o is not equal to unity. For case 7, the soil unit weight is 20 KN/m^3 and K_o is two, while for case 8, the soil unit weight is equal to zero.

Figure 6.7 shows the contact pressures for these two cases at the safety factors equal to 4 and 1.3. Generally,

omitting the soil unit weight from the analysis (like the case with K_o equal to unity which will be discussed later) tends to increase the contact pressure at the central section of the footing, and to decrease it near the edges. In Fig. 6.7, the maximum differences between the contact pressures from case 7 and case 8, are near the edges and equal to 8% at the safety factor equal to 4, and 20% at the safety factor equal to 1.3.

Also, in Fig. 6.7 the results for case 8, at the safety factor equal to 4, are compared with the results given by Milovic et al (1970) which also assume zero unit weight for the soil. At the central section of the footing, the agreement between the finite element results and those given by the elastic solution is good. The contact pressure for case 8 is a maximum of 6% greater than the contact pressure given by Milovic et al (1970), at the central section of the footing. However, near the edges, due to material non-linearity and local failure, the finite element results are much smaller than the results given by elastic solution.

K_o Two undrained cases 5 and 6 (Table 5.2, Chapter 5) were considered to study the effect of K_o on the contact pressure. For both cases, the shear strength and modulus increase linearly with depth, the applied load is inclined and eccentric, and the shear unloading modulus is equal to the tangent modulus at the same state of stress (see Fig. 5.1a of Chapter 5). For case 5, the soil unit weight is equal

to 20 KN/m³ and K_o is two, while for case 6, the soil unit weight is 20 KN/m³ and K_o is one.

Figure 6.8 shows the contact pressures distributions for these two cases. The contact pressure for case 6 ($K_o = 1$) is greater than the contact pressure for case 5 ($K_o = 2$), for the central section of the footing. Near the edges, the contact pressure for case 6 is less than that for case 5. The maximum differences between the contact pressures from these two cases are 6% at the safety factor equal to 2, and 20% at the safety factor equal to unity.

By comparing the effects of soil unit weight and K_o on the contact pressures, it is clear that the soil unit weight has no effect on the undrained behaviour of shallow foundations, provided that K_o is equal to unity.

Shear unloading modelling   For a shallow foundation, which is loaded monotonically, the shear unloading can only occur if K_o is not equal to unity. This shear unloading occurs in the early stages of loading.

Two undrained cases 4 and 9 (Table 5.2, Chapter 5) were considered to investigate the effect of shear unloading modelling on the contact pressure. For both cases, the shear strength and modulus increase linearly with depth, applied load is vertical, the soil unit weight is 20 KN/m³ and K_o is two. In case 4, the shear unloading path is on the first loading curve (i.e. $E_u = E_t$, see Fig. 5.1a of Chapter 5), while in case 9, the unloading modulus is equal to the initial modulus (i.e. $E_u = E_i$, see Fig. 5.1b of Chapter 5). In both cases, the reloading curve is parallel

to the first loading curve.

Figure 6.9 shows the contact pressures distributions for these two cases, at the safety factors equal to 2.15 and 1.08. At the safety factor equal to 2.15, the contact pressure for case 9 is greater than that for case 4, at the central section of the footing. Near the edge, the contact pressure for case 9 is smaller than that for case 4. At the safety factor equal to 1.08, both cases give the same contact pressures at the central section of the footing. Near the edges, the contact pressure for case 9 is greater than that for case 4. The difference between the contact pressures from these two cases depends on K_o and the non-linearity of the early section of the stress-strain curve.

For these two cases, as the early section of stress-strain curve used is close to linearity (see Fig. 5.15 of Chapter 5), therefore, the contact pressures differences are small. The maximum difference is 7% at a distance equal to B/12 from the edge, for the safety factor equal to 2.15. Obviously, this difference decreases as the ultimate failure is approached.

For case 4, local failure starts at the safety factor equal to 2.15 (see also Figures 6.45b and 6.57a). Case 9, as discussed above, affects the stresses, but as this effect is small for the cases considered, therefore, the load required for the initiation of first local failure is not affected by the correct modelling of the shear unloading.

Variaton of E with σ_3 To investigate the effect of linear

variation of the Young's modulus with the minor principal

stress, two linear elastic cases 51A and 51B (Table 5.4,

Chapter 5) were considered.   For case 51A, the modulus is

constant, while for case 51B, it increases linearly with

σ_3, and the rate of increase in modulus with σ_3 is modest

when compared with the modulus for σ_3 equal to zero (Table

5.4 of Chapter 5).

Figure 6.10 shows the contact pressures for these two

cases.   The contact pressure for case 51B is greater than that

for case 51A, at the central section of the footing.   Near

the edge, the contact pressure for case 51B is smaller than

that for case 51A.   However, as the rate of increase in

modulus with σ_3, in case 51B, is small compared to the

modulus of case 51A, therefore, the difference between the

stresses from these two cases is small.

Stress-strain relationship   Three undrained cases 43, 45

and 46 (Table 5.2, Chapter 5) were considered to investigate

the effect of the stress-strain relationship on the contact

pressure.   For all three cases, the soil unit weight is

20 KN/m^3, K_o is one, and the shear strength and modulus

increase linearly with depth.   The stress-strain curves

used in these three cases are shown on Fig. 5.18 of Chapter 5.

Figure 6.11 shows the contact pressures for these

cases.   At the safety factor equal to 3.56, and before the

local failure occurs (for these cases, local failure starts

at the safety factor equal to 2.15, see also Fig. 6.51), the
effect of stress-strain relationship on the contact pressures
is small. At a safety factor equal to 1.09, the contact
pressure for case 45 (stiffer curve) is greater than that
for case 46 (softer curve), at the central section of the
footing. Near the edge, the contact pressure for case 45
is smaller than that for case 46. The maximum difference
between the contact pressures for these cases, is 7% at a
distance equal to B/6 from the edge, at the safety factor
equal to 1.09.

Nonhomogeneity Two undrained cases 43 and 44 (Table 5.2,
Chapter 5) were considered to investigate the effect of the
nonhomogeneity on the contact pressure. For case 43, the
shear strength and modulus increase linearly with depth,
while for case 44, both are constant. For both cases, the
soil unit weight is 20 KN/m^3 and K_o is one.

Figure 6.12 shows the contact pressures for these
two cases, at the safety factors equal to 9.6, 2.4 and 1.12.
For case 43, local failure starts at the safety factor
equal to 2.15, while for case 44, local failure starts at
the safety factor equal to 1.66 (see also Fig. 6.45c).

The form of the nonhomogeneity considered for case 43
results in stiffer soil than the uniform case 44. The
contact pressures for case 43 are greater than the contact
pressures for case 44, at the central section of the footing
(central 2/3 of the footing width). Near the edges, the
contact pressures for case 43 are smaller than those for
case 44.

Figure 6.12 shows that the ratio $E_o/\lambda B$ (see Eq. 3.10, Chapter 3) has a marked effect on the contact pressures. On the footing centre line, the contact pressure for case 43 ($E_o/\lambda B = 0.28$) is 12% more than that for case 44 ($E_o/\lambda B = \infty$), at the safety factor equal to 9.6. Near the edges, the contact pressure for case 43 ($E_o/\lambda B = 0.28$) is 19% less than that for case 44 ($E_o/\lambda B = \infty$), at the safety factor equal to 9.6. These differences increase as the safety factors decrease, and their values are 18% and 39% for a safety factor equal to 1.12, on the centre line and near the edge, respectively.

Carrier and Christian (1973) have also showed that the effect of $E_o/\lambda D$ (D is footing diameter) on the stress distribution for a circular footing is significant in producing more uniform contact stresses (see Fig. 3.33 of Chapter 3).

6.2.1.2 Stress Distribution

Figures 6.13 to 6.27 represent the vertical and horizontal stresses distributions for different cases. The stresses in these figures are those corresponding to the average of four Gauss points stresses, minus the initial stresses.

Discussion on these results will be conducted from the following points of view (bearing in mind that some of the comments on contact pressures, discussed in section 6.2.1.1, are also valid for the stresses):

1. Comparison with available solutions (drained
    and undrained);

2. stress level (undrained);

3. layer thickness (undrained);

4. side boundaries (undrained);

5. shear unloading modelling (undrained);

6. variation of E with σ_3 (drained);

7. nonhomogeneity (undrained); and

8. K_o (undrained).

<u>Comparison with available solutions</u>   Figures 6.13 and 6.14
show the vertical and horizontal stresses for drained case
1 (Table 5.1, Chapter 5), at the safety factor equal to
46, and compare the finite element for this case with the
results given by Poulos (1967) and Milovic <u>et</u> <u>al</u> (1970) for
$\nu = 0.33$.

Generally, the agreement between the drained results
from the finite element analysis, at the safety factor equal
to 46, and those given by the elastic solutions is good,
except for the vertical stresses near the edges.   Near the
footing centre line (Fig. 6.13), the vertical stresses at
great depths from the finite element analysis are almost
the same as those given by Poulos (1967) and Milovic <u>et</u> <u>al</u>(1970).
For shallow depths, the vertical stresses given by Poulos
(1967), for uniform loading, are greater than those from
the finite element analysis, and the vertical stresses given
by Milovic <u>et</u> <u>al</u> (1970) are smaller than those given by
the finite element analysis.   The maximum difference in

vertical strsses is near the ground surface, and the finite

element results are 10% less than the results given by

Poulos (1967), and they are 7% more than the results given

by Milovic et al (1970). However, as the effect of material

non-linearity is to increase the stresses near the centre

line (see Fig. 6.15), therefore, the difference between the

vertical stresses from the finite element analysis and Milovic

et al (1970) must be less than 7% at the higher safety

factors. Near the centre line, the horizontal stresses

from the finite element analysis are a maximum of 20% and 30%

greater than those given by Milovic et al (1970) and Poulos

(1967).

Near the edges (Fig. 6.14), horizontal stresses from

the finite element analysis for great depths are almost the

same as those given by Poulos (1967). The vertical stresses

from the finite element analysis are a maximum of 50% more

than those given by Poulos (1967) for a uniform loading.

Comparison of the results for undrained case 3 (Table

5.2, Chapter 5), at the safety factor equal to 5.14, and

the elastic solutions for $\nu = 0.5$, is made in Figs. 6.15 and

6.16. Near the centre line, vertical stresses from the

finite element analysis are a maximum of 19% and 8% smaller

than those given by Poulos (1967) and Milovic et al (1970).

The horizontal stresses from the finite element analysis

are almost the same as those given by Milovic et al (1970),

and they are a maximum of 40% greater than the Poulos

results, near the centre line. Near the edges, vertical

stresses from the finite element analysis are a maximum of

50% greater than those given by Poulos (1967) for a uniform loading, and the horizontal stresses at great depths are almost the same as those given by Poulos (1967).

Stress level Figures 6.15 and 6.16 show the effect of stress level on the stress distribution for undrained non-linear case 3 (Table 5.2, Chapter 5). By increasing the applied load, vertical stress increases at the central section of the footing, and decreases near the edges. This effect is a maximum near the ground surface, and decreases with depth (Fig. 6.15).

By increasing the applied load, horizontal stress increases in whole domain, except at very shallow depths near the edges. At depths more than the footing width near the centre line, the opposite occurs (see Figs. 6.16 and 6.17).

Layer thickness Two undrained cases 15 and 16 (Table 5.2, Chapter 5) were considered to investigate the effect of layer thickness on the stresses. For both cases, the shear strength and modulus increase linearly with depth, and the applied load is inclined and eccentric. For case 15, the layer thickness is equal to the footing width, while for case 16, the layer thickness is twice the footing width.

Figures 6.17 and 6.18 show the stress distribution for these two cases, at the safety factors equal to two and one. At the safety factor equal to two, by reducing the layer thickness, vertical stresses increase at the central section of the footing and decrease near the edges, while

horizontal stresses increase at great depths and decrease
at shallow depths. At the safety factor equal to one, by
reducing the layer thickness, vertical and horizontal
stresses decrease at shallow depths and increase at great
depths.

Side boundaries   Three undrained cases 9, 11 and 12 (Table
5.2, Chapter 5) were considered to study the effect of the
side boundaries on the stresses. For all three cases, the
shear strength and modulus vary linearly with depth. The
horizontal distances from the footing centre line to the
side boundary are 2B for case 12, 4.17B for case 9, and 6B
for case 11.

Figures 6.19a and b show the stress distribution for
these cases. At the safety factor equal to 2.15 (Fig.
6.19a), the side boundaries have no effect on the vertical
stresses, except at very shallow depths near the edge, where
by almost doubling the horizontal distance from the centre
line to the side boundaries, the vertical stress is reduced
about 4%. Horizontal stresses are the same for all three
cases near the centre line, but they are on average 10%
greater for case 12 than for cases 9 and 11 for the rest
of domain. This effect is reduced a little as failure is
approached (Fig. 6.19b).

Shear unloading modelling   As discussed in the contact
pressure section, by monotonic loading of a footing, shear
unloading can only occur if K_o is not equal to unity. For
two undrained cases 4 and 9 (Table 5.2, Chapter 5), which

were considered to investigate the effect of correct shear

unloading modelling on the stresses, the soil unit weight

is 20 KN/m^3 and K_o is two. For both cases, the shear

strength and modulus increase linearly with depth. In

case 4, E_u is equal to E_t (see Fig. 5.1a), and in case 9,

E_u is equal to E_i (see Fig. 5.1c).

The correct shear unloading modelling affects the

solution itself, rather than affecting the validity of the

solution. Obviously, the value of K_o and the initial

section of the stress-strain curve used in the analysis

influence this effect.

Figures 6.20a and b show the stress distribution for

these two cases. First, it may seem that the correct

shear unloading modelling does not affect the stresses, but,

by considering that the initial section of the stress-strain

curve used in these cases (Fig. 5.15 of Chapter 5) is very

close to linearity, therefore, this effect is small.

However, correct shear unloading modelling tends to increase

the vertical stress at the central section of the footing,

and to decrease it near the edges, and this process is

reversed as the failure is approached (see also Fig. 6.9).

Also, correct shear unloading modelling tends to decrease

the horizontal stresses.

Variation of E with σ_3 Two linear elastic cases 51A and

51B (Table 5.4, Chapter 5) were considered to study the

effect of the linear variation of E with σ_3 on stresses.

All parameters are the same for both cases, except the

modulus.   For case 51A, the modulus is constant, while

for case 51B, it increases linearly with σ_3.

Figures 6.21 to 6.23 show the principal stresses for

these two cases.   Near the footing centre line (Fig. 6.21),

the principal stresses for case 51B are greater than those

for case 51A.   For the major principal stress this diffe-

rence is 3%, and for the minor principal stress it is 2%.

These effects decrease toward the edges (Fig. 6.22), and

near the edges, the principal stresses for case 51A are a

maximum of 2% greater than those for case 51B.   As dis-

cussed before in the contact pressure section, these effects

are small, because the rate of increase in E with σ_3 is

small compared to E itself.

Nonhomogeneity   In order to investigate the effect of the

linear variation of undrained strength and modulus with

depth, two undrained cases 43 and 44 (Table 5.2, Chapter 5)

were considered.   All parameters are the same for both

cases, except the strength and the modulus.   For case 44,

strength and modulus are constant, while for case 43, they

increase linearly with depth.

Figures 6.24 to 6.26 show the stresses for these two

cases.   Vertical stresses for case 43 are greater (at the

central section of the footing), and are smaller (near the

edges), than those for case 44, at all values of the safety

factors.   The maximum differences between the stresses

from these two cases are near the centre line (18%) and

edges (39%), at very shallow depths for the safety factors

equal to 1.12. They decrease as the depth or the safety factor increase.

Horizontal stresses for case 43 are greater than those for case 44, except at very shallow depths near the edges, and at great depths. The average value of the difference in horizontal stresses is 25%.

K_o Two undrained cases 5 and 6 (Table 5.2, Chapter 5) were considered to study the effect of K_o on the stress increases due to loading. All parameters are the same for these two cases, except the value of K_o. For case 5, K_o is two, and for case 6, it is one.

Figures 6.27a and b show the stresses for these two cases, at the safety factors equal to two and one. Vertical stresses for case 6 ($K_o = 1$) are greater (at the central section of the footing), and are smaller (near the edges), than those for case 5 ($K_o = 2$). Horizontal stresses for case 6 are greater than those for case 5, except at great depths. These effects increase at shallow depths and decrease at great depths for vertical stresses, and increase at mid-depth for horizontal stresses, as the failure is approached.

The maximum differences in vertical stress changes are 6% and 20% for the safety factors equal to two and one, respectively. The average differences in horizontal stress changes are 8% for the safety factors equal to two, and 15% for the safety factors equal to one.

6.2.2 Displacements

Figures 6.28 to 6.44 show the displacements for different cases. Discussion on these plots will be conducted from the following points of view:-

1. stress level (drained);

2. layer thickness (undrained);

3. side boundaries (undrained);

4. shear unloading modelling (undrained);

5. footing rigidity (undrained); and

6. nonhomogeneity (undrained).

Comparison of the undrained results with available solutions, and the effect of stress level on undrained results are discussed during studies of the effect of other parametres.

Stress level Figures 6.28 and 6.29 show the vertical and horizontal displacements for drained case 1 (Table 5.1, Chapter 5). Figure 6.28 indicates that by reducing the safety factor, vertical displacements concentrate at the central section of the footing. Figure 6.29 shows that the maximum horizontal displacements are around mid-depth, and concentration of the horizontal displacements around mid-depth increases, as the safety factor decreases.

Layer thickness Figure 6.30 shows the settlements profiles for two undrained cases 15 and 16 (Table 5.2, Chapter 5) at the safety factors equal to two. For both cases, the shear strength and modulus increase linearly with depth, and the applied load is inclined and eccentric. All

parameters are the same for both cases, except the layer thickness. For case 15, the layer thickness is equal to the footing width, while for case 16, it is twice the footing width.

By decreasing the layer thickness, settlement decreases and heave increases (Fig. 6.30). However, in this figure, the heave for case 16 is greater than that for case 15 near the side boundaries, and this is due to the increasing side boundary effect.

In Fig. 6.30, the finite element results are compared with the results given by Milovic et al (1970) using an average modulus. For case 15 (D=B), the settlement from the finite element analysis is 8% less than that given by Milovic et al (1970). For case 16 (D=2B), the centre settlements from both solutions are the same, but the tilt from the finite element analysis is 25% more than that given by Milovic et al (1970).

Side boundaries   The effect of the side boundaries on the settlement was considered for both inclined and eccentric loading and vertical loading. Figure 6.31a shows the settlements profiles for three undrained cases 10, 13 and 14 (Table 5.2, Chapter 5). In all three cases, the applied load is inclined and eccentric, and all parameters are the same, except the side boundary distance from the centre line, H.   For case 10, H is 2.5B, for case 13, H is 4B, and for case 14, H is 1.5B.

Figure 6.31b shows the settlements profiles for three

undrained cases 9,11 and 12 (Table 5.2, Chapter 5). In all three cases, the applied load is vertical, and all parameters are the same, except H. For case 9, H is 4.17B, for case 11 , H is 6B, and for case 12, H is 2B.

These two figures indicate that by decreasing the side boundary distance from the centre line, the settlement decreases and the maximum heave increases.

In Fig. 6.31a, the settlements for cases 10 and 13 are the same, and the heave for case 13 is slightly less than that for case 10. This indicates that the more economical distance from the centre line to the side boundaries is equal to 2.5B.

In Fig. 6.31b, the finite element results at the safety factor equal to 2.15 are compared with the results given by the elastic solutions using an average modulus. The settlement for case 9 is 10% less than the settlement given by Poulos (1967), using an average modulus and Eq. 3.17 of Chapter 3 for relating the settlement of a rigid footing to the settlement of a flexible footing. The settlement given by Milovic et al (1970), using an average modulus, is 40% more than that for case 9.

Shear unloading modelling   In Fig. 6.32, settlements for two undrained cases 4 and 9 (Table 5.2, Chapter 5) are shown. All parameters are the same for these two cases, except the unloading modulus. For case 4, the E_u is equal to E_t (see Fig. 5.1a), while for case 9, the E_u is equal to E_i (see Fig. 5.1b). For both cases, K_o is two.

Figure 6.32 indicates that the effect of correct shear unloading modelling is to decrease both the settlement and the heave (provided that $K_o > 1$).

Also, in Fig. 6.32, the finite element results are compared with the results given by the elastic solutions using an average modulus. The settlement for case 4 is equal to that given by Poulos (1967) using an average modulus, and Eq. 3.17 of Chapter 3 for relating the settlement of a rigid footing to the settlement of a flexible footing. The settlement given by Milovic et al (1970), using an average modulus, is 30% more than that for case 4.

Footing rigidity   Two undrained cases 39 and 40 (Table 5.2, Chapter 5) were considered to investigate the effect of footing rigidity on the settlement. For both cases, the shear strength and modulus increase linearly with depth, and the applied load is inclined and eccentric. The relative stiffness (see Eq. 6.1) for case 39 is 2.1, and for case 40 is 16.8.

Figure 6.33 shows the settlements for these two cases at the safety factors equal to 1.98 and 0.85. One important feature of this figure is that, for the safety factor equal to 1.98, the tilt is not affected by the footing rigidity. But the effect of footing rigidity on the tilt becomes significant as the failure is approached.

Also, Fig. 6.33 shows a good agreement between the settlement given by the Milovic et al (1970) using an average modulus, and the settlement for case 40 at a safety factor equal to 1.98.

<u>Nonhomogeneity</u>   Figures 6.34 to 6.37 show displacements
for two undrained cases 43 and 44 (Table 5.2, Chapter 5).
For case 44, the undrained strength and modulus are constant,
while for case 43, they increase linearly with depth.

Figures 6.34 and 6.35 show that the effect of non-
homogeneity (case 43) is to reduce both the settlement and
the heave (compared to uniform case 44).   Figures 6.36 and
6.37 indicate that nonhomogeneity tends to decrease both
vertical and horizontal displacements.   The effect on
horizontal displacements increases with depth, because the
modulus increases with depth (Fig. 6.37).

Also, in Fig. 6.34, the settlements for cases 43 and
44 at the safety factor equal to 9.6, are compared with
those given by the elastic solutions.   For uniform case
44, the settlement given by Poulos (1967), using Eq. 3.17
of Chapter 3 for settlement of rigid footing, is 5% less
than the settlement from case 44.   For the same case, the
result given by Milovic <u>et</u> <u>al</u> (1970) is 20% more than that
for case 44.

For nonhomogeneous case 43, the settlement given by
Milovic <u>et</u> <u>al</u> (1970), using an average modulus, is 6%
greater than that for case 43.

In Figures 6.38 to 6.44, some typical displacements
vectors are given for drained case 2, and undrained cases
3 and 40 (Tables 5.1 and 5.2, Chapter 5).   In Figures 6.38
to 6.42, the applied load is vertical and a wedge of rigid
material, which is moving down with the footing, can be
seen clearly.

The important feature of Figures 6.43 and 6.44 is to show that the displacement vector field can be used to evaluate the ultimate failure load, more accurately. These figures show displacements vectors for an inclined and eccentric load at the safety factors equal to 0.89 and 0.88. By comparing the settlements of the footings in these two figures, it is clear that, at the safety factor equal to 0.88, there is a sudden change in the direction of the displacement vector. Therefore, the ultimate failure for this case must occur between these two loads (see also Fig. 6.61).

6.2.3 The Failure Load

6.2.3.1 Definition of the Failure Load

In Chapter 4, the failure load was defined as the load at which the slope of the load-settlement curve first reaches a steady minimum value. Also, it was mentioned that in some cases, this slope increases continuously, and it is difficult to define the failure load more accurately. In these cases, consideration of three different plots, namely, load-settlement curve, load-settlement curve in a log-log scale, and displacement vector field is recommended for defining the failure load more accurately.

An example of the use of displacement vector fields was shown in the previous section. In the following section the load-settlement curves will be discussed.

6.2.3.2 Load-settlement Curves

Figures 6.45 to 6.51 represent some typical load-settlement curves and the effect of different parameters on them.

In Fig. 6.45a, the load-settlement curve for drained case 2 (Table 5.1, Chapter 5) is given. In this case, as mentioned in Chapter 5, the load was only increased up to 11% of the ultimate failure load. The first local failure occurs at a safety factor equal to 46 (see also Fig. 6.55a).

Figure 6.45b represents the load-settlement curves for two undrained cases 3 and 4 (Table 5.2, Chapter 5). For case 3, undrained strength is constant, the initial modulus is 1400 C_u and K_o is one. For case 4, undrained strength increases linearly with depth, E_i is 300 C_u and K_o is two. Also, in Fig. 6.45b, the results from the closed form solutions are given, in order to compare them with the finite element results.

By considering that, in principle, an incremental elastic finite element solution predicts a lower bound to the failure load, the comparison between the failure loads from the finite element analyses, and those given by the plasticity solutions is very good.

In Fig. 6.45c, the load-settlement curves for two undrained cases 43 and 44 (Table 5.2, Chapter 5) are given. For case 44, the undrained strength is constant and E_i is 300 C_u, while for case 43, undrained strength increases linearly with depth, and E_i is 300 C_u. For both cases K_o is one.

Figures 6.45b and c indicate that the nonhomogeneous cases 4 and 43 give higher values for the safety factors at first local failure than the uniform cases 3 and 44. For uniform cases 3 and 44, the local failure starts at the safety factor equal to 1.66 (which is in good agreement with the value 1.64 given by Davis and Poulos, 1968, for K_o equal to 1). For the nonhomogeneous cases 4 and 43, the local failure starts at the safety factors equal to 2.15.

The safety factors at first local failure for two nonhomogeneous cases 4 and 43 are coincidently equal. However, this does not necessarily mean that the ratio $C_{uo}/\rho B$ (see Eq. 4.33, Chapter 4) has no effect on the value of safety factor at first local failure.

The safety factor at first local failure is a function of the ratio $f = (1-K_o)\sigma'_{vo}/2C_u$ (Davis and Poulos, 1968). Its value is a minimum for f equal to zero, and it increases by increasing or decreasing the value of f.

Figure 6.45d shows the load-settlement curves for two undrained cases 9 and 23 (Table 5.2, Chapter 5). For both cases, undrained strength and modulus increase linearly with depth, and all parameters used are the same, except a slight difference in the grading of the meshes (see Table 5.2, Chapter 5), and K_o. The effect of the difference in the grading of the meshes on the value of safety factor at first local failure, is negligible. For case 9, the soil unit weight is 20 KN/m^3 and K_o is two, while for case 23, the soil unit weight is 20 KN/m^3 and K_o is one. This

figure indicates that, from the qualitative point of view, for nonhomogeneous clay, the ratio f has the same effect on the safety factor at first local failure, as for the uniform clay.

For case 23 (Fig. 6.45d), the safety factor at first local failure is 1.86, the ratio $C_{uo}/\rho B$ is 0.67 and K_o is one, while for case 43 (Fig. 6.45c), the safety factor at first local failure is 2.15, the ratio $C_{uo}/\rho B$ is 0.28, and K_o is one. Therefore, from these results, it may be concluded that by increasing the ratio $C_{uo}/\rho B$, the safety factor at first local failure decreases, provided that the ratio f is equal to zero. At the limit for $C_{uo}/\rho B = \infty$. (i.e. $\rho = 0$, uniform clay) the safety factor at first local failure is equal to $(\pi+2)/\pi$ for f = 0.

Figures 6.46a and b show that the side boundaries and the shear unloading modelling do not affect the magnitude of the ultimate failure pressure, as should be the case. However, the fixed side boundaries produce a confining effect in the domain, and by moving the boundaries toward the centre line the horizontal stresses increase (see Fig. 6.19a), resulting in a decrease in the value of safety factor at first local failure (Höeg et al, 1968). The same effect is shown in Fig. 6.46a, where load-settlement curves for cases 9, 11 and 12 (Table 5.2, Chapter 5) are given. In these three undrained cases, all parameters are the same, except the side boundary distances from the centre line, which are 4.17B, 6B and 2B for cases 9, 11 and 12,

respectively.   In this figure, the results for cases 9 and
11 are the same, but for case 12, the safety factor at
first local failure is slightly decreased.

The correct modelling of the shear unloading has not
affected the value of the load required for the initiation
of local failure (Fig. 6.46b).

Also, Figures 6.47a and b show that the layer thickness
has no effect on the value of ultimate failure pressure.
But, as discussed in section (6.2.2), by increasing the
layer thickness, pre-failure settlement is increased.

Smith (1976) showed that, in vertical loading, the
ultimate failure load for a rigid footing increases as the
thickness of the uniform clay foundation becomes smaller
than the footing diameter.   Also, he showed that the ulti-
mate failure load for a "uniform stress" footing (completely
flexible), on homogeneous clay, is lower than that for a
"uniform displacement" footing (completely rigid), in verti-
cal loading.

The ultimate failure pressures predicted by the finite
element solutions are found to be independent of the assumed
initial stresses (Figures 6.48 to 6.50).   However, the
safety factor at first local failure is affected by the
assumed initial stresses as shown on Fig. 6.45d.   Figures
6.48 to 6.50 also show that by decreasing the value of K_o,
or by omitting the soil unit weight from the analysis
(compared to the case with K_o equal to 2), settlements are
increased.

However, as the undrained strength of a cohesive soil
varies with the rotation of principal stresses, and this
rotation is a function of both the stress changes due to
the applied load and the initial stresses in the ground,
therefore, the ultimate failure pressure will be dependent
on K_O (D'Appolonia and Lambe, 1970).

Figure 6.51 shows the load-settlement curves for
three undrained cases 43, 45 and 46 (Table 5.2, Chapter 5).
In these three cases, all parameters are the same, except
the initial modulus and the strain at failure.   The initial
moduli are 300 C_u, 1000 C_u, and 300 C_u, and the strains at
failure are 1.0%, 0.53% and 3.0% for cases 43, 45 and 46,
respectively.   For all three cases, shear strength and
modulus increase linearly with depth, and K_O is one.

This figure indicates that the ultimate failure
pressures and the safety factors at first local failure for
all three cases are equal.   However, as the stress-strain
curve becomes softer, the settlement is increased.

6.2.4 Stress-Strain Curves

Undrained case 40 (Table 5.2, Chapter 5) is considered
to study the stress-strain curve followed by the programme,
and to comapre that with the nominated stress-strain curve
as given to the computer.   The shear strength and modulus,
for this case, increase linearly with depth, the soil unit
weight is 20 KN/m^3 and K_O is 1.5.

Figures 6.52 and 6.53 show the stress paths at two

different points for this case. The coincidence between the nominated stress-strain curves as given to the computer and the stress-strain curves followed by the programme is excellent.

6.2.5 Effects of the Load Eccentricity and Inclination
   on the Failure Load

In Chapter 4, the effects of load eccentricity and inclination on the bearing capacity for both uniform and nonhomogeneous clays were discussed.

The common practice for the effect of load eccentricity on the bearing capacity is to use a reduced footing width in the analysis. The finite element results for the vertical eccentric loading on either uniform or non-homogeneous clays are plotted on Fig. 6.54. Equivalent eccentricity factors were deduced from the failure loads predicted by these calculations, by applying Equations 4.35 and 4.37 of Chapter 4. In this figure the eccentricity factors from the finite element analyses are compared with the eccentricity factor given by the reduced width concept. The agreement between the finite element results and the reduced width concept is good. The eccentricity factor from the finite element analysis is 3% less than that from the reduced width concept, at e/B equal to 0.083 for the uniform clay.

For the bearing capacity of a central inclined load on either uniform or nonhomogeneous clays, the inclination

factors are given on Fig. 4.8 of Chapter 4. For the eccentric and inclined loading, a combination of the eccentricity and inclination factors must be used, as discussed in Chapter 4, section (4.10.3).

The finite element results, for both central inclined and eccentric and inclined loads on either uniform or non-homogeneous clays, are plotted on Fig. 4.8 of Chapter 4, and they are compared with the results given by Vaughan et al (1976). In this figure, equivalent inclination and eccentricity factors were deduced from the failure loads predicted by these calculations, by applying Equations 4.35 to 4.39 of Chapter 4. Generally, the results from the finite element analyses are in good agreement with those given by Vaughan et al (1976), and the maximum difference between these results is less than 10 per cent.

6.2.6 Failure Zones and Rupture Figures

Figures 6.55 to 6.64 represent some failure zones for different cases, and compare them with the rupture figures given by the closed form solutions.

Figure 6.55a shows the failure zone for drained case 2 (Table 5.1, Chapter 5). The applied load is vertical, and it is increased up to 11% of the ultimate failure load. Figure 6.55a shows that the local failure starts from the edge of the footing at a safety factor equal to 46. At the safety factor equal to 9.2, the failure zone is slightly expanded.

In Figures 6.55b to e, the principal stress and strain rotations are given for case 2 at the safety factors equal to 15.3 and 9.2 (in these figures, the extension is marked with an arrow). Although the applied load has not reached the ultimate failure load, the principal stress and strain rotations plots indicate that a wedge of rigid soil is being produced under the footing (Figures 6.55d and e).

Figures 6.56a and b show the failure zones for a vertical load on uniform clay (case 3, Table 5.2, Chapter 5). In Fig. 6.56a, the failure zone starts from the footing edge at a safety factor equal to 1.66 (see also Fig. 6.45b, case 3), and by increasing the load it spreads downward and towards the footing centre line. At the safety factor around 1.17 the failure zone has just reached the centre line. At this point the footing and an adjacent elastic wedge are separated by a band of failed material from the remainder of the unfailed zone. The spread of the failure zone to the centre line is usually coincident with a sharp break in the load-settlement curve (see Fig. 6.45b, load-settlement curve for case 3, $q/q_f = 0.86$). By further increase of the applied load the failure zone continues to spread outward from the footing and upward toward the footing. Figure 6.56b represents the failure zone at the safety factor equal to unity, and the planes of maximum shear stress for case 3, which may be compared with the Prandtl rupture figure.

An identical failure zone to one shown on Fig. 6.56b, at the safety factor equal to one, is reported by Smith

(1978) for the vertical uniform loading on homogeneous clay.

Figure 6.56c shows the principal stress rotations at failure, for case 3.

Figures 6.57a and b show the failure zones for a vertical load on the clay layer whose undrained strength and modulus increase linearly with depth (case 4, Table 5.2, Chapter 5). In Fig. 6.57a, the failure zone starts from the footing edge at the safety factor equal to 2.15 (see also Fig. 6.45b, case 4). By increasing the applied pressure, the failure zone spreads downward and toward the footing centre line, and at the safety factor around 1.09 it reaches the centre line. This safety factor corresponds to a sharp break in the load-settlement curve (see Fig. 6.45b, load-settlement curve for case 4, $q/q_f = 0.92$).

Figure 6.57b represents the failure zone at the safety factor equal to unity, and the planes of maximum shear stress for case 4. The failure zone and these planes may be compared with the typical rupture surfaces postulated by Davis and Booker (1973).

In Fig. 6.58 the principal stress rotations at failure are given for case 4.

Figures 6.56 and 6.57 show that the failure zones in both uniform clay and nonhomogeneous clay cases spread to below the footing, and the boundary between the unfailed rigid wedge and the failed clay does not pass through the footing edges (see also Fig. 6.59 for the contact shear stresses for case 4). This suggests that, in order to satisfy the basic condition of the kinematical admissibility

(Hansen, 1965), the boundary between the unfailed rigid wedge and the failed clay must be tangent to the footing base, and cannot be a straight line (as discussed in Chapter 4, section 4.5).

By comparing Figures 6.56 and 6.57, it is clear that the failure zone for case 4 (non-homogeneous clay) is shallower than the failure zone for case 3 (uniform clay).

Figure 6.60 represents the failure zone for the eccentric and inclined loading on a nonhomogeneous clay (case 40, Table 5.2, Chapter 5). In this figure the applied load required to give a continuous failure zone (at the safety factor equal to 0.9) is 10% higher than the calculated failure load (using Fig. 4.8, Chapter 4) given in Table 6.1.

Figure 6.61 gives the load-settlement curve for case 40 (Table 5.2, Chapter 5), in a log-log scale, and indicates that, for this case, the calculated failure load (using Fig. 4.8, Chapter 4), given in Table 6.1, is 10% less than the ultimate failure load from the finite element analysis. It has to be mentioned that in calculating the ultimate failure load using Fig. 4.8 of Chapter 4, it is assumed that the adhesive contact is maintained over the full width of the footing (as the case for finite element analysis), and the horizontal component of the load is distributed over the full width of the footing. Thus a reduced load inclination is used together with the reduced width concept to reproduce the effect of load eccentricity (see section 4.10.3, Chapter 4).

Figure 6.62a represents the failure zone and the planes of maximum shear stress for case 40, at the safety factor equal to 0.88. The failure zone and planes of maximum shear stress may be compared with the rupture figure given in Fig. 4.9 of Chapter 4.

The principal stress values and rotations for case 40, is given on Fig. 6.62b, at the safety factor equal to 0.9.

These results indicate that the failure zones and the planes of maximum shear stress given by the finite element analysis are in reasonable agreement with the rupture figures given by Prandtl (1920) for uniform clay, Davis and Booker (1973) for nonhomogeneous clay, and the rupture figure for the eccentric and inclined loading given in Fig. 4.9 of Chapter 4. However, in the failure zone given by the finite element analysis for the case of eccentric and inclined loading (Fig. 6.62a), the zone A'CB (Fig. 4.9, Chapter 4) is not an elastic rigid wedge, and it is at the state of failure. Also, the finite element results do not produce the complete failure zone which contains the whole passive zone (see Figures 6.56b, 6.57b and 6.62a). This indicates that, in the finite element analysis, the rupture is produced by a local shear failure mode (section 4.2) of Chapter 4), where the ultimate failure is achieved in a load-settlement plot, but the rupture figure is not yet completed (see Fig. 4.1 of Chapter 4).

By using a stiffer stress-strain curve, the failure zone from the finite element analysis can be enlarged and the general shear failure mode (section 4.2 of Chapter 4)

can be achieved. Figure 6.63 shows the failure zones for two undrained cases 45 and 46 (Table 5.2, Chapter 5) at safety factors equal to unity. This figure indicates that the failure zone for case 45 (stiffer stress-strain curve) is laterally greater than the failure zone for case 46 (softer stress-strain curve). By further increase of the applied load, the failure zone for case 46 expands laterally, and at the safety factor equal to 0.94, the lateral boundaries of the failure zones are the same for both cases. However, for these two cases the stress-strain curves were not stiff enough to produce a general shear failure mode.

Also, in Fig. 6.64, the failure zone from the finite element analysis for an inclined and eccentric load on a nonhomogeneous clay (case 7, Table 5.2, Chapter 5) is compared with the rupture figure given in Chapter 4, section (4.10.4). The agreement between this rupture figure and the failure zone from the finite element analysis is good.

6.3 Finite Element Results, Cyclic Loading

6.3.1 General

This section is concerned with the finite element results for cyclic loading. The cyclic loads may occur rapidly (earthquakes, explosive loads etc.) or at slower rates (wave loads) where dynamic effects are negligible. From these, the latter form is considered in these studies.

In studying the behaviour of off-shore structures under dead weight loading and cyclic wave loading, as

mentioned by Vaughan et al (1976), clays, in beds of modest thickness, may remain substantially undrained during both dead weight loading and the critical design wave loading, and thus the undrained loading of clays is likely to be the critical design condition for the off-shore structures.

The progressive weakening of the soil properties due to cyclic loading (as the effective stresses are decreasing) is not considered in these analyses, and in all cases studied, a stable rocking is achieved after a few cycles.

Figures 6.65 to 6.129 represent the finite element results for the cyclic loading of the clay under undrained conditions. In these figures, the numbers on the curves designate the loading stages, as discussed in Chapter 5, section (5.3.2). Properties and geometries of the different cases are given in Table 5.3 of Chapter 5.

Discussion of the results is divided into two subsections, namely, displacements and stresses. In each subsection, the effects of cyclic loading, correct shear unloading and reloading modelling, non-linearity, and an increase in the overall safety factor against ultimate failure on displacements and stresses are considered.

6.3.2 Displacements

Figures 6.65 to 6.82 represent the displacements for different cases. For all cases, except the linear case 48 (Table 5.3, Chapter 5), undrained shear strength and modulus increase linearly with depth. For cases 42, 48 and 49,

the shear unloading and reloading modelling is according to Fig. 5.1c of Chapter 5, and both unloading and reloading moduli are equal to 3.5 times the initial modulus. For cases 47 and 47,1 both unloading and reloading moduli are equal to the tangent modulus at the corresponding stress level (see also Fig. 5.1a of Chapter 5).

Discussion on the results will be presented from case 42 to case 49, respectively.

Case 42   Figures 6.65 to 6.69 represent the displacement plots for case 42 (Table 5.3, Chapter 5). Figure 6.65 shows the vertical and horizontal settlements of the footing, under cyclic loading, and compares them with those given by Milovic et al (1970) using an average modulus. For the first half cycle of the wave load, a load reduction factor equal to 4.5/11 is used, which is calculated from the theory of subgrade reaction (see section 5.3.2 of Chapter 5). This figure indicates that the rocking of the footing is stable after 1.5 complete load cycles.

Figure 6.65 also shows that the settlements and the tilt given by Milovic et al (1970), using an average modulus, are greater than those for case 42. For the vertical load, the difference in settlements is 7%. After the first half load cycle, the footing tilt given by Milovic et al (1970) is almost three times the tilt for case 42. This difference in footing tilt increases by further rocking, because the shear unloading and reloading modelling of case 42 tends to decrease the tilt, before a stable

situation is achieved, as the rocking is continued.

Figure 6.66 shows the settlement and heave for case 42, and it indicates that the effect of cyclic loading is to increase both settlement and heave. After a stable rocking is achieved, centre settlement is increased 15%, and the maximum increase in heave is 40% compared to the values at the end of previous cycle. These effects decrease by depth as shown on Fig. 6.67.

The horizontal displacements for case 42 are shown on Fig. 6.68. This figure indicates that the horizontal displacements are stable after 1.5 complete cycles.

Figure 6.69 represents the centre horizontal and vertical settlements plus the differential settlement between two edges of the footing. This figure shows that, before a stable rocking is achieved, the centre vertical settlement increases, the centre horizontal settlement and the differential settlement between two edges decrease, as the rocking continues. Obviously, this effect is due to a larger unloading and reloading modulus, compared to the tangent modulus.

Cases 47 and 47,1   For these two cases, unloading and reloading paths are on the first loading curve (see Fig. 5.1a of Chapter 5). All the parameters are the same for both cases, except the load reduction factor used at the first half loading cycle. For case 47, this reduction factor is 4.5/11, while for case 47,1 it is 0.5.

The rocking in these two cases is stable after the

first complete load cycle (Figures 6.70 and 6.71). The symmetry of displacements is achieved in case 47,1 (see Fig. 6.71). Also, in Figures 6.70 and 6.71 the results for case 47 and 47.1 are compared with those given by Milovic et al (1970), using an average modulus. After application of the vertical load (like case 42), the settlement given by Milovic et al (1970) is 7% greater than the settlements for these two cases. The tilt of the footing given by Milovic et al (1970) is almost twice that of those for case 47 and 47,1.

Figures 6.72 and 6.73 show the settlement, the heave, and the horizontal displacement for case 47. Obviously, as the unloading, reloading and loading moduli are equal, a stable rocking is achieved after the first complete load cycle.

Figure 6.74 represents the centre vertical and horizontal settlements, and the differential settlement between two edges, for case 47.

By comparing the results for case 42 (Figures 6.65 to 6.69) with the results for case 47 (Figures 6.70 to 6.74), it can be concluded that the correct shear unloading and reloading modelling (case 42) tends to:-

1. increase the number of load cycles required for the achievement of a stable rocking, and

2. decrease displacements and tilt of the footing.

Case 48   Figures 6.75 to 6.78 represent the displacements for case 48 (Table 5.3, Chapter 5). For this case, the

behaviour is linear, both unloading and reloading moduli are equal to 3.5 E_i, and the load reduction factor, used at the first half load cycle, is 4.5/11.

Figure 6.75 shows that the rocking is stable after the first complete load cycle. Also, in this figure the finite element results are compared with those given by Milovic et al (1970). After application of the vertical load, the settlement given by Milovic et al (1970) is 25% more than the settlement for case 48. After first half cycle of the rocking, the footing tilt given by Milovic et al (1970) is almost 5 times the tilt for case 48. By further increase of the rocking, and before the achievement of a stable situation, this difference in tilt increases.

Figures 6.76 and 6.77 give the settlement, the heave and horizontal displacements for case 48. In both figures the rocking is stable after the first complete cycle. However, the interesting feature of Fig. 6.76 is that, at the end of the first complete cycle, the footing is almost horizontal (zero tilt).

Figure 6.78 gives values of centre vertical and horizontal settlements, and the differential settlement between two edges. This figure also indicates that the rocking is stable after the first complete cycle, and at the end of each complete cycle (loading stages 3, 5 etc.), the differential settlement between the two edges is zero.

By comparing the results for case 42 (Figures 6.65 to 6.69) with the results for case 48 (Figures 6.75 to 6.78), for the effects of non-linearity on displacements, it can be

concluded that the non-linearity tends to increase the number of cycles required for the achievement of a stable rocking, and to increase the displacements.

Case 49   Figures 6.79 to 6.82 represent displacements for case 49 (Table 5.3, Chapter 5).   All parameters for case 49 are the same as those for case 42, except the horizontal load.   The applied horizontal load for case 49 is 60% of that for case 42, which results in an increase for the overall safety factor against ultimate failure from 1.57 to 2.57 (see also Table 5.3 of Chapter 5).

By comparing the results for case 49 (Figures 6.79 to 6.82) with those for case 42 (Figures 6.65 to 6.69), it is clear that the overall behaviour is the same in both cases, and 40% reduction in horizontal load does not affect the behaviour from the qualitative point of view.   Therefore, the conclusions for case 42 will also be valid for case 49, for displacements.

6.3.3 Stresses

Figure 6.68 shows the distribution of contact pressure, contact shear stress, vertical stress and horizontal stress given by Milovic et al (1970), using the same loading stages as for cases 42, 47, 48 and 49.   These stresses will be compared to those from the finite element analyses, later in this section.

Discussion on the stresses from the finite element analyses are divided into the following subsections:-

1.   contact pressure and shear stress,

2.   stress distribution,

3.   stress changes and stress paths, and

4.   mobilized shear stress.

6.3.3.1 Contact Pressure and Shear Stress

Figures 6.84 to 6.93 represent the contact pressures and contact shear stresses for different cases.   The contact pressures considered in these figures are equal to the average of four Gauss points stresses, minus the vertical initial stresses at the same level.

In Figures 6.84 and 6.85 the contact stresses for case 42 (Table 5.3, Chapter 5) are given.   For this case, both unloading and reloading moduli are equal to 3.5 E_i. For these stresses, the rocking is stable after 1.5 complete load cycles.

By comparing the contact stresses for case 42 with those given by Milovic et al (1970) in Fig. 6.83, it is clear that the contact pressures for case 42 are a maximum of 10% greater than those given by Milovic et al (1970), on the footing centre line.   Near the edges, due to the non-linearity effect in case 42, the contact pressures from the finite element analysis are smaller than those given by Milovic et al (1970).   The contact shear stresses for case 42 are on average 10% less, on the centre line, and on average 25% more, near the edges, than those given by Milovic et al (1970).

Figures 6.86 to 6.89 represent the contact pressures and the contact shear stresses for cases 47 and 47,1 (Table 5.3, Chapter 5). For these two cases, unloading and reloading paths are on the first loading curve (see Fig. 5.1a of Chapter 5). All parameters are the same for both cases, except the load reduction factors, which are 4.5/11 for case 47 and 0.5 for case 47,1.

Figures 6.86 to 6.89 show that in these two cases, stresses are stable after first complete cycle. For case 47,1, symmetry is achieved.

By comparing the results for case 42 ($E_u = E_r = 3.5 E_i$) with the results for case 47 ($E_u = E_r = E_t$), Figures 6.84 to 6.87, it is clear that correct unloading and reloading modelling (case 42) tends to:-

1. increase the contact pressure at the central section of the footing and decrease near the edges,

2. increase the number of load cycles required for the achievement of the stable stresses, and

3. increase the contact shear stress in the loaded half section of the footing, and decrease in the other half.

Figures 6.90 and 6.91 give the contact pressures and the contact shear stresses for case 48 (Table 5.3, Chapter 5). The behaviour is linear for this case, and both unloading and reloading moduli are equal to 3.5 E_i. These figures show that the stresses are stable after first com-

plete load cycle.

By comparing these figures with the results for case 42 (Figures 6.84 and 6.85), it is clear that the non-linearity (case 42) tends to:

1. increase the contact stresses at the central section of the footing, and decrease near the edges, and

2. increase the number of cycles required for the achievement of the stable stresses.

In Figures 6.92 and 6.93 the contact pressures and contact shear stresses for case 49 (Table 5.3, Chapter 5) are given. All parameters used in case 49, are the same as those for case 42, except the applied horizontal load, which is 60% of that for case 42.

By comparing the results for case 42 (Figures 6.84 and 6.85) with the results for case 49 (Figures 6.92 and 6.93), it is clear that by 40% reduction in horizontal load, the overall behaviour is not changed from the qualitative point of view, and for case 49 (like case 42) the stable stresses are achieved after 1.5 complete load cycles. However, obviously, the contact shear stresses are reduced for case 49.

6.3.3.2 Stress Distribution

Figures 6.94 to 6.106 represent the principal stress distribution for different cases. The stresses considered in these figures are equal to the average of four Gauss

points stresses, minus the initial stresses at the same level.

Figures 6.94 to 6.96 represent the principal stresses for case 42 (Table 5.3, Chapter 5). These figures indicate that the principal stresses become stable after 1.5 complete load cycles. Also, from these figures, it is clear that the effect of rocking on stresses is a minimum near the centre line, and it increases towards the edges and outside the loaded area. The effect of rocking on minor principal stresses decreases very rapidly with depth.

As the principal stress rotation is very small near the centre line, therefore Fig. 6.94 can be compared with Fig. 6.83c given by Milovic et al (1970). This comparison indicates that the stresses from case 42 (at the end of dead weight loading) are 12% more than the stresses given by Milovic et al (1970), near the ground surface. At great depths (e.g. near the underlying bedrock), the stresses from case 42 (at the end of dead weight loading)are 10% smaller than those given by Milovic et al (1970).

Figures 6.97 to 6.99 show the principal stresses for case 47 (Table 5.3, Chapter 5). These stresses are stable after the first complete load cycle. The effect of rocking on the stresses is a minimum near the footing centre line, and it increases toward the edges and outside the loaded area. For minor principal stresses, the effect of rocking decreases very rapidly with depth.

By comparing the results for case 42 ($E_u = E_r = 3.5 E_i$) with the results for case 47 ($E_u = E_r = E_t$), Figures 6.94

to 6.99, it is clear that the correct shear unloading and reloading modelling (case 42) tends to:-

1. increase the number of load cycles required for the achievement of stable stresses during rocking,

2. decrease the minor principal stresses at shallow depths, and

3. increases the major principal stresses at the central section of the footing, and decrease them near the edges and outside the loaded area.

Figures 6.100 to 6.103 represent the principal stresses for linear case 48 (Table 5.3, Chapter 5). For this case, both unloading and reloading moduli are equal to 3.5 E_i. Stresses are stable after the first complete load cycle. The effect of the rocking on stresses is minimum near the footing centre line and increases towards edges, and outside the loaded area. The effect on the minor principal stresses decreases very rapidly with depth.

By comparing the results for non-linear case 42 (Figs. 6.94 to 6.96) with the results for linear case 48 (Figs. 6.100 to 6.103), it is clear that the non-linearity (case 42) tends to:-

1. increase the number of load cycles required for the achievement of the stable stresses,

2. increase the major principal stresses at the central section of the footing, and decrease

near the edges and outside the loaded area, and

3. increase the minor principal stresses at shallow
depths and decrease at great depths.

Figures 6.104 to 6.106 represent the principal stresses
for case 49 (Table 5.3, Chapter 5). Stresses are stable
after first 1.5 complete load cycles. The effect of the
rocking on stresses is a minimum near the footing centre
line and increases toward the edges, and outside the loaded
area. The effect on the minor principal stresses decreases
very rapidly with depth.

6.3.3.3 Stress Changes and Stress Paths

Figures 6.107 to 6.111 represent the principal stress
changes and rotations during dead weight and cyclic loading,
for different cases. The stresses considered in these
figures are the stresses in one of the Gauss points minus
the initial stresses at the same level.

All these figures show large rotations of principal
stresses beneath and outside the loaded area. However,
toward the outside of the loaded area, these rotations
increase considerably. In all cases, large stress changes
occur just under the edge of the footing.

By comparing the results for case 42 ($E_u = E_r = 3.5\ E_i$)
and case 47 ($E_u = E_r = E_t$), Figures 6.107 and 6.108, it is
clear that the correct unloading and reloading modelling
(case 42) leads to smaller principal stress rotations and
changes compared to the case without unloading and reload-
ing modelling (case 47). Outside the loaded area, the

principal stress rotations for case 42 are almost half of those for case 47, when the cyclic loading causes a reduction in shear stress below that caused by dead weight loading (loading stages 2,4 etc. in these figures).

By comparing Figures 6.107 and 6.110 (cases 42 and 48), it is clear that the non-linearity (case 42) tends to decrease the principal stress changes near the edges, and to decrease the principal stress rotations beneath the footing and to increase them outside the loaded area. Outside the loaded area, the principal stress rotation for case 42 is almost twice the rotation for case 48 when the cyclic loading causes a reduction in shear stress below that caused by the dead weight loading (loading stages 2,4 etc. in these figures).

By comparing Figures 6.107 and 6.111, it is clear that, just outside the loaded area, the principal stress rotations for case 49 (overall safety factor against ultimate failure = 2.57, Table 5.3, Chapter 5) are a maximum of 50% more than those for case 42 (overall safety factor against ultimate failure equal to 1.57, Table 5.3, Chapter 5), when the cyclic loading causes a reduction in shear stress below that caused by the dead weight loading.

Figures 6.112 to 6.116 represent some total stress paths for different cases. For all cases, the maximum stress changes occur just under the footing edge.

These figures also indicate that the non-linearity and the correct unloading and reloading modelling tends to increase the shift in the stress paths per cycle. The

linear case 48 gives greater deviatoric stresses than the non-linear case 42.

Figures 6.112 and 6.116 show that the slope of cyclic stress paths for case 42 (overall safety factor against ultimate failure = 1.57, Table 5.3, Chapter 5) are less than those for case 49 (overall safety factor against ultimate failure = 2.57, Table 5.3, Chapter 5). In other words, the change in deviatoric stress during rocking is greater for case 49 than that for case 42. Also, a 40% reduction in the horizontal load (case 49) does not increase the safety factor against local failure (see also Figures 6.126 and 6.129).

6.3.3.4 Mobilized Shear Stress

Figures 6.117 to 6.125 represent the contours of mobilized shear stress ratio for different cases. In Fig. 6.117 the stress ratios after application of the vertical load are shown. Figures 6.118 to 6.120 give the contours of shear stress ratio for case 42. In Figures 6.121 and 6.122 these contours for case 47 are given. Finally, Figures 6.123 to 6.125 represent these contours for case 49 (for differences between cases, see Table 5.3, Chapter 5).

These figures indicate that the rocking tends to increase the size of mobilized shear stress ratio contours, before a stable situation is achieved. At shallow depths, during rocking, the mobilized shear stress ratio contours spread downward under the loaded edge of the footing, and they spread sideways under the unloaded edge of the footing (see Figures 6.117 to 6.125).

6.3.4 Behaviour of the Solution

Figures 6.126 to 6.129 represent the stress-strain curves for different cases. In all cases, the stress-strain curves followed in the programme coincide well with the nominated stress-strain curves as given to the computer.

However, in Figures 6.126 and 6.129, when the correct unloading and reloading modelling is used, during reloading, a small error in stress path, due to rather large load increments, occurred. This error can be corrected by using much smaller load increments, obviously, with higher computer cost.

6.4 Application of the Analyses to Actual Structures

The real foundation problem is three-dimensional, and non-linear finite element analyses in three dimensions require very large computer capacities. It is thus desirable to consider ways of applying the two dimensional analysis to the three dimensional problem. The simplest method, for stability analyses only and as used in bearing capacity theory, is to deal with load eccentricity by assuming an equivalent rectangle, to deal with load inclination and foundation variability by two dimensional theory and to use an empirical shape factor to allow for three dimensional effects. An alternative, suitable for stress analyses, is to establish an equivalent rectangle for the actual foundation, and to perform a two-dimensional analysis of a strip of the same width as the rectangle. A second alternative is to use a linear elastic analysis, which can

be performed more readily in three dimensions, to predict the proportion of the load which is carried by the central strip of the actual foundation, and to perform a non-linear analysis using this proportion of the total load as the load per unit length on a strip foundation with a width the same as the central strip of the actual foundation (Vaughan et al, 1976).

For cyclic loading, the results of three-dimensional analysis could be deducted from the results of two-dimensional analysis by using the proper coefficients, which are (for a point) function of the zone (El-Ghamrawy, 1978).

6.5   Conclusions

The non-linear finite element technique was used to study the undrained behaviour of shallow foundations under monotonic and cyclic loadings.

The conclusions made from these studies will be considered in two groups, namely, monotonic loading and cyclic loading.

6.5.1 Monotonic Loading

The finite element results were compared with the closed form solutions.   Reasonable agreement was found between the finite element results, prior to local failure occurring, and the elastic solutions.   The agreement was good between the ultimate failure loads and the failure zones from the finite element analyses (for both vertical, and inclined and eccentric loading on either uniform clay

or nonhomogeneous clay) with those from the plasticity solutions.

Effects of the layer thickness, the side boundaries and footing rigidity on stresses, displacements and failure loads were studied, and the same results as reported in the literature (e.g. Höeg et al, 1968; and D'Appolonia and Lambe, 1970) were found. Thus, soundness of the technique used was confirmed.

The effect of the material non-linearity is to increase the vertical stress at the central section of the footing and to decrease it near the edges and outside the loaded area; also, to increase the horizontal stresses, and displacements.

Correct modelling of the shear unloading (with K_o greater than one) tends to decrease settlement and heave; and to increase the vertical stress at the central section of the footing and decrease it near the footing edges. The effects on stresses are small, for the cases considered, and decrease as the ultimate failure is approached.

The ratio $E_o/\lambda B$ (nonhomogeneity) has a marked effect on stresses and displacements.

It was found that the side boundaries distance from the footing centre line, layer thickness, initial stresses and correct modelling of the shear unloading have no effect on the ultimate failure load. However, the safety factor at first local failure is affected by the side boundary distance from the centre line and by the assumed initial stresses.

The ratio $C_{uo}/\rho B$ (nonhomogeneity) has a marked effect on the ultimate failure load and the safety factor at first local failure. It was found that by increasing the ratio $C_{uo}/\rho B$, the safety factor at first local failure is decreased, provided that the ratio $f = (1-K_o)\sigma'_{vo}/2C_u$ is equal to zero.

From the qualitative point of view, the effect of the ratio f on the safety factor at first local failure of a nonhomogeneous clay is the same as for a uniform clay.

For a rigid footing with vertical load, on either uniform clay or nonhomogeneous clay, the failure zone starts from the footing edge, and by increasing the applied load it spreads downward and toward the footing centre line. The spread of the failure zone to the centre line is usually coincident with a sharp break in the load-settlement curve. By further increase of the applied load the failure zone continues to spread outward from the footing and upward toward the footing. For the nonhomogeneous clay, the failure zone is shallower than the failure zone for uniform clay.

These failure zones, in both uniform and nonhomogeneous clays, spread to the underneath of footing, and the boundary between the unfailed rigid wedge and the failed zone does not pass through the footing edges. This suggests that, in order to satisfy the basic condition of the kinematical admissibility,the boundary between the unfailed rigid wedge and the failed clay must be tangent to the footing base, and cannot be a straight line.

These studies indicate that the results are highly sensitive to soil modulus, strength and in-situ stresses. Therefore, in a stress analysis the greatest attention must be given to the correct selection of the parameters used, in order to obtain results as close to the reality as possible.

6.5.2 Cyclic Loading

The effects of the cyclic loading, correct shear unloading and reloading modelling (Fig. 5.1c, Chapter 5), and the material non-linearity on stresses and displacements were studied, using the finite element method. Findings from these studies are as follows:-

The effects of rocking (before a stable situation is achieved) are to:

1. increase both settlement and heave, but decrease the footing tilt, and

2. increase the size of the mobilized shear stress ratio contours.

Also, it was found that the effect of rocking on the principal stress changes is considerable near the footing edges, and the effect on the principal stress rotations is considerable outside the loaded area.

The effects of correct unloading and reloading modelling (compared to case without unloading and reloading modelling) are to:

1. increase the number of load cycles required
    for the achievement of a stable rocking,

2. decrease displacements and tilt of the footing,

3. decrease the minor principal stresses at shallow
    depths, and increase the major principal stresses
    at the central section of the footing and
    decrease them near the edges and outside the
    loaded area, and

4. decrease the principal stress rotation.

The effects of material non-linearity (compared to the
linear case) are to:-

1. increase the number of load cycles required for
    the achievement of a stable rocking,

2. increase displacements,

3. increase the major principal stresses at the
    central section of the footing and decrease them
    near the edges, and outside the loaded area,

4. increase the minor principal stresses at shallow
    depths and decrease them at great depths, and

5. decrease the principal stress rotations beneath
    the footing and increase them outside the loaded
    area.

Table 6.1   Values of Failure Pressures (from theory)

Case No.	Failure Pressure KN/M²	Reference	Case No.	Failure Pressure KN/M²	Reference
1	46300	Eq. 4.7	25	170	Eq. 4.37
2	4630	Eq. 4.7	26	149	Eq. 4.37
3	257	Eq. 4.31	27	129	Eq. 4.37
4	215	Eq. 4.34	28	144	Eq. 4.38
5	77.1	Eq. 4.39	29	62.6	Eq. 4.38
6	77.1	Eq. 4.39	30	30.3	Eq. 4.38
7	160	Eq. 4.39	31	9.3	Eq. 4.38
8	160	Eq. 4.39	32	81.7	Eq. 4.39
9	215	Eq. 4.34	33	35.8	Eq. 4.39
10	160	Eq. 4.39	34	17.3	Eq. 4.39
11	215	Eq. 4.34	35	5.3	Eq. 4.39
12	215	Eq. 4.34	36	212	Eq. 4.38
13	160	Eq. 4.39	37	133.5	Eq. 4.39
14	160	Eq. 4.39	39	356	Eq. 4.39
15	160	Eq. 4.39	40	356	Eq. 4.39
16	160	Eq. 4.39	42	315	Eq. 4.39
18	270	Eq. 4.31	43	890	Eq. 4.34
19	247	Eq. 4.35	44	514	Eq. 4.31
20	225	Eq. 4.35	45	890	Eq. 4.34
21	202.5	Eq. 4.35	46	890	Eq. 4.34
22	180	Eq. 4.35	47	315	Eq. 4.39
23	215	Eq. 4.34	49	427.5	Eq. 4.39
24	192	Eq. 4.37			
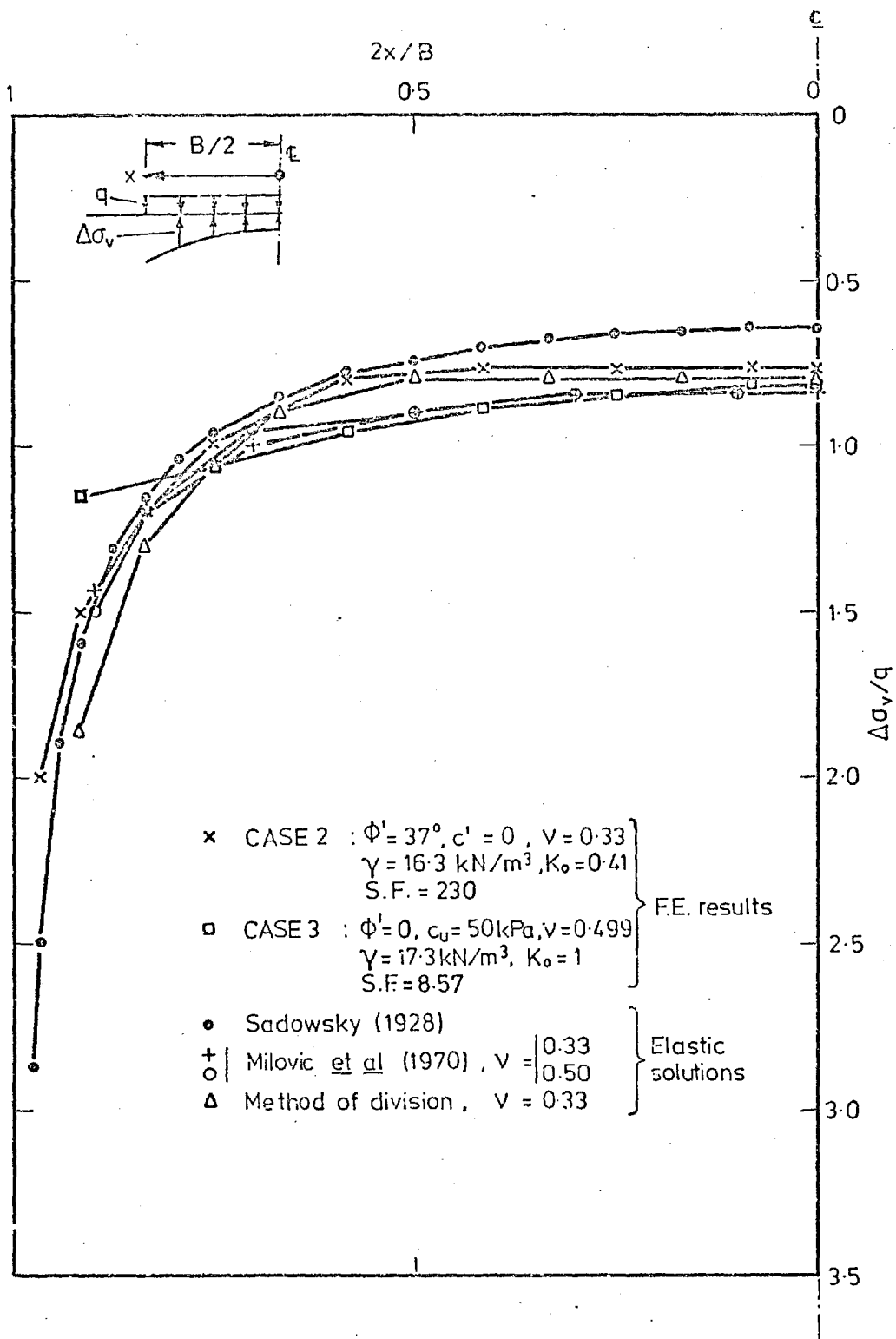
Fig. 6.1 Contact pressure distribution.
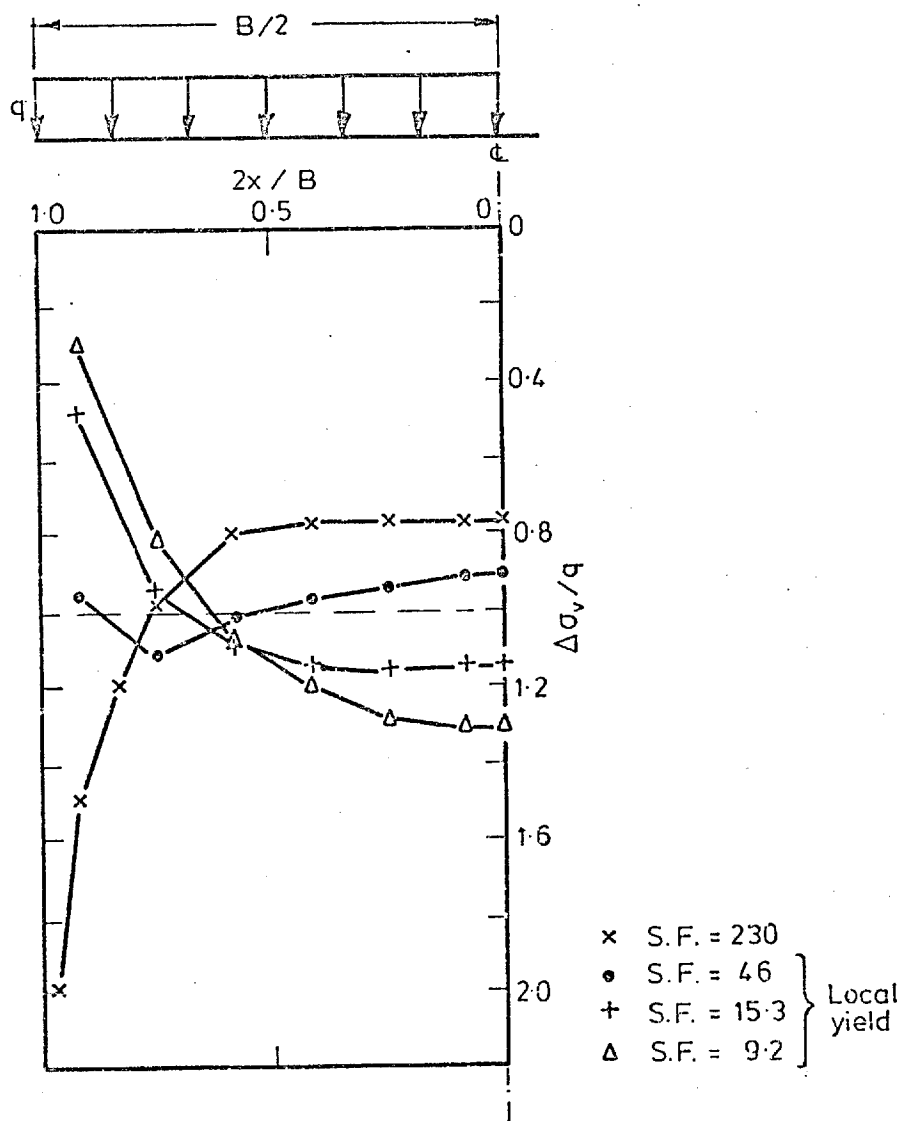
CASE 2

$\Phi' = 37°$, $c' = 0$, $\gamma = 16\cdot3$ kN/m³

$K_o = 0\cdot41$, $\nu = 0\cdot33$

Fig. 6.2   Effect of the stress level on the contact
pressure distribution (drained).
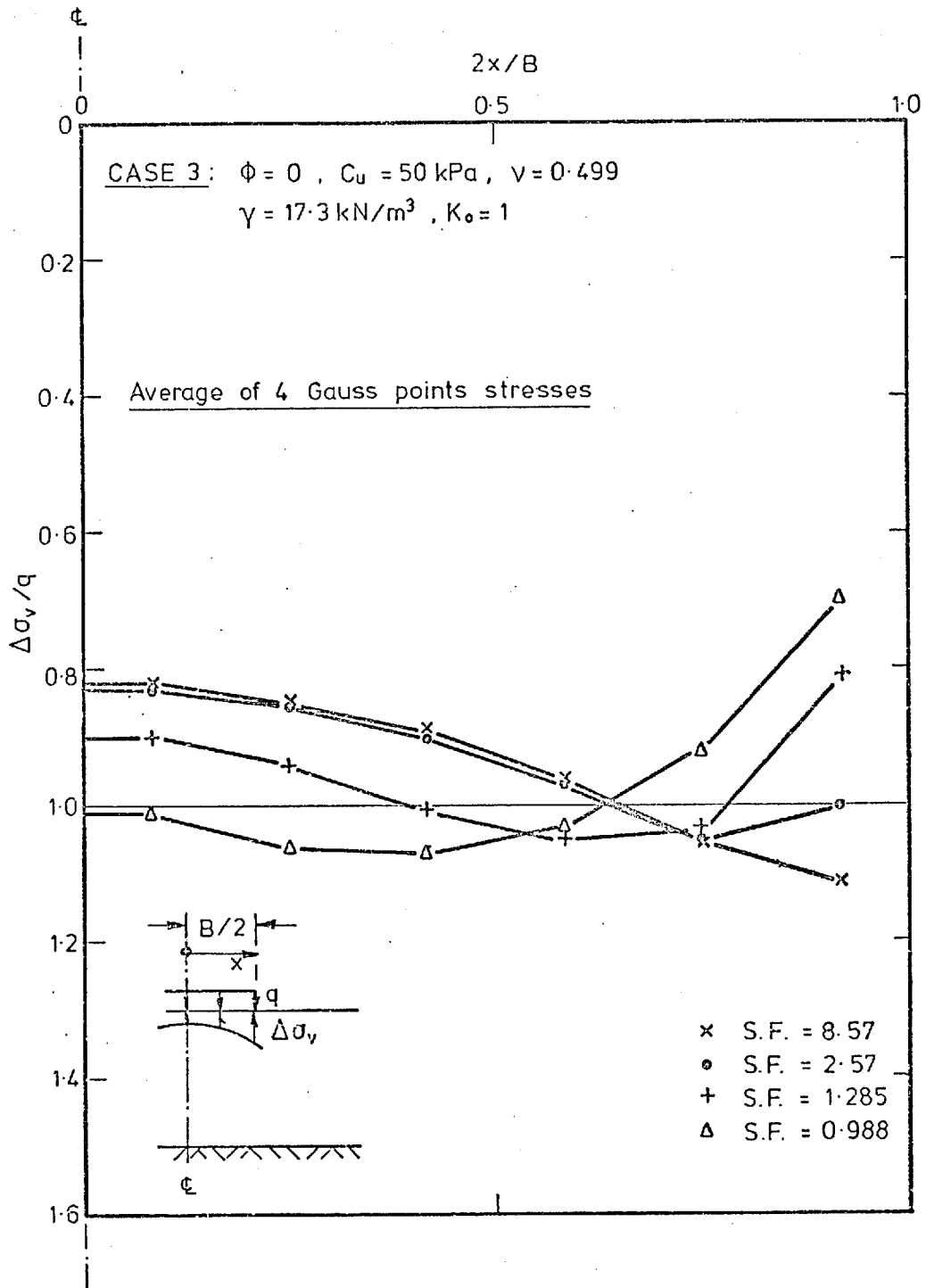
Fig. 6.3a   Effect of the stress level on the contact
pressure distribution (undrained).
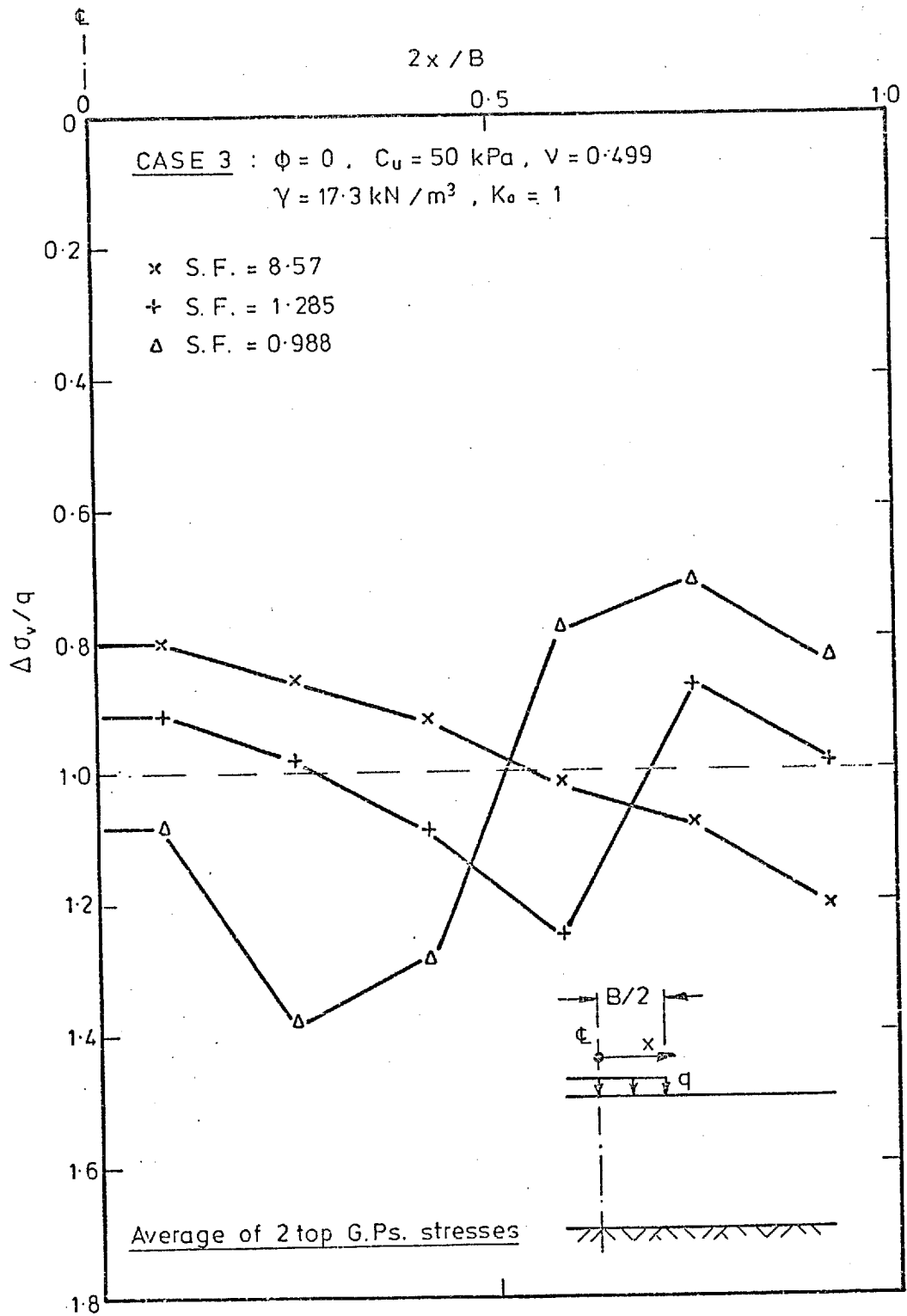
Fig. 6.3b   Effect of the stress level on the contact
pressure distribution (undrained).
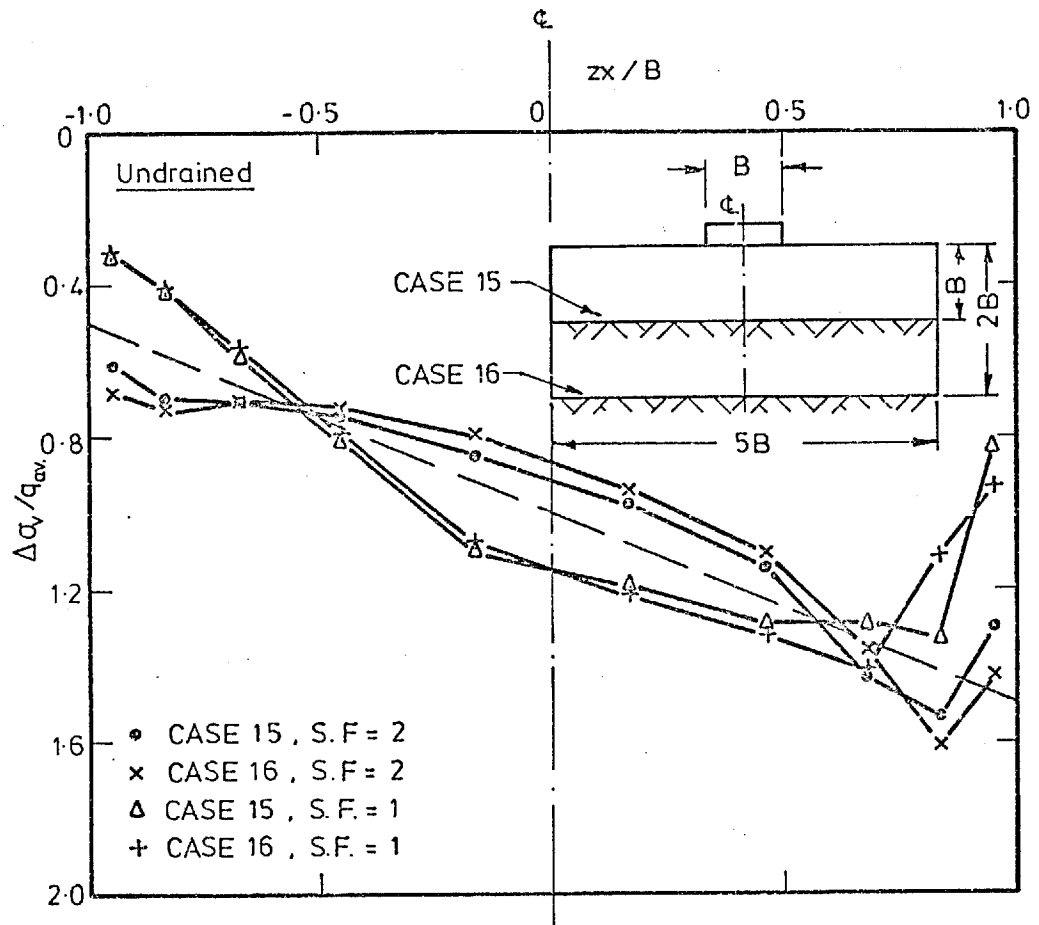
Fig. 6.4   Effect of layer thickness on the contact
            pressure distribution (eccentric and inclined
            load).
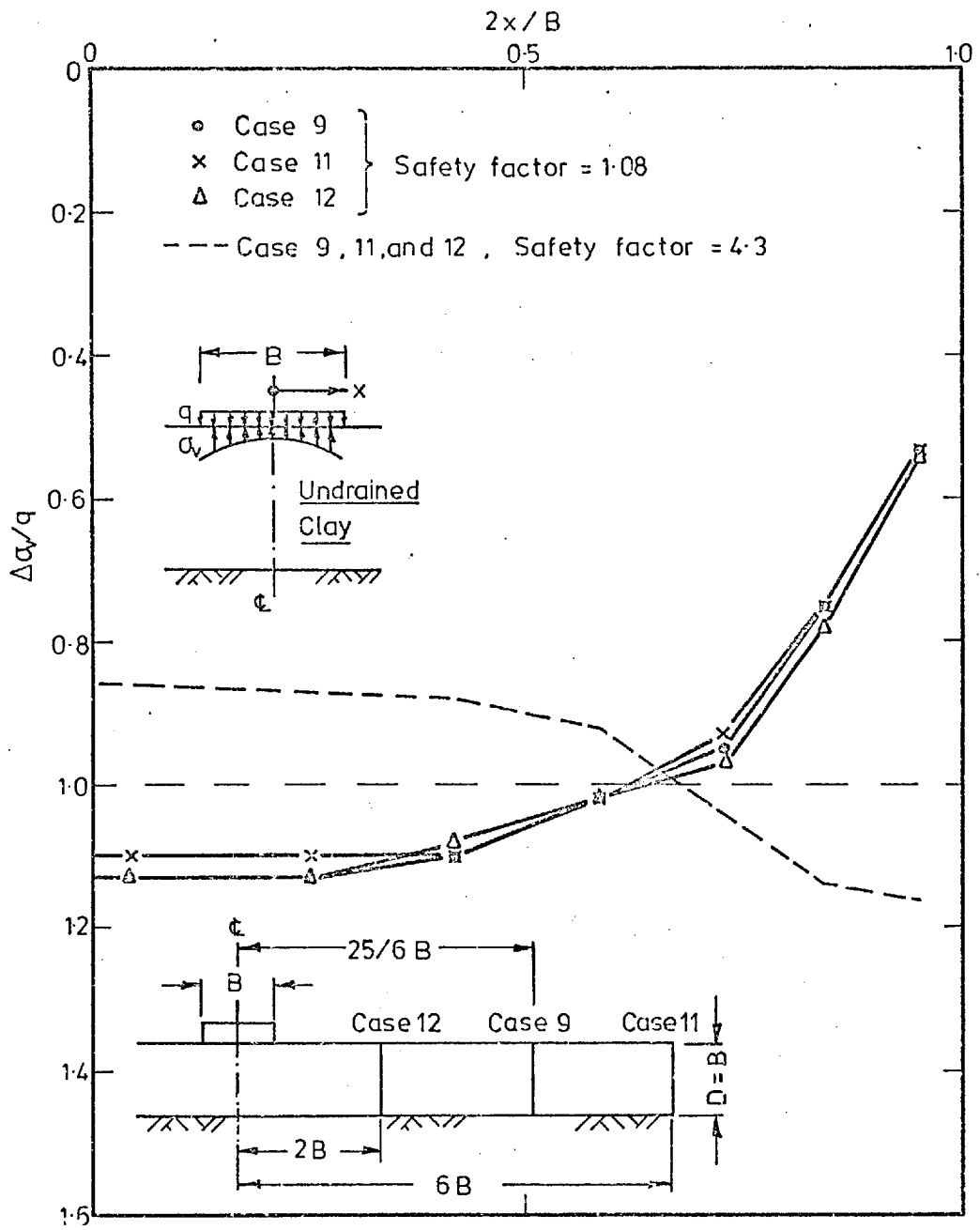
Fig. 6.5 Effect of the side boundaries on the contact pressure distribution.
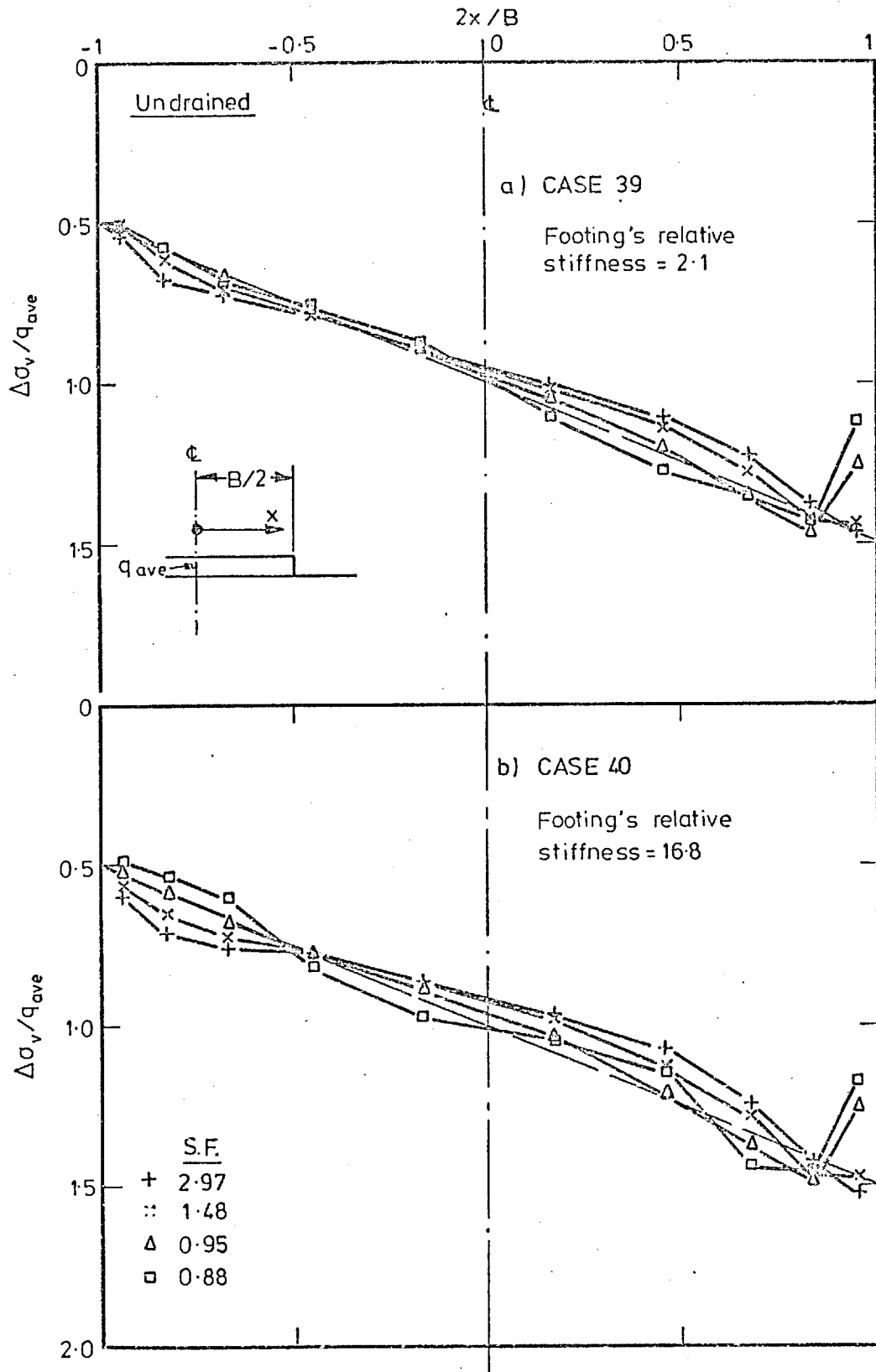
Fig. 6.6   Effect of footing rigidity on the contact
            pressure distribution (eccentric and inclined
            load).
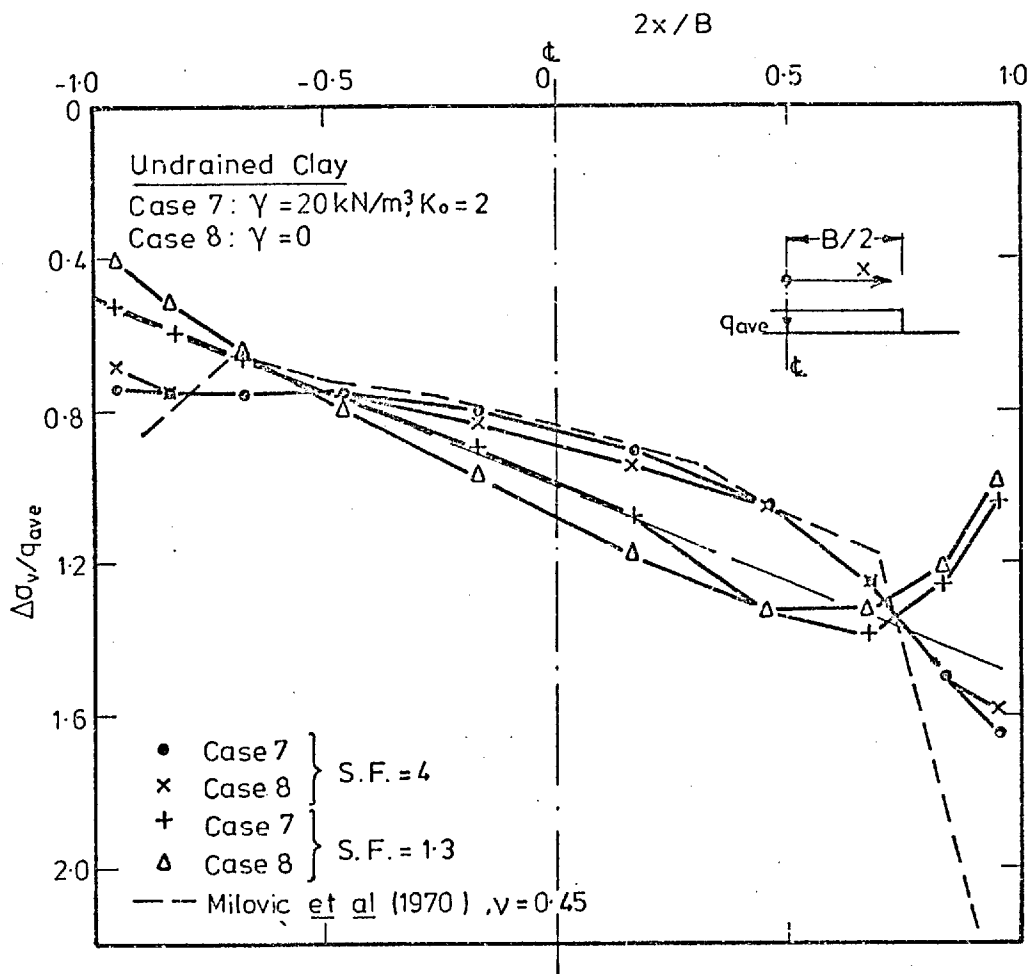
Fig. 6.7 Effect of the soil unit weight on the contact pressure distribution (eccentric and inclined load).
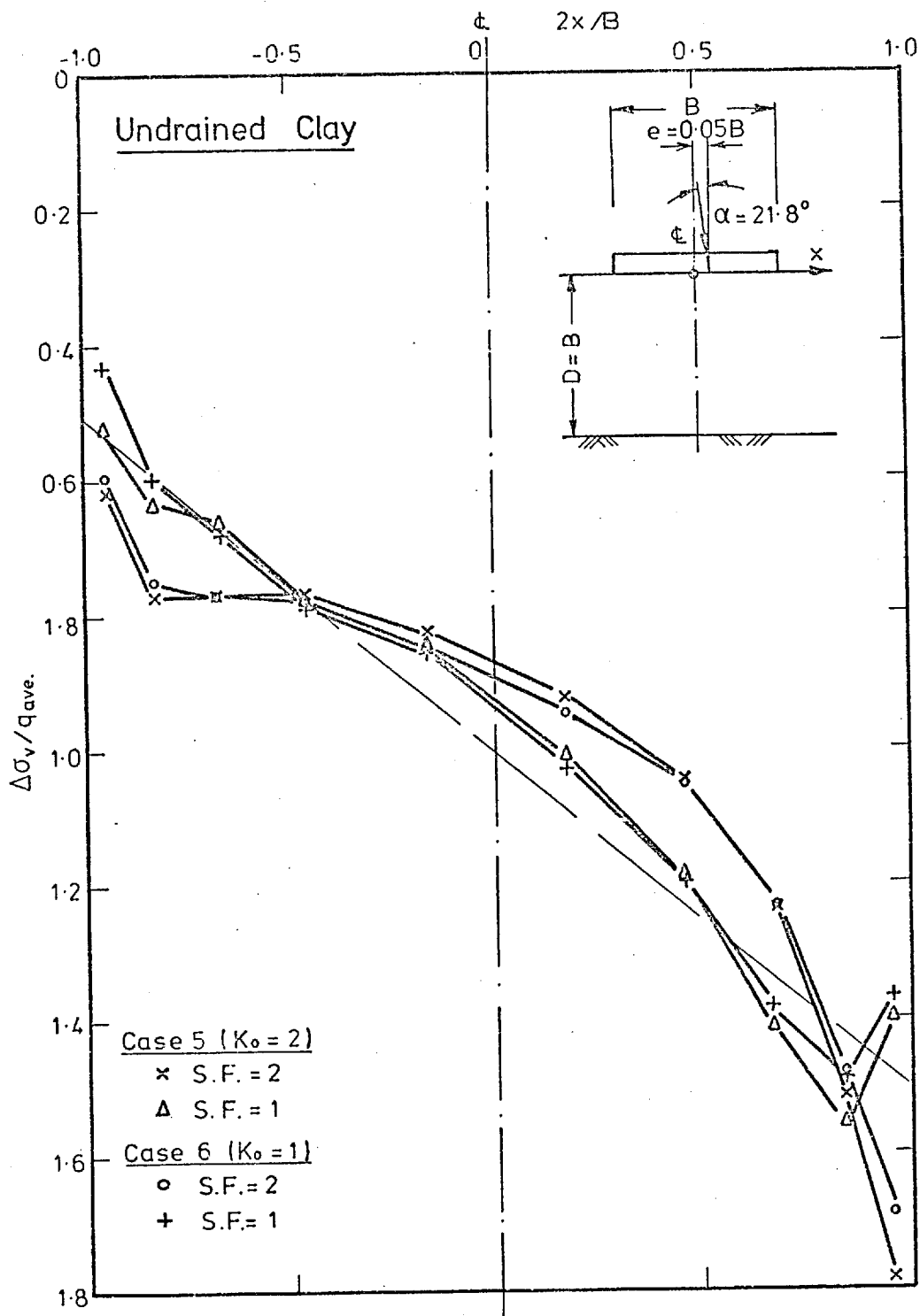
Fig. 6.8   Effect of K_o on the contact pressure distribution (eccentric and inclined load).
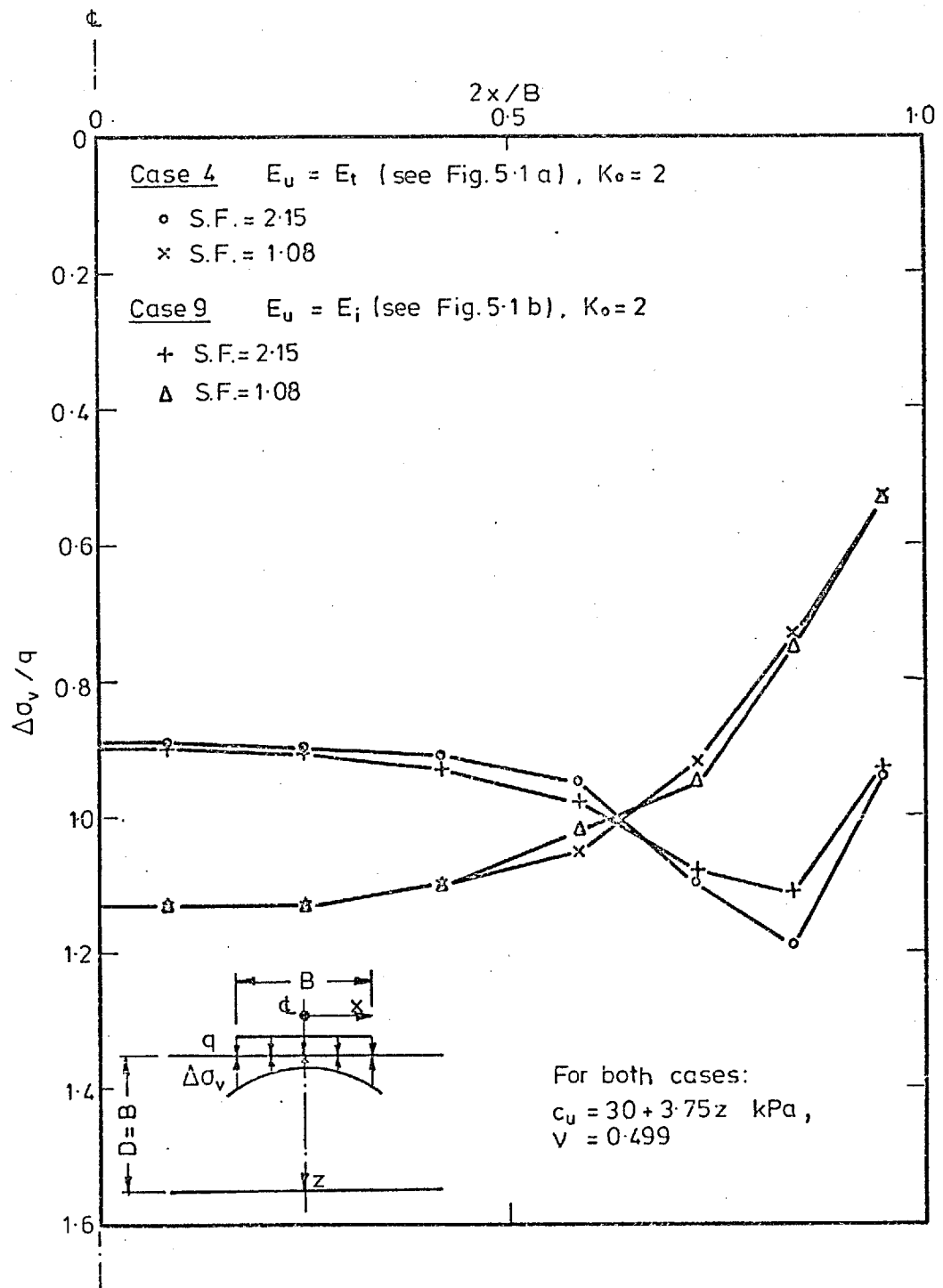
Fig. 6.9 Effect of the shear unloading modelling on the contact pressure distribution (undrained).
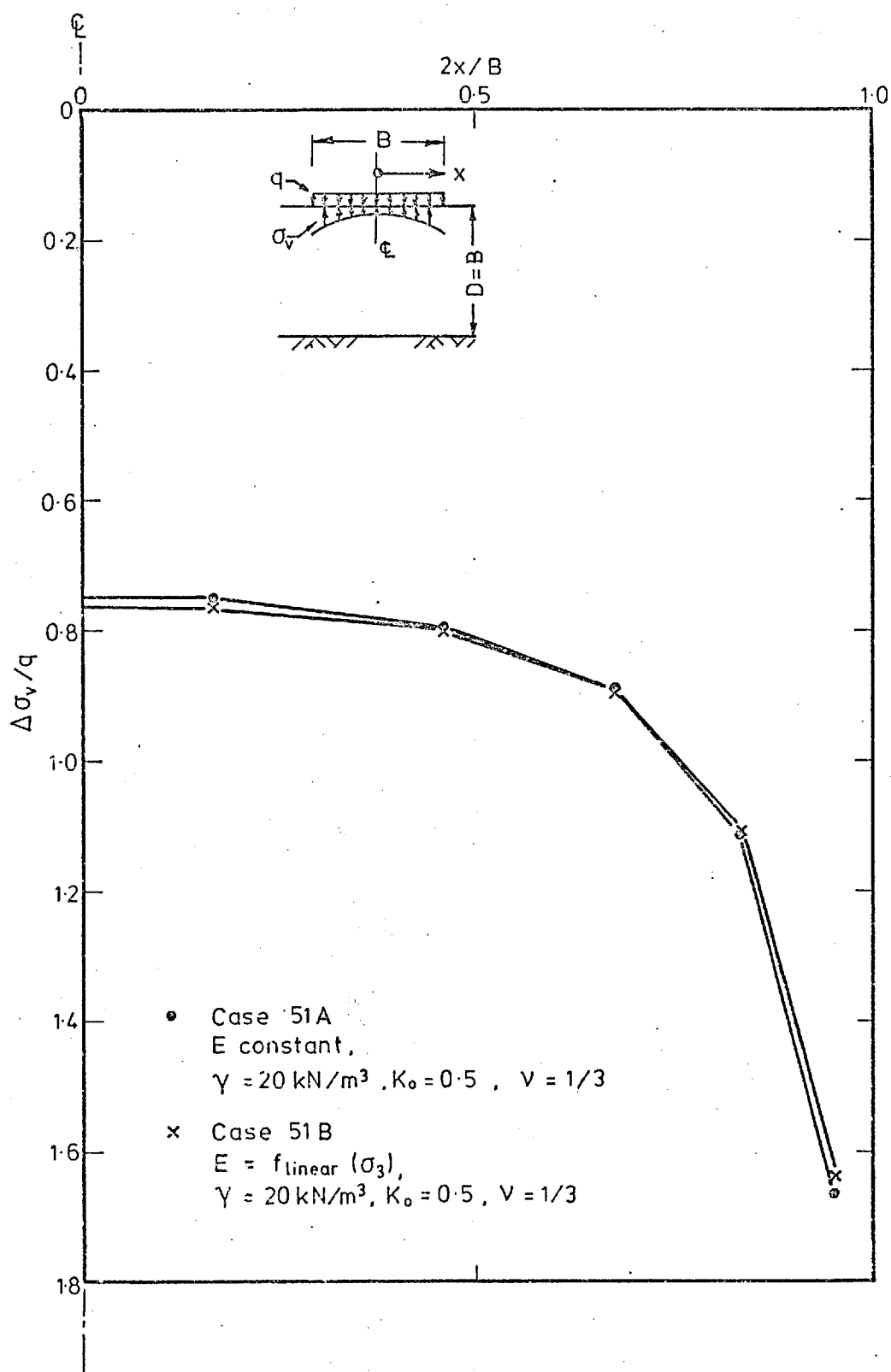
Fig. 6.10 Effect of the variation of Young's modulus with minor principal stress on the contact pressure distribution.
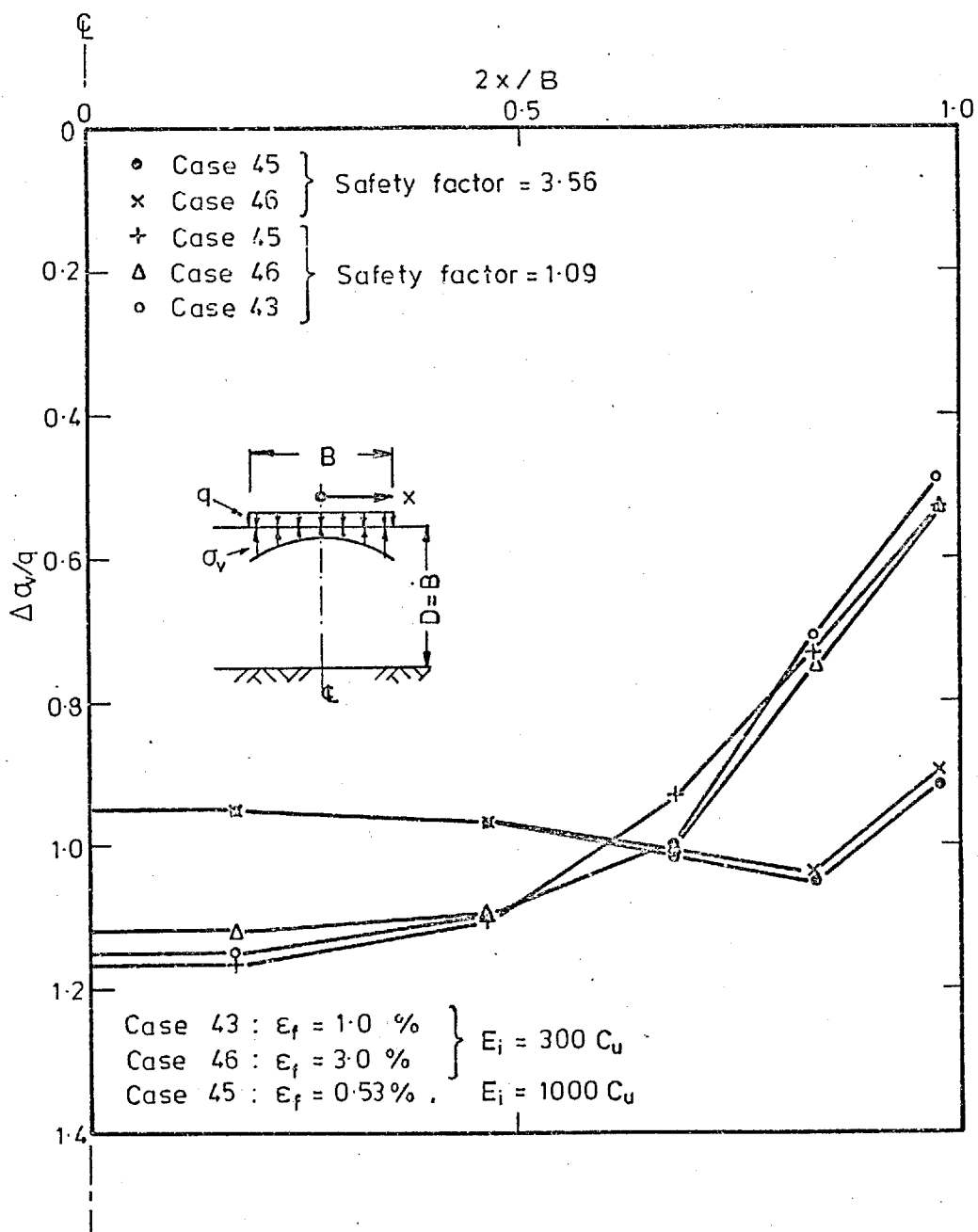
Fig. 6.11   Effect of the stress-strain relationship on
the contact pressure distribution(undrained).
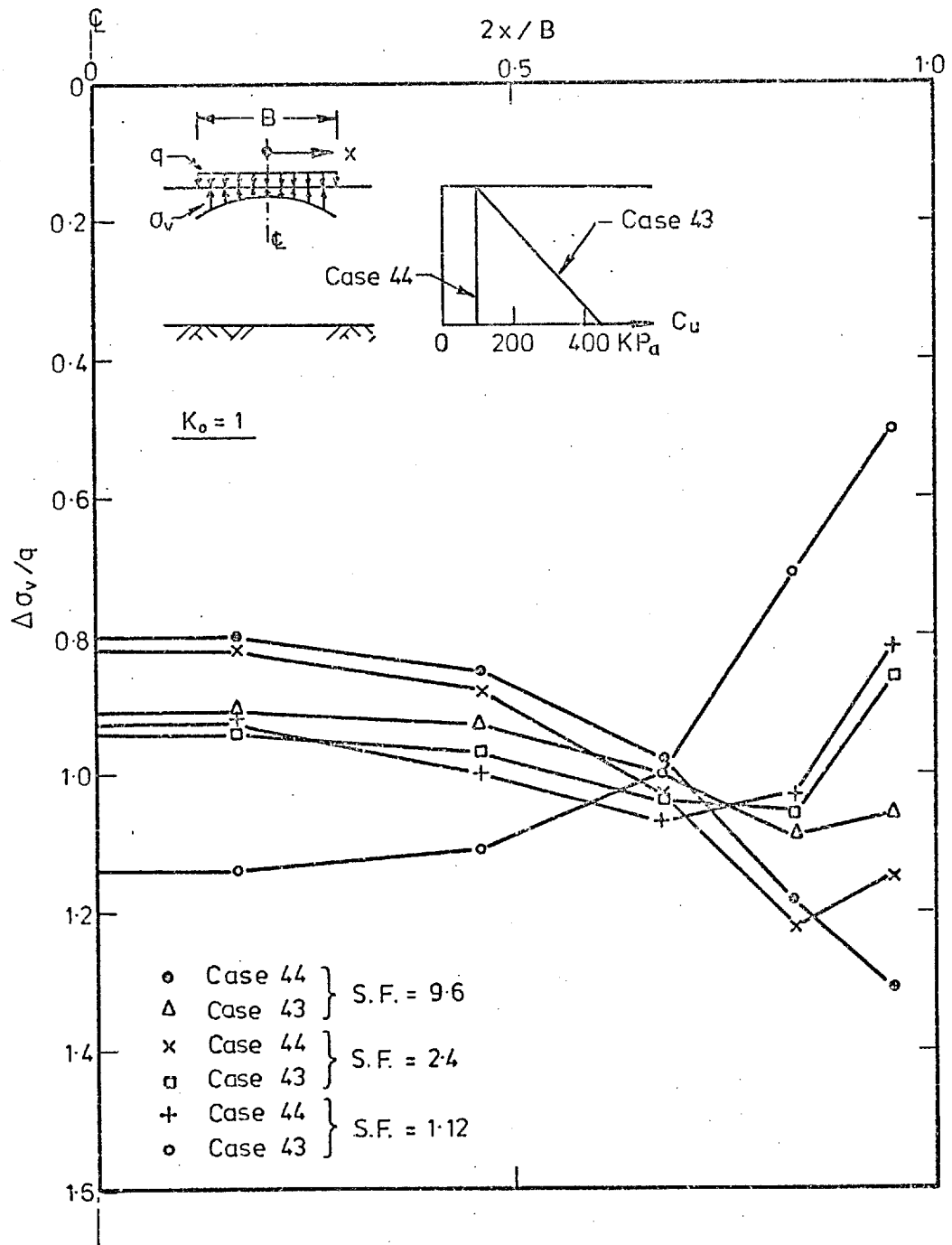
Fig. 6.12 Effect of nonhomogeneity on the contact pressure
distribution (undrained).
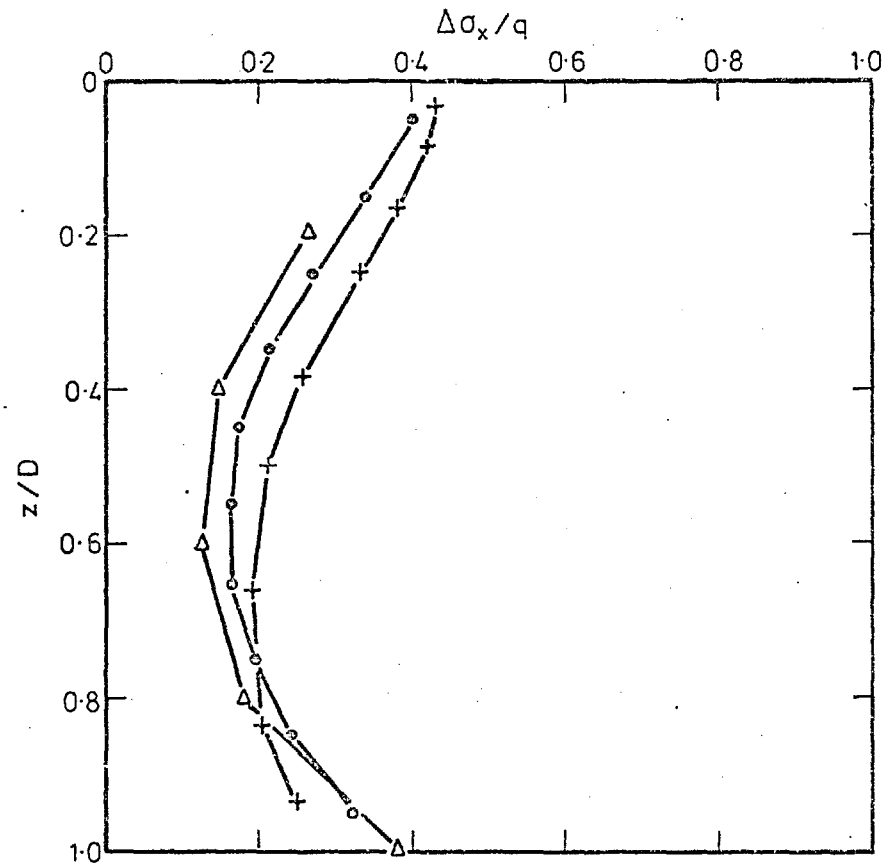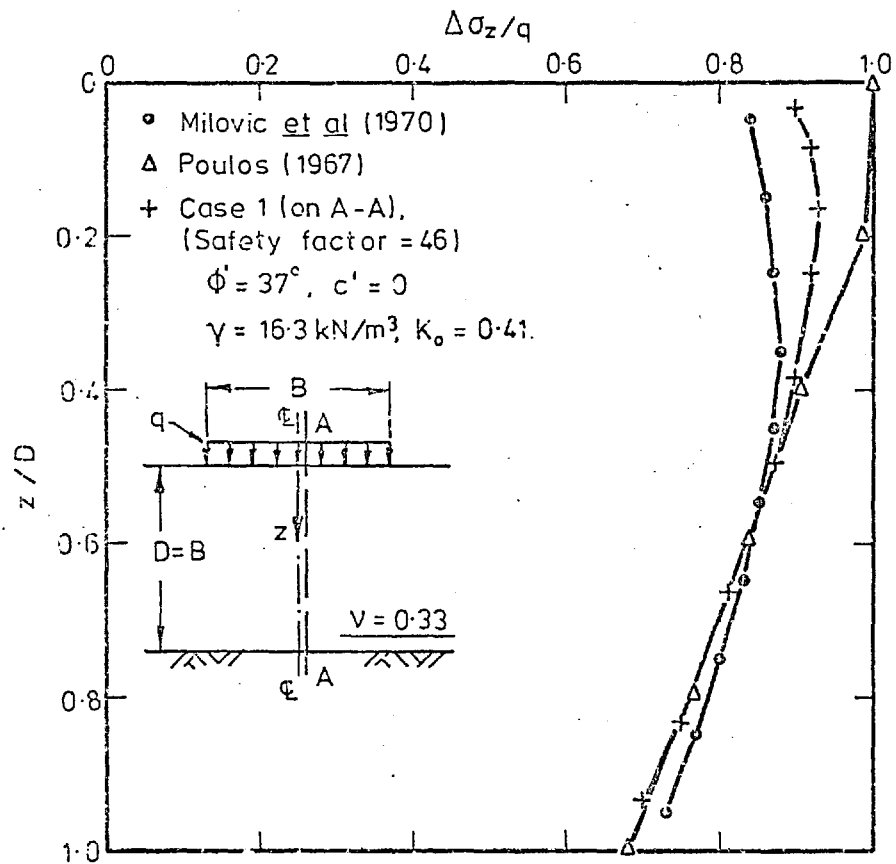
Fig. 6.13 Stress distribution near the centre line.
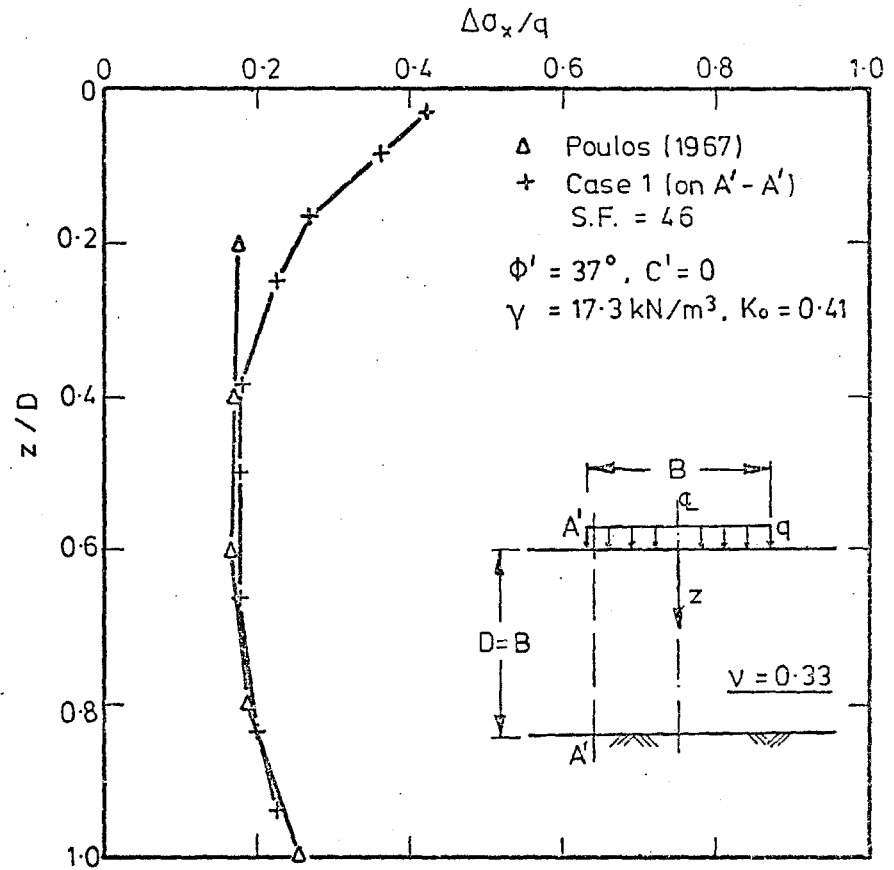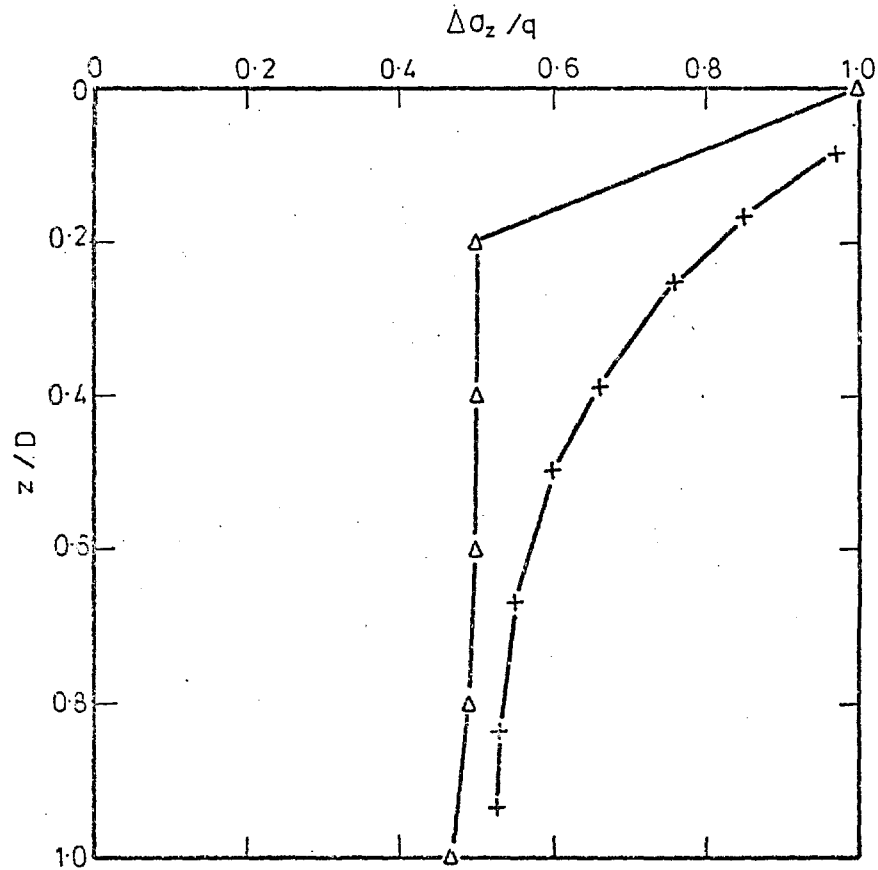
Fig. 6.14 Stress distribution near the edge.
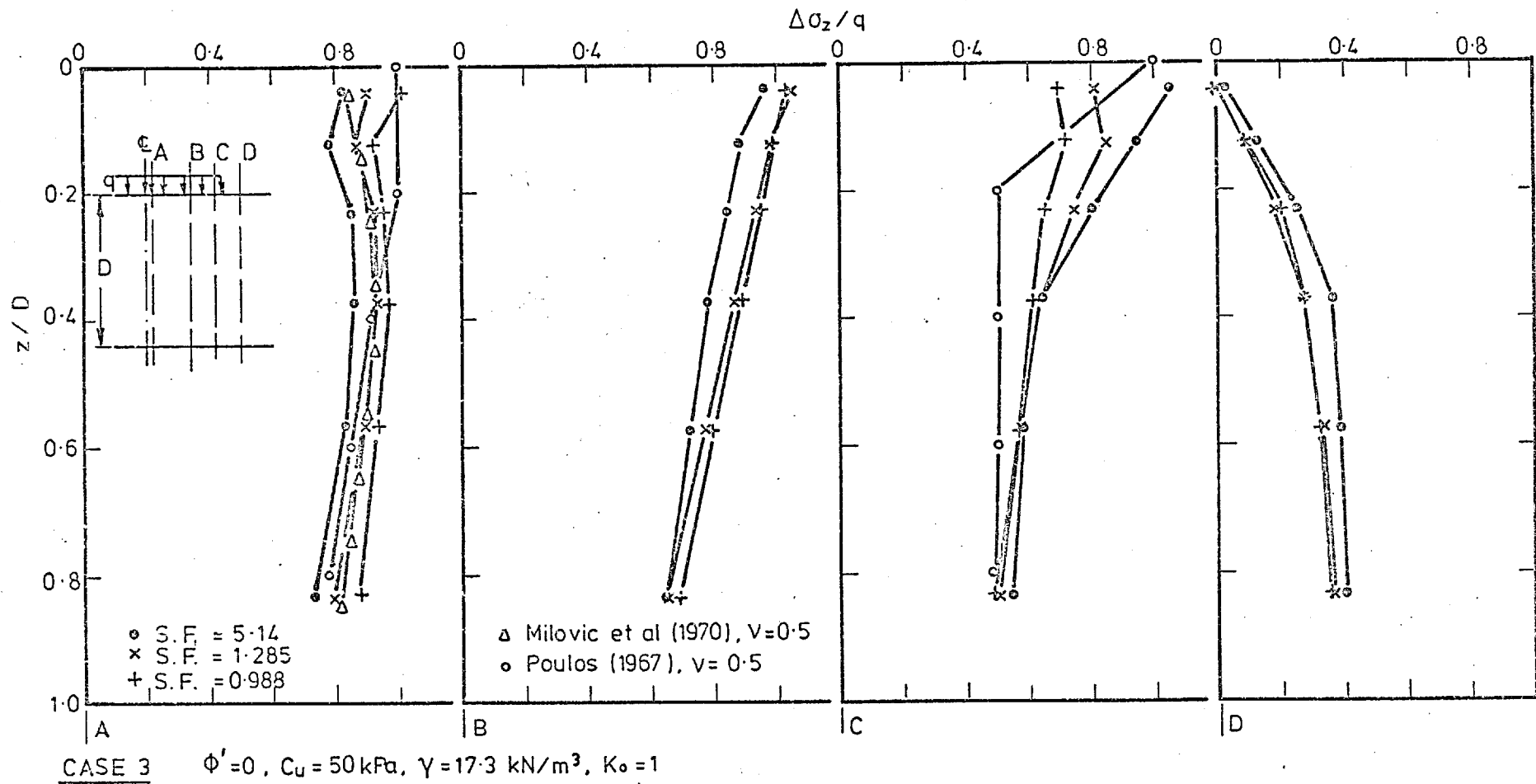
Fig. 6.15 Effect of stress
level on the vertical stress
distribution(undrained).
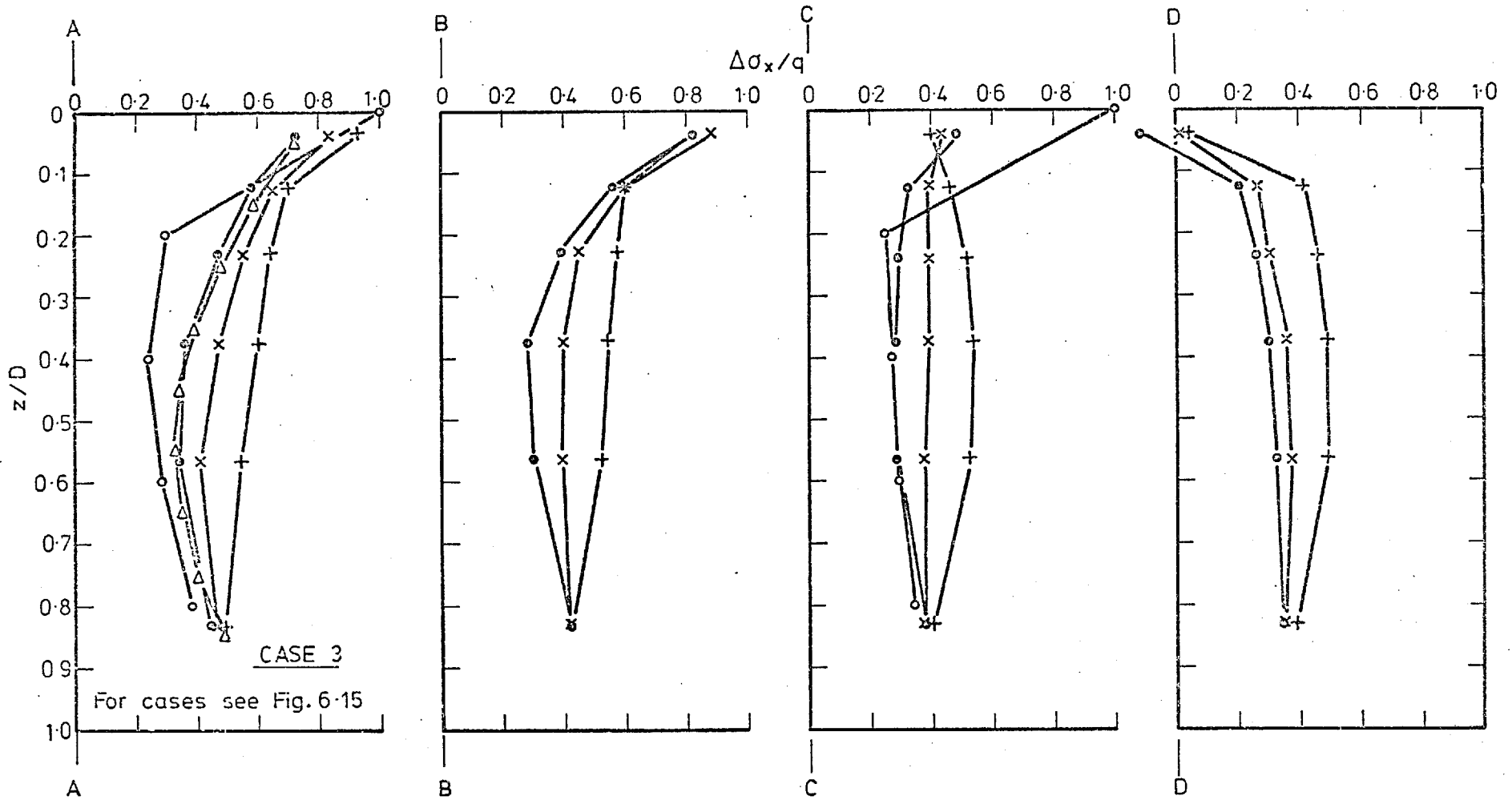
Fig. 6.16 Effect of stress level on the horizontal stress distribution, (undrained).
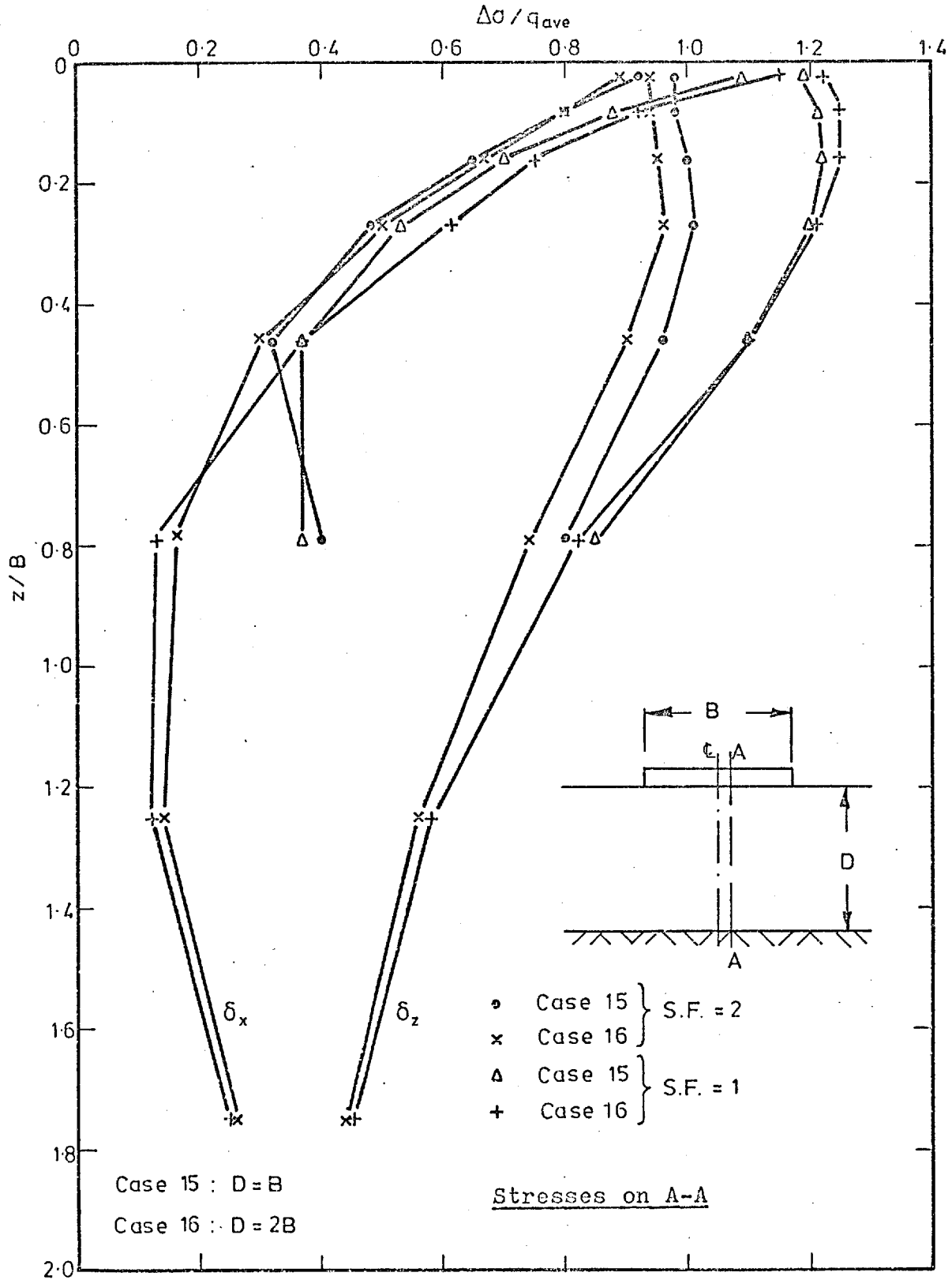
Fig. 6.17 Effect of the layer thickness on the stress
distribution (eccentric and inclined load).
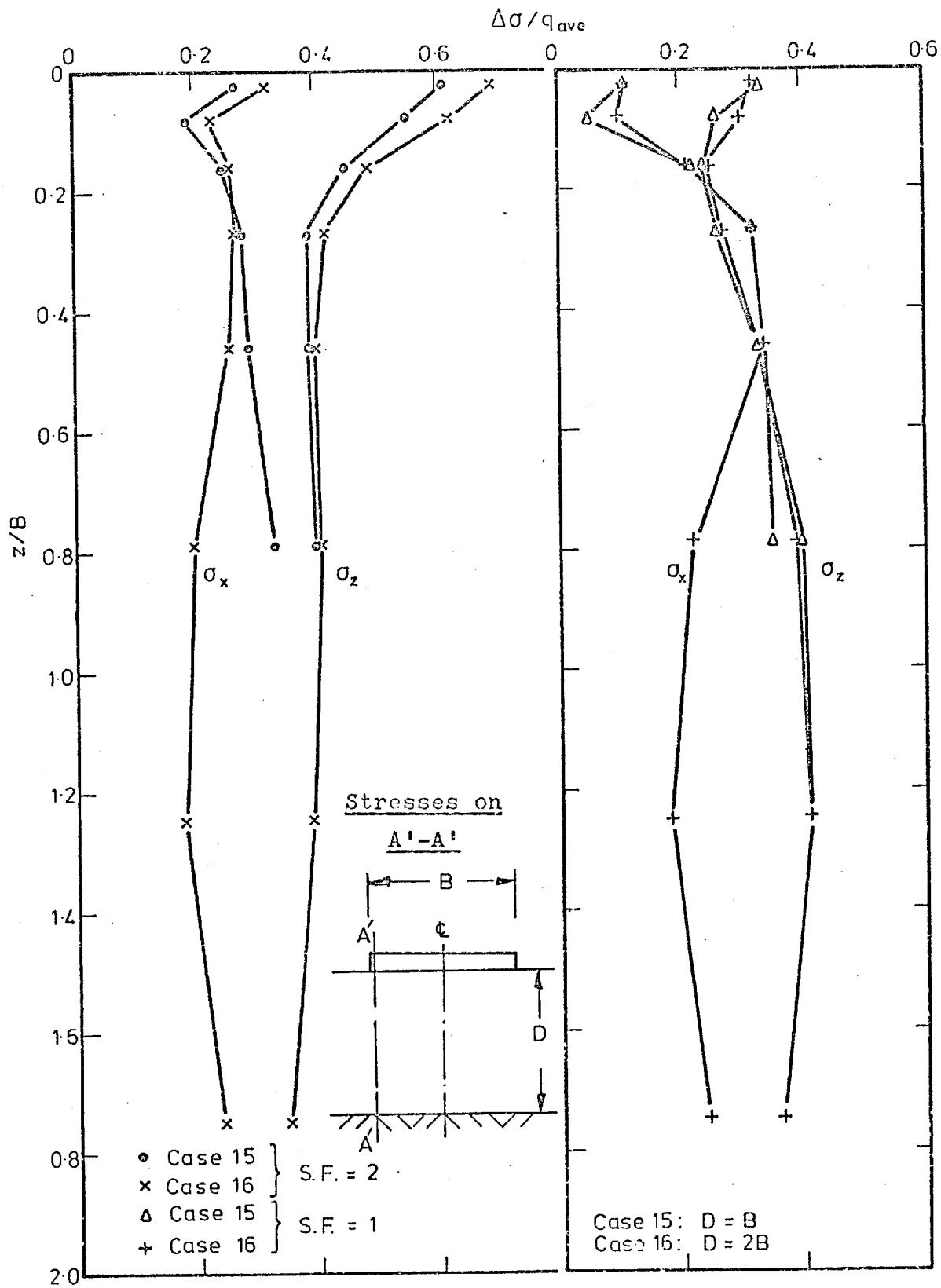
Fig. 6.18   Effect of the layer thickness on the stress
distribution (eccentric and inclined load).

Fig. 6.19a Effect of the side boundaries on the stress distribution (safety factor equal to 2.15).
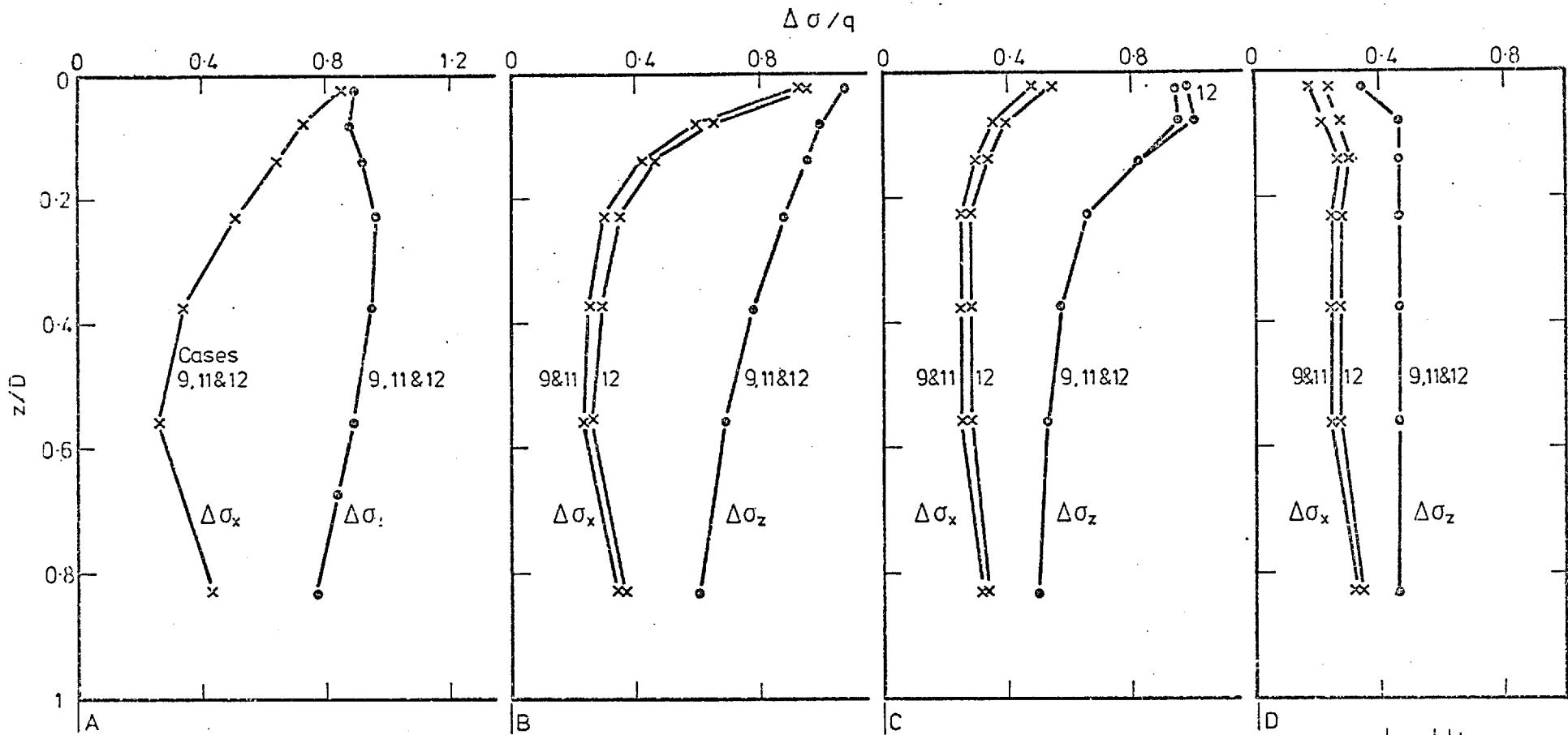
For geometry see Fig. 6·5
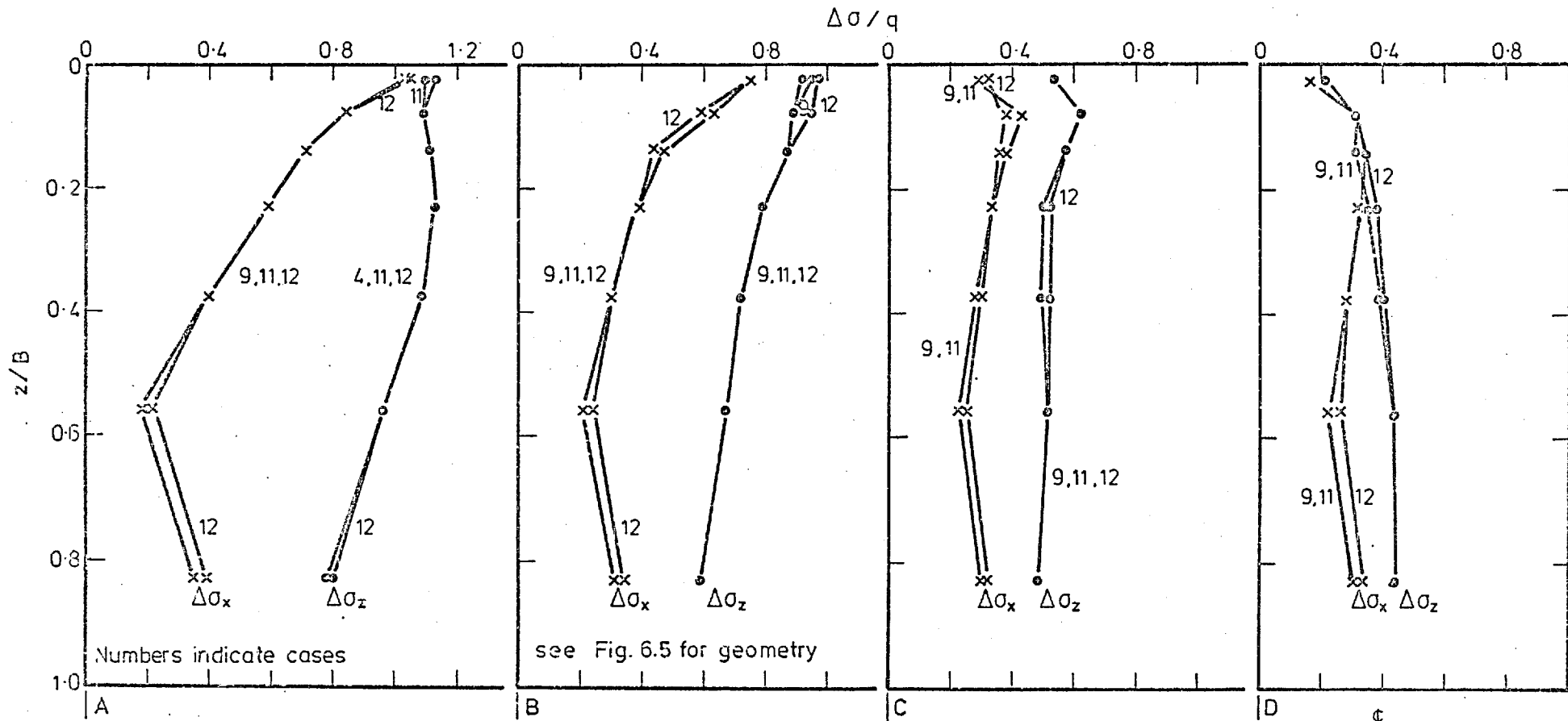
Fig. 6.19b Effect of the side
boundaries on the stress
distribution (safety factor
equal to 1.08).

250

Fig. 6.20a Effect of shear
unloading modelling on the
stress distribution,
(safety factor equal to 2.15).
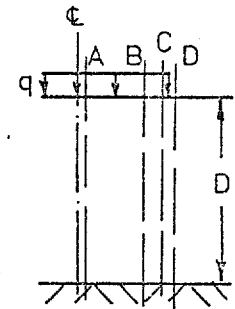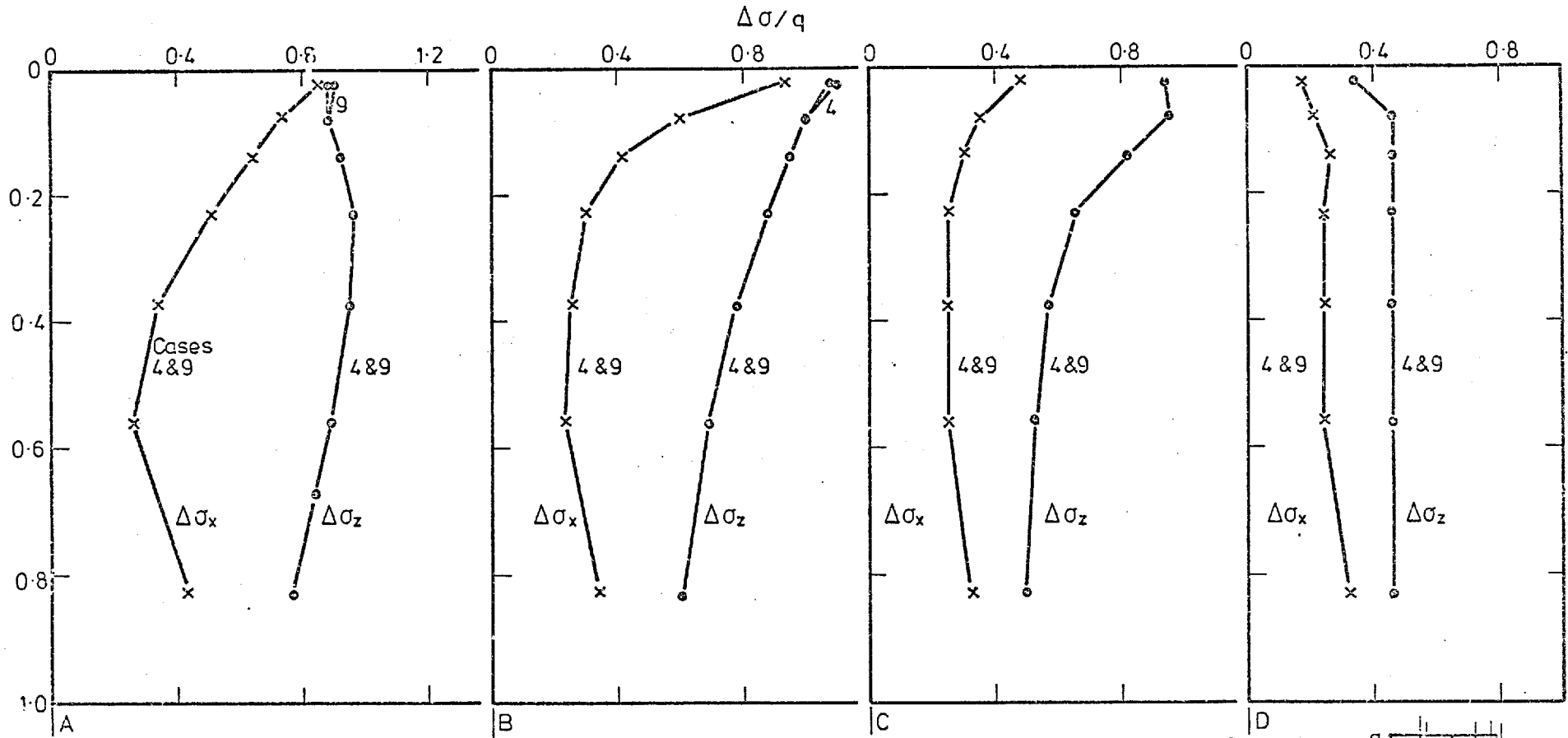
CASE 4 : $E_u = E_t$ } see Fig. 5.1
CASE 9 : $E_u = E_i$

For geometry see Fig. 5.6
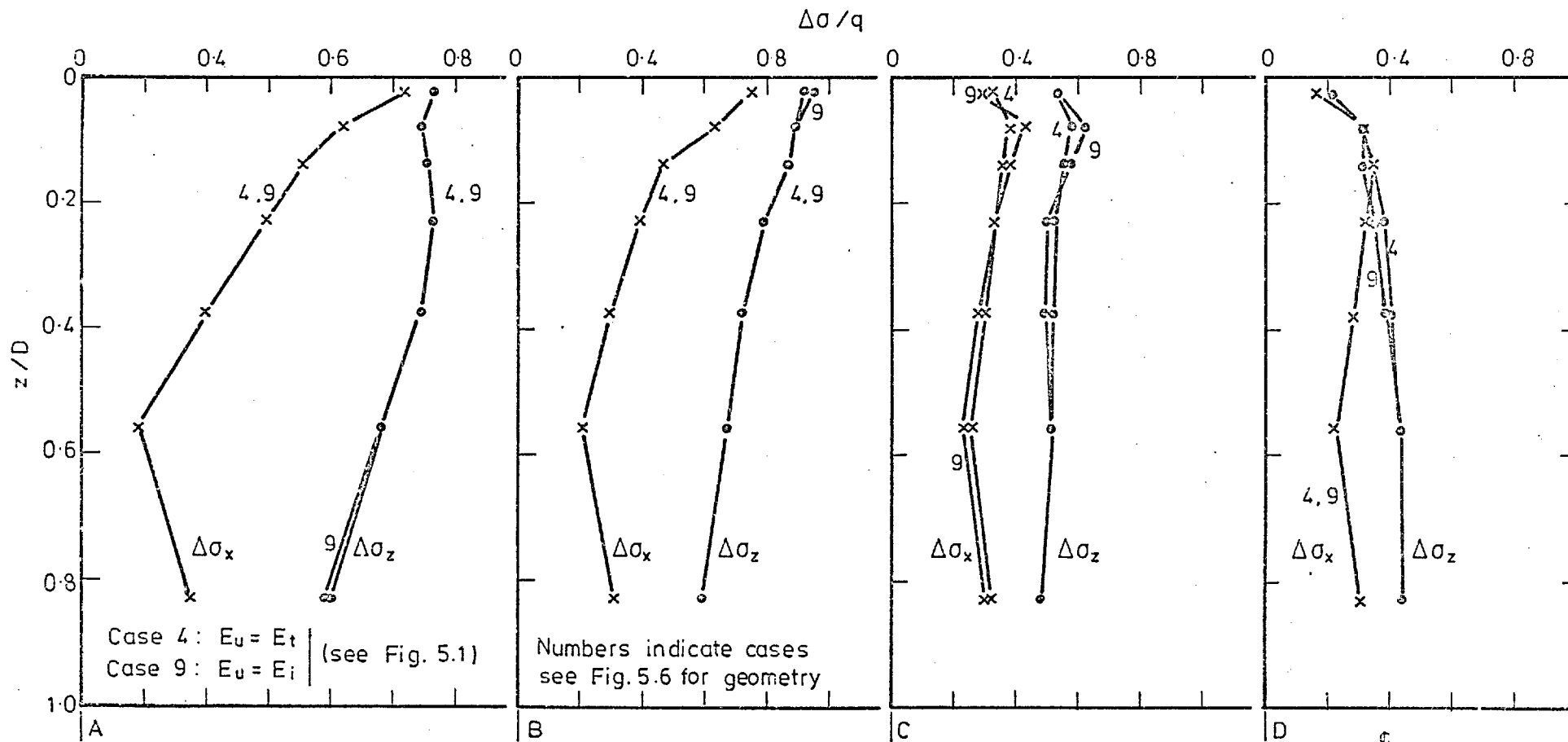
$\gamma = 20 \ KN/m^3$

$K_o = 2$
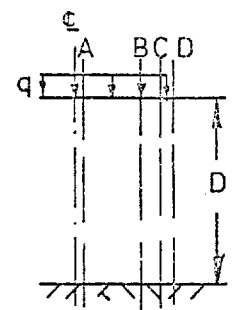
Fig. 6.20b Effect of shear
unloading modelling on the
stress distribution,
(safety factor equal to 1.08).

252

Fig. 6.21   Effect of variation
of modulus with σ_3 on the
principal stress distribution.
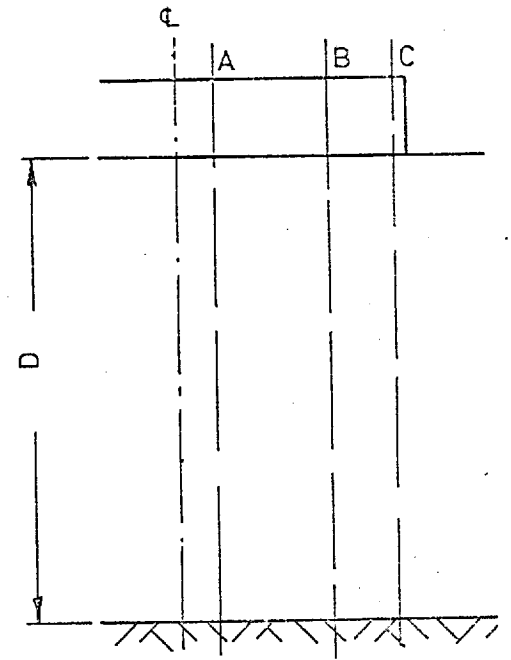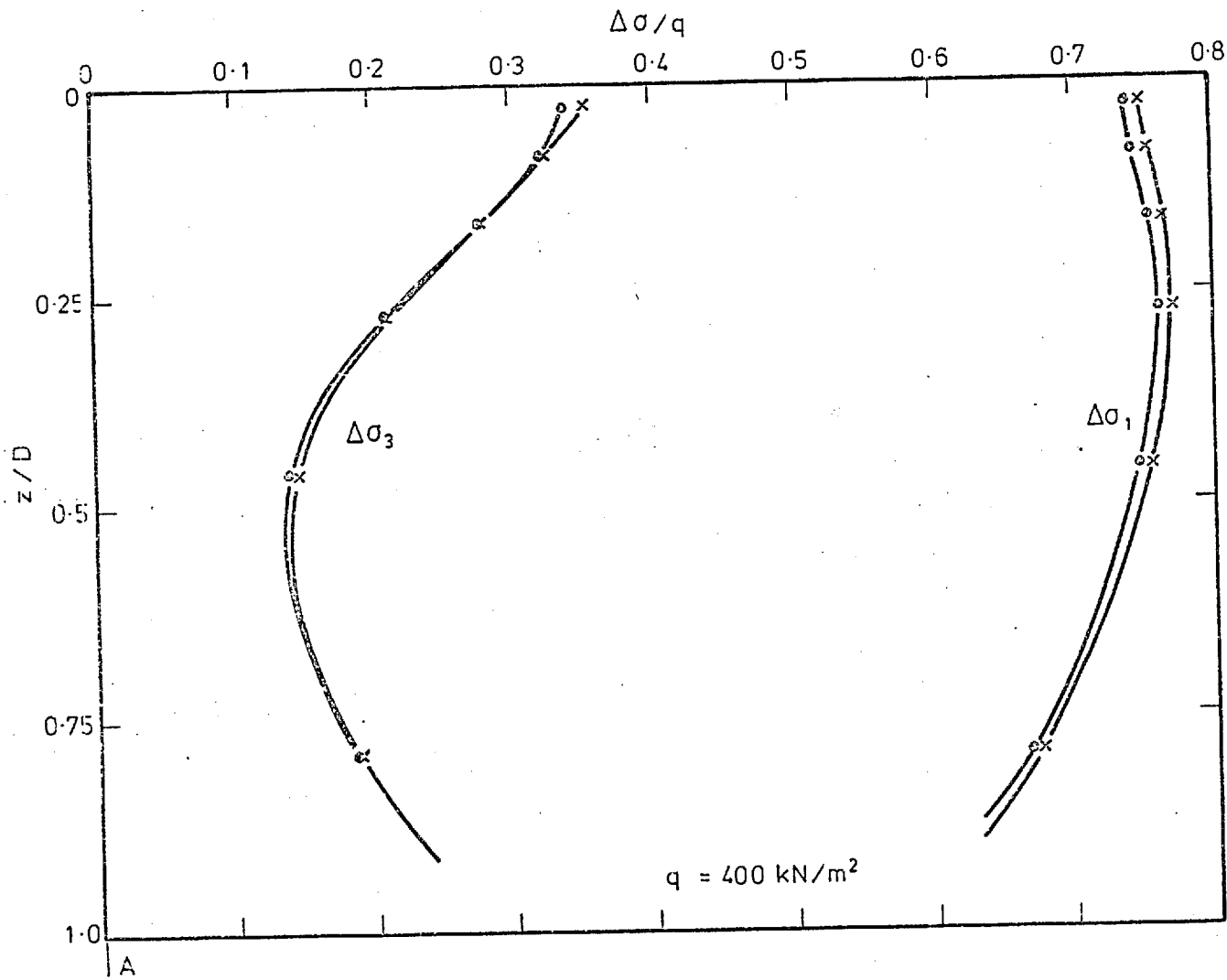
o Case 51 A . E constant
x Case 51 B . E varies linearly with σ_3
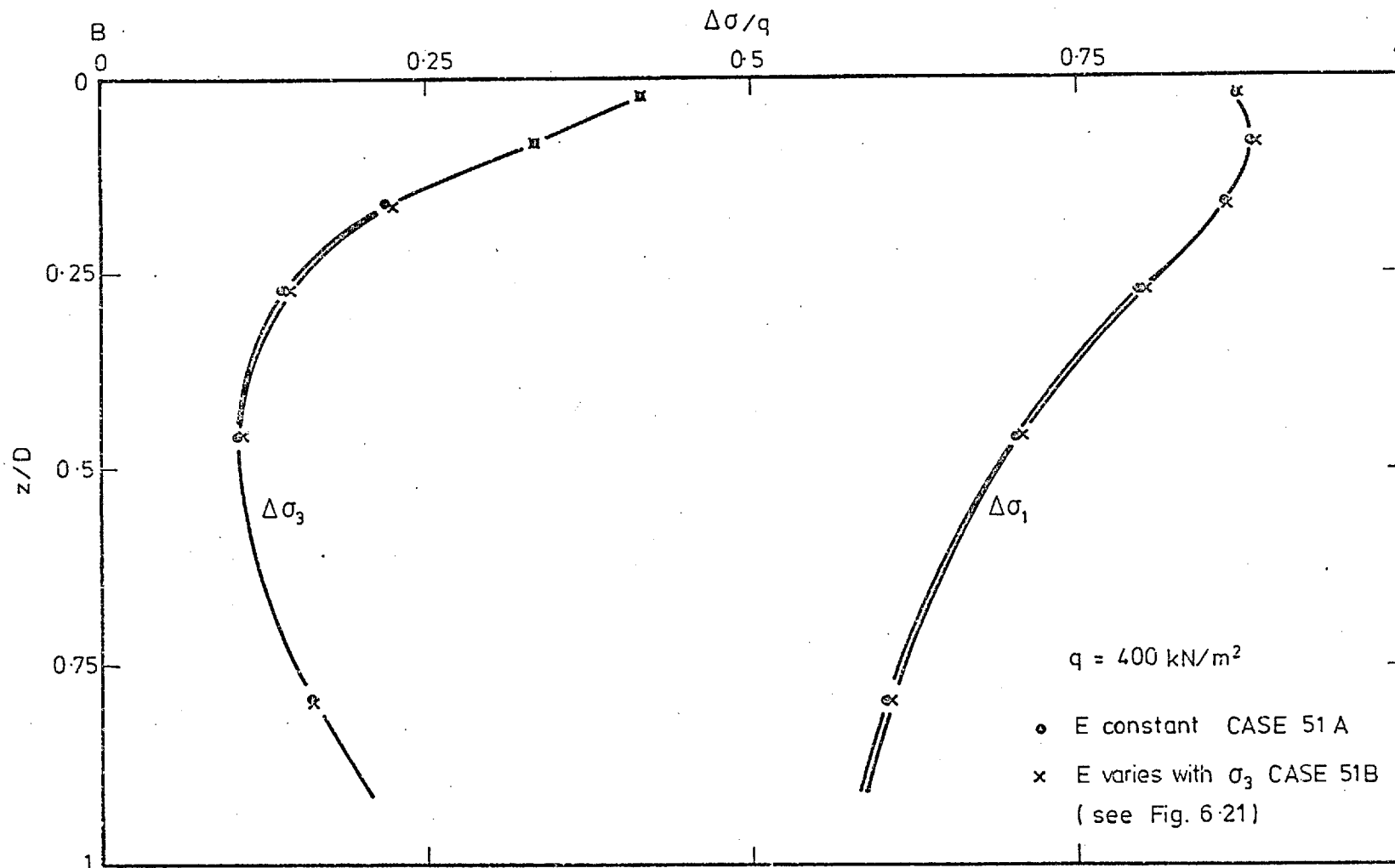
Fig. 6.22 Effect of variation
of modulus with σ_3 on the
principal stress distribution.
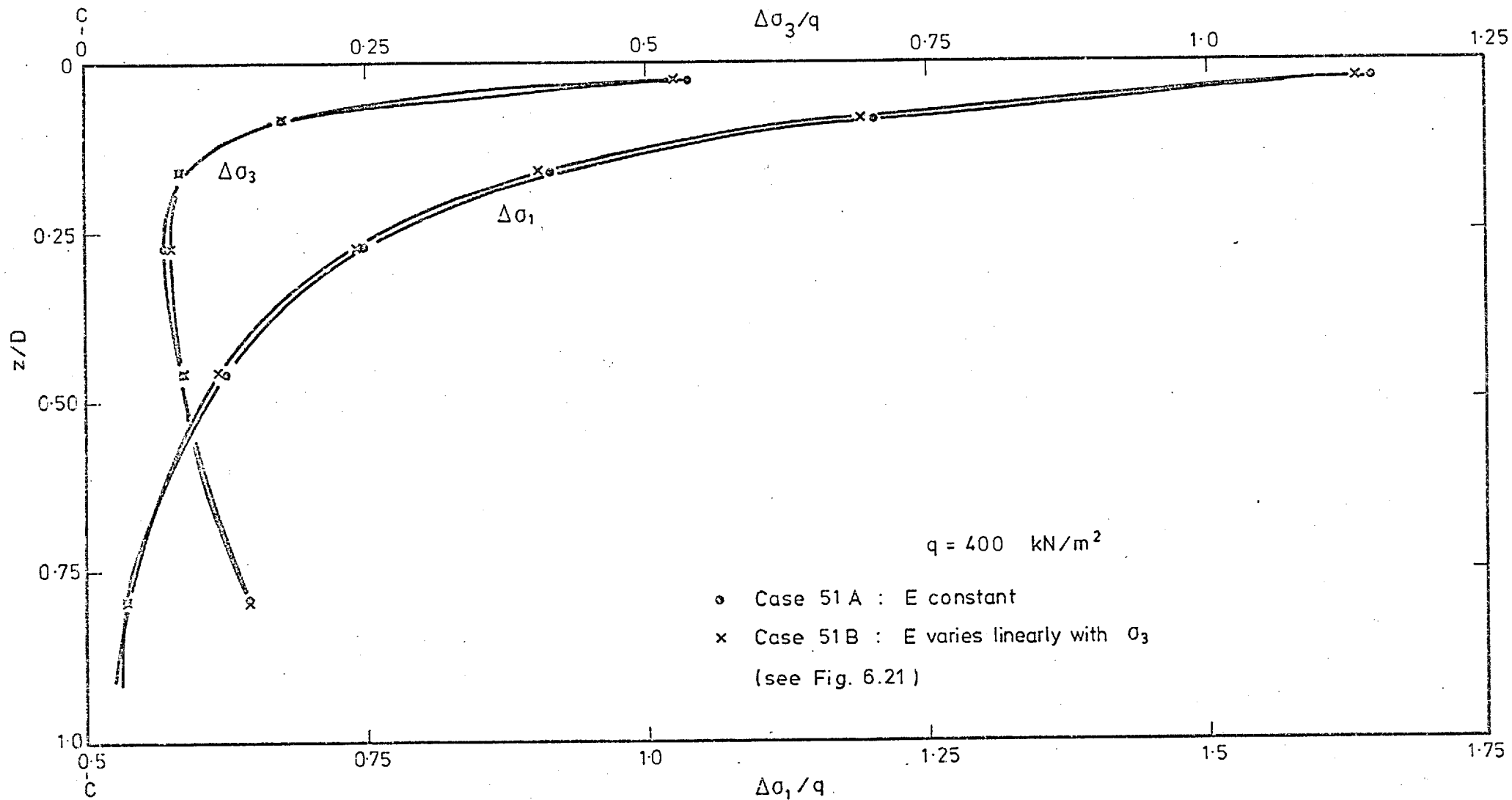
Fig. 6.23 Effect of variation
of modulus with σ_3 on the
principal stress distribution.
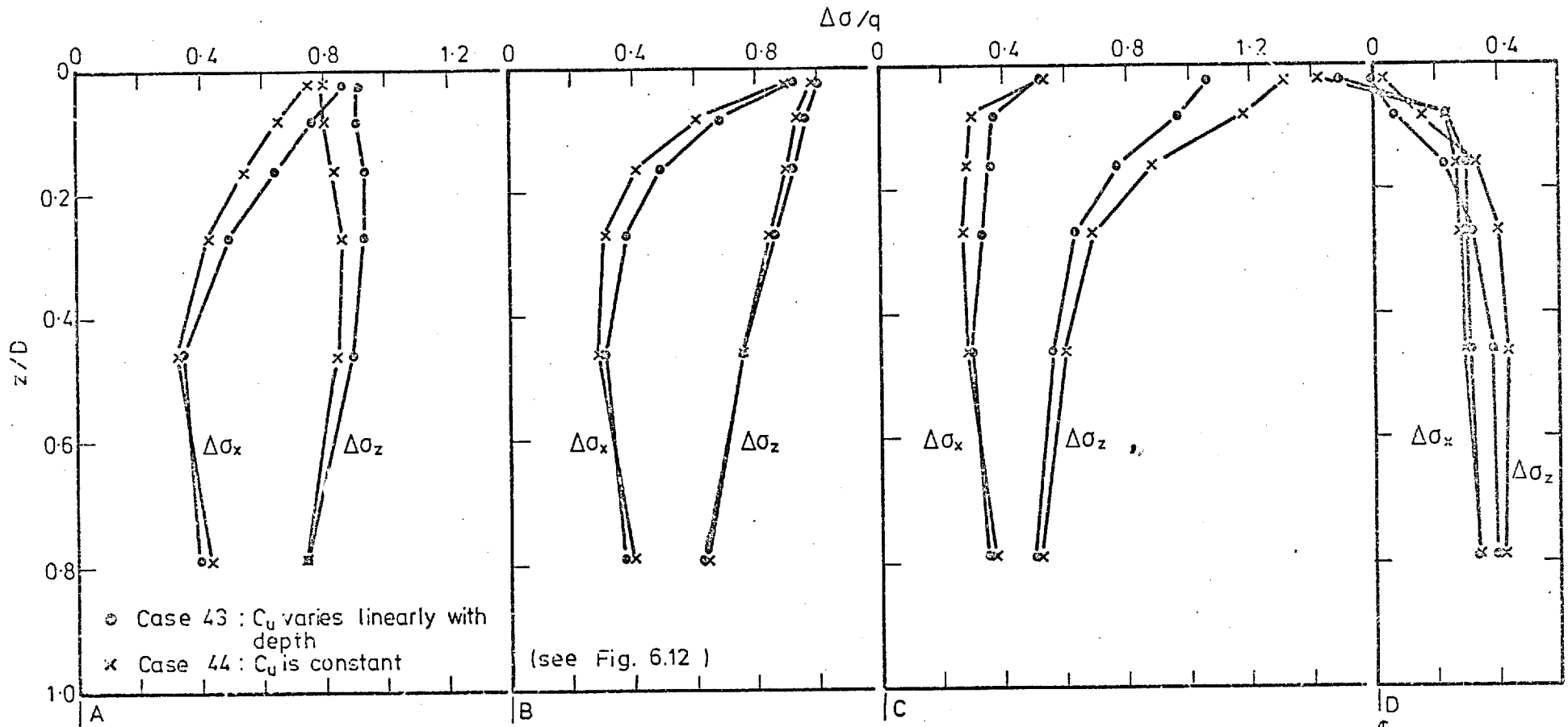
Fig. 6.24 Effect of the non-homogeneity on the stress distribution (safety factor equal to 9.6).

○ Case 43 : C_u varies linearly with depth
× Case 44 : C_u is constant

(see Fig. 6.12)

$K_o = 1$

$\Delta\sigma/q$

o Case 43 (C_u varies linearly with depth)

x Case 44 (C_u is constant)

see Fig. 6.12

$\Delta\sigma_x$ $\Delta\sigma_z$
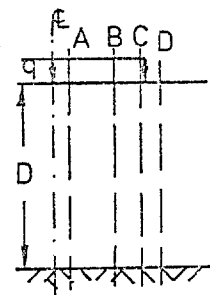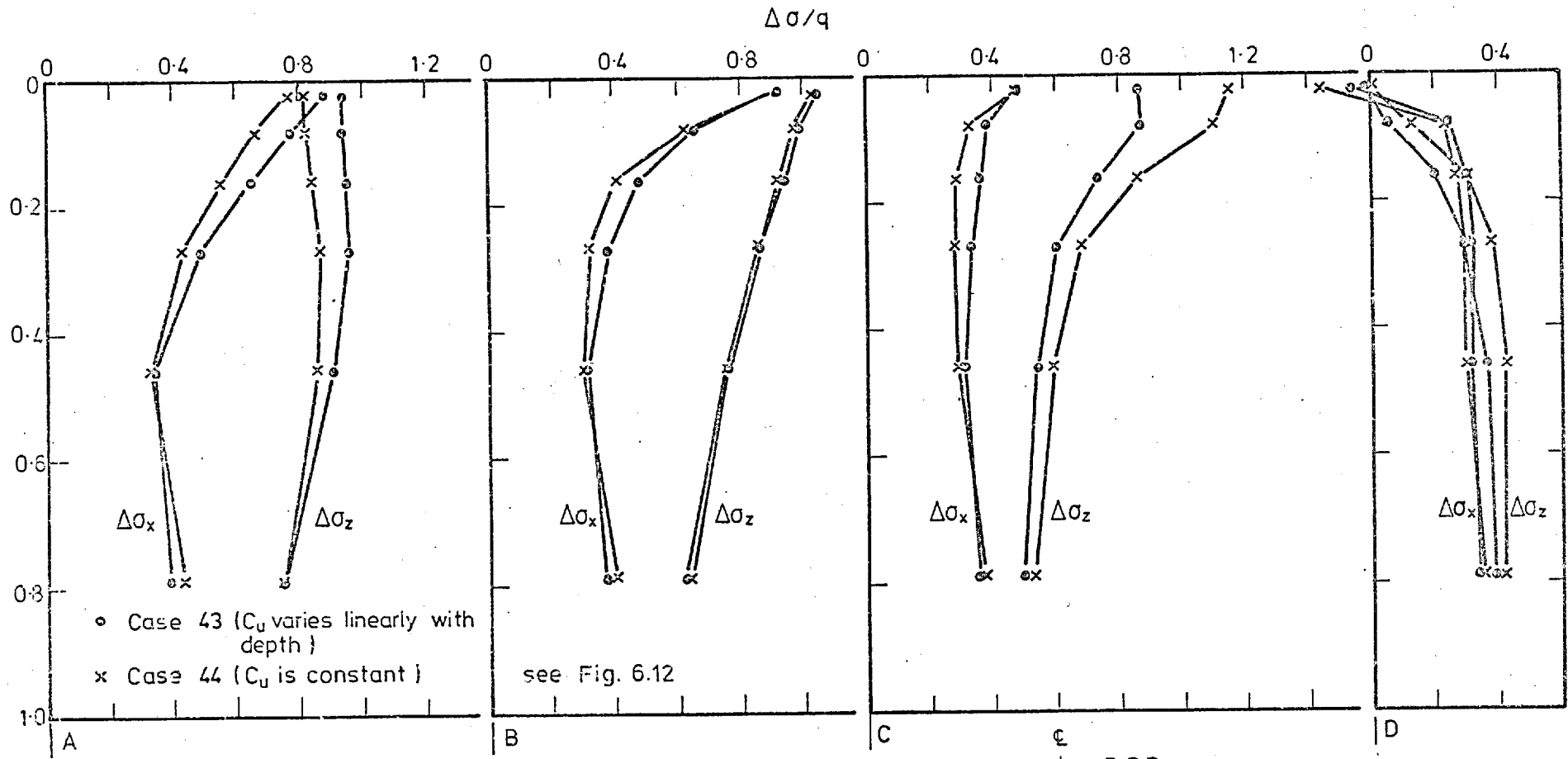
Fig. 6.25 Effect of the non-homogeneity on the stress distribution, (safety factor equal to 2.4).
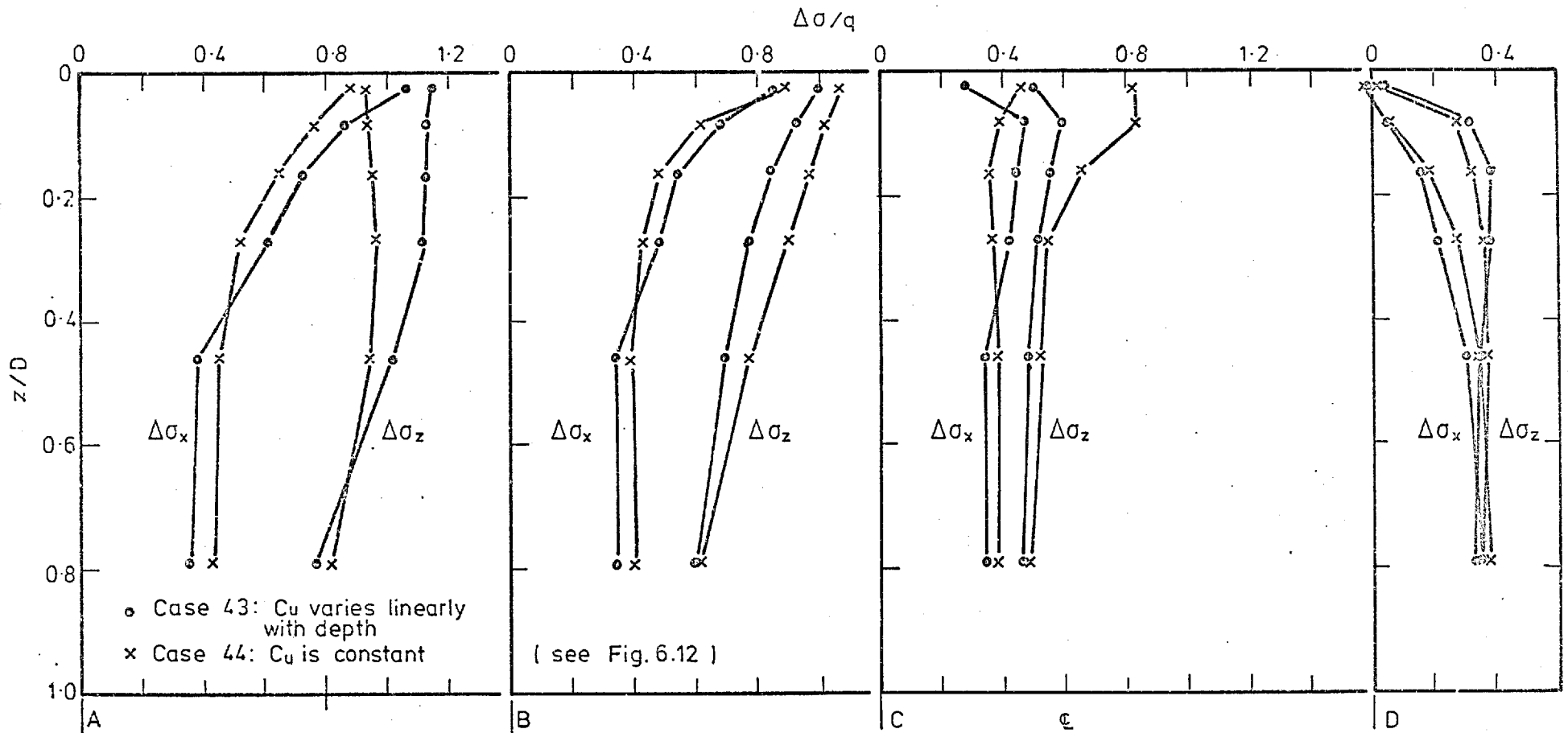
$K_o = 1$

Fig. 6.26 Effect of the non-homogeneity on the stress distribution, (safety factor equal to 1.12).

Legend within figure:
- Case 43: Cu varies linearly with depth
- Case 44: Cu is constant
- (see Fig. 6.12)

Axis labels: $\Delta\sigma/q$, z/D, $\Delta\sigma_x$, $\Delta\sigma_z$, $K_o = 1$
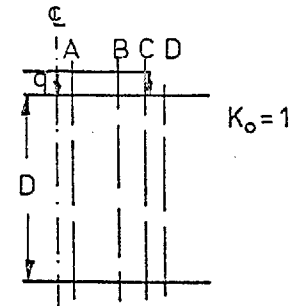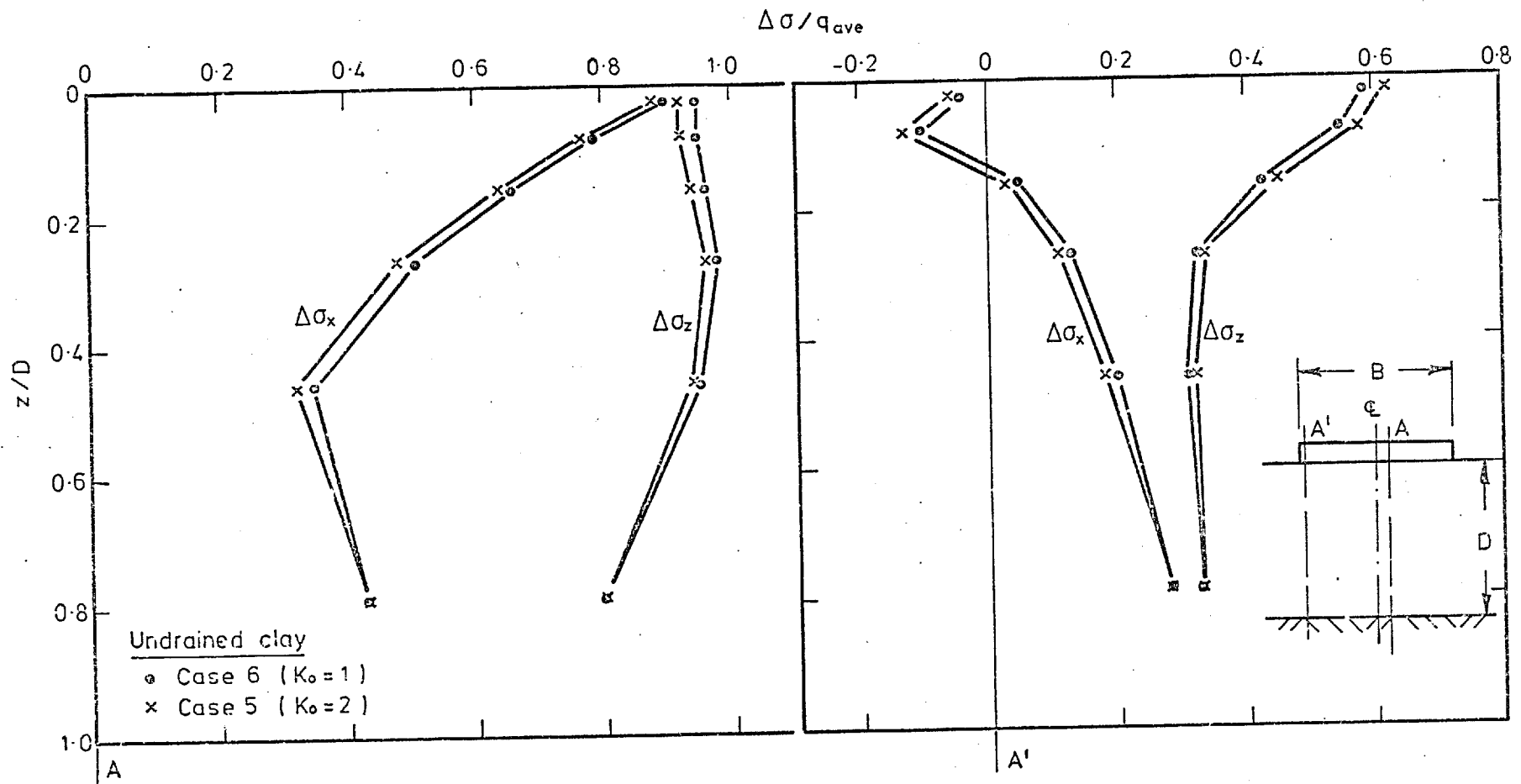
Fig. 6.27a Effect of K_o on
the stress distribution(<u>safety
factor equal to 2</u>).
<u>Eccentric and inclined load.</u>
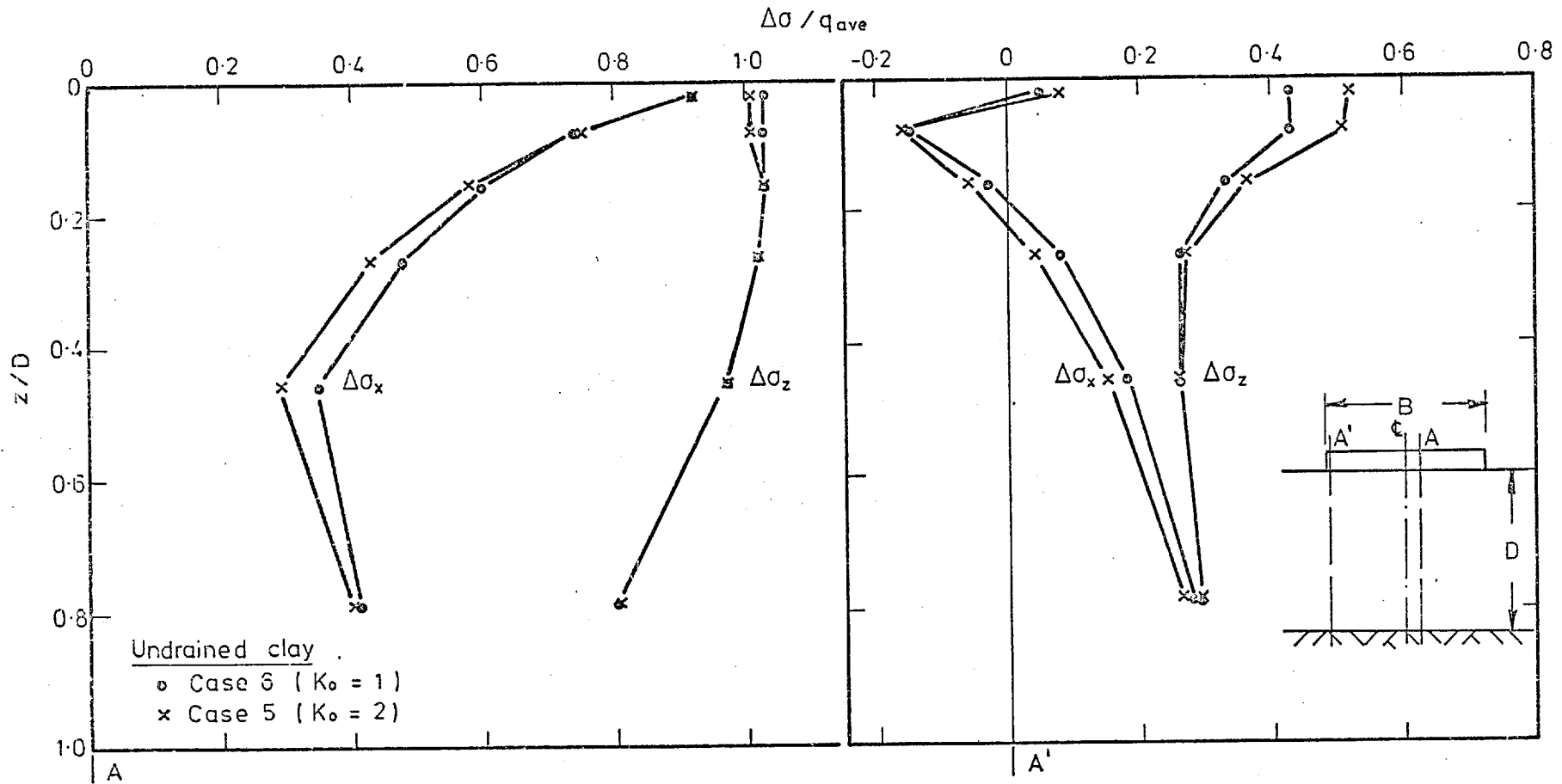
Fig. 6.27b Effect of K_o on
the stress distribution(safety
factor equal to 1).
Eccentric and inclined load.
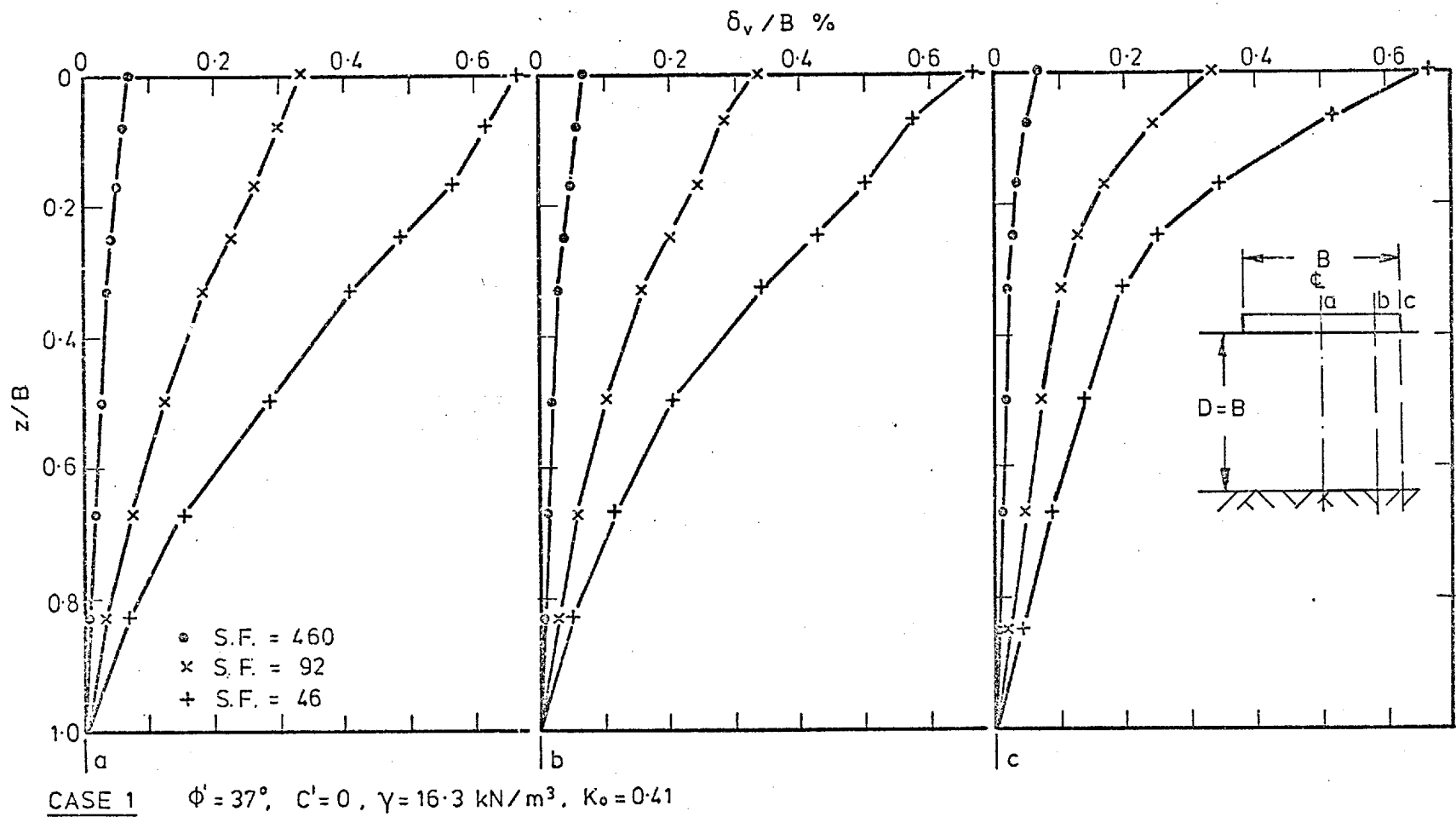
Fig. 6.28   Vertical displacements profile
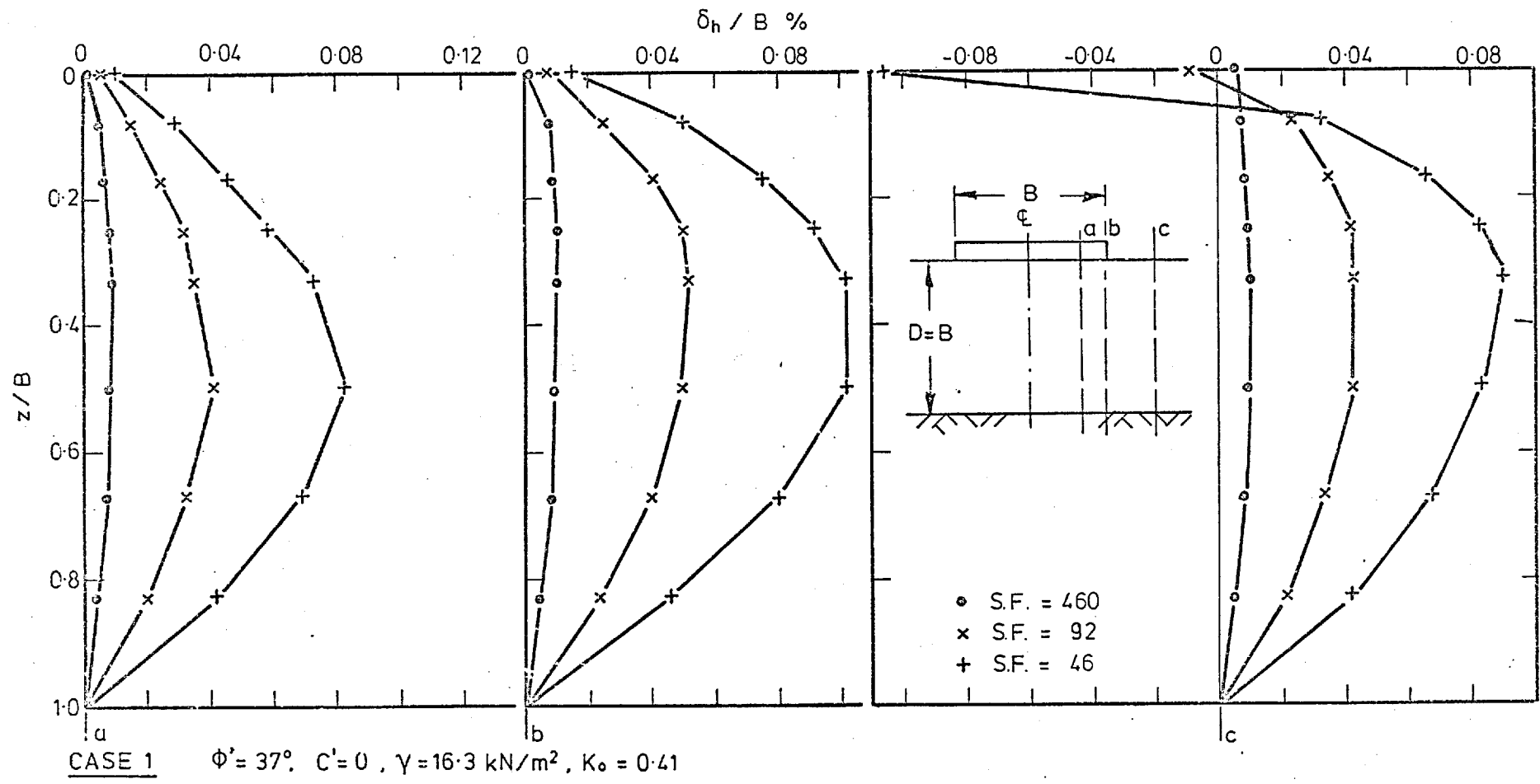
Fig. 6.29   Horizontal displacements profile
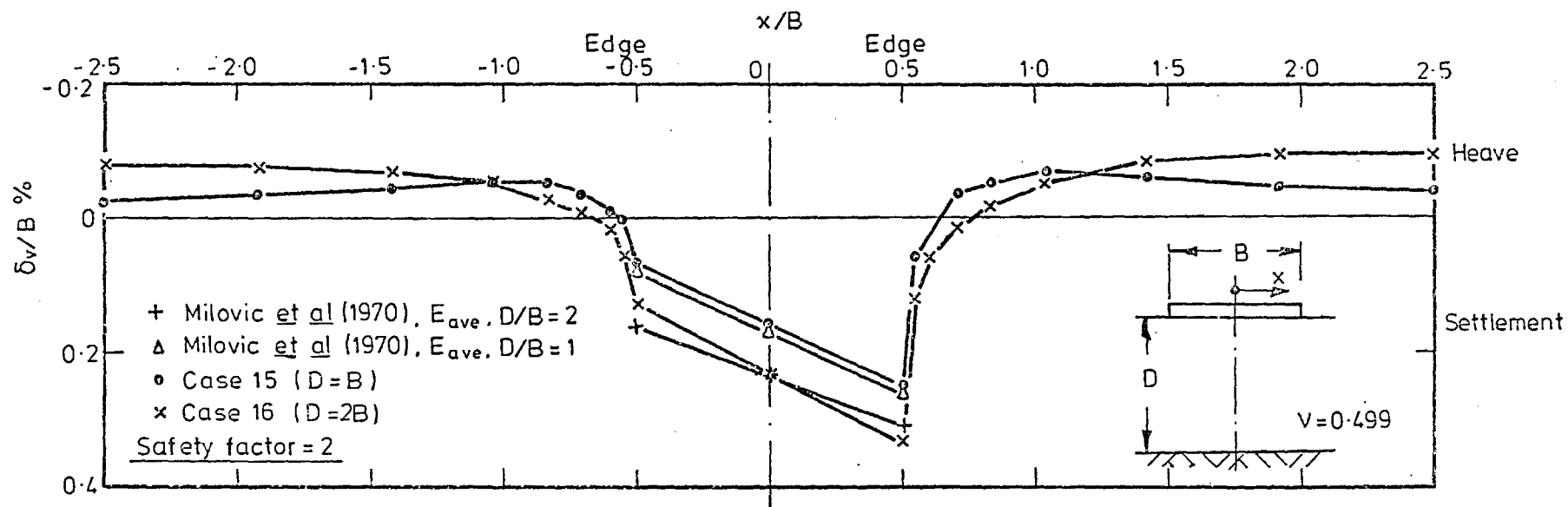
Fig. 6.30   Effect of the layer thickness on the settlement,
              inclined and eccentric loading
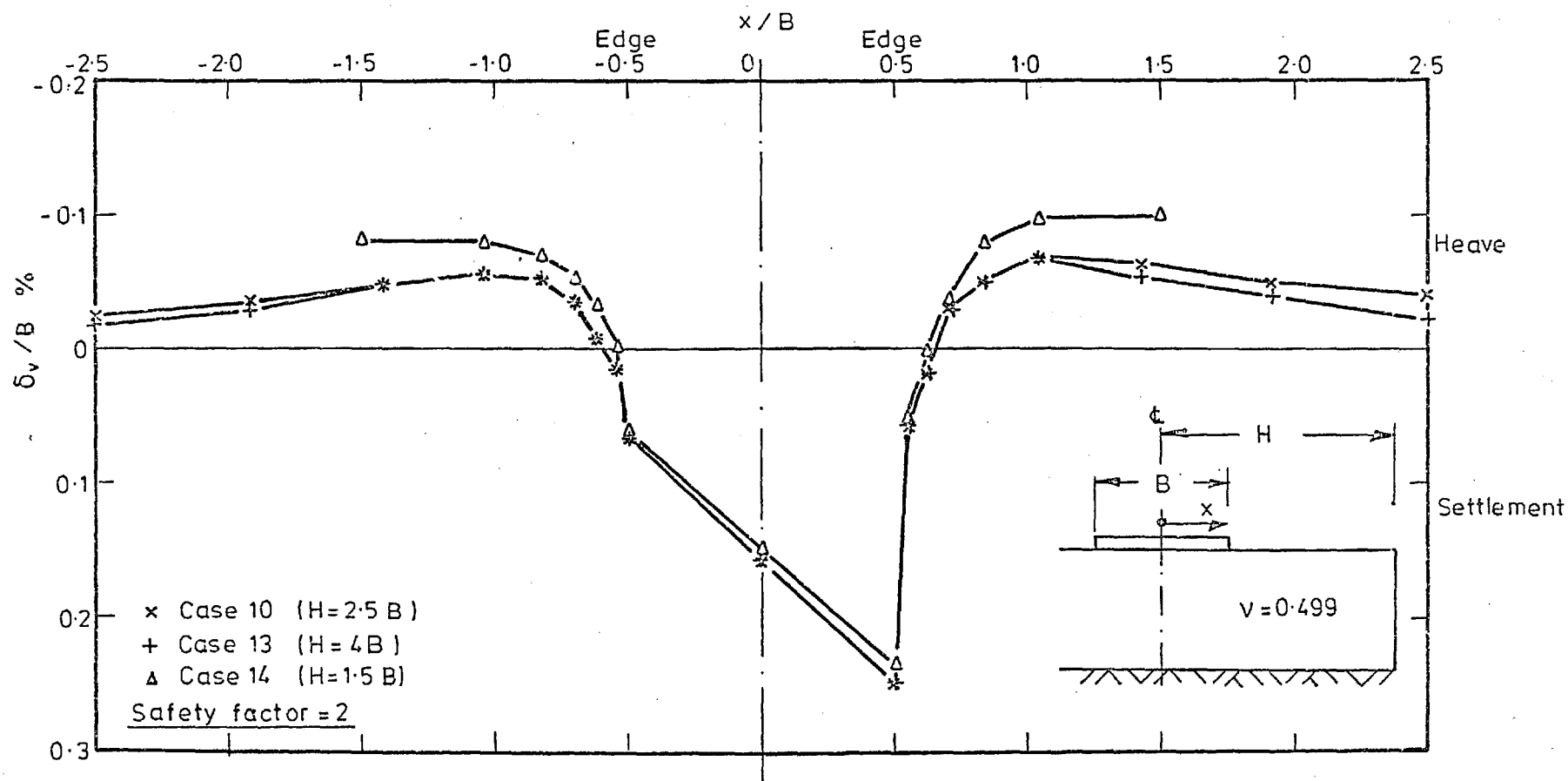
Fig. 6.31a   Effect of the side boundaries on the settlement,
              inclined and eccentric loading
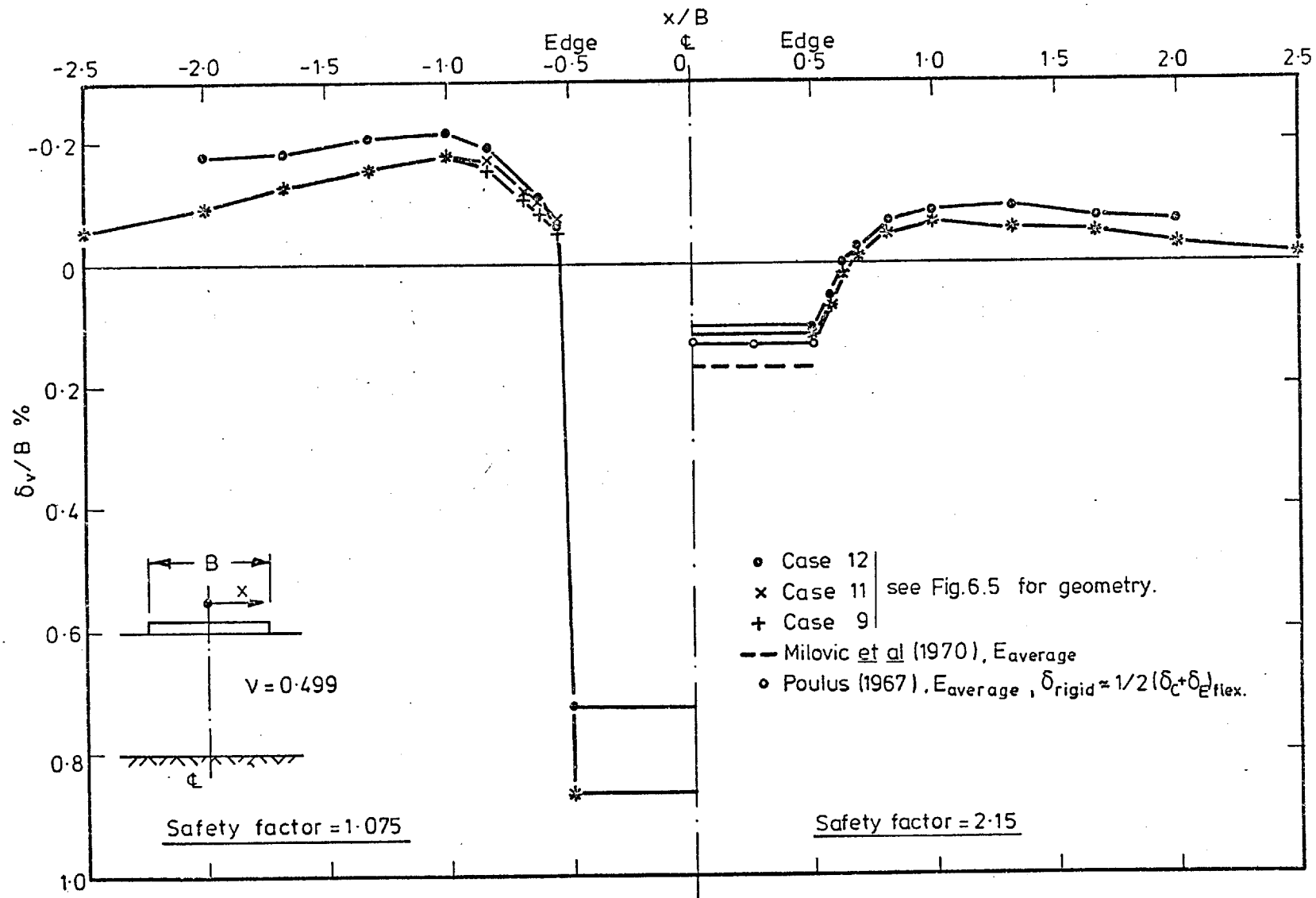
Fig. 6.31b   Effect of the side boundaries on the settlement,
              vertical loading
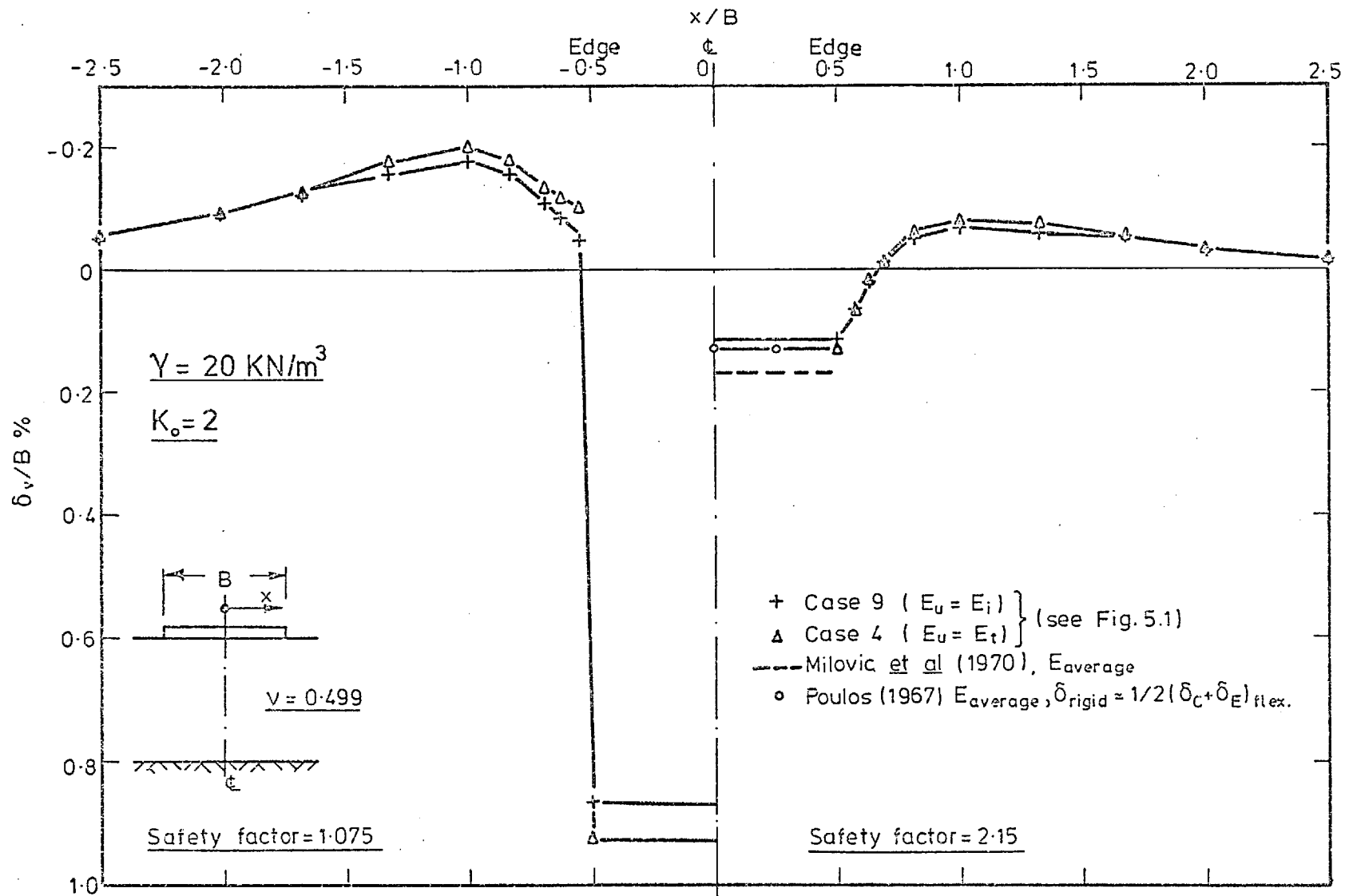
Fig. 6.32   Effect of the shear unloading modelling on the settlement, vertical loading
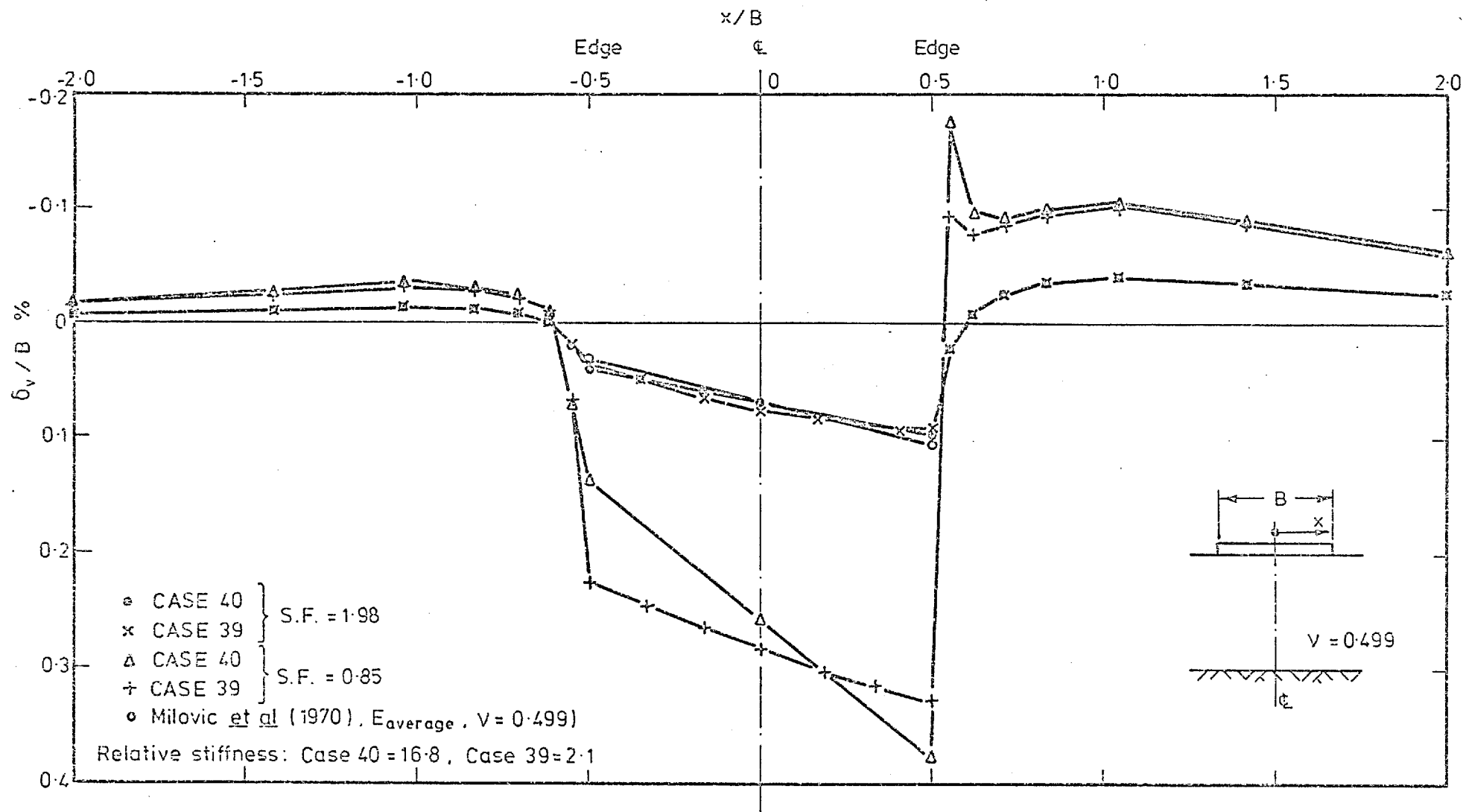
Fig. 6.33   Effect of footing rigidity on the surface settlement
             (eccentric and inclined load)

x / B

Edge
-0.5

¢
0

Edge
0.5

-2.0   -1.5   -1.0   0   1.0   1.5   2.0

δ_v / B %

-0.1

-0.05

0

0.05

0.1

0.15

0.2

Safety factor = 9.6

⊚ Case 44   (C_u is constant)
✕ Case 43   (C_u varies linearly with depth), (see Fig. 6.12)
△ Milovic et al (1970), E for case 44
+ Poulos (1967), E for case 44 , $\delta_{rigid} \simeq 0.5 \, (\delta_C + \delta_E)_{flex.}$
○ Milovic et al (1970), $E_{average}$ for Case 43

B

x

$\nu = 0.499$

¢
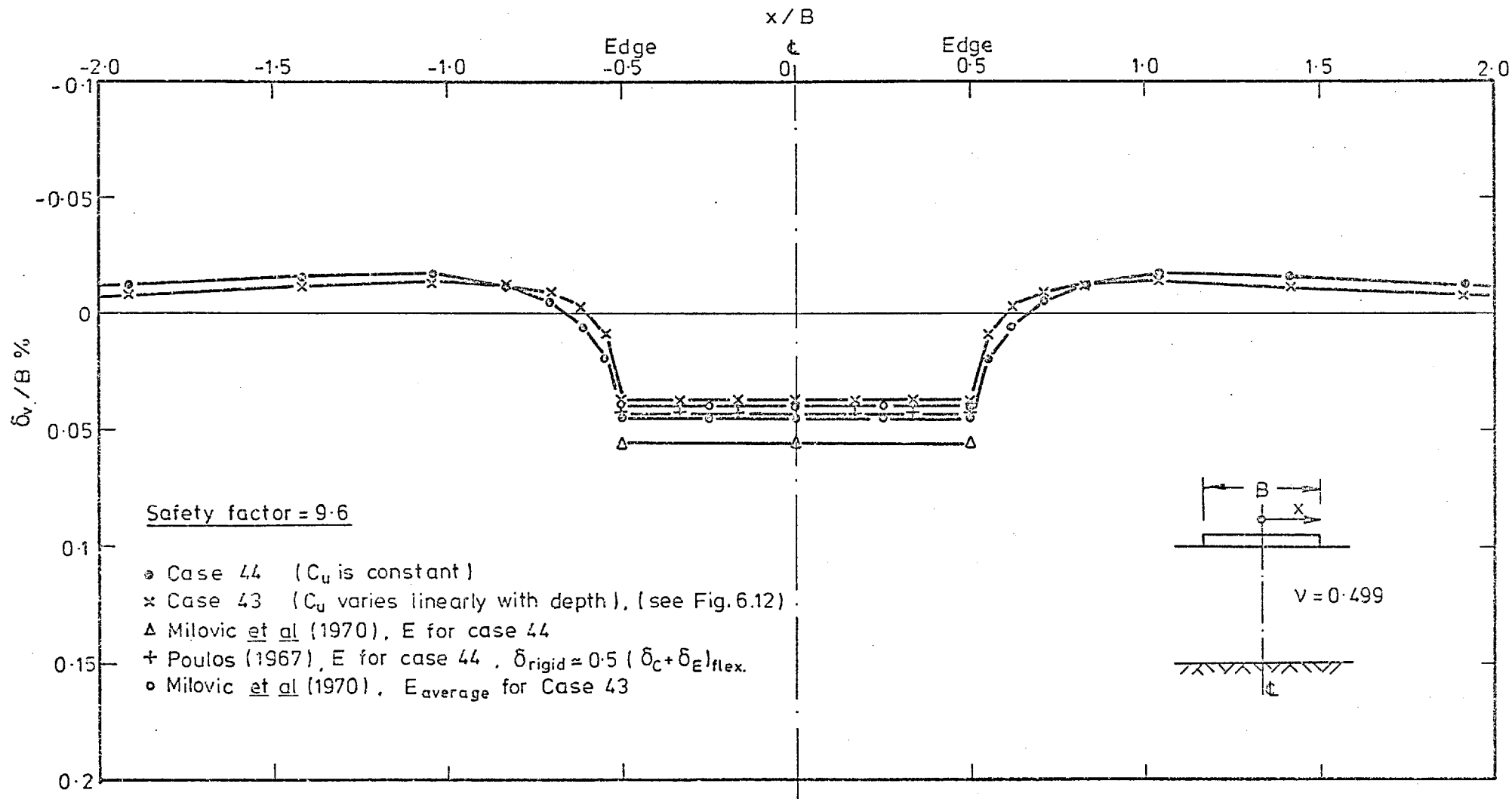
Fig. 6.34   Effect of the non-homogeneity on the surface settlement

268
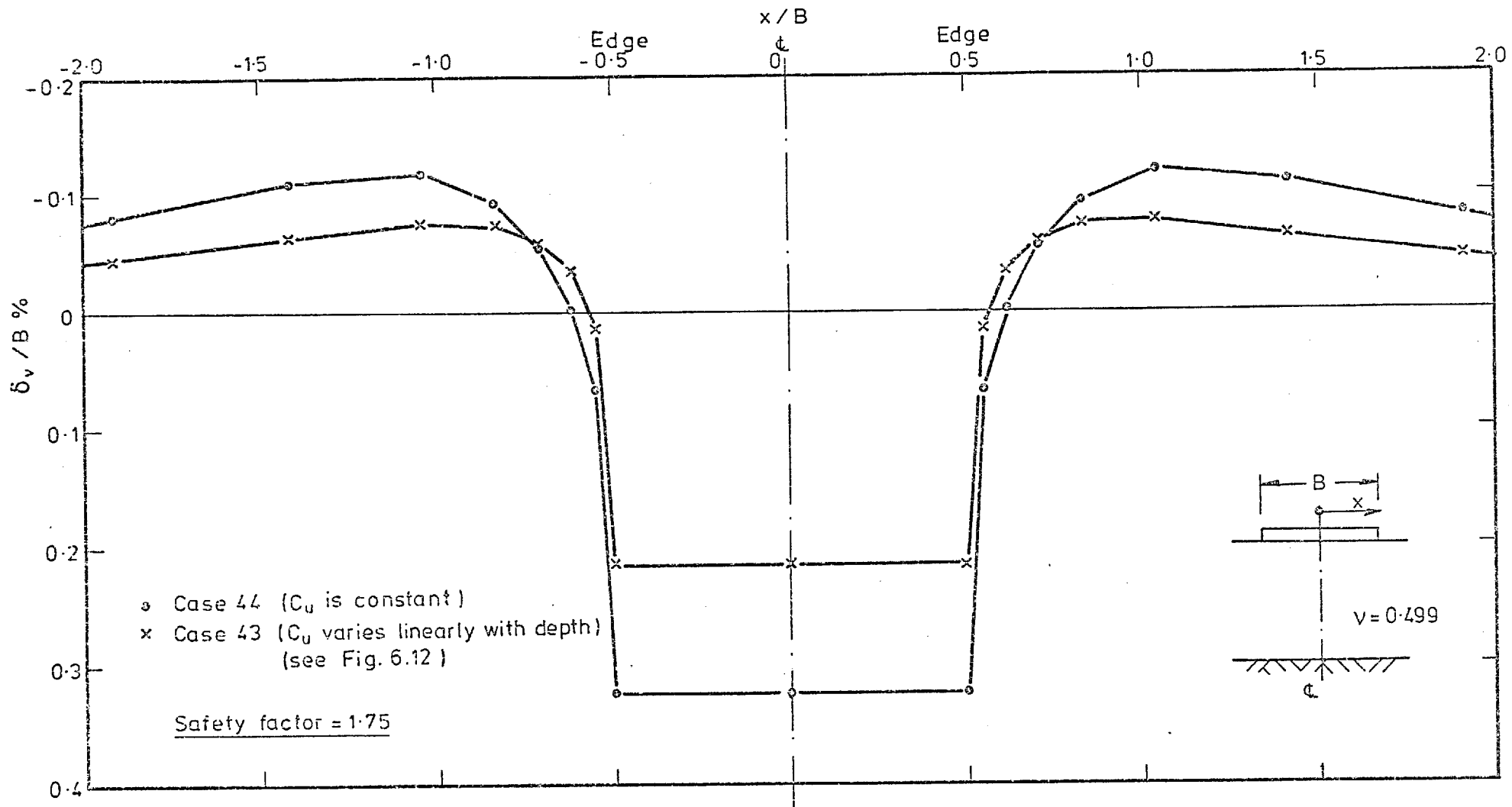
Fig. 6.35   Effect of the non-homogeneity on the surface settlement
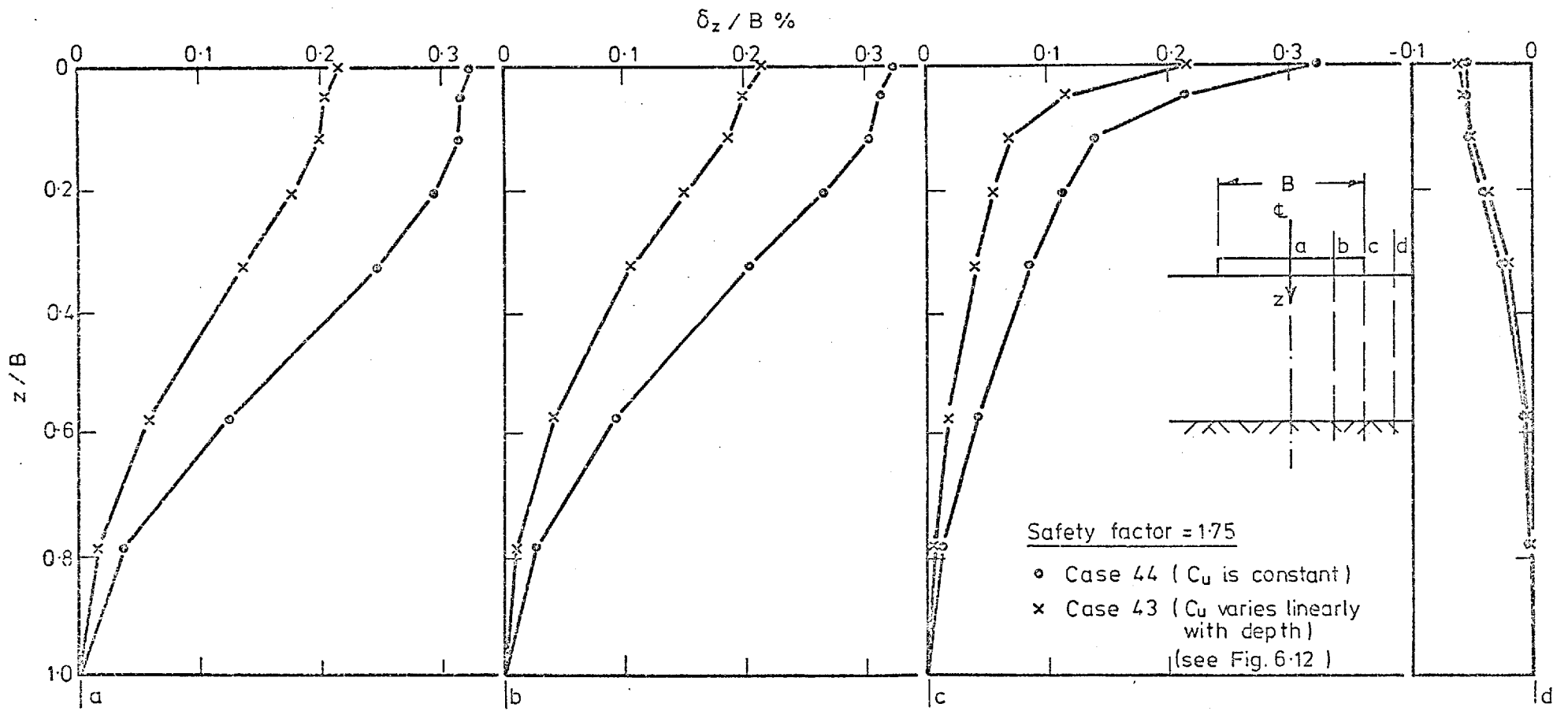
Fig. 6.36   Effect of the non-homogeneity on the vertical displacements

$\delta_x / B \%$

Safety factor = 1·75

CASE 44 ⊙ } (see Fig. 6·36)
CASE 43 × }
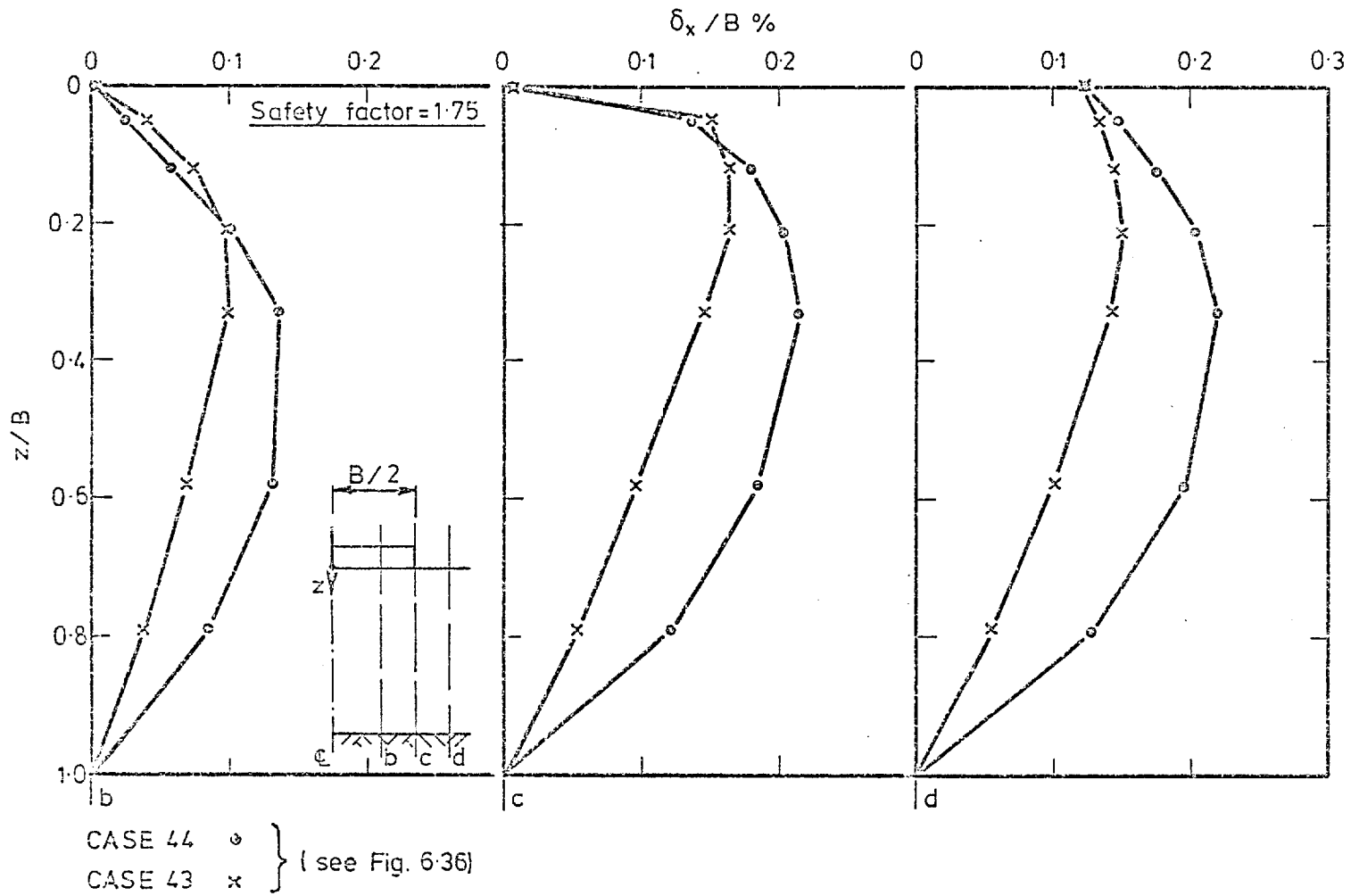
Fig. 6.37   Effect of the non-homogeneity on the horizontal displacements
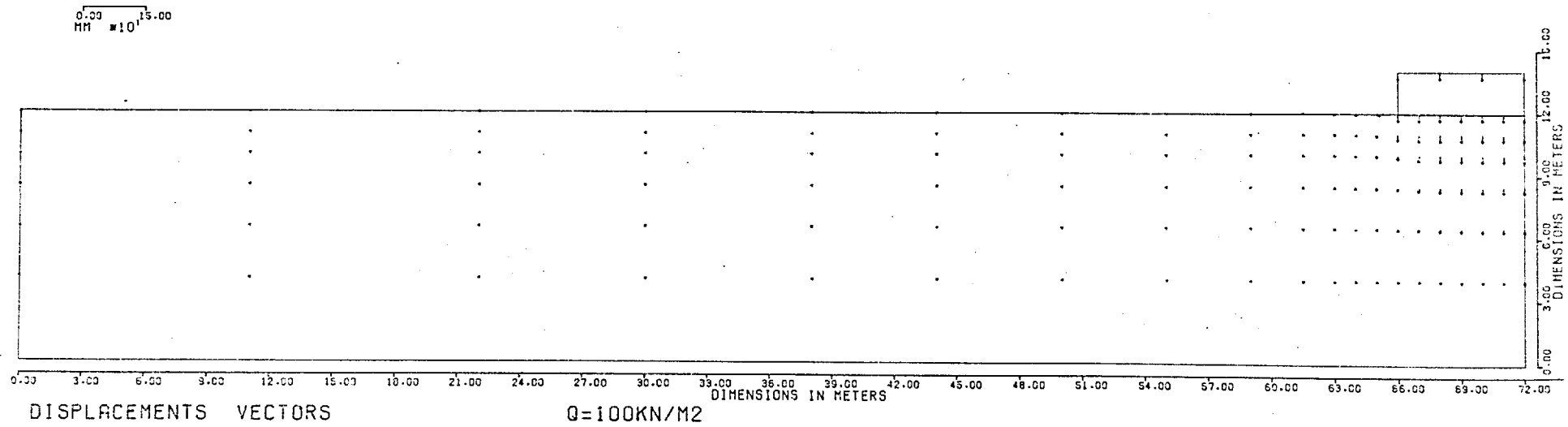
Fig. 6.38   Case 2 ($\phi' = 37°$, $c' = 0$, $\gamma = 16.3$ Kn/m^3, $K_o = 0.41$, $\nu = 0.33$),
Safety Factor = 46

```
0.00      15.00
MM  ×10¹
```

DISPLACEMENTS VECTORS   Q=300KN/M2
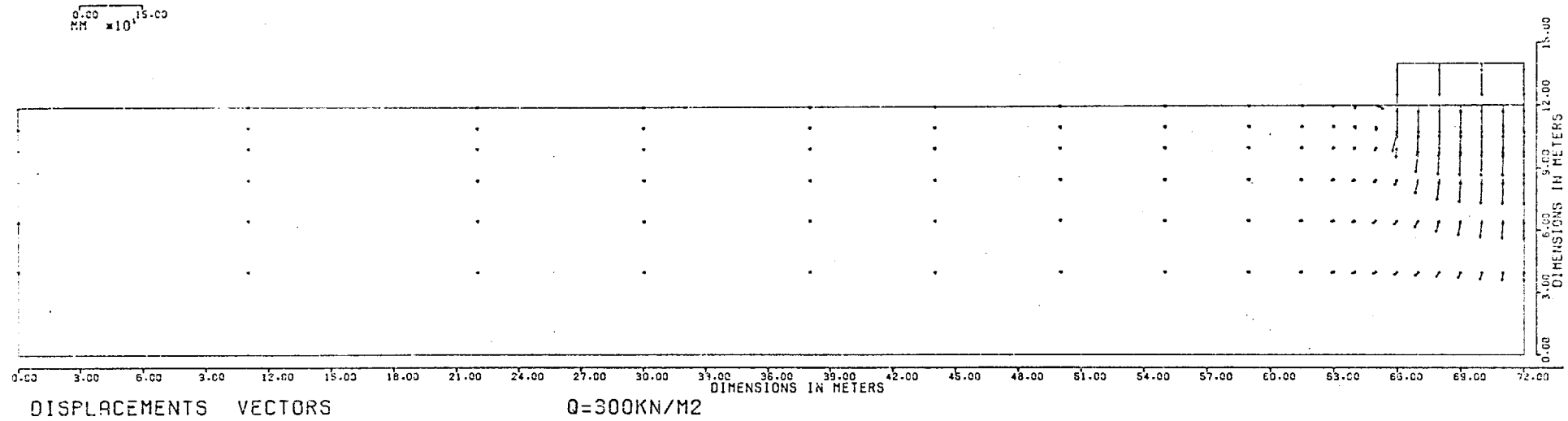
Fig. 6.39   Case 2 ($\phi' = 37°$, $c' = 0$, $\gamma = 16.3$ KN/m³, $K_o = 0.41$, $\nu = 0.33$),

Safety Factor = 15.3

273.

DISPLACEMENTS VECTORS   Q=500KN/M2

Fig. 6.40   Case 2 ($\phi' = 37^O$, $c' = 0$, $\gamma = 16.3$ KN/m^3, $K_o = 0.41$, $\nu = 0.33$),
            Safety Factor = 9.2
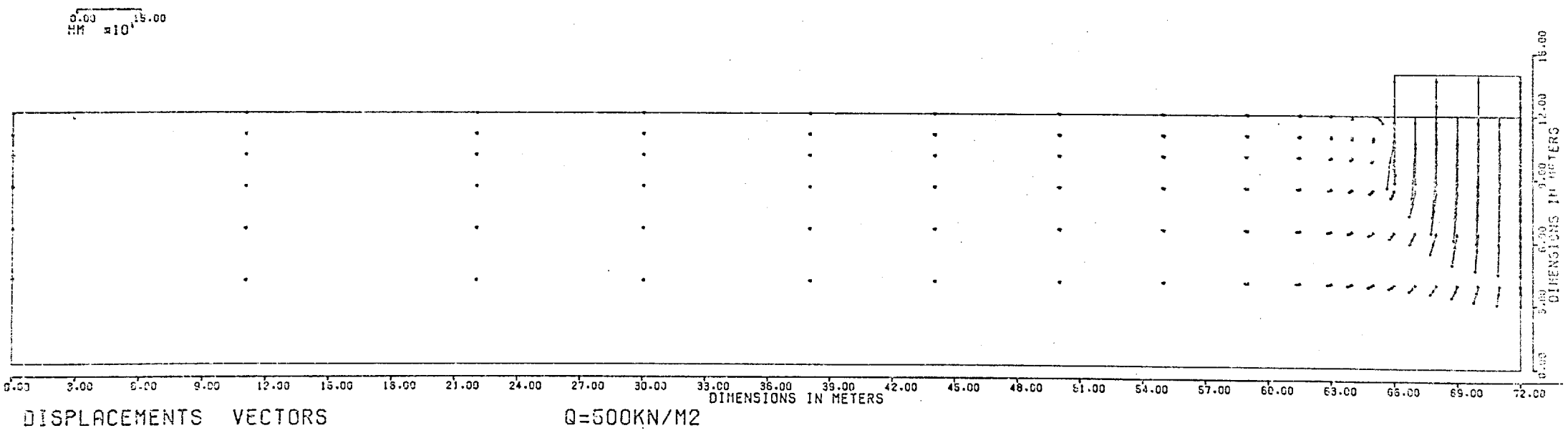
DISPLACEMENTS VECTORS   Q=200KN/M2
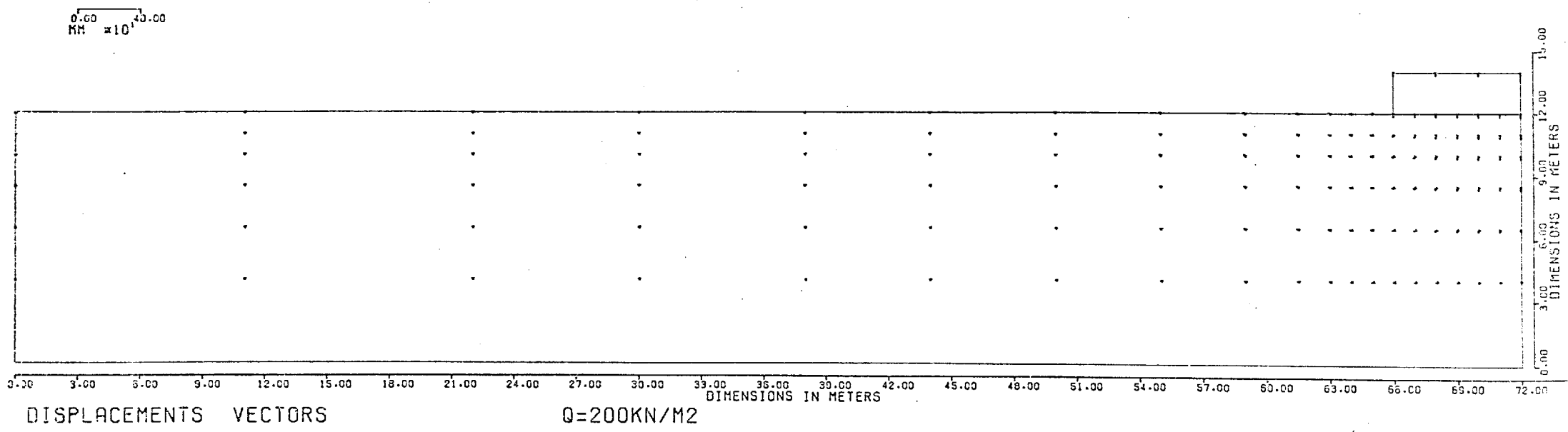
Fig. 6.41   Case 3 ($\phi = 0$, $C_u = 50$ KPa, $\gamma = 17.3$ KN/m^3, $K_o = 1$),
             Safety Factor = 1.29

DISPLACEMENTS   VECTORS   Q=260KN/M2
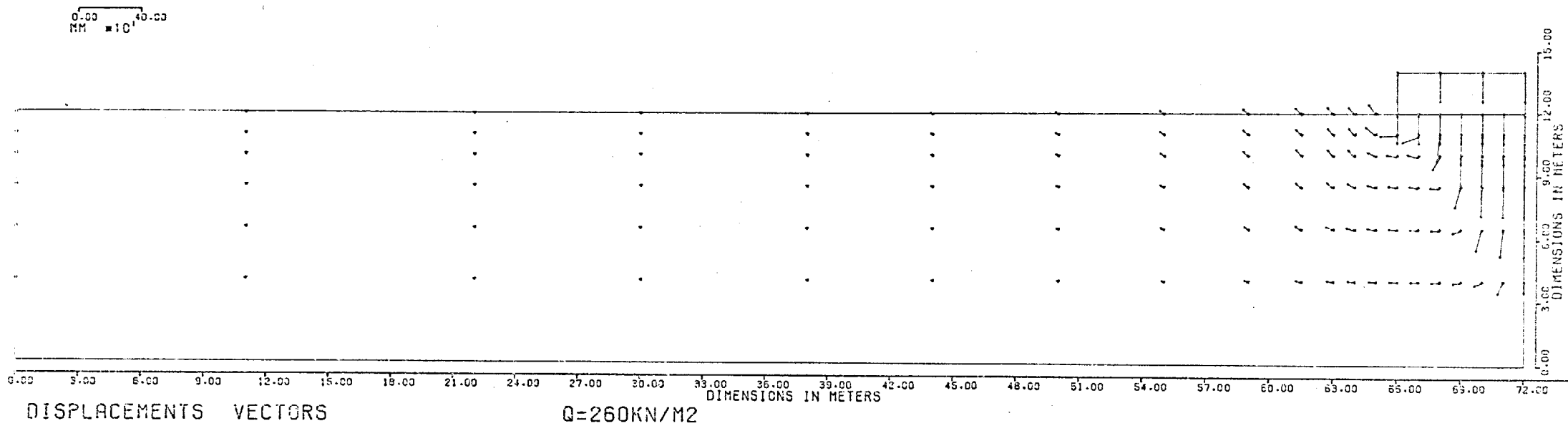
Fig. 6.42   Case 3 ($\phi = 0$, $C_u = 50$ KPa, $\gamma = 17.3$ KN/m^3, $K_o = 1$),
Safety Factor = 0.99

DISPLACEMENTS VECTORS   Q=400KN/M2
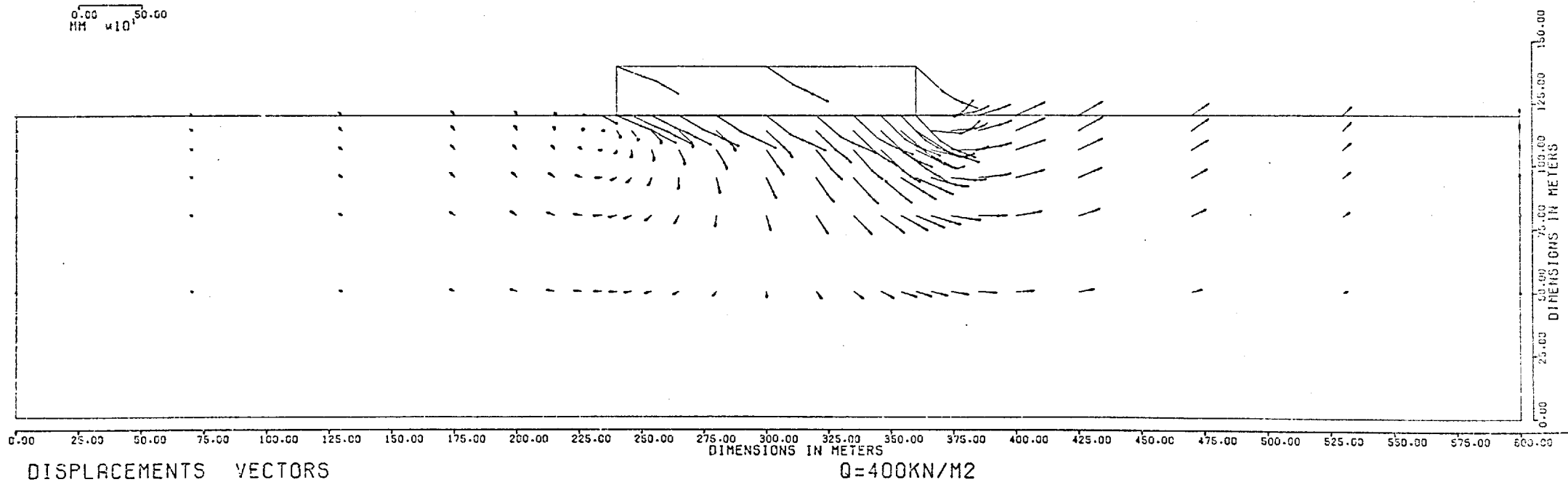
Fig. 6.43   Case 40 (see Table 5.2), Safety Factor = 0.89

DISPLACEMENTS VECTORS

Q=405KN/M2
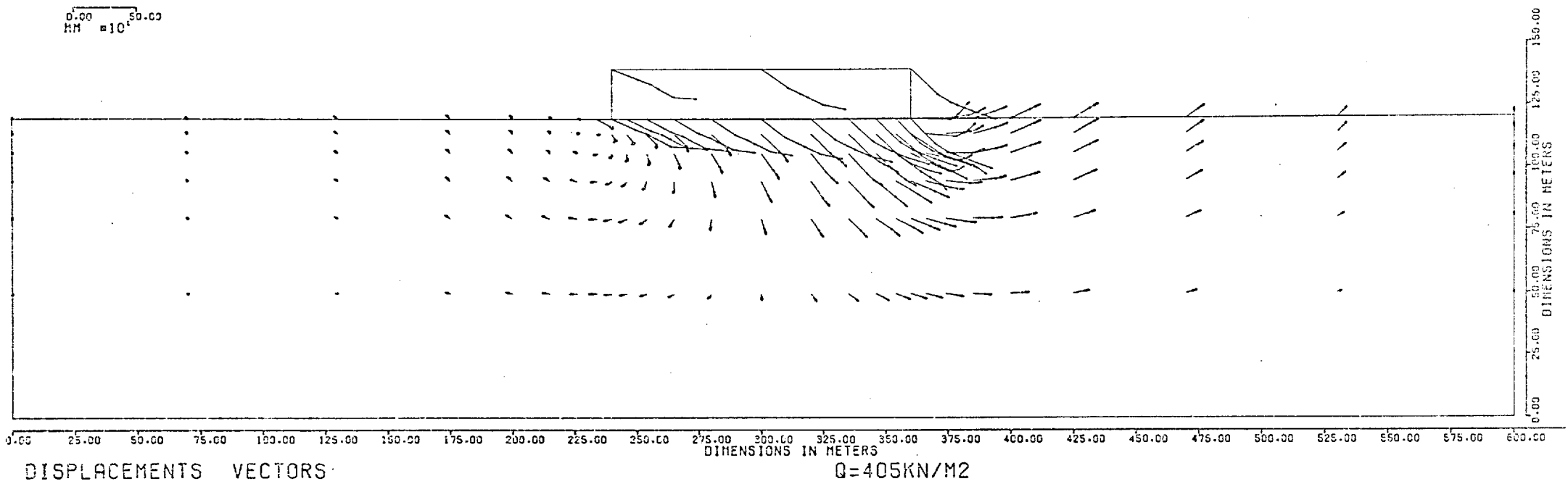
Fig. 6.44   Case 40 (see Table 5.2), Safety Factor = 0.88

q/q_f axis: 0   0·02   0·04   0·06   0·08   0·10   0·12

Linear

First local failure

F.E.

δ_{zc} = centre settlement

B = footing width

q_f is given in Table 6.1

CASE 2

$\Phi' = 37°$, $c' = 0$

$\gamma = 16\cdot3\ kN/m^3$, $K_o = 0\cdot41$
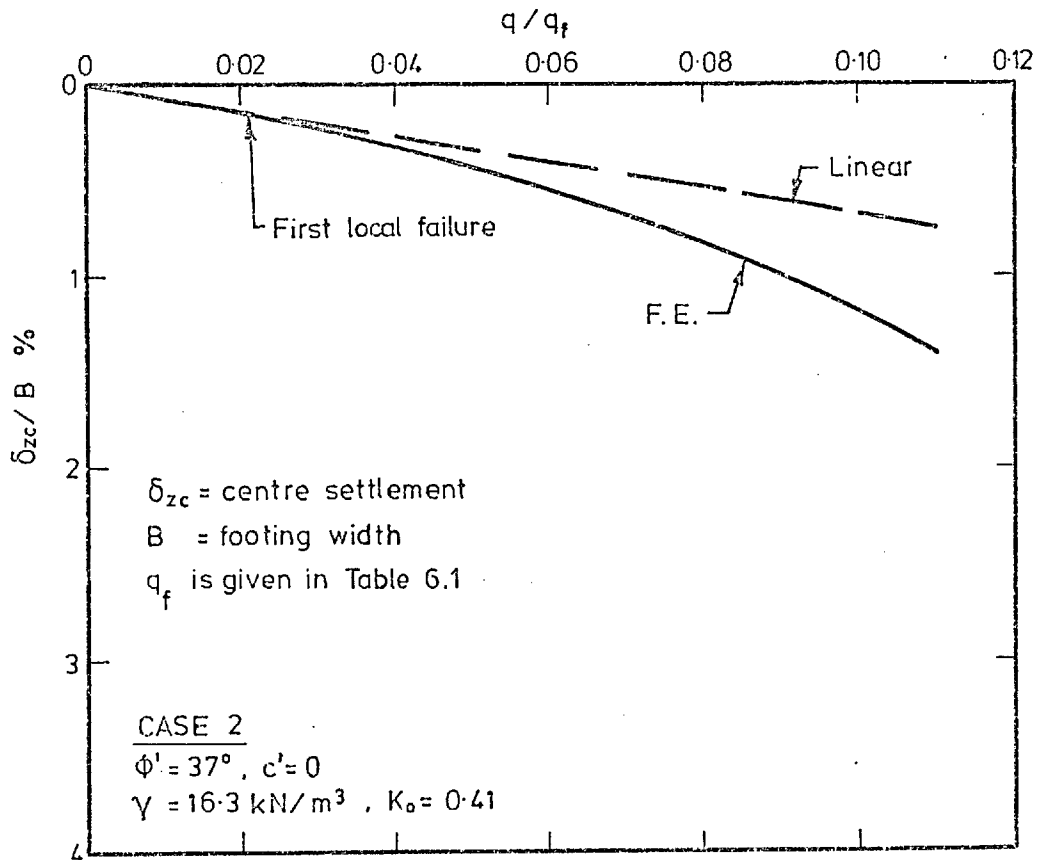
Fig. 6.45a   Load-Settlement Curve
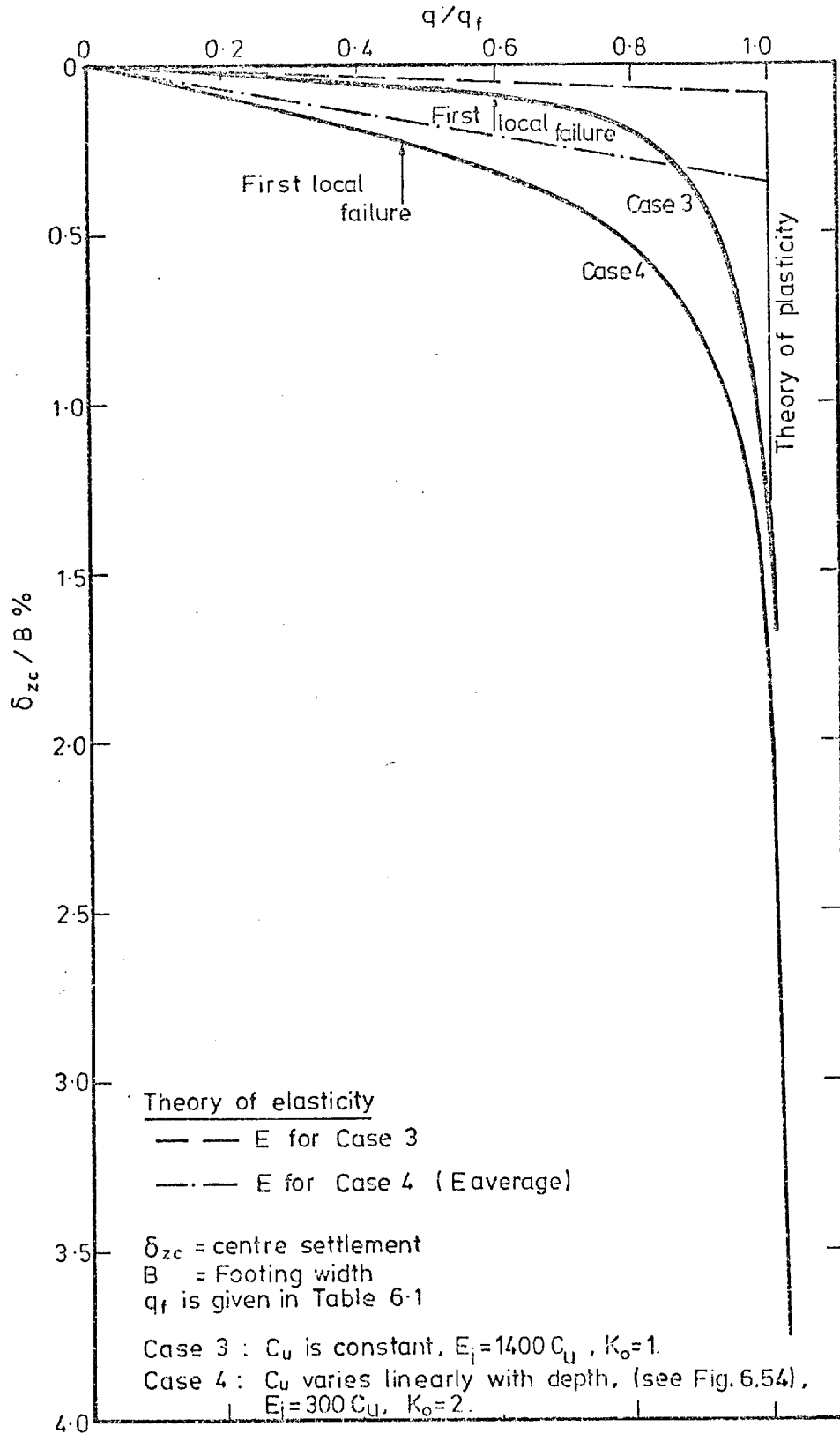
Fig. 6.45b   Load-Settlement Curves
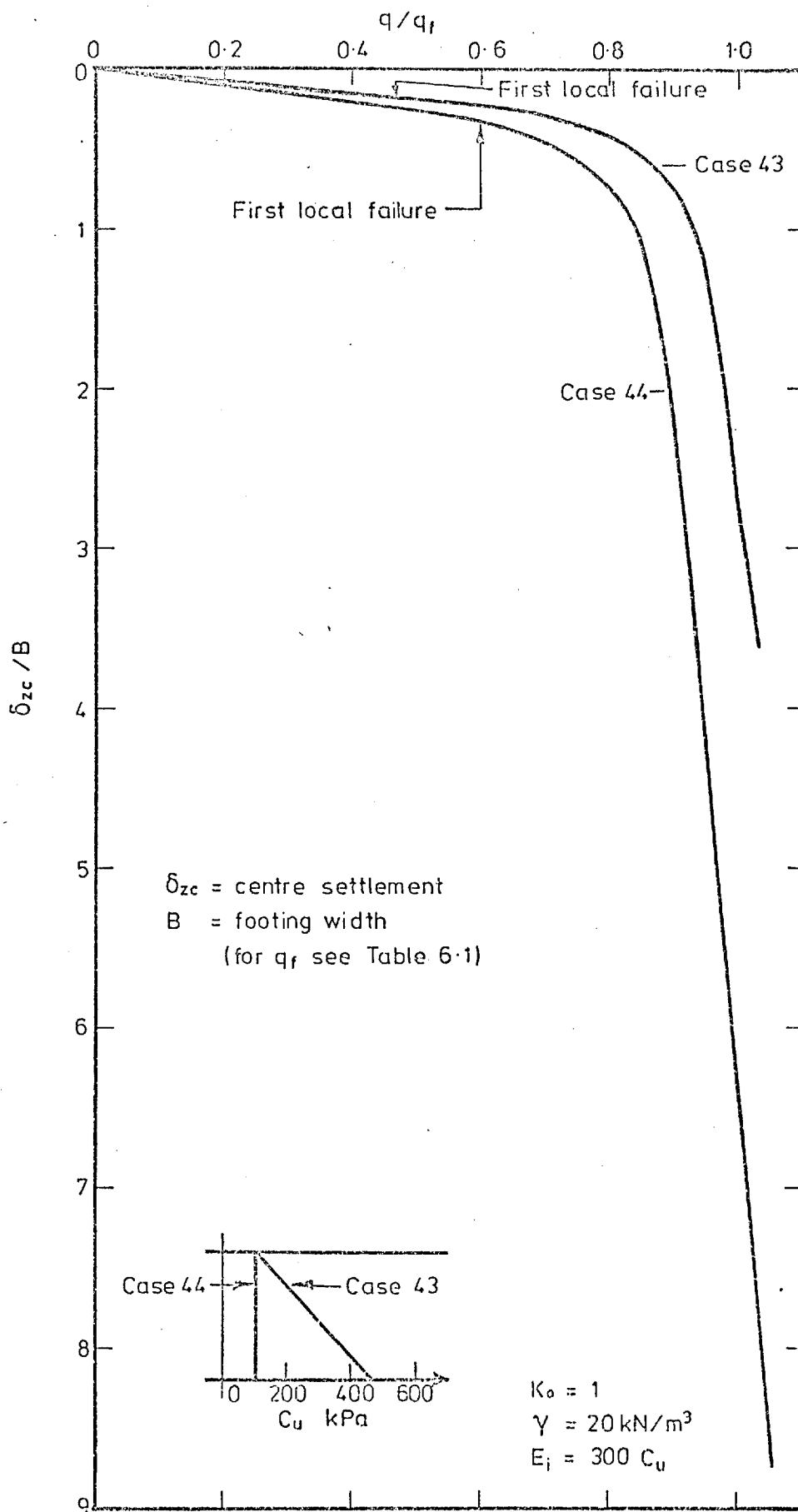
Fig. 6.45c Effect of the Non-homogeneity on the Safety Factor at First Local Failure

Fig. 6.45d   Effect of K_O on the Safety Factor at
First Local Failure

q/q_f

δ_{zc}/B %

First local failure
(Case 12)

First
local
failure (Cases 9&11)

Case 12

Case 9&11

q_f is given in Table 6.1

For geometry see Fig. 6·5

$E_u = E_i$ (see Fig. 5·1)

δ_{zc} = centre settlement

B = footing width
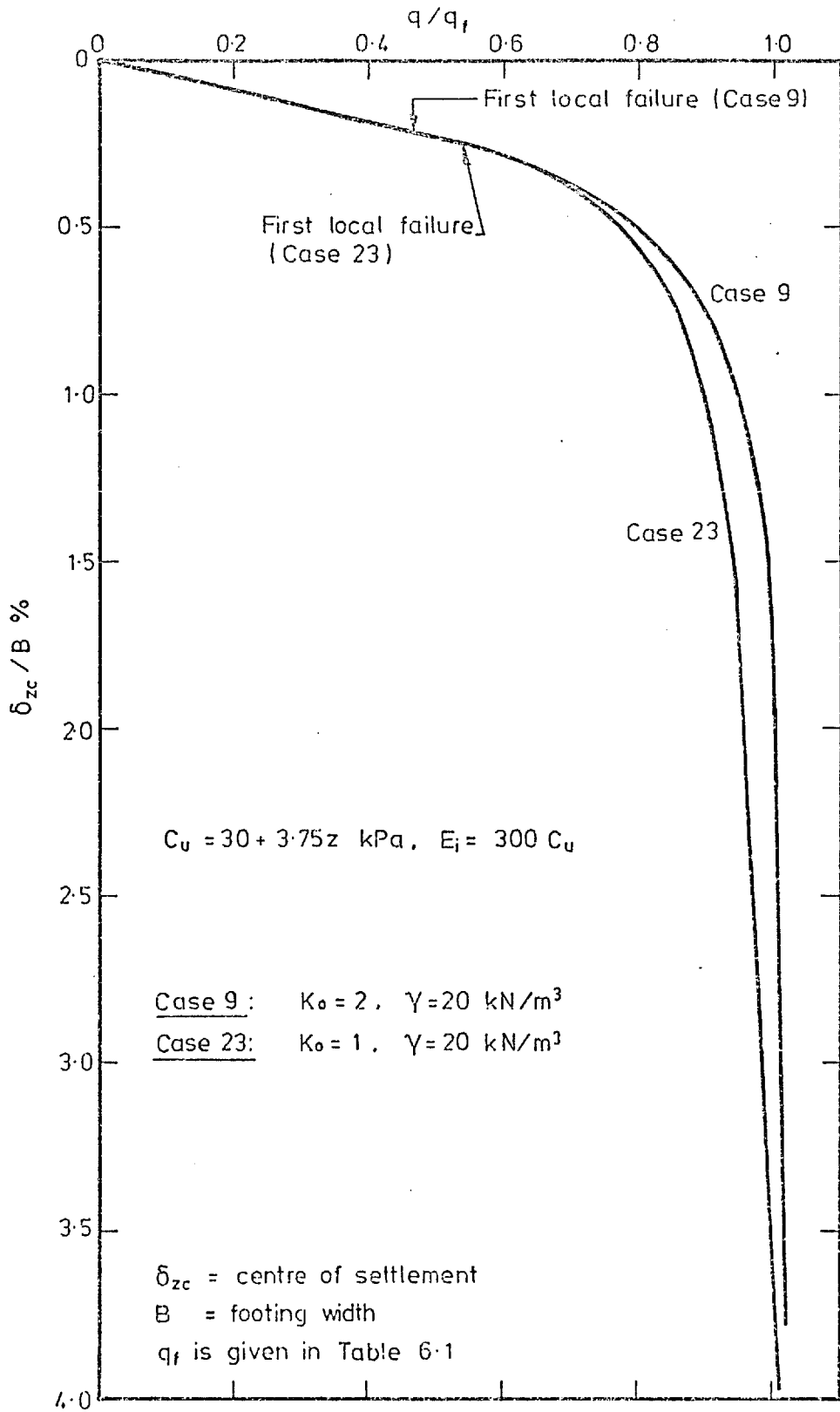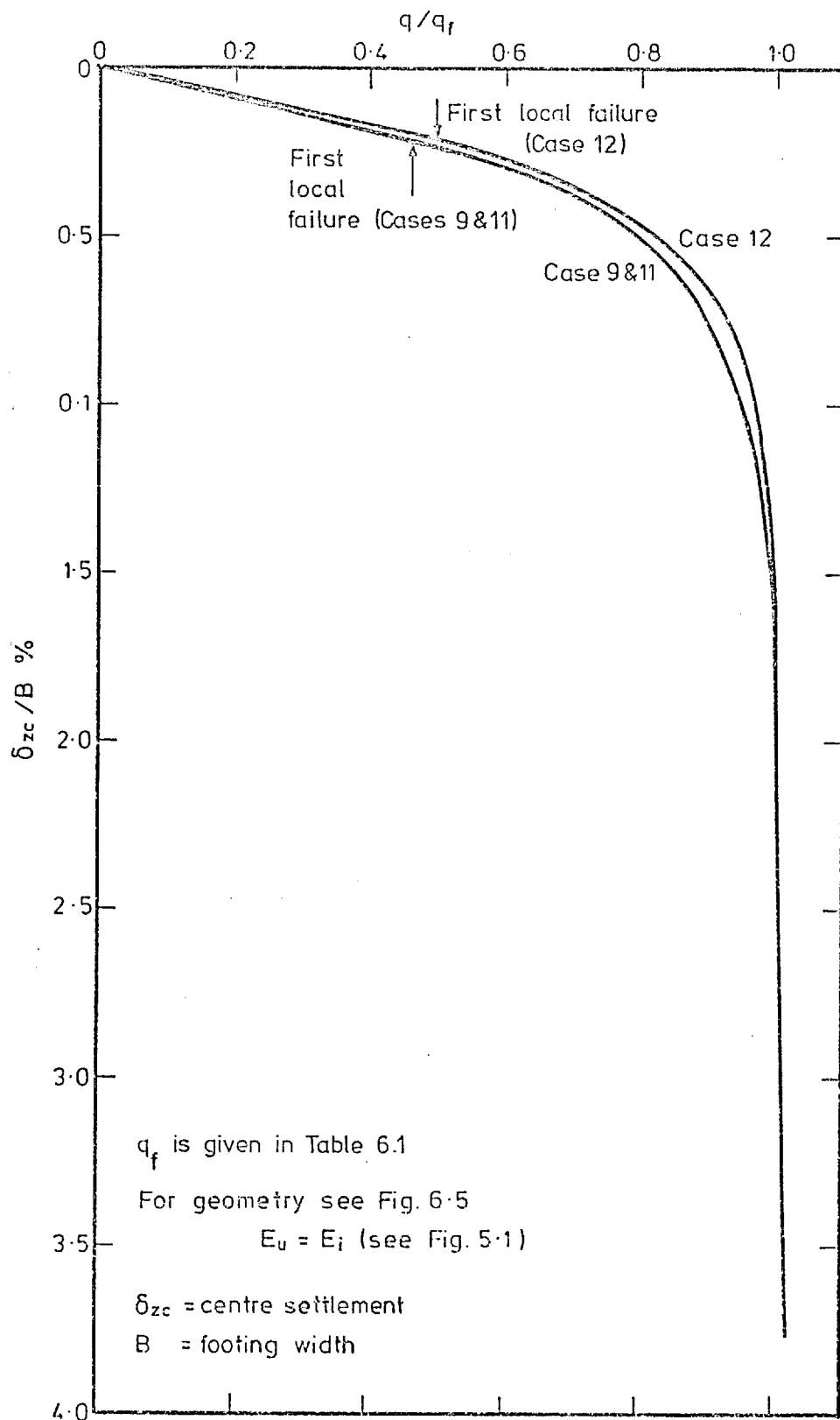
Fig. 6.46a   Effect of the Side Boundaries on
the Load-Settlement Curve

For geometry see Fig. 5.6

CASE 4 : $E_u = E_t$

CASE 9 : $E_u = E_i$ (see Fig. 5.1)

q_f is given in Table 6.1

δ_{zc} = centre settlement

B = footing width
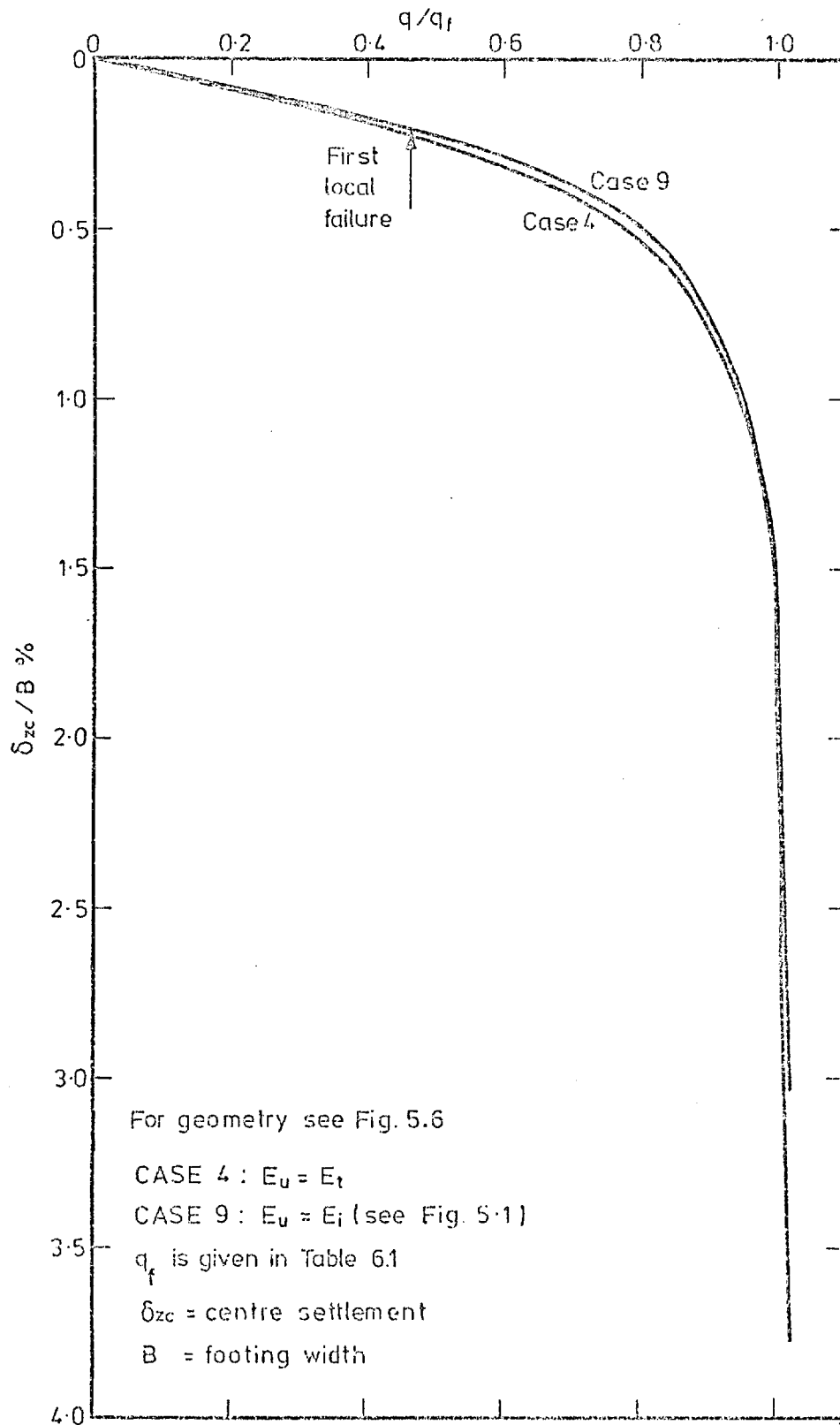
Fig. 6.46b   Effect of the Shear Unloading Modelling
on the Load-Settlement Curve

CASE 15   Depth = footing width , $K_o = 1.5$

CASE 16   Depth = twice footing width , $K_o = 1.5$

q_f is given in Table 6.1

δ_d = Differential settlement between two edges
B = Footing width
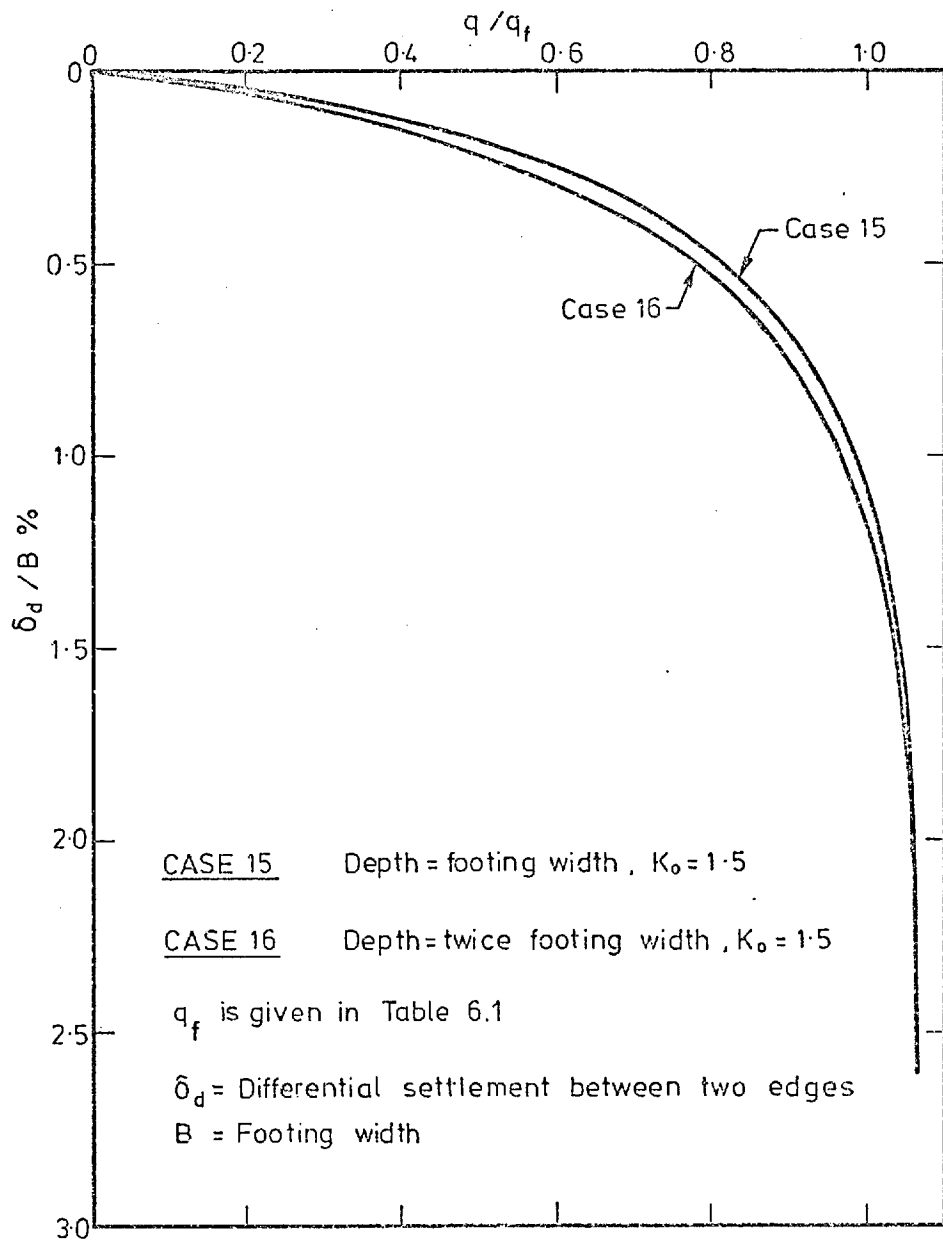
Fig. 6.47a   Effect of Layer Thickness on the
Load-Settlement Curve (Eccentric and
Inclined Load)
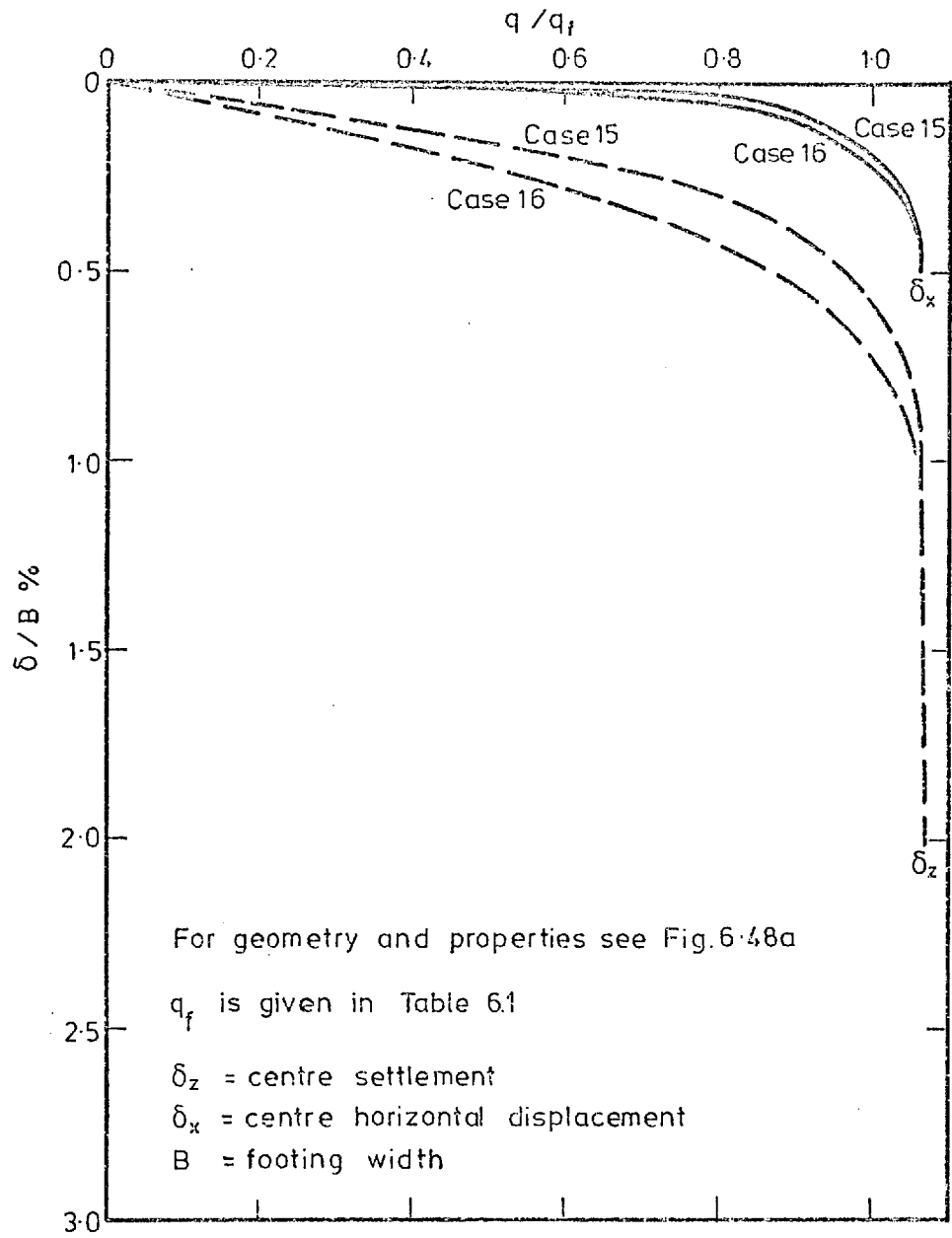
Fig. 6.47b Effect of Layer Thickness on the
Load-Settlement Curve (Eccentric and
Inclined Load)
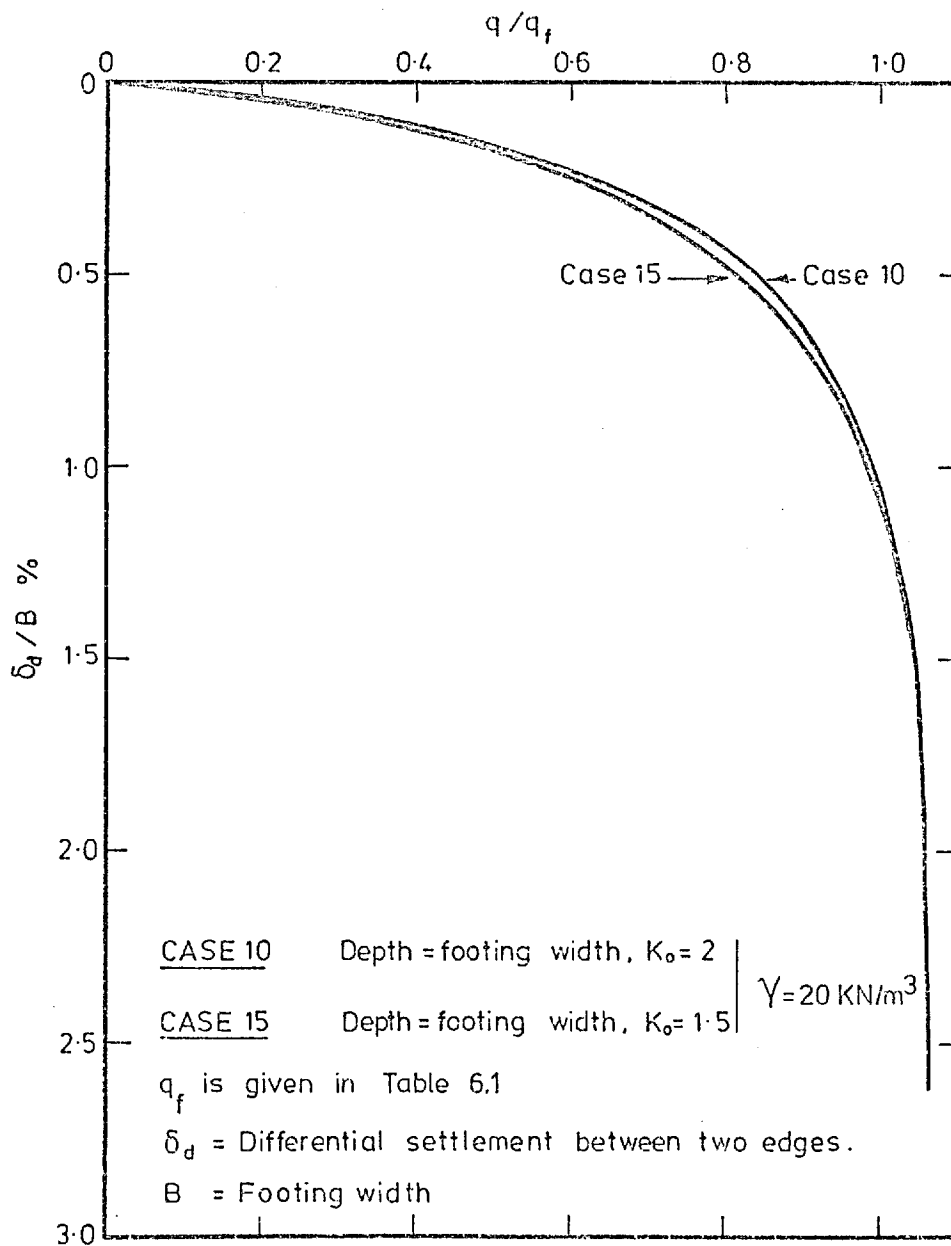
Fig. 6.48a   Effect of K_O on the Load-Settlement Curve
(Eccentric and Inclined Load)
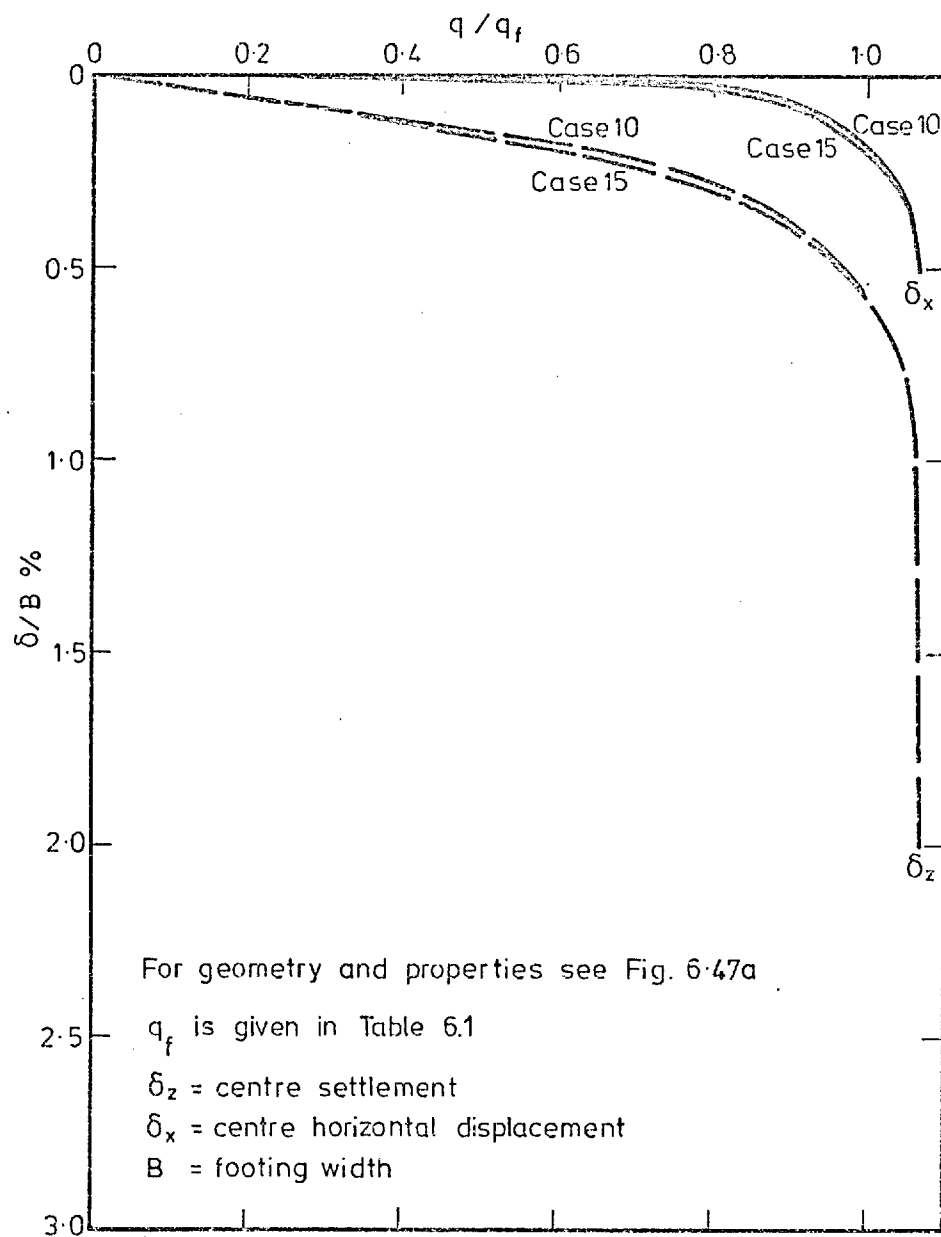
Fig. 6.48b   Effect of K_O on the Load-Settlement Curve
(Eccentric and Inclined Load)
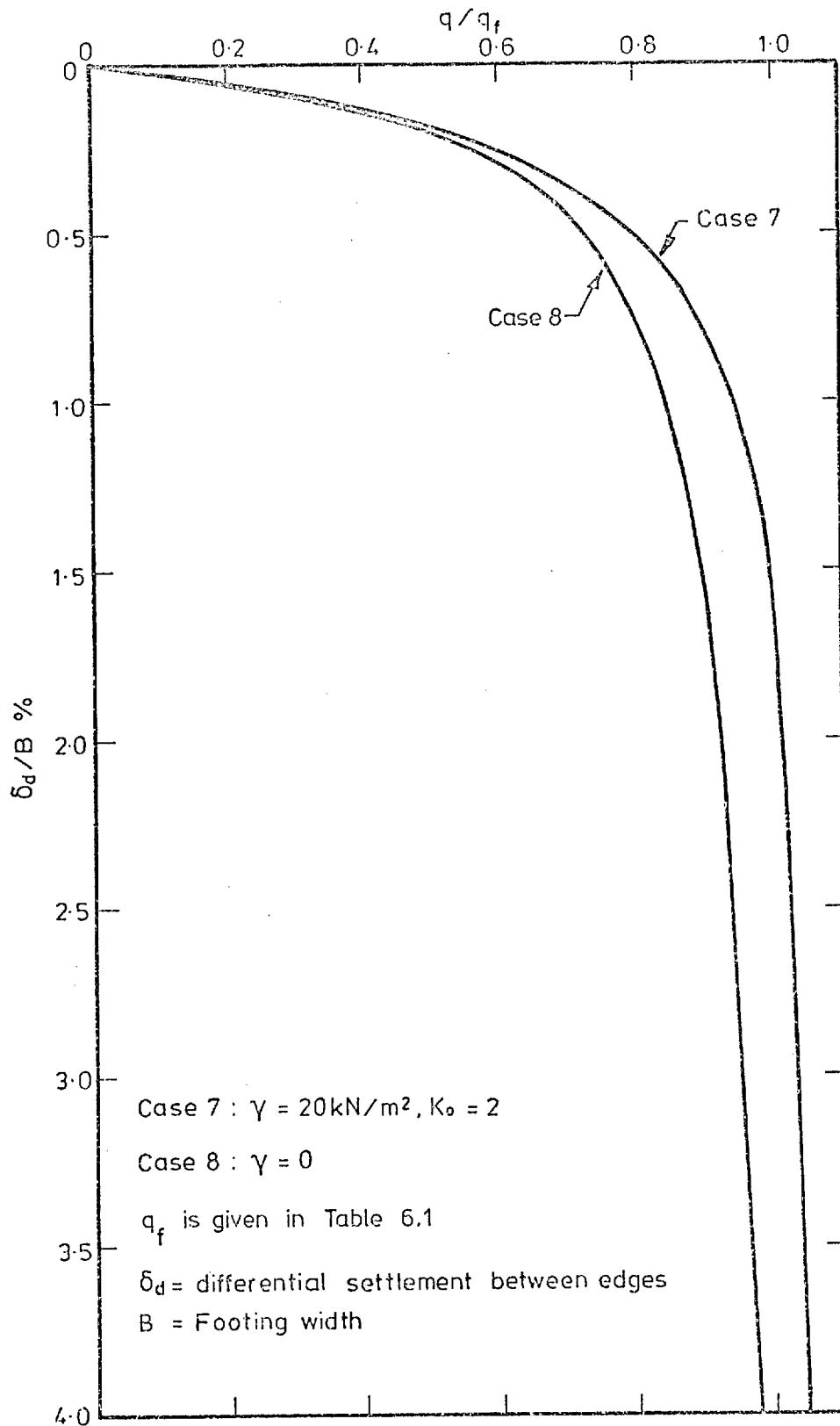
Fig. 6.49   Effect of the Soil Unit Weight on the Load-Settlement Curve (Eccentric and Inclined Load)
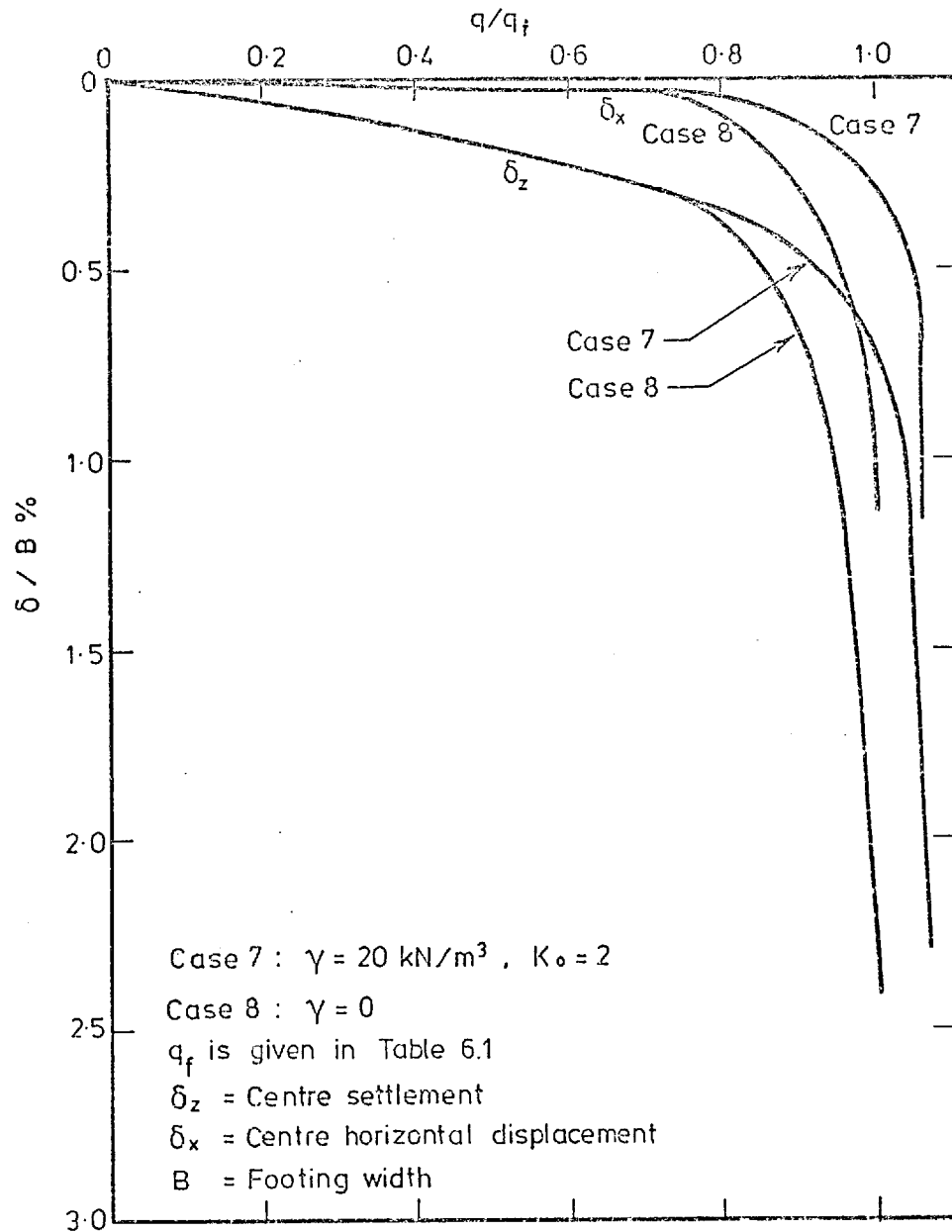
Fig. 6.50 Effect of the Soil Unit Weight on the Load-Settlement Curve (Eccentric and Inclined Load)
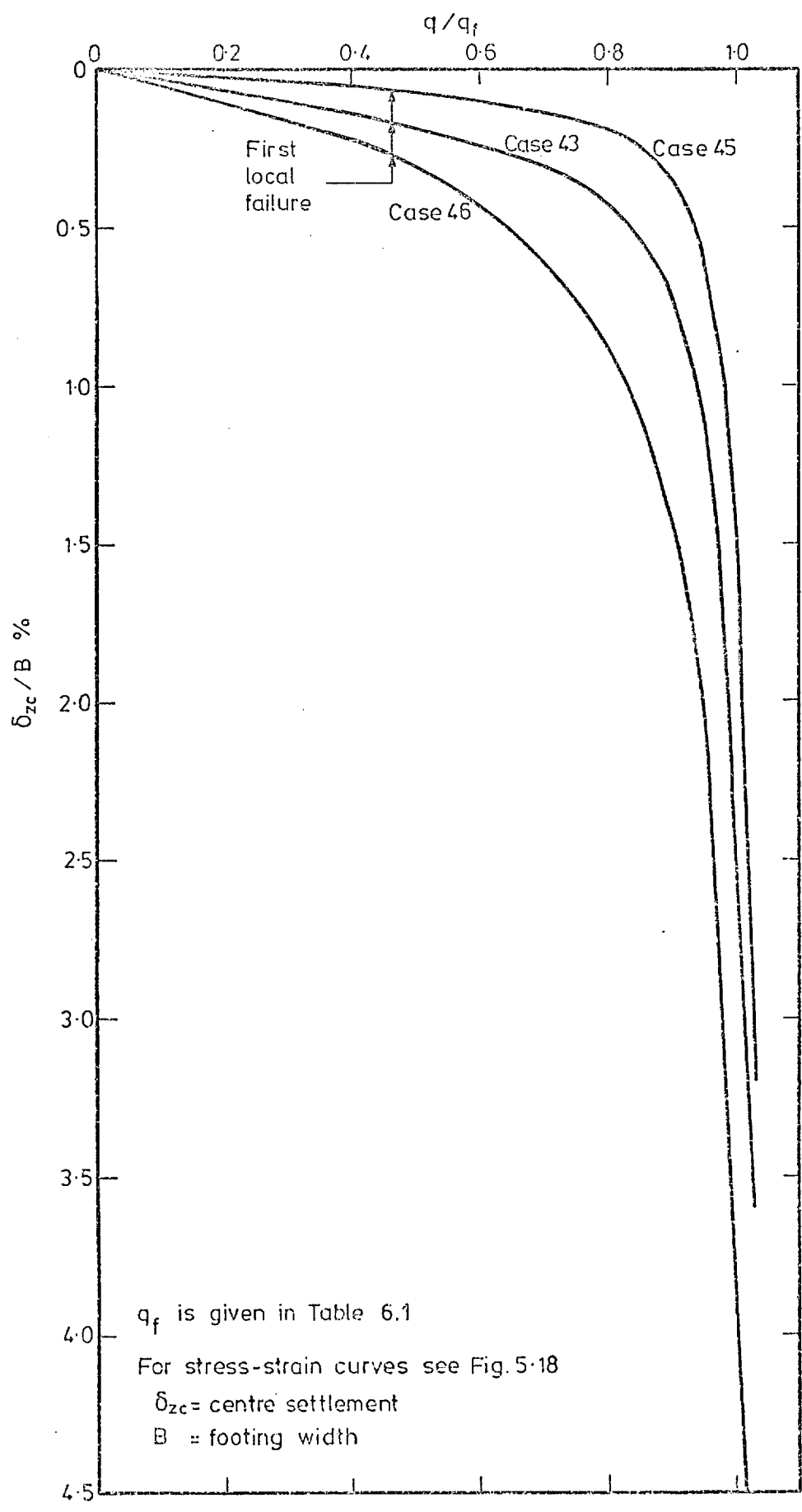
Fig. 6.51 Effect of the Stress-Strain Relationship on the Load-Settlement Curve
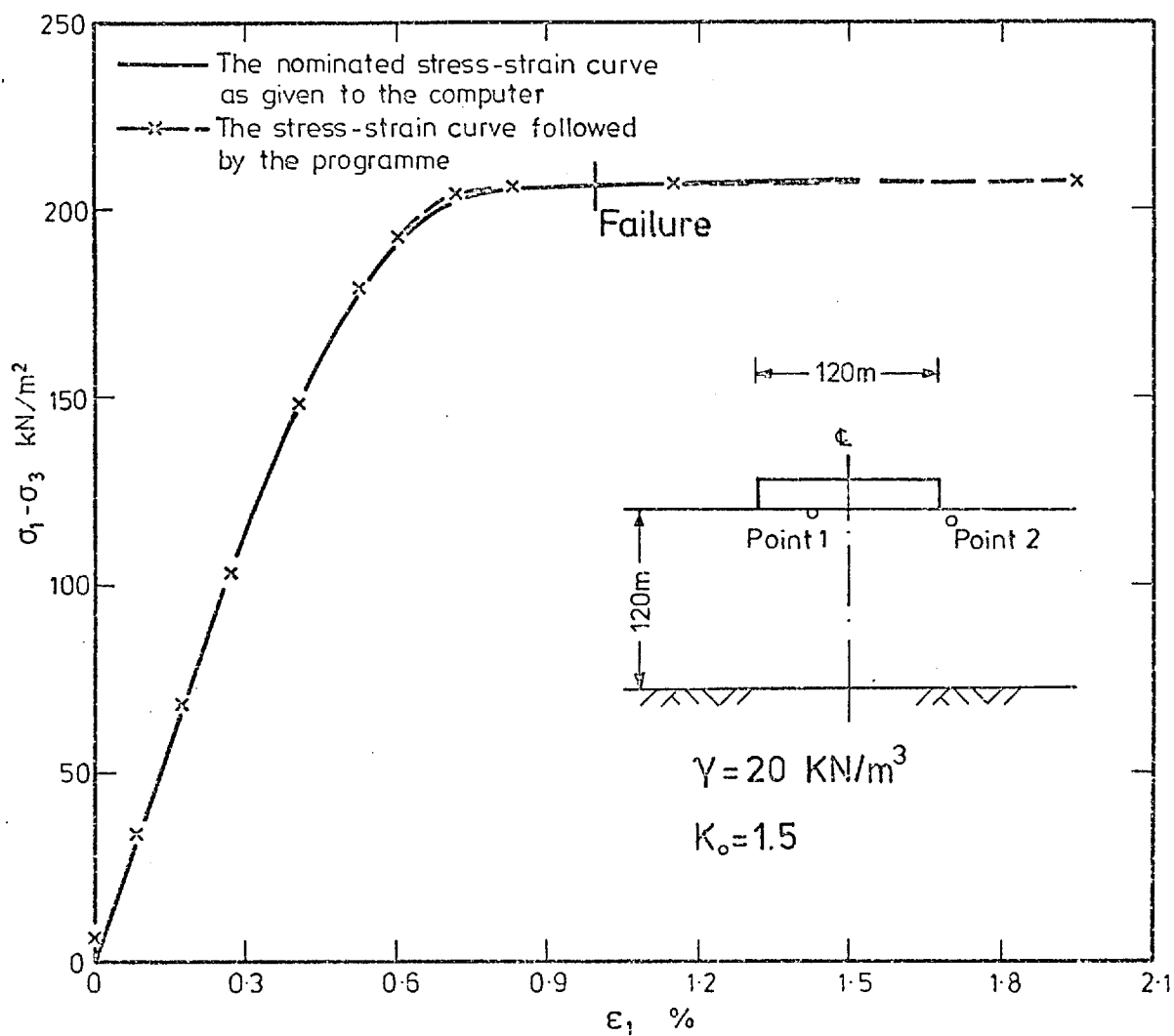
CASE 40 (see Table 5·2)

Point 1

Fig. 6.52   Stress-Strain Curve
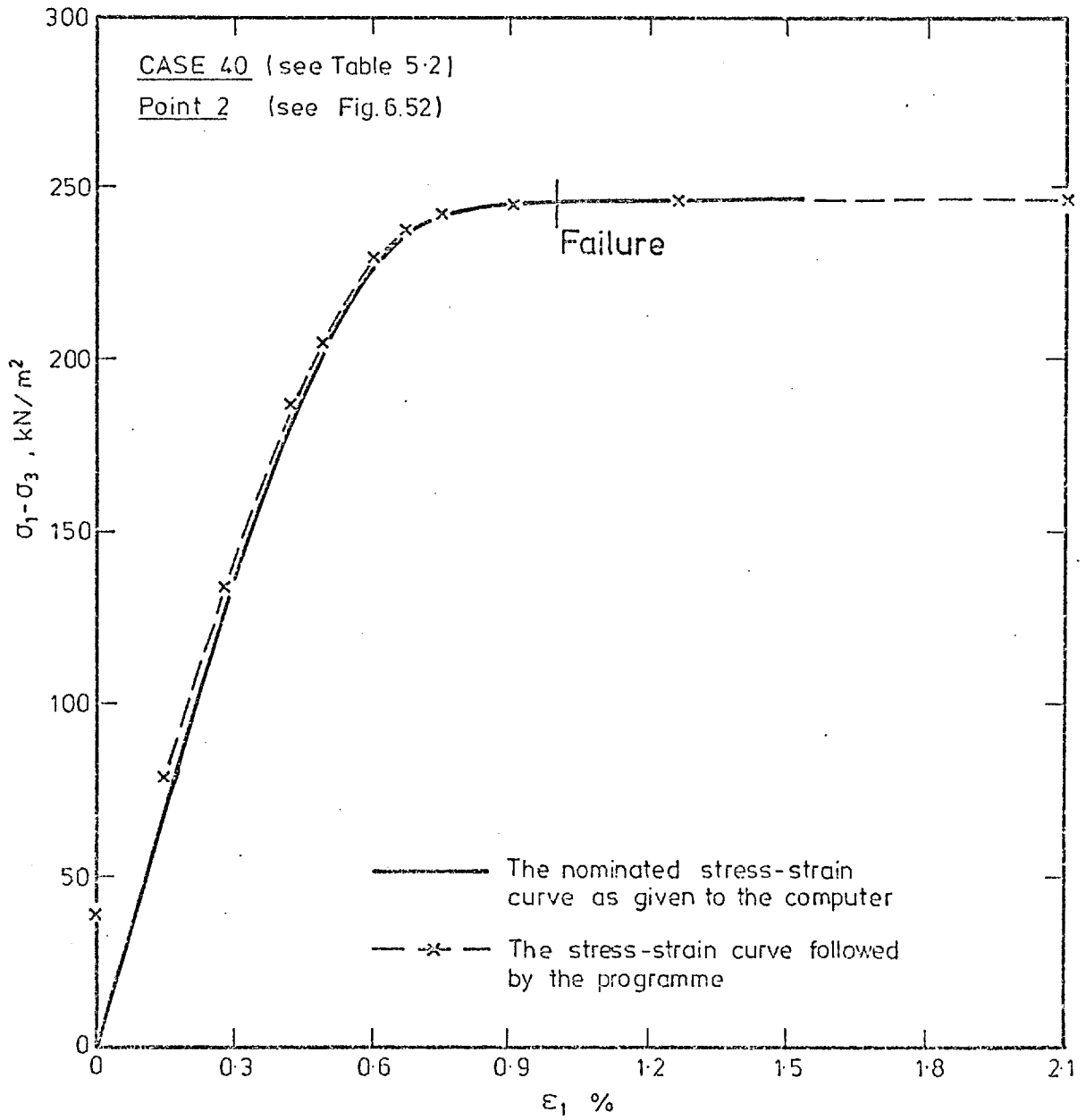
Fig. 6.53   Stress-Strain Curve
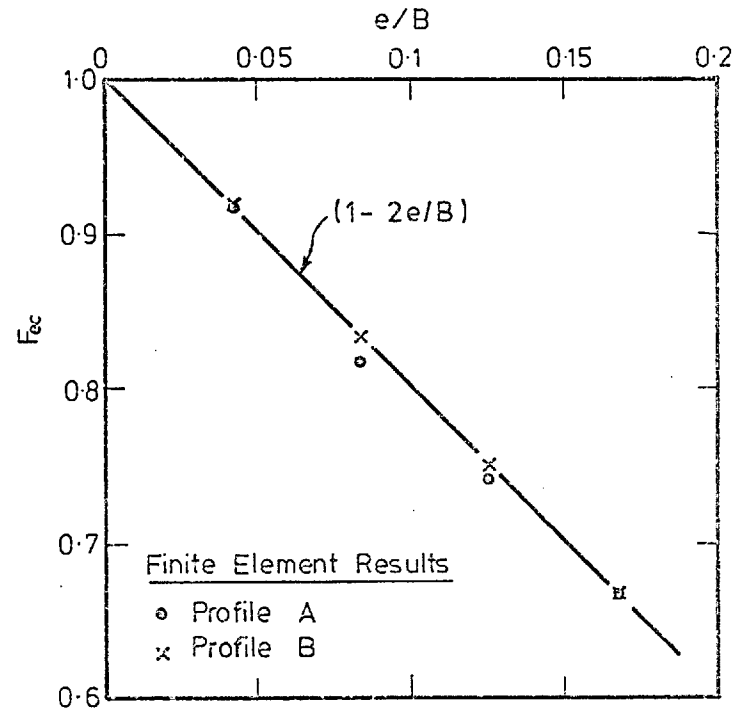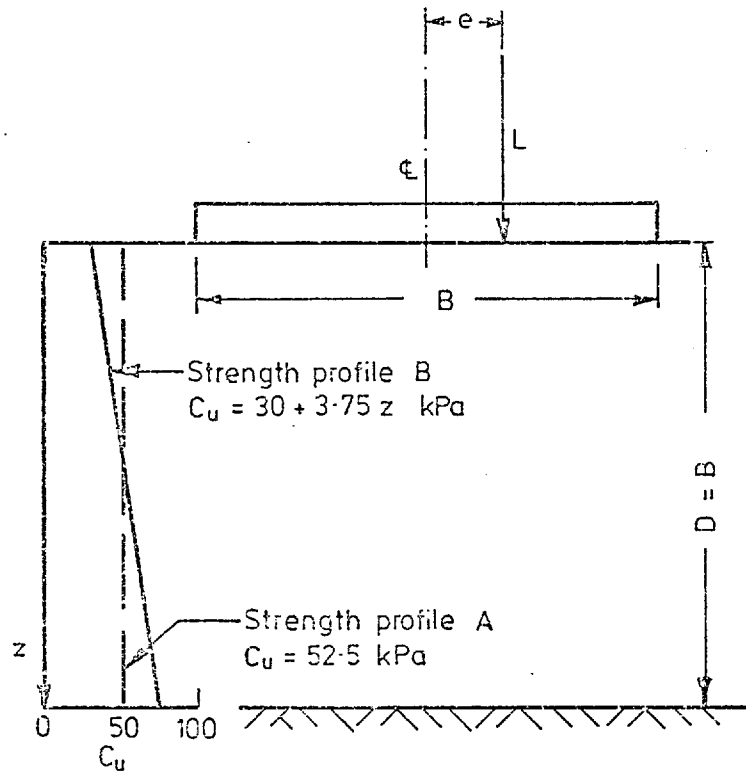
Fig. 6.54   Failure Pressure for Eccentric Vertical Load,
Load Eccentricity Factor, F_{ec}

CASE 2 ($\phi' = 37°$, $C' = 0$, $\gamma = 16.3$ kN/m³
$K_o = 0.41$, $\nu = 0.33$)

S. F. = 46
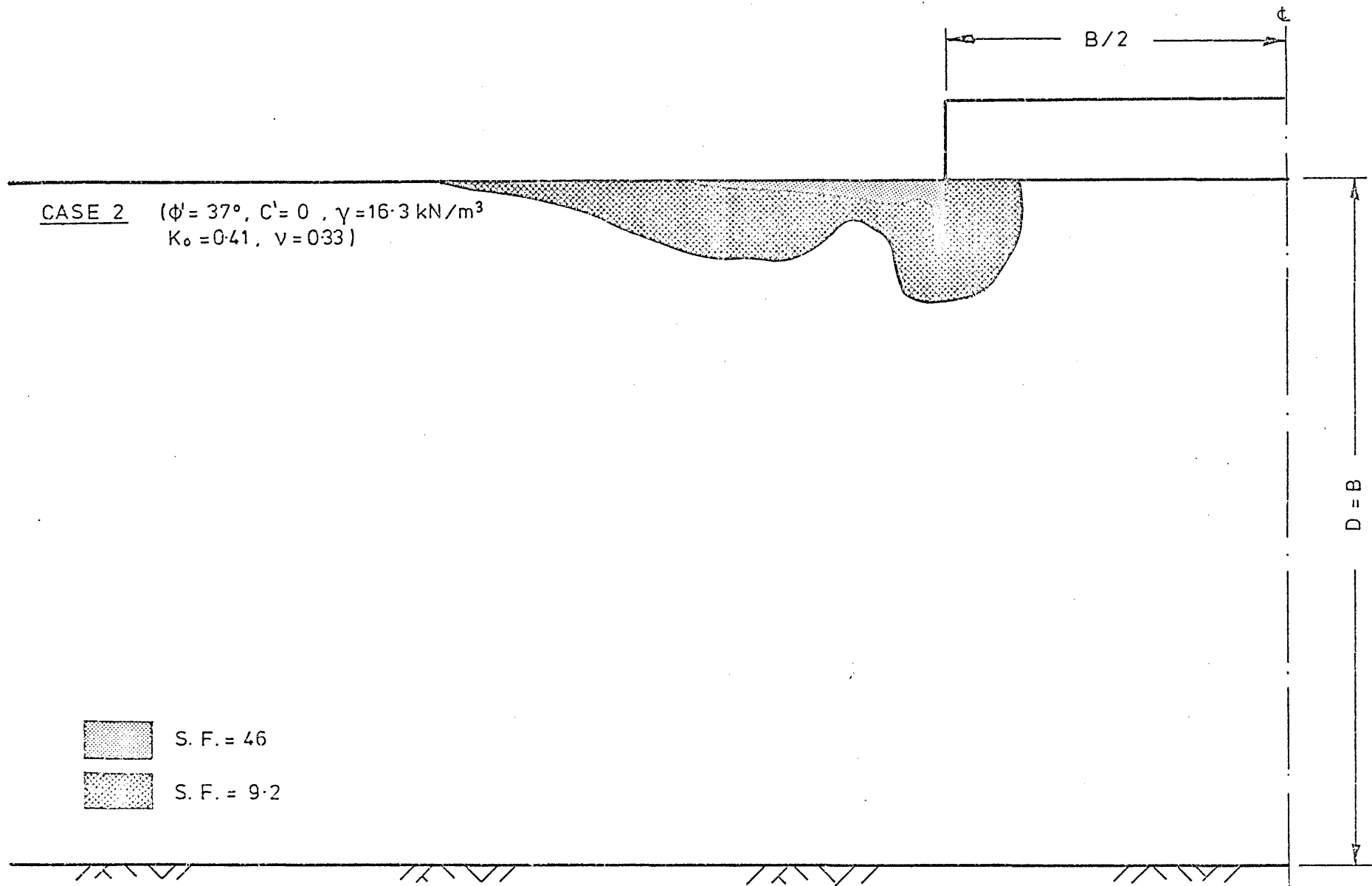
S. F. = 9·2

Fig. 6.55a   Failure Zone
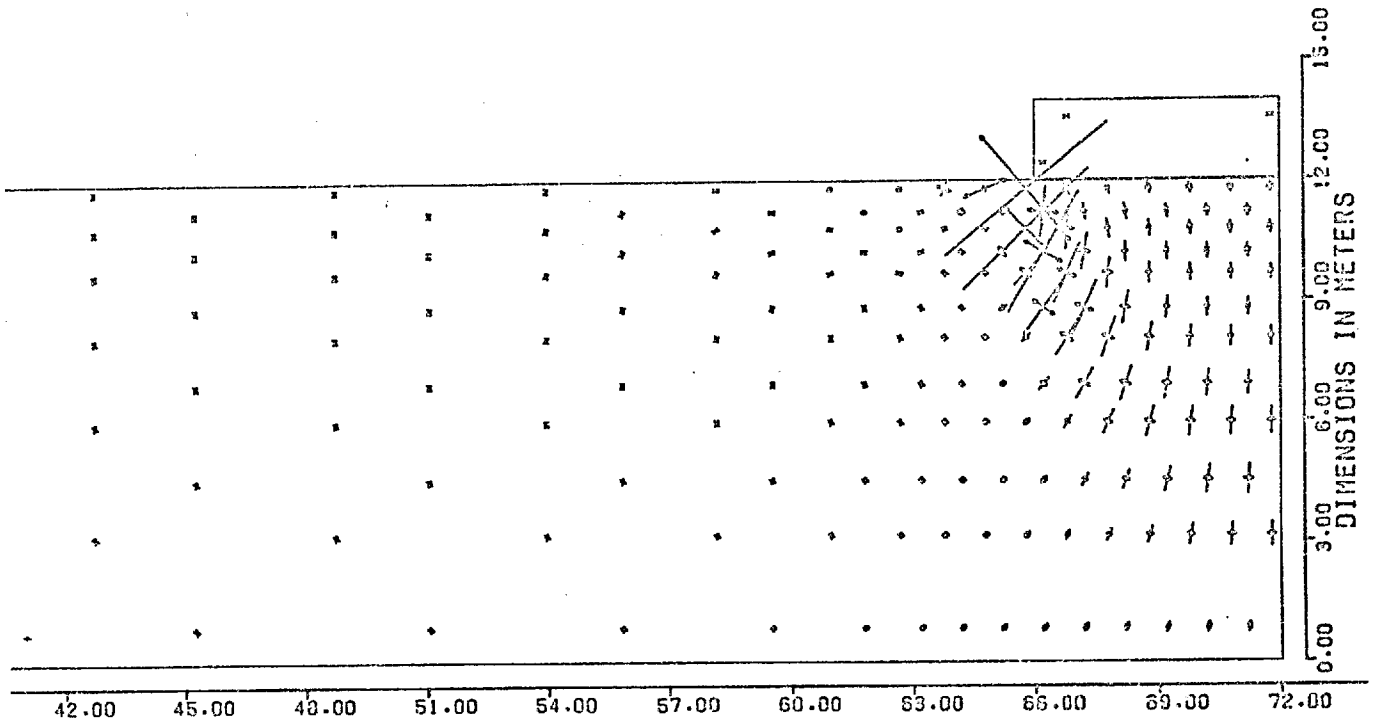
Fig. 6.55b Principal strain rotations for Case 2,
(S.F. = 15.3)
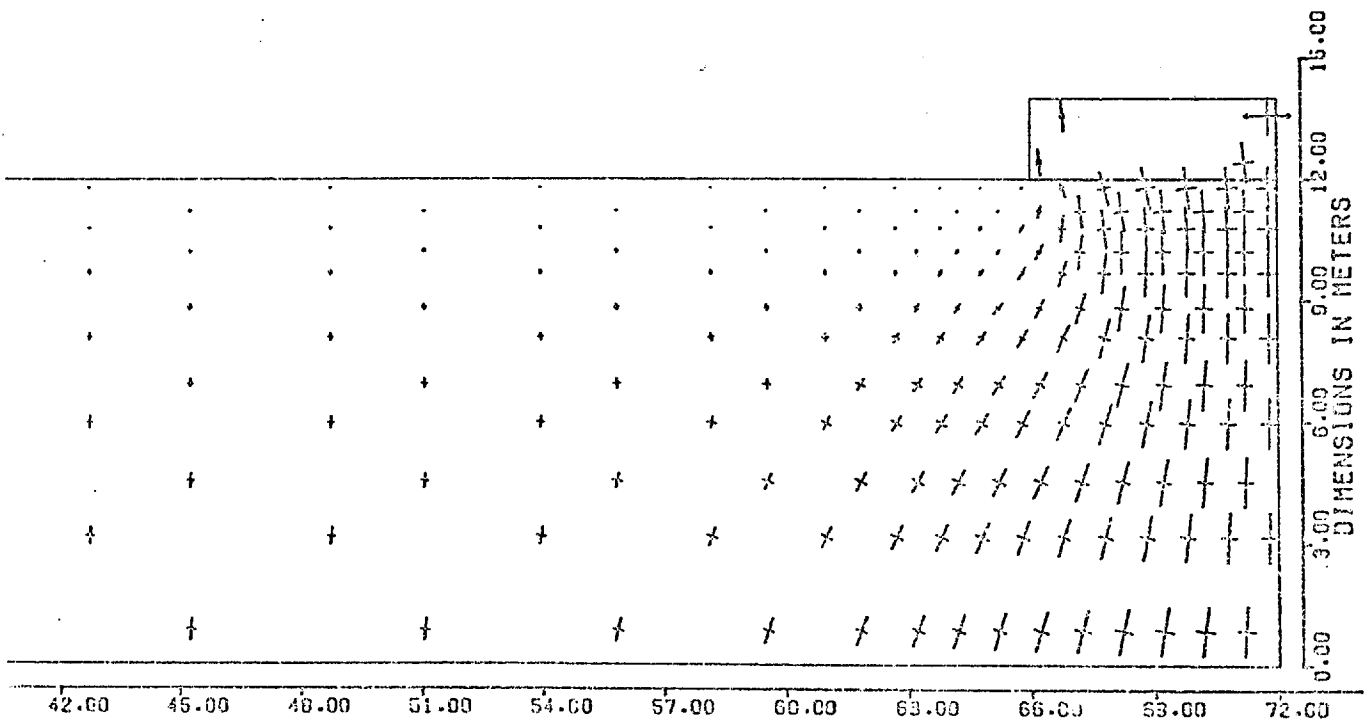
Fig. 6.55c Principal stress rotations for Case 2,
(S.F. = 15.3)
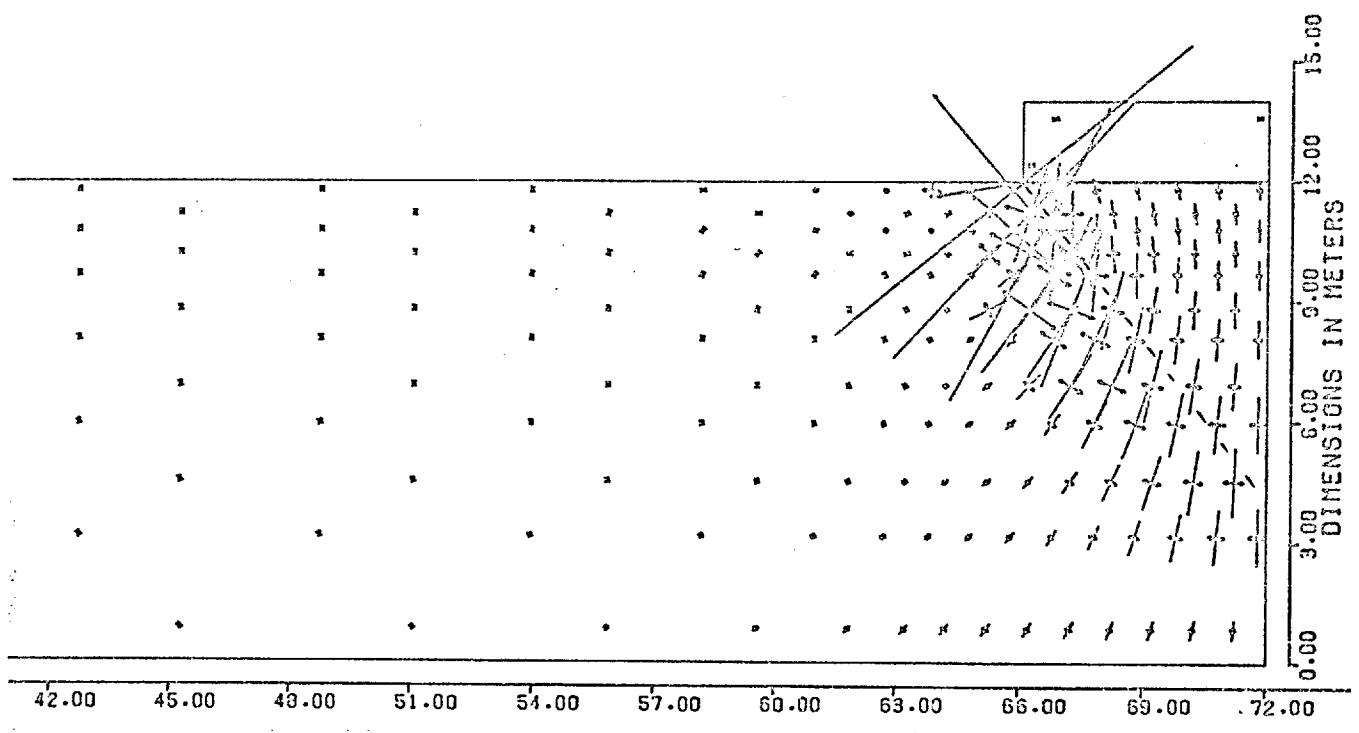
Fig. 6.55d   Principal strain rotations for Case 2
              (S.F. = 9.2)
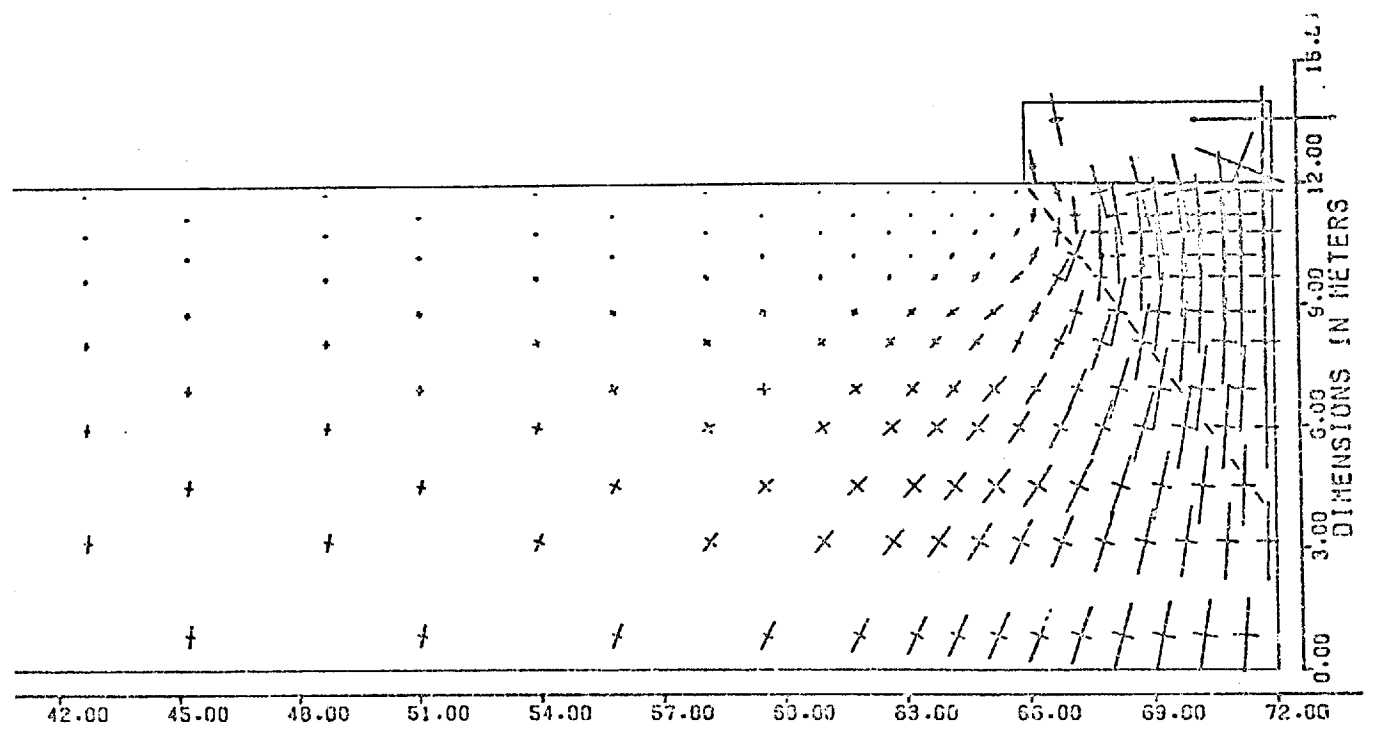
Fig. 6.55e   Principal stress rotations for Case 2
              (S.F. = 9.2)

CASE 3 ($\phi = 0$, $c_u = 50$ kPa , $K_o = 1$)

S.F. = 1·66

S.F. = 1·17

S.F. = 1·12
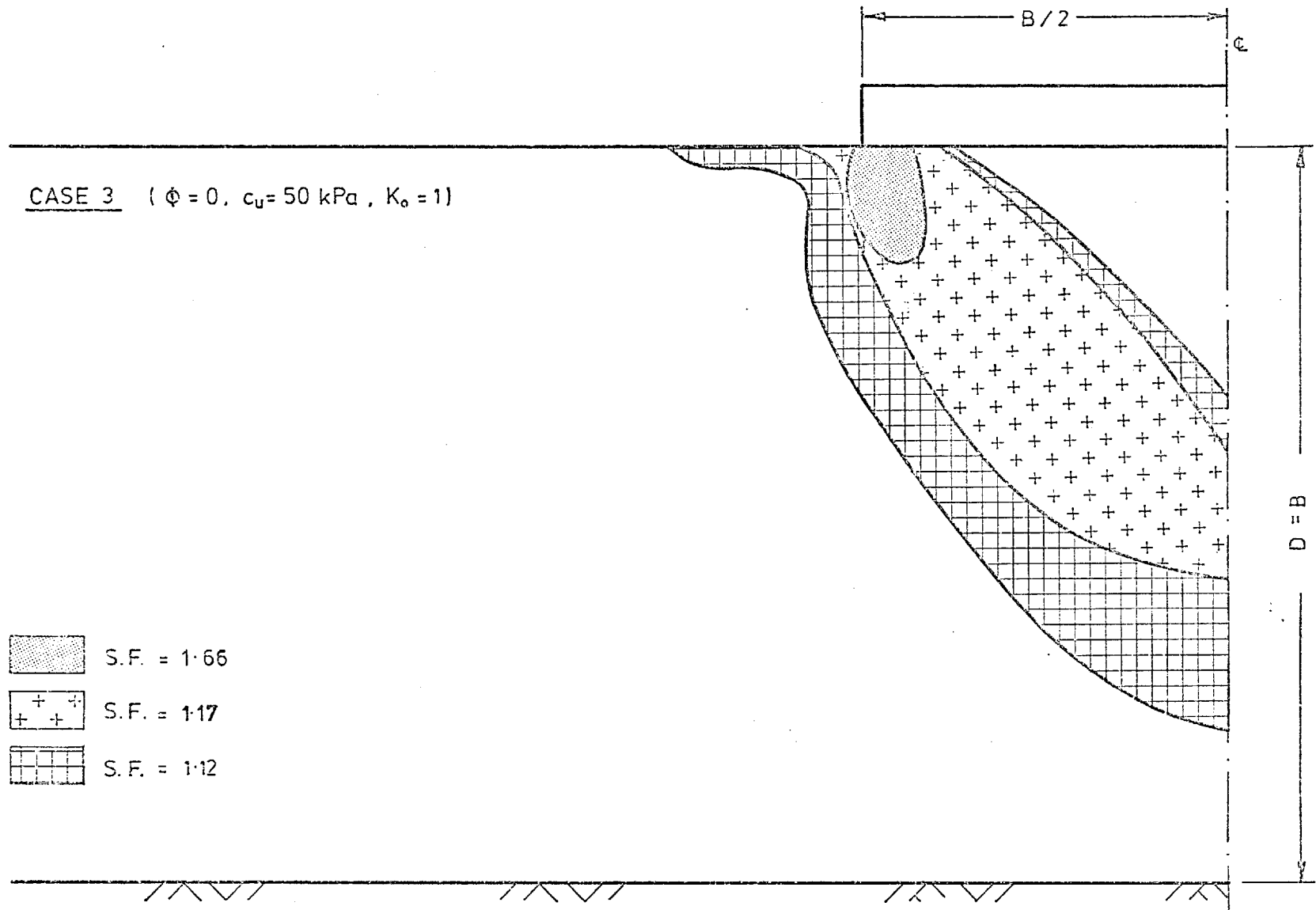
Fig. 6.56a   Progress of Failure Zone by Increasing the Applied Pressure (homogeneous clay)
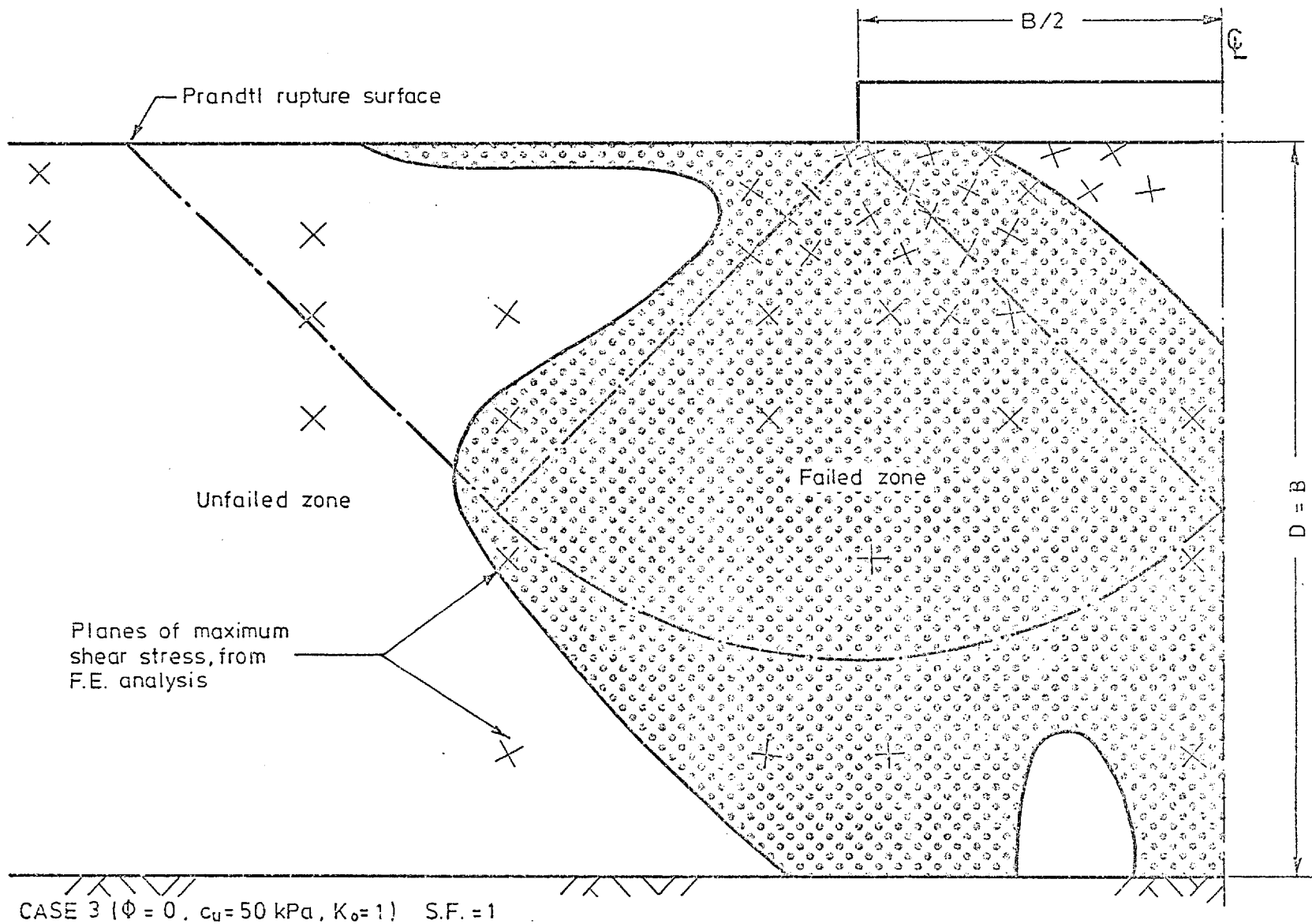
Fig. 6.56b   Failure Zone from the F.E. Analysis Compared to the Prandtl Rupture Figure

CASE 3 ($\phi = 0$, $c_u = 50$ kPa, $K_o = 1$)   S.F. = 1

Prandtl rupture surface

Unfailed zone

Failed zone

Planes of maximum shear stress, from F.E. analysis

$B/2$

$D = B$
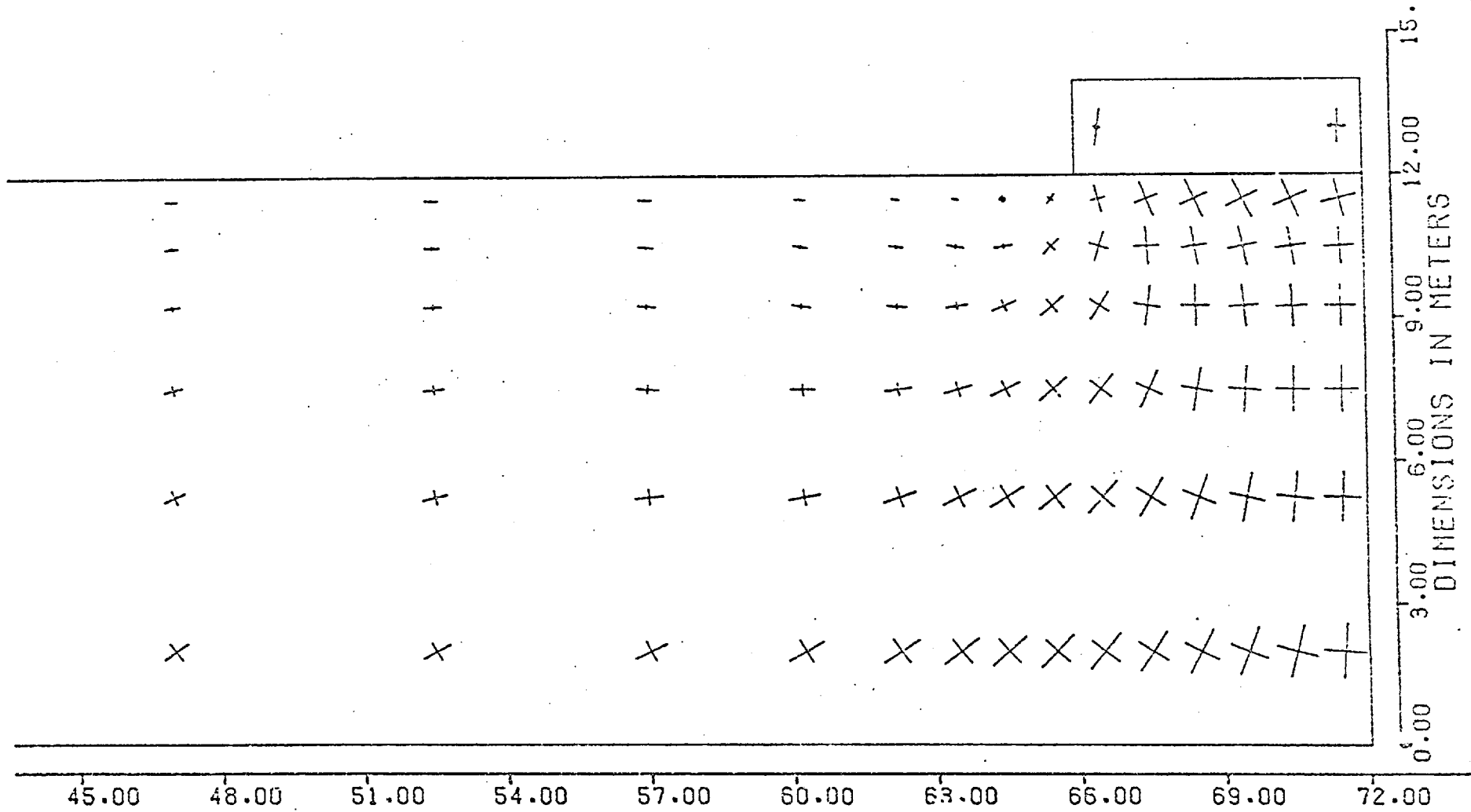
Fig. 6.56c   Principal stress rotations for Case 3 (S.F. = 1)

CASE 4 $(\Phi = 0 , c_u = 30 + 3.75z , K_o = 2)$

S.F. = 2.15

S.F. = 1.43

S.F. = 1.075
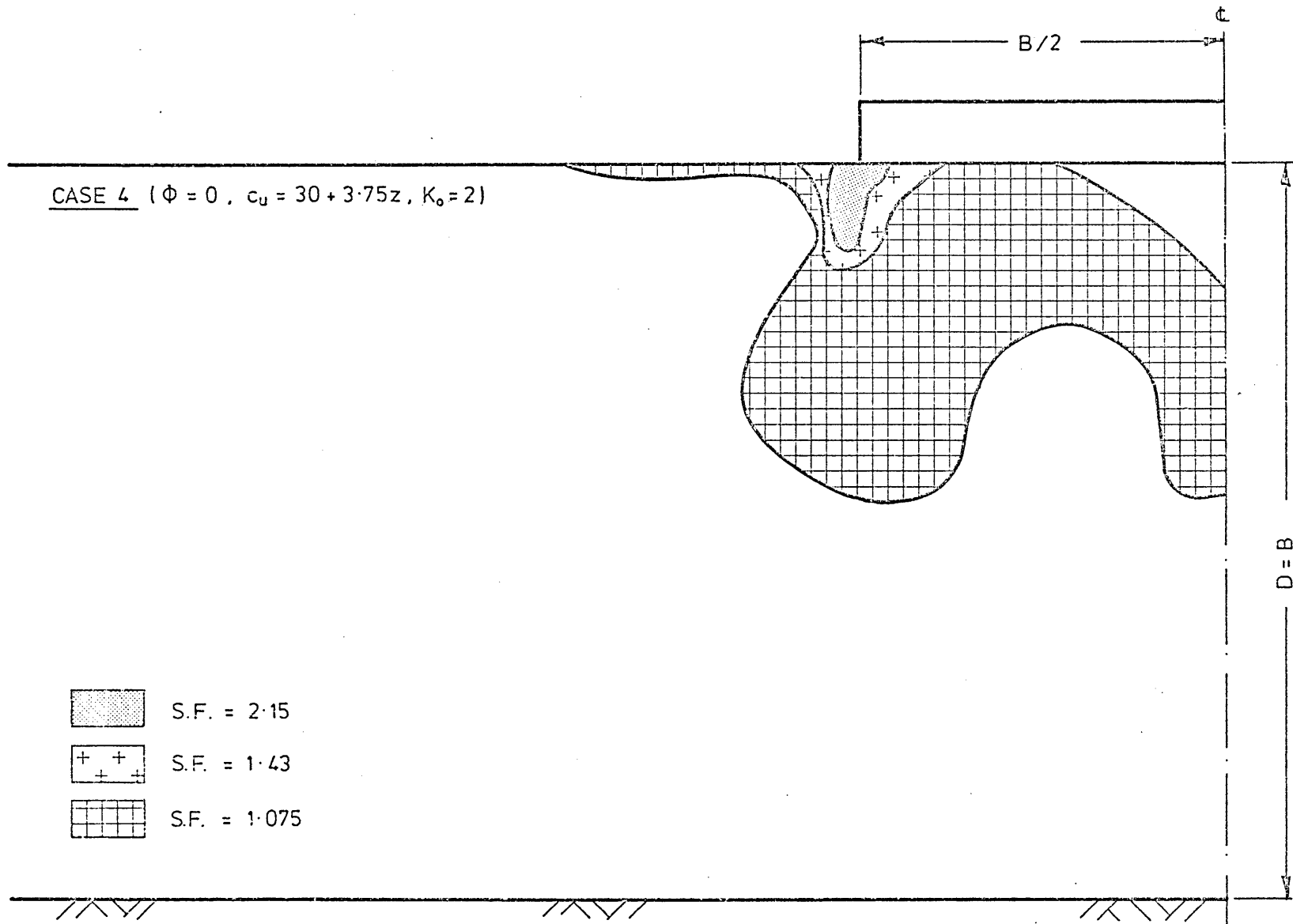
Fig. 6.57a   Progress of Failure Zone by Increasing the Applied Pressure (non-homogeneous clay)

6 m

12 m

Rupture surfaces,
after Davis & Booker

Tensile stress zone

Planes of maximum shear stress
(from F.E. analysis)

Boundary between clay at
failure and unfailed clay

CASE 4 (see Table 5.2)

Safety factor = 1

0   20   40   60   80

C_u , kN/m²
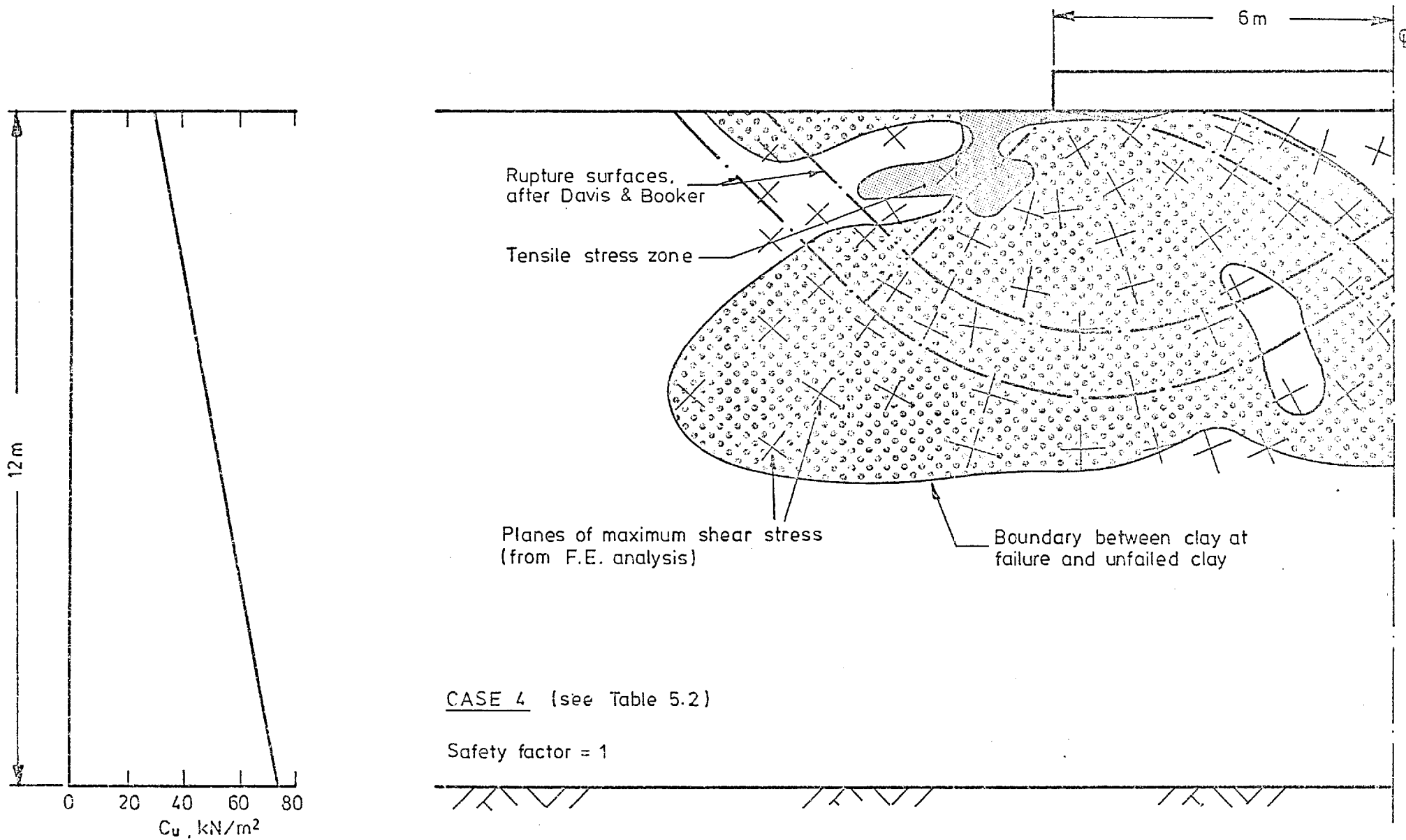
Fog. 6.57b   Failure Zone Compared to the Rupture Figure from the Theory of Plasticity
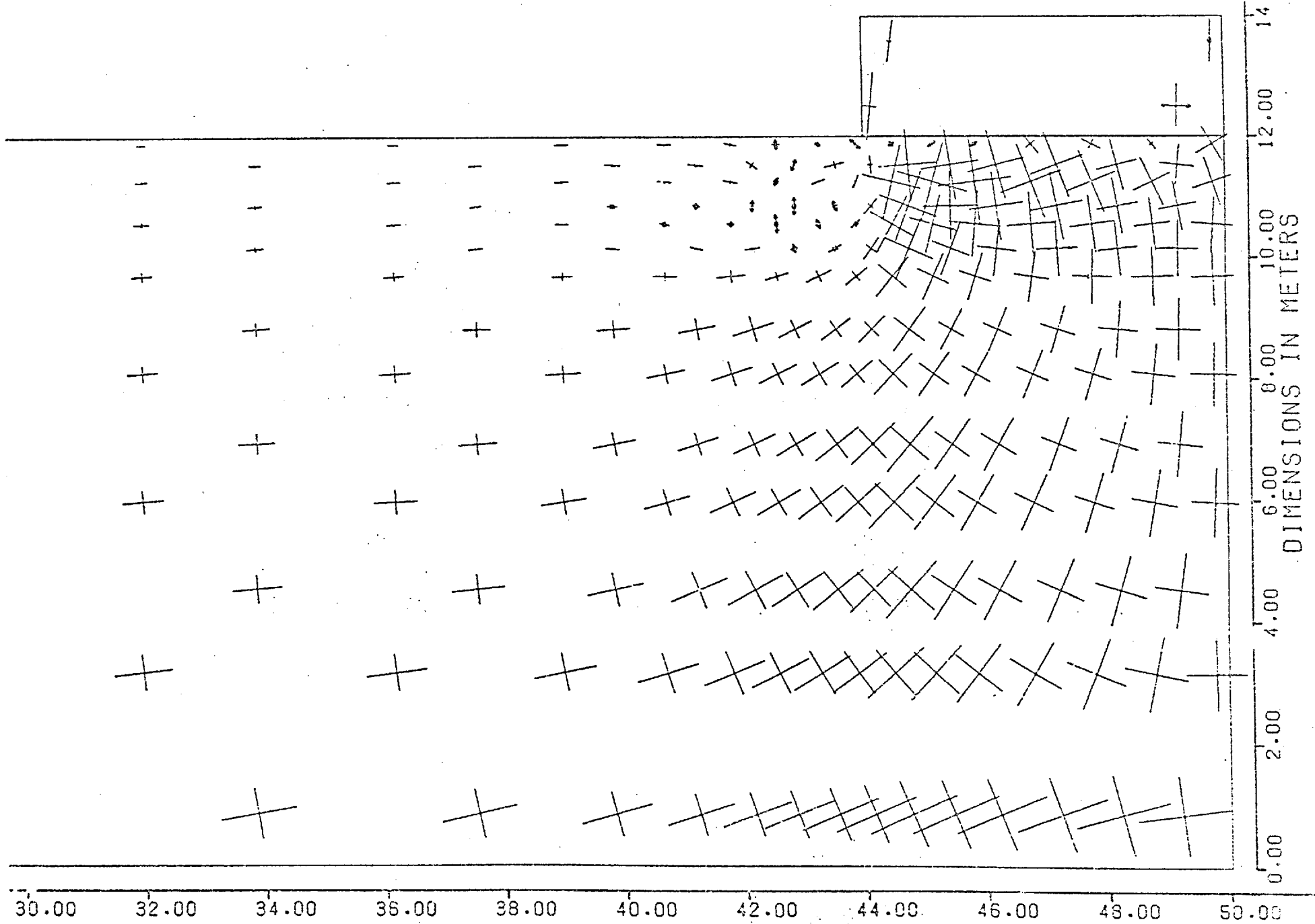
Fig. 6.58   Principal stress rotations for Case 4 (S.F. = 1)

DIMENSIONS IN METERS

303
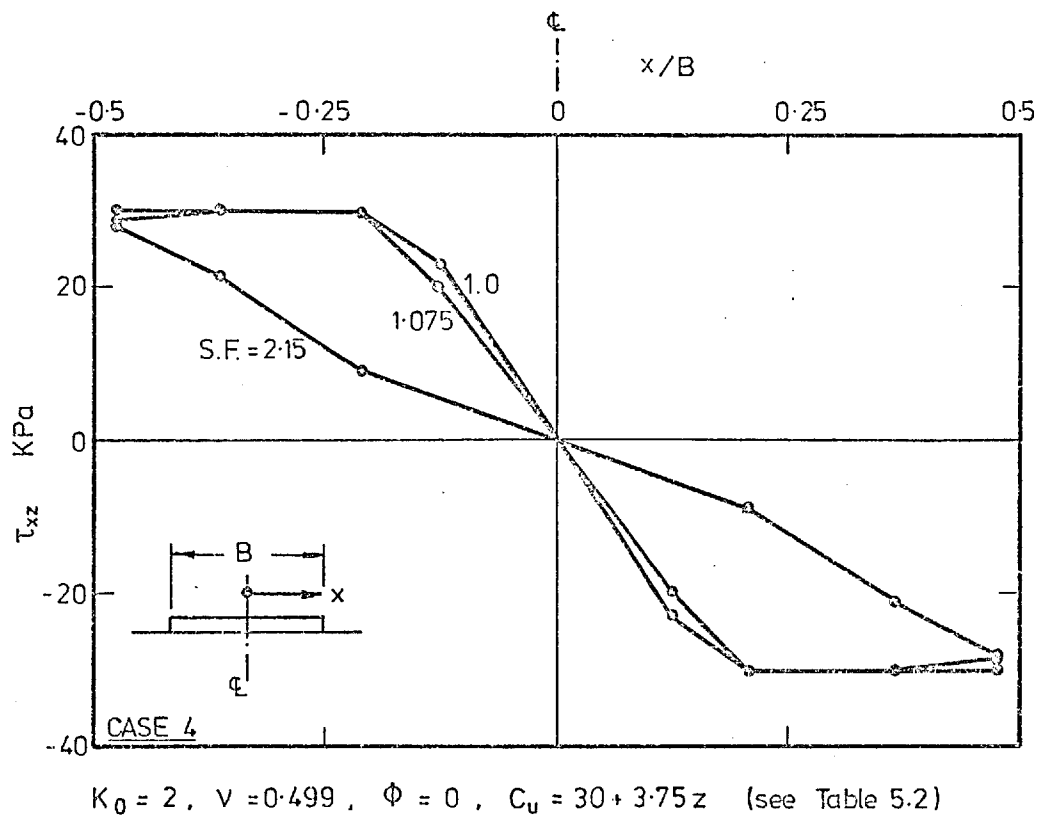
Fig. 6.59   Contact Shear Stresses   CASE 4
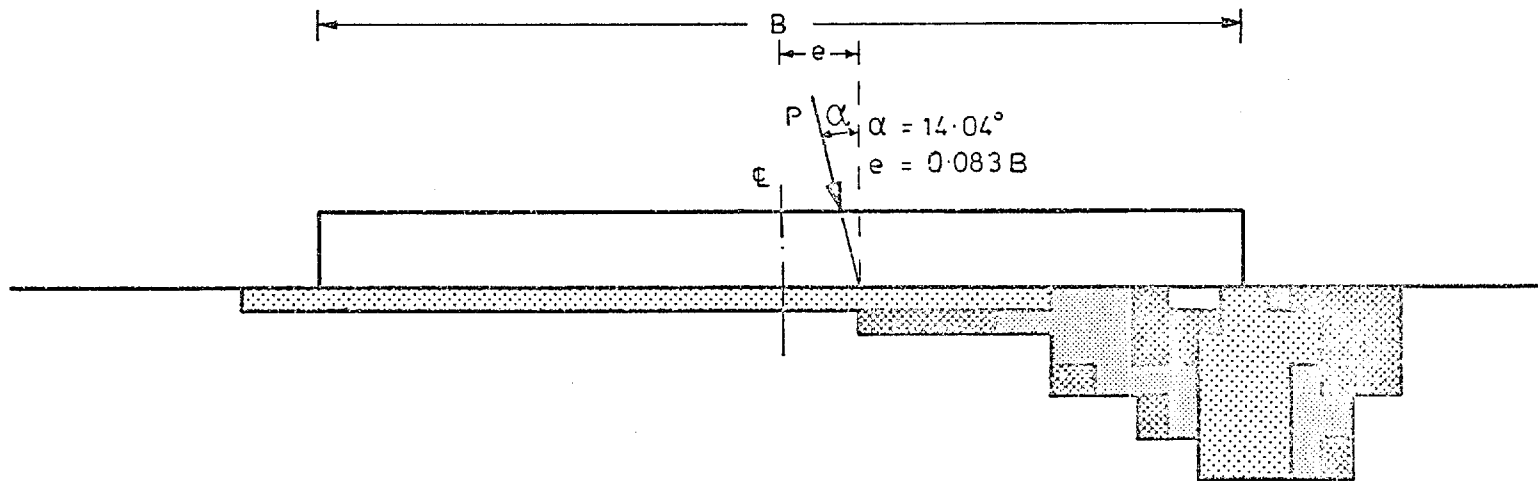
CASE 40   ($\Phi = 0$, $C_u = 100 + 3z$, $K_a = 1.5$), (see Table 5.2)

Safety factor = 0.95

Safety factor = 0.90

Safety factor = 0.88
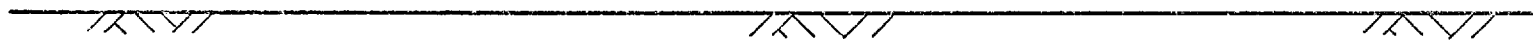
Fig. 6.60   Progress of Failure Zone by Increasing the Applied Load
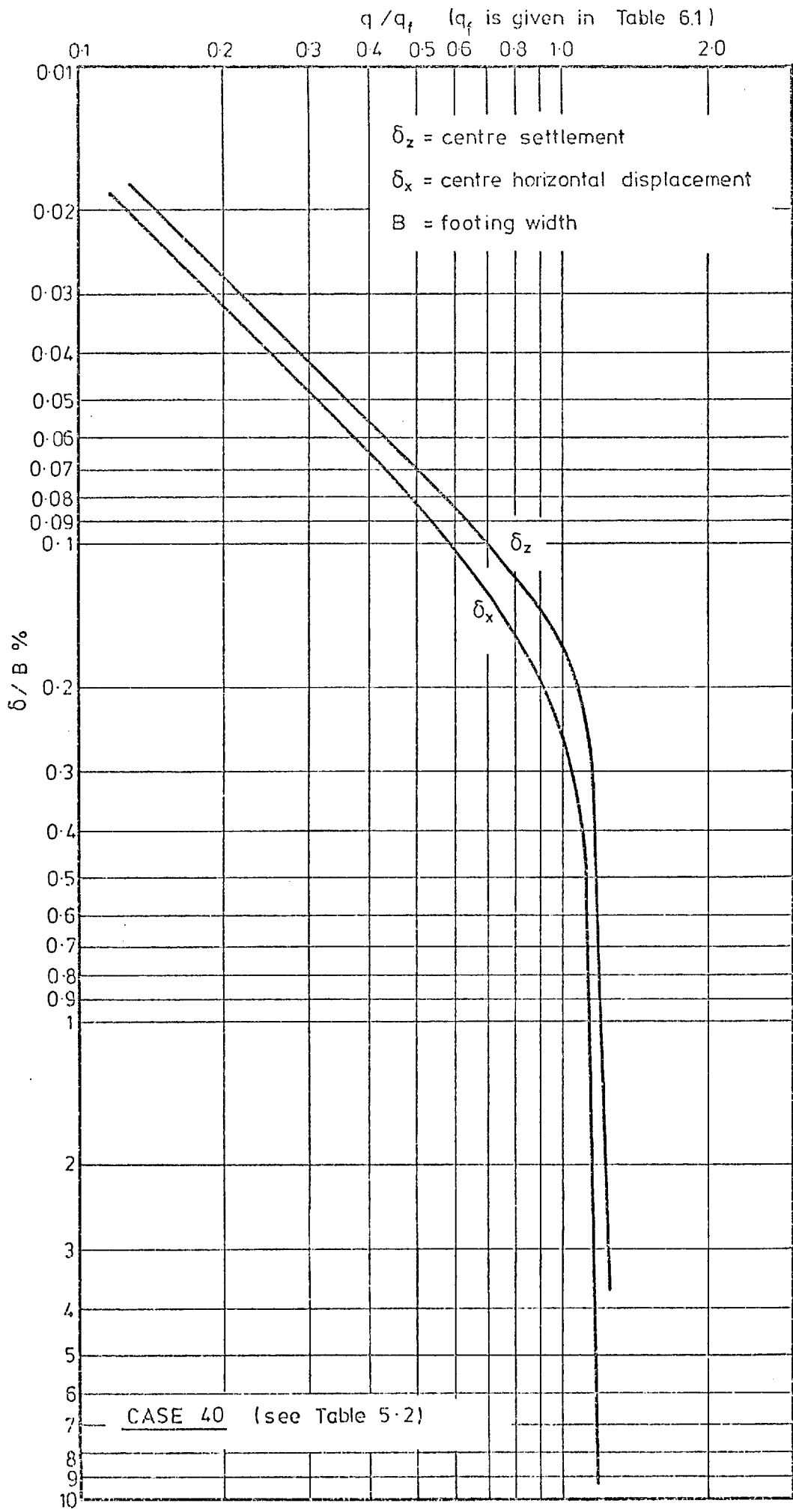
Fig. 6.61   Load-Settlement Curve (Eccentric&Inclined Load)
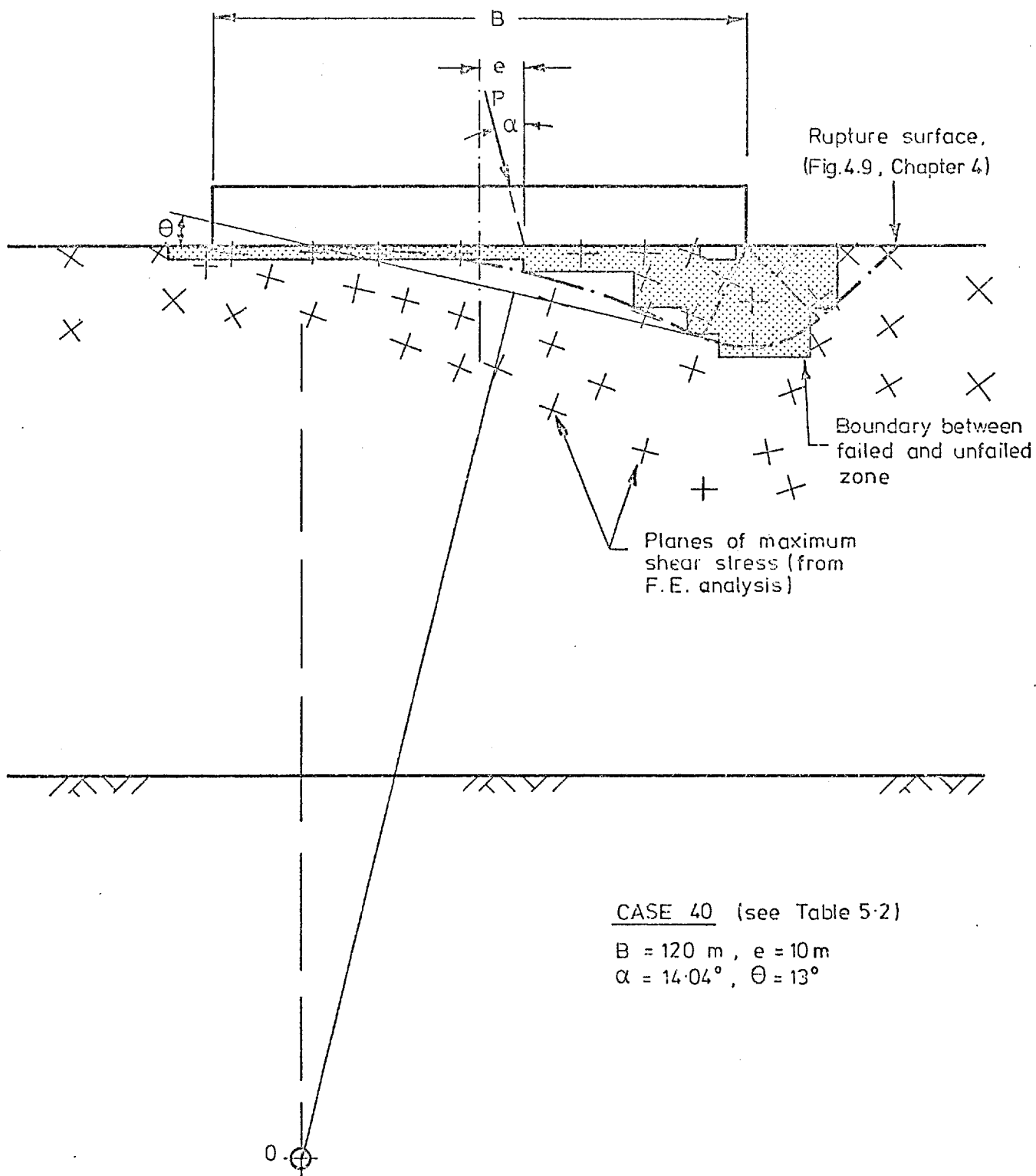
Fig. 6.62a   Failure Zone and Planes of Maximum Shear
              Stress from F.E. Analysis Compared to the
              Rupture Figure for Eccentric and Inclined
              Loading

PRINCIPAL STRESSES VALUES AND ROTATIONS   Q=400KN/M2
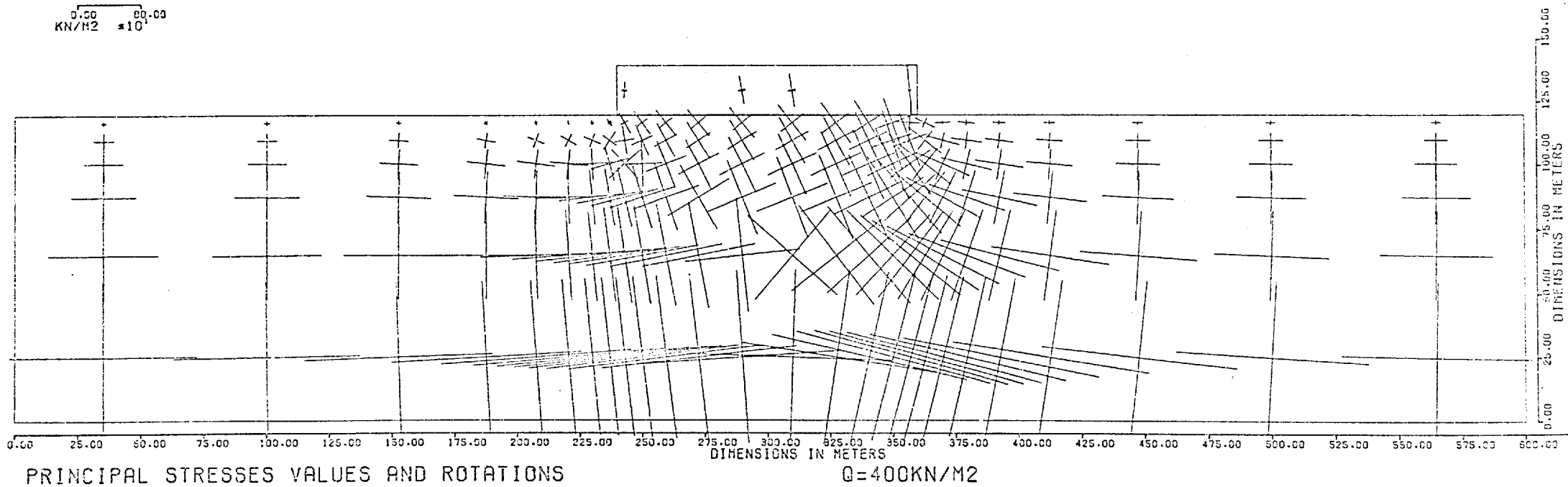
Fig. 6.26b   Case 40 (see Table 5.2), eccentric and inclined load, S.F. = 0.89
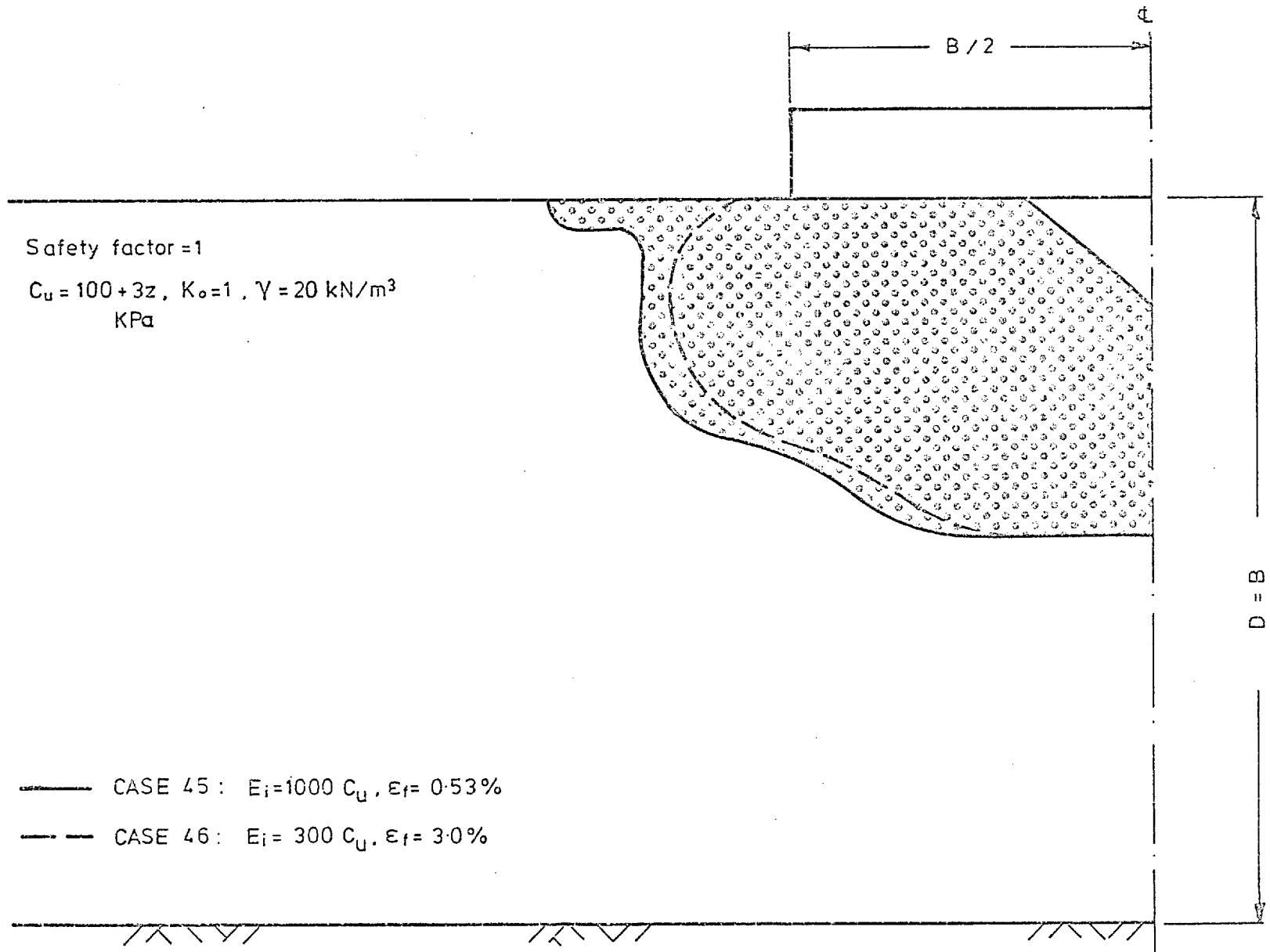
Fig. 6.63   Effect of the Stress-Strain Relationship on the Failure Zone

The figure contains the following labels:

Safety factor = 1

$C_u = 100 + 3z$, $K_o = 1$, $\gamma = 20$ kN/m³
     KPa

$B/2$

$D = B$

CASE 45 : $E_i = 1000\ C_u$, $\varepsilon_f = 0.53\%$

CASE 46 : $E_i = 300\ C_u$. $\varepsilon_f = 3.0\%$
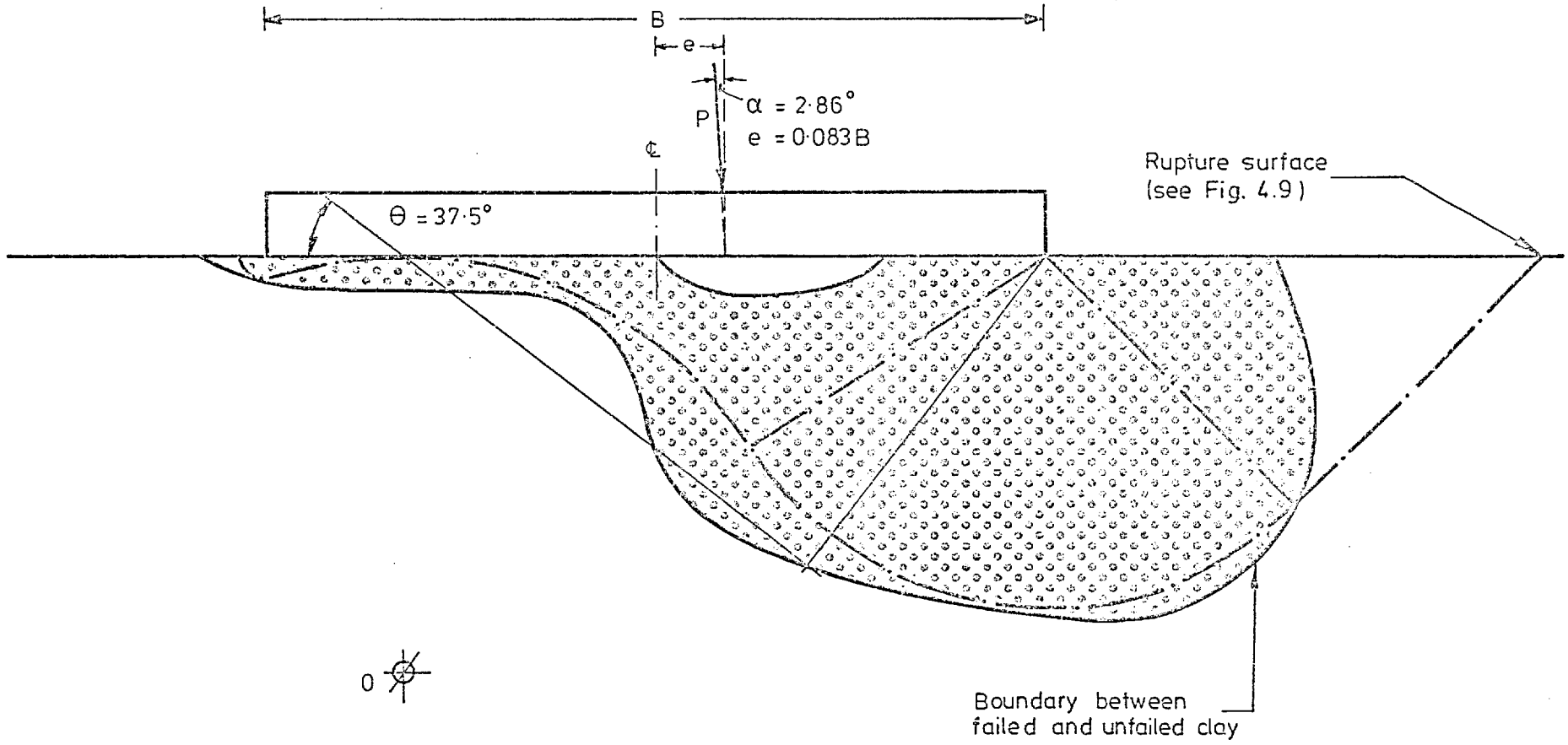
CASE 7 $\Phi = 0$. $C_u = 30 + 3.75\,z$, $E_i = 300\,C_u$.

$\gamma = 20\,kN/m^3$, $K_o = 2$ (see Table 5.2)

Safety factor = 1

Fig. 6.64   Failure Zone (Inclined and Eccentric Load on the Non-homogeneous Clay)

¢

A
-0·5

0

B
0·5

x / B

0

δz / B %

0·05

0·1

A

A

B

B 1

1

2

2
B

3

3,5&7

4,6&8

A

δx / B %

δz / B %

— — — Milovic et al (1970), E average

0   0·025   0·05
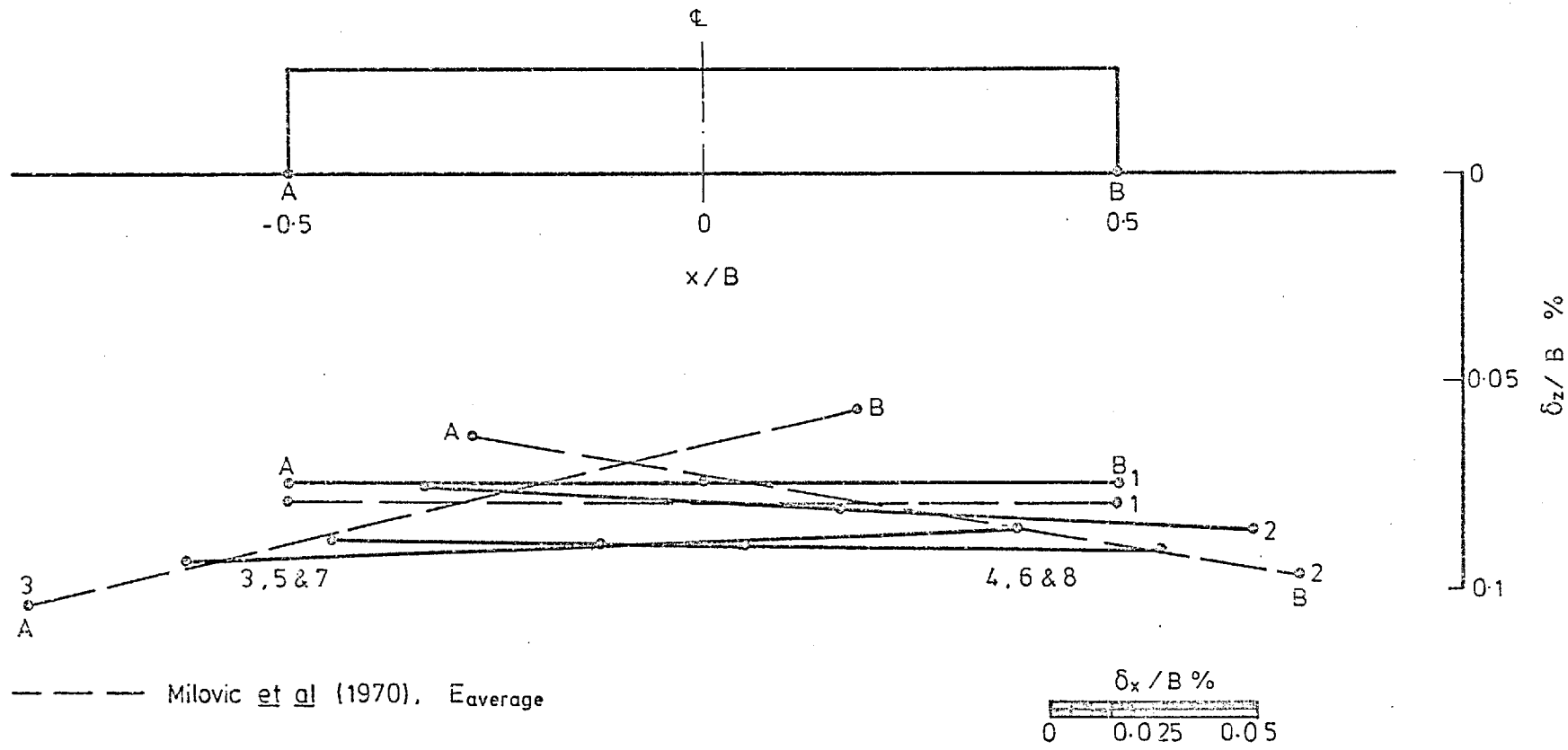
CASE 42 ———— (see Table 5.3)

Fig. 6.65   Surface Horizontal and Vertical Displacements

Numbers denote loading stages (see Chapter 5, Section 5.3.2 and Table 5.3)
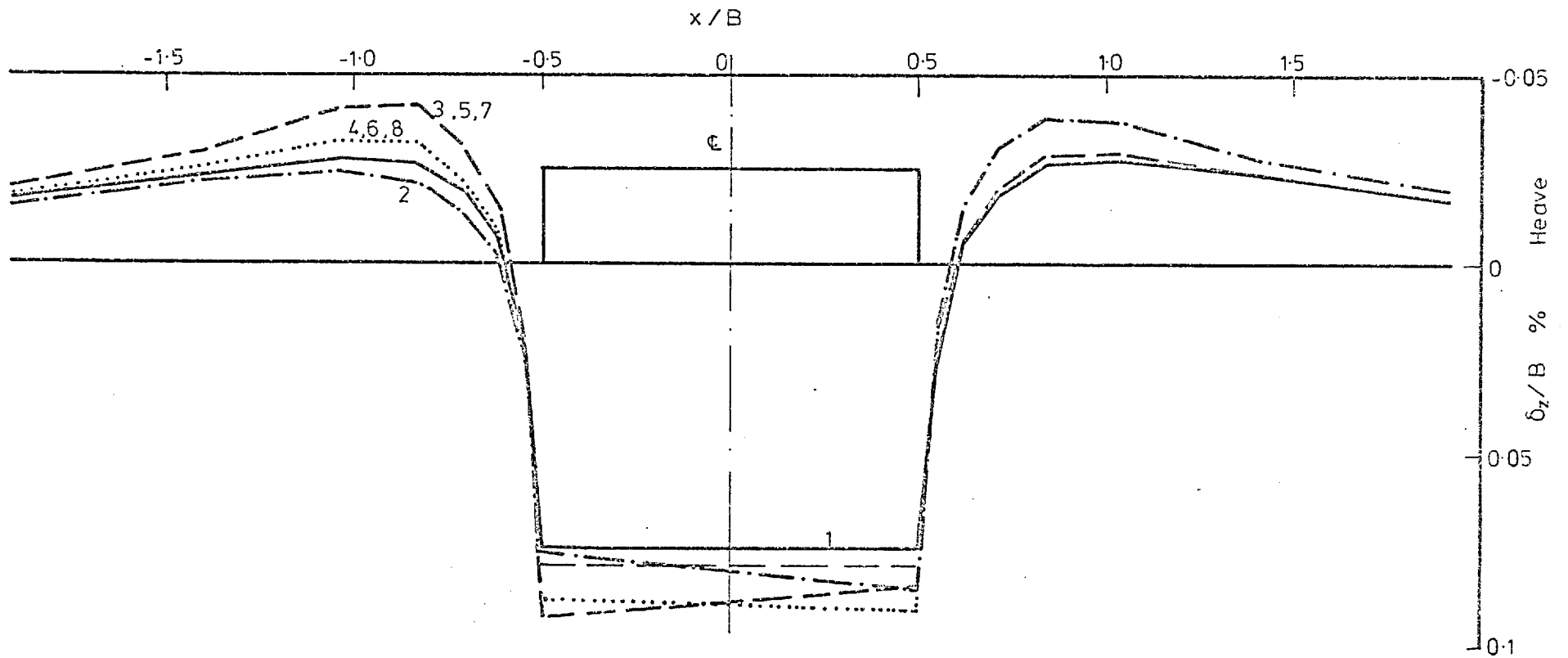
CASE 42 (see Table 5.3)

Fig. 6.66   Surface Settlement Distribution (Depth = 0)

Numbers denote the loading stages (see Chapter 5, section 5.3.2 and Table 5.3)

x/B

Edge   Edge

D=B/3

Heave

δ_z / B %

3

2,4,6,8

2

1

7,5,3

₵
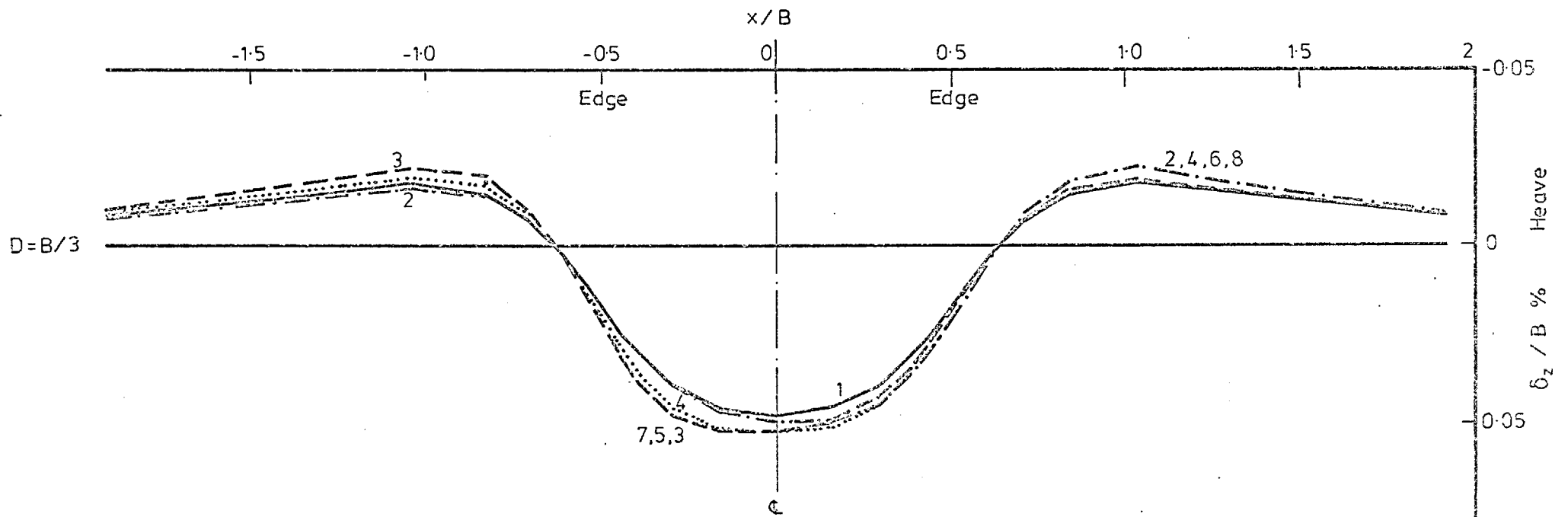
CASE 42   (see Table 5.3)

Fig. 6.67   Vertical Displacement Distribution (Depth = B/3)
Numbers denote loading stages (see Chapter 5, section 5.3.2 and Table 5.3)

313

δ_x / B %
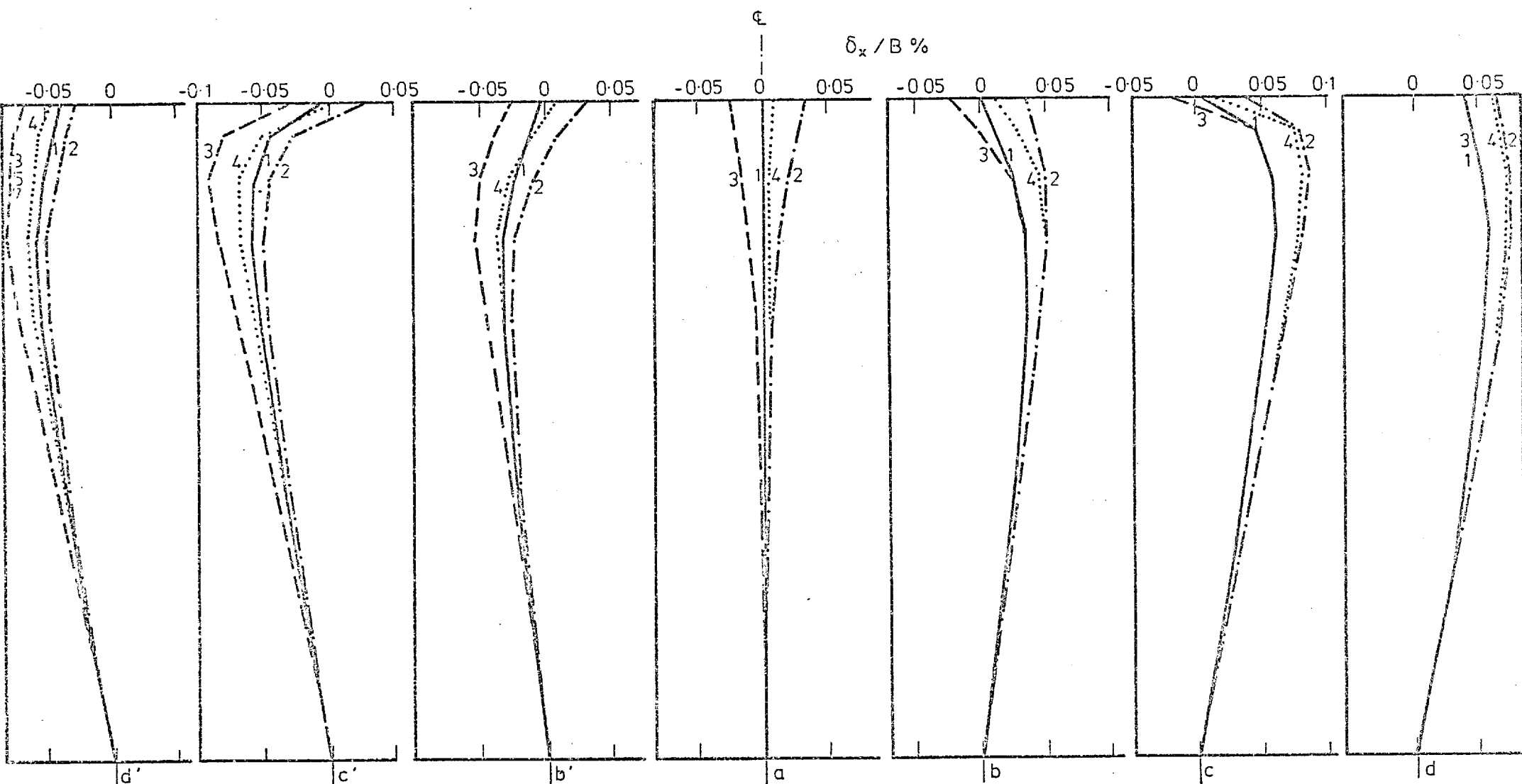
CASE 42

$4 = 6.8$
$3 = 5.7$
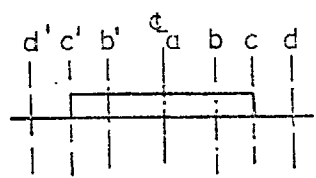
Fig. 6.68   Horizontal Displacement

Numbers denote loading stages (see Chapter 5, section 5.3.2 and Table 5.3)
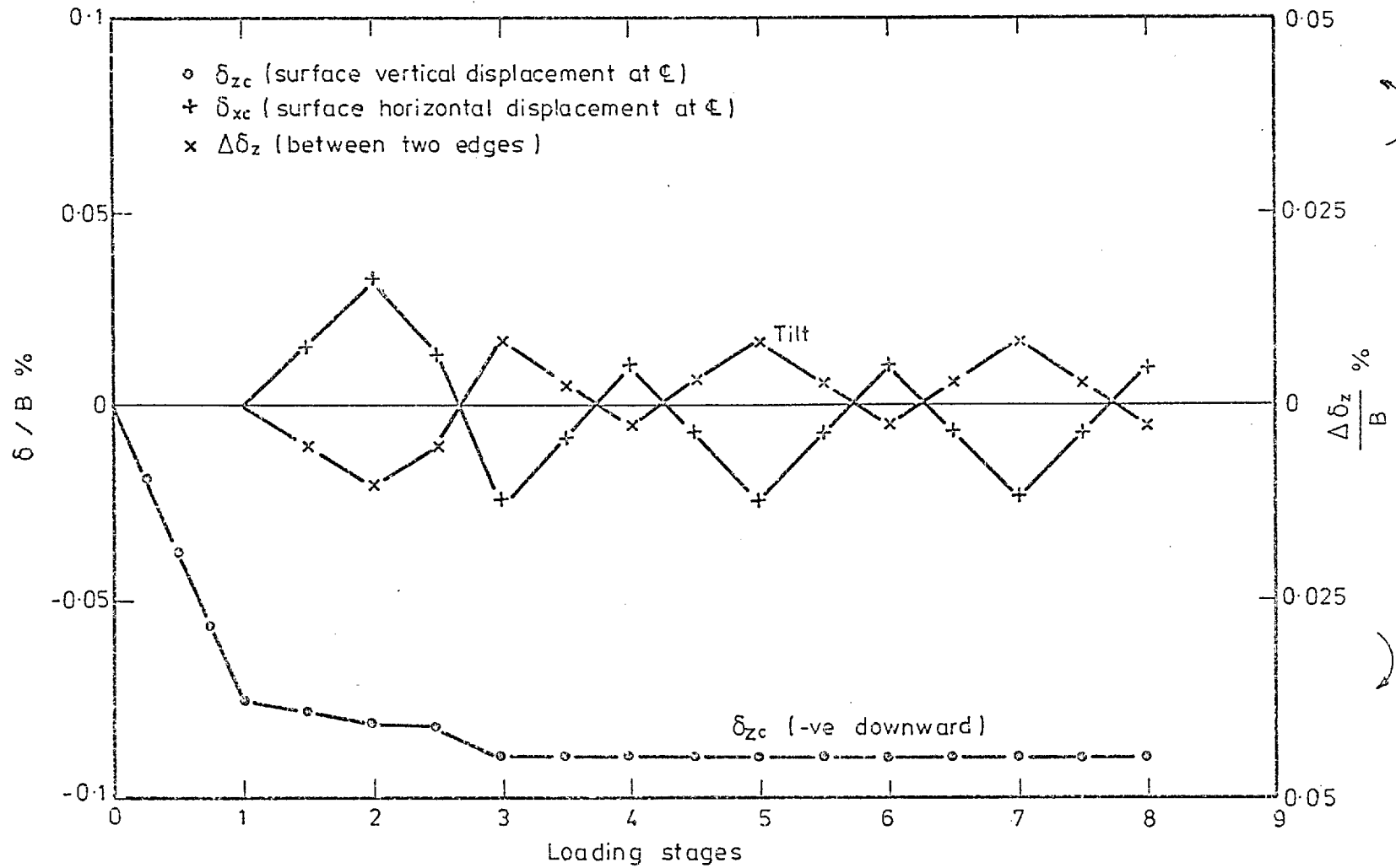
CASE 42

Fig. 6.69 Displacements   Numbers denote loading stages (see Chapter 5, section 5.3.2 and Table 5.3)
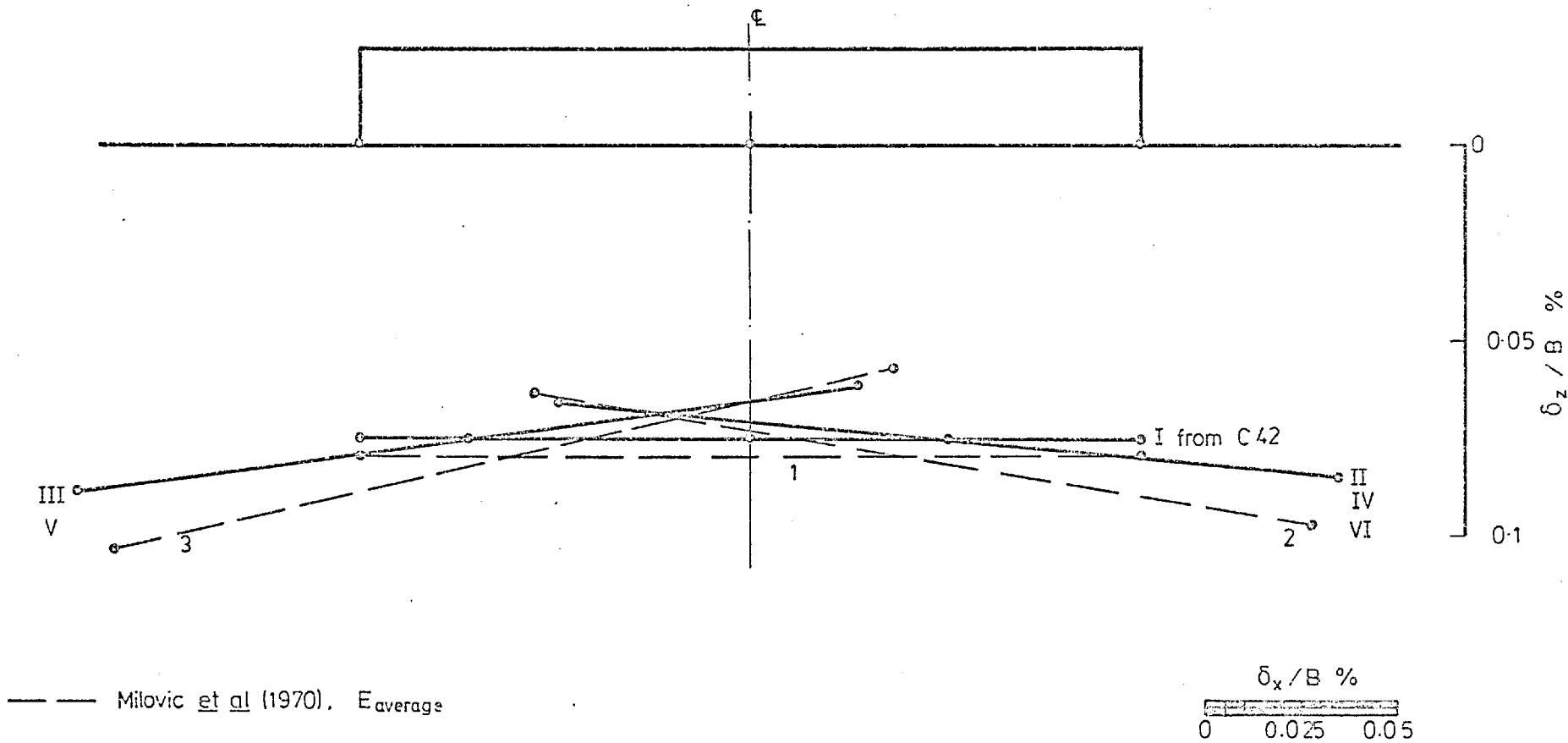
Fig. 6.70   Surface Horizontal and Vertical Displacements

Numbers denote loading stages (see Chapter 5, section 5.3.2 and Table 5.3)

CASE 47   (see Table 5.3)

— — — Milovic et al (1970). E average
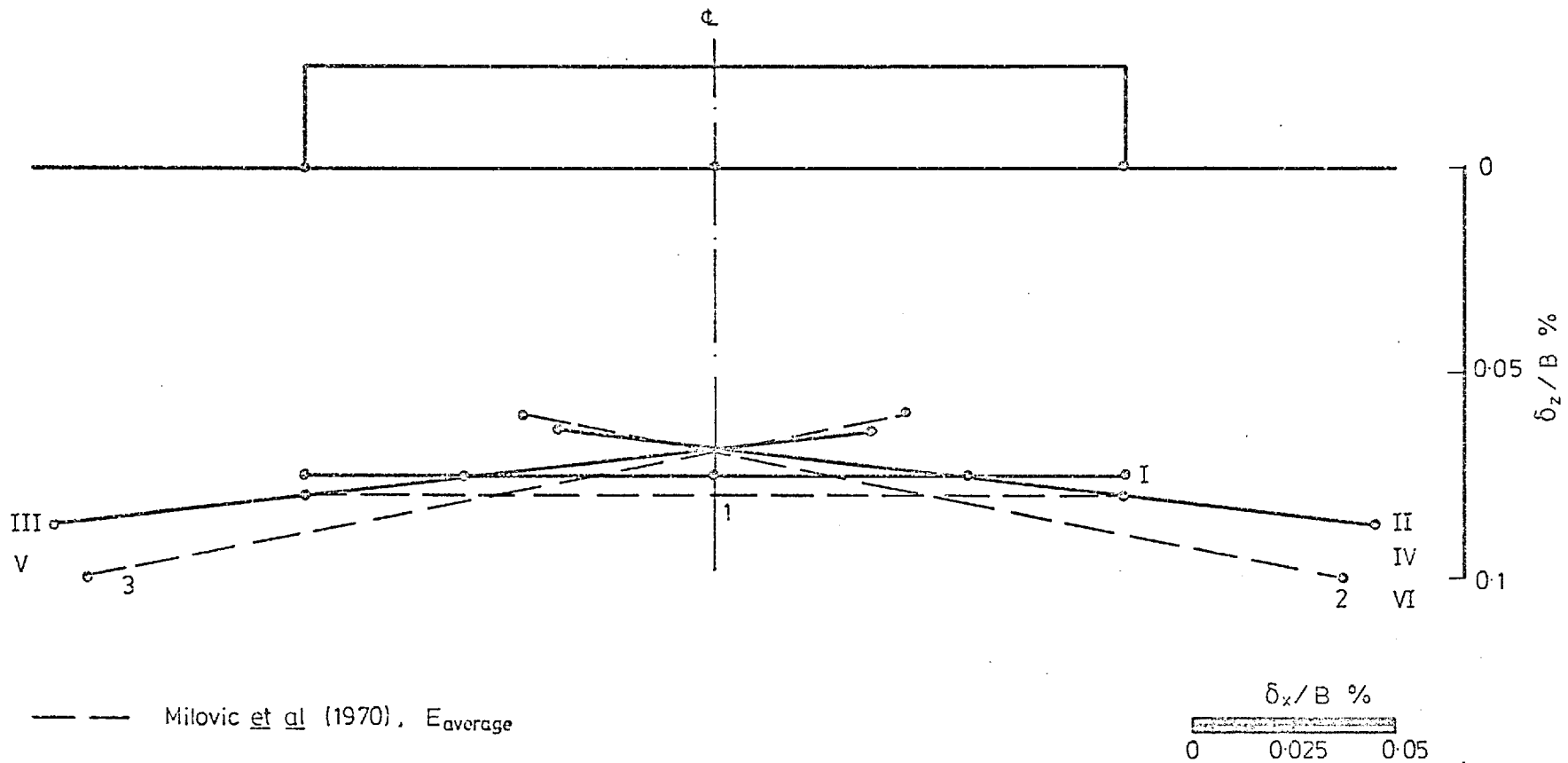
CASE 47.1 (see Table 5.3)

Fig. 6.71   Surface Horizontal and Vertical Displacements
             Numbers denote loading stages (see Chapter 5, section 5.3.2 and Table 5.3)

Figure labels: 3,5 / 1 / 2,4,6 / Edge / ¢ / Edge / D=0·0

Right axis (upper): -0·05 / 0% / 0·05 / 0·1 — Heave — δ_z/B %

Right axis (lower): -0·025 / 0 % / 0·05 — δ_z/B %

Lower plot labels: 3,5 / 1 / 2,4,6 / D=B/3
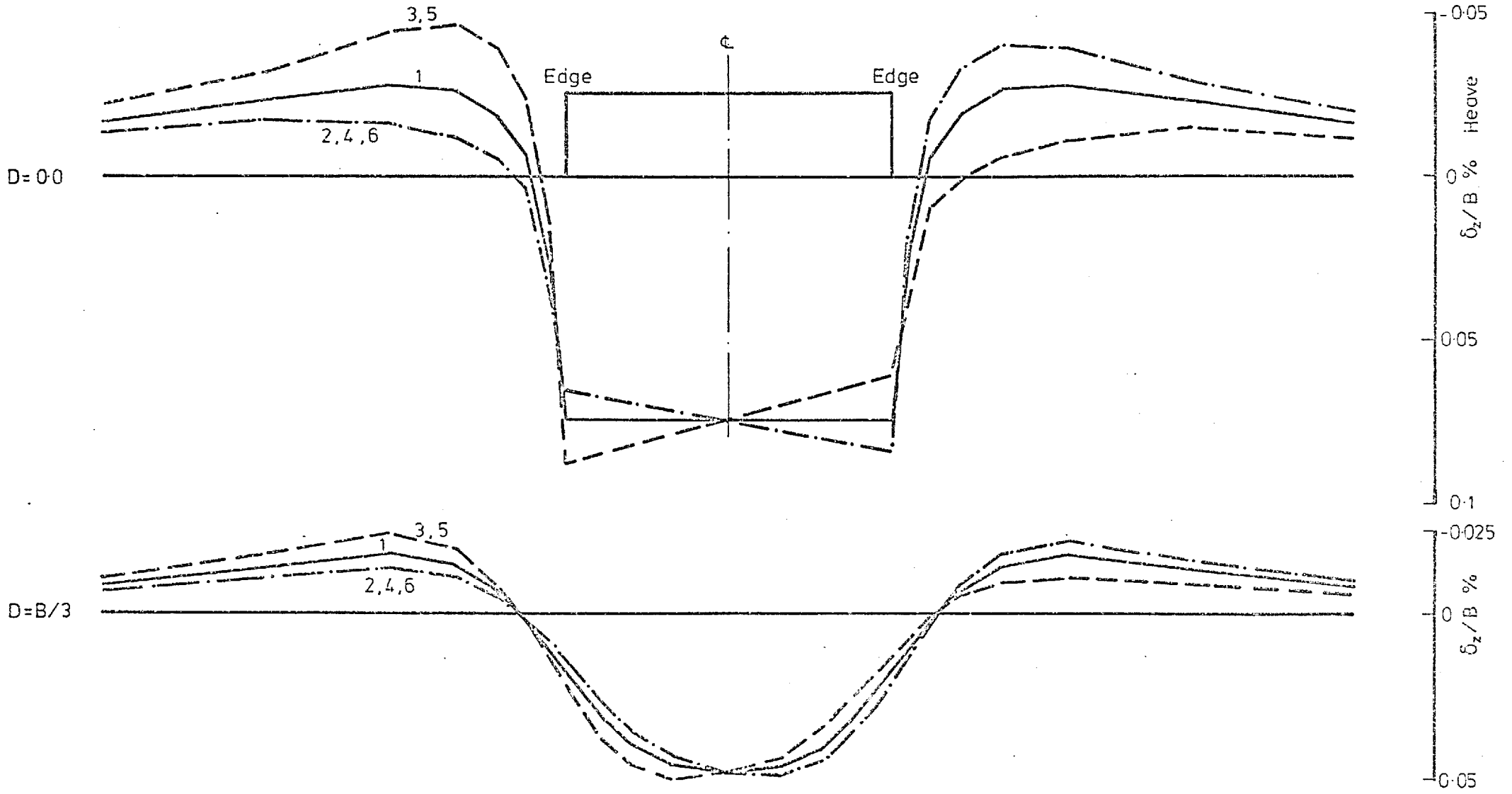
CASE 47   (see Table 5.3)

Fig. 6.72   Values of Vertical Displacements   Numbers denote loading stages
(see Chapter 5, section 5.3.2 and Table 5.3)

318
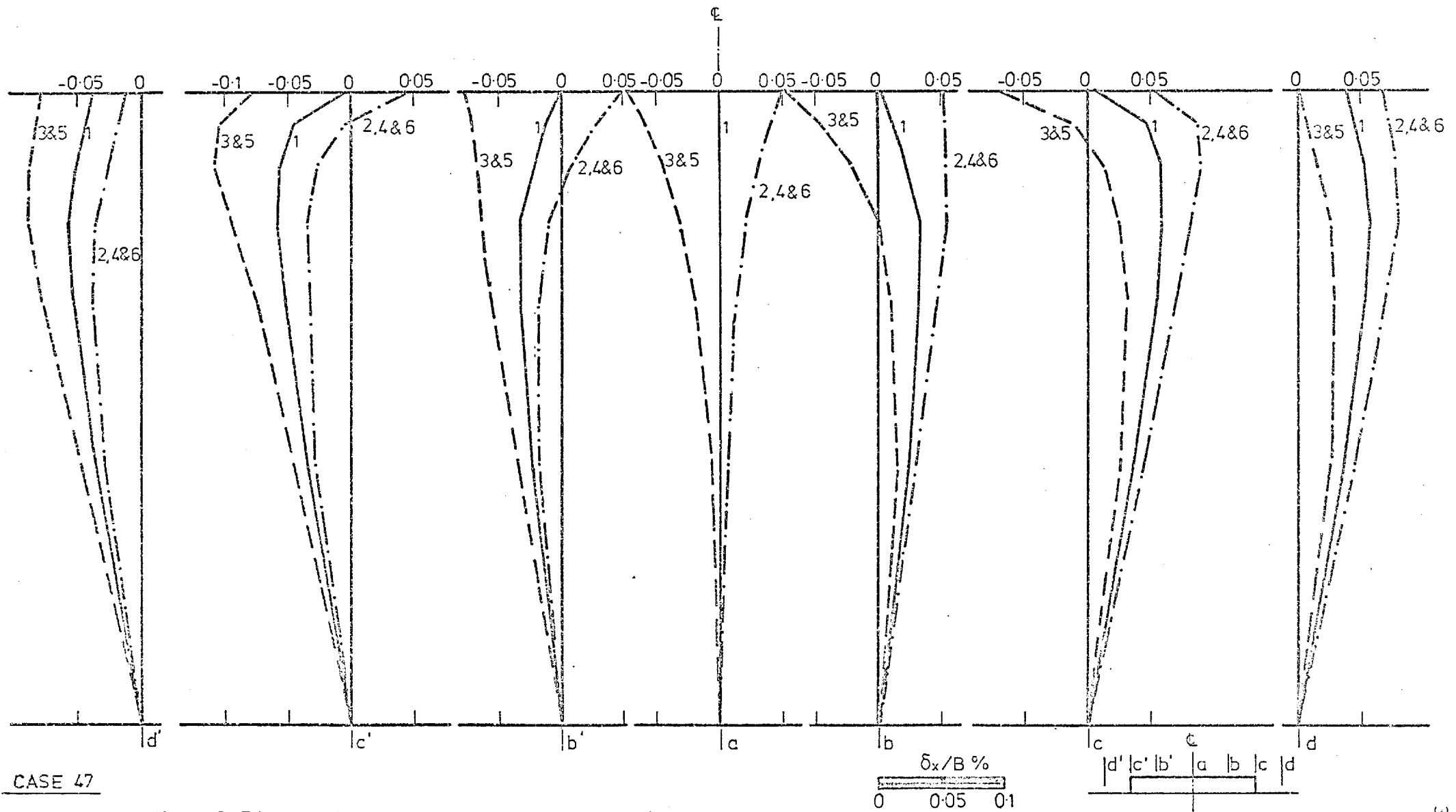
CASE 47

Fig. 6.73   Value of Horizontal Displacements

Numbers denote loading stages (see Chapter 5, section 5.3.2 and Table 5.3)

319
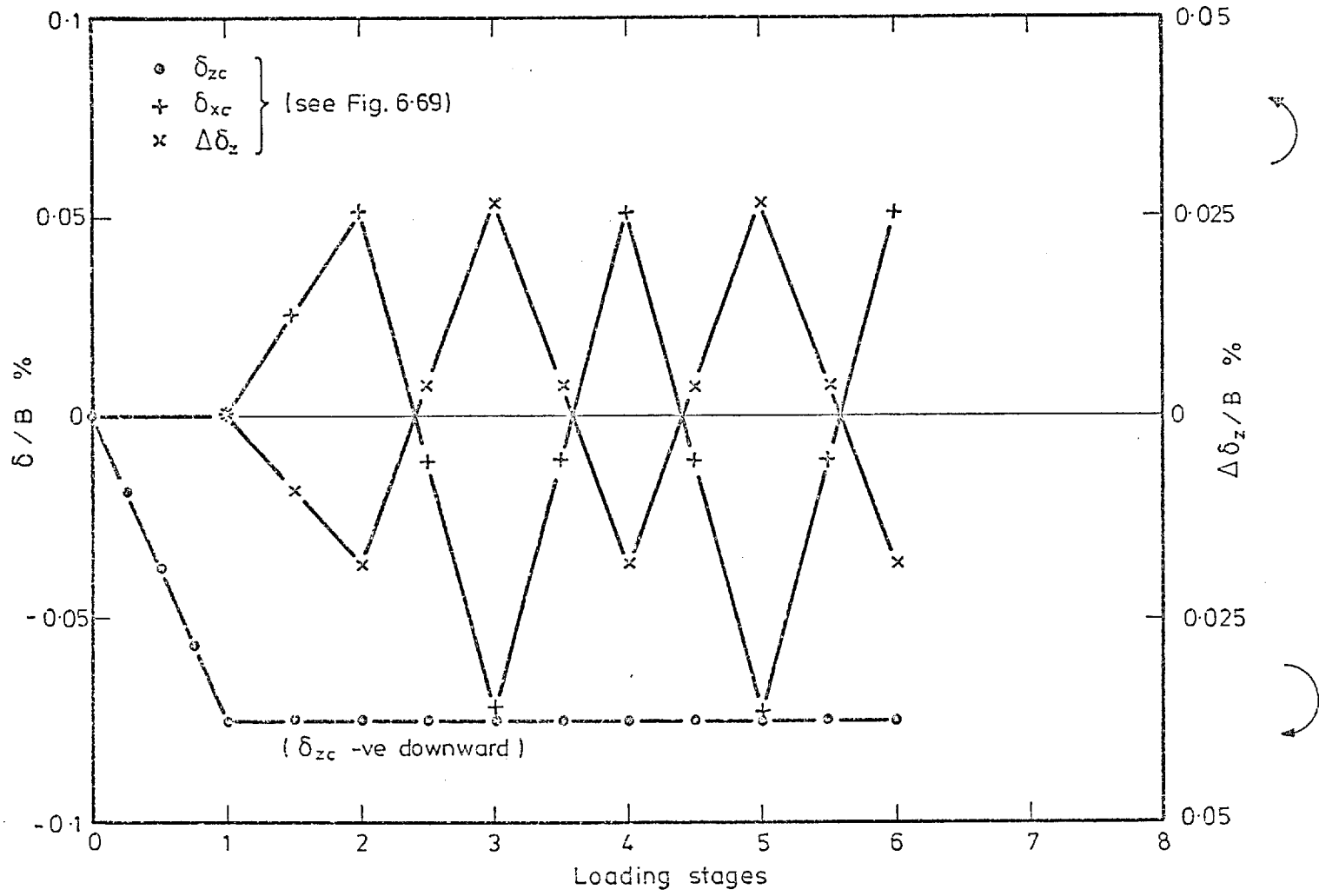
CASE 47   (see Table 5.3)

Fig. 6.74   Displacements   Numbers denote loading stages (see Chapter 5, section 5.3.2 and
Table 5.3)

7,5&3

2,4,6&8

1

3

2

1

δ_z / B %

0

0.05

0.1

0.15

0.2

0.25

——— ——— Milovic et al (1970)

δ_x/B %

0   0.05   0.1
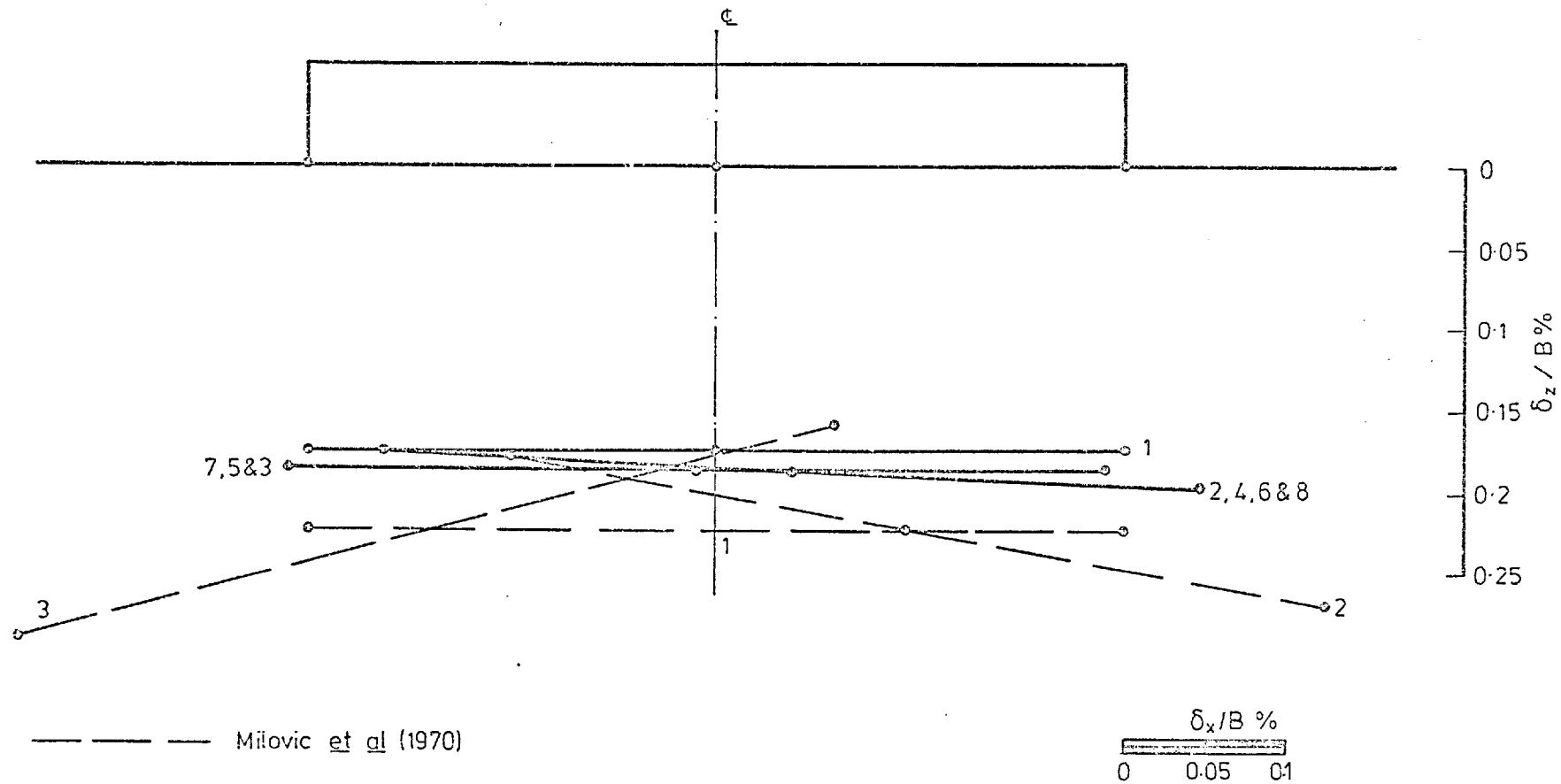
CASE 48

(see Table 5.3)

Fig. 6.75   Surface Horizontal and Vertical Displacements
Numbers denote loading stages (see Chapter 5, section 5.3.2 and Table 5.3)
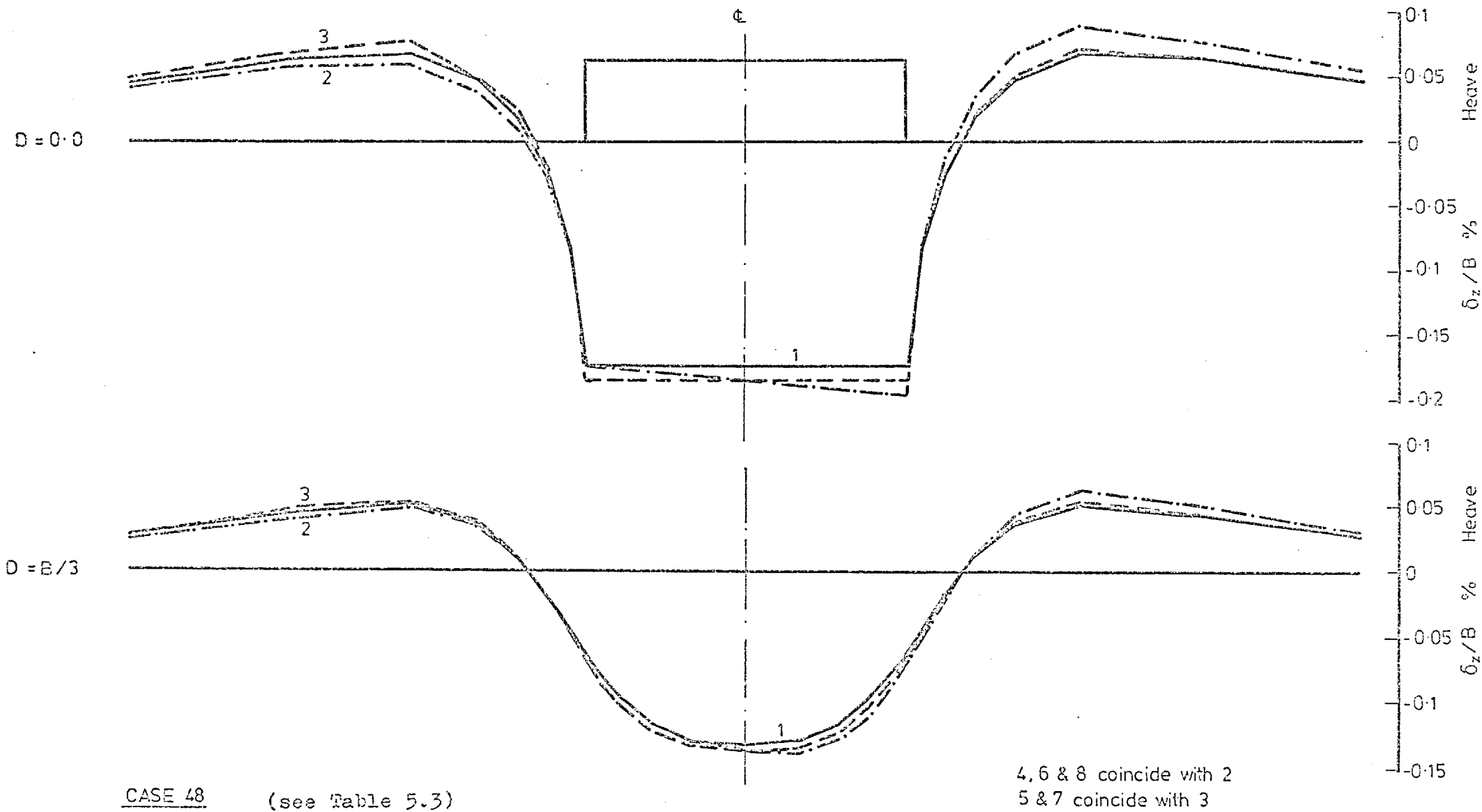
CASE 48   (see Table 5.3)

4, 6 & 8 coincide with 2
5 & 7 coincide with 3

Fig. 6.76   Values of Vertical Displacements, δz Numbers denote loading stages
(see Chapter 5, section 5.3.2 and Table 5.3)

322
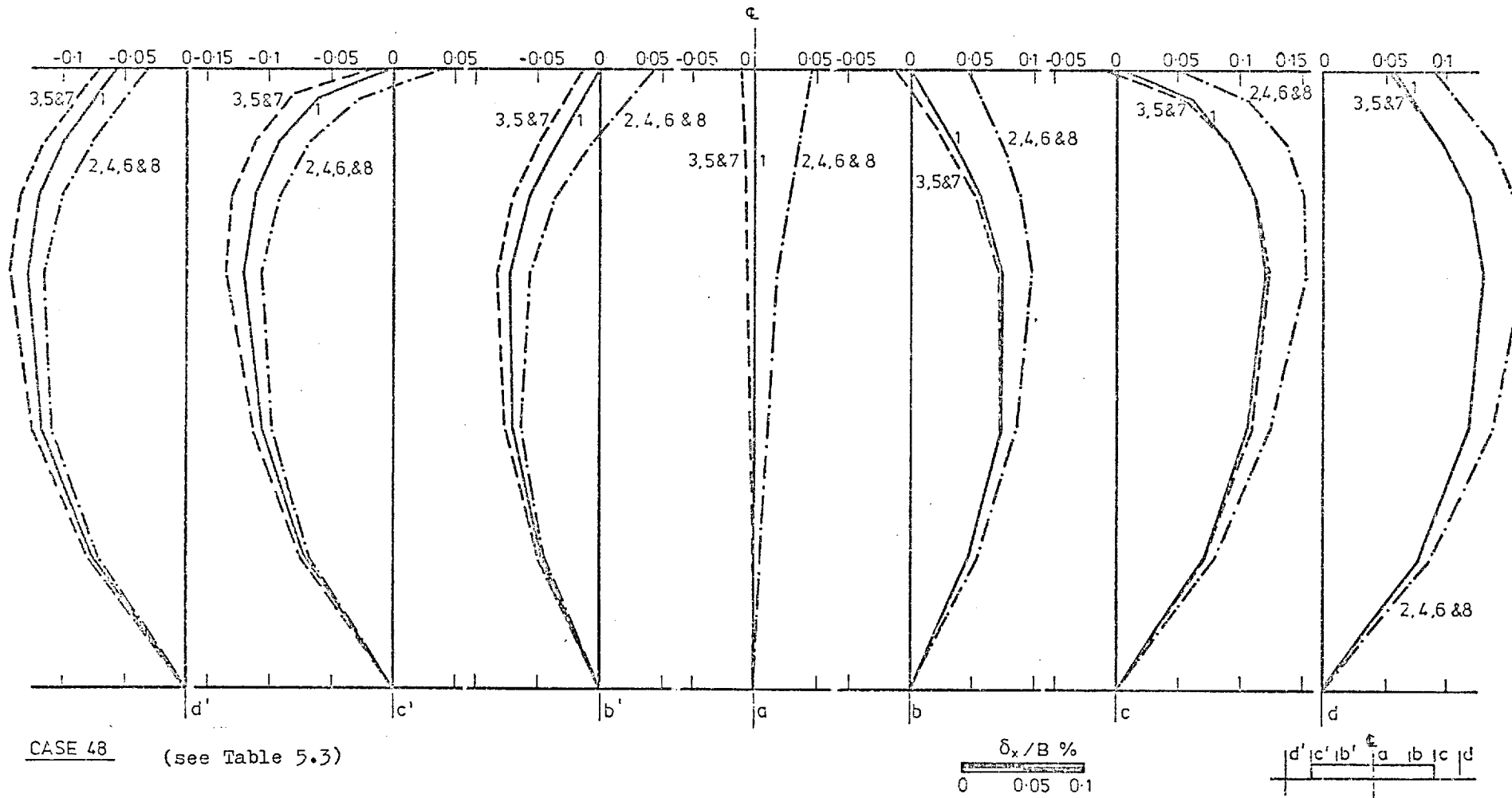
Fig. 6.77   CASE 48   Values of Horizontal Displacements
Numbers denote loading stages (see Chapter 5, section 5.3.2 and Table 5.3)

CASE 48   (see Table 5.3)

δ_x /B %
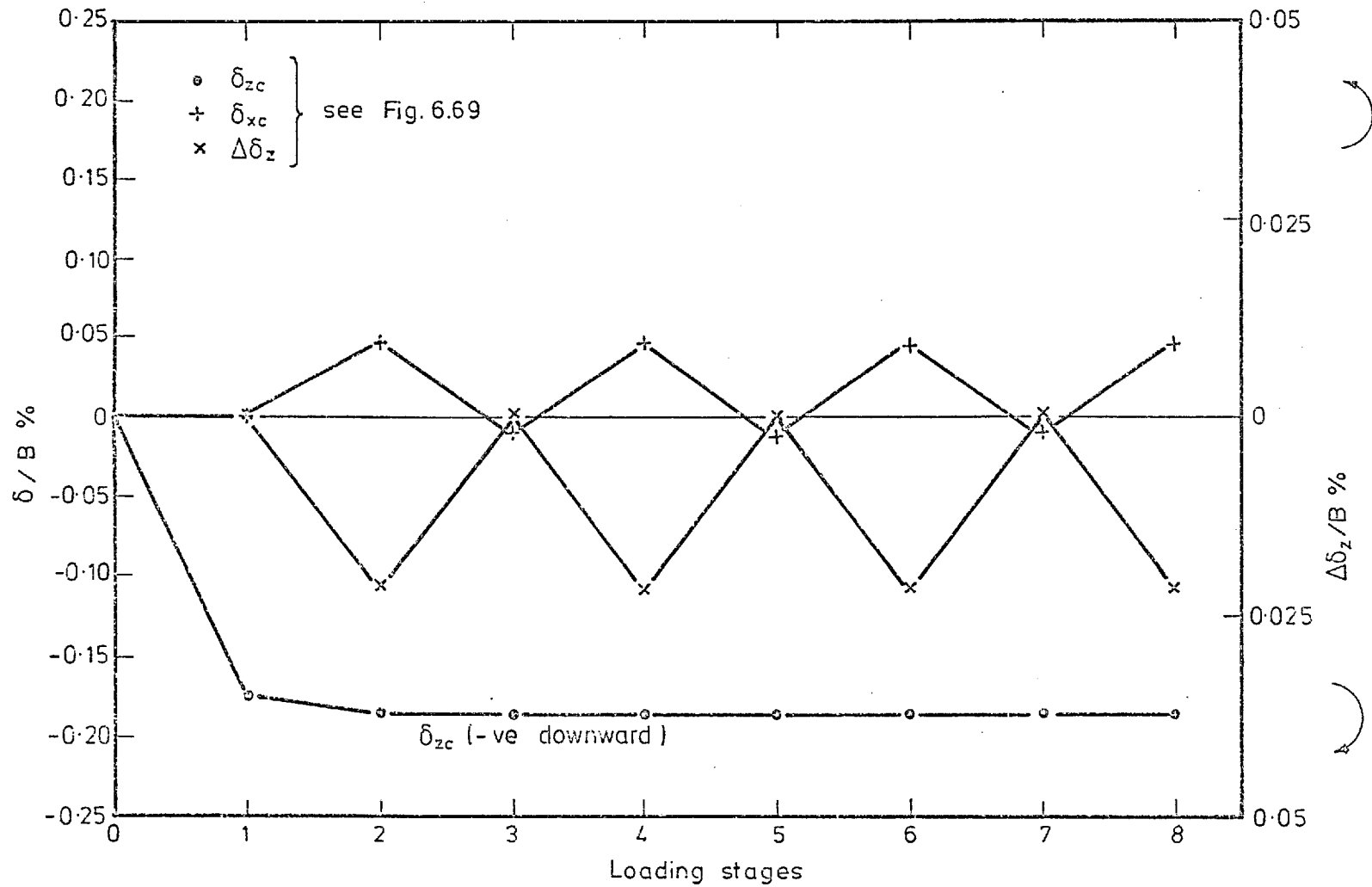
CASE 48   (see Table 5.3)

Fig. 6.78   Displacements   Numbers denote loading stages (see Chapter 5, section 5.3.2

and Table 5.3)

δ_z / B %

δ_x / B %

— — — — — Milovic et al (1970), $E_{average}$
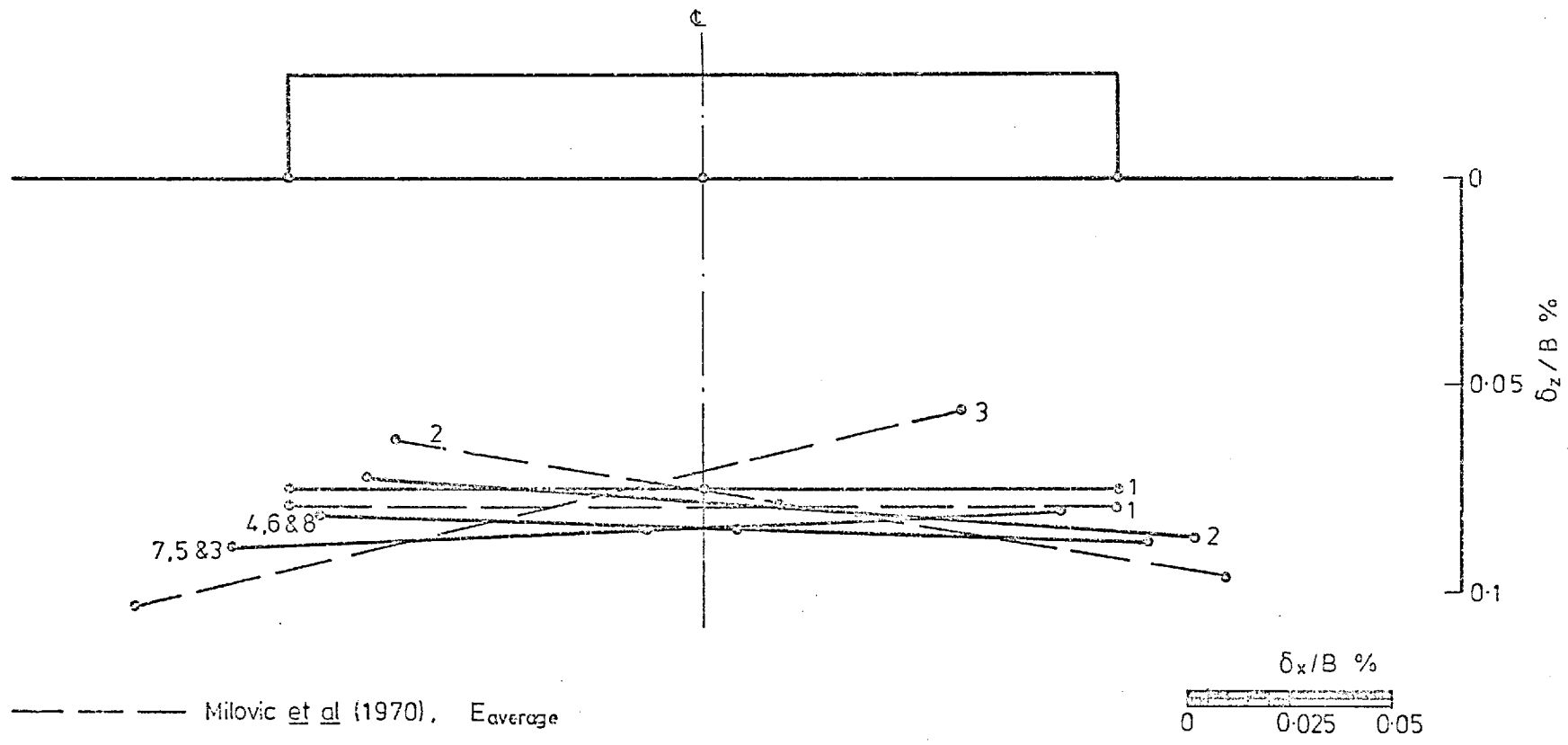
<u>CASE 49</u>   (see Table 5.3)

Fig. 6.79   Surface Horizontal and Vertical Displacements
            Numbers denote loading stages (see Chapter 5, section 5.3.2 and Table 5.3)
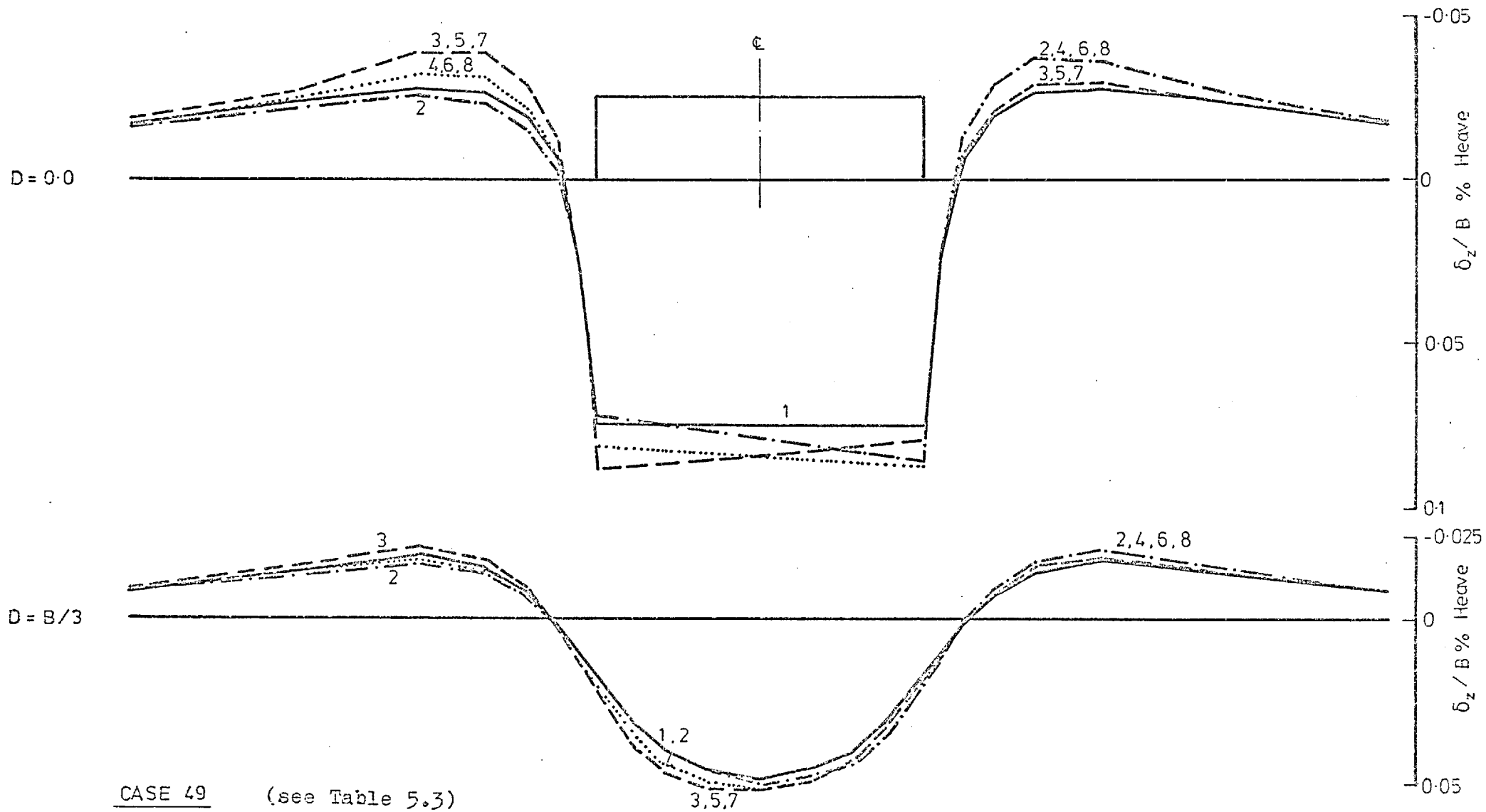
Fig. 6.80   Values of Vertical Displacements

Numbers denote loading stages (see Chapter 5, section 5.3.2 and Table 5.3)
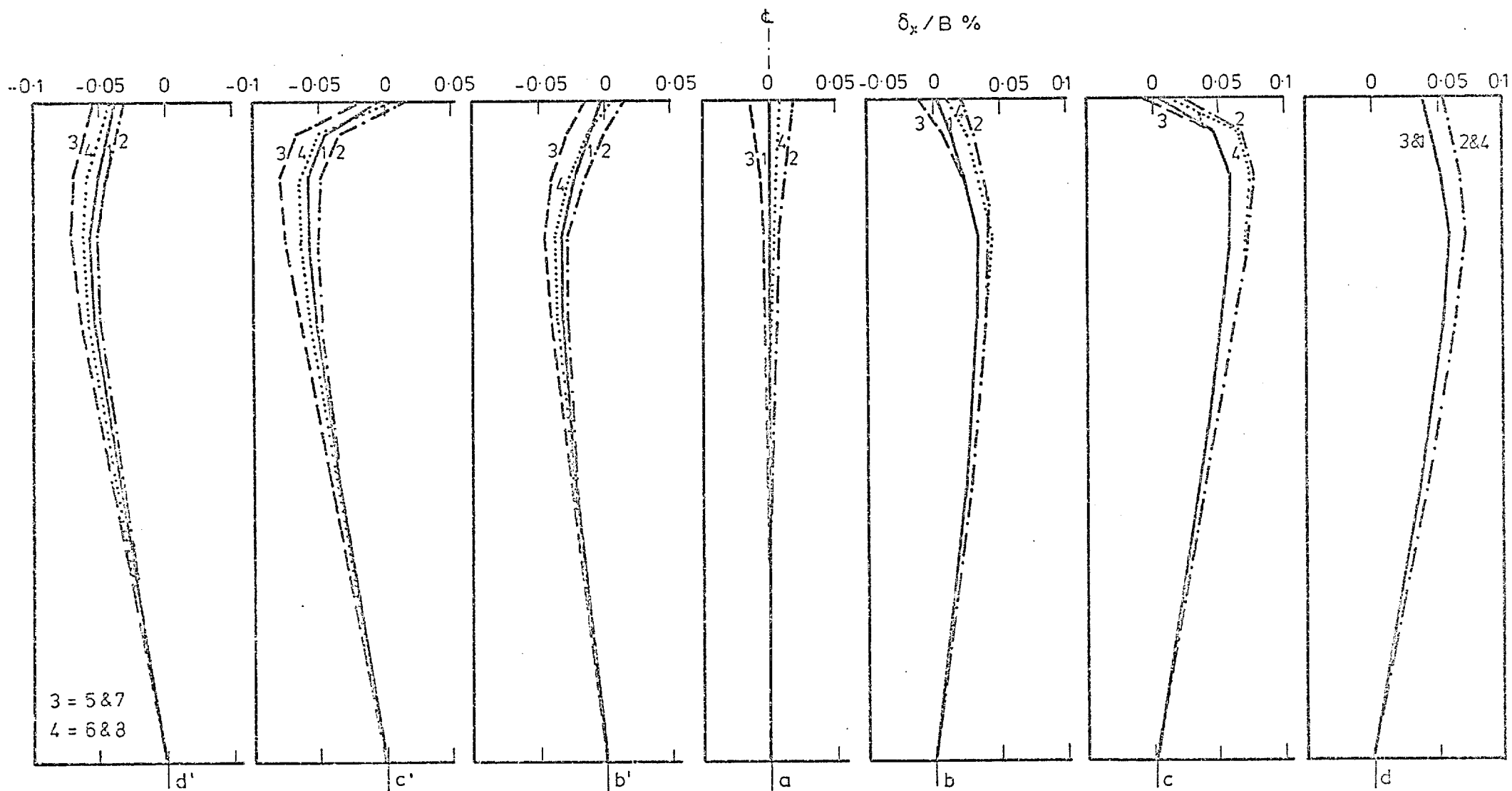
CASE 49   (see Table 5.3)

CASE 49 (see Table 5.3)

Fig. 6.81   CASE 49   Values of Horizontal
                       Displacements
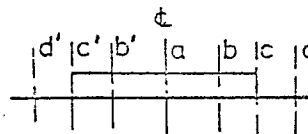
Numbers denote loading
stages (see Chapter 5,
section 5.3.2 and
Table 5.3)

327
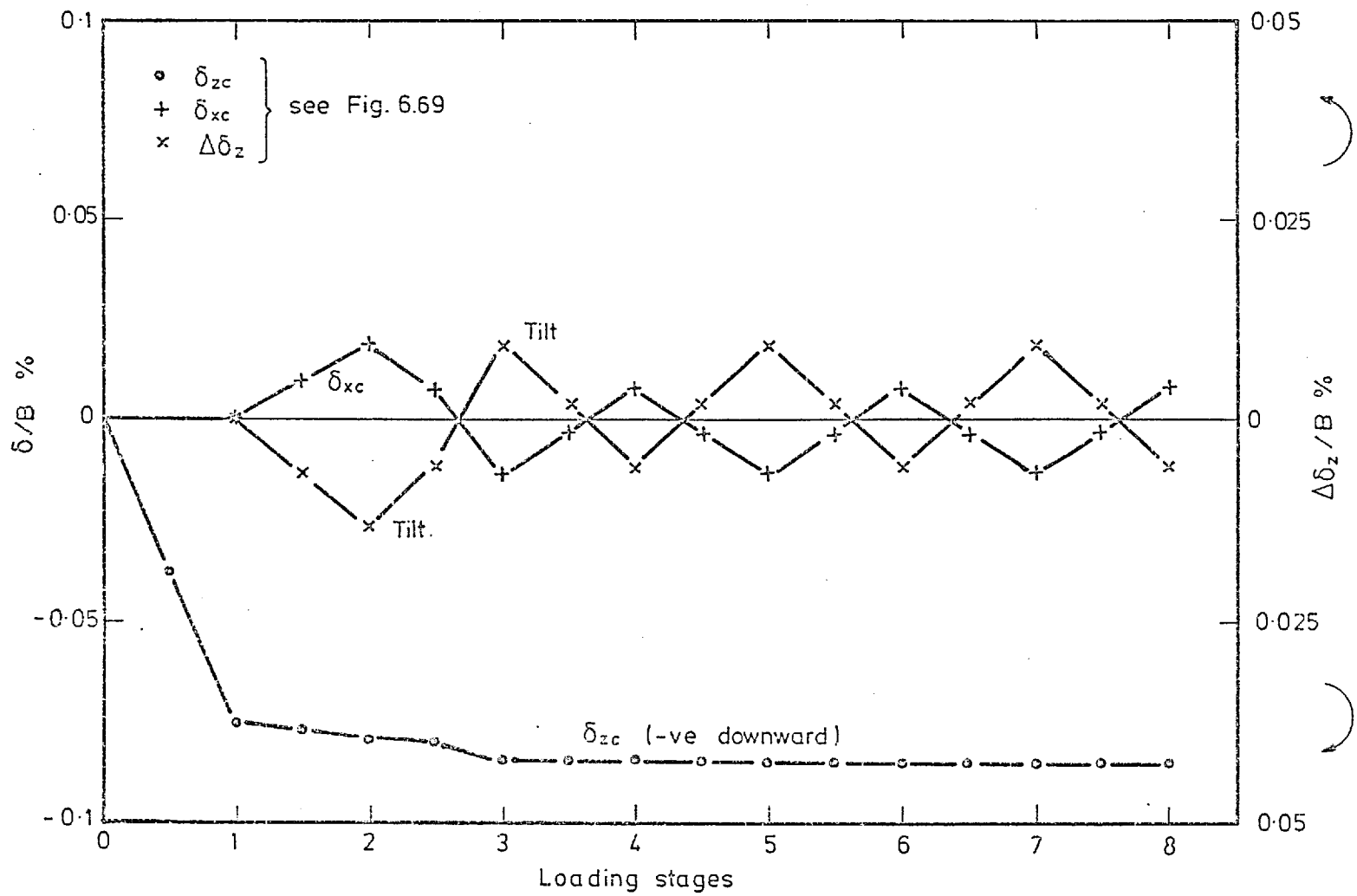
CASE 49   (see Table 5.3)

Fig. 6.82   Displacements   (see Section 5.3.2)
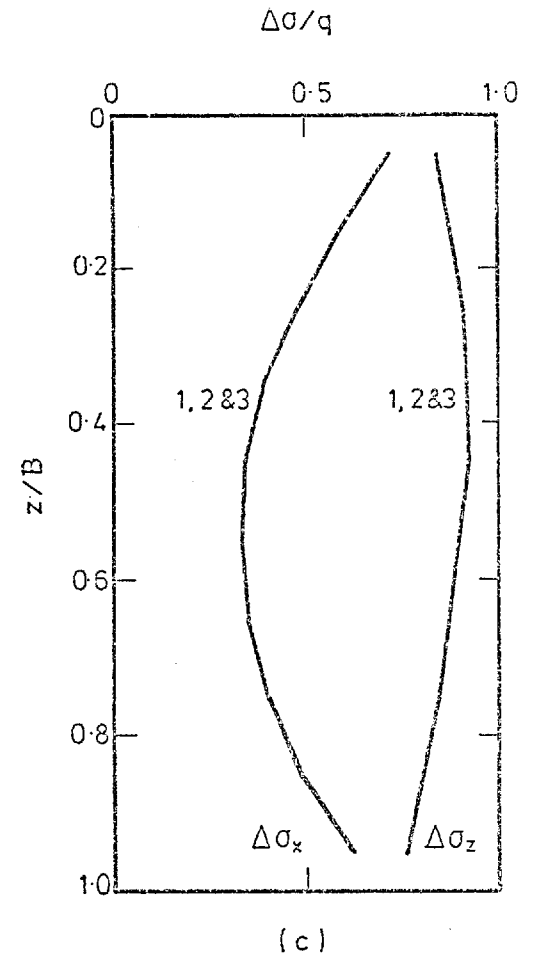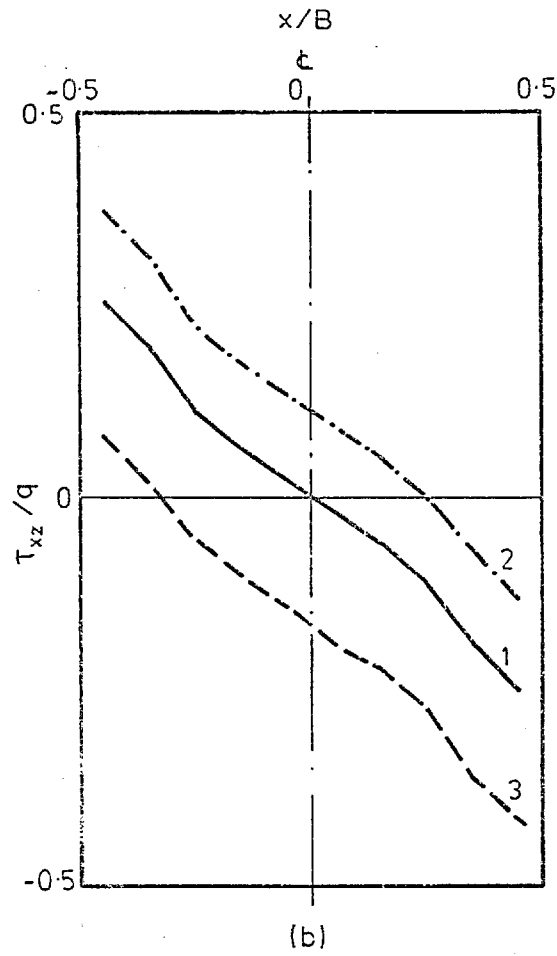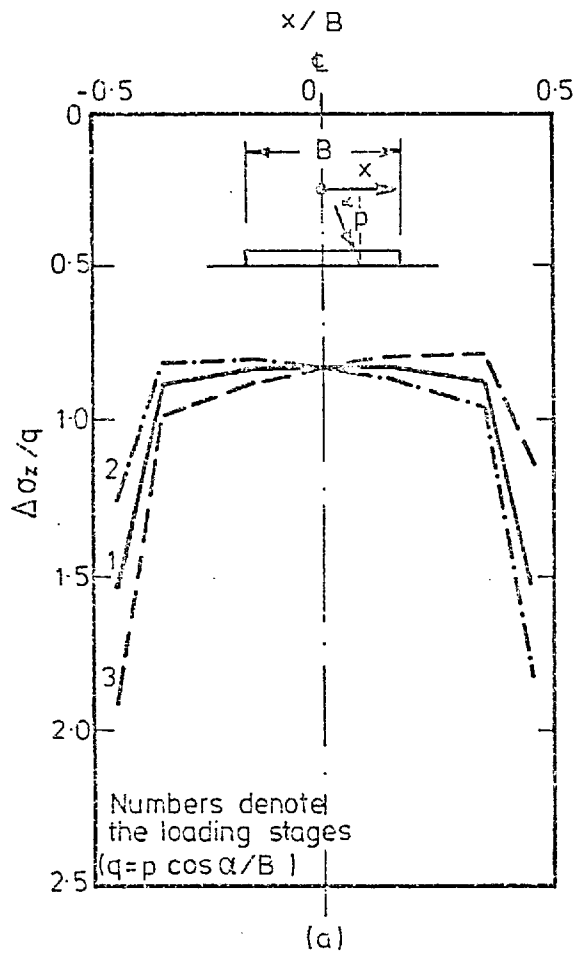
Fig. 6.83   Values of the Contact Vertical and Shear Stresses, and Stress Distribution
at the Centre-Line, after Milovic et al (1970)
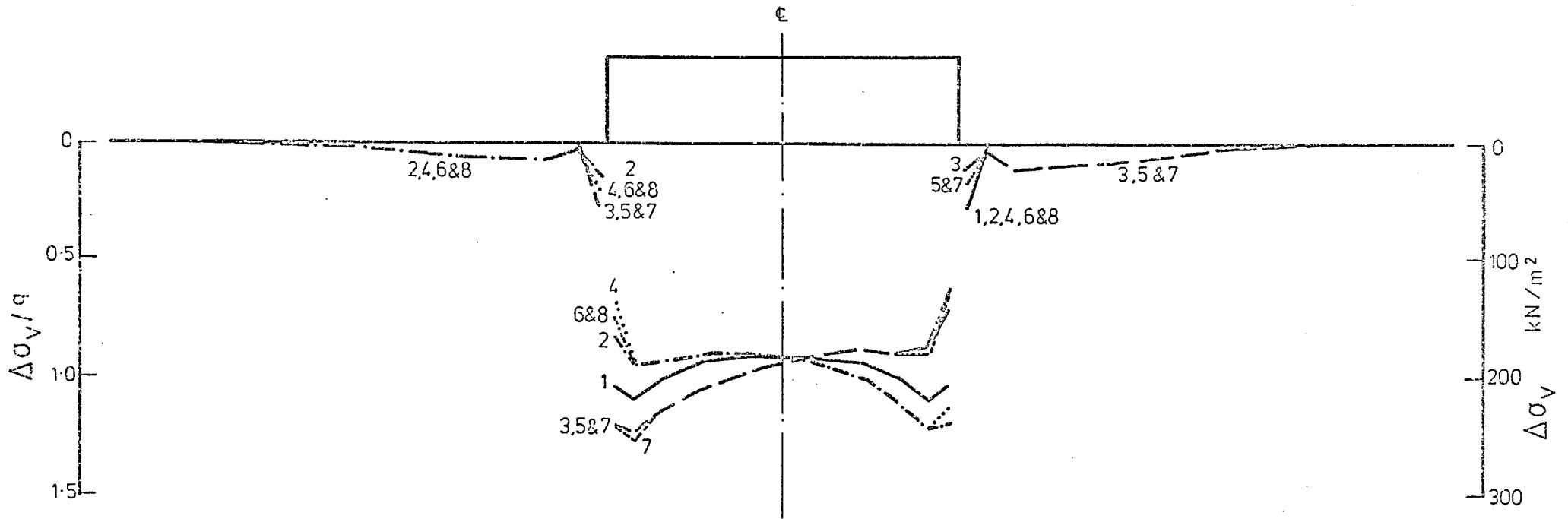
CASE 42   q = P cos α/ B   P = applied load

(see Table 5.3)

Fig. 6.84   Contact Pressure

Numbers denote loading stages,
(see Section 5.3.2).

Edge   ₵   Edge
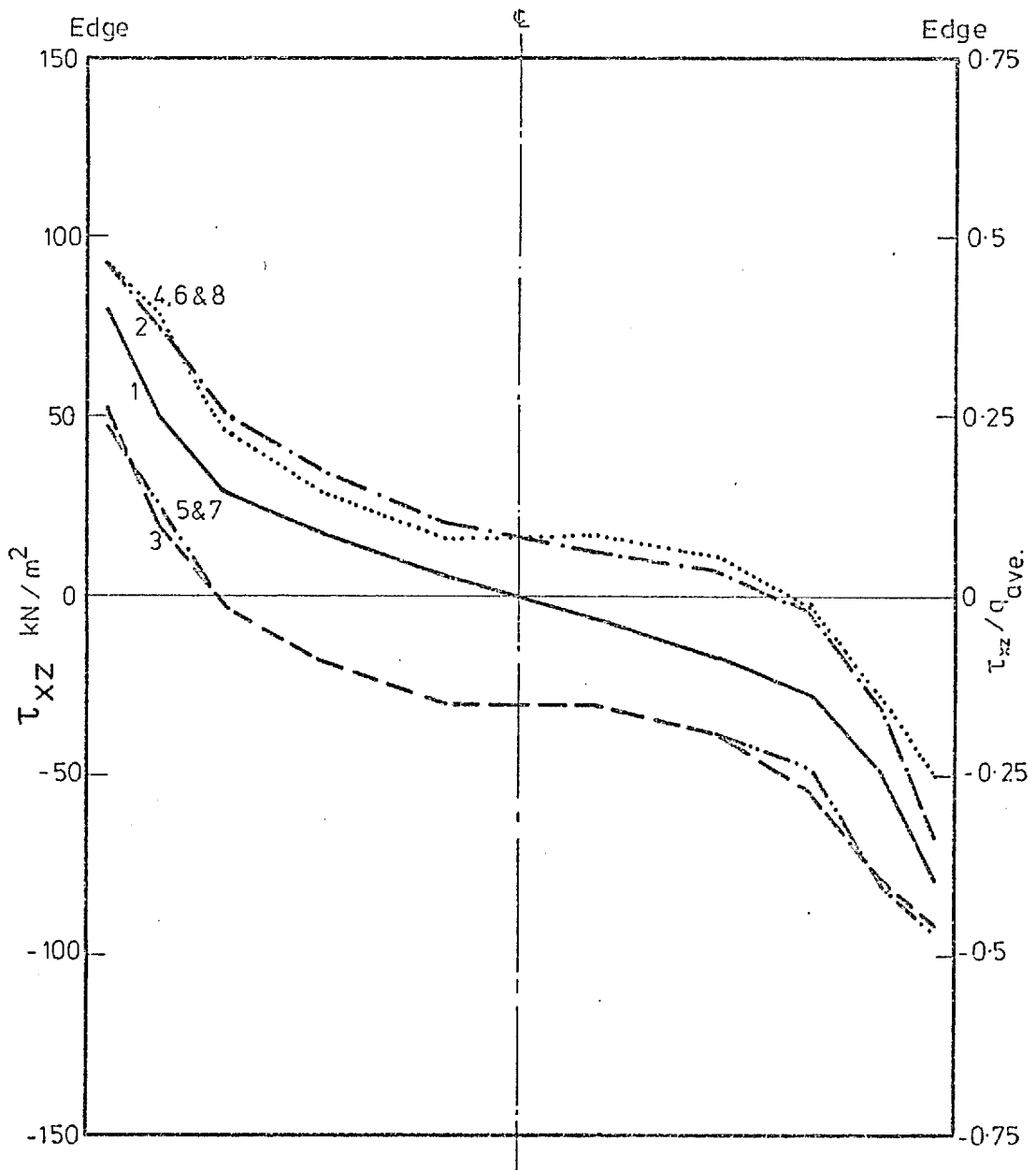
CASE 42   (see Table 5.3)

Fig. 6.85   Contact Shear Stresses

Numbers denote loading stages,
(see Section 5.3.2).
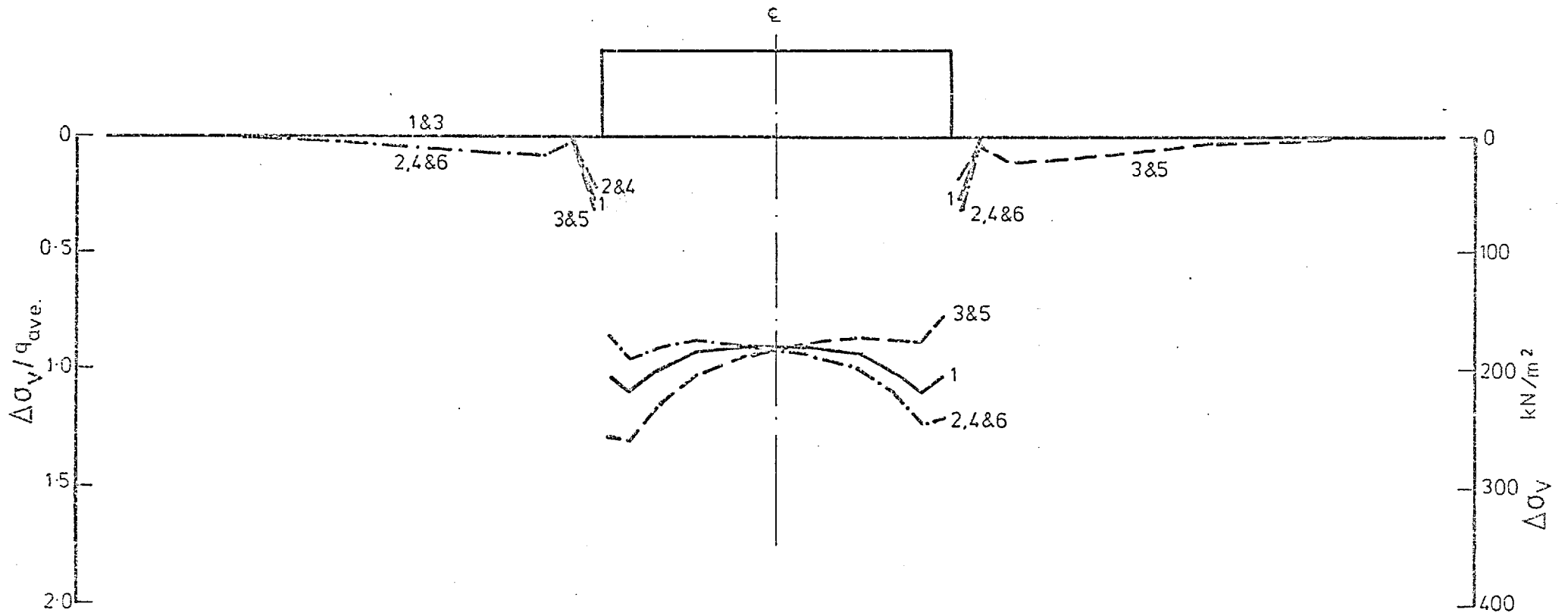
CASE 47   (see Table 5.3)

Fig. 6.86   Contact Pressure

Numbers denote loading stages,
(see Section 5.3.2).
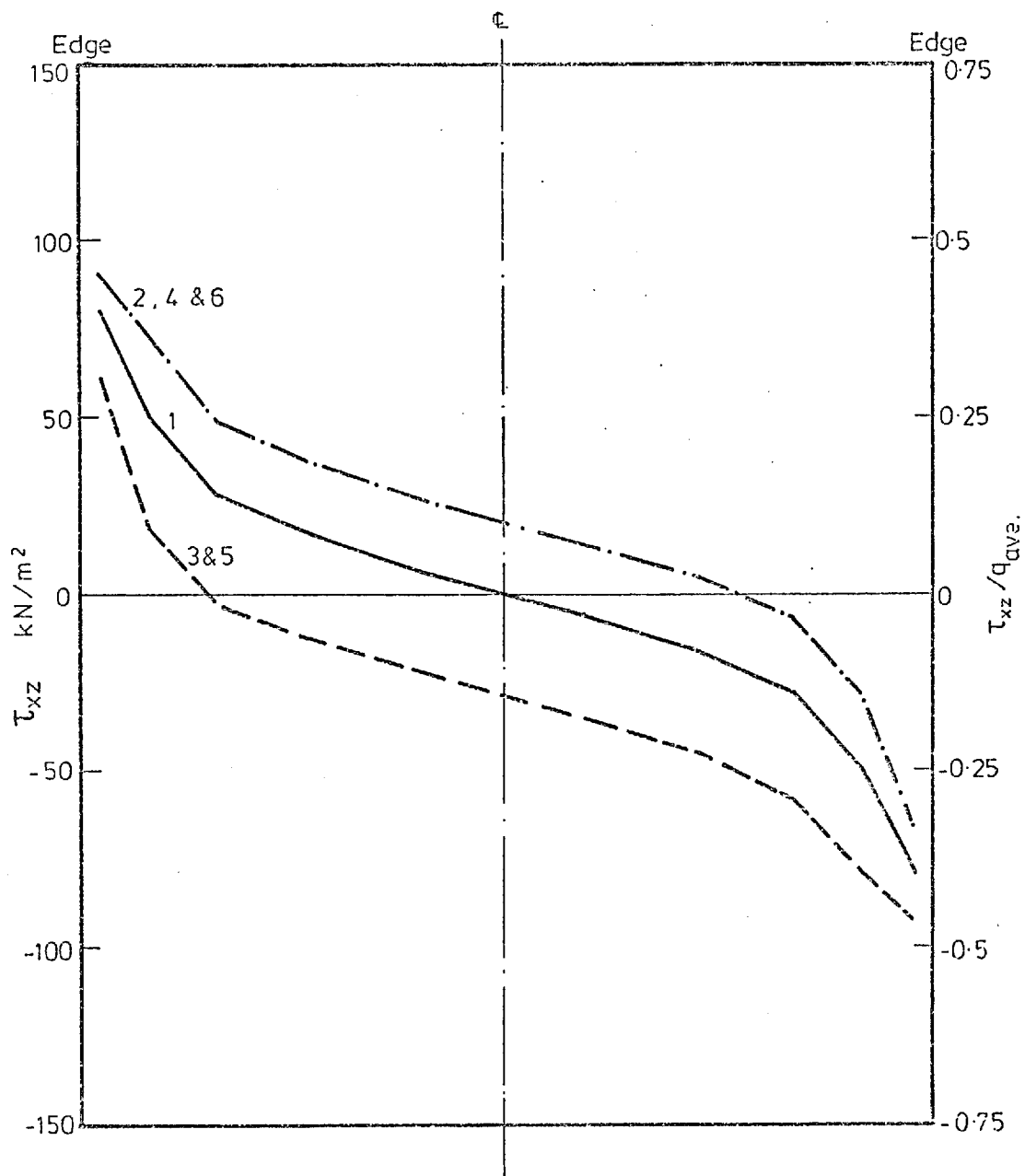
CASE 47   (see Table 5.3)

Fig. 6.87   Contact Shear Stresses

Numbers denote loading stages,
(see Section 5.3.2).
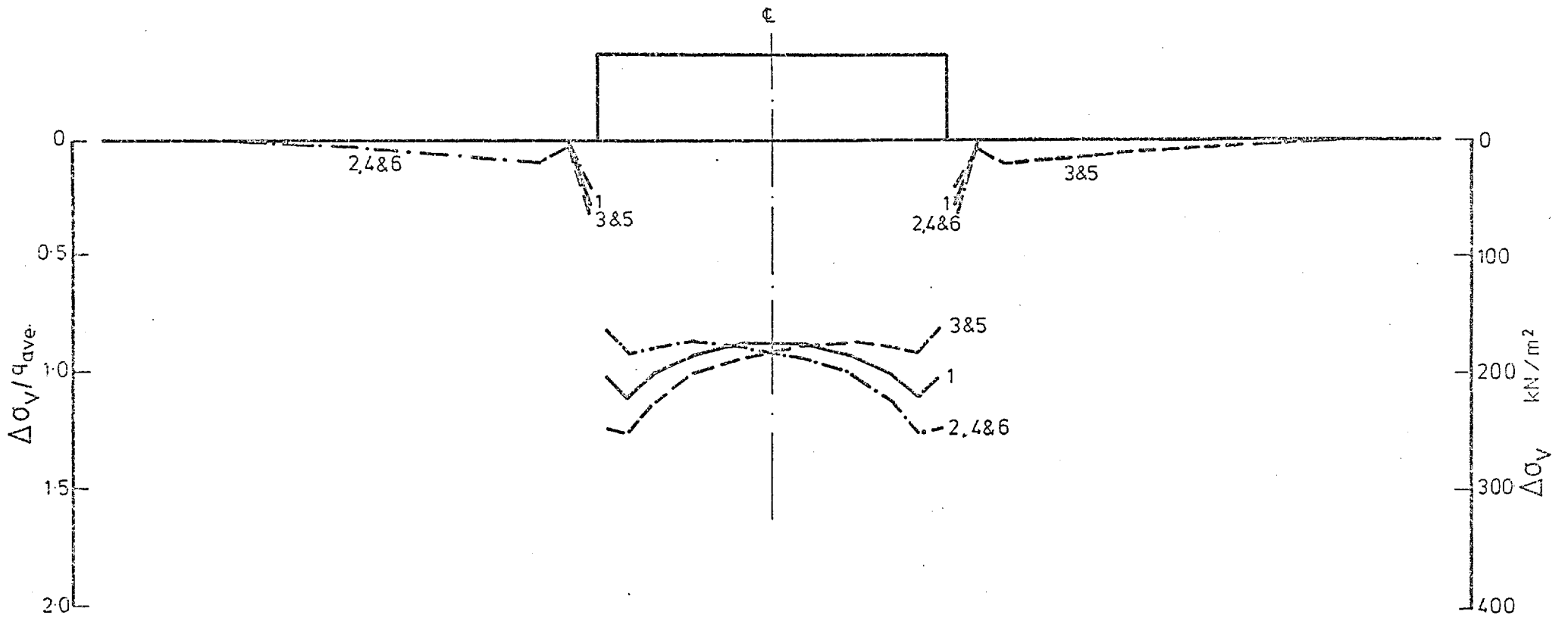
Fig. 6.88   Contact Pressure

Numbers denote loading stages,
(see Section 5.3.2).
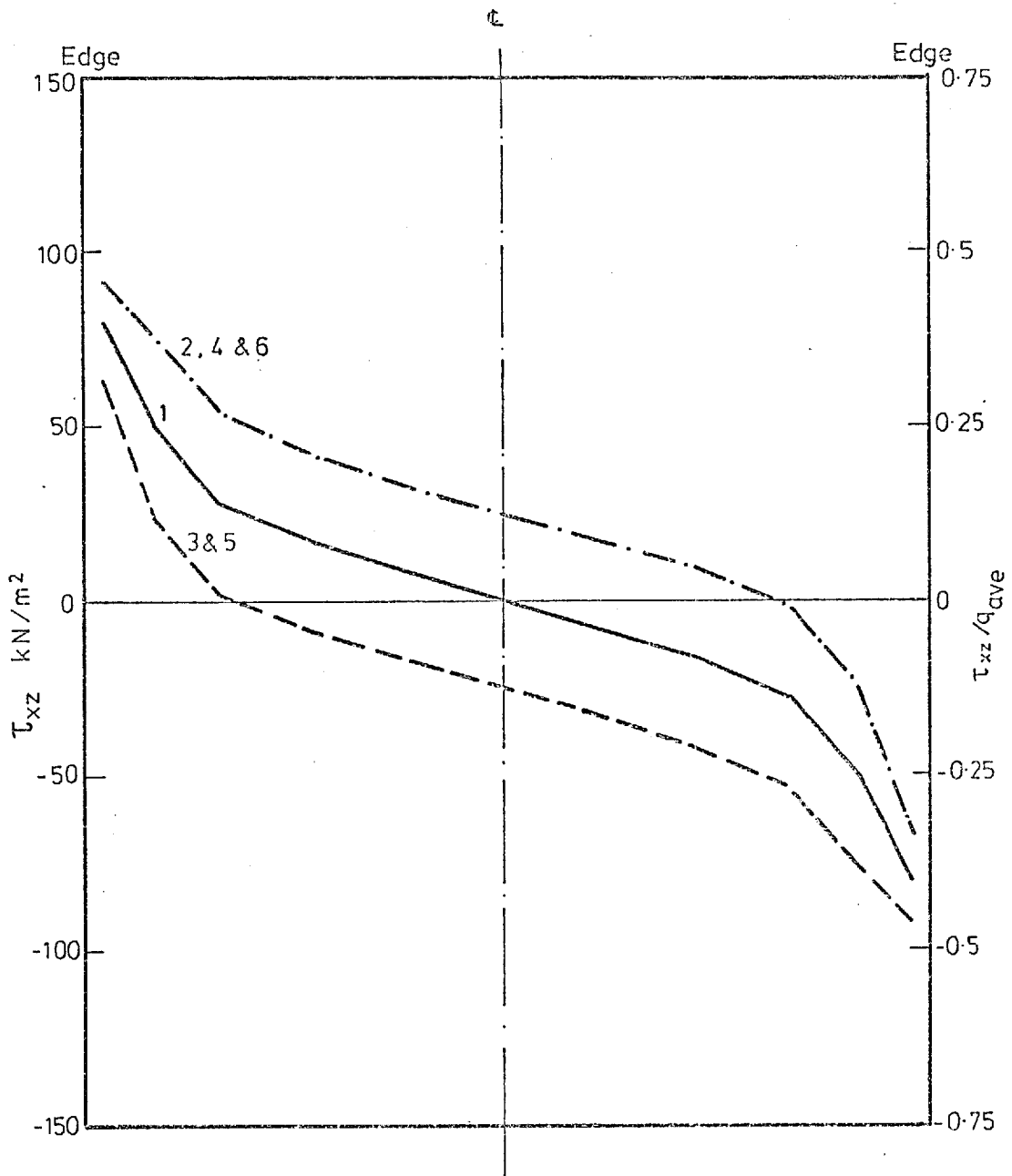
CASE 47.1   (see Table 5.3)

Fig. 6.89   Contact Shear Stresses
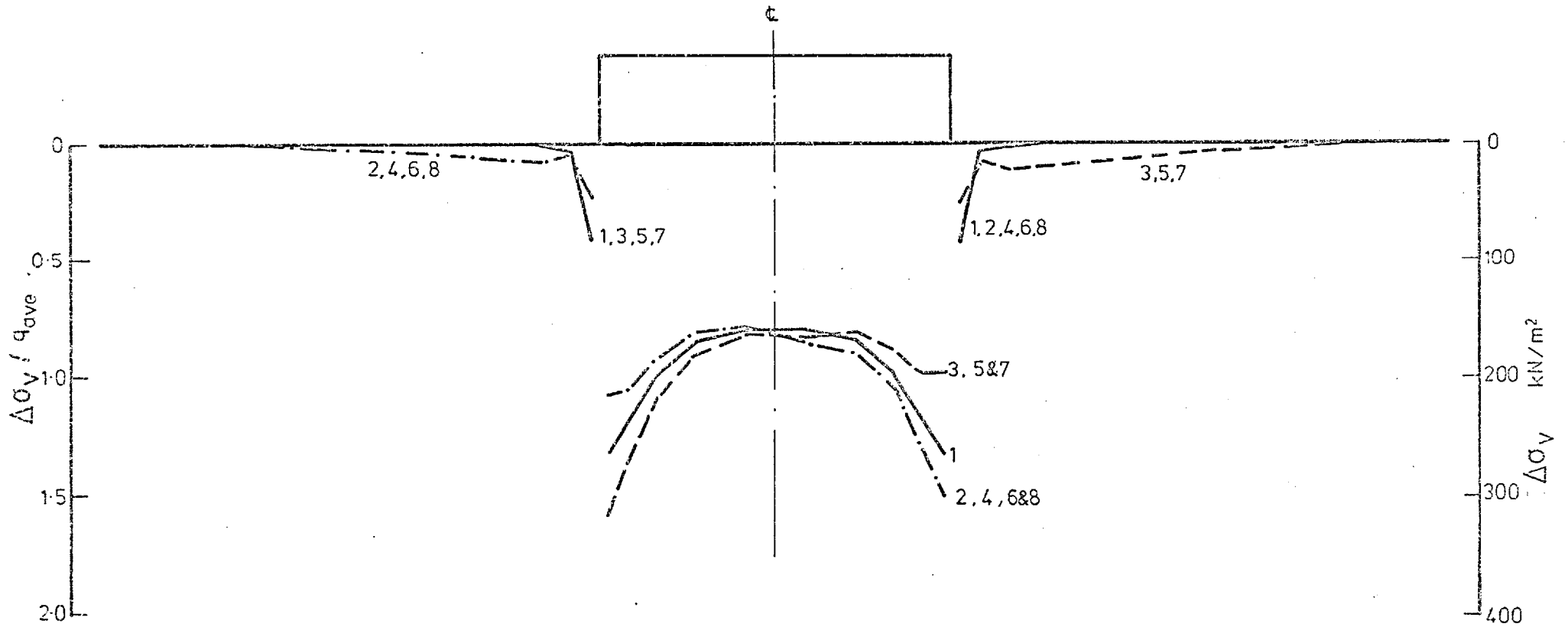
CASE 48 (see Table 5.3)

Fig. 6.90 Contact Pressure

Numbers denote loading stages,
(see Section 5.3.2).

336.
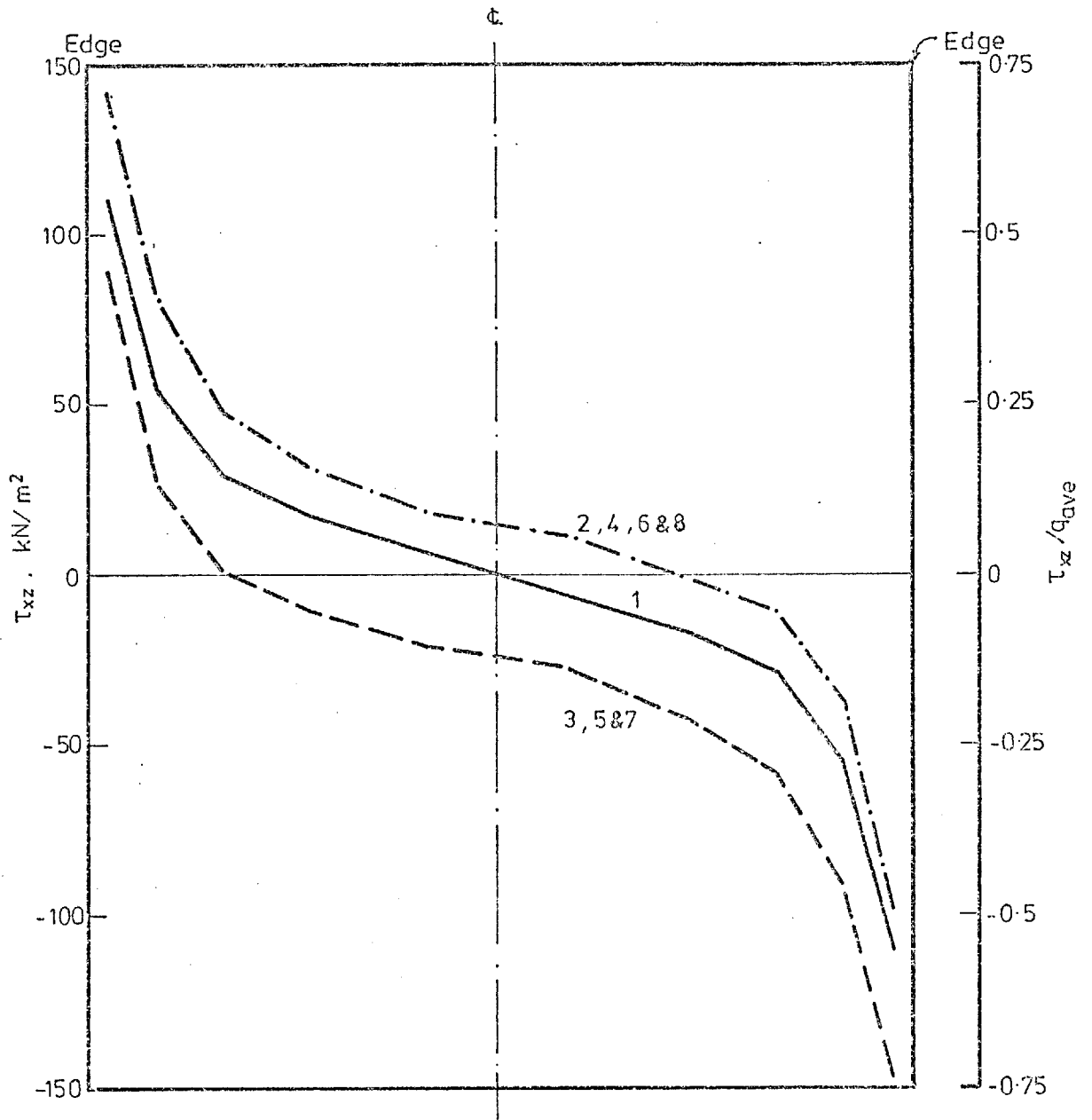
CASE 48   (see Table 5.3)

Fig. 6.91   Contact Shear Stresses

Numbers denote loading stages,
(see Section 5.3.2).
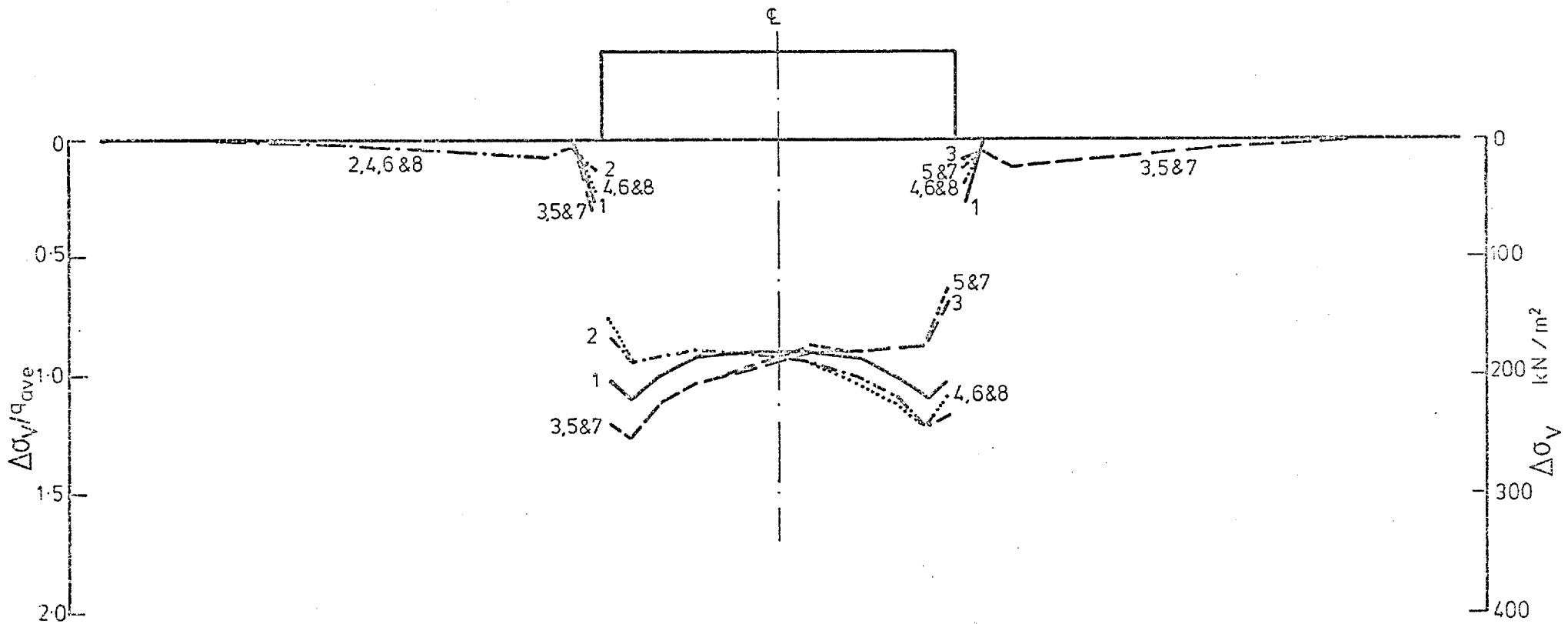
CASE 49   (see Table 5.3)

Fig. 6.92   Contact Pressure

Numbers denote loading stages,
(see Section 5.3.2).
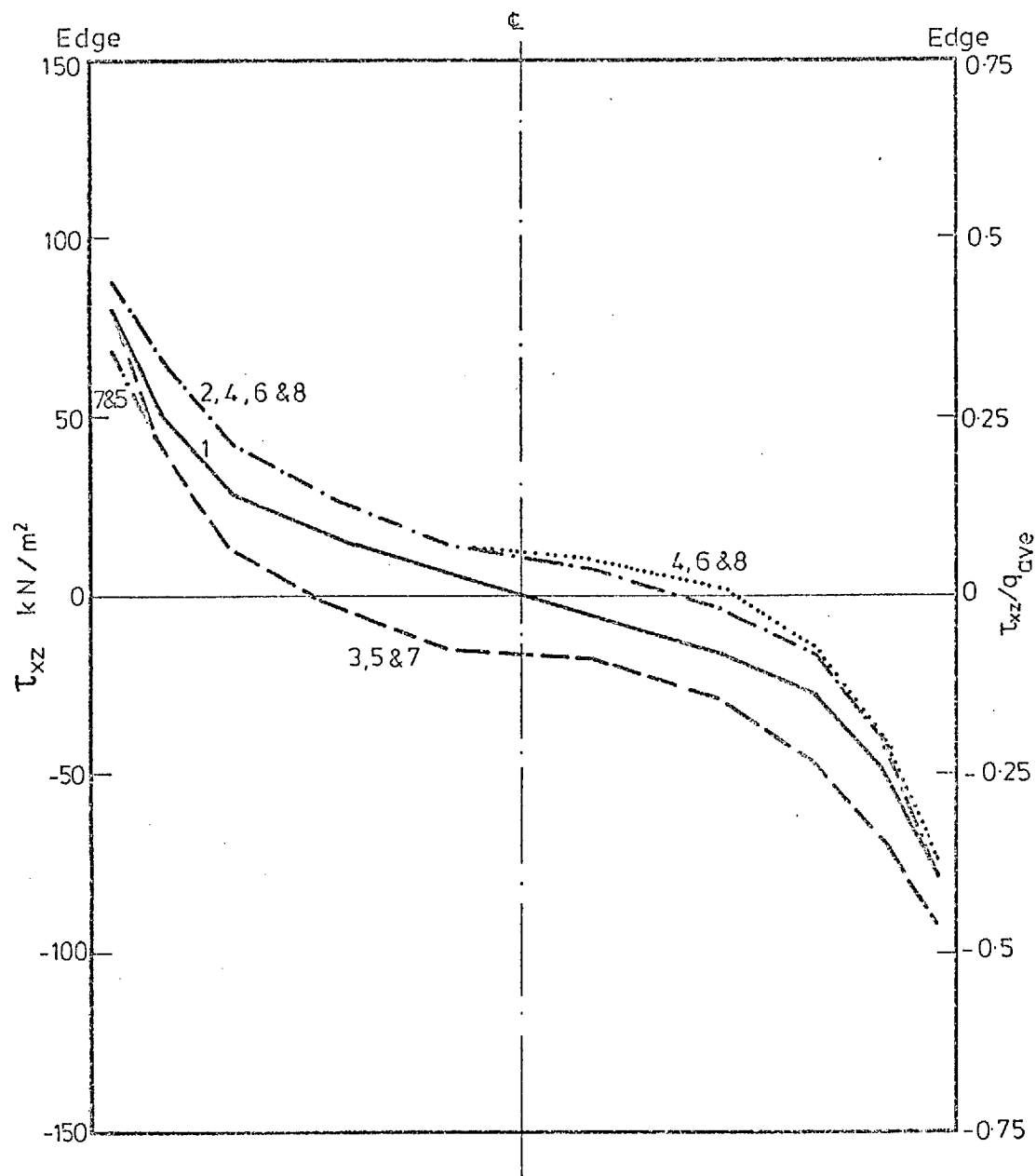
CASE 49   (see Table 5.3)

Fig. 6.93   Contact Shear Stresses

Numbers denote loading stages,
(see Section 5.3.2),

$\Delta\sigma/q$
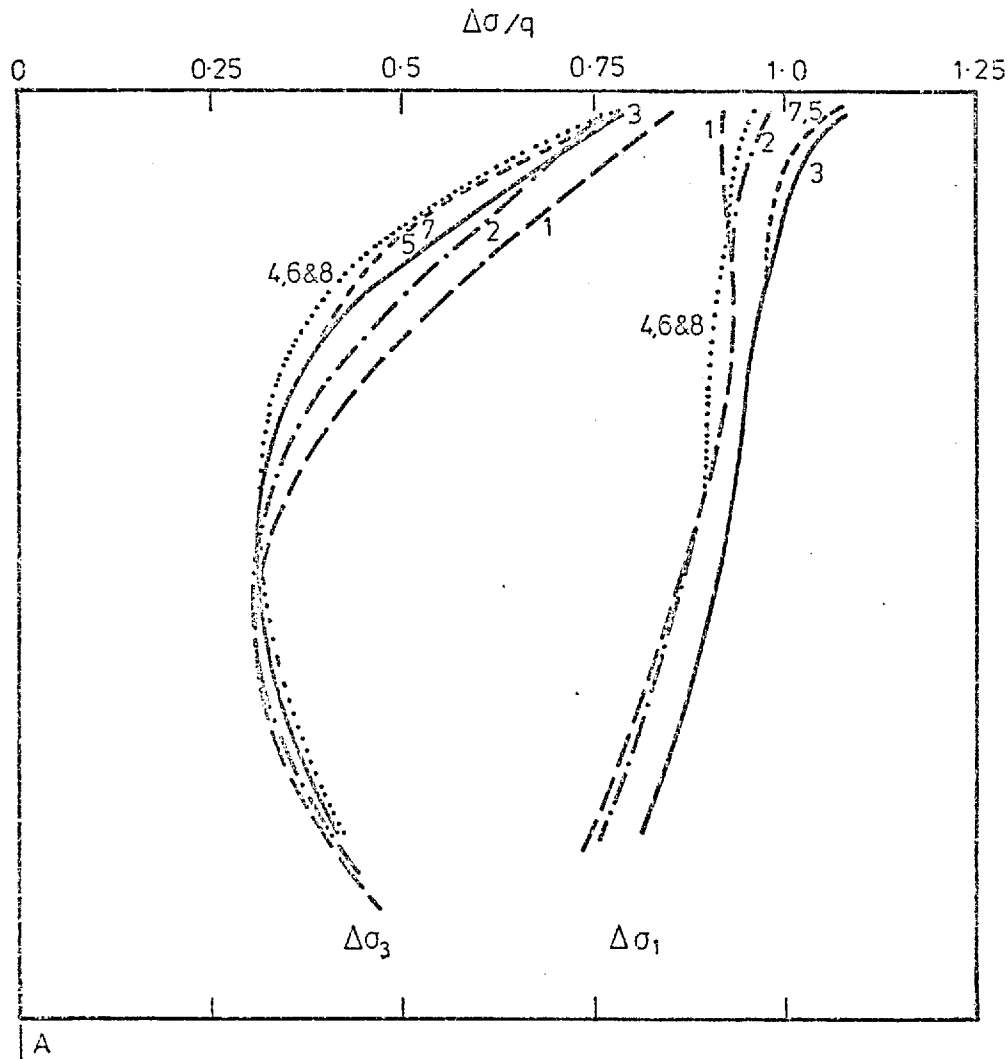
CASE 42 (q = 200 kPa)   (see Table 5.3)

Fig. 6.94   Principal Stress Changes
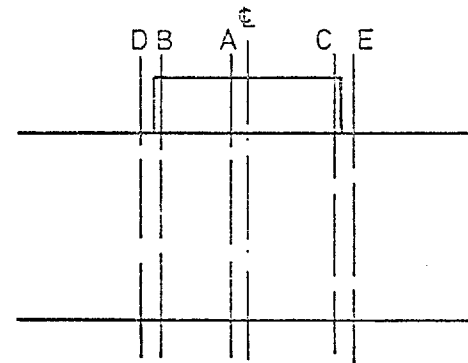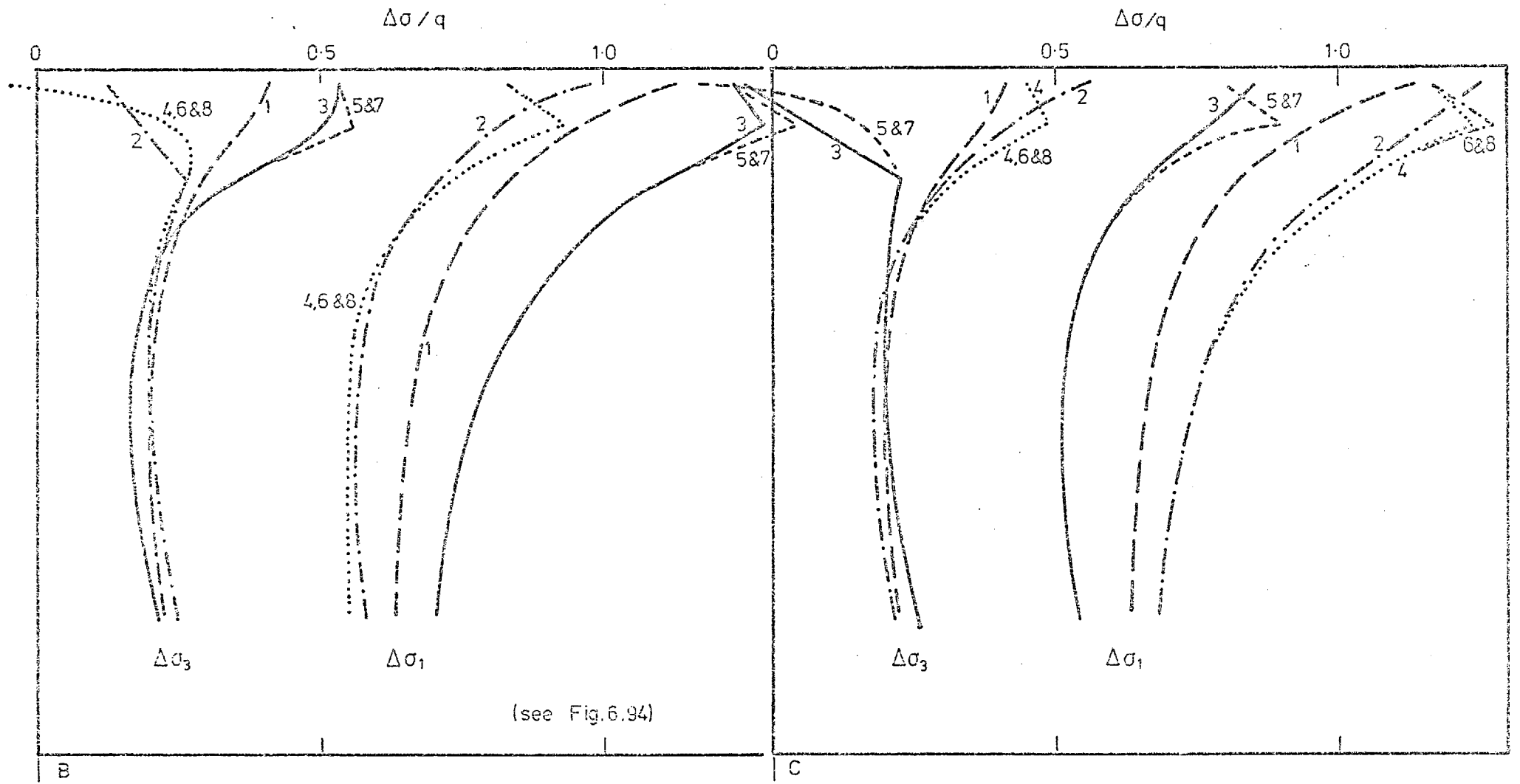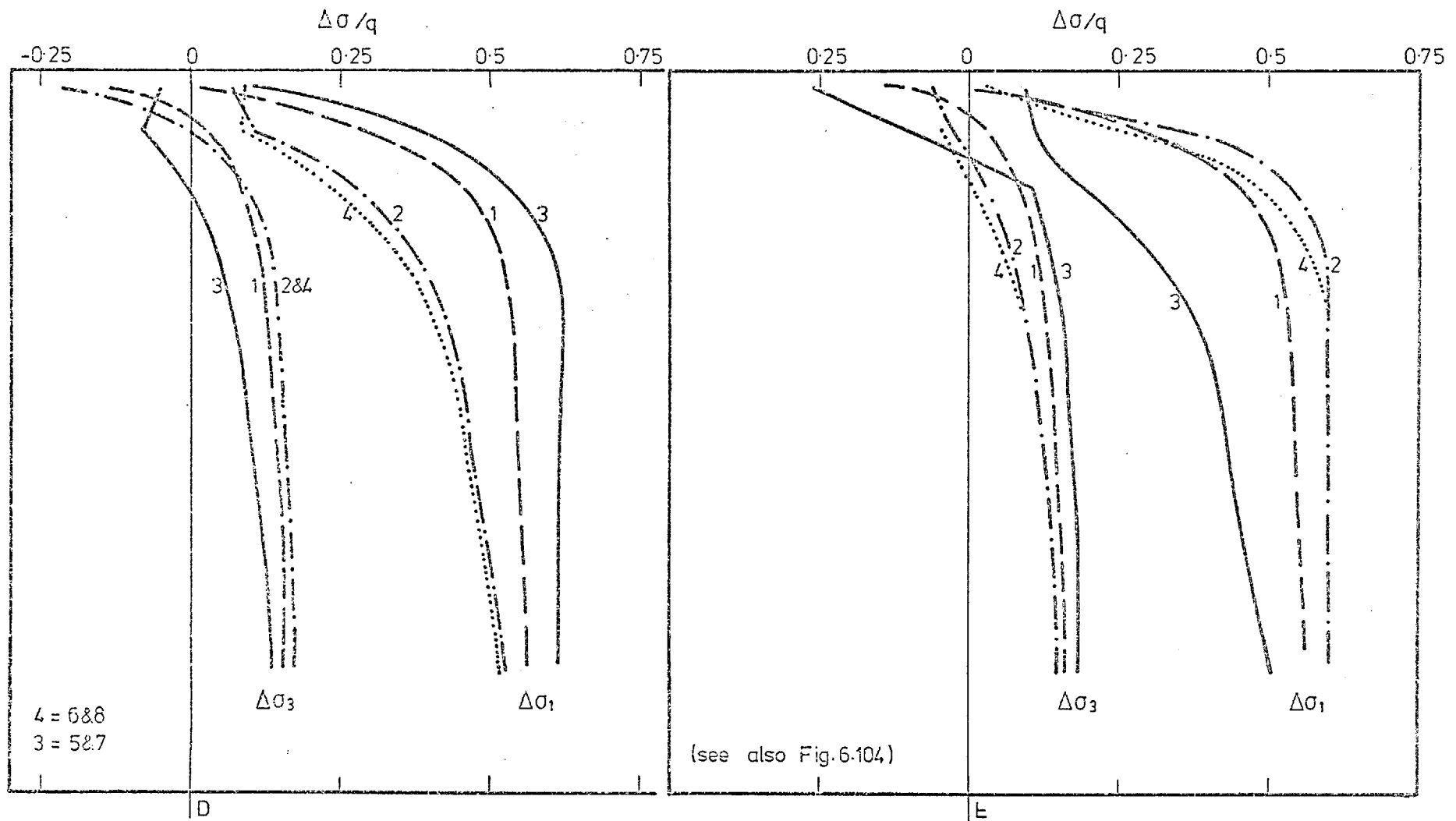
Numbers denote loading stages,
(see Section 5.3.2).

Fig. 6.95   Principal Stress Changes

CASE 42   (q = 200 kPa)

(see Table 5.3)

Numbers denote loading stages,
(see Section 5.3.2).

Fig. 6.96   Principal Stress Changes

CASE 42   (q = 200 kPa)   (see Table 5.3)

Numbers denote loading stages,
(see Section 5.3.2).

Δσ/q

0   0·5   1·0

5&3   1
6,4&2   3&5

2,4&6

Δσ₃   Δσ₁
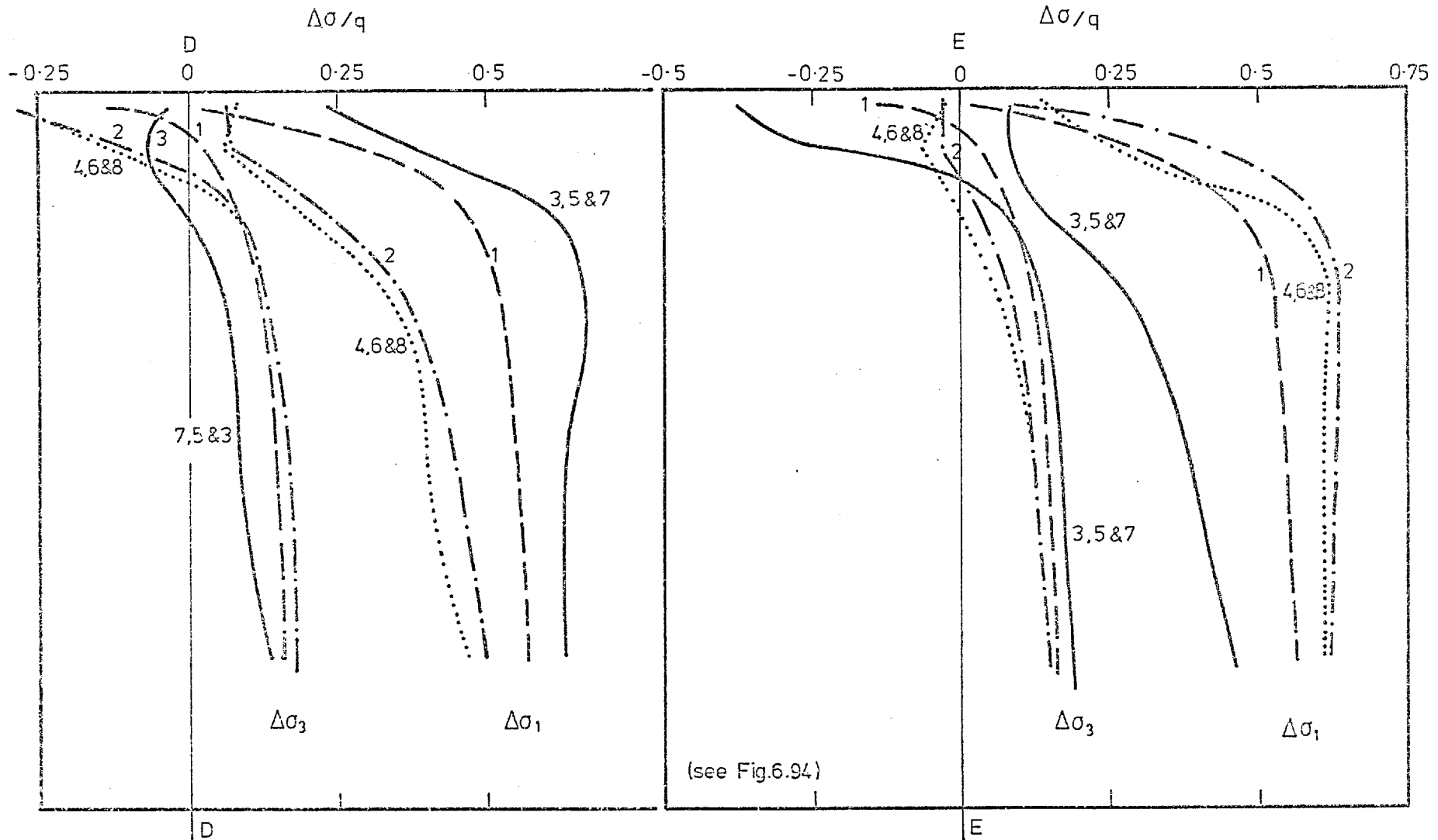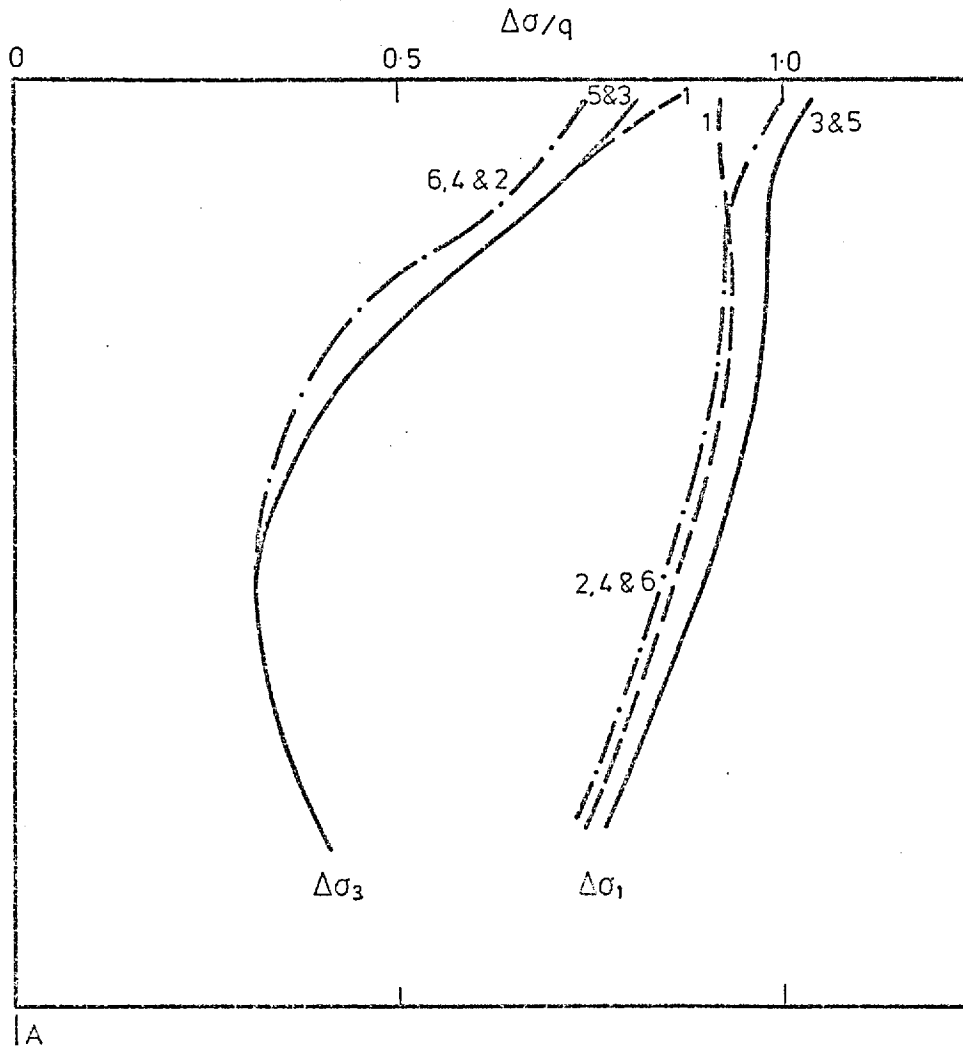
CASE 47   (q = 200 kPa)   (see Table 5.3)

Fig. 6.97   Principal Stress Changes

D B   A   ℄   C E

Numbers denote loading stages,
(see Section 5.3.2).

343
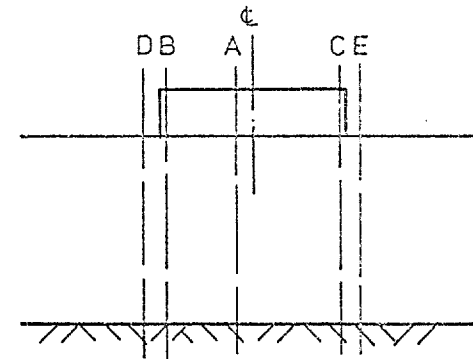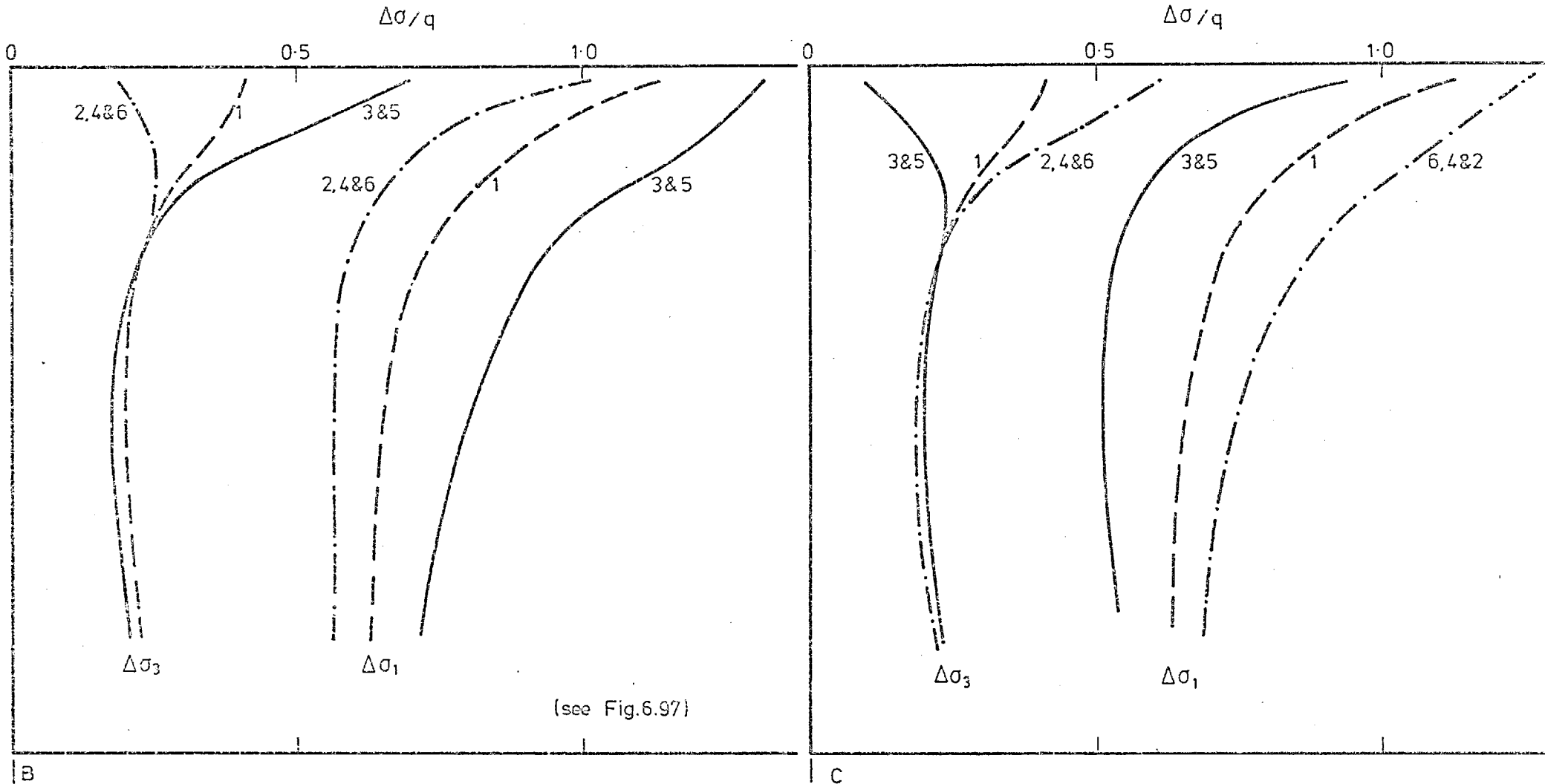
CASE 47   (q=200 kPa)   (see Table 5.3)

Fig. 6.98   Principal Stress Changes
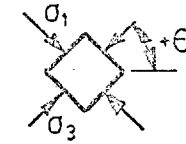
Numbers denote loading stages,
(see Section 5.3.2).
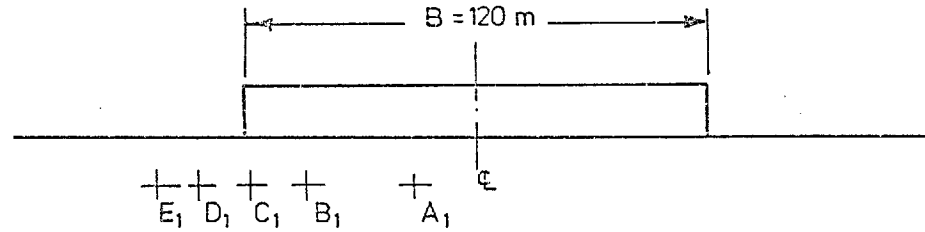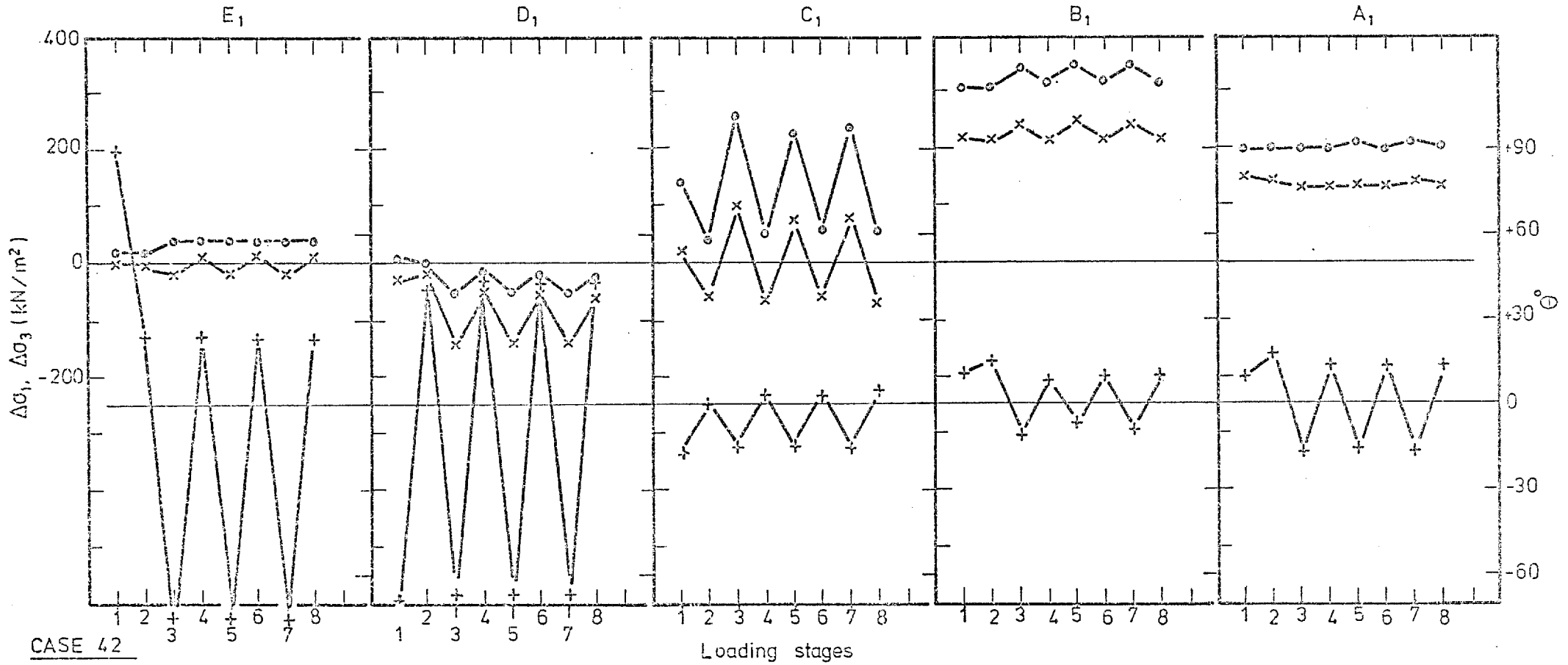
Δσ/q   Δσ/q

D   E

-0·25   0   0·25   0·5   0·75   -0·25   0   0·25   0·5   0·75

2,4&6   3&5   3&5   1   2   2,4&6

3&5   2,4&6   1   3&5   1

1   4   6

$\Delta\sigma_3$ $\Delta\sigma_1$ $\Delta\sigma_3$ $\Delta\sigma_1$

(see Fig.6.97)

D   E
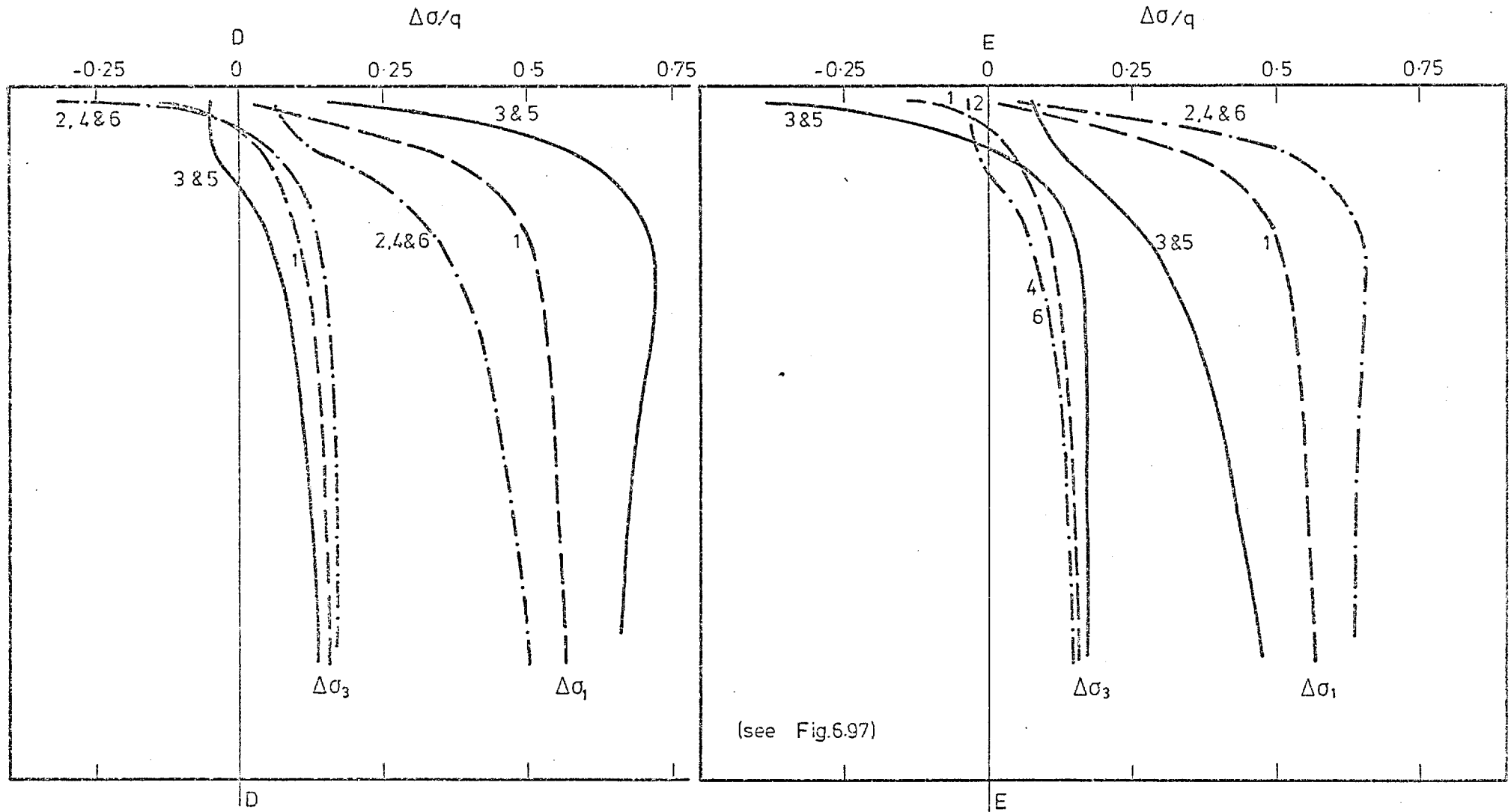
CASE 47   (q = 200 kPa)   (see Table 5.3)

Fig. 6.99   Principal Stress Changes   Numbers denote loading stages, (see Section 5.3.2).

345

$\Delta\sigma/q$

0   0·5   1·0

2 = 4, 6 & 8
3 = 5 & 7

$\Delta\sigma_3$ $\Delta\sigma_1$

A
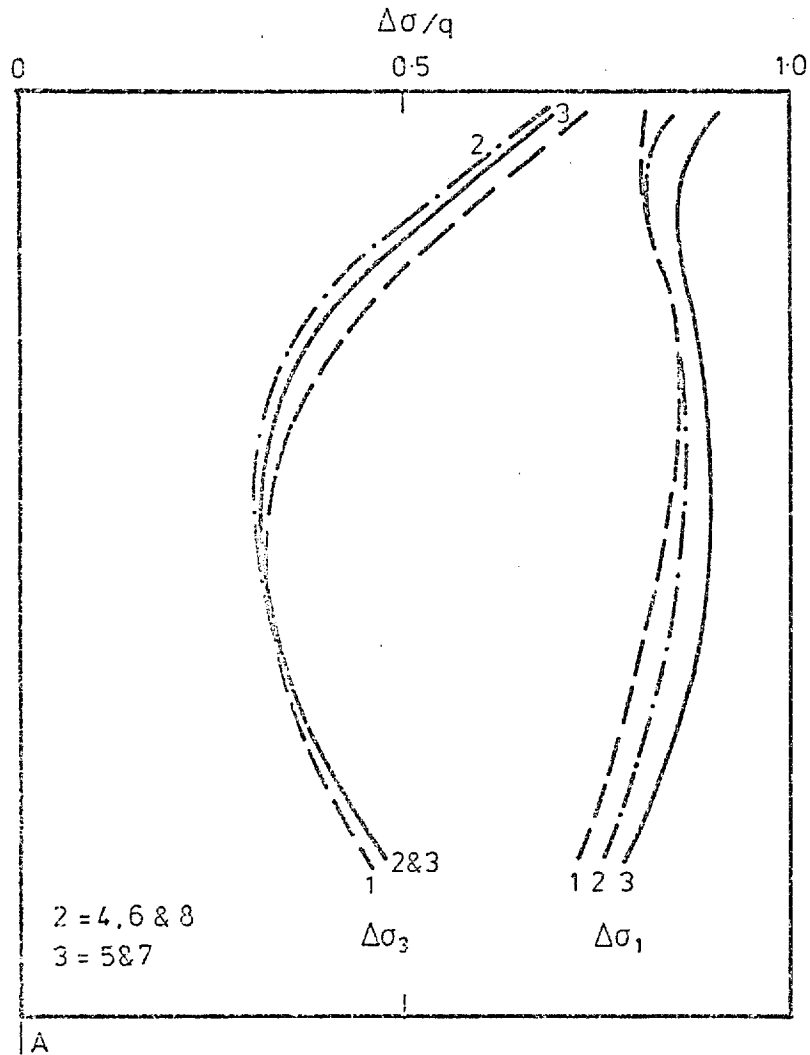
CASE 48   (q = 200 kPa)   (see Table 5.3)

Fig. 6.100   Principal Stress Changes

Numbers denote loading stages,
see Section 5.3.2.

$\Delta\sigma/q$

2 = 4,6 & 8
3 = 5 & 7

$\Delta\sigma_3$ $\Delta\sigma_1$

(see   Fig.6.100)
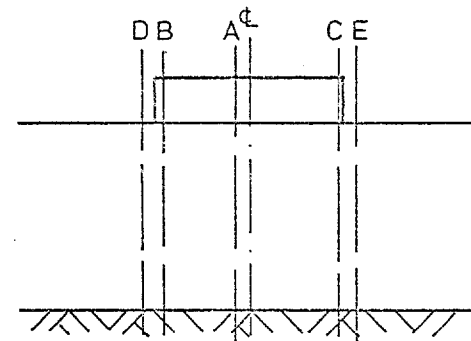
CASE 48   q = 200 kPa   (see Table 5.3)
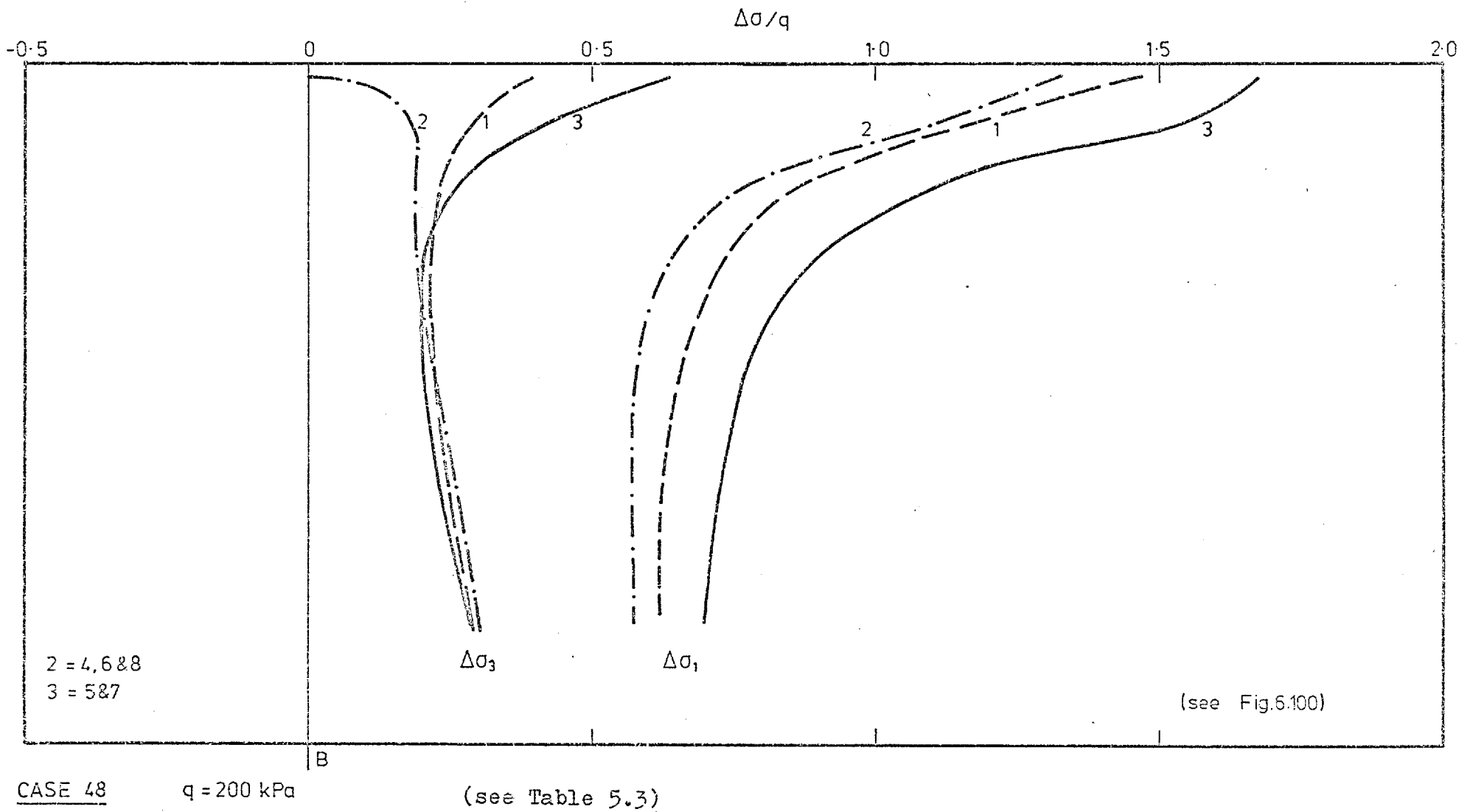
Fig. 6.101   Principal Stress Changes   Numbers denote loading stages,
(see Section 5.3.2).

$\Delta \sigma / q$

-0·5   0   0·5   1·0   1·5   2·0

3   1   2   3   1   2

2 = 4,6 & 8
3 = 5 & 7

$\Delta \sigma_3$ $\Delta \sigma_1$

(see   Fig.6.100)

C
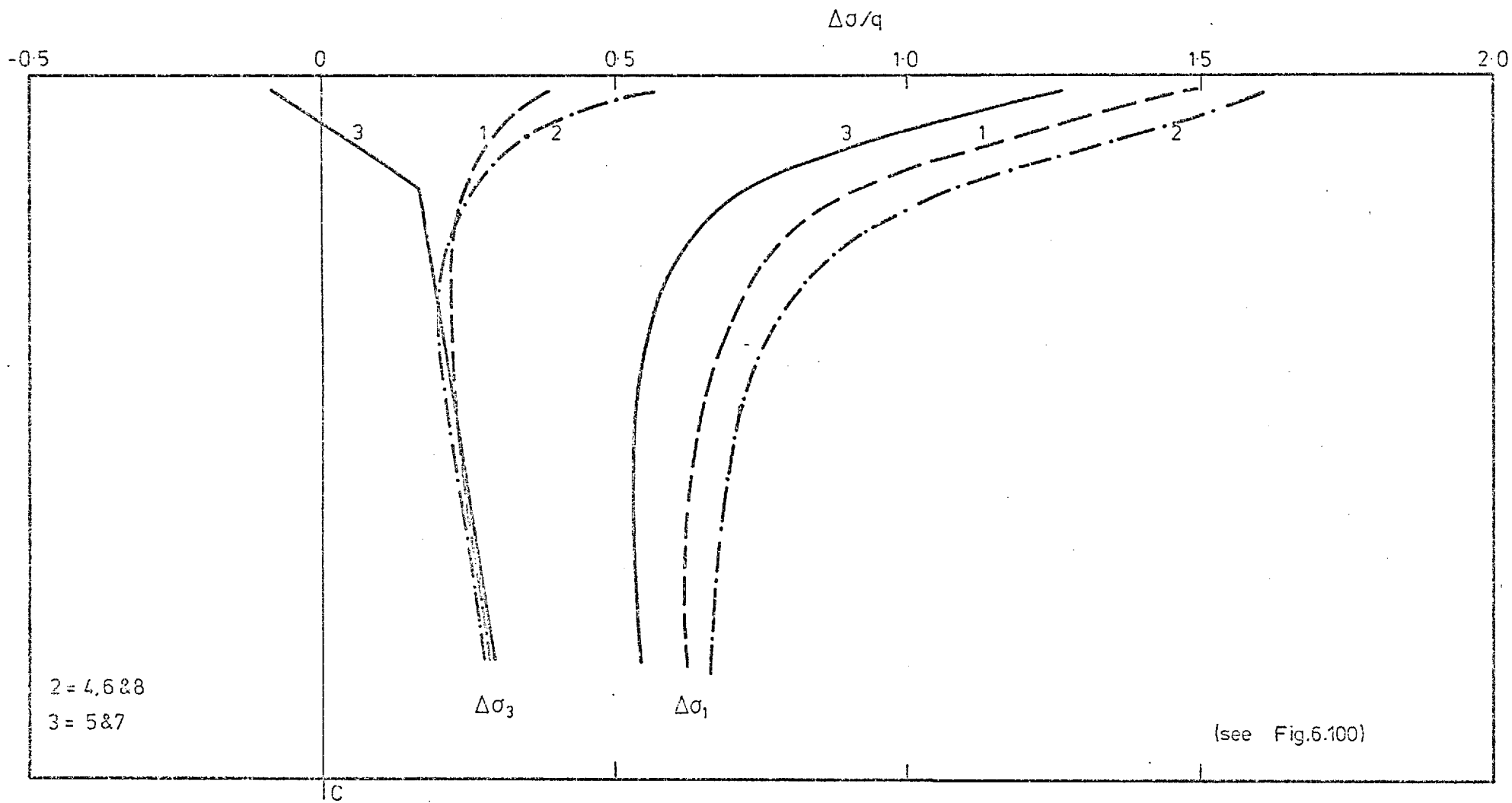
CASE 48   q = 200 kPa   (see Table 5.3)

Fig. 6.102   Principal Stress Changes

Numbers denote loading stages,
(see Section 5.3.2).

$\Delta\sigma/q$ ... $\Delta\sigma/q$

2 = 4, 6 & 8
3 = 5 & 7

$\Delta\sigma_2$ ... $\Delta\sigma_1$

(see also Fig.6.100)

$\Delta\sigma_3$ ... $\Delta\sigma_1$
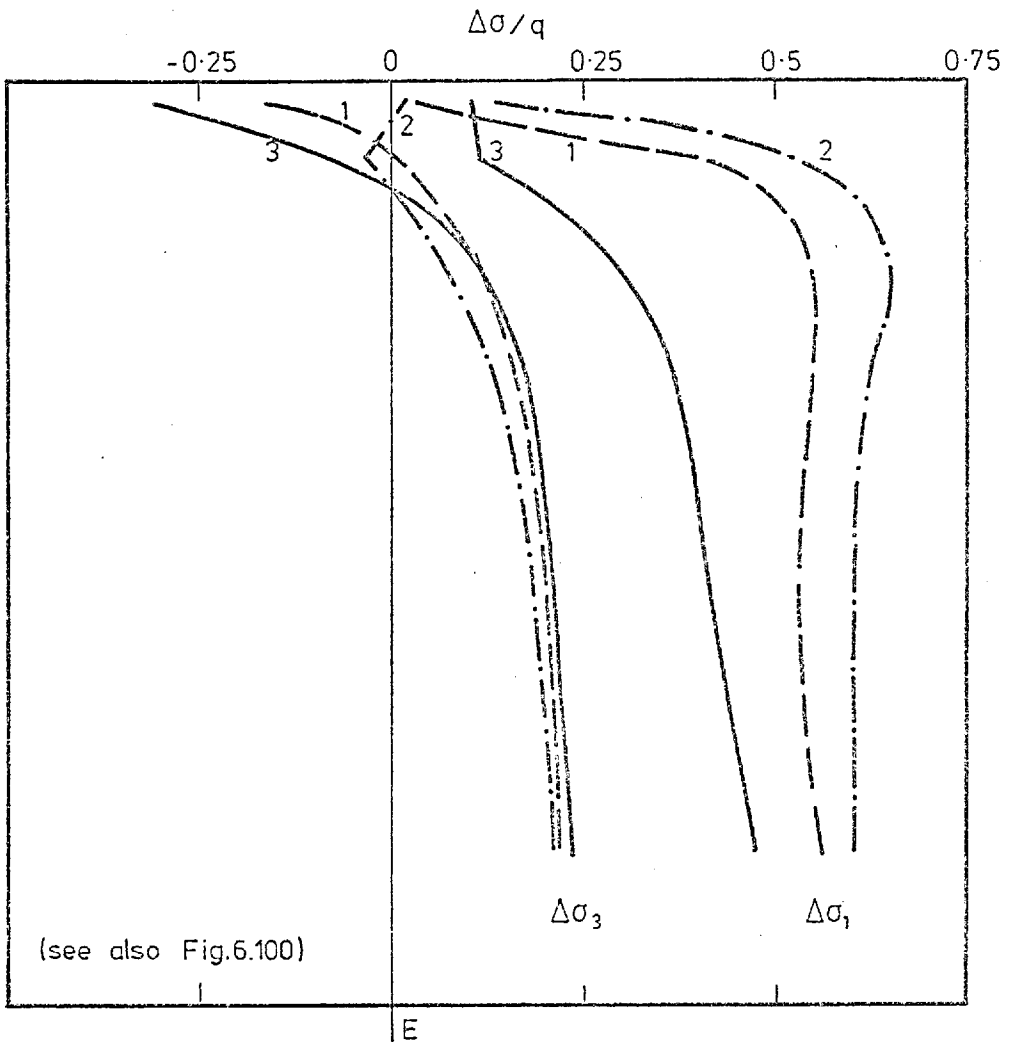
CASE 48   q = 200 kPa

(see Table 5.3)

Fig. 6.103   Principal Stress Changes

Numbers denote loading stages,
(see Section 5.3.2).

$\Delta\sigma/q$

120 m

$3 = 5\&7$

$4 = 6\&8$

$\Delta\sigma_3$ $\Delta\sigma_1$

CASE 49   q = 200 kPa
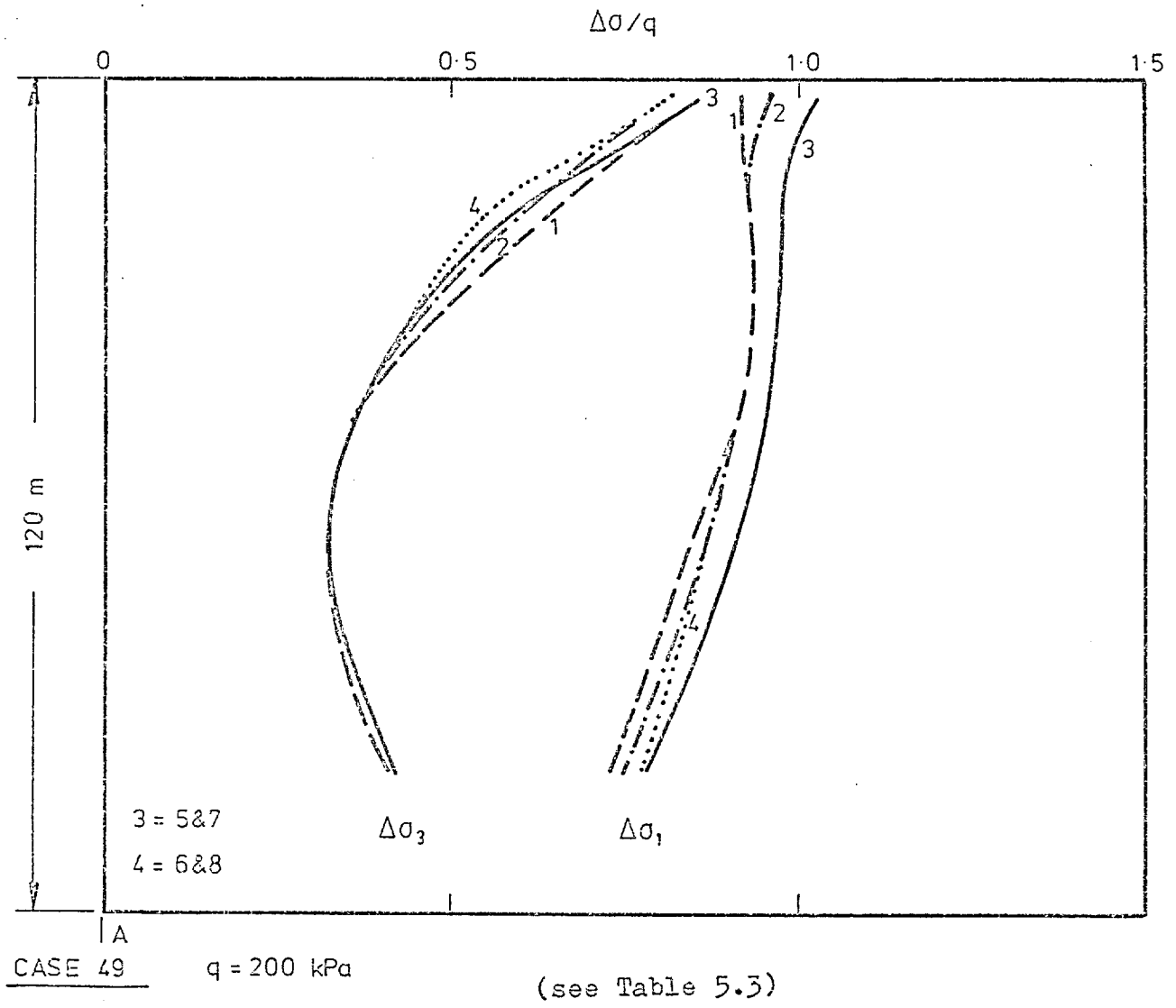
(see Table 5.3)

Fig. 6.104   Principal Stress Changes

Numbers denote loading stages,
(see Section 5.3.2).

350
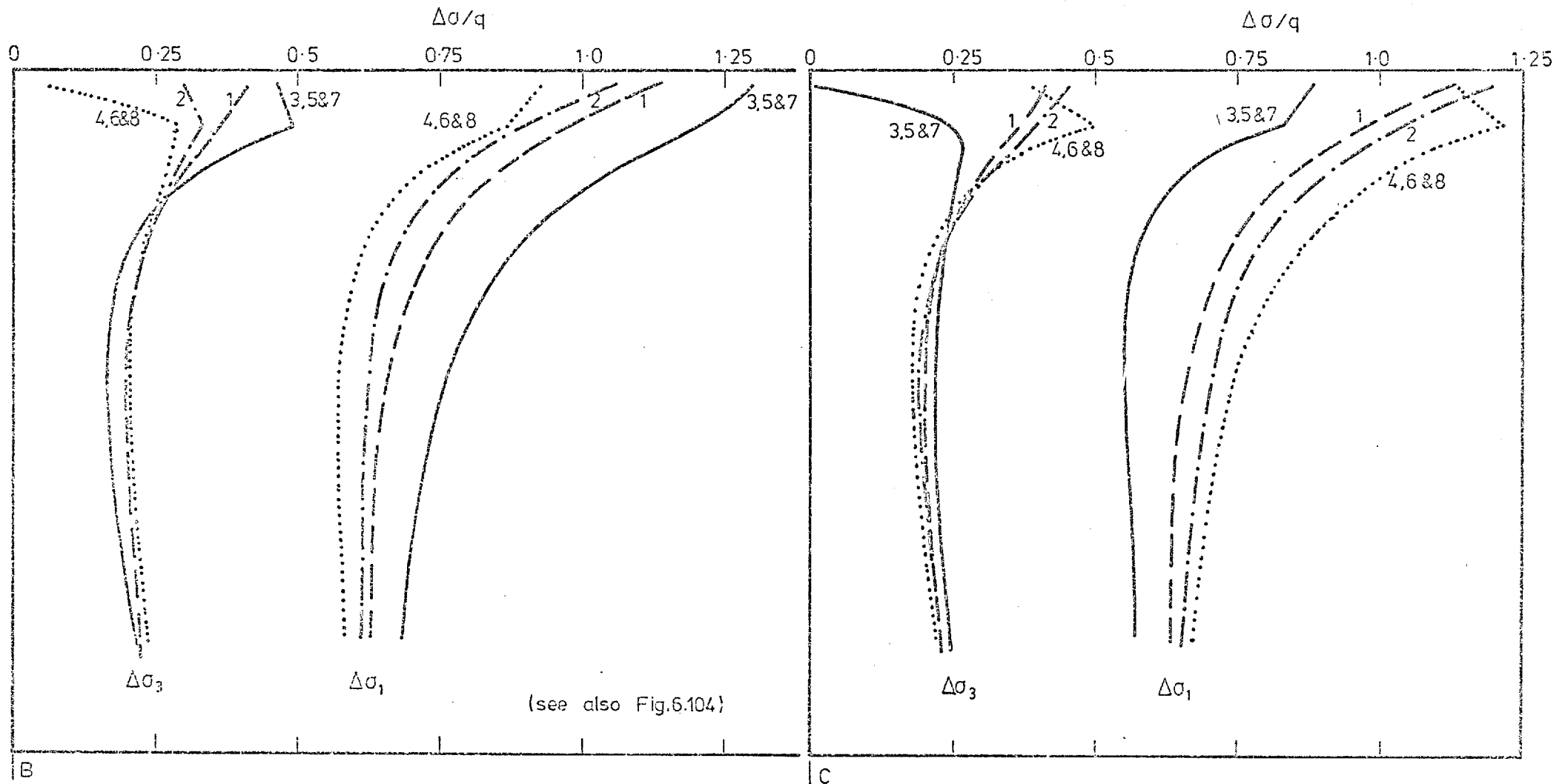
Fig. 6.105   Principal Stress Changes

CASE 49   q = 200 kPa   (see Table 5.3)

(see also Fig.6.104)

Numbers denote loading stages,
(see Section 5.3.2).

$\Delta\sigma/q$

-0.25   0   0.25   0.5   0.75

4 = 6&8
3 = 5&7

$\Delta\sigma_3$ $\Delta\sigma_1$

D

$\Delta\sigma/q$

0.25   0   0.25   0.5   0.75

(see also Fig.6.104)

$\Delta\sigma_3$ $\Delta\sigma_1$

E

CASE 49   (q = 200 kPa)   (see Table 5.3)

Fig. 6.106   Principal Stress Changes

Numbers denote loading stages,
(see Section 5.3.2).

$\bullet \quad \Delta\sigma_1$
$\times \quad \Delta\sigma_3$
$+ \quad \Theta$

$\sigma_{zo} = \sigma_{xo} = 286 \text{ kN/m}^2$

B = 120 m

$E_1 \quad D_1 \quad C_1 \quad B_1 \qquad A_1$

$E_1 \qquad\qquad D_1 \qquad\qquad C_1 \qquad\qquad B_1 \qquad\qquad A_1$

$\Delta\sigma_1, \Delta\sigma_3 \text{ (kN/m}^2)$

Loading stages

CASE 42

(see Table 5.3)   Fig. 6.107   Principal Stress Changes and Rotations

353
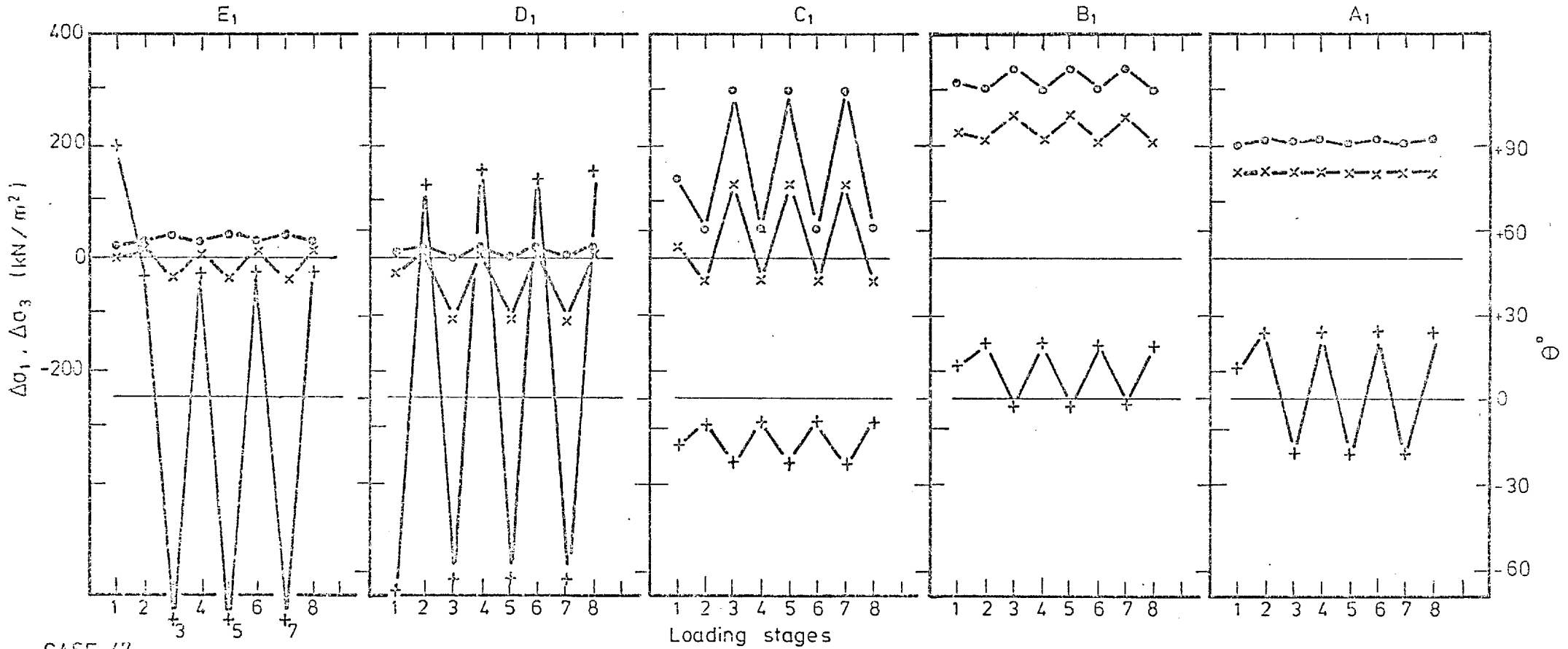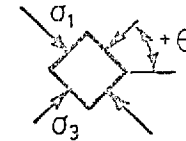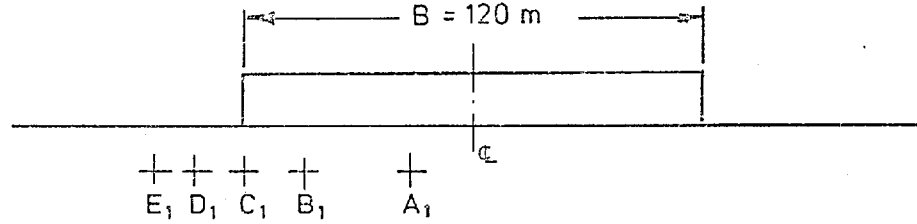
(see Section 5.3.2)

CASE 47

Fig. 6.108   Principal Stress Changes and Rotations

(see Table 5.3)

(see Section 5.3.2)

354

$\sigma_{zo} = \sigma_{xo} = 285 \text{ kN/m}^2$

$\Delta \sigma_1 \quad \circ$

$\Delta \sigma_3 \quad \times$

$\theta \quad +$
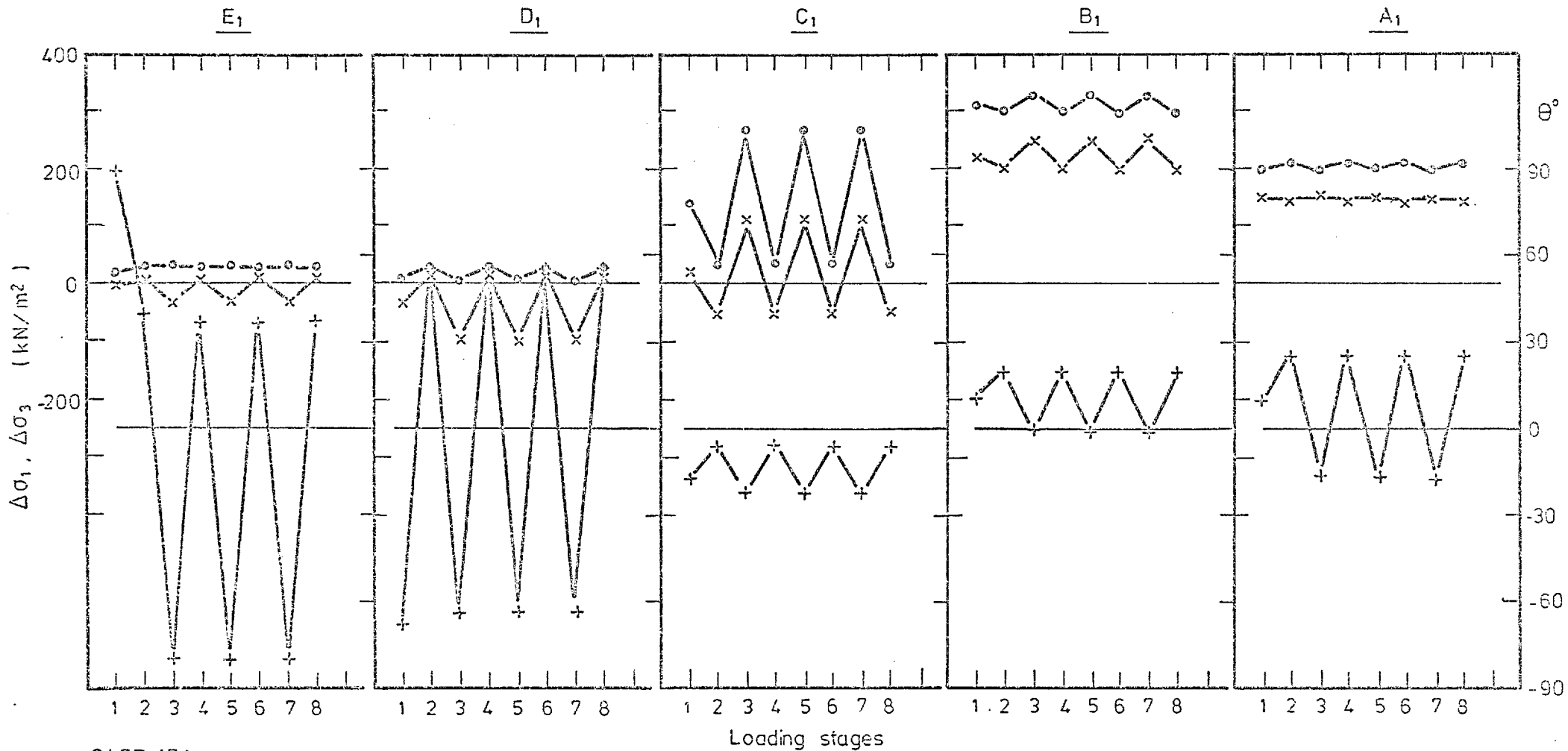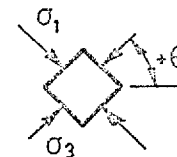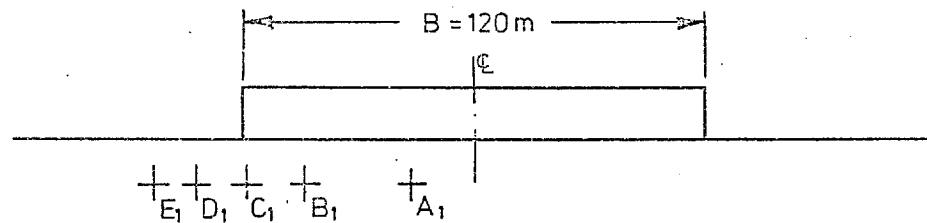
CASE 47.1

Fig. 6.109   Principal Stress Changes and Rotations
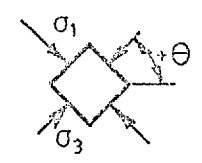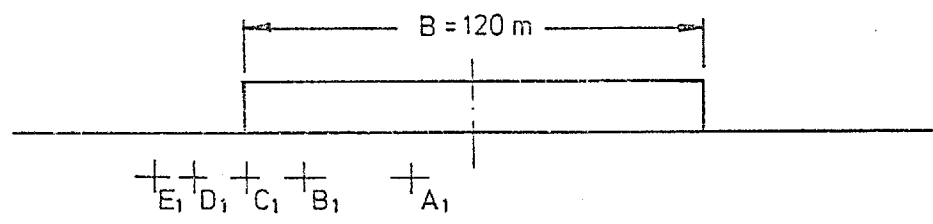
(see Table 5.3)
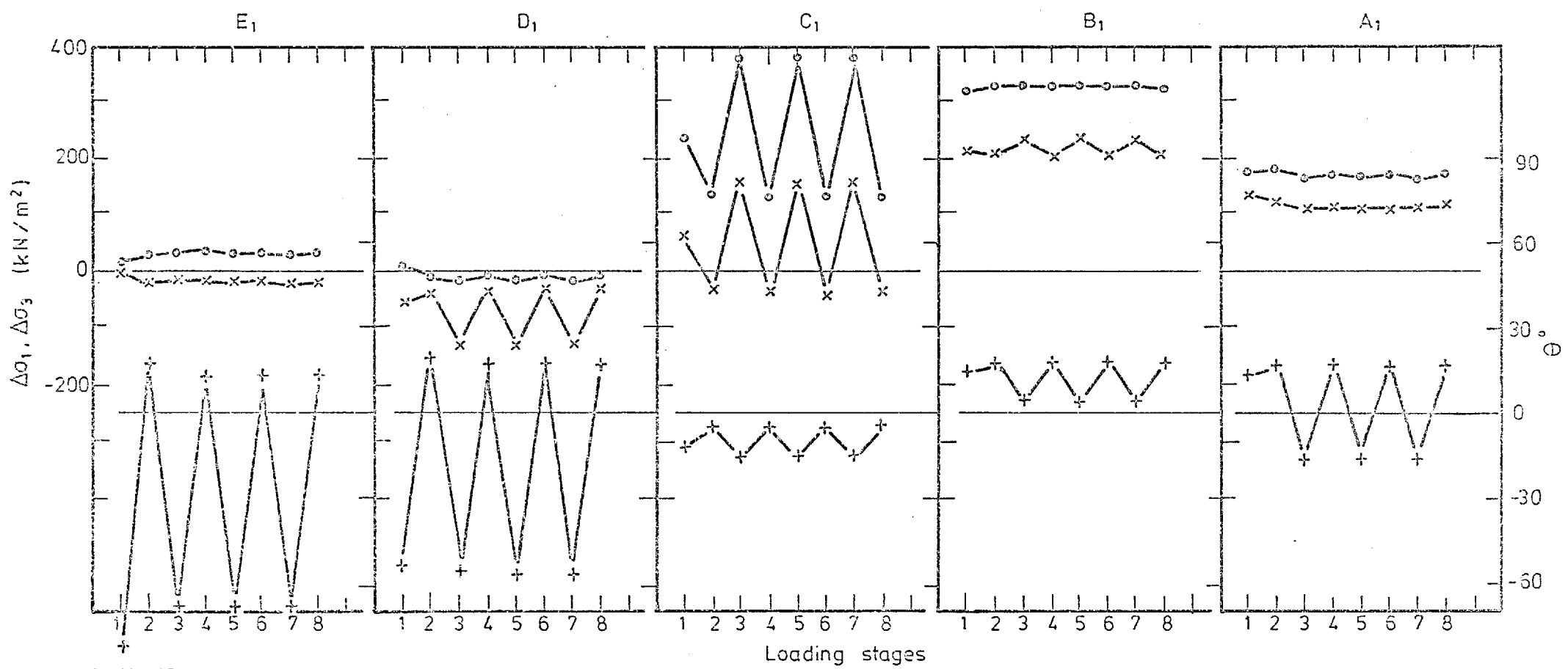
(see Section 5.3.2)

Fig. 6.110   Principal Stress Changes and Rotations

CASE 48

(see Table 5.3) (see Section 5.3.2)
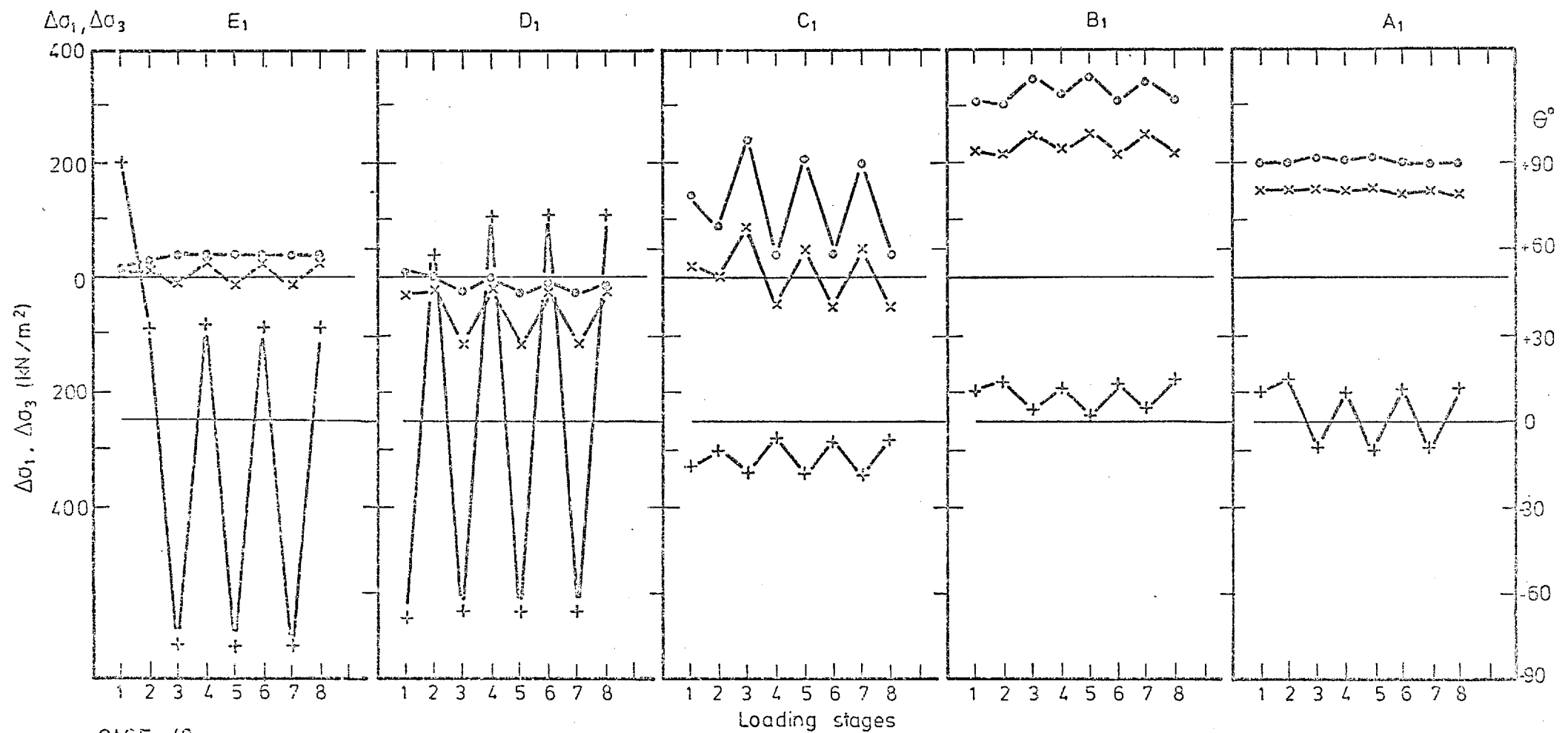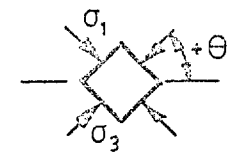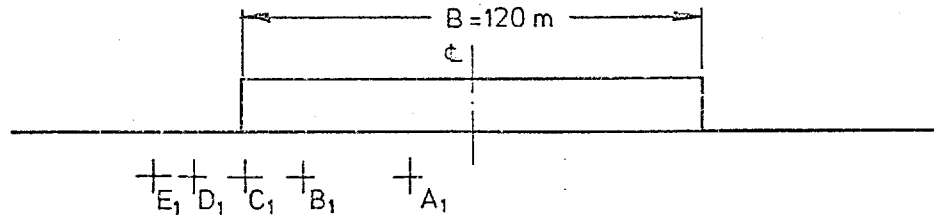
Fig. 6.111 Principal Stress Changes and Rotations

CASE 49

357

CASE 42 $C_u = 137$ kPa for $z = 12·3$ m
(see Table 5·3)

○ Point B_1
✕ Point C_1 } (see Fig. 6·107)
✛ Point D_1

Numbers denote loading sequences
(see section 5.3.2)

$\dfrac{\sigma_1 - \sigma_3}{2}$. kPa

$\dfrac{\sigma_{1o} + \sigma_{3o}}{2}$
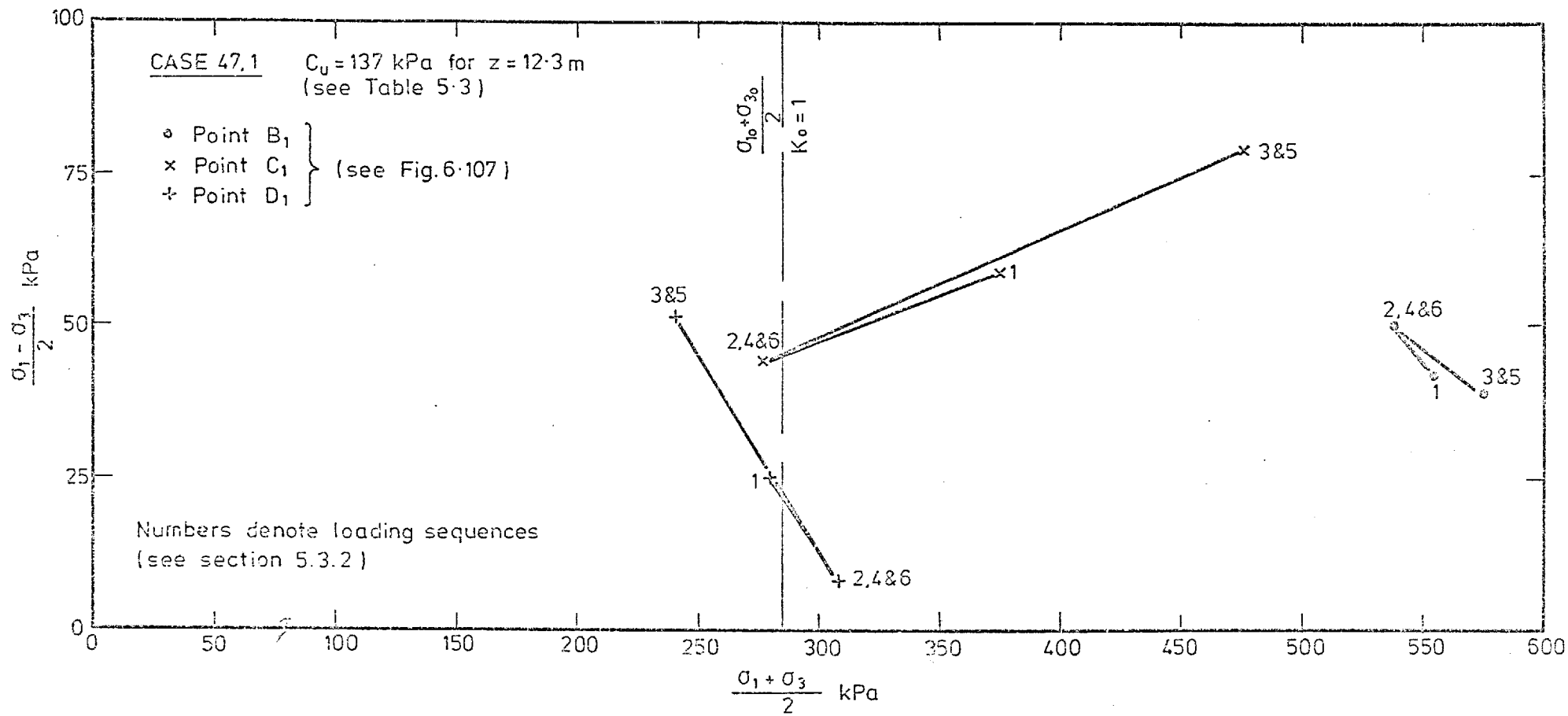
$K_o = 1$

$\dfrac{\sigma_1 + \sigma_3}{2}$ kPa
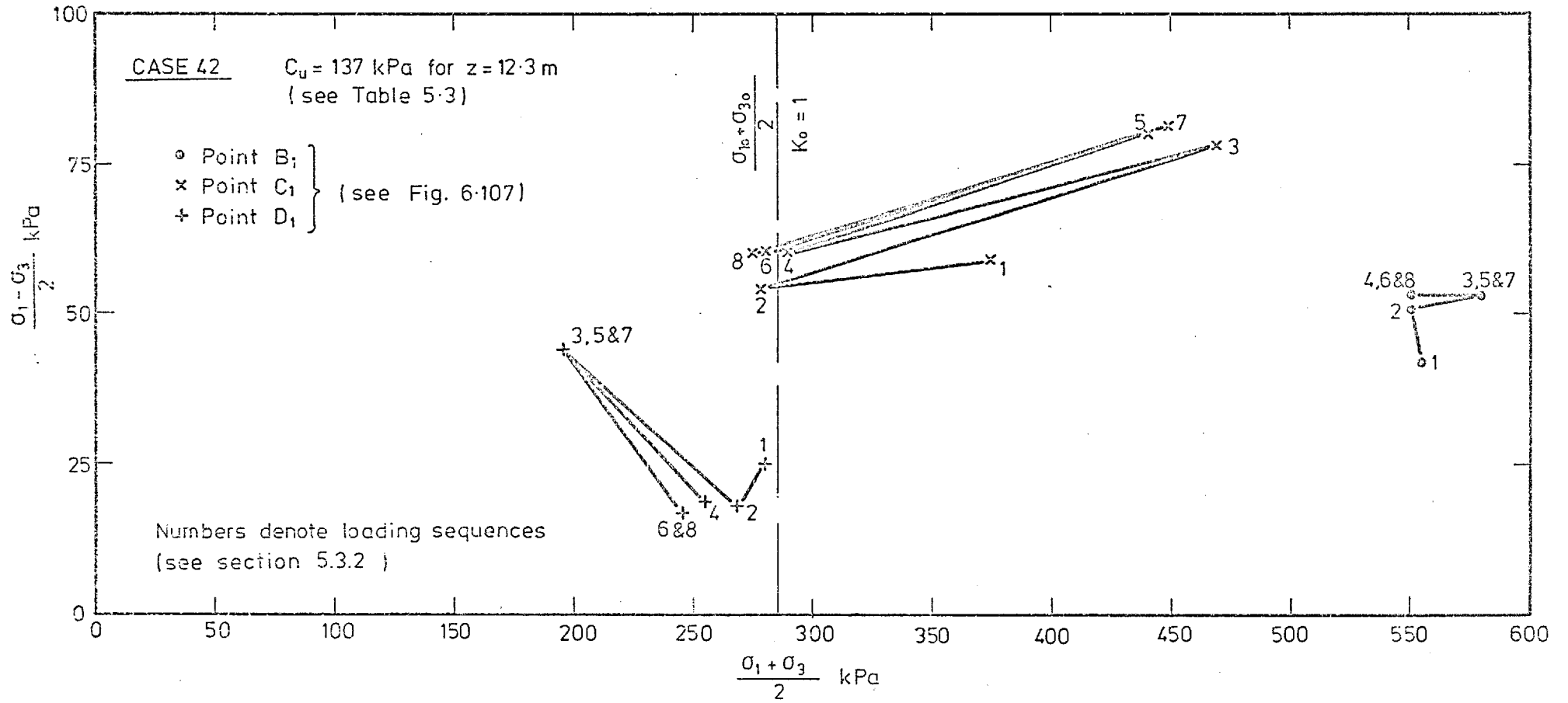
Fig. 6.112   Stress Paths
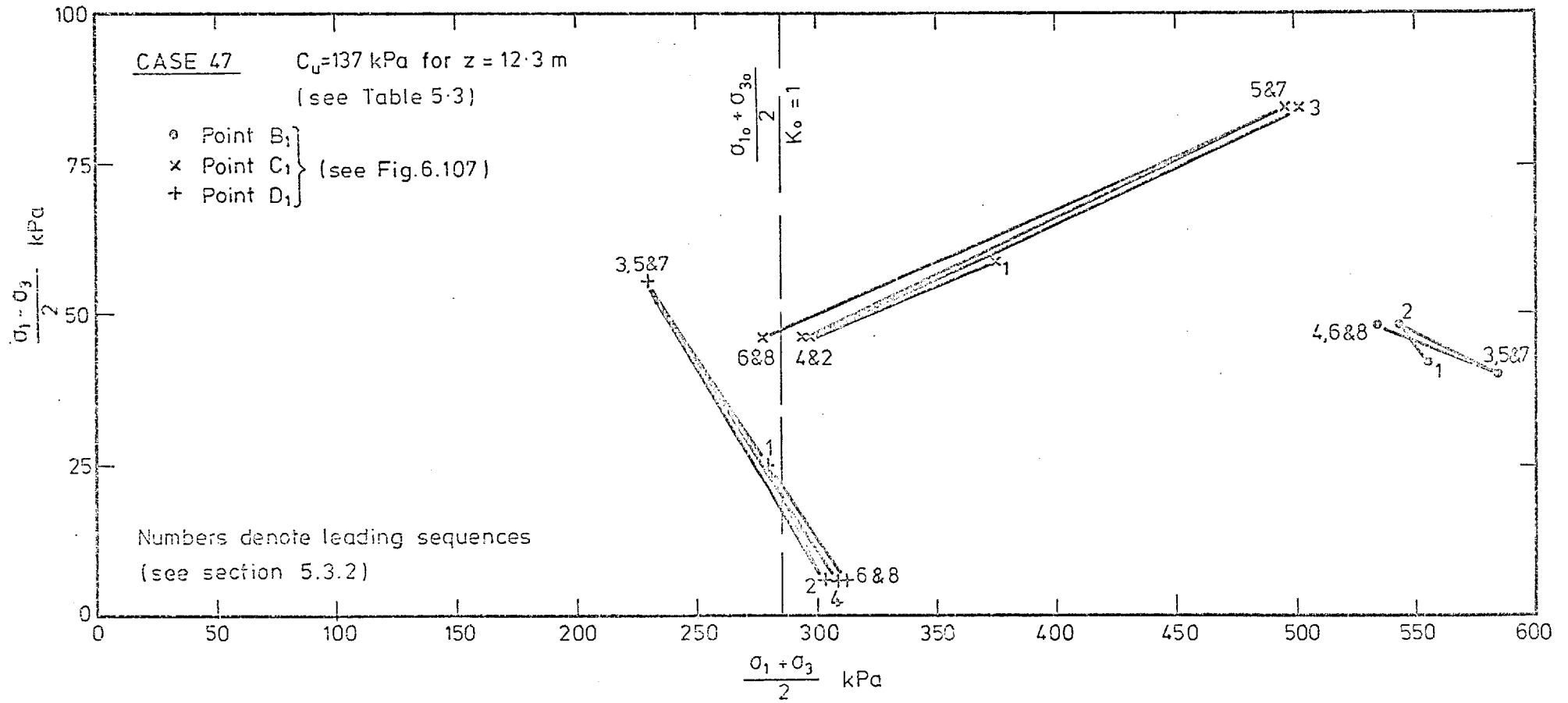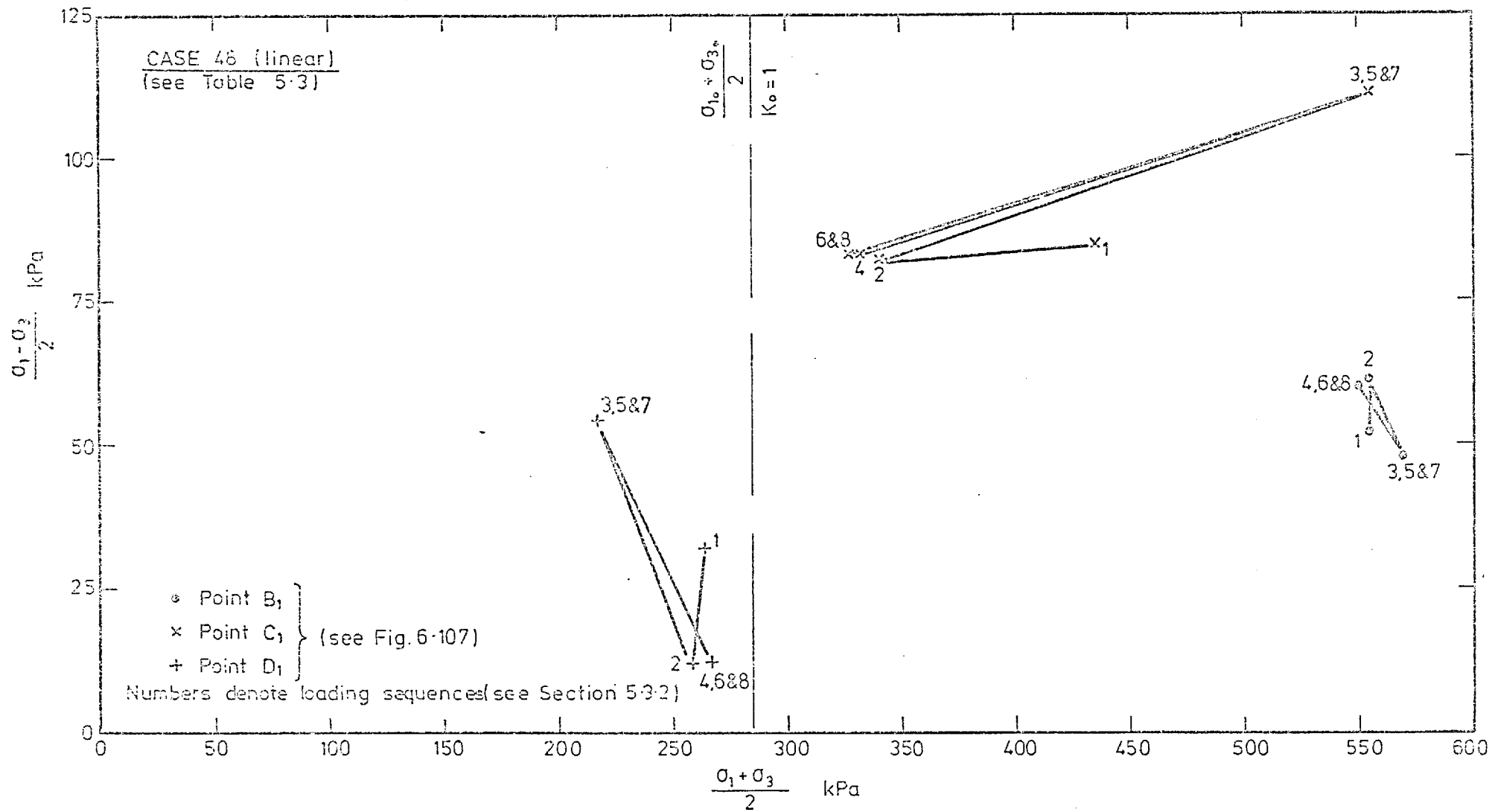
Fig. 6.113   Stress Paths
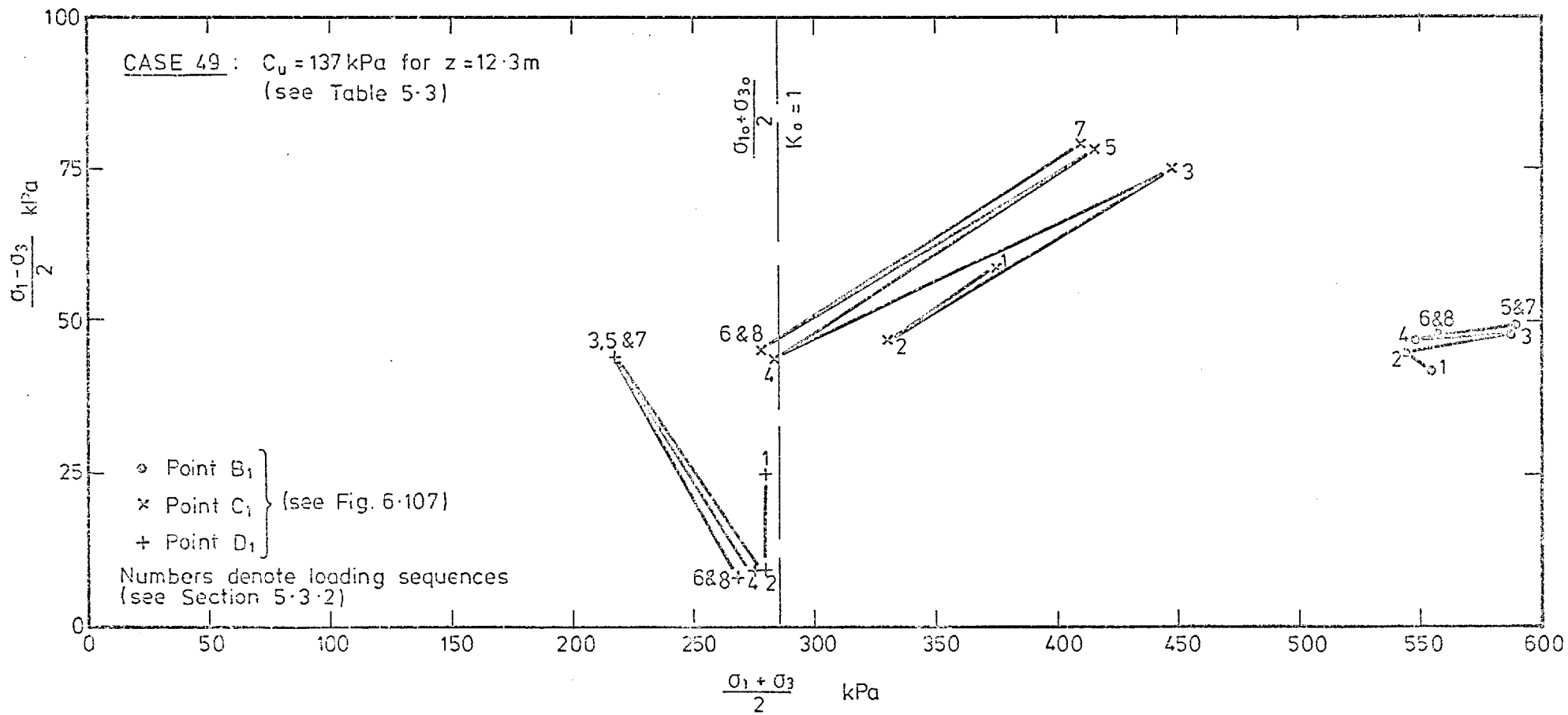
Fig. 6.114   Stress Paths
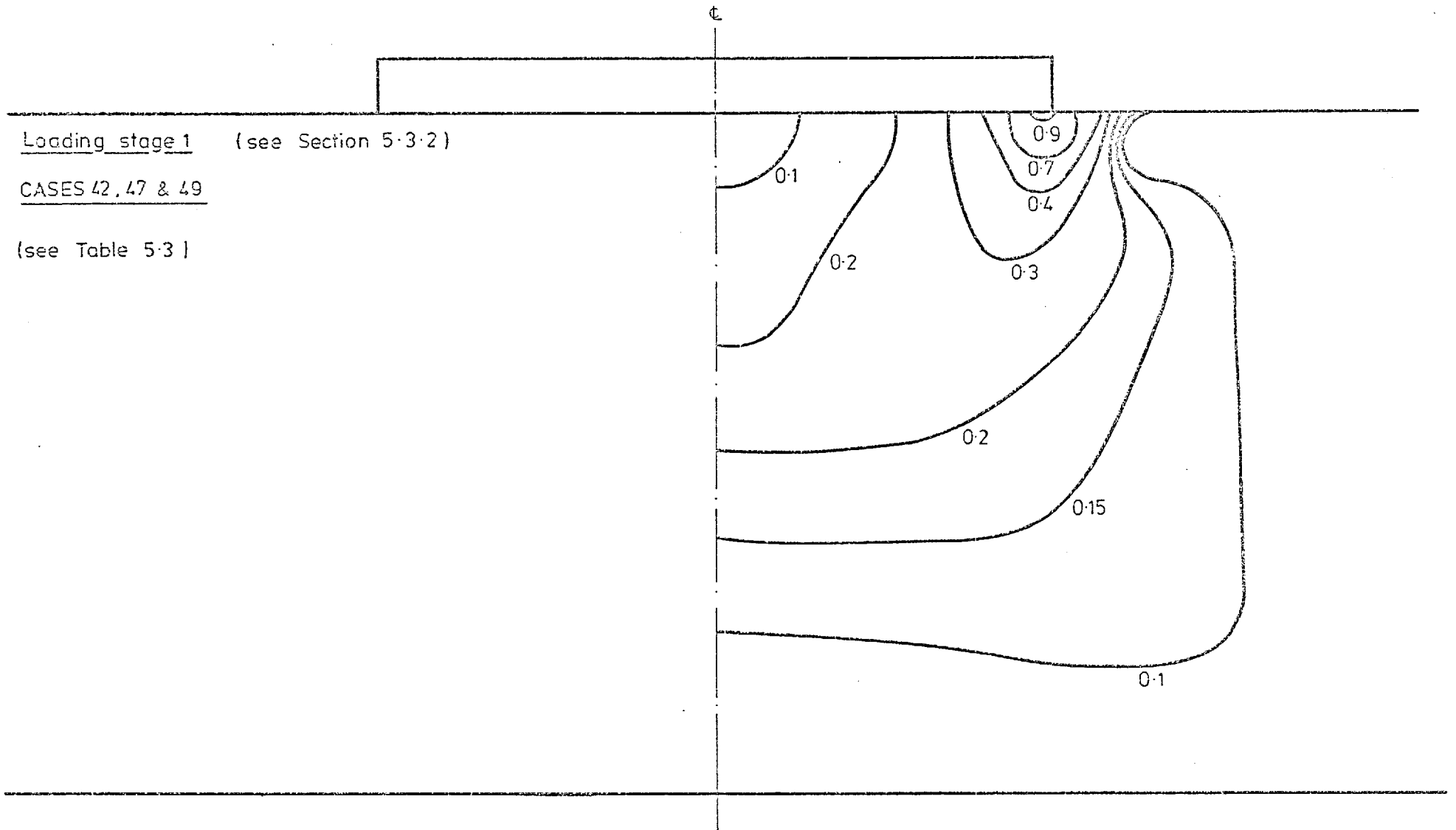
Fig. 6.115   Stress Paths

Fig. 6.116   Stress Paths

Loading stage 1   (see Section 5·3·2)

CASES 42, 47 & 49

(see Table 5·3)

Fig. 6.117   Contours of Mobilized Shear Stress

₵

0·9
0·7
0·1
0·4
0·2
0·3
0·7
0·2
0·4
0·3
0·2
0·1

Loading stage 2   (see Section 5.3.2)

CASE 42   (see Table 5.3)

Fig. 6.118   Contours of Mobilized Shear Stress

Loading stage 3   (see Section 5.3.2)

CASE 42   (see Table 5·3)

Fig. 6.119   Contours of Mobilized Shear Stress

Loading stage 4   (see Section 5.3.2)

CASE 42   (see Table 5·3)
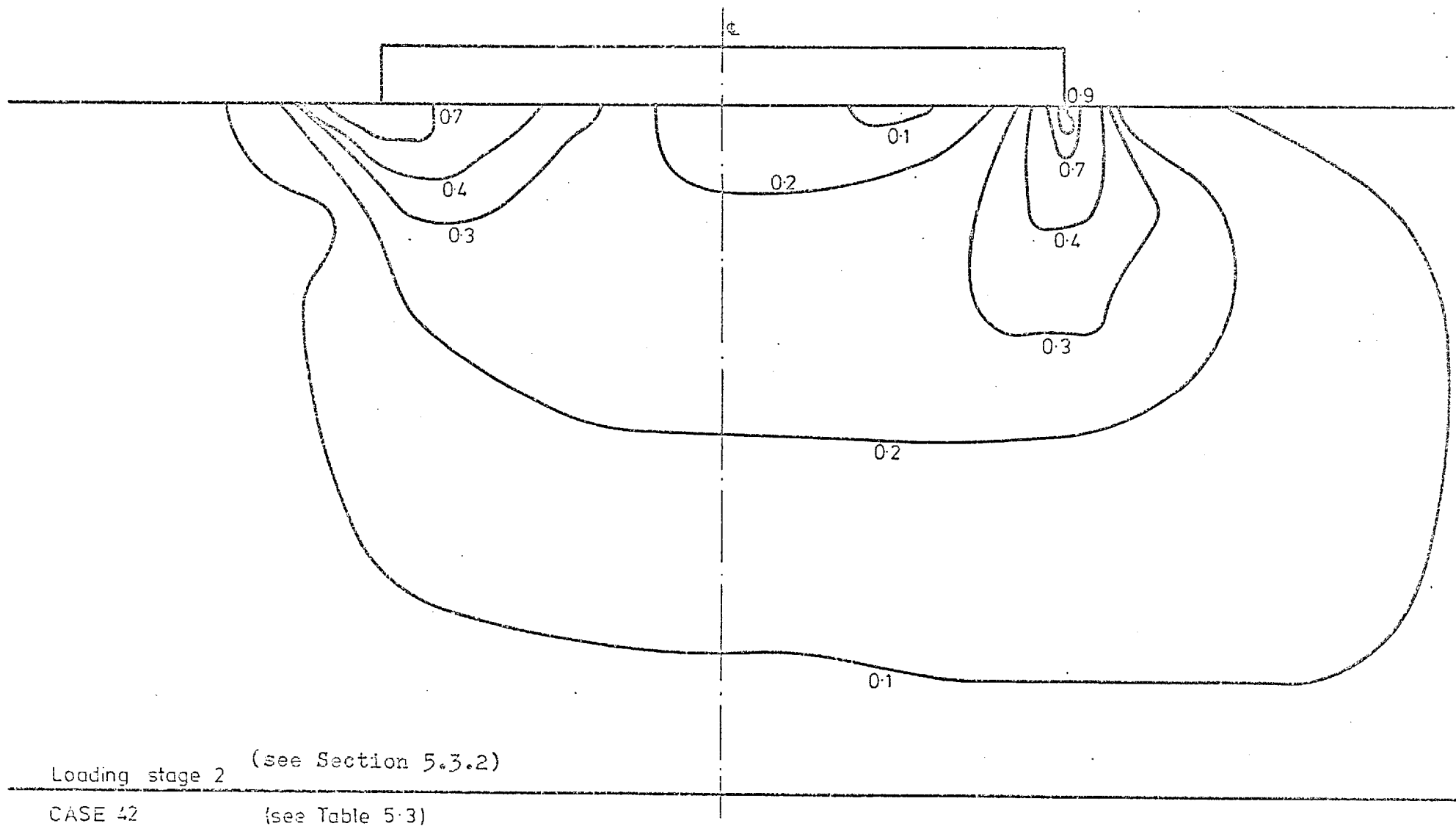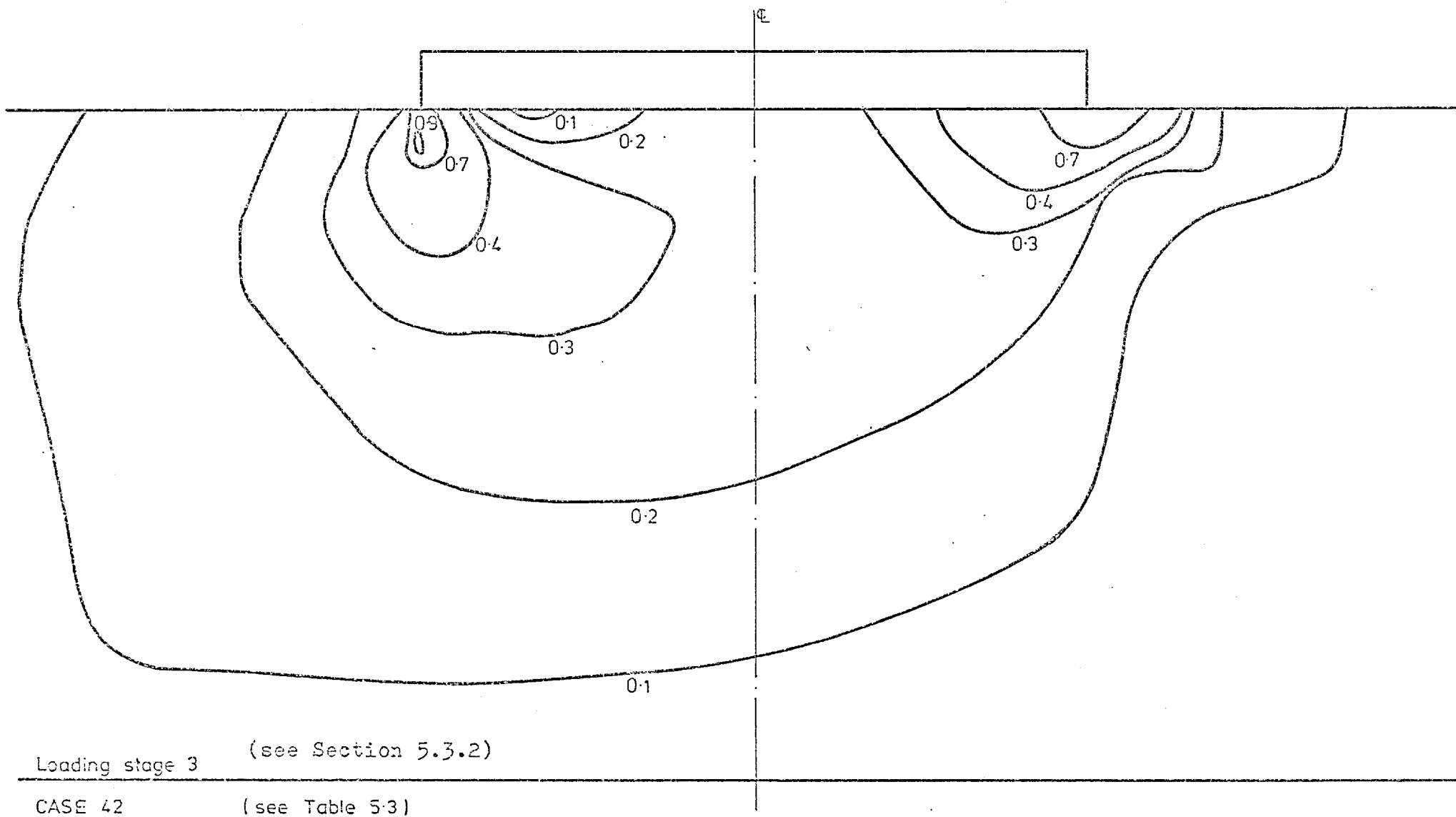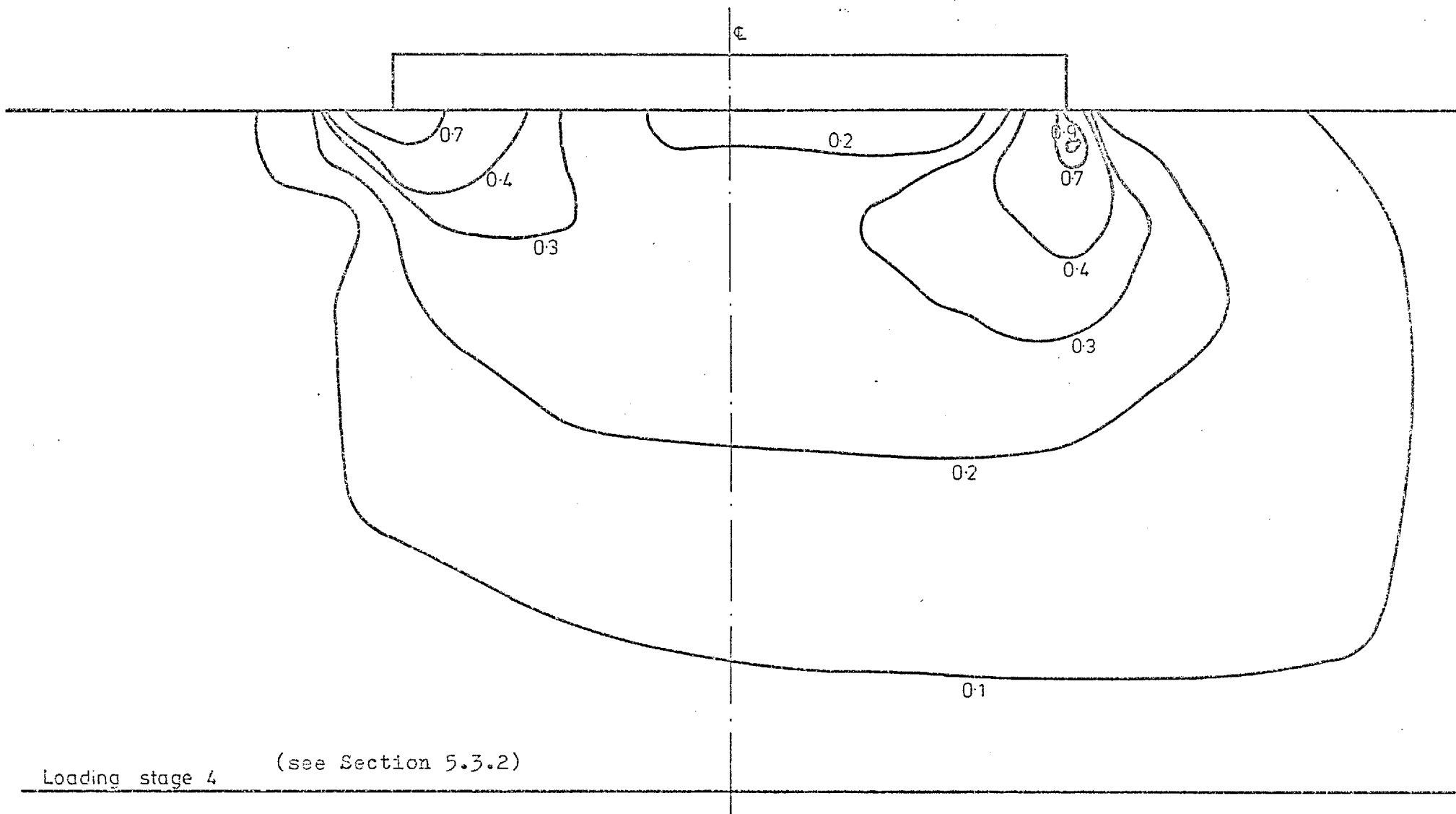
Fig. 6.120   Contours of Mobilized Shear Stress

Fig. 6.121   Contours of Mobilized Shear Stress

Loading stage 2   (see Section 5.3.2)
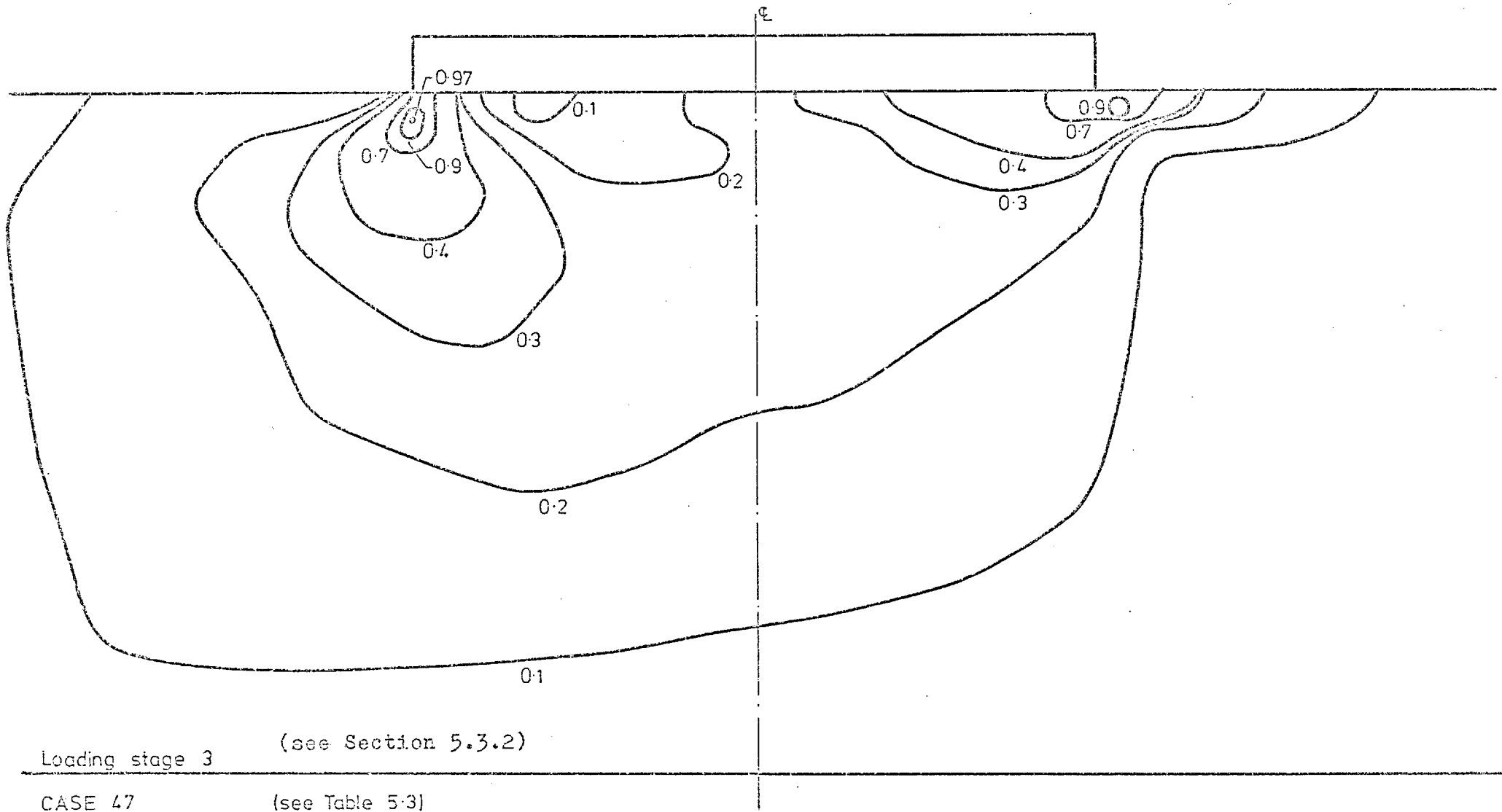
CASE 47   (see Table 5·3)

Fig. 6.122   Contours of Mobilized Shear Stress

Loading stage 2   (see Section 5.3.2)
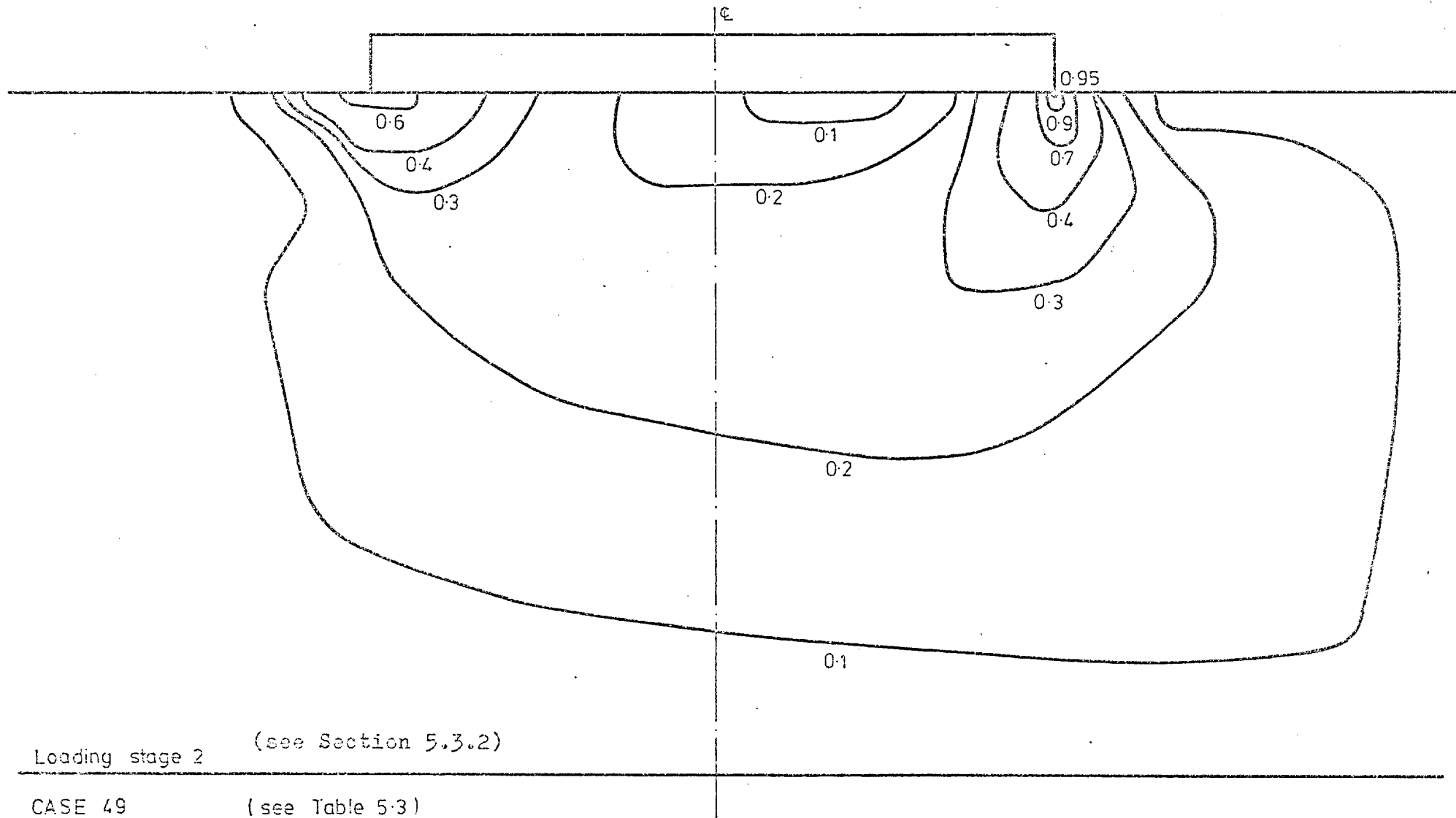
CASE 49   (see Table 5·3)

Fig. 123   Contours of Mobilized Shear Stress

Loading stage 3   (see Section 5.3.2)
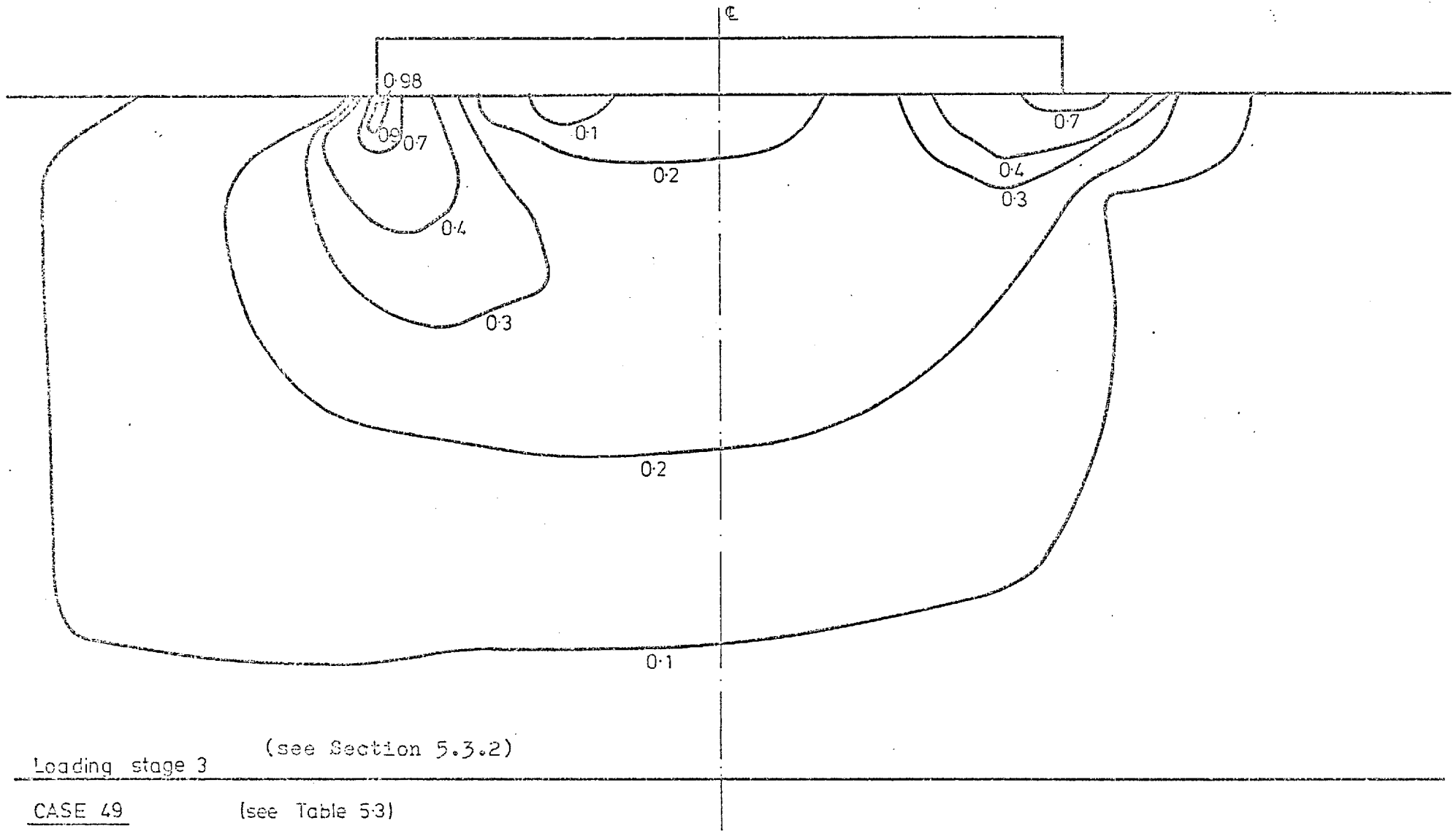
CASE 49   (see Table 5.3)

Fig. 6.124   Contours of Mobilized Shear Stress

Loading stage 4   (see Section 5.3.2)
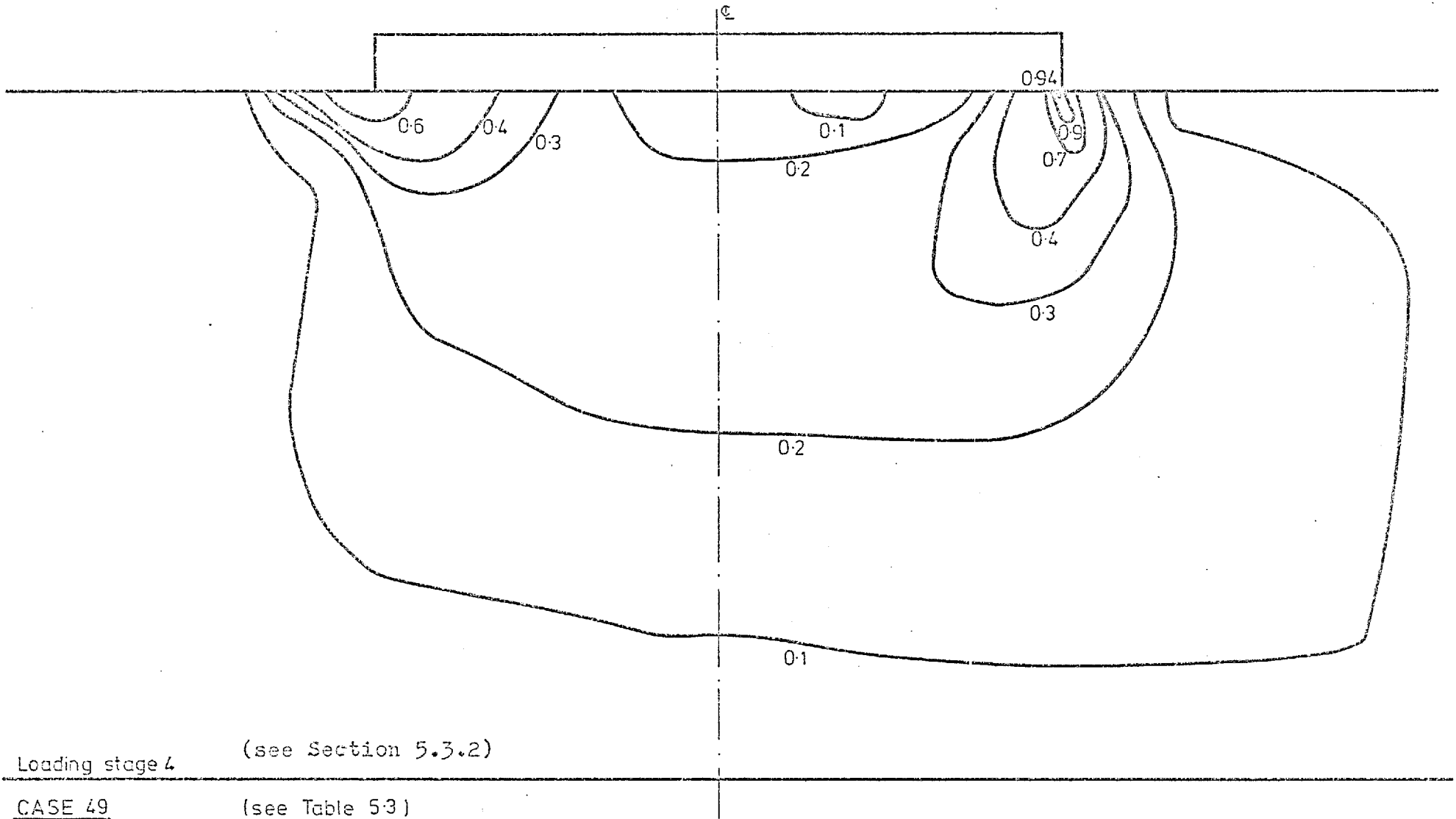
CASE 49   (see Table 5·3)
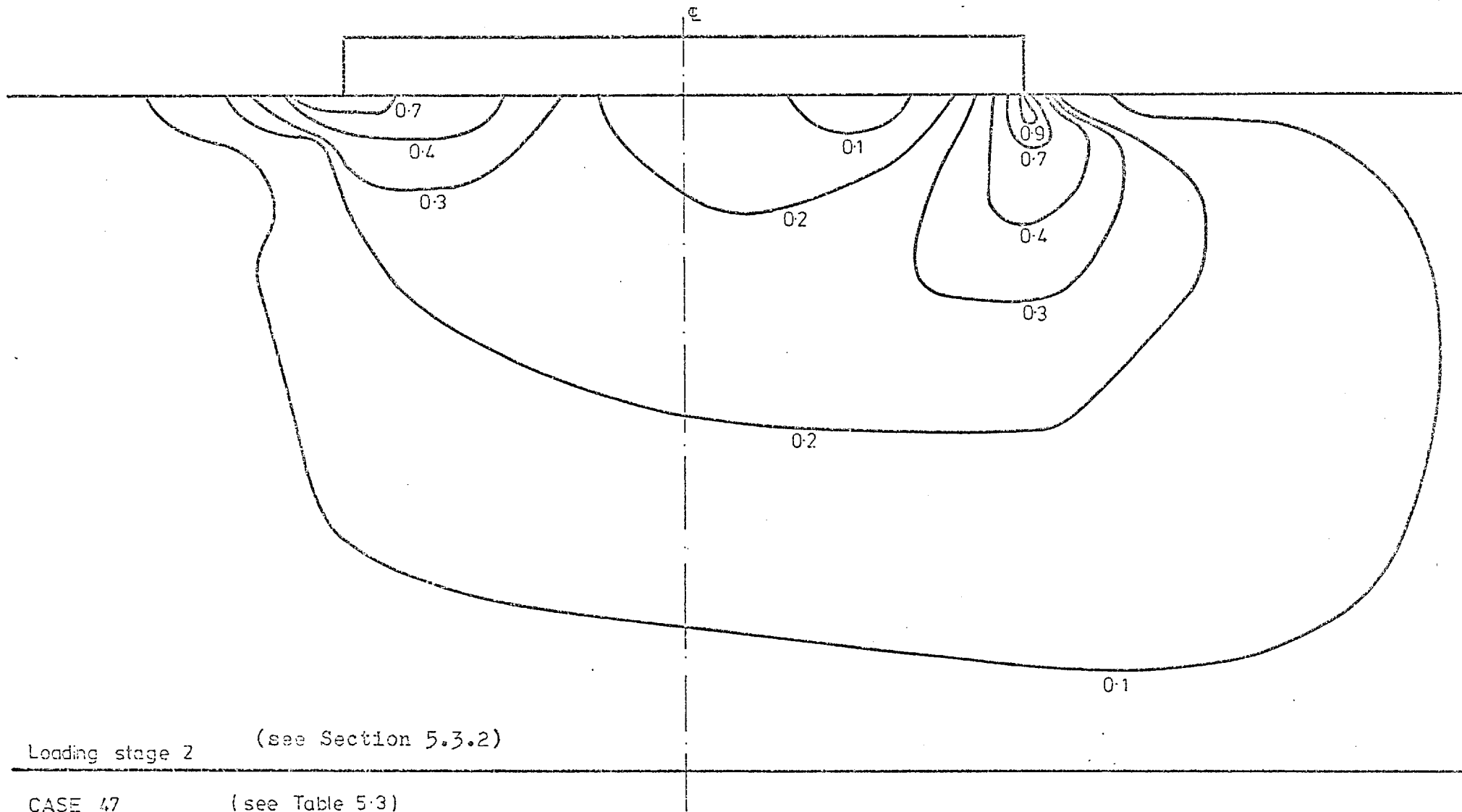
Fig. 6.125   Contours of Mobilized Shear Stress
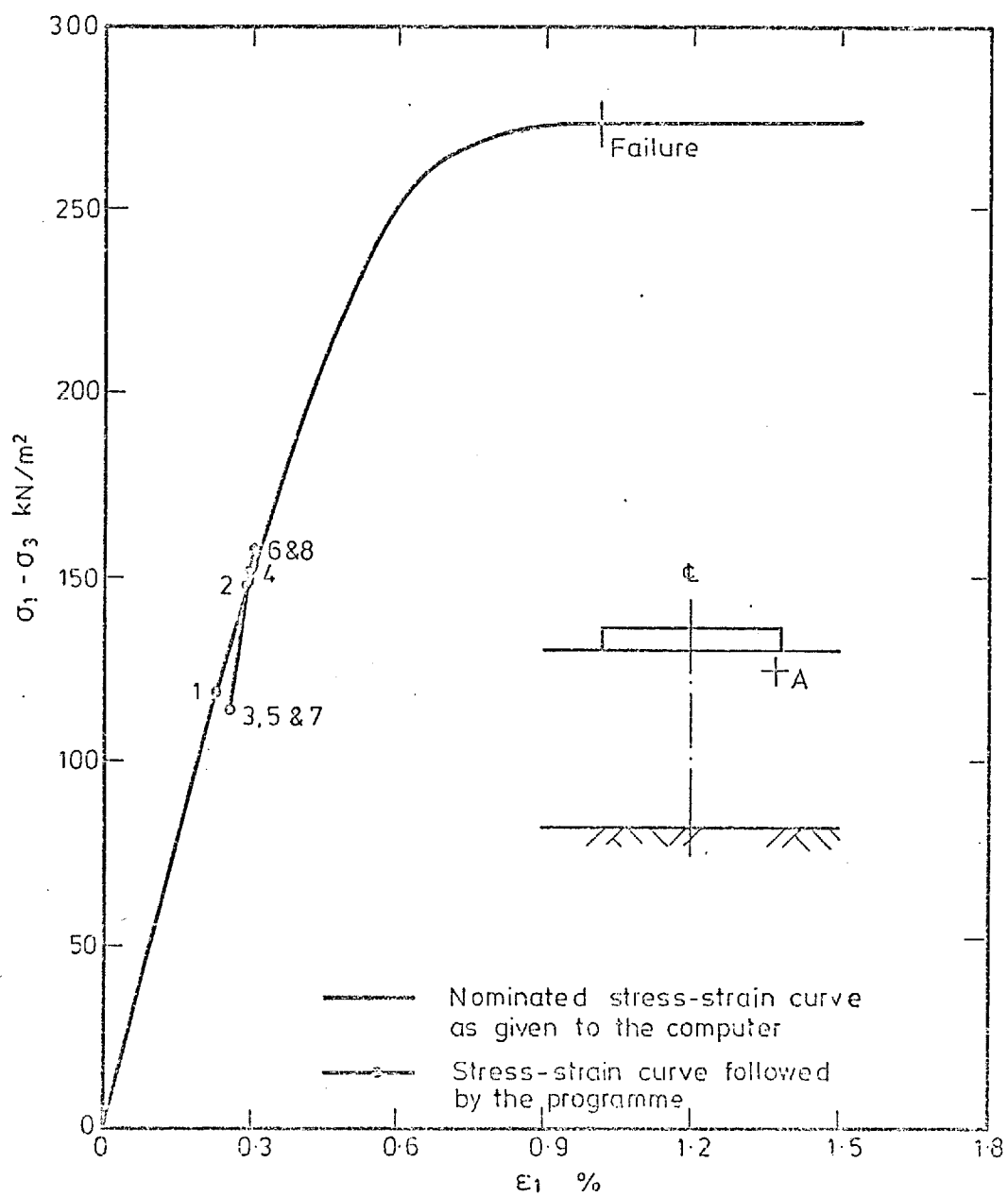
CASE 42 (see Table 5·3)

Point A

Fig. 6.126 Stress-Strain Curve
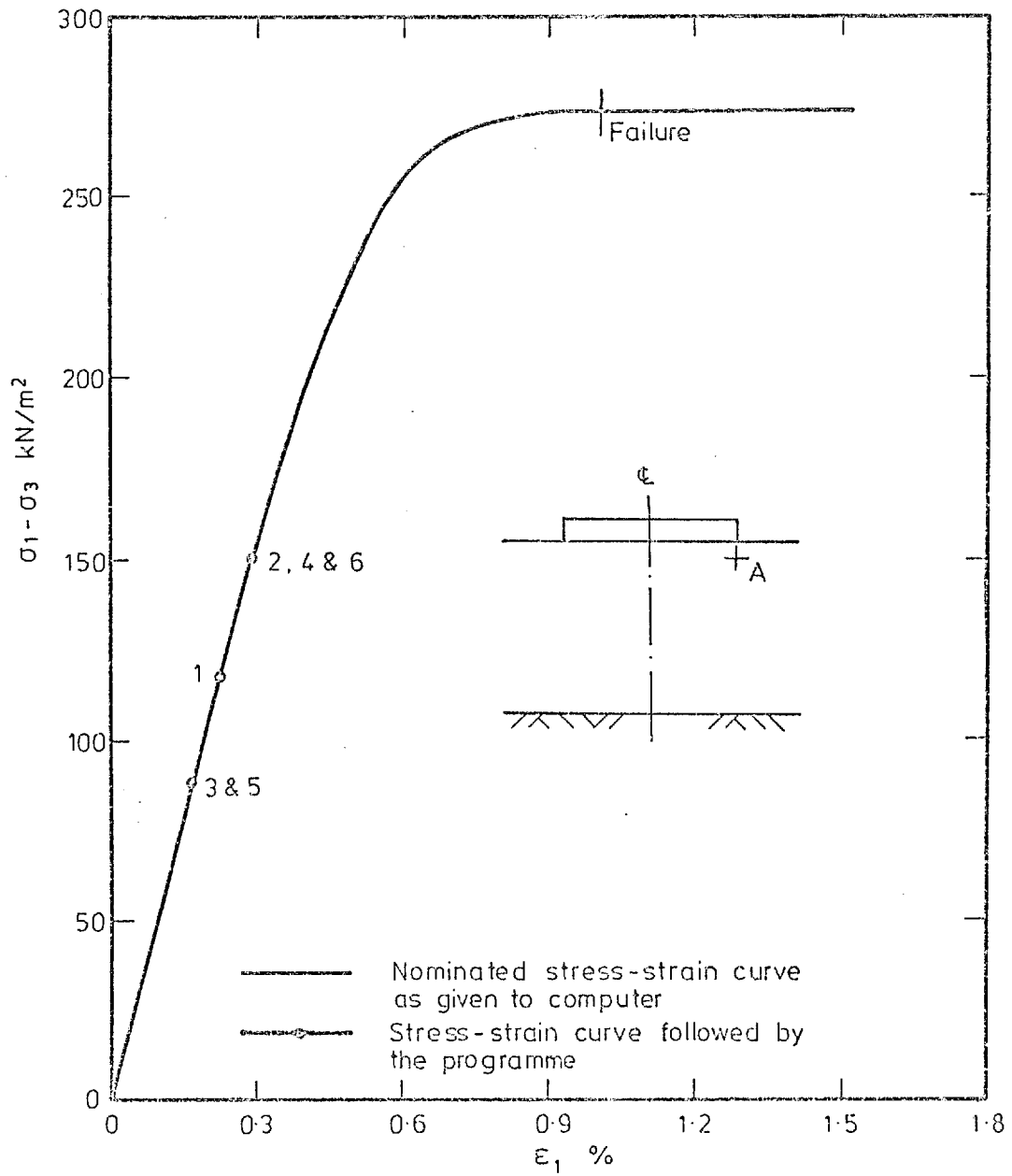
CASE 47 (see Table 5·3)

Point A

Fig. 6.127   Stress-Strain Curve

Numbers denote loading stages (see Chapter 5, section 5.3.2)

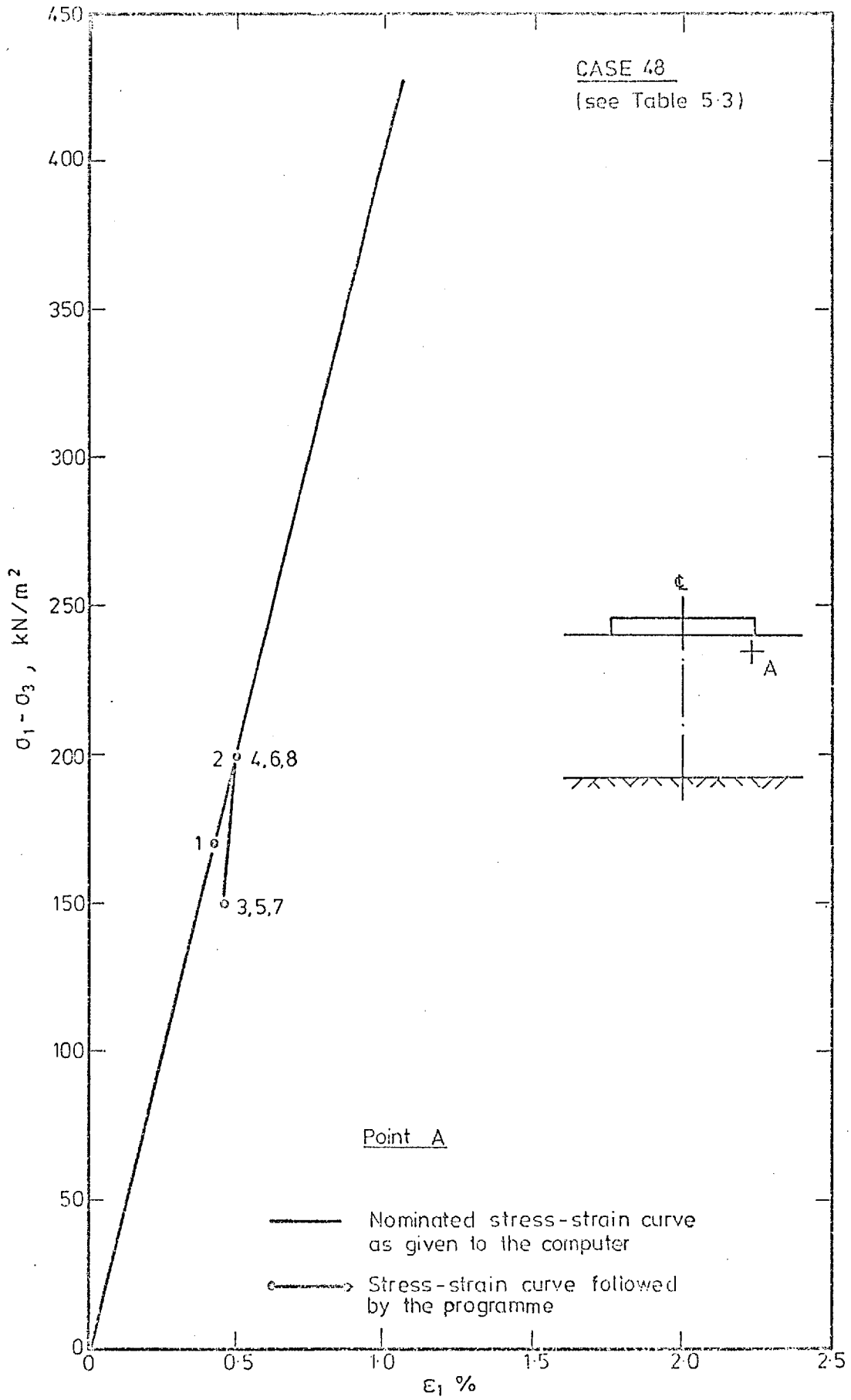Fig. 6.128   Stress-Strain Cuve
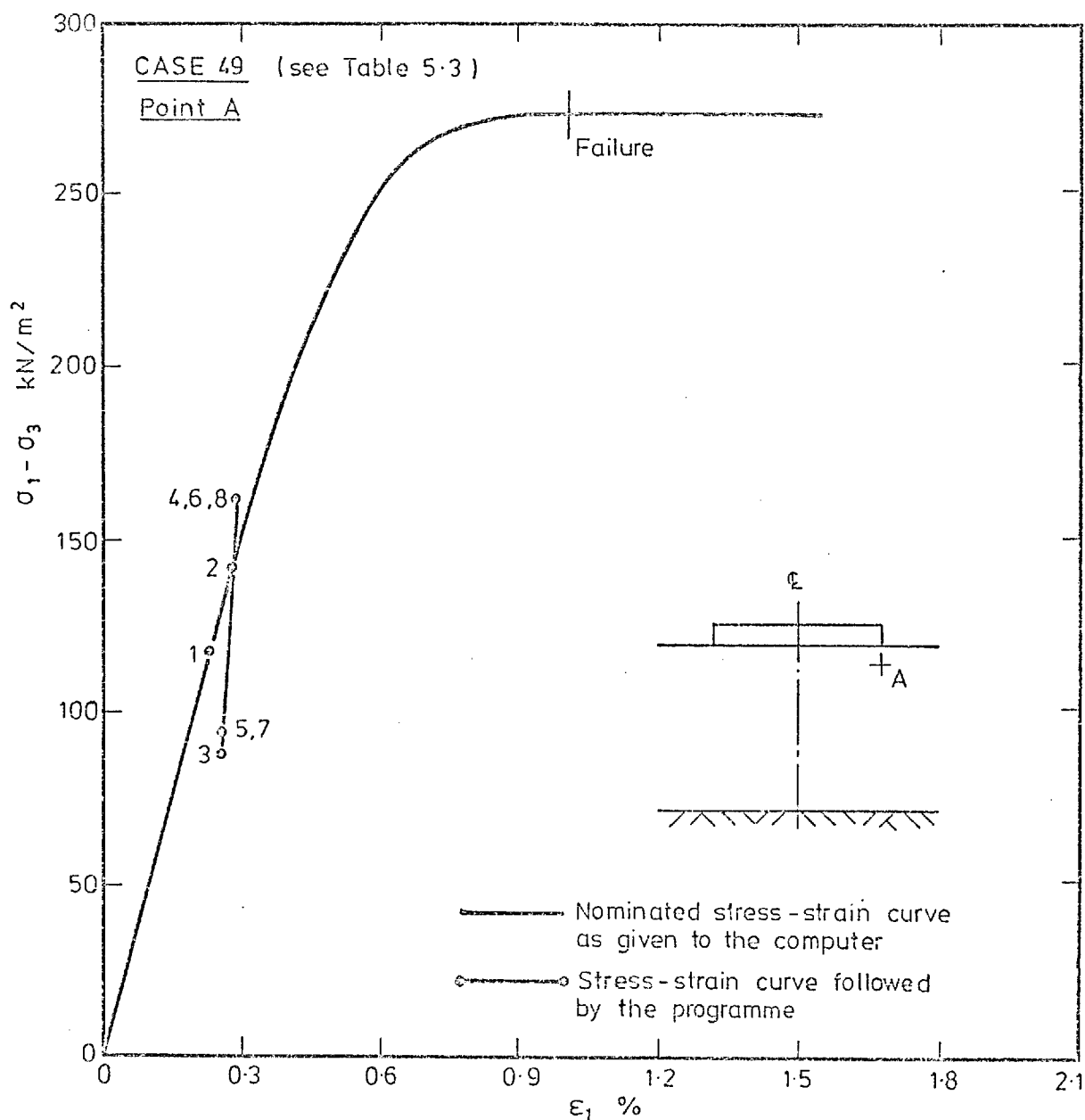
Fig. 6.129   Stress-Strain Curve

Numbers denote loading stages,
(see Section 5.3.2).

PART III

STUDY OF HYDRAULIC FRACTURE

CHAPTER 7

CRACKING OF EMBANKMENT DAM CORES

7.1 Introduction

The function of an embankment dam, namely the retention of water with acceptable leakage and without shear failure or sliding, leads to the following stability considerations:-

1. Stability of slopes and foundations and a reserve against failure by sliding.

2. Internal stability of the embankment soils when their particles are subjected to drag forces as seepage from the reservoir occurs.

The internal stability can be ensured by the proper design of transitions from one material to another, but a special problem arises when cracks form in the core of a dam.

In this chapter a brief review of the cracking, load transfer, and hydraulic fracture is given.

7.2 Brief Description of Cracking

7.2.1 General

It is now generally known that apart from overtopping by flood water, internal erosion by seepage is the most common cause of the catastrophic failures of embankment dams. As a large portion of seepage failures are due to piping which has been initiated by cracks in the embankment (Sherard et al, 1963), cracking is seen to be one of the

main causes of failure in embankment dams.

A crack is considered to be an opening in the fill, and it is formed when the tensile strength of the soil is exceeded. This tensile strength is generally small, and its value may depend on negative pore pressure which will be destroyed by seepage. The crack remains open if the water pressure in it equals the total pressure on the plane of the crack (Nonveiller and Anagnosti, 1961).

As the formation of a crack results in a redistribution of stresses and strains in the vicinity of the crack (Vaughan, 1970), therefore, once a crack has formed the damage cannot necessarily be undone by returning the loads on the structure to the state they were in before the crack occurred.

7.2.2 Causes of Cracking

Cracks can occur during construction and operation of an embankment dam due to a number of causes, such as, differential foundation settlement, irregularities in a rigid foundation, arching of the core, differences in the properties of core material, shrinkage, and hydraulic fracture. In Table 7.1 a selection of the mechanisms which are considered to cause cracking have been tabulated, and for each case a sketch and a brief description of the cracking mechanism is given. The names of a few dams for which these mechanisms have been observed (or postulated) to be the cause of cracking, are also given as examples.

Table 7.1 considers separately the transverse and the

longitudinal cracking. The transverse cracks are likely to constitute a greater threat to the safety of an embankment dam than longitudinal cracks, for they may provide a path for leakage through the impermeable core which could result in a piping failure.

A more general discussion of the causes of cracking has been given by Truscott (1977).

It has to be mentioned that the existence of cracks through the core of a dam does not necessarily mean that the performance of the dam is adversely affected. The soil around the crack may either swell or collapse to seal it, or, with effective filter and transition zones, material may be deposited in the crack to heal it. In fact, it is suspected that a considerable number of dams may have cracked and subsequently sealed themselves without anyone's knowledge. However, as cracks are one of the main causes of disastrous failures in embankment dams, efforts must be made either to prevent their occurrence or to minimize their effects.

The ASCE Committee on Earth and Rockfill Dams (1967) has given the basic defensive and construction procedures to protect against the cracking and the resultant hazards of the piping as follows:-

1. Use of a wide transition zone, or of properly graded filter zones of adequate width.

2. Special treatment of foundation and abutment conditions to reduce sharp differential settlement.

3.   Arching the dam horizontally between steep
     abutment slopes.

4.   Adjustment of construction sequence for the
     different zones or sections.

5.   Requiring special placement methods for
     questionable materials.

6.   Thorough compaction of rock shells to avoid
     inducing tensile stresses in adjacent core
     material.

7.2.3 Mechanism of Cracking

Typically, stresses within an ideal homogeneous
embankment in plane strain will always be compressive, and
there will be no cracks during its construction.   However,
the minor principal stresses within the fill will generally
be less than the maximum seepage pressure which may occur,
and thus there is a potential risk of cracks forming by
hydraulic fracture when the reservoir is filled (Vaughan,
1974).

Furthermore, the stresses within dam cores will
generally depart from the ideal case, due to differences in
stiffness of the different fill types in non-homogenous dams
and due to discontinuities in the geometry of the dam section
in both the transverse and the longitudinal directions.
In some cases the stresses may reduce sufficiently to form
the cracks.

The load transfer and hydraulic fracture will be
considered later, but first it is necessary to consider the

situation in which cracks can form and remain open.

This section considers (1) cracks under "dry" conditions i.e. cracks which form above reservoir level and which contain air, and (2) cracks under "wet" conditions, below reservoir level during impounding, which contain water.

Vaughan (1976b) has given four situations for crack formation (Fig. 7.1):-

(1) Dry cracks, formed by undrained failure. Such cracks are likely only during construction. A substantial negative pore pressure is implied. The undrained cracking is only likely in fills of very low permeability. The presence of negative pore pressure may give a fine grained soil a substantial tensile strength, which must be overcome before tensile cracking occurs.

(2) Dry cracks, formed by drained failure. Again, they are likely only during construction. A negative pore pressure may exist, maintained by capilliary effects at exposed seepage boundaries, and the tensile strength in terms of total stress, which must be overcome before cracking can occur, will depend on the magnitude of the negative pore pressure and the grading of the soil. Such cracks can form in most soils, if the tensile strength in terms of total stress is sufficient for the crack to be stable and remain open.

(3) Wet cracks, formed by undrained failure. Such cracks can only form during or after impounding of the reservoir. If the seepage pressure is applied rapidly

within some initial crack or imperfection then tensile failure may occur by undrained failure.

(4) Wet cracks, formed by drained failure. Such cracks may form during or after impounding, when there is a general increase in seepage pressure in the core. The tensile strength to be overcome will be negligeably small in most instances. Generally, tensile failure must be preceded by shear failure.

If dry cracks form during construction, they are unlikely to be closed by the increasing water load on the dam, and thus they will eventually be subjected to seepage flow through them.

7.3 Arching of the Core and Load Transfer

If the material of the core is more compressible than that of the adjacent shells or abutments, the differential settlement across the boundaries between these zones is likely to inhibit the settlement of the core, transferring load from the core to the shells or abutments. Hence the vertical stresses in the core are reduced and those in the shells or abutments are increased until the difference reaches the shear strength of the weaker material. This reduction in the stresses in the core is known as the arching or load transfer and may cause transverse cracks.

Various modes of arching and load transfer and changes in modes may occur in an earth and rockfill embankment during its lifetime. Load transfer may exert a significant influence on the characteristics of embankment behaviour

which are the displacements and the strains as well as the earth pressure and the pore water pressure that are observed. The effects of load transfer on the dam behaviour are a function of the compressibility of the core materials in conjunction with the settlement characteristics of the shell materials. The width of the core has also some effects on the degree of load transfer.

A comprehensive discussion of the different modes of load transfer has been given in a paper by Squier (1970).

Pressure cell measurements have revealed a significant reduction in both vertical and horizontal stresses at depth in thin cores of several rockfill dams. This was attributed to greater compressibility of the core with respect to the shells. The lower than expected settlements and pore water pressure of puddled clay core in Selset Dam were attributed to the greater downward movement of the core with respect to the shells and transfer of load from the core to the shells (Bishop and Vaughan, 1962).

In the papers by Vaughan (1970 & 1972), Vaughan et al (1970), and Kjaernsli and Torblaa (1968) developments of serious cracks in the cores of two dams, Balderhead Dam and Hyttejuvet Dam, have been reported. In both cases the cause of cracking has been attributed to a combination of two mechanisms: arching at the core-shoulder boundaries, and a form of hydraulic fracturing due to the pressure of the impounded water.

If the zoned dam has a soft shell and a stiff core,

then the load transfer occurs from the shell onto the core. This mode of load transfer could cause a local over-stress in the core leading generally to additional resistance to cracking.

Kulhawy and Gurtowski (1976) analysed the phenomenons of load transfer and hydraulic fracturing using the finite element method. Their conclusions for the effect of soil properties and dam's geometry on the arching are as follows:-

(1) A dam with a dense shell, regardless of geometry, will exhibit a large load transfer.

(2) As the core becomes wetter, the load transfer increases.

(3) For core compacted dry of optimum, the load transfer is nearly constant for the central 2/3 to 3/4 height of the core. But for core compacted at optimum water content or wet of optimum, the greatest load transfer from the core to the shells occurs near the base of the dam. This load transfer decreases with increasing height until near the crest where the load is transferred from the shells onto the core.

(4) A higher dam will exhibit slightly less load transfer.

(5) Steeper side slopes to the core will cause more load transfer.

(6) The effects of transition zone's properties and thickness are very minor in all respects in influencing cracking.

(7)   Thinner (steeper) vertical core leads to more arching.

(8)   Equivalent vertical and sloping core dams exhibit essentially the same effect.

(9)   A thinner sloping core leads to more arching.

· From these effects Kulhawy and Gurtowski (1976) concluded that the dam with less cracking potential will be one with:-

(1)   Medium dense shells;

(2)   flatter side slopes;

(3)   a thicker core (with flatter core slopes);

(4)   a core compacted drier than optimum; and

(5)   a sloping core (a vertical core leads to greater potential for hydraulic fracturing).

7.4   Hydraulic Fracture

7.4.1 General

In recent years, cracking leading to excessive loss of drill water in the cores of a number of embankment dams has been attributed to the phenomenon of hydraulic fracturing; that is, a condition leading to the creation and propagation of a crack in a soil whenever the hydraulic pressure exerted on a surface of the soil exceeds the stress on that surface and the tensile strength of the soil.

7.4.2 Mechanism of Hydraulic Fracture

Hydraulic fracture may either occur under undrained or drained conditions.

7.4.2.1 Undrained Hydraulic Fracture

Undrained cracking can only occur if the seepage or swelling face has only penetrated a small distance into the core at the time the reservoir pressure reaches the value required for hydraulic fracture. Thus the reservoir level must rise very rapidly relative to the rate of advance of the seepage or swelling front. This form of cracking is unlikely, as the rate of impounding in relation to the permeability of the core will almost always ensure that there is a general increase in seepage pressure in at least the upstream side of the core before cracking can occur.

Thus, the cases where undrained hydraulic fracture is considered a serious possibility are adjacent to bore-holes and in small rapidly filled flood control dams where both filling and through going cracks occur in a matter of hours (Vaughan, 1972).

Hydraulic fracture could also occur due to the water penetrating preferentially into the core via some irregularities such as a crack or more pervious layer (see next section).

7.4.2.2 Drained Hydraulic Fracture

For drained hydraulic fracturing, the seepage or swelling face must have advanced a significant distance into a low stressed area of the core before the reservoir reaches the level at which undrained fracturing would have occurred.

Drained hydraulic fracture is considered to have

occurred at Hyttejuvet Dam (Kjaernsli and Torblaa, 1968);

Balderhead Dam (Vaughan et al, 1970); and Teton Dam (Report

of the Independent Panel on Failure of Teton Dam, 1976).

A comprehensive discussion of drained hydraulic

fracture is given by Vaughan (1970, 1976a and 1976b), and

the remainder of this section is derived from his analysis.

Drained hydraulic fracture is illustrated in Fig. 7.2.

The critical feature is the changes in stress which must

accompany increasing seepage pressures. Figure 7.2 shows

potential stress changes at a typical point Z within a core

if the reservoir first applies a water load to the upstream

face of the core and the seepage pressure within the core

builds up slowly. The total stresses (A) before impounding

are assumed to be compressive but less than the eventual

seepage pressure. There will be a small increase in

stress (A-B) due to the water load on the upstream side of

the core. There will then be a reduction in effective

stress (B'-C') as the seepage pressure increases, which

might well produce a further increase in total stress (B-C).

When the effective stresses are reduced to C' shear failure

must occur. To cause tensile failure at D' there must be

a reduction in shear stress and substantial deformation of

the soil, which will modify the total stress, and probably

increase it (C-D). Such an increase may prevent tensile

fracture occurring. Thus a critical situation is likely
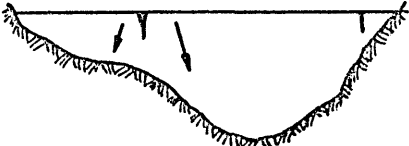
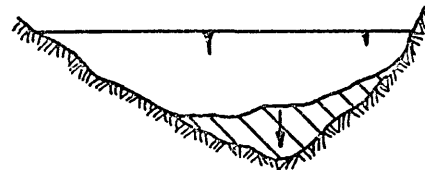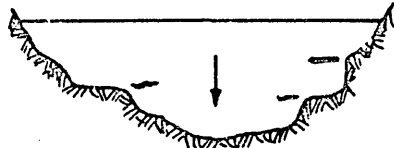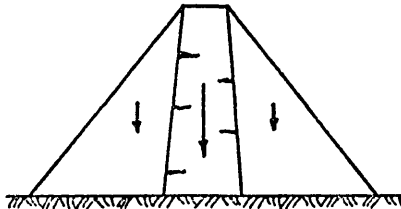only if this increase is insufficient to prevent fracture.

Drained hydraulic fracture is complicated by the

difficulty in predicting the stress changes due to shear failure induced by an increasing pore pressure. However, a simple elastic model (shown on Fig. 7.3) can be considered to study this effect (Vaughan, 1976b).

From this analysis, Vaughan (1976b) has given two conclusions, which are likely to be valid for the real situation. Firstly, hydraulic fracture will only occur if the pore pressure due to seepage increases to a value equal to or greater than the average total stress before impounding. Secondly, the effects of the water load (ignored in Fig. 7.3) and of swelling are likely to increase the average total stress and so prevent cracking. It further follows that soils with a low swelling potential present the greatest risk of hydraulic fracture.

As shear failure results in redistribution of total stress and an increase in minimum stress, so it can be concluded that hydraulic fracture is more likely when the initial stresses in the core at the end of construction are very non-uniform, and low stress zones are local. Then fracture may occur locally, before general shear failure and the stress redistribution accompanying it are induced (Vaughan, 1976b).

Table 7.1   Some Causes of Cracking in Embankment Dams

(from Laing, 1971)

Sketch of Mechanism	Description of Mechanism	Example Dams*
Part I: Transverse Cracks 1. 	Varying Embankment Height Variations in the embankment height due to varying foundation level and/or steep abutments causes differential settlement and cracks	3 7 9 12 13
2. 	Varying Depth of Compressible Foundation Differential Settlement of the foundation causes transverse cracks in the dam	11 14
3. 	Uneven Abutments Uneven and overhanging areas of the abutments develop localized differential settlements causing cracks to form	4
4. 	Arching of the Core Greater compressibility of the core than of the shells reduces the stresses in the core sufficiently to form cracks	1 6

* These numbers refer to dams which have cracked due to the given mechanisms.   The dams are listed in Part III.
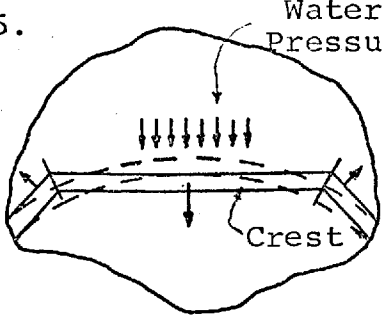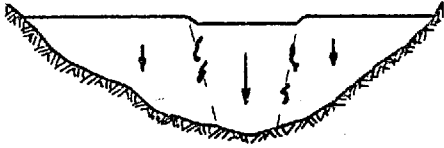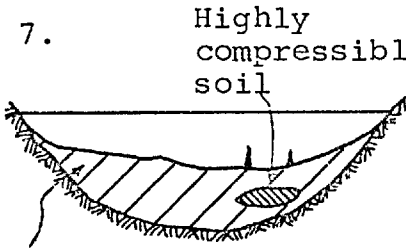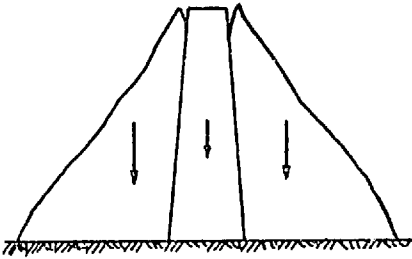
Table 7.1 Continued

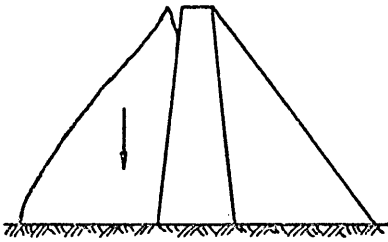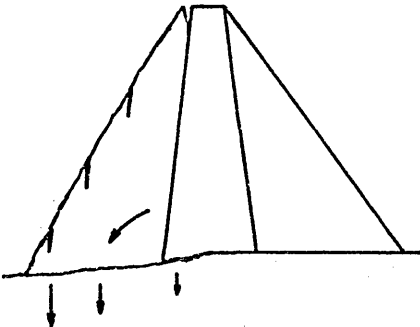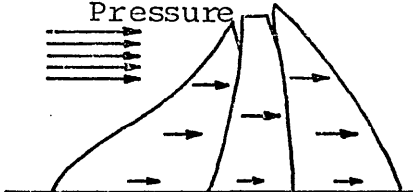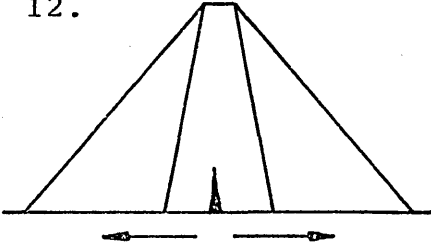| Sketch of Mechanism	Description of Mechanism	Example Dams
5.	**Differential Crest Deflection** The crest initially deflects upstream due to saturation, and then the centre of the crest deflects downstream due to the water load. This causes transverse cracks near the abutments.	12 5
6.	**Poor Construction Procedures** Poor Construction may cause differential settlements and cracks. For example, a rapidly built closure section settles more than the remainder of the dam, causing cracks.	15
7. Highly compressible soil Soil of low compressibility	**Localized Foundation Discontinuity** For example, a local lense of highly compressible soil in the foundation, or a stiff rolled-fill cutoff trench through a compressible foundation cause differential settlements and cracks	16
Part II: Longitudinal Cracks 8.	**Settlement of Shells** Greater compressibility of the shells than of the core develops longitudinal cracks at the dam crest, over the edges of the core.	2 10 13

Table 7.1 Continued

Sketch of Mechanism	Description of Mechanism	Example Dams
9.	**Collapse of Upstream Shell on Saturation** The upstream shell settles due saturation on first filling developing longitudinal cracks at the crest	3
10.	**Collapse of Foundation Soils on Saturation** Settlement of the foundation soils due to wetting starts at the upstream toe of the dam and progresses downstream as the foundation becomes saturated on first filling. This rotates the upstream shell about the core and develops longitudinal cracks	8 11
11. Water Pressure	**Downstream Crest Deflection** The reservoir water pressure deflects the embankment downstream, causing longitudinal cracks to form at the crest	13
12.	**Spreading of a Soft Foundation** The soft foundation deforms laterally, forming a vertical crack in the base of the embankment	17

Table 7.1   Continued

Part III: The Dams given as examples above

No	Name of Dam	References
1.	Balderhead Dam	Vaughan (1965), (1967), (1970); Vaughan et al (1970); Kennard, Knill and Vaughan (1967); Kennard, Penman and Vaughan (1967)
2.	Cherry Valley Dam	Sherard et al (1963)
3.	Cougar Dam	Pope (1967)
4.	East Branch Dam	Bertram (1967)
5.	El Infiernillo Dam	Marsal and de Arellano (1967)
6.	Hyttejuvet Dam	Kjaernsli and Torblaa (1968)
7.	Leobardo Reynoso Dam	Marsal (1959)
8.	Marte R. Gomez Dam	Marsal (1959)
9.	Miguel Aleman Dam	Marsal (1959)
10.	Mud Mountain Dam	Sherard et al (1963)
11.	Portland Dam	Leonards and Narain (1963)
12.	Rector Creek Dam	Leonards and Narain (1963)
13.	Round Butte Dam	Patrick (1967)
14.	Shek Pik Dam	Carlyle (1965)
15.	Wister Dam	Bertram (1967)
16.	Woodcrest Dam	Leonards and Narain (1963)
(17.)	(Sea Embankments on the North Kent Coast)	Bishop (1966c), Toms (1954)

DRY CRACKS

Undrained $\sigma_3 < t_u$ Drained $\sigma_3 < t_{ud}$

WET CRACKS

Undrained $\sigma_{3E} < t_u$ [or $p_w > \sigma_3$]   Drained $\sigma_3' < t'$
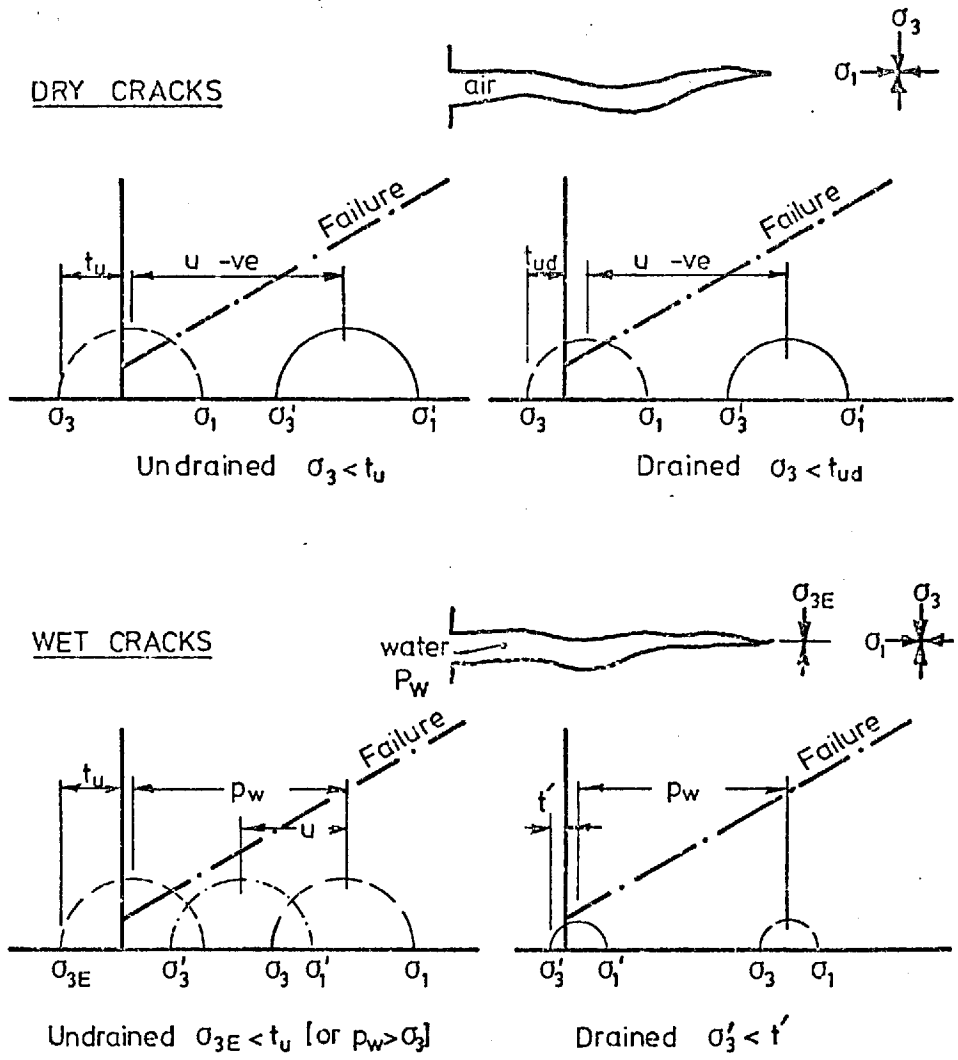
Fig. 7.1   Idealised Stresses Causing Cracking
            (from Vaughan, 1976b)
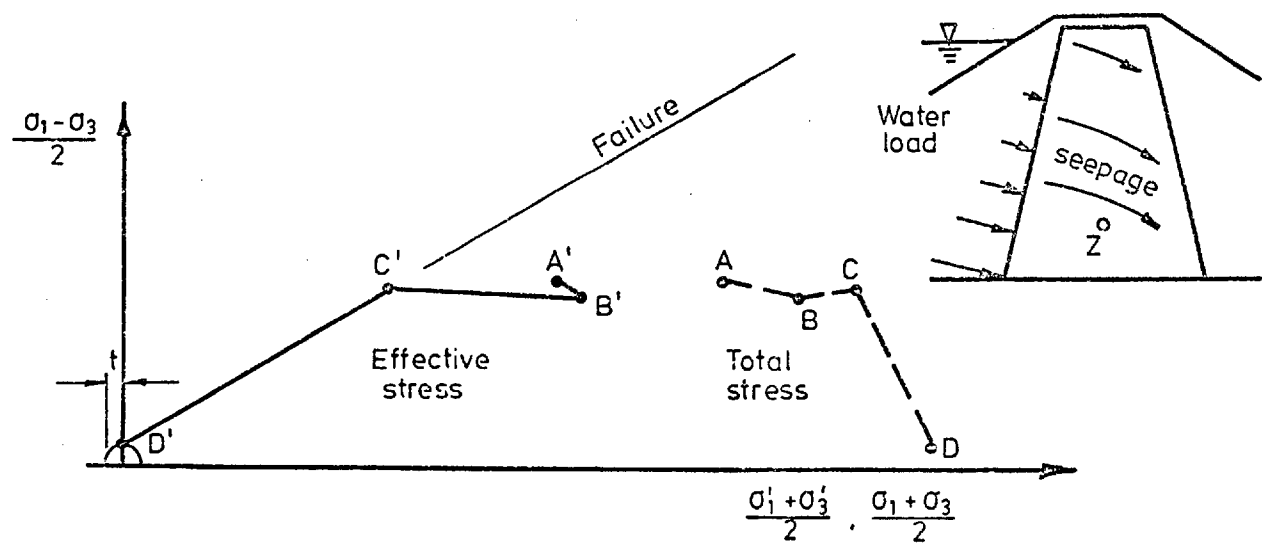
Fig. 7.2   Stress Changes Leading to Drained Hydraulic Fracture
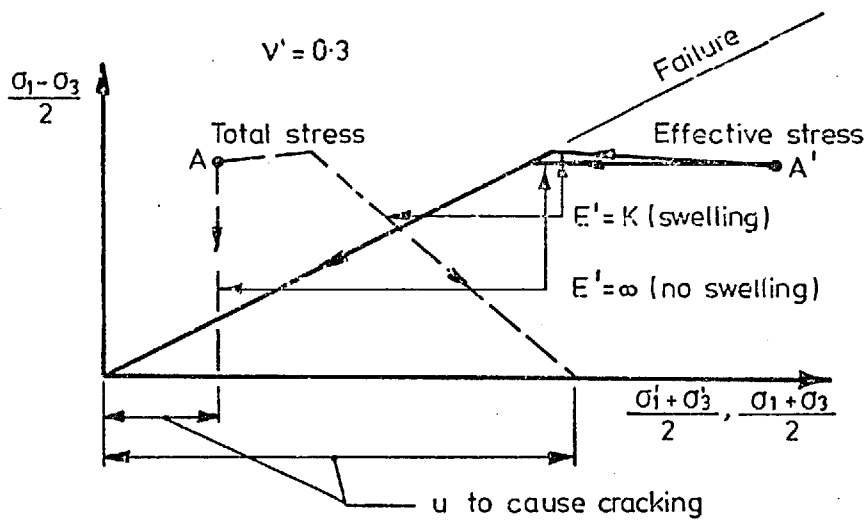
(from Vaughan, 1976b)
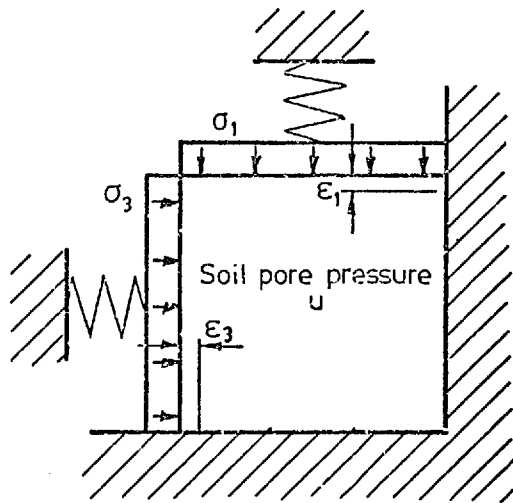
Fig. 7.3 Simplified Calculations of Stress Changes due to Increasing Pore Pressure (from Vaughan, 1976b)

CHAPTER 8

STRESS ANALYSIS OF EMBANKMENT DAM CORE WITH

EMPHASIS ON HYDRAULIC FRACTURE

8.1   Introduction

In Chapter 7 a brief review of cracking of embankment dam cores was presented, together with the phenomena of load transfer and hydraulic fracture in the core.

The stresses and stress changes in the core at the end of construction and after impounding can be analysed using the non-linear finite element method.   From these analyses it is possible to investigate the areas of low stress and the likelihood of crack formation.

The main purpose of this chapter is to demonstrate that the development of seepage pressures throughout the core during impounding reduces the risk of hydraulic fracture (as predicted by Vaughan, 1976b).   Therefore, the analyses carried out in this chapter, consider the stresses and the stress change in an idealised core with vertical sides at the end of construction and during impounding.   For impounding three different forms of seepage were simulated, namely, flooding (with hydrostatic water pressure gradient everywhere), transient flow (with horizontal and vertical head gradients), and local flow (with horizontal head gradient only in a local layer).   Of these three forms of impounding the latter two are much closer to reality than the first one.   The flooding is a fictitious form of impounding, and

it is simulated to study the effect of the hydrostatic water pressure gradient on stresses and stress changes in the core.

In the analyses performed, both undrained and drained soil properties were considered. Where undrained properties were assumed, stresses at the end of construction only were analysed, and with drained properties, both construction and impounding were modelled. Both undrained and drained results at the end of construction were compared to the results given by closed form plasticity solutions.

8.2   The Finite Element Mesh

In order to minimize the computer cost and to concentrate more elements in those areas of the dam which are of prime interest for cracking and hydraulic fracture, only the core of the dam was considered in the analyses. Effects of shells on the core were modelled by applying springs at the side boundaries.

Figure 8.1 shows the finite element mesh used in the analyses. The effects of the shells are modelled by applying springs horizontally and fixed vertically at the side boundaries. For all cases considered, the spring stiffness was assumed to be equal to 4×10^3 KPa. This value was calculated from the theory of subgrade reaction by assuming that if a force equal to 200 KN/mrun is applied to the spring, a displacement equal to 0.05 m will be produced. This is probably less stiff than typical embankment shells but was adopted to ensure that arching would occur.

8.3   Cases Considered in the Analyses

Three main cases were considered in these analyses, together with two minor cases for the side boundary conditions.   Table 8.1 gives the soil properties used in the main cases.   The soil properties used in the minor cases are given in section (8.6).

The first major case considered (case U1, Table 8.1) was undrained and the construction only was modelled.   Two values for the undrained shear strength (C_u = 60 KPa and 30 KPa) were used, together with the non-linear stress-strain curve shown on Fig. 8.2.   The comparison was made between the results of this case and those given by closed form plasticity solutions, which will be discussed in section (8.7.1).

Two cases D1 and ST1 (Table 8.1) were drained and modelled the construction together with the following impounding.   For both cases, the pore water pressure at the end of construction was assumed to be equal to zero.   Figure 8.3 shows the family of non-linear stress-strain curves used for case D1.   Also, for case D1, the tangential Poisson's ratio was assumed to vary with the state of stress as given in Table 8.1

In order to simplify the analysis and to minimize the computer cost, the bi-linear stress-strain curves (Fig. 8.4) were used for case ST1.   Poisson's ratio was constant (equal to 0.2) before the failure, and it was equal to 0.499 at failure.

For case D1, the unloading modulus and the reloading modulus were the same and equal to the initial modulus ($E_u = E_r = E_i$, see Chapter 5, Fig. 5.1c). For case ST1, the unloading modulus was equal to the initial modulus and the reloading modulus was equal to the tangent modulus at the same state of stress ($E_u = E_i$, $E_r = E_t$, see Chapter 5, Fig. 5.1.b).

8.4 Analysis Procedures

For accurate analyses of the embankment dams, it is necessary to simulate the placement of successive layers of the embankment dam material. Clough and Woodward (1967) have examined the usefulness of both "layered" finite element analyses (in which the placement of successive layers was simulated) and "single-lift" finite element analyses (in which the gravity body forces were applied to the entire structure in one step). Their studies, for homogeneous embankment dams with linear elastic material properties, indicate that the "single-lift" analyses provide reasonable stress distributions, but displacement patterns are different from those calculated by means of "layered" analyses and measured in real embankments.

Hamza (1976) showed that the material non-linearity amplifies these differences in deformations.

However, by considering that in these analyses the stresses are of prime interest, and the undrained shear strength is not a function of the state of stress, for

undrained case U1 (Table 8.1) single-lift analysis was employed for construction. The material non-linearity was dealt with using the incremental quasi Runge-Kutta method (explained in Chapter 2).

For drained cases D1 and ST1 (Table 8.1), as the drained shear strength is a function of the state of stress, so layered analyses were simulated for both construction and impounding. As the result of this technique, the probable progressive build up in stress due to placing the layers causes gain in strength which closely simulates the actual sequence of construction.

The material non-linearity was dealt with using the incremental quasi Runge-Kutta method for case D1, and a combination of the incremental tangential method and the Newton-Raphson iterative method (explained in Chapter 2 and Appendix 2) for case ST1, in each layer.

8.5   Loading Sequences

The loading sequences employed in the analyses, were construction and impounding. Impounding could have three different forms, namely, flooding, transient flow and local flow. In the following section these loading sequences are discussed.

Construction   In simulating the construction of an embank-ment dam, the loads applied due to placing a layer represent the weights of the added elements. The weight of each element is distributed equally among its nodes, in accordance

with the usual procedures for applying body forces (soil

unit weight). In drained analyses, for each step of placing

a layer, drained soil properties were used for the new

layer, with zero weight and small stiffness (E = 5 KPa)

assumed for the layers above.

A more general discussion of simulating the construc-

tion in layers using this technique is given by Hamza (1976).

For undrained case U1, where single-lift analysis

was employed, the undrained soil properties were used for

the whole domain.

Flooding   In simulating the application of water loads to

the embankment dam, the loads are considered in two forms -

buoyancy forces (due to flooding) and seepage forces (due

to transient and local flows). The buoyancy forces are

equal to the unit weight of water multiplied by the area of

the submerged elementes. These forces act vertically

upward, and are distributed equally among the nodes of each

element, in the same manner as the body forces. In the

programme the gradients of water pressures due to these

buoyancy forces were calculated and then applied as body

forces (see Appendix 2). Drained soil properties were

used for all layers and in all steps.

Transient Flow   In simulating the transient flow, seepage

forces were calculated from a flow net which consists of

postulated horizontal flow lines, in order to simplify the

calculation of the pore water pressure. Figure 8.5 shows

this flow net. In the analyses, water pressures were calculated from this flow net and input at the nodes. In the programme the gradients of these water pressures were calculated and applied as body forces (see Appendix 2). Drained soil properties were used for all layers and in all steps.

Local Flow   If the reservoir is filled very quickly, the core remains under undrained conditions. By supposing that there is a local layer which is much more permeable than the rest of the core, then water penetrates into the core at this layer. It has been postulated in Chapter 7 that this local flow or drainage can be more critical in producing hydraulic fracture (see also section 8.7.2.1). In simulating the local flow, the following assumptions were made:

1. Full reservoir height at the upstream side.

2. Water penetrates into the core generally at the upstream face to a slight extent, which was modelled by a column of thin elements at the upstream side (see Fig. 8.1).

3. One layer in the core (in this study layer number 7 from the bottom, Fig. 8.1) is affected by seepage. The water pressure varies linearly from the reservoir height at the upstream side to zero at the downstream side, across this layer.

By these assumptions, the water pressures were calculated and input at the nodes. In the programme gradients of these pressures were calculated and applied as body

forces (see Appendix 2). Drained soil properties were used for whole domain.

Flooding and transient flow were simulated in layers after the embankment has reached its full height. Local flow was simulated in increments after completion of the construction sequence.

8.6 Effects of the Side Boundary Conditions on the Stresses

The requirement of zero vertical deformations at the core sides imposed by the side boundary conditions shown in Fig. 8.1, has a tendency to magnify the load transfer effects compared to a real situation. The amount of load transfer from the core to the side supports (shells) can be reduced by decreasing the shear strength of the core material to produce a zone of failed soil at the side boundaries between the core and supports (this effect will be discussed in sections 8.7.1 and 8.7.2).

In order to make a preliminary study of the effects of the side boundary conditions assumed for these analyses (see Fig. 8.1) on the stresses and stress paths, two minor cases (cases A and B) were considered. In both cases, a linear material with E = 50000 KPa and ν = 0.33 was used. The soil unit weight was equal to $20 KN/m^3$, and the water unit weight was assumed to be equal to 10 KN/m^3. The construction was followed by transient flow, and layered analyses were simulated. Both construction and impounding were completed in 15 layers for the full height of 30 m.

Figure 8.1 shows the mesh used for both cases, except for the side boundary conditions. For case A, the side boundaries were free vertically and fixed horizontally. Case B had the same side boundary conditions as shown on Fig. 8.1

Figures 8.6 to 8.8 show the stress paths for these two cases. From these figures the following observations are made:-

Case B produces large negative average effective stresses at the upstream side at the end of impounding (transient flow), which may result in zero or negative shear strength for drained non-linear analyses. The negative average effective stress at the end of transient flow is about 1.5 times the average stress at the end of construction, near the base of the core. This value is approximately constant for about 2/3 of the core height, then it decreases towards the top of the core.

Case B gives smaller deviatoric and average effective stresses than case A, both at the end of construction and impounding, except near the top of the core where the deviatoric stresses for case B are greater than for case A. This reduction in stress is due to the arching effect in case B. Also, it suggests that near the top of the core, reduction in major principal stress due to the arching effect is much greater than the reduction in minor principal stress.

Values of the average effective stresses at the end of construction for case B are about 6% (near the base of

the core), about 10% (around the core mid-height) and about 38% (near the top of the core) of the average effective stresses at the end of construction for case A. These values indicate a large arching effect in case B. However, as will be discussed later in this chapter (sections 8.7.1 and 8.7.2), the amount of load transfer from the core to the side supports decreases if a proper strength is considered for the soil.

For case A, impounding tends to decrease the values of the average effective stresses. The average effective stresses, near the upstream side, at the end of transient flow are between 50%, near the top of the core, and 55%, near the base of the core, of the average stresses at the end of construction. Near the downstream side of the core, these values are between 95%, near the base, and 99% near the top of the core.

For case B, transient flow tends to decrease the average effective stresses near the upstream side and to increase them near the downstream side of the core. The average effective stresses, near the upstream side, at the end of transient flow are between -150%, near the base, and 15%, near the top of the core of the average effective stresses at the end of construction. Near the downstream side of the core, the average effective stresses at the end of transient flow are between 2 times, near the top, and 3 times, near the base of the core, of the average stress at the end of construction.

It has to be mentioned that the values of the average

effective stresses (at the end of construction and impounding) for case B are almost constant for about 2/3 of the core height.

From these parametric studies, it is clear that the side boundary conditions used in case B are more critical than those used in case A, from the point of view of the arching and hydraulic fracture. As the side boundary conditions used in case B are closer to reality than those used for case A, and also, they model effects of the shells in the analyses, for the main analyses of this chapter, the side boundary conditions shown on Fig. 8.1 are used.

8.7 The Finite Element Results and Discussion

8.7.1 Results for Undrained Construction

Undrained analysis is used to get the stresses at the end of construction. These stresses are useful in studying the hydraulic fracture phenomenon.

Nobari and Duncan (1972), and Kulhawy and Gurtowski (1976) determined the end of construction stresses by undrained analyses. Nobari and Duncan showed that the stress on a horizontal plane through the core at the end of construction was not significantly affected by impounding and postulated that hydraulic fracture would occur if the reservoir pressure exceeded this stress. Kulhawy and Gurtowski assumed that the intermediate principal stress would not change on impounding and postulated hydraulic fracture when the reservoir pressure exceeded this stress.

However, as it will be discussed in section (8.7.2), drained impounding tends to increase the total stresses and so reduce the risk of hydraulic fracture.

For undrained construction, only one case (case U1, Table 8.1) with two values for the undrained shear strength (C_u = 60 KPa and 30 KPa) was considered.

As mentioned in section (8.6), the requirement of zero vertical deformation at the core sides imposed by the side boundary conditions shown on Fig. 8.1 magnifies the amount of the load transfer from the core to the side supports (shells). This arching effect on stresses can be reduced by decreasing the shear strength of the core material. When the shear strength is reduced enough to produce a zone of failed soil at the sides between the core and supports (see Fig. 8.9a), then the vertical stress in the core becomes equal to about half of that due to the full weight of the soil. Figure 8.9b shows the values of vertical stresses at the end of undrained construction, at the core centre line, for two different values of the shear strength. This figure indicates that by reducing the shear strength of the core material from 60 KPa to 30 KPa the amount of load transfer from the core to the side supports is decreased almost three times.

Bishop (1952), and Nonveiller and Anagnosti (1961) have given the values of vertical stresses in the core, using the theory of plasticity. In Fig. 8.9b, comparisons are made between the values of vertical stresses from the

non-linear finite element analysis (C_u = 30 KPa) and those given by Bishop (1952), and Nonveiller and Anagnosti (1961). Note that equation (2.19) for the values of vertical stresses in the Nonveiller and Anagnosti paper was wrong. This has been corrected and used for calculating the vertical stresses.

Generally, the agreement between the results from the non-linear finite element analysis and those given by the plasticity solutions is good for C_u = 30 KPa. The reason why the non-linear elastic finite element analysis gives results which are in good agreement with those given by the plasticity solution, is that the non-linear finite element analysis satisfies the equilibrium conditions, and near the centre line the principal stress rotations are very small.

For the shear strength equal to 30 KPa, the results from the finite element analysis are a maximum of 30% greater, near the top of the core, and a maximum of 8% smaller, near the base of the core, than the results given by Nonveiller and Anagnosti (1961). Bishop's results are a maximum of 15% greater than the results given by the finite element analysis, for C_u = 30 KPa.

For C_u = 60 KPa, the Nonveiller and Anagnosti method gives the values of vertical stresses equal to zero. Bishop's method gives a constant value for the vertical stress which is not a function of the depth. This value of the vertical stress is equal to 25 KPa (for no tension crack). For this strength the plasticity solutions are

clearly invalid, as negligible shear failure occurs.

8.7.2 Results for Drained Conditions

Two drained cases (cases D1 and ST1, Table 8.1) were considered in the analyses. For case D1, the solution technique was not adequate to deal with the strain-softening behaviour. For case ST1, the programme was extended to deal with the strain-softening behaviour (see Appendix 2).

The construction and impounding were simulated with layered analyses. In case D1, two different numbers of layers (9 and 15 layers) for the full height of 30 m were used. In case ST1, 5 layers for the full height of 10 m were modelled.

8.7.2.1 Drained Case before Strain-Softening Modelling

Only one case (case D1, Table 8.1) was analyzed in this subgroup. The values of vertical stresses at the core centre line from the finite element analysis, at the end of drained construction, are given on Fig. 8.10. For simulating the construction, both 9 and 15 layers were used. With a 9-layered analysis, the first three layers consisted of one row of elements and subsequent layers consisted of two rows of elements.

By comparing the 9- and 15-layered analyses (Fig. 8.10), it is clear that the 15-layered analysis gives a much smoother curve for the vertical stress distribution than the 9-layered analysis. The 9-layered analysis gives smaller stresses for the lower half of the core, and greater

stresses for the upper half of the core. The maximum difference in stresses is just above the core mid-height, where the vertical stress from 9-layered analysis is 25% less than the vertical stress from 15-layered analysis.

Also, the values of vertical stresses from 9-layered analysis are scattered around the core mid-height. This is due to the large size of the layers around the core mid-height which cause overshooting of the shear strength in some Gauss points.

As the vertical stresses from 15-layered analysis are not scattered, therefore, the 15-layered analysis has been used for modelling of the construction and impounding in this section.

In Fig. 8.10 the vertical stresses at the core centre line from the non-linear finite element analysis, at the end of drained construction, are compared with the vertical stress given by Nonveiller and Anagnosti (1961). The agreement between the finite element results and results given by the plasticity solution is very good. The vertical stresses from the finite element analysis are 2% more than the vertical stresses from the plasticity solution for the lower 1/3 of the core height.

Figure 8.11 represents zones of the soil at failure at the end of construction, flooding and transient flow for case D1. At the end of construction, existence of the zone of failed material at the sides between the core and supports results in the proper amount of the load transfer

from the core to the side supports, shown on Fig. 8.10.
At the end of flooding, the zone of failed soil is changed
a little. The transient flow concentrates the zone of
failed material at the upstream side of the core.

Figures 8.12 and 8.13 show the distribution of the
average stress with depth for case D1, at the end of con-
struction and flooding. The average stresses (total and
effective) at the end of construction are less than the
eventual water pressure due to flooding, except near the
top section of the core, where these stresses are greater
than the eventual water pressure. But, as shown on Figs.
8.12 and 8.13, impounding tends to increase the average
total stresses prior to fracture, and so reduce the risk of
hydraulic fracture occurring (as predicted by Vaughan, 1976b).
The average total stress at the end of flooding near the
core sides at a depth between 6 to 8 m (Fig. 8.13) is equal
to the eventual water pressure, and if the tensile strength
of the core material is ignored, there is a possibility of
drained hydraulic fracture in this area.

In Figs. 8.14 to 8.16 some stress paths for the con-
struction followed by flooding (case D1) are given. Point
A represents the total and effective stresses at the end of
construction. There is a small increase in stress (A-B)
due to the application of the water pressure to the zone
beneath the point considered (this stress path is both
total and effective). As the water pressure continues to
increase (after flooding reaches the point considered) there

will then be a reduction in average effective stress (B-D'),
and an increase in average total stress (B-D). Such an
increase in average total stress may prevent drained
hydraulic fracture occurring. Thus, a critical situation
is likely only if this increase is insufficient to prevent
fracture. Such a critical area was shown on Fig. 8.13, at
depth between 6 to 8 m, where the average total stress at
the end of impounding is equal to the eventual water pressure.

In the effective stress path during flooding (Figs.
8.14 to 8.16), when the effective stress is reduced to C',
shear failure must occur. Obviously, post-failure stress
path must be on the failure envelope. However, as will
be discussed later in this chapter (section 8.7.2.2),due to
shortcomings of the incremental non-linear methods used,
the post-failure stresses in these figures followed hori-
zontal paths.

Figures 8.17 and 8.18 show the distribution of the
average stress for construction followed by transient
flow (case D1). Near the core centre line, the average
stress at the end of construction is greater than the even-
tual seepage pressure. Transient flow tends to decrease
the average effective stress in the top 1/3 section of the
core, and to increase the average total stress.

Figure 8.18 gives the average stress distribution
near the upstream side of the core. The average stress
at the end of construction (total and effective) is less
than the eventual seepage pressure for the lower 2/3 of
the core height. This does not necessarily mean that there

is a possibility of drained hydraulic fracture in this area,
like the case of flooding, transient flow leads to greater
average total stress than those at the end of construction,
and so reduces the risk of cracking.

A more detailed discussion of the stress changes due
to impounding, shown on Figs. 8.17 and 8.18, is given in
section 8.8.

By comparing Figs. 8.13 and 8.18, it is clear that
reduction in the average effective stress at the end of
impounding (compared to the stresses at the end of con-
struction) due to flooding is greater than that due to
transient flow.

In Figs. 8.19 and 8.20 the stress paths for constuc-
tion followed by transient flow are given. Point A is
the end of construction (total and effective). Like the
case of flooding, impounding increases the average total
stress. Again, in these figures, the post-failure stress
paths are horizontal, instead of laying on the failure
envelope. Also, in Figs. 8.19 and 8.20, the construction
stress path shows some overshooting of the shear strength.

The overshooting during construction is due to the
incremental non-linear method used, as this method (unlike
the interative method) is not able to prevent overshooting,
unless very small load increments are applied.

During impounding, the average effective stress in
the core decreases. In general, this decrease (unloading)
can occur from any state of stress including the state of

failure, and it will be accompanied by a drop in strength.
If this stress path induced softening (or strain-softening)
is not modelled correctly, a stress path which violates
the failure criterion will be followed.

In Fig. 8.21 the p'-q and q-ε_1 stress paths for a
typical point which should exhibit strain-softening behaviour
are given.   From this figure, it is clear that when the
stress path reaches the failure envelope, as there is no
shear unloading, so it maintains a horizontal path on the
q-ε_1 and p'-q plots,while due to the reduction in average effec-
tive stress,it should be loosing strength, resulting in an
overshooting which is increasing as impounding continues.

The incremental non-linear solution techniques are
inadequate to model the post-failure behaviour.   So, in
analyses presented in this section, the strain-softening
behaviour due to an increasing pore pressure is not repro-
duced.   As a result, in Figs. 8.14 to 8.16 and 8.19 to
8.21, when the effective stress path has reached the failure
envelope during impounding, it has followed a horizontal
path.

As discussed in Appendix 2, the programme was extended
to deal with this strain-softening behaviour.   The stress
analysis of the core was then continued, as discussed in
section 8.7.2.2.

Also, in this section, the stress analysis and the
possibility of hydraulic fracture occurring in a core due
to local flow are considered.

Shear failure transfers stress from areas of high stress to those of low stress, and results in an averaging of the stresses in the core and an increase in stress in the critical zones. Therefore, as postulated in Chapter 7, hydraulic fracture is most likely when the initial stresses in the core at the end of construction are very non-uniform, and low stress zones are local. Then fracture may occur locally, before general shear failure and the stress redistribution accompanying it are induced (Vaughan, 1976b). Such a critical situation for hydraulic fracture may occur due to the water penetrating preferentially into the core via some irregularities such as a crack or more pervious layer.

Figures 8.22 and 8.23 (note that for these two figures $E_i = 1000\tau_{max}$) show distribution of the average effective stress in the core for construction followed by local flow (layer 7 from the bottom in Fig. 8.1 is the assumed drained layer). After impounding, the average effective stress increases except in the drained layer, where a large reduction in average effective stress has occurred. The local drainage, due to the existence of these low stress areas, can be more critical for hydraulic fracture occurring than a fully drained core. As in a fully drained core, general shear failure and swelling result in redistribution of stress and an increase in low total stress, so reducing the risk of cracking.

8.7.2.2 Drained Case after Strain-Softening Modelling

8.7.2.2.1 Modelling of the strain-softening behaviour

In many geotechnical problems, the stress-strain curves exhibit strain-softening behaviour. Considering this post-failure behaviour in the finite element analysis is one of the problems which has not yet (1977) been solved with complete satisfaction, although some promising starts have been made. In the case of non-linear elastic models using the tangent modulus approach in the incremental scheme, the required modulus becomes negative once peak strength is passed.

Girijavallabhan and Reese (1968), and Hoyaux and Ladanyi (1970) have introduced an approach for the non-linear elastic models which used the secant modulus instead of the tangent modulus.

Many efforts have been made to model the strain-softening behaviour using the plasticity concepts. Höeg (1972) attempted to model undrained strain-softening of clays. Nayak and Zienkiewicz (1972) have presented a generalization of existing elasto-plastic constitutive relations including strain-softening. More recently, Prévost and Höeg (1975a, b and c) have used the theory of plasticity to model the strain-softening behaviour in geotechnical problems.

Desai (1974) has presented a hypothesis for defining the softening behaviour after peak and a numerical procedure based on iterative relaxation scheme of the Newton-Raphson type. The distinguishing feature of the Desai

approach is that the strain-softening phenomenon is viewed as a process of modification (reduction) in the strength of the material rather than as a change in the moduli computed as gradients of the stress-strain curves, as is done in other strain-softening studies. This technique was used by Desai (1977) to study the behaviour of deep foundations.

In these analyses, to prevent overshooting during construction, and to model the strain-softening behaviour encountered in this research, the iterative solution using the Newton-Raphson method was utilized. During analysis, it was found that in some iterations, for some of the Gauss points the behaviour is shear unloading, bearing in mind that the overall behaviour can be loading (e.g. construction). The iterative technique uses the tangent modulus, which can result in large strains for points near or at the failure, if they are shear unloaded. These large strains can cause numerical problems resulting in non-convergence of the solution (see Fig. A.3, Appendix 2).

As discussed in Appendix 2, the Newton-Raphson iterative technique was modified to deal with the shear unloading. Also, in Appendix 2, the form of the strain-softening behaviour encountered in this research and the development in the programme to deal with this behaviour are explained.

The typical stress path for strain-softening is shown in Fig. A.5 of Appendix 2: as the point a-A is at failure, so a horizontal path is continued to point b-B, then at

this point the shear stress level is checked with the shear strength, and as this shear stress is greater than the shear strength, so the point is brought down to the failure envelope (point c-C) by keeping the average effective stress and the principal stress rotation constant. The excess stress is transferred to other points that have not reached failure in the following iterations.

8.7.2.2.2 Drained Case Results

Only one drained case (case ST1, Table 8.1) was analysed after extending the programme to deal with the shear unloading during iteration and the strain-softening behaviour. In this analysis, only five layers (height equal to 10 m) of the mesh shown on Fig. 8.1 were considered, in order to cut the computer time and cost. The construction and following transient flow were simulated in 5 layers (for the full height of 10 m), using the layered analysis.

Figures 8.24 and 8.25 show zones of the failed soil at the end of construction and impounding. By comparing these two figures, it is clear that the transient flow leads to the concentration of the failed soil at the upstream side of the core. This is due to the horizontal gradient of the water pressure and the higher water pressure at the upstream side. Also, comparison of these two figures indicates that, at the end of transient flow the size of the failed soil zone has been reduced. This effect is due to the shear unloading of some of Gauss points from the state of failure (that was reached at the end of construc-

tion) during impounding, which results in the state of pre-failure for these points at the end of impounding. However, some of the Gauss points may remain at the state of failure at the end of transient flow, even if they are shear unloaded.

As discussed in the section (8.7.2.1) and Appendix 2, some of the Gauss points exhibit strain-softening behaviour (or stress path induced softening) during impounding. Figure 8.26 shows zone of the points exhibiting strain-softening behaviour at the end of transient flow. It is obvious that, for the points which are not included in this figure, the behaviour is shear unloading during impounding, and at the end of impounding they are still at the state of failure.

Also, Fig. 8.24 indicates that a thin zone of failed soil has been produced at the sides between the core and supports, which results in proper load transfer from the core to the supports at the end of construction (see Fig. 8.34).

Figures 8.27 to 8.33 give the stress paths for some of the points exhibiting strain-softening behaviour. For Figs. 8.27 to 8.29 and 8.33, point A represents the total and effective stresses at the end of construction. Application of the water pressure tends to decrease the average effective stress (A-B'), and to increase the average total stress (A-B). When the effective stress is reduced to B', shear failure occurs. As the water pressure increases, the average effective stress and the shear stress decrease

(B'-C'), which cause the redistribution of stresses and an increase in the total stress (B-C). In the corresponding q-ε_1 plots (Figs. 8.27 to 8.29 and 8.33), point a is the end of construction. By increasing the water pressure, the shear stress decreases. The early section of the stress path during impounding shows shear unloading (a-b). After shear failure has occurred, the stress path shows strain-softening (b-c).

In Figs. 8.30 to 8.32, point A is the end of construction (total and effective). There is a small increase in stress (A-B) due to the application of the water load to elements lower than these points. As the seepage pressure increases, the average effective stress decreases (B'-C') and the average total stress increases (B-C). When the effective stess path is reached to the failure envelope (point C'), shear failure occurs, except for the effective stress path on Fig. 8.31, where the state of failure is reached at the end of construction. By further increase in the water load, the average effective stress decreases (C'-D') and the average total stress increases (C-D). In the q-ε_1 plots (Figs. 8.30 to 8.32), the behaviour is loading from a to b, it is shear unloading from b to c, and it is strain-softening from c to d.

During the strain-softening path, volumetric strains are zero, as Poisson's ratio is assumed to be 0.499 at the state of failure.

Figure 8.34 shows the distribution of the average

stress in the core at the end of construction and after transient flow. Near the upstream side of the core, the average stress at the end of construction is less than the eventual seepage pressure for the lower half of the core height. This does not necessarily mean that there will be hydraulic fracture in these areas after impounding, as impounding increases the average total stress and reduces the risk of cracking.

8.8   Effects of the Strain-softening Modelling on the
       Stresses

In order to investigate the effects of the strain-softening modelling on the stresses, two cases D1 and ST1 must be compared. Direct comparison of these two cases, due to different geometries, is not possible. However, the major effect of the strain-softening modification is to correct the stress path. For case D1, post-failure stress paths are horizontal lines resulting in overshooting of the specified strengths (Figs. 8.14 to 8.16 and 8.19 to 8.21). For case ST1, there is no overshooting which results in a redistribution of stresses, and therefore, increase in stresses at those Gauss points that have not reached failure (Figs. 8.27 to 8.34). Also, this redistribution of stress may increase the size of the zone of failed soil.

For both cases D1 and ST1, impounding tends to increase average total stresses. For case D1, near the upstream

side of the core, the average effective stress at the end of transient flow is on average 89% of the average stress at the end of construction (Fig. 8.18). While for case ST1, near the upstream side of the core, the average effective stress at the end of transient flow is on average 60% of the average stress at the end of construction (Fig. 8.34). Near the upstream side of the core, for case D1 (Fig. 8.18) the mean stress at the end of construction is, on average, 45% of the mean total stress at the end of transient flow. For case ST1 (Fig. 8.34) this becomes 60% near the core centre line, for case D1 (Fig. 8.17), the average effective stress at the end of transient flow is greater for the lower 2/3 of the core height, and is smaller for the upper 1/3 of the core height than the average stress at the end of construction. For case ST1 (Fig. 8.34), near the core centre line, the average effective stress at the end of transient flow is smaller than the average stress at the end of construction, for the core's full height.

For case D1, near the upstream side of the core, the mean effective stress at the end of flooding is, on average, 65% of the mean stress at the end of construction, and the mean stress at the end of construction is, on average, 52% of the mean total stress at the end of flooding (Fig. 8.13). Near the core centre line, these percentages are 64% and 56% respectively (Fig. 8.12).

From comparison of these results, it is clear that for case D1, where the strain-softening behaviour is not

modelled, the flooding is more critical than the transient flow, from the point of view of drained hydraulic fracture. However, after correct modelling of the strain-softening behaviour, the transient flow can be more critical than flooding for drained hydraulic fracture to occur.

8.9   Conclusions

The non-linear finite element programme (explained in Chapter 2) was used to analyse the stresses and stress changes in an idealised vertical core.   The effects of the shells on the core were modelled by using the side boundary conditions shown on Fig. 8.1.

From these studies it is concluded that:

1.   The special side boundary conditions used in these analyses tends to magnify the amount of load transfer from the core to the side supports (shells).   This arching effect can be reduced by decreasing the shear strength of the core material to produce a zone of failed soil at the sides between the core and supports.

2.   Generally, the agreement between values of vertical stresses from the finite element analysis (undrained and drained) and those given by plasticity solutions is good, provided that failure has occurred.

3.   At the end of undrained construction, the finite element results for C_u = 30 KPa are a maximum of 30% greater near the top of the core, and a maximum of 8% smaller near the base of the core, than those given by

Nonveiller and Anagnosti (1961). Results given by Bishop (1952) are a maximum of 15% greater than the finite element results for C_u = 30 KPa.

4.   At the end of drained construction, the finite element results are about 2% more than those given by Nonveiller and Anagnosti (1961) for the lower 1/3 of the core height. For the upper 2/3 of the core height, both solutions give the same value for the vertical stress.

5.   There is a possibility of drained hydraulic fracture for areas where the average total stress at the end of construction is less than the eventual seepage pressure. However, impounding tends to increase the total stress prior to hydraulic fracture and so reduce the cracking risk (as predicted by Vaughan, 1976b). Thus a critical situation is likely only if this increase is insufficient to prevent fracture.

6.   During impounding, stress predictions show stress paths exhibiting strain-softening behaviour. If this behaviour is not modelled correctly, a stress path which violates the failure criterion will be followed.

7.   Correct modelling of the strain-softening behaviour results in the redistribution of stresses. This stress redistribution reduces the risk of cracking.

Table 8.1   Main Cases for the Embankment Dam Core

Case No.	Stress-Strain Curve (Fig.No.)	Soil Unit Weight γ_t KN/M³	Water Unit Weight γ_w KN/M³	Loading Sequences	Soil Properties		
					Poisson's* Ratio ν	Strength	Initial Modulus
U1	8.2	20	10	Construction	0.499	$C_u = 60$ KPa & $C_u = 30$ KPa	$E_i = 300\ C_u$
D1	8.3	20	10	Construction followed by impounding	$\nu_i = 0.2$ $\nu_t = \nu_i (1-\sigma_r) + 0.5\sigma_r$	$C' = 10$ KPa & $\phi' = 25^O$	$E_i = 300\ \tau_{max}$
ST1	8.4	20	10	Construction followed by impounding	0.2 At Failure 0.499	$C' = 20$ KPa $\phi' = 32^O$	$E_i = 300\ \tau_{max}$

* $\sigma_r = (\sigma_1 - \sigma_3)/(\sigma_1 - \sigma_3)_f$

6 m

℄

Total number
of elements = 120

Total number
of nodes = 407

K_s

K_s

30 m
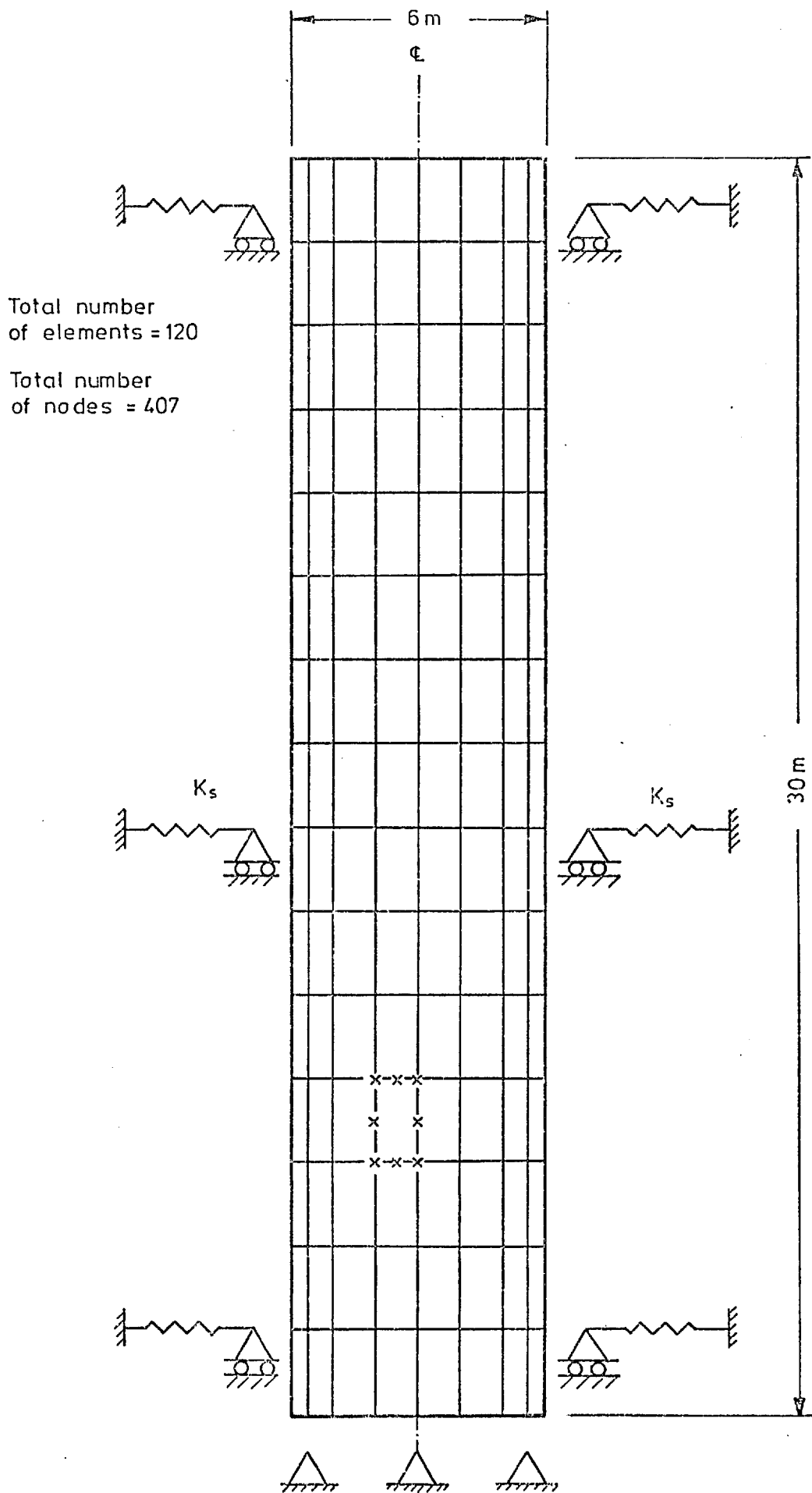
Fig. 8.1   The mesh used for the embankment core
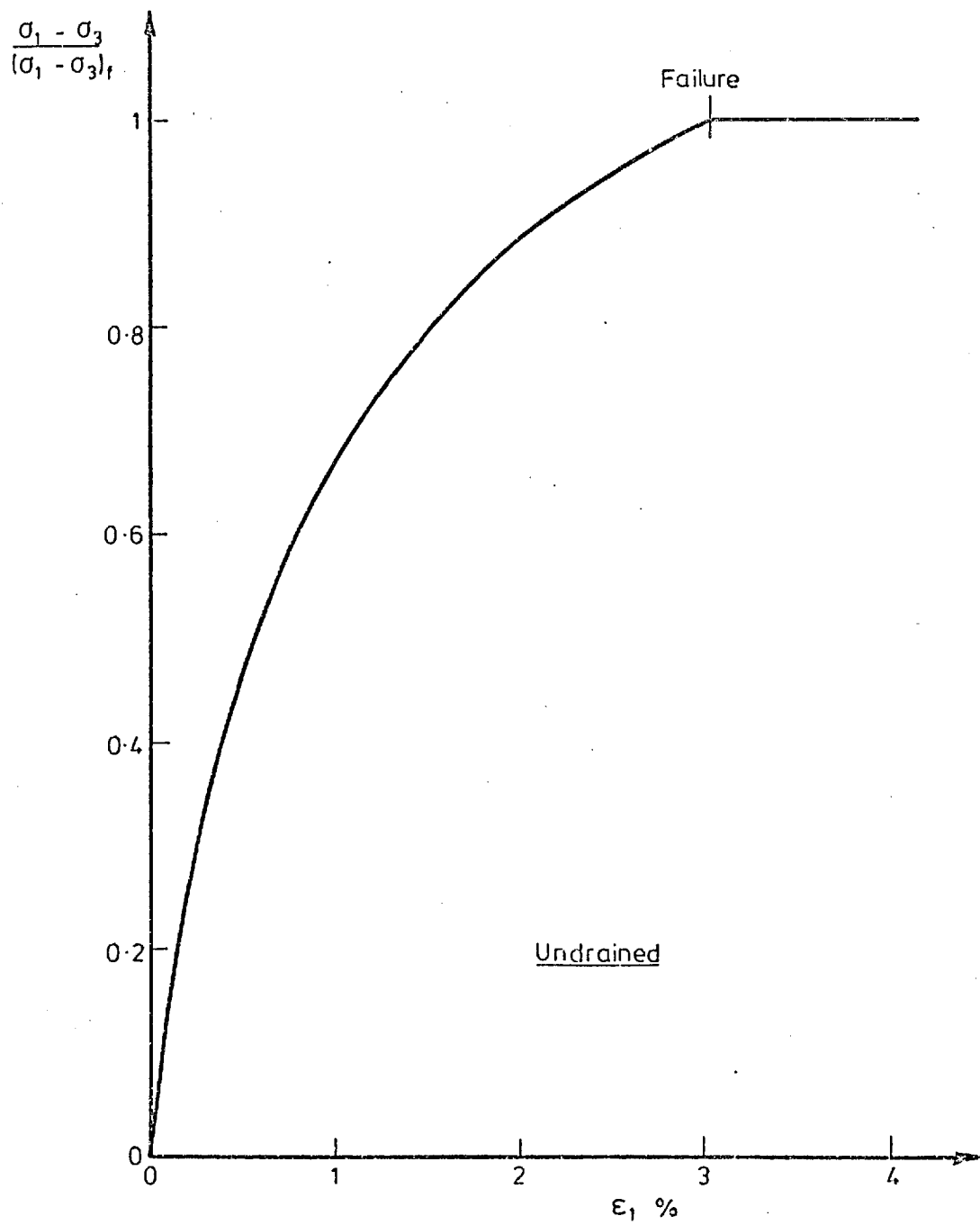
Fig. 8.2   The Stress-Strain Curve (Plane Strain)
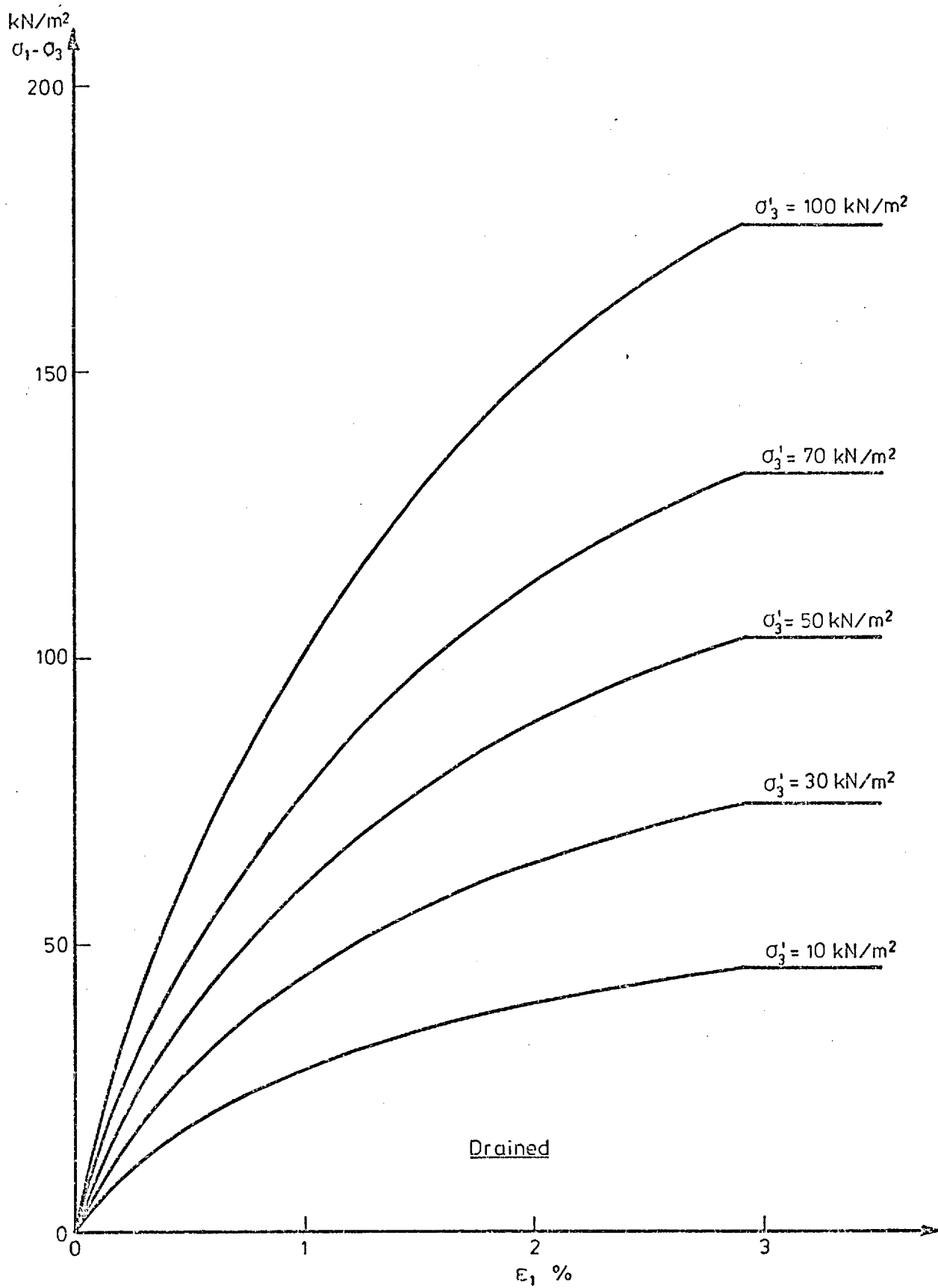
Fig. 8.3   The Stress-Strain Curve (Plane Strain)
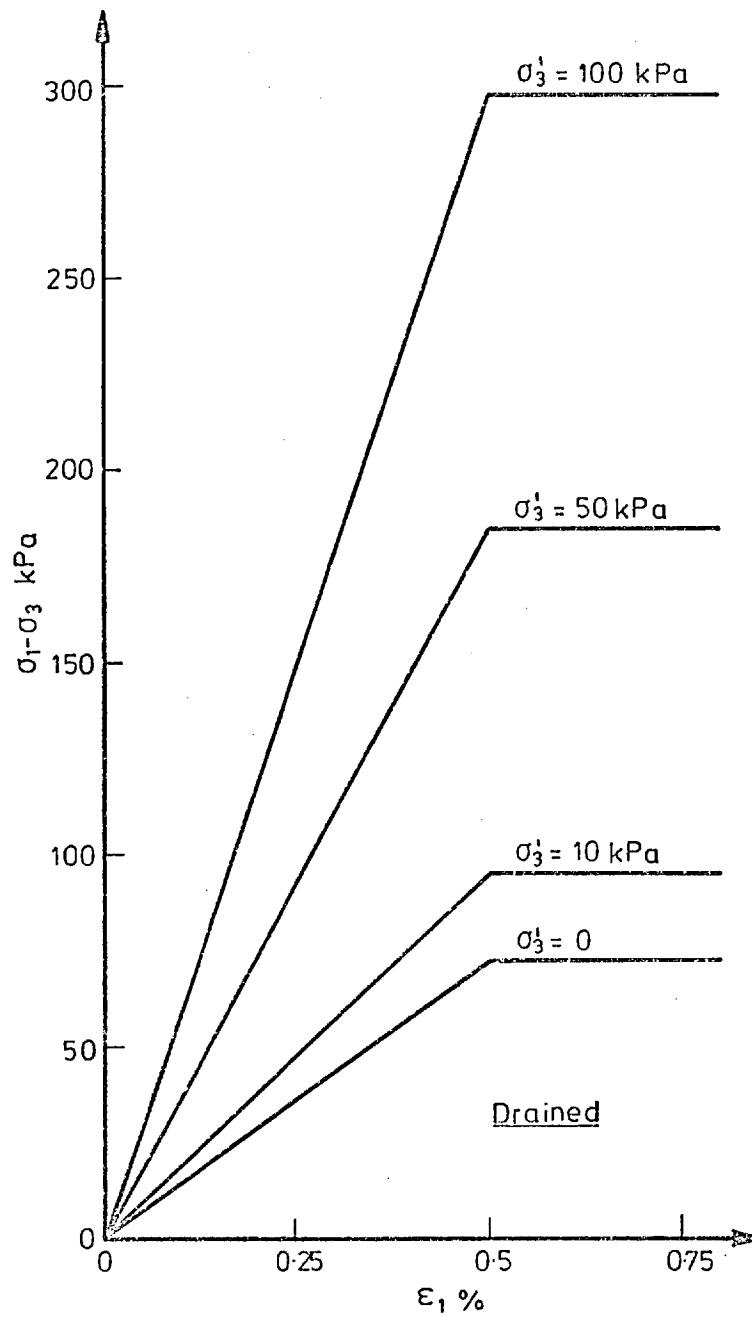
Fig. 8.4   The Stress-Strain Curve (Plane Strain)
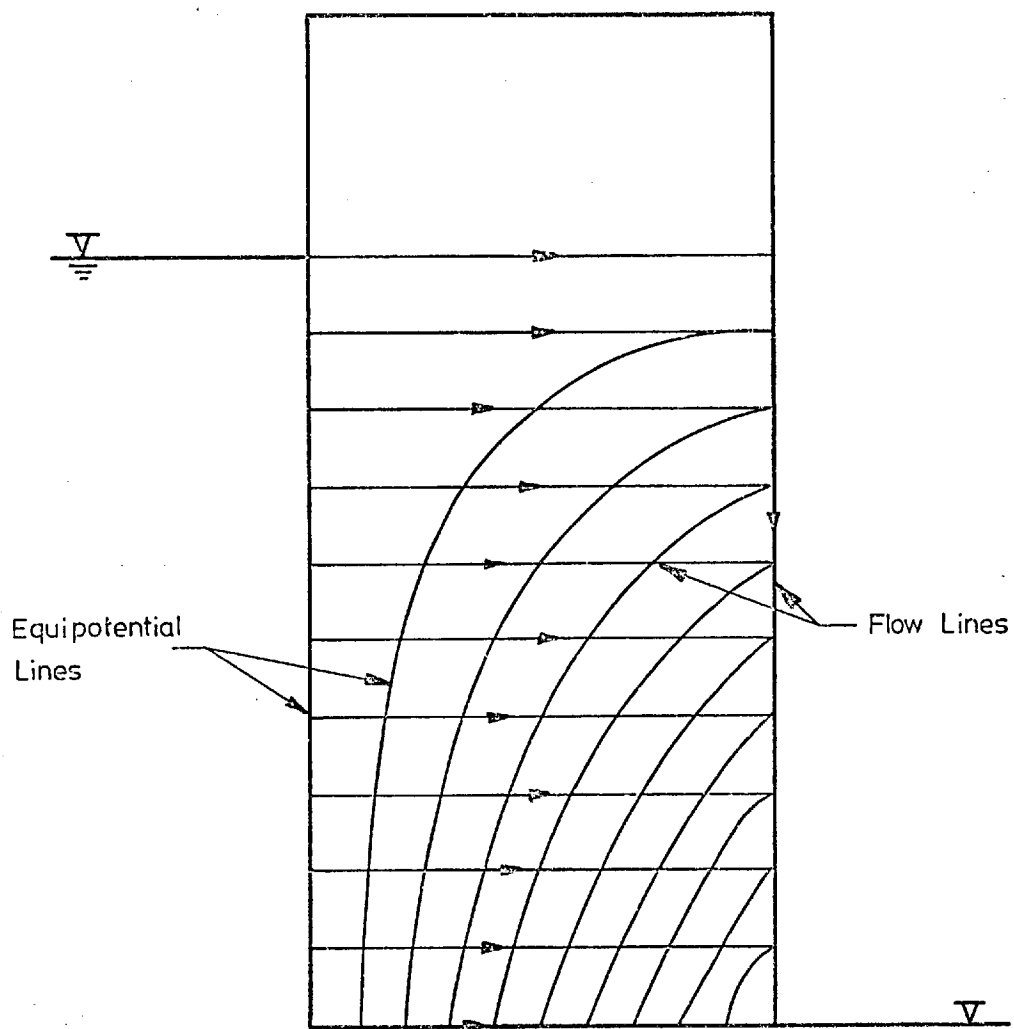
Fig. 8.5   The Flow Net for Impounding of the
Transient Flow Form

a) Point 1

b) Point 2

Case A: the side boundaries, vertically free and horizontally fixed
Case B: the side boundaries as shown on Fig. 8·1
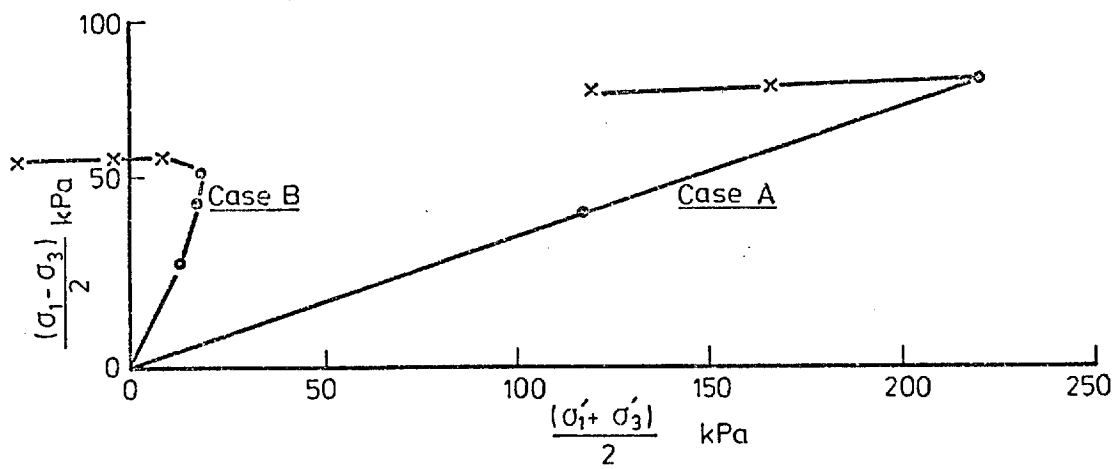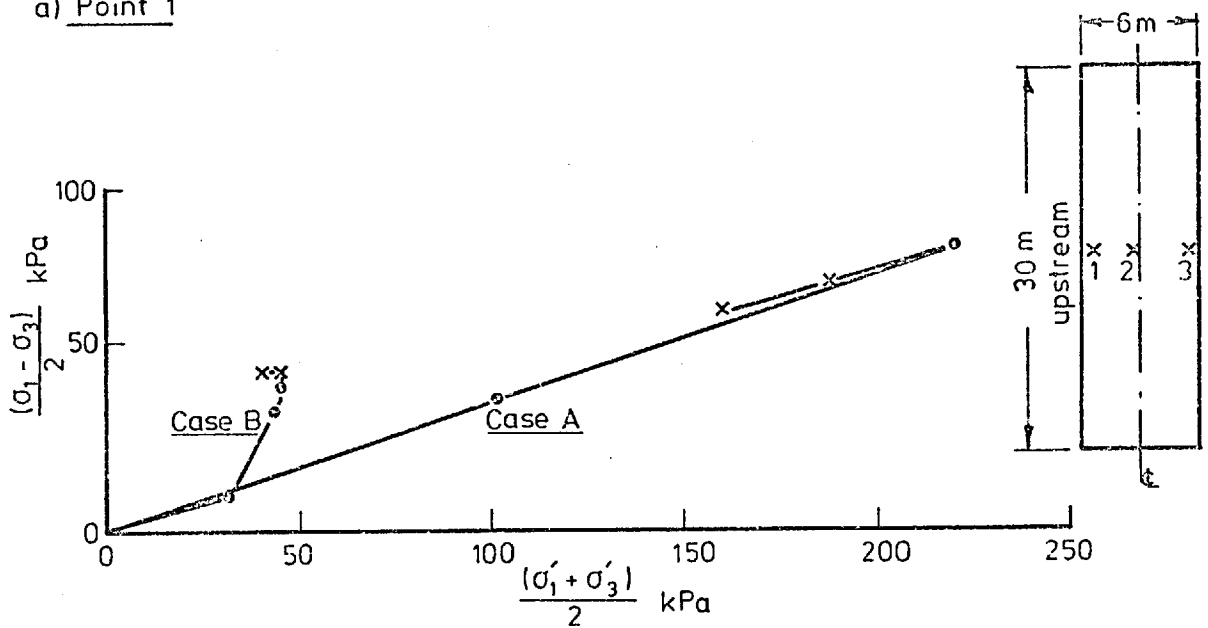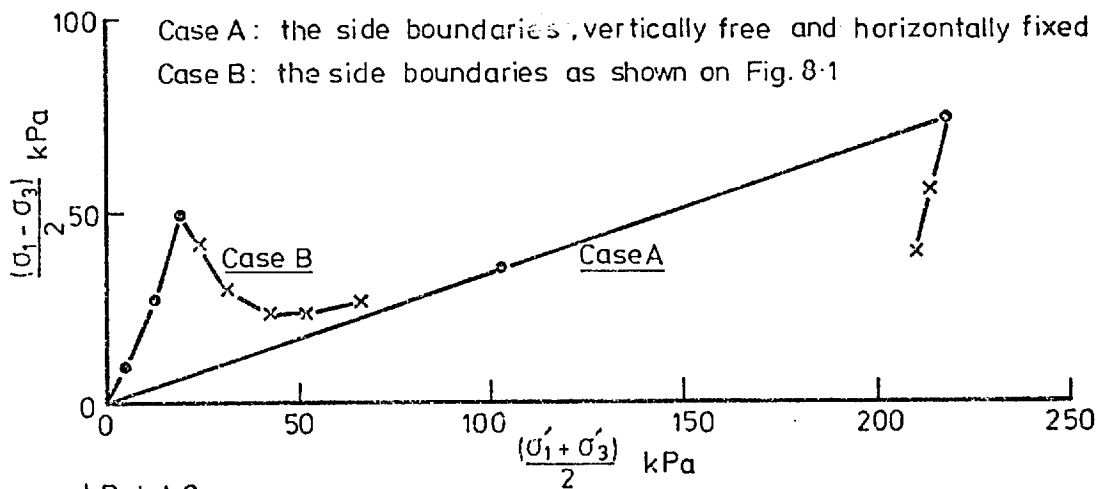
c) Point 3

Construction   o
Transient flow   x

Fig. 8.6   Effect of the Side Boundary Conditions on the Stress Paths
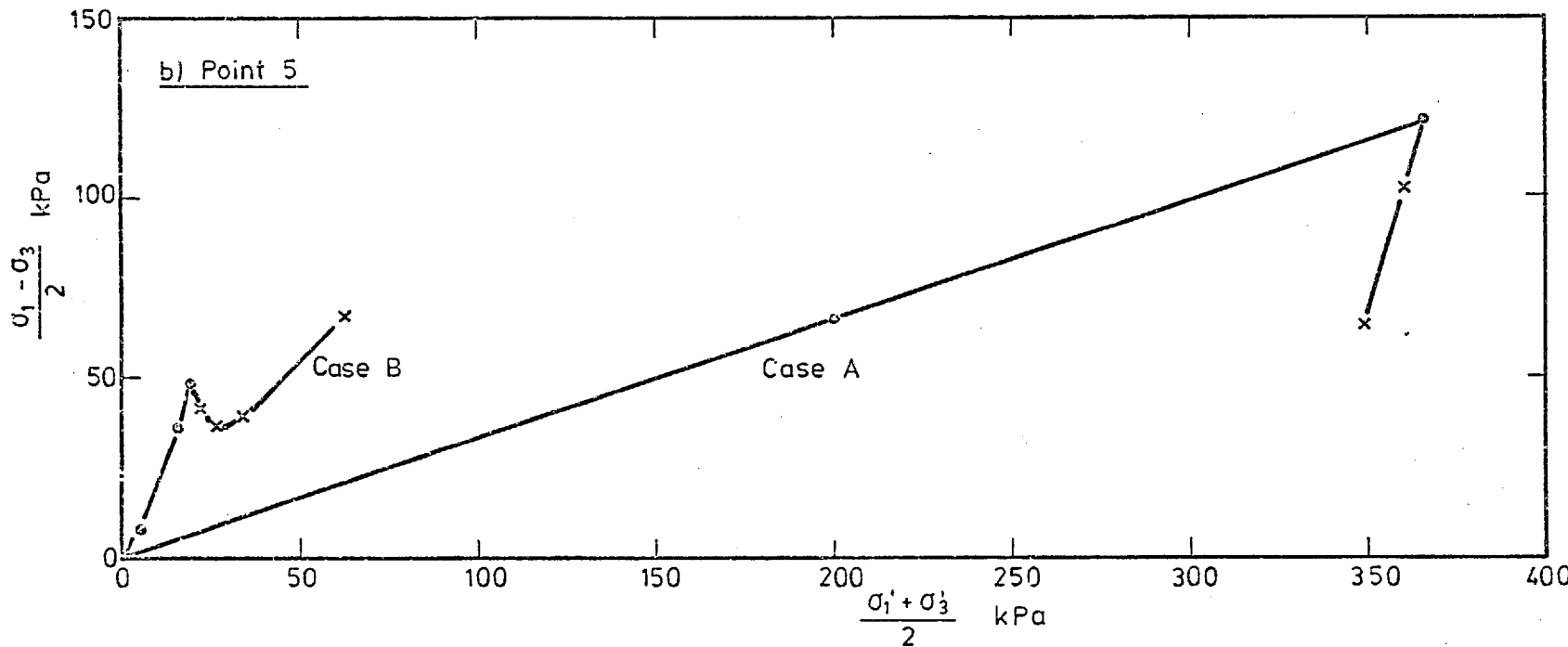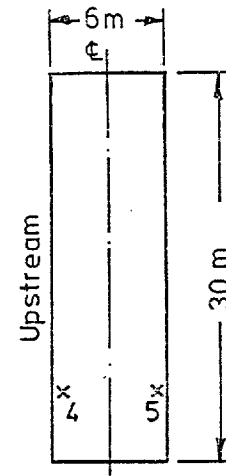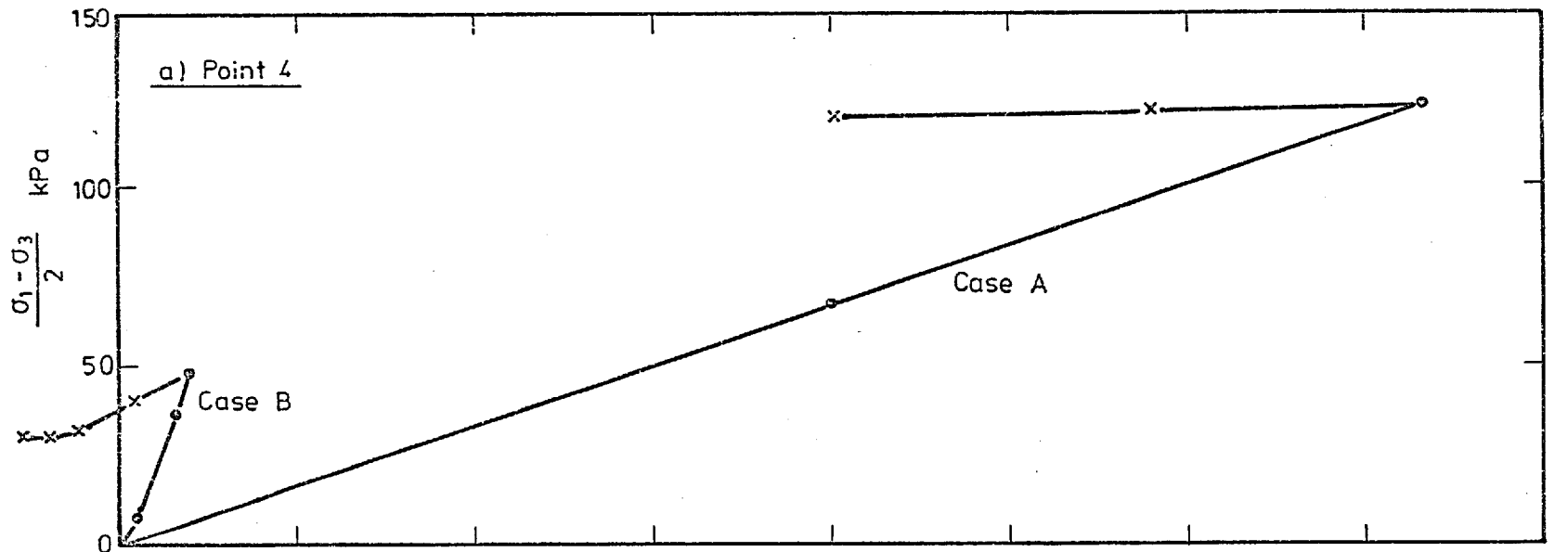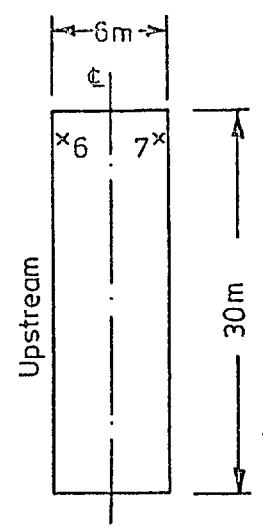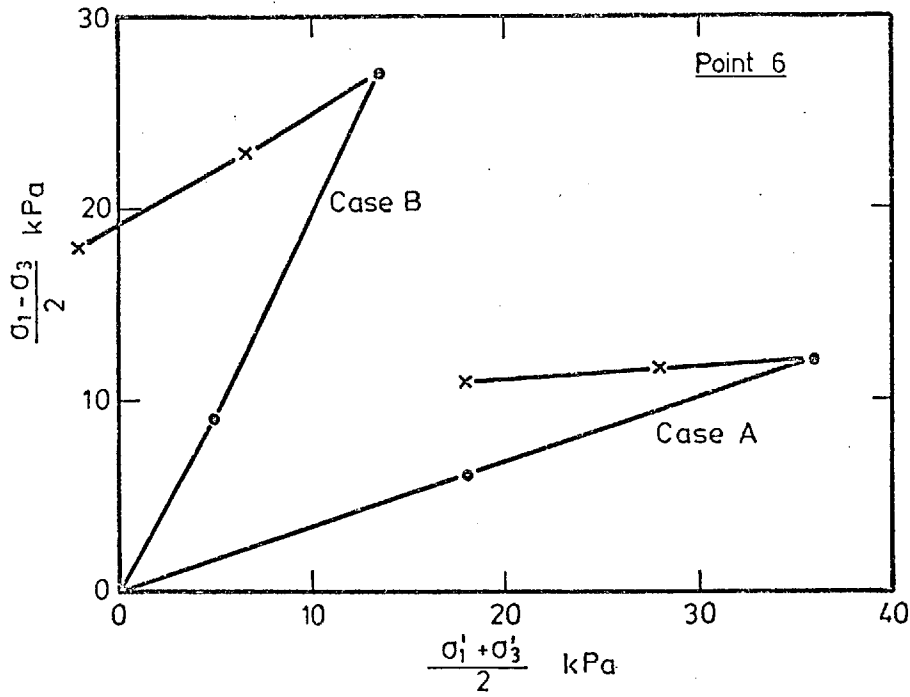
Fig. 8.7   Effect of the Side Boundary Conditions on the Stress Path
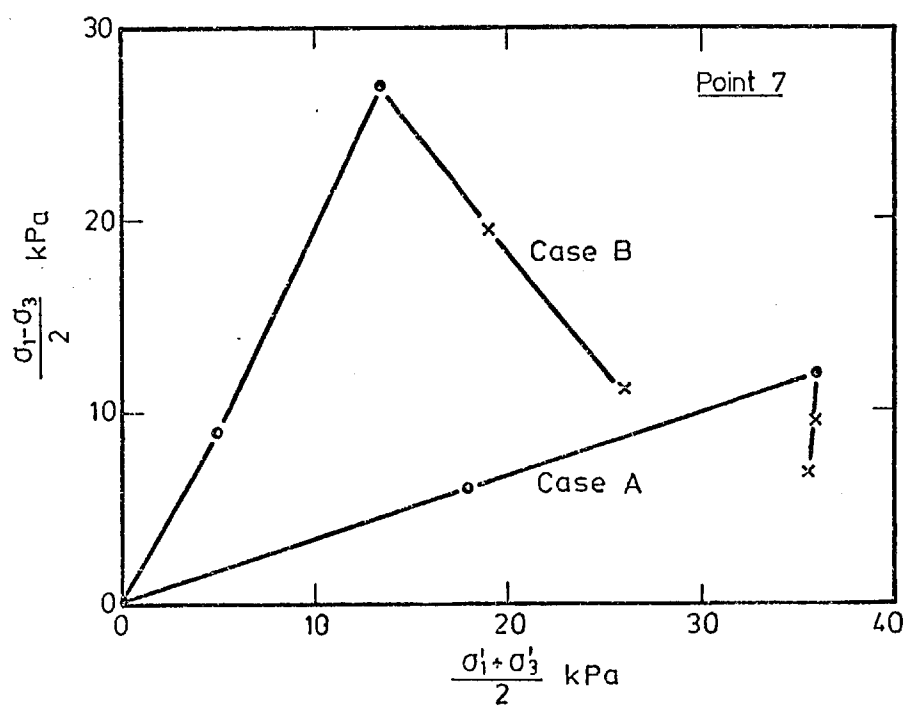
Fig. 8.8 Effect of the Side Boundary Conditions on the Stress Paths

Fig. 8.9a   Zones of the Failed Soil at the End of
            Undrained Construction (Case U1)
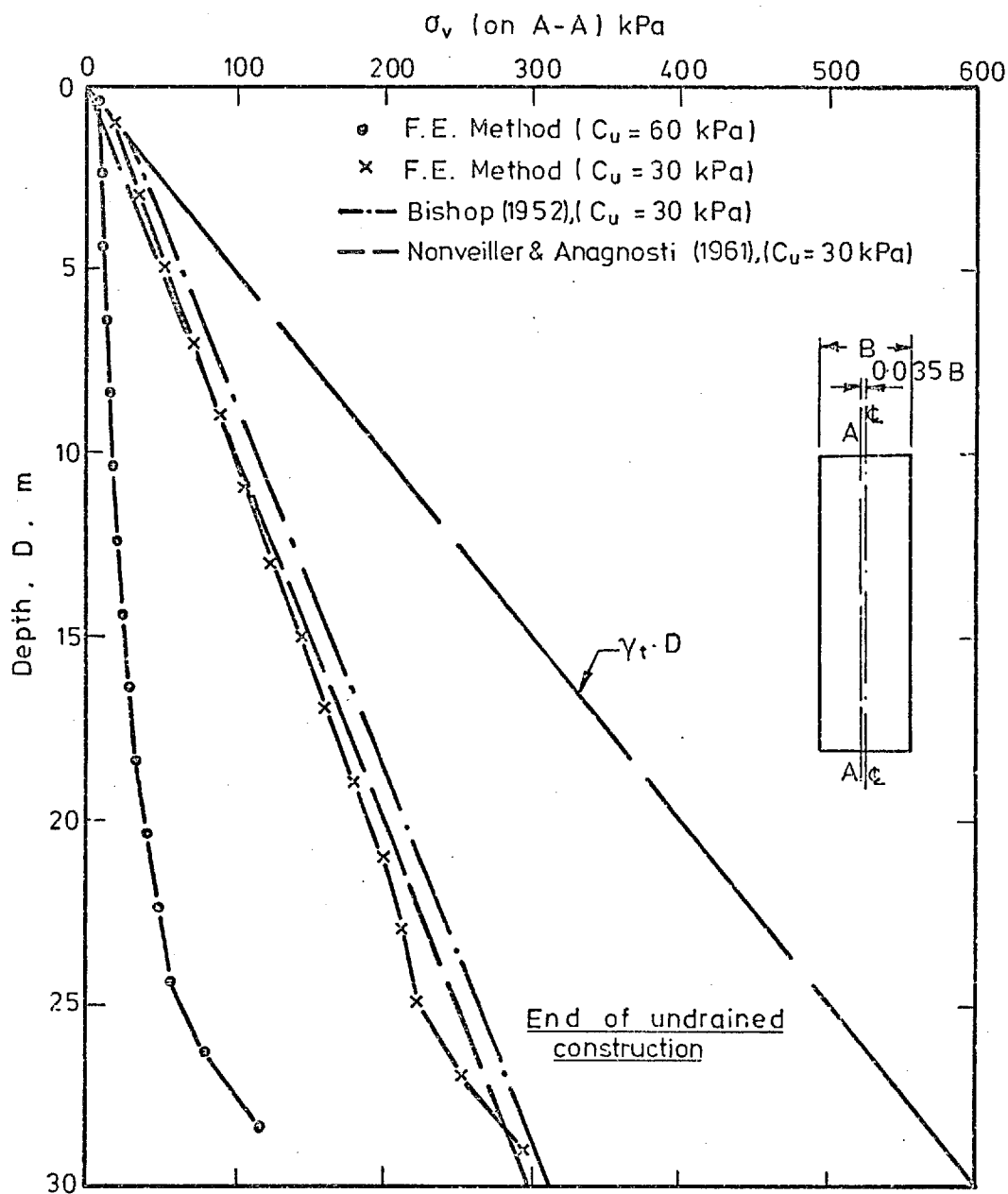
Fig. 8.9b   Values of the Vertical Stresses (Undrained)
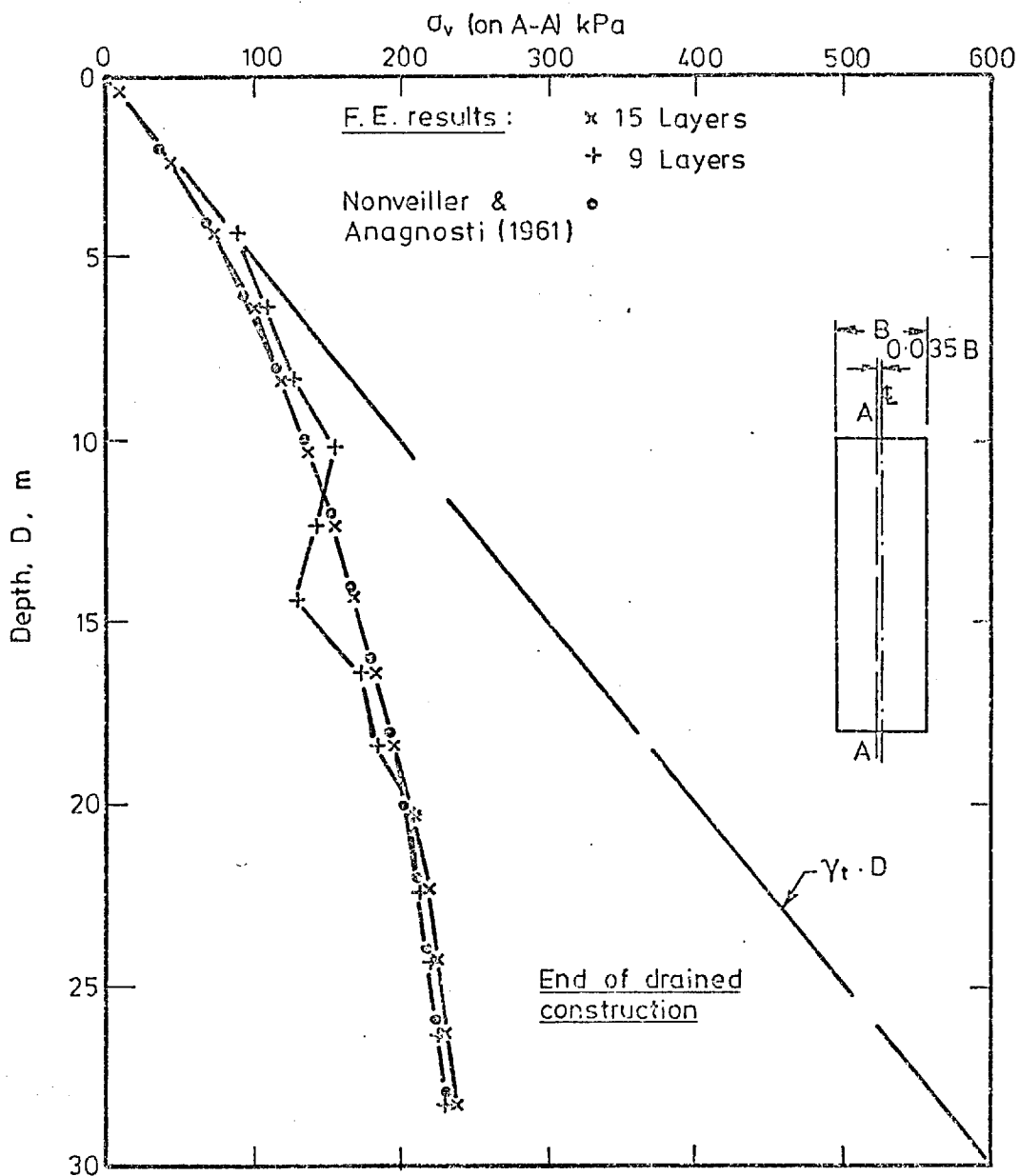
Fig. 8.10   Values of the Vertical Stresses (Drained)

a) End of   b) End of
   construction   flooding

c) End of transient flow
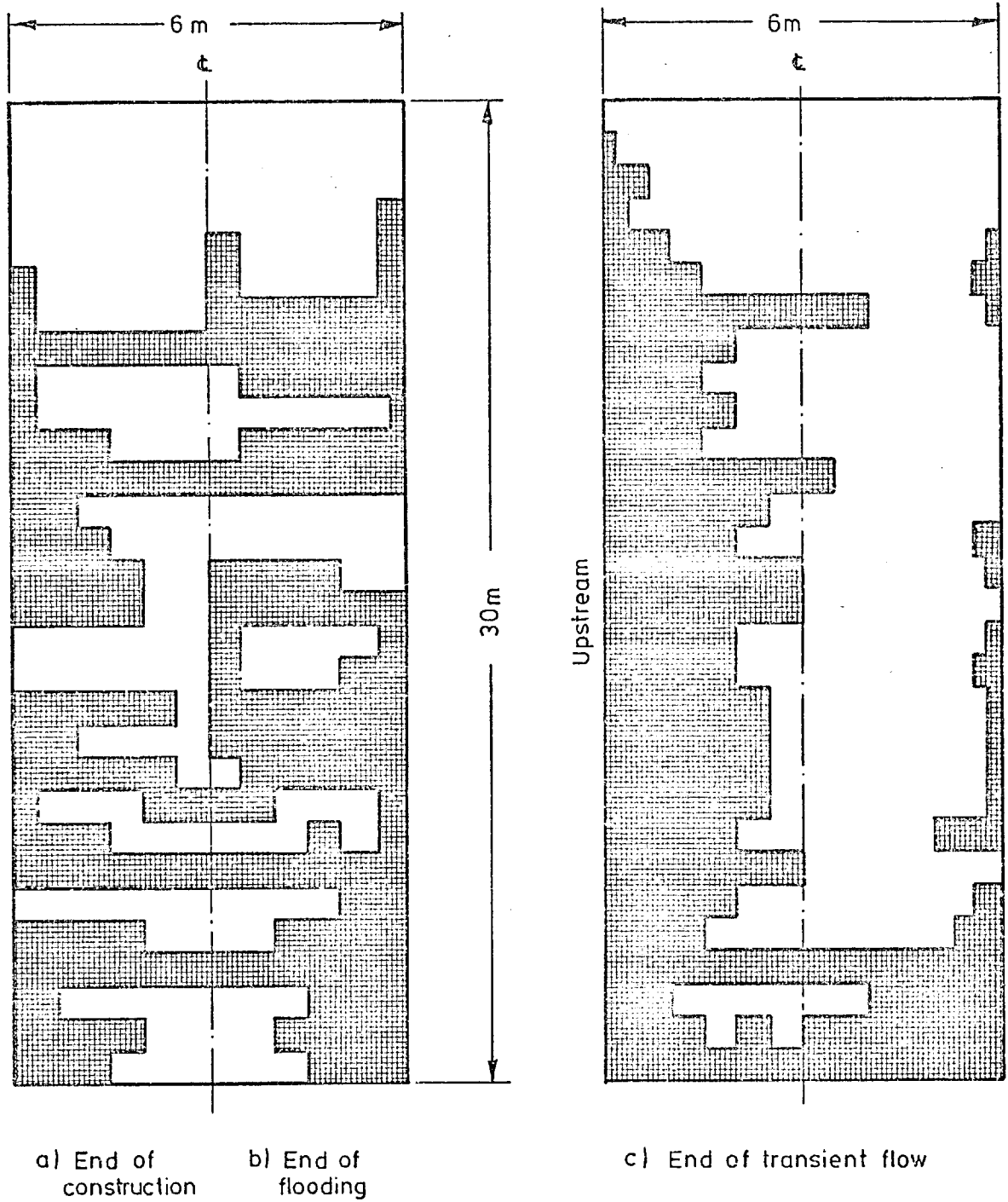
Fig. 8.11   Zone of the Soil at Failure (Case D1)
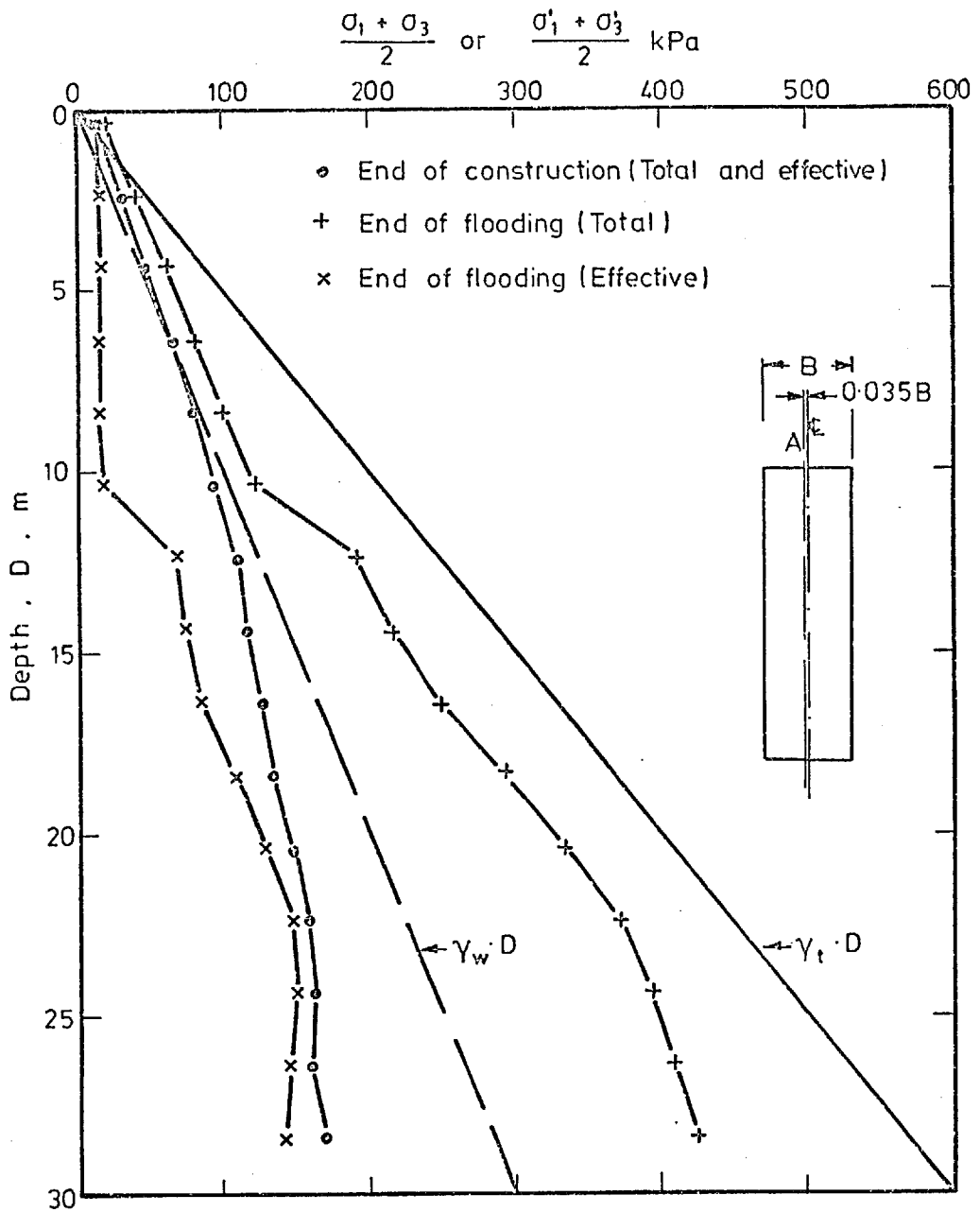
Fig. 8.12 Values of the Average Stresses on A-A
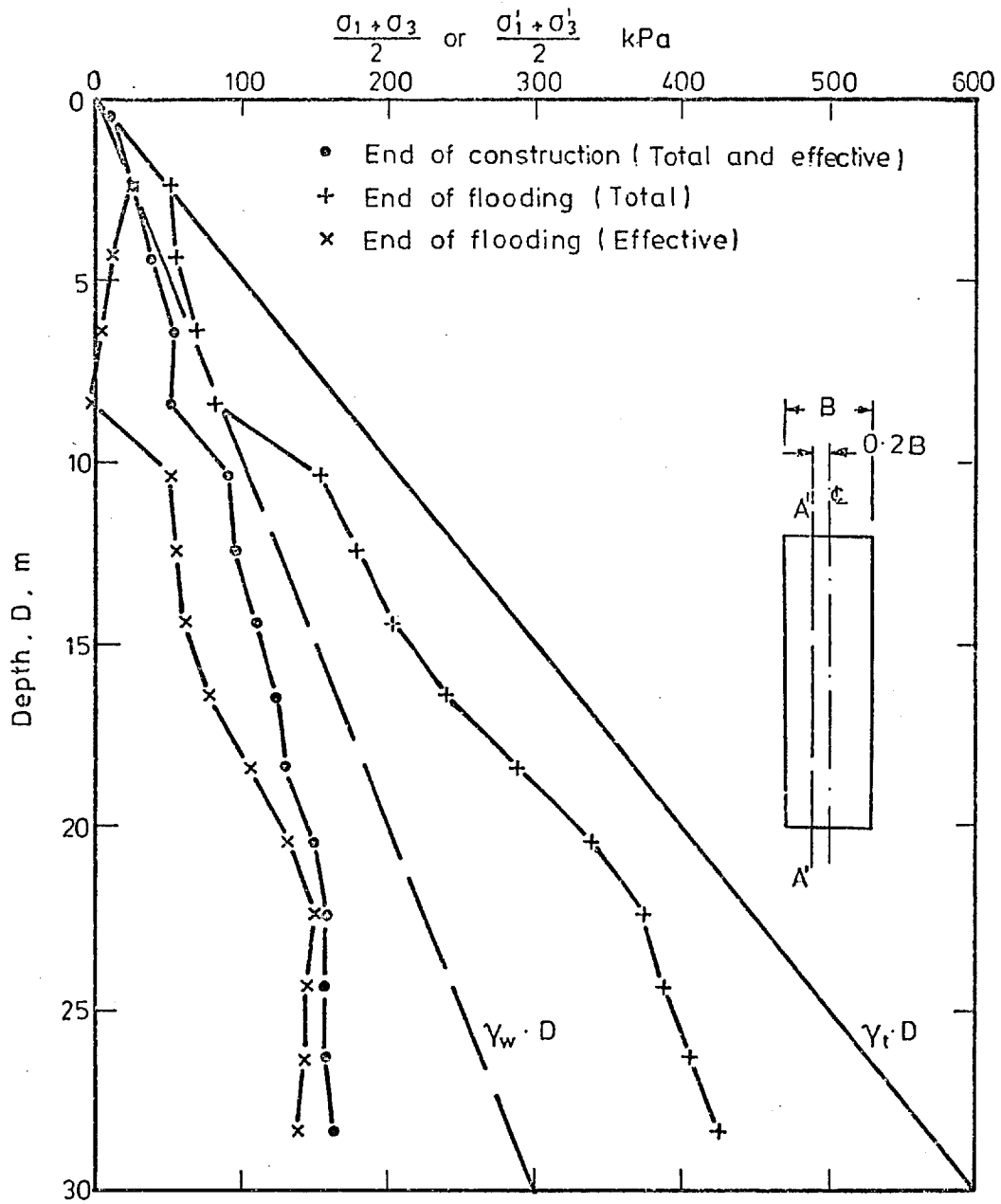
Fig. 8.13   Values of the Average Stresses on A'-A'
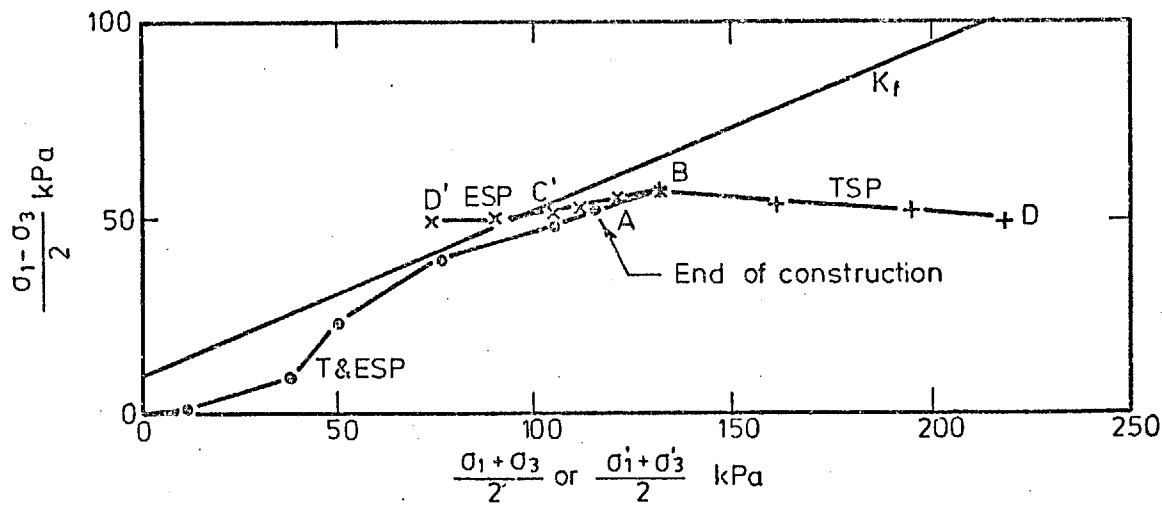
Fig. 8.14   The Stress Path at <u>Point 1</u>
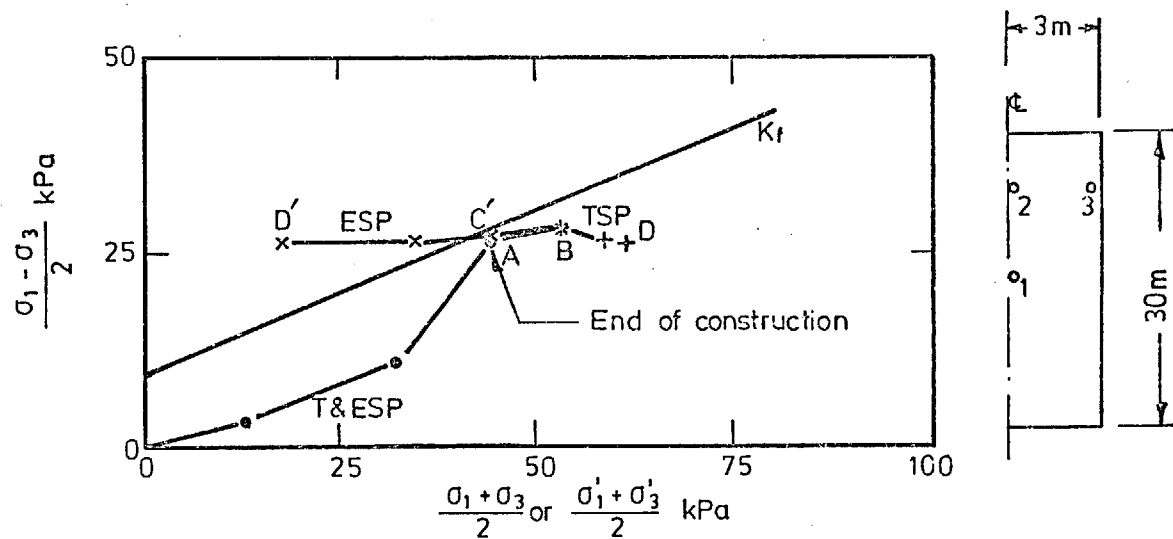
Fig. 8.15   The Stress Path for <u>Point 2</u>
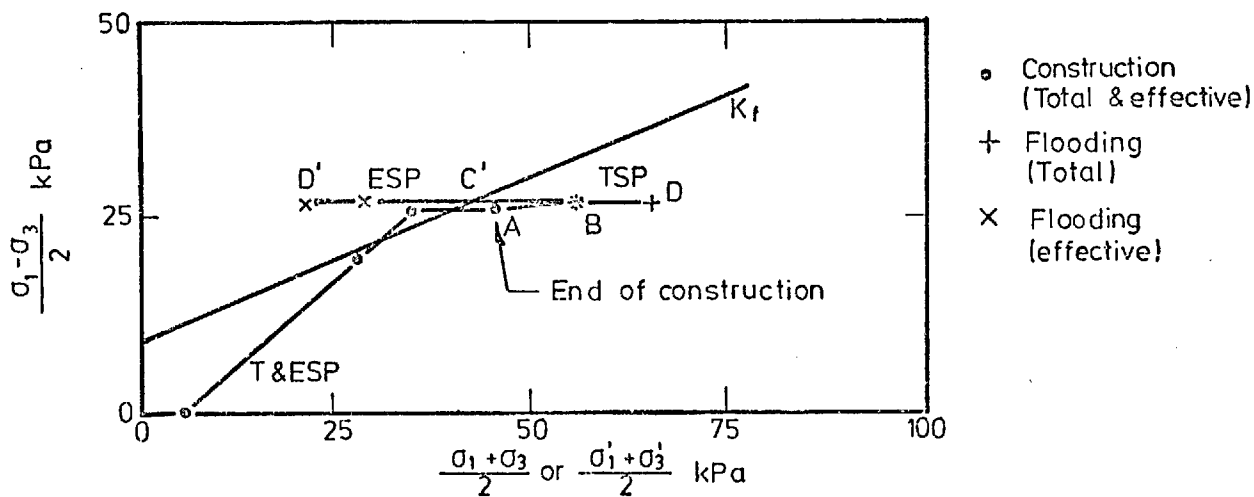
Fig. 8.16   The Stress Path for <u>Point 3</u>
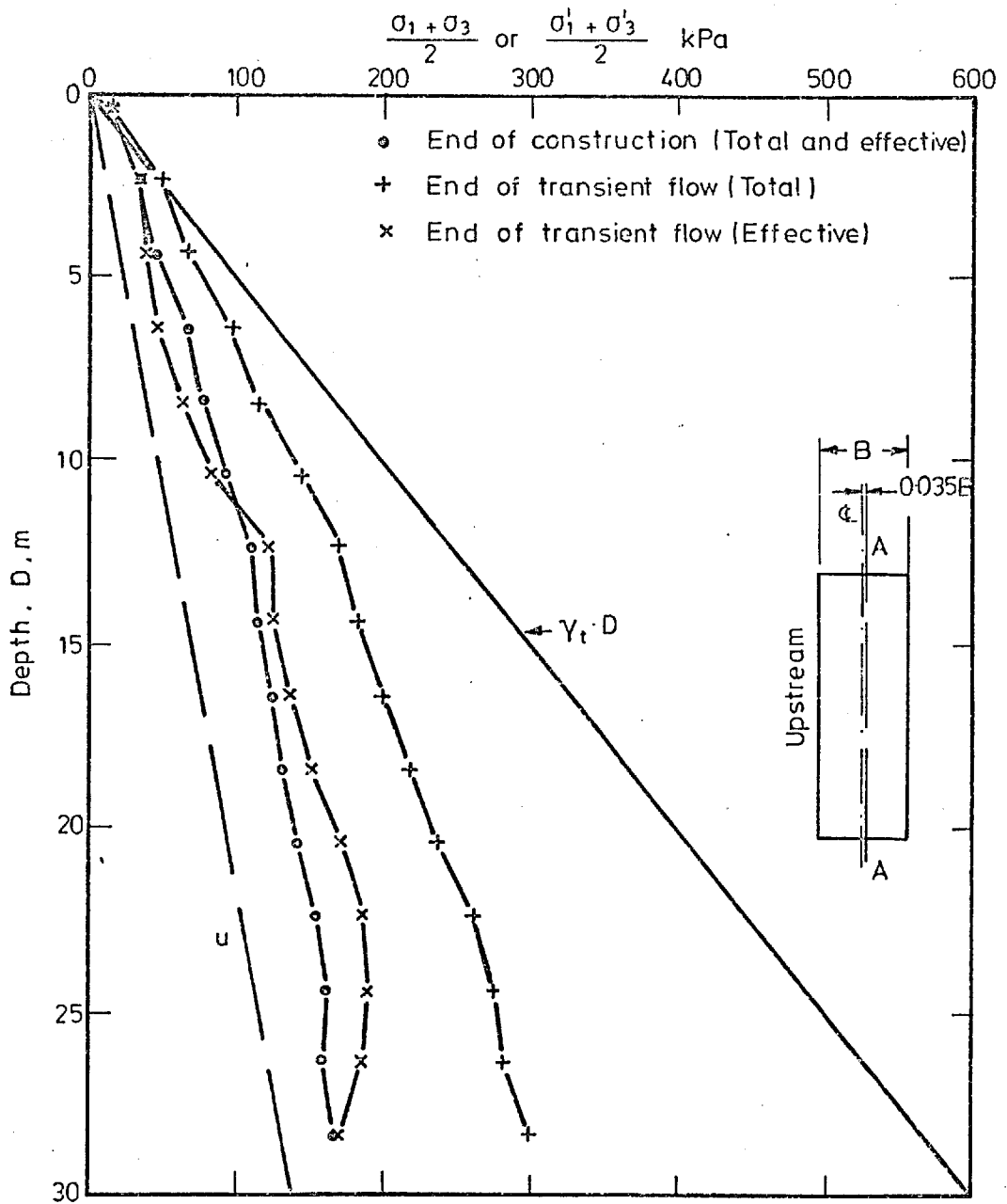
Fig. 8.17 Values of the Average Stresses on A-A
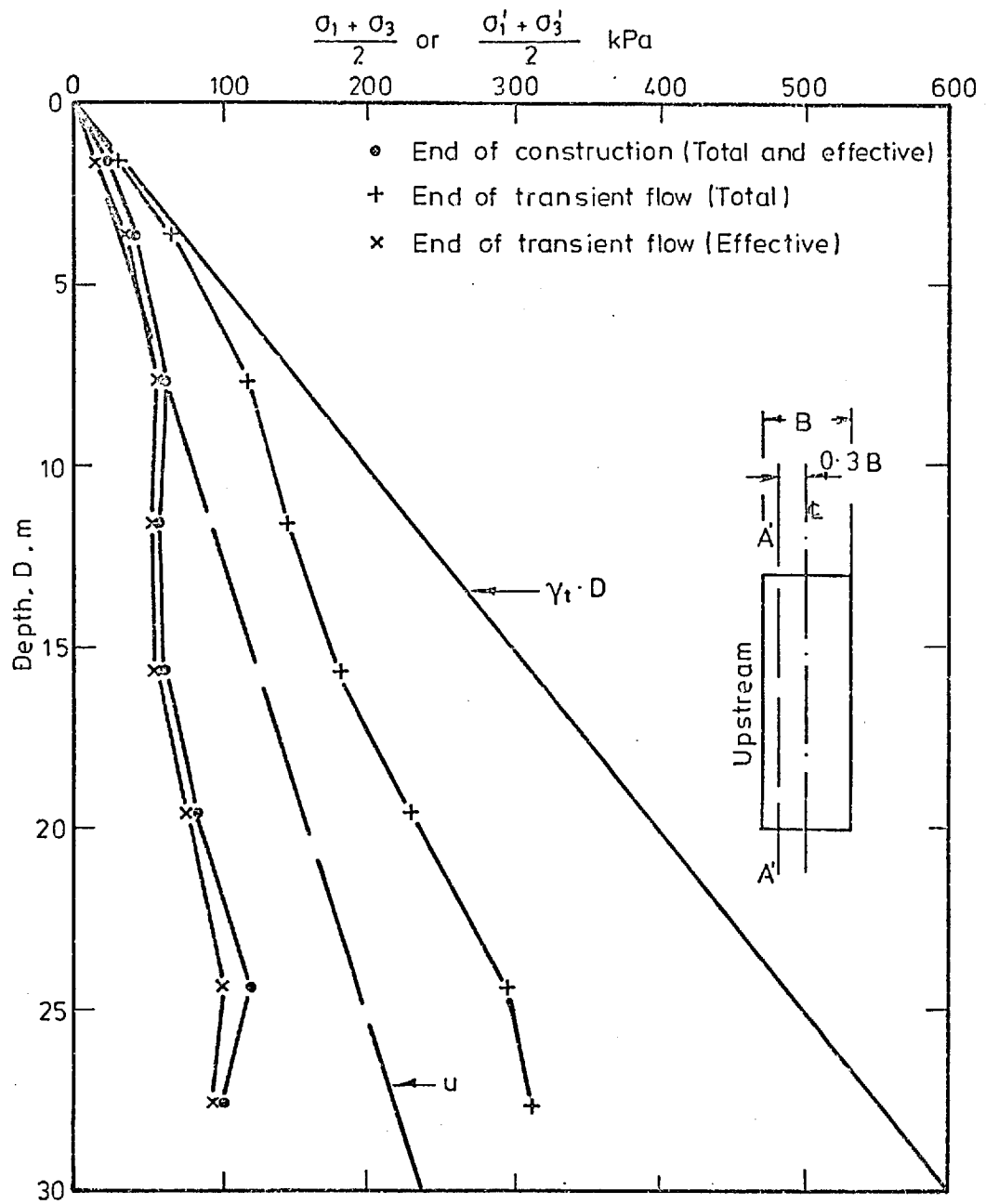
Fig. 8.18   Values of the Average Stresses on A'-A'

Fig. 8.19   The Stress Path for <u>Point 1</u>
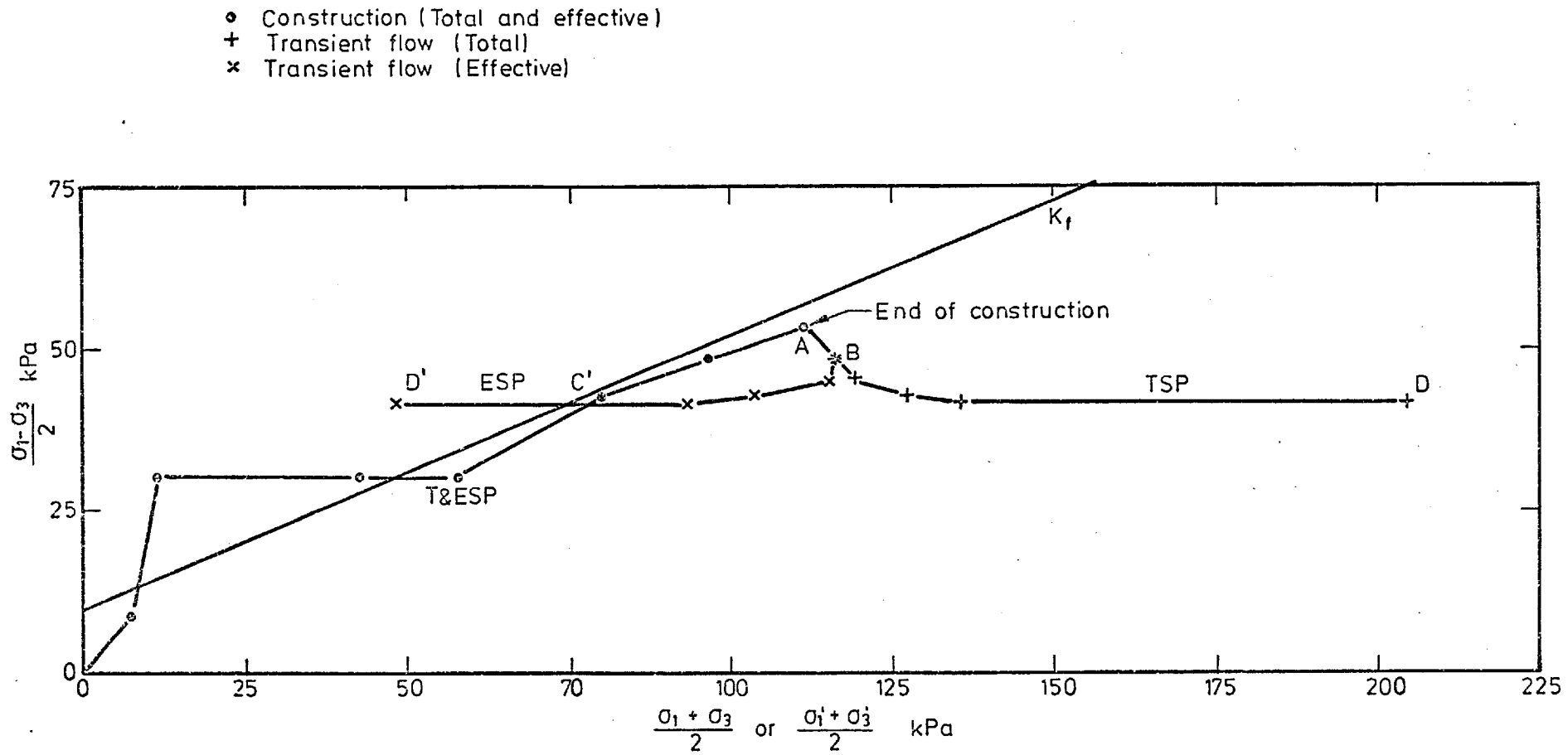
CASE   D1

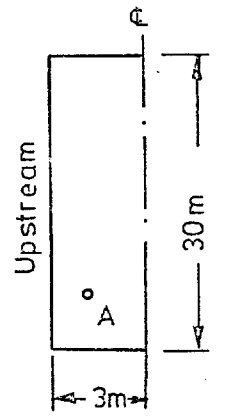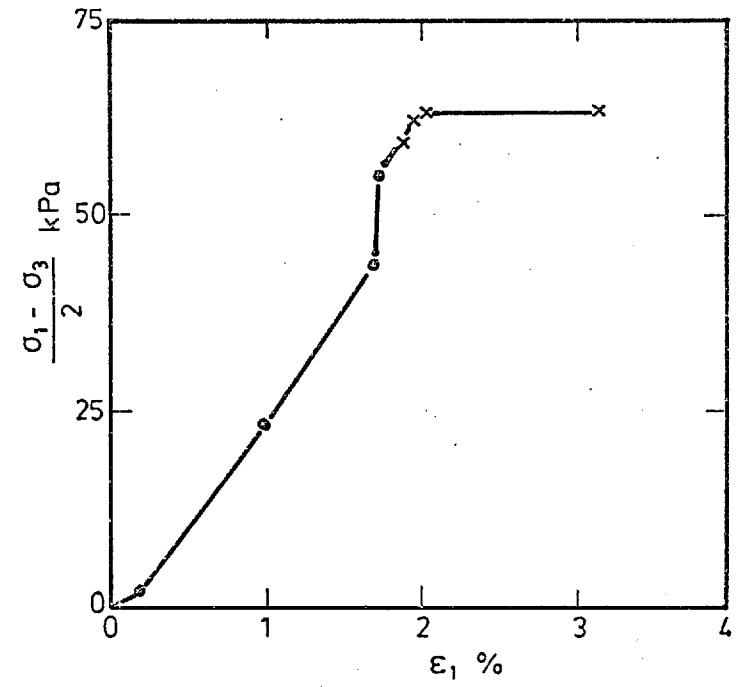Fig. 8.20   The Stress Path for Point 2

CASE   D1

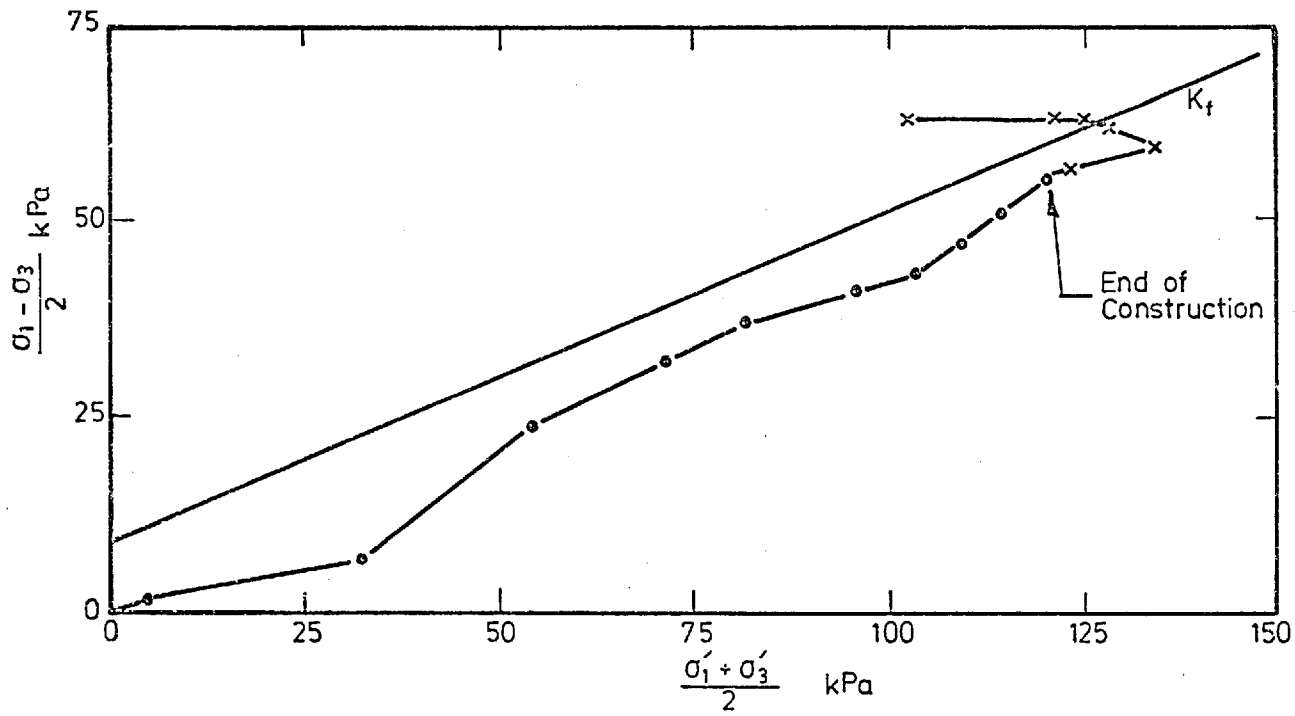Fig. 8.21   The Stress Path for Point A

CASE   D1

Fig. 8.22   Values of the Average Effective Stresses
on A-A
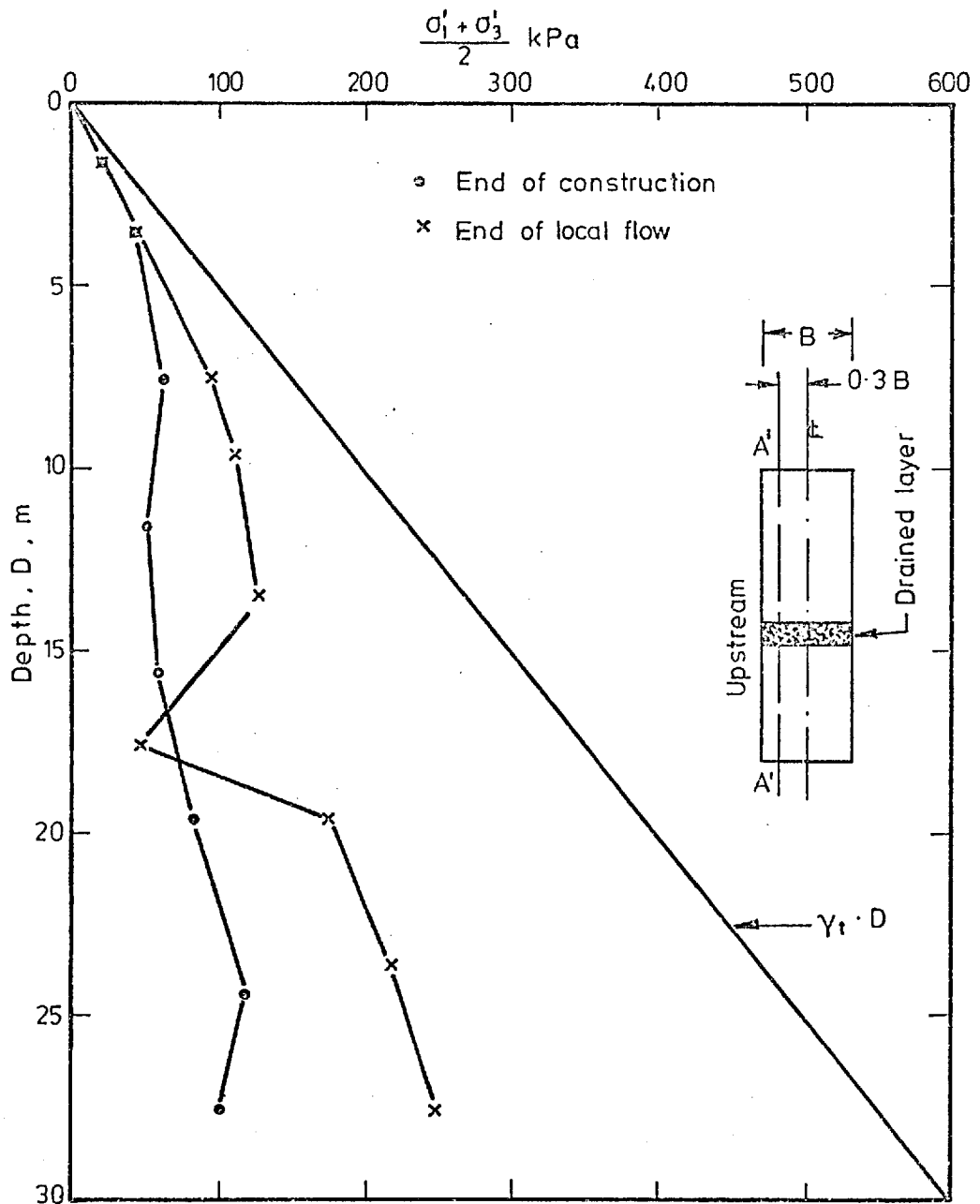
Fig. 8.23   Values of the Average Effective Stresses
on A'-A'
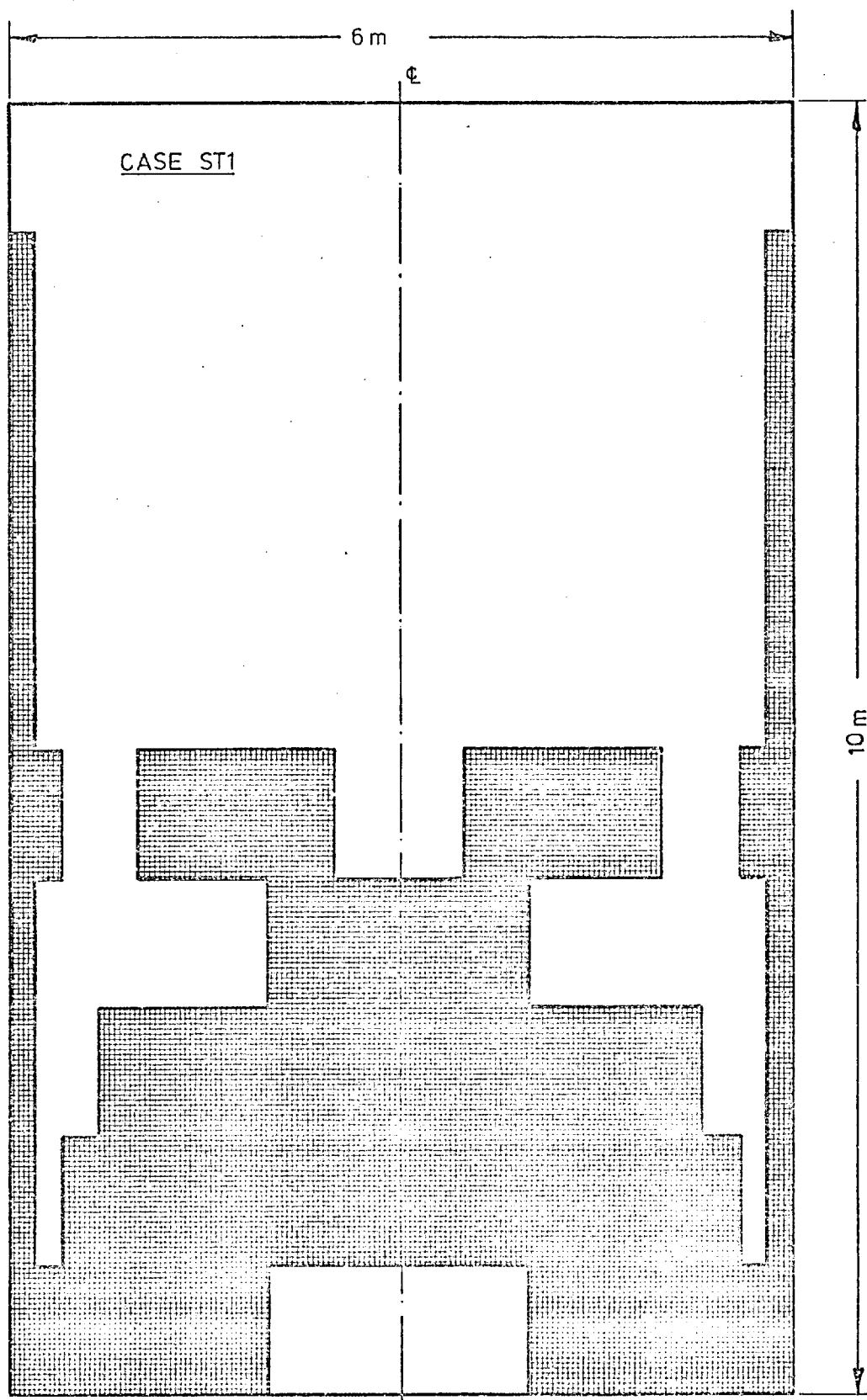
Fig. 8.24   Zone of the Soil at Failure
(End of Construction)
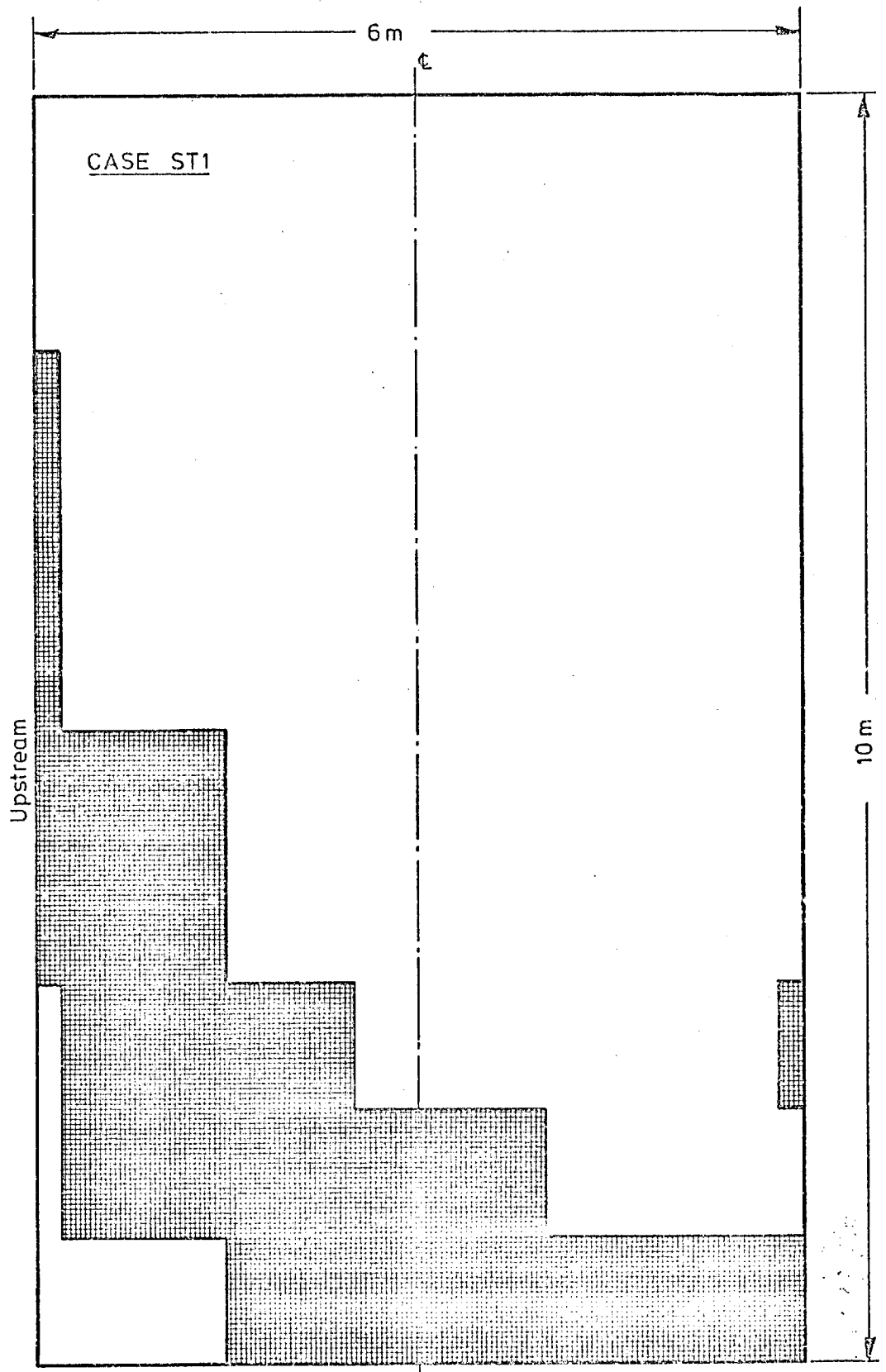
Fig. 8.25 Zone of the Soil at Failure
(End of Transient Flow)
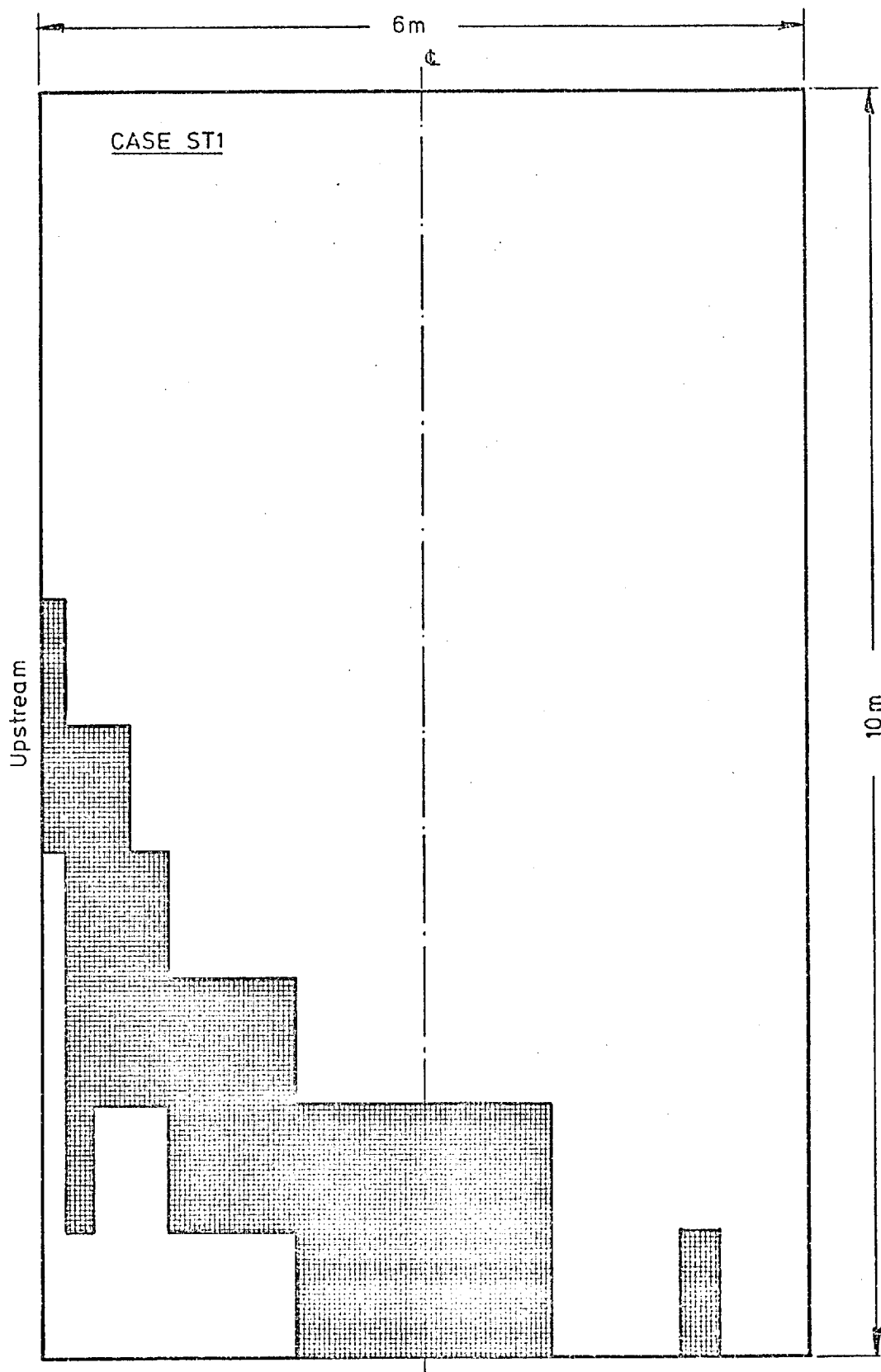
Fig. 8.26   Zone of the Soil Exhibiting Strain-
Softening Behaviour
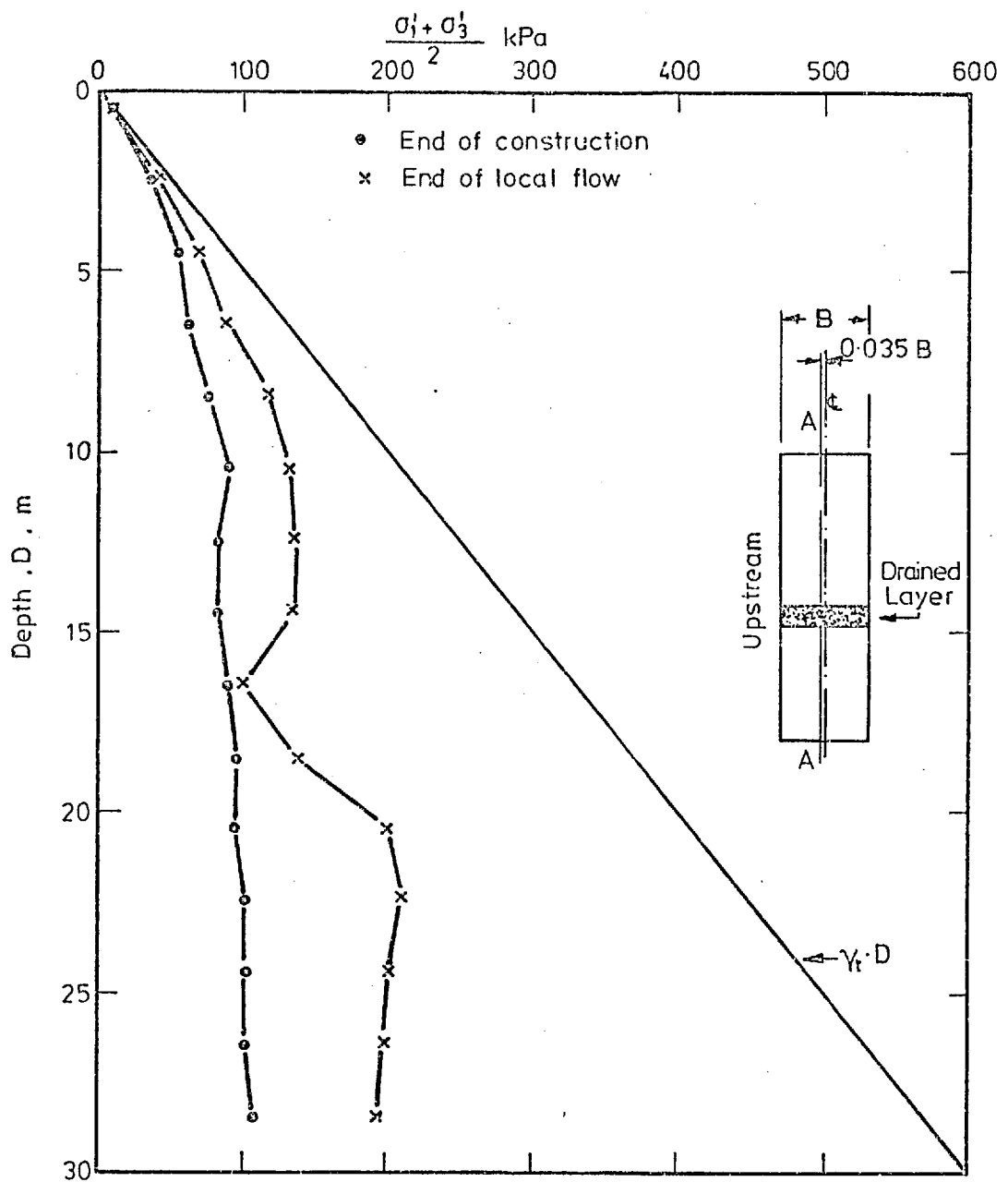(End of Transient Flow)

Fig. 8.27   The Stress Path for <u>Point 1</u>

CASE ST1

450

Fig. 8.28   The Stress Path for <u>Point 2</u>

CASE   ST1

Fig. 8.29   The Stress Path for Point 3

CASE   ST1

Fig. 8.30 The Stress Path for Point 4

CASE ST1

Fig. 8.31   The Stress Path for Point 5

CASE ST1

Fig. 8.32   The Stress Path for <u>Point 6</u>

CASE ST1

455
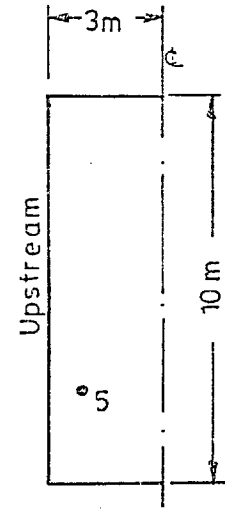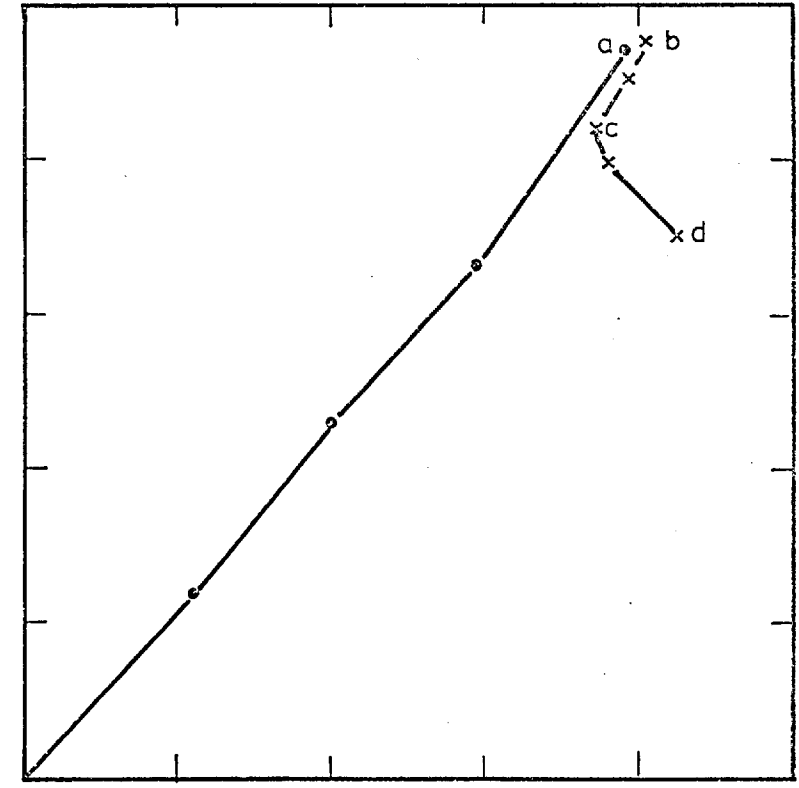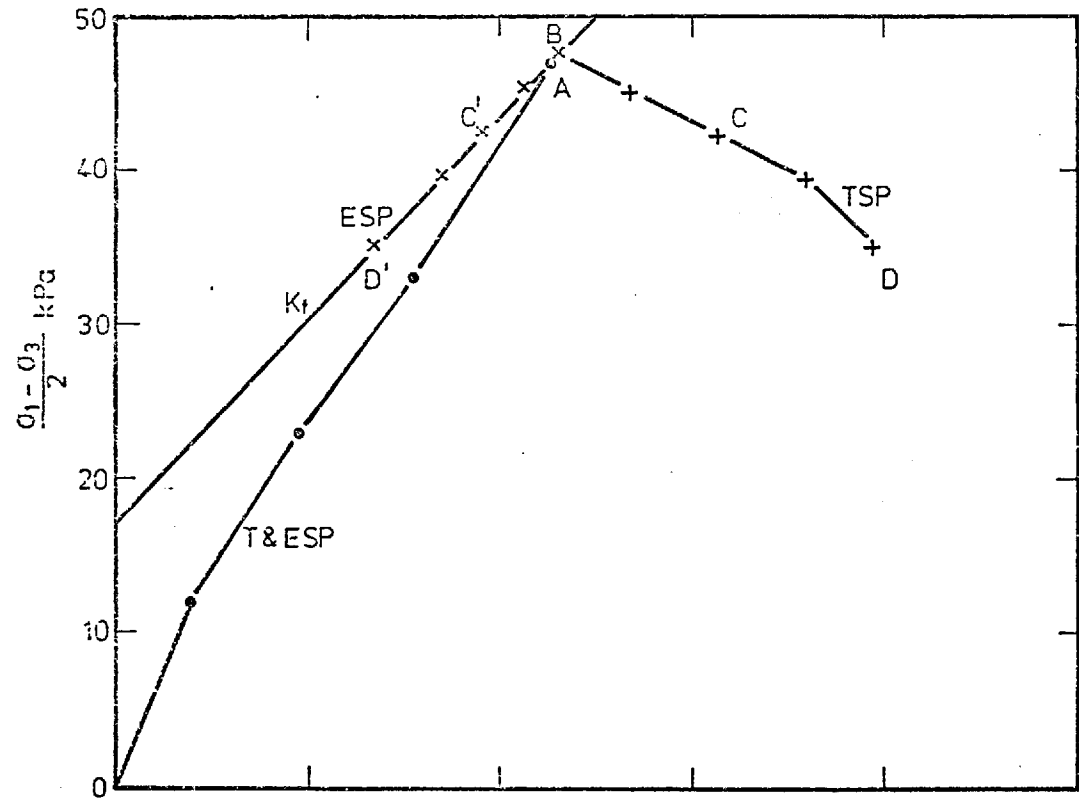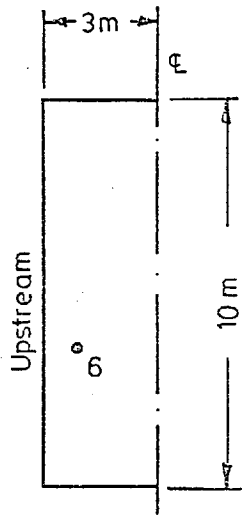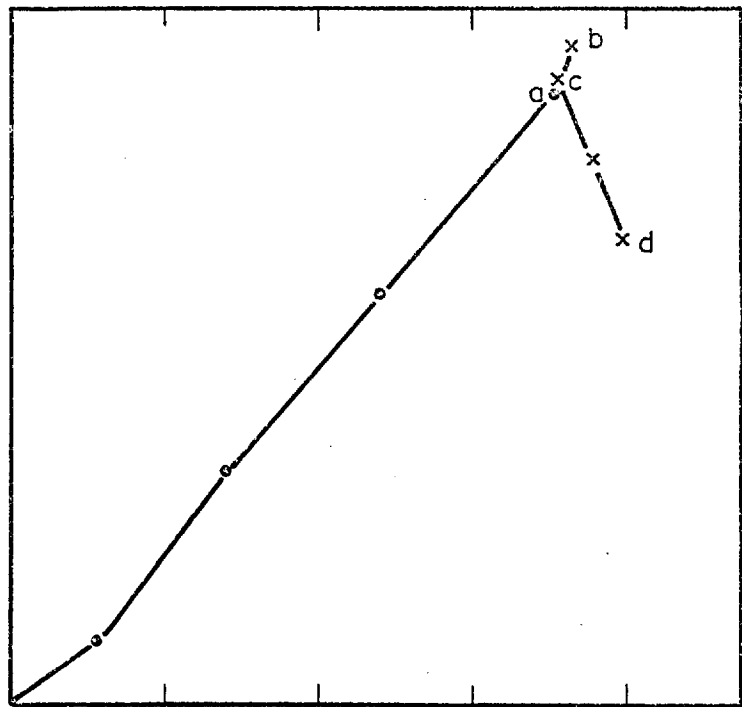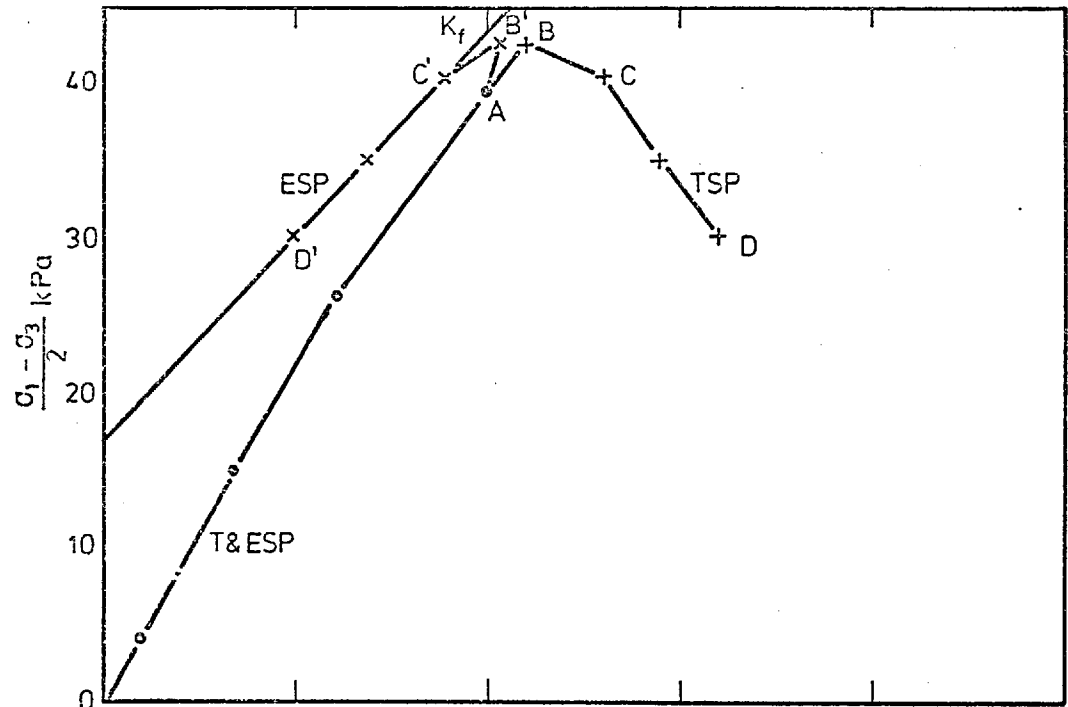
- ● Construction (Total and effective)
- + Transient flow (Total)
- × Transient flow (Effective)
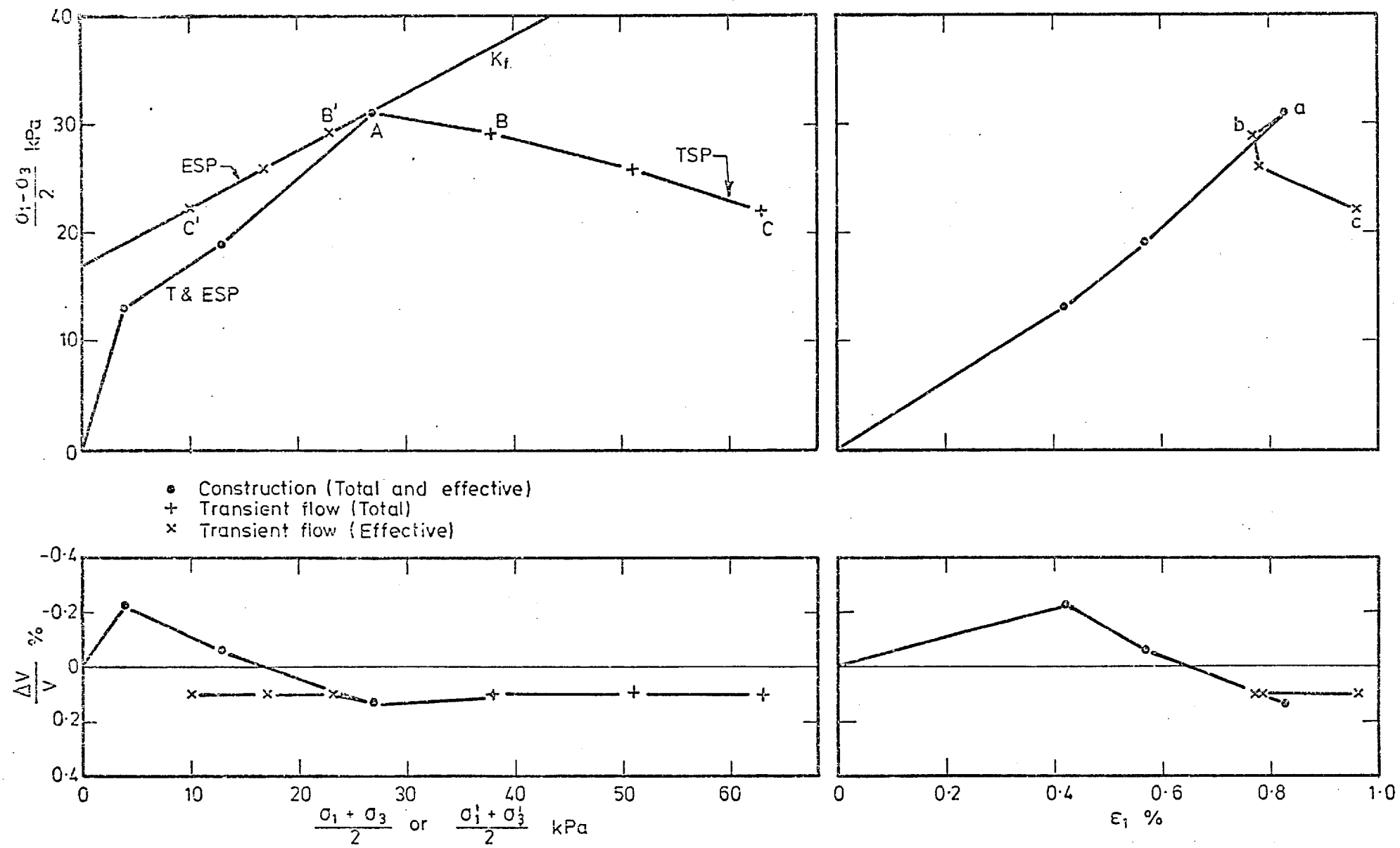
Fig. 8.33   The Stress Path for <u>Point 7</u>   CASE ST1

Left graph axis: $\dfrac{\sigma_1 + \sigma_3}{2}$ or $\dfrac{\sigma_1' + \sigma_3'}{2}$ kPa

Average stresses on A-A

Depth, D, m

$\gamma_t \cdot D$

u
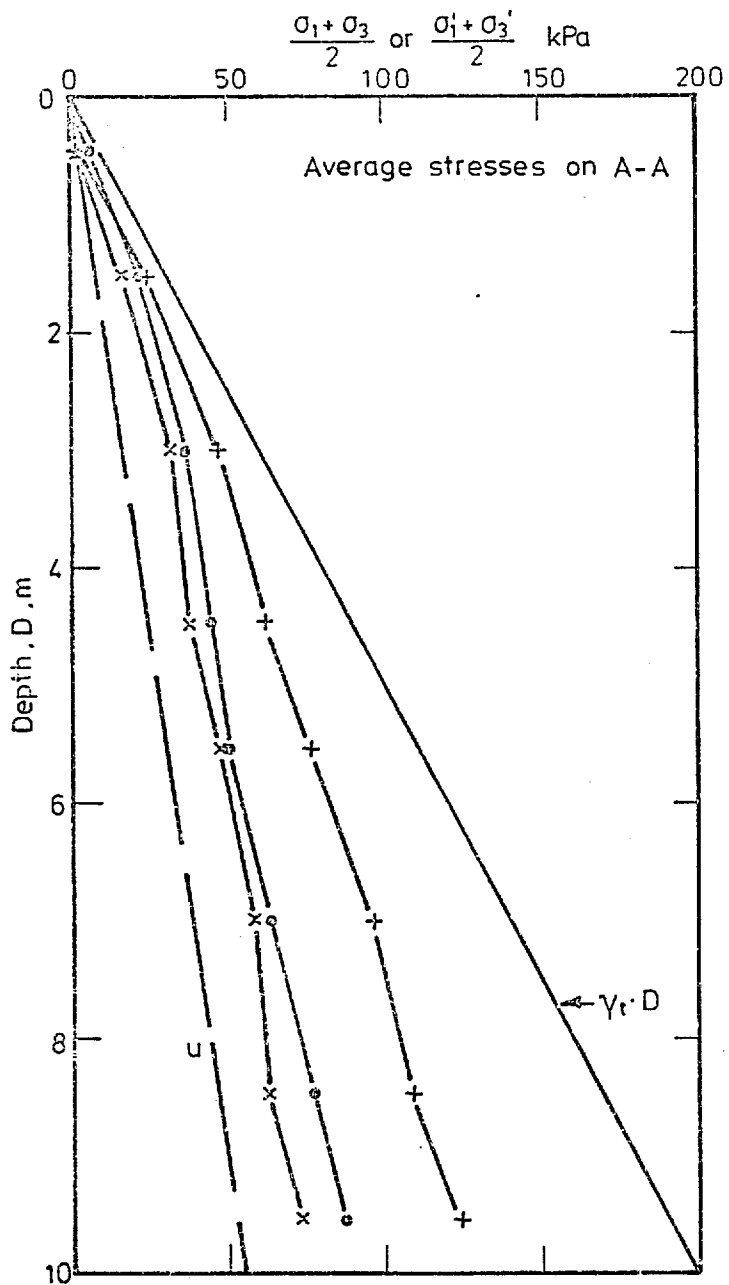
∘ End of construction (Total and effective)

+ End of transient flow (Total)

× End of transient flow (Effective)

6 m

0·21 m

A'   A

Upstream

10 m

2·13 m

A'   A
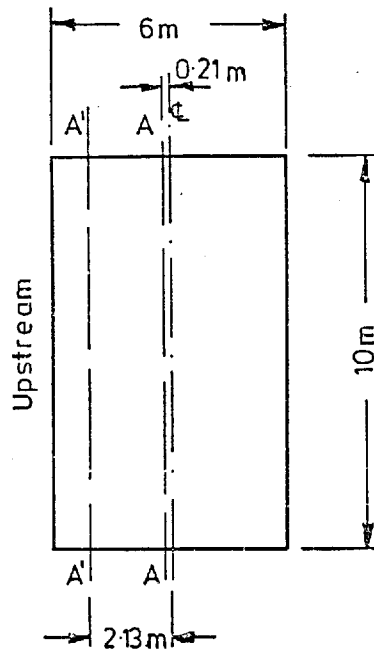
Fig. 8.34   Values of the Average Stresses

Right graph axis: $\dfrac{\sigma_1 + \sigma_3}{2}$ or $\dfrac{\sigma_1' + \sigma_3'}{2}$ kPa

Average stresses on A'-A'

Depth, D, m

$\gamma_t \cdot D$

u

CASE   ST1
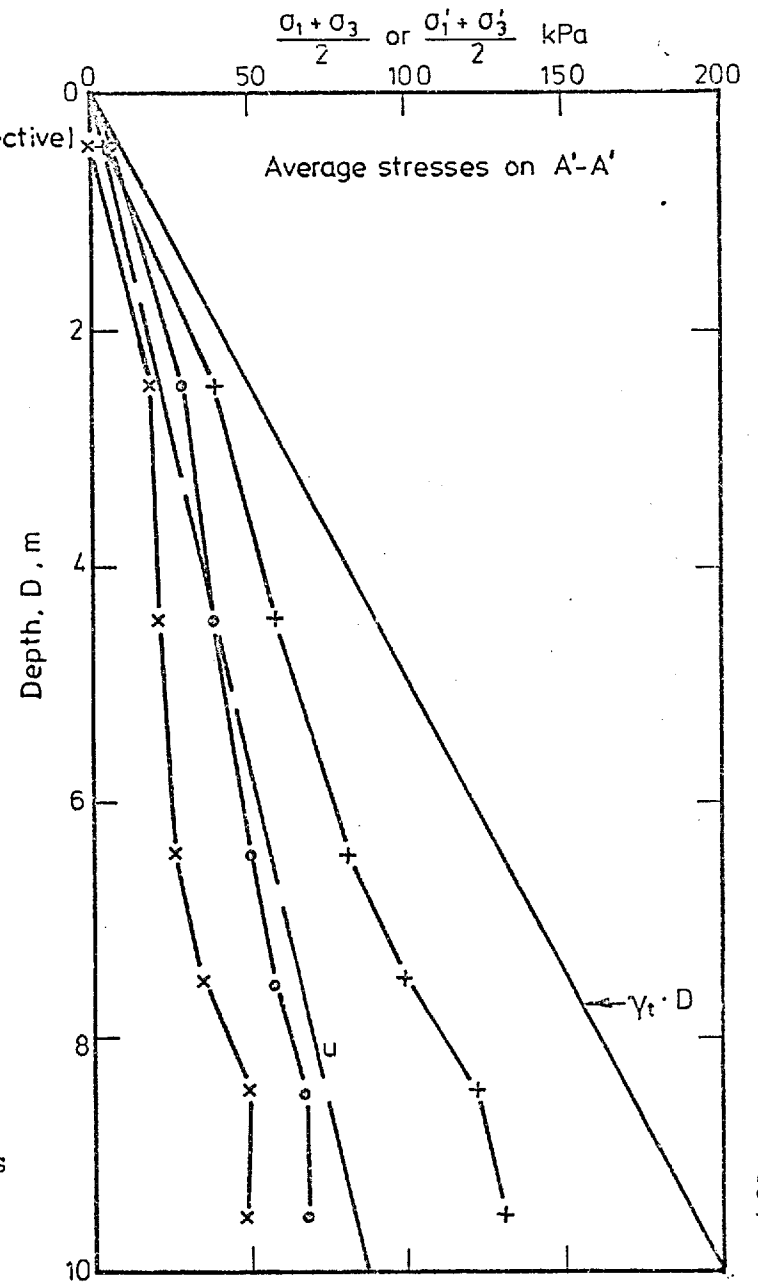
APPENDIX ONE

FLOW CHART OF THE PROGRAMME

A brief description of the function of the SUBROUTINES appearing in the flow chart is given in the following section:-

GINPUT, MIDNOD: Read geometrical, material properties and boundary conditions. Store the input in the relevant disc and memory storage.

SHAPEF, SFR, AUX: Calculate shape function and its derivatives for each element using numerical integration and store them in disc file.

SINPUT: Reads the initial stresses and strains from cards and/or magnetic tape. Converts the initial stresses to nodal forces, and stores them in the memory.

ELSTIF, NLELAS, SPRING: Calculate the stiffness matrix for each element according to its state of stress and the stiffness of the boundary spring, and store it in disc file.

LINPUT: Reads the loading pressure and forces. Converts the loads into nodal forces and stores them in the memory.

SOLVE: Assembles the overall stiffness matrix and reduces it by elimination.

RESOLV: Modifies the new R.H.S., and reduces the stiffness matrix by elimination.

BSUB: Obtains the displacement vector.

SELECT: Selects the state of stress for the first

                    solution of the Quasi Runge-Kutta method.

RESID: Calculates the nodal forces corresponding

                    to the total state of stress, and compares

                    with the external applied loads.

ITSLCT: Performs the pilot iteration, and records

                    the number of the points which are shear

                    unloaded.

ITELAS: Calculates the increment of stress corres-

                    ponding to the increment of strain using

                    Euler-Cauchy method.   Also, treats the

                    points with the strain-softening behaviour.

STRAIN: Calculates strains from the displacements

                    of the nodes.

CORSTN: Corrects the values of strains due to the

                    use of the dense liquid technique for

                    layering analysis.

STRESS: Calculates stresses from strains.

NODOUT: Outputs the values of the residual forces,

                    boundary springs stiffnesses, and displace-

                    ments at the nodes.

STOUT: Outputs stresses and strains at the

                    required elements and points.

MAGOUT: Stores the values of stresses and strains

                    in disc file or magnetic tape for graphics

                    and/or future reference.

Flow Chart of the Programme.
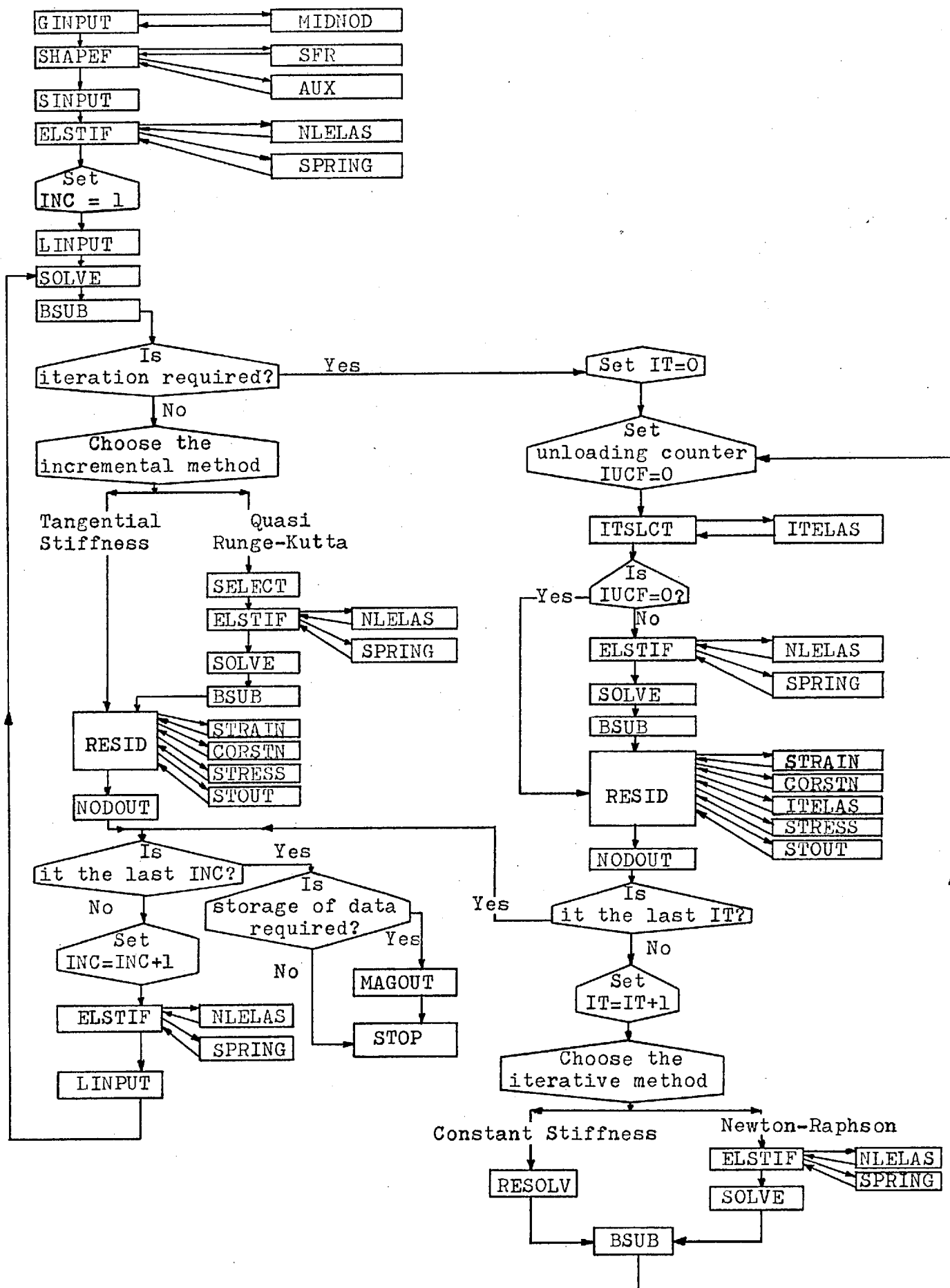
APPENDIX TWO

DISCUSSION ON THE MODIFICATIONS AND DEVELOPMENTS IN THE

PROGRAMME

In Chapter 2, a list of the principal parts of the programme specially written for this research is given. In the following section descriptions and algorithms of these parts are considered.

A.1   Shear Unloading and Reloading

In the first solution of the Quasi Runge-Kutta non-linear method (Chapter 2, Fig. 2.3), it is established whether the shear stress will increase or decrease, and the Gauss points at which a decrease will occur are identified. For these points a linear modulus is adopted during the second solution of this method.

The previous maximum shear stress at the end of each increment is recorded for checking the shear reloading. For a Gauss point if the shear stress increases after unloading or reloading, and the maximum shear stress from the previous increment is less than the previous maximum shear stress, a linear modulus is adopted during the second solution of the Quasi Runge-Kutta method. The unloading modulus may or may not be equal to the reloading modulus.

In the programme it is possible to select whether both the unloading modulus and reloading modulus or only one of them, in the second solution, will be linear or will

follow the first loading stress-strain curve (see Fig. 5.1, Chapter 5).

The algorithm for choosing the shear unloading and reloading moduli is as follows:-

In subroutine RESID (see Appendix one for descriptions of subroutines and the flow chart of the programme) the maximum shear stress $(\sigma_1-\sigma_3)/2$ is checked at the end of each increment with the previous maximum shear stress and the greater one is saved.

a.   First solution (subroutines ELSTIF and NLELAS)
      Enter element loop.

a.1.   Read stresses corresponding to the end of the previous increment or initial values (subroutine ELSTIF).
      Enter Gauss point loop.

a.2.   Look up the previous maximum shear stress (subrouting ELSTIF).

a.3.   Calculate principal stresses and the shear strength for stresses from (a.1), (subroutines NLELAS).

a.4.   Calculate the maximum shear stress and the mobilized shear stress ratio $\left(\frac{\sigma_1-\sigma_3}{2}\text{ and }\frac{\sigma_1-\sigma_3}{(\sigma_1-\sigma_3)_f}\right)$ for stresses from (a.1), (subroutine NLELAS).

a.5.   (i) If the maximum shear stress is less than the previous maximum shear stress, then take the unloading modulus, (RETURN), (subroutine NLELAS).

      (ii) If the mobilized shear stress ratio is greater than or equal to unity, then give a very small

value for modulus, (RETURN), (subroutine NLELAS).

(iii) If the mobilized shear stress ratio is less than unity, then take the tangent modulus (equation 2.3, Chapter 2), or, if this ratio is greater than 0.95, take half of the tangent modulus, (RETURN), (subroutine NLELAS).

End of Gauss point loop.

End of element loop.

b.   Second solution (subroutines SELECT, ELSTIF and NLELAS)

Enter element loop.

b.1.   Read stresses corresponding to the start of the increment (subroutine ELSTIF).

Enter Gauss point loop.

b.2.   Look up the previous maximum shear stress (subroutine ELSTIF).

b.3.   Retrieve the stress vector corresponding to half of the displacement increment obtained in the first solution (subroutine SELECT).

b.4.   With the initial stresses corresponding to the start of the increment (step b.1), repeat steps (a.3) and (a.4), (subroutine NLELAS).

b.5.   Multiply the stresses from step (b.3) by a factor F (for the start of the second solution F is equal to unity).   The output is, say, $\Delta\sigma^*$ (subroutine NLELAS).

b.6.   Add $\Delta\sigma^*$ to the initial stresses at the start of the increment (subroutine NLELAS).

b.7. Calculate the principal stresses and the shear strength for the stresses resulting from (b.6), (subroutine NLELAS).

b.8. Calculate the maximum shear stress $(\sigma_1 - \sigma_3)/2$ and the mobilized shear stress ratio $\dfrac{\sigma_1 - \sigma_3}{(\sigma_1 - \sigma_3)_f}$ corresponding to step (b.7), (subroutine NLELAS).

b.9. (i) If the maximum shear stress from (b.8) is less than the maximum shear stress from (b.4), then choose unloading modulus, (RETURN), (subroutine NLELAS).

(ii) If the maximum shear stress from (b.8) is greater than the maximum shear stress from (b.4), and the maximum shear stress from (b.4) is less than the previous maximum shear stress, then choose reloading modulus, (RETURN), (subroutine NLELAS).

(iii) With the results from (b.4) repeat steps a.5(i) and a.5(ii), (subroutine NLELAS).

(iv) If the mobilized shear stress ratio from (b.8) is less than unity, then the modulus is calculated from equation (2.3), and, if this ratio is greater than 0.95, take half of this modulus, (RETURN), (subroutine NLELAS).

(v) If the mobilized shear stress ratio from (b.8) is equal to unity, then choose a very small value for modulus, (RETURN), (subroutine NLELAS).

(vi) If the mobilized shear stress ratio from (b.8) is more than unity, then set factor F equal to 0.5F and (GO TO) step (b.5), (subroutine NLELAS).

End of Gauss point loop.

End of element loop.

Step b.9(vi) is the start of an iterative process which is performed for each Gauss point. Steps b.9(iv) to b.9(vi) ensure that there is no significant overshooting if the stresses are near failure, which would otherwise occur in a one-step, non-iterative method.

A.2 Poisson's Ratio Varying with Stress

The value of the Poisson's ratio in a non-linear stress analysis may be expressed as a function of the confining pressure, and during shear it would be a function of axial strain. In order to have zero volume change during failure, the Poisson's ratio must be equal to 0.5 at failure.

For many soils, the value of initial Poisson's ratio ν_i (at zero shear strain) has been reported to decrease as the confining pressure is increased. Based on experimental data, Kulhawy et al (1969) suggested the following equation for the variation of ν_i with σ_3:-

$$\nu_i = M - N \log_{10}\left(\frac{\sigma_3}{P_a}\right) \qquad (A.1)$$

where M is the value of ν_i at a confining pressure of one atmosphere, P_a is the atmospheric pressure, and N is a parameter representing the rate of decrease in ν_i with increasing σ_3.

During shear, the following equation is used for the

variation of the tangential Poisson's ratio ν_t:-

$$\nu_t = \nu_i (1 - \sigma_r) + 0.5\sigma_r \qquad (A.2)$$

where

$$\sigma_r = \frac{\sigma_1 - \sigma_3}{(\sigma_1 - \sigma_3)_f} \qquad (A.3)$$

Thus $\nu_t = \nu_i$ under isotropic stress and $\nu_t = 0.5$ at failure.

In the programme (subroutines NLELAS and ITELAS) the Poisson's ratio is selected and modified for each loading increment according to equations (A.1) to (A.3) and the state of stress.

A.3   Spring as the Boundary Condition

The programme is modified to deal with the spring boundary condition.   The springs are only possible in the horizontal and/or vertical directions with constant stiffnesses, and they could also be applied to nodes within the domain.

In the programme (subroutines ELSTIF and SPRING) the stiffness of the spring at a node is added only to the corresponding diagonal term in the stiffness matrix.   At the end of the increment, in subroutine RESID, the nodal force at a point with the spring is equated to the product of the corresponding displacement and spring stiffness.

A.4   Applying the Seepage Forces

The programme is modified to consider the effect of dissipating an increment of pore water pressure (either

after an interval of time or after the steady state is achieved) on the state of stress of the soil skeleton, by using the pore water pressure increment as the case of loading, as follows:-

The general equation of equilibrium of an element of soil in x direction is:

$$\frac{\partial \sigma_x}{\partial x} + \frac{\partial \tau_{xy}}{\partial y} + \frac{\partial \tau_{xz}}{\partial z} + X = 0 \qquad (A.4)$$

There are two other similar equations for y and z directions. In equation (A.4), X represents the total body force per unit gross volume of the material. But:-

$$\sigma_x = \sigma_x' + u \qquad (A.5)$$

Thus:-

$$-\frac{\partial \sigma_x'}{\partial x} + \frac{\partial \tau_{xy}}{\partial y} + \frac{\partial \tau_{xz}}{\partial z} + (X - \frac{\partial u}{\partial x}) = 0 \qquad (A.6)$$

This equation is identical in form to the equation (A.4), but the body force terms have now been changed by the amount:

$$-\frac{\partial u}{\partial x} , \quad -\frac{\partial u}{\partial y} \quad \text{and} \quad -\frac{\partial u}{\partial z}$$

in the appropriate directions, and the analysis can be carried out after converting the gradient of the pore water pressure into an equivalent body force. The values of pore water pressures are input at the nodes (subroutine LINPUT), and, in the programme, their gradients are calculated and applied as body forces.

The soil parameters used during these analyses are the effective stress parameters E', ν', and they may be non-linear, in which case E' and ν' are related to $\Delta\sigma_3'$ or $(\Delta\sigma_1' + \Delta\sigma_3')$ and $(\Delta\sigma_1 - \Delta\sigma_3)$ by a family of curves.

The procedure described above is valid whether the dissipation is consolidation or swelling. In the case of consolidation, the soil skeleton will exhibit a decrease of volume due to an increase in the compressive effective stress; in the case of swelling, the soil skeleton will increase in volume due to the decrease in the compressive effective stress, thus the volume change and the causative stresses have the same sign, and so the analysis for swelling does not imply $\nu' > 0.5$. But it must be pointed out that the swelling process is an unloading one in terms of volumetric stresses, so unloading parameters should be used in the analysis; also, in some cases, it may exhibit strain-softening.

A.5   Iteration Modified for Shear Unloading

The programme is extended for cases which need an iterative or incremental-iterative solution technique. The Newton-Raphson or the Constant Stiffness methods are used. The root mean squares of the residual forces at the nodes are used as the measure of convergence, which should decrease and become very small as the iteration proceeds. The iteration is terminated when the root mean square reaches a pre-set value, or when a pre-set number

of iterations have been performed.

The programme, if terminated at an arbitrary residual error, will result in a situation where the stresses are in agreement with the stress-strain curve but the finite element structure is not in equilibrium with the applied loads. In this situation, the engineering significance of the errors is difficult to evaluate.

The analyses were carried out for the footing on undrained clay with 826 degrees of freedom (case 3, Table 5.2, Chapter 5), using both the Newton-Raphson and the Constant Stiffness methods. Figure A.1 shows the plots of the maximum residuals and the root mean square of the residuals. From this figure it is clear that, for the same computer time, the Newton-Raphson method gives better results than the constant stiffness method. The root mean square of the residual and the maximum residual from the Newton-Raphson method at t = 4280 secs are about 75 per cent of those from the constant stiffness method.

The same analyses were carried out with the incremental-iterative technique, using both the Newton-Raphson and the Constant stiffness methods. Figure A.2 shows the plots of the maximum residuals and the root mean square of the residuals for the same load as Fig. A.1, but it was applied in 3 increments (note that for increment one the residuals were zero).

Comparison of Figs. A.1 and A.2 indicates that the incremental-iterative technique gives much better results than the iterative method for about half of the computer

time used by the iterative method. The root mean square of the residual and the maximum residual from the incremental-iterative method (3 increments) at t = 2000 secs are about 5% (for the Newton-Raphson method) and 14% (for the constant stiffness method) of those from the iterative method.

Again, for the incremental-iterative method, the Newton-Raphson method is better than the constant stiffness method. The root mean square of the residual and the maximum residual from the Newton-Raphson method at t = 2000 secs are about 20% of those from the constant stiffness method.

However, the problems which include the shear unloading cannot be handled using these iterative methods, as they cause numerical trouble due to the use of the tangential stiffness, which predicts large strains for the unloaded region at the state of stress close to, or at, failure.

The programme is extended to deal with the shear unloading by introducing a pilot solution for each iteration. During this pilot iteration, the tangential stiffnesses are assumed for the whole region.

The stresses derived from this first solution (iteration) are calculated to correspond to the full displacement vector obtained from the pilot iteration. These stresses are stored in a local disc and are not added to the initial stresses from the start of the iteration. By using these

stresses, it is established whether the shear stresses will increase or decrease, and the number of the unloaded Gauss points are recorded. If the unloading counter is zero, then this solution (iteration) is treated as the correct one and stresses are added to initial stresses from the start of the iteration.

If the unloading counter is not zero, then the iteration is repeated, and stresses from the pilot solution are used to identify the unloaded Gauss points, and a linear modulus is adopted for these points during the second solution (iteration).

For reloading, the first loading stress-strain curve is followed.

The algorithm of this procedure is as follows:-

Set unloading counter IUCF equal to zero.

a.   Pilot iteration (subroutines ITSLCT and ITELAS).

Enter element loop.

a.1.   Read stresses corresponding to the start of iteration (subroutine ITSLCT).

Enter Gauss point loop.

a.2.   Choose the tangent modulus corresponding to the state of stress at the start of iteration. Solve, and get displacements.

a.3.   Get strains from displacements, and calculate stresses from strains using the modulus from step (a.2).

Add these stresses to the stresses from step (a.1) and save the results on a local file. These final

stresses correspond to the end of pilot iteration, (subroutine ITELAS).

a.4. If the maximum shear stress from stresses corresponding to step (a.3) is less than the maximum shear stress from step (a.1), then set IUCF = IUCF + 1 (subroutine ITELAS).

End of Gauss point loop.

End of element loop.

a.5. If IUCF is equal to zero, (RETURN). Results from step (a.3) are the final results for this iteration and no second iteration is required (i.e. iteration has only one solution).

a.6. If IUCF is not equal to zero, then enter second solution (iteration), storing the stresses from the first solution (iteration).

b. Second iteration (subroutines ELSTIF, NLELAS, SOLVE, BSUB and RESID).

Enter element loop.

b.1. Read stresses corresponding to the start and end of the pilot iteration (subroutine ELSTIF).

Enter Gauss point loop.

b.2. With stresses from (b.1), and according to the algorithm explained in the second solution of the Quasi Runge-Kutta method (section A.1), choose the correct modulus (subroutine NLELAS).

b.3. Solve and get displacements, strains, and stresses using the modulus from (b.2), (subroutines SOLVE,

BSUB, RESID and ITELAS). These displacements, strains, and stresses correspond to the end of second iteration.

End of Gauss point loop.

End of element loop.

Figures A.3 and A.4 show the values of the maximum residuals and root mean square of the residuals for case ST1 (Table 8.1, Chapter 8) with 294 degrees of freedom.

In Fig. A.3, three layers of the core of the dam were considered, where each layer had 3 increments, except layer one which had one increment. In each increment the Newton-Raphson method (without modification for shear unloading) was used. In Fig. A.4, five layers of the core of the dam (same problem) were considered, where each layer had 4 increments, except layer one which had one increment. In each increment this modified form of the Newton-Raphson method was used (which considers the shear unloading and adopts a correct modulus for each Gauss point).

Comparison of these two figures indicates that the iterative method without the shear unloading modification does not converge. This is due to the numerical trouble caused by the use of the tangential stiffness, which predicts large strain for the unloaded Gauss points with state of stress at, or close to, failure.

A.6   Strain-Softening

In many geotechnical problems (e.g. dams, tunnels,

retaining walls and rocking footings) stress predictions

show stress paths exhibiting shear or an average effective

stress reduction (unloading) during construction and/or

operation.   In general, this unloading can occur from any

state of stress including the state of failure.   In case

of shear unloading, from or near the failure, the soil

will suddenly grossly increase its stiffness, a condition

which, if not modelled correctly, may cause very large errors

or even numerical break-down of the solution.   Alternatively,

if the failure state persists while the average effective

stress is reducing, a drop in the strength will occur.   If

this stress path induced softening is not modelled correctly,

a stress path which violates the failure cirterion will be

followed.   A combination of both conditions may occur in

reality.

Available non-linear solution techniques are inade-

quate to cover these groups of problems.   Incremental

methods can only model the shear unloading which has been

discussed in section (A.1).   From the iterative solution

techniques, the Newton-Raphson method was selected and

modified to deal with both cases of the shear unloading

and the stress path induced softening.   The shear unload-

ing modification and its importance have been discussed in

section (A.5).   The modification for the stress path

induced softening is discussed in the following section.

The form of the strain-softening behaviour encountered

in this research (see Chapter 8) is shown on Fig. A.5.

In the Newton-Raphson iterative method, the modulus becomes

very small at the state of failure. Post-failure stress path, if there is no shear unloading, will follow an almost horizontal path. By decreasing the average effective stress, the shear strength decreases, and this horizontal stress path, if not modelled correctly, will violate the failure criterion.

In order to have a stress path which does not violate the failure criterion, in the programme (subroutine ITELAS), at the end of each iteration and for each Gauss point the maximum shear stress, $(\sigma_1 - \sigma_3)/2$, is compared with the corresponding shear strength. If, for a point, the maximum shear stress exceeded the shear strength and the average effective stress, $(\sigma_1' + \sigma_3')/2$, at the end of iteration is less than the average effective stress at the start of iteration, then the point is brought down to the failure envelope by keeping the average effective stress and the principal stress rotation constant (see Fig. A.5). For a point with no strain-softening behaviour, if the maximum shear stress exceeded the shear strength, then the point is brought back to the failure envelope, on the same stress path that it was following, by reducing both the maximum shear stress and the average effective stress.

The algorithm of this strain-softening behaviour modification is as follows:-

At the end of each iteration (subroutine ITELAS)

Enter element loop.

1. Read stresses corresponding to the start and end of this iteration.

Enter Gauss point loop.

2. Calculate the shear strength, the maximum shear stress and the average effective stress corresponding to the stresses at the end of this iteration.

3. Calculate the average effective stress corresponding to stresses at the start of this iteration.

4. If the average effective stress from step (2) is less than the average effective stress from step (3), and the maximum shear stress from step (2) is greater than the shear strength from step (2),then deal with strain-softening by following steps (5) to (7). Otherwise RETURN (i.e. no strain-softening).

5. Assume that the average effective stress and the principal stress rotation from step (2) remain constant.

6. By using this average effective stress and the shear strength from step (2), calculate the principal stresses.

7. By using these principal stresses and the principal stress rotation from step (2), calculate the stresses.

End of Gauss point loop.

End of element loop.

As shown on Figs. 8.27 to 8.33 (Chapter 8), this modification results in stress paths which do not violate the failure criterion.
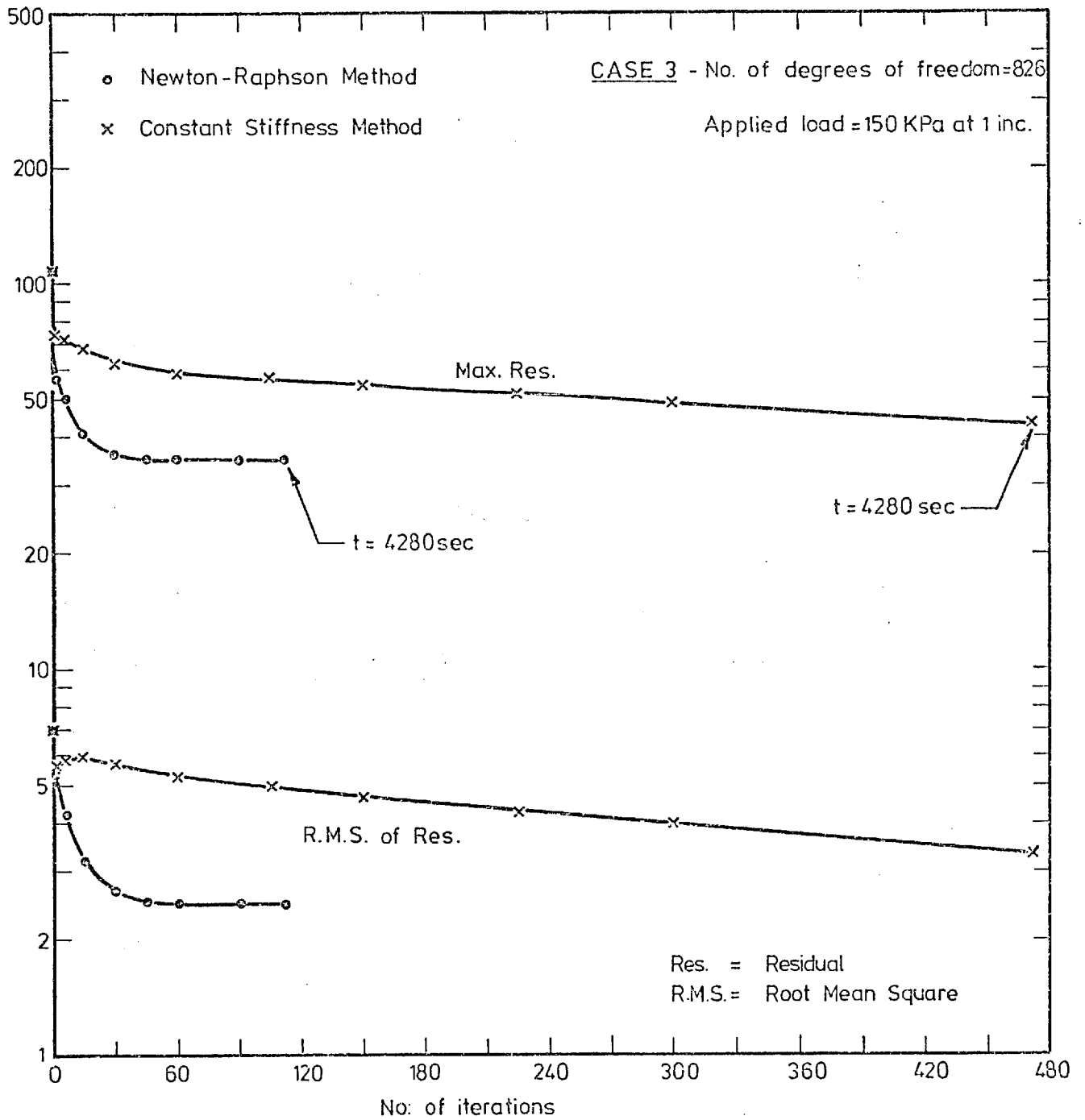
Fig. A.1   Comparison of Newton-Raphson Method with
            Constant Stiffness Method
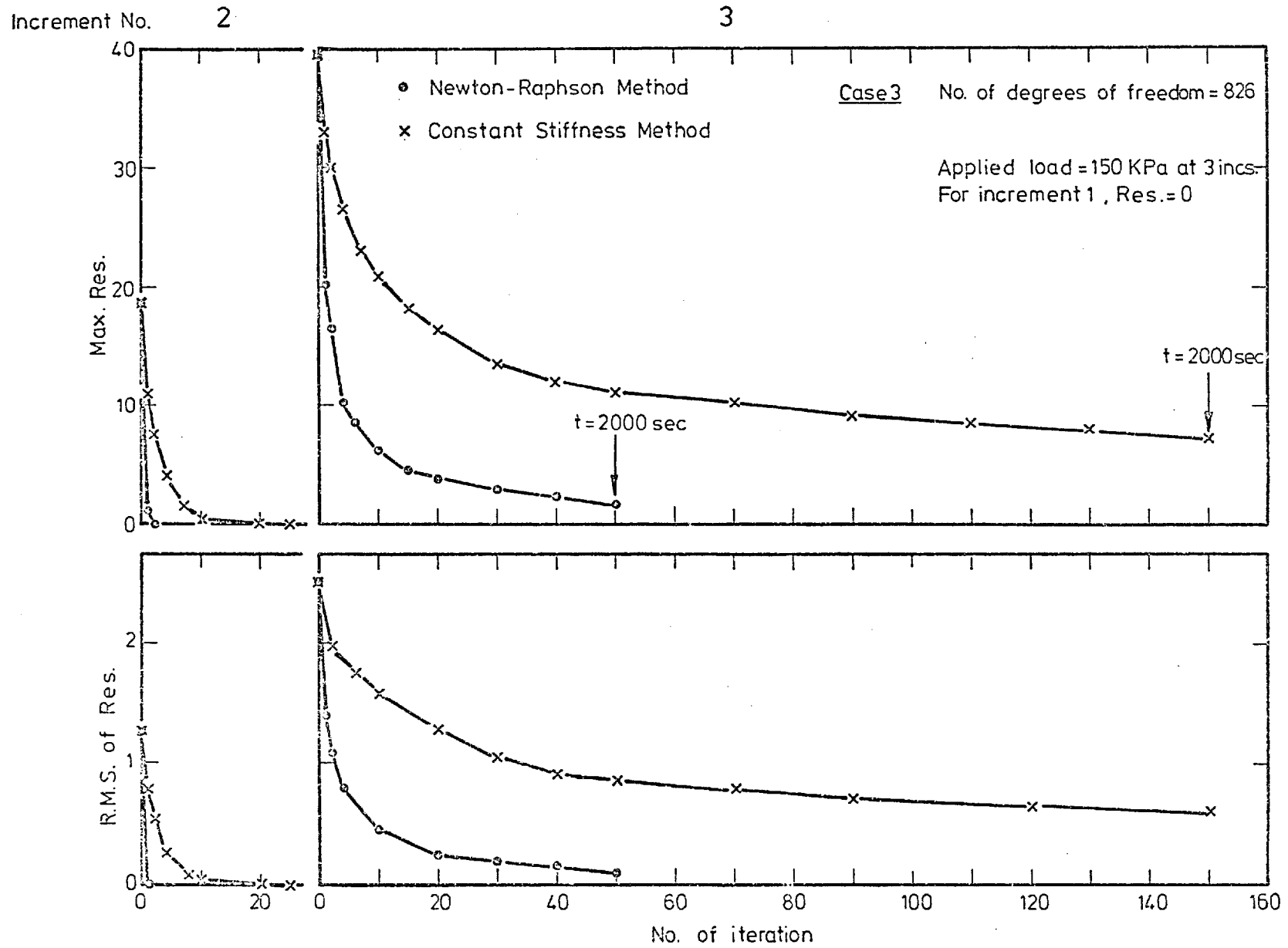
Fig. A.2   Comparison of the Newton-Raphson Method with Constant Stiffness Method

CASE ST1. No. of degrees of freedom = 294, 3 layers of the core, body force, t = 2400 sec

No. of iterations

No. of increments

No. of layers
(Layer 1 has only 1 increment)
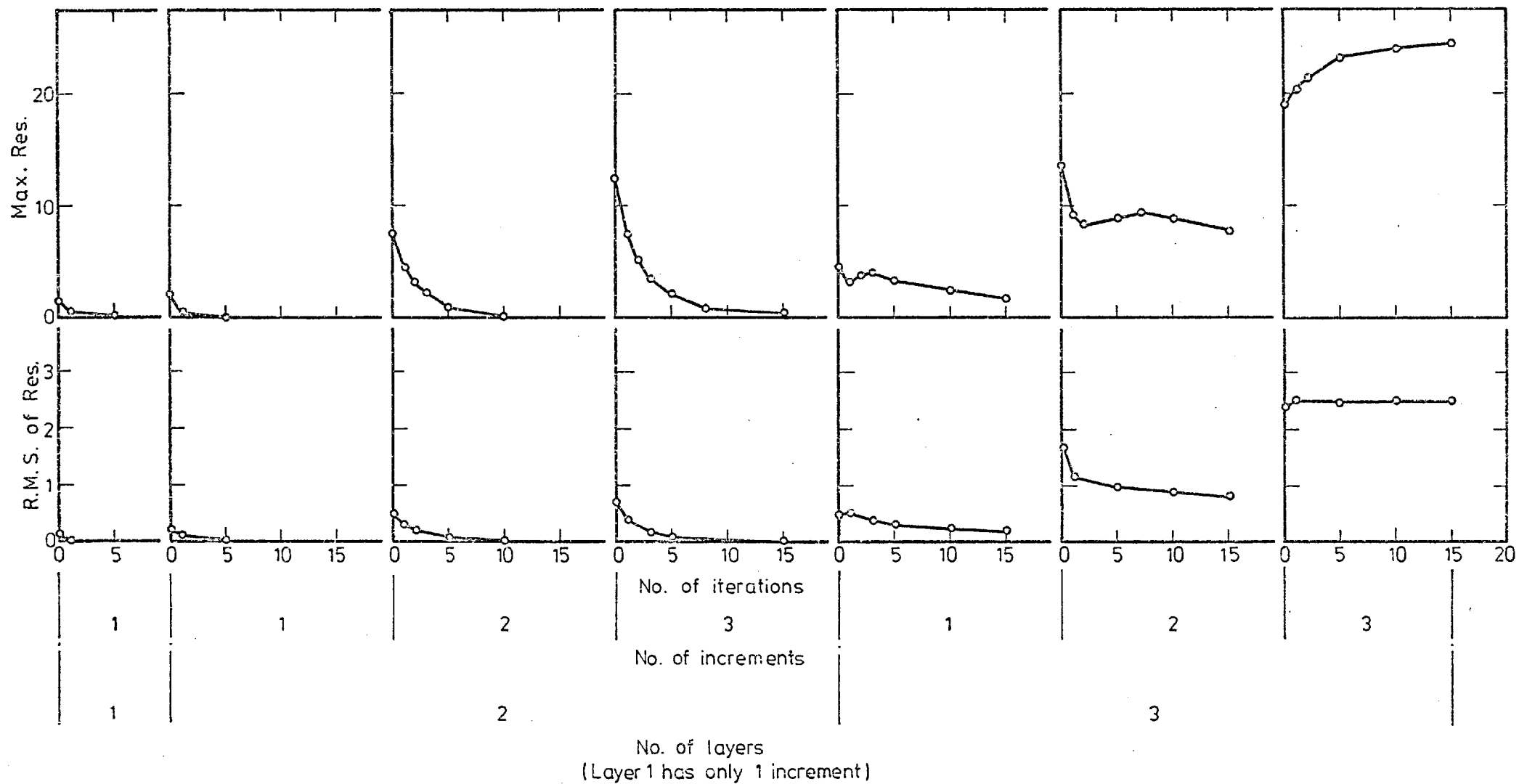
Fig. A.3   The Newton-Raphson Method without the Shear Unloading Modification

CASE ST1. No. of degrees of freedom = 294 , 5 layers of the core , body force, t = 4200 sec
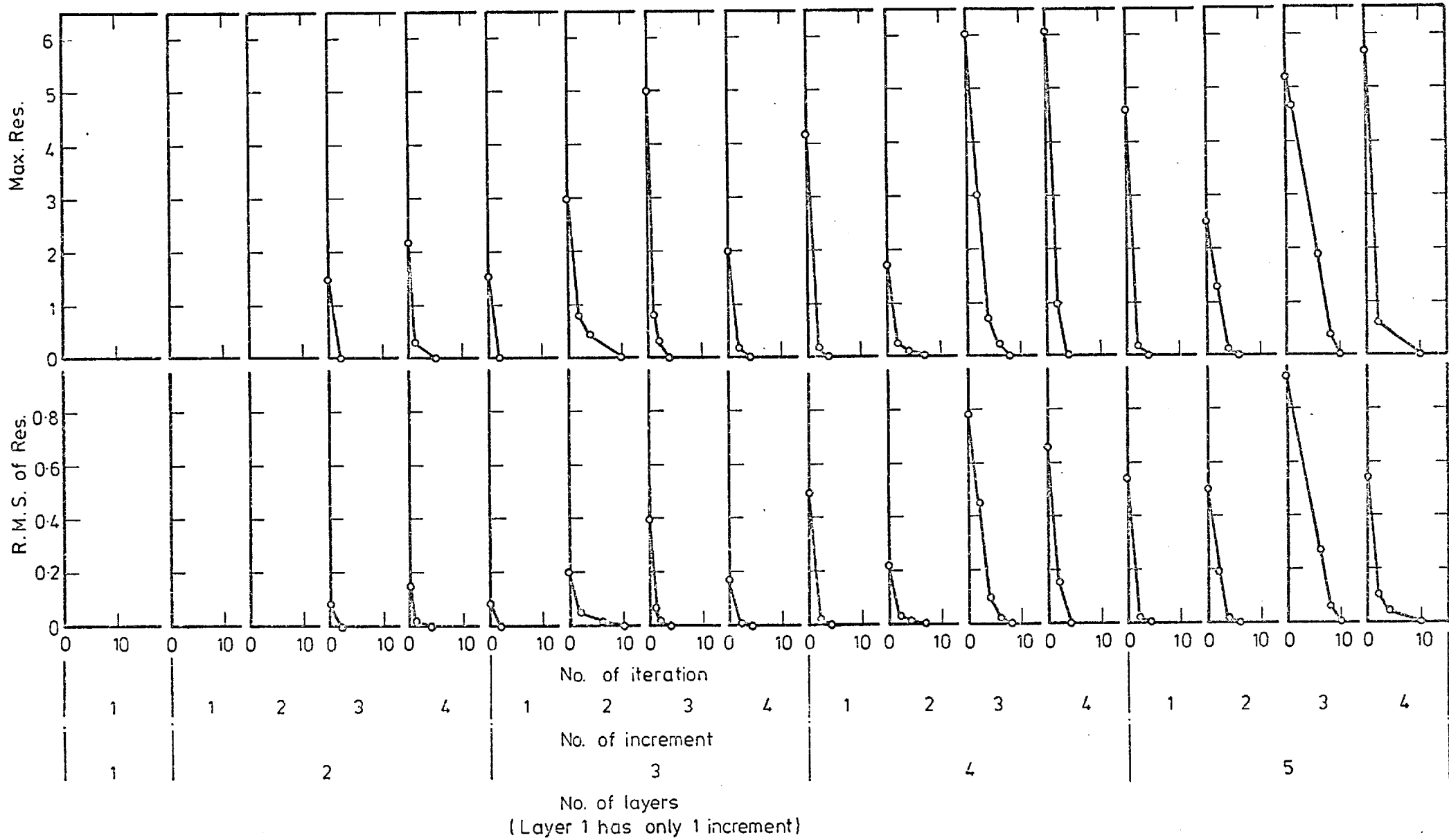
Fig. A.4   The Newton-Raphson Method with the Shear Unloading Modification
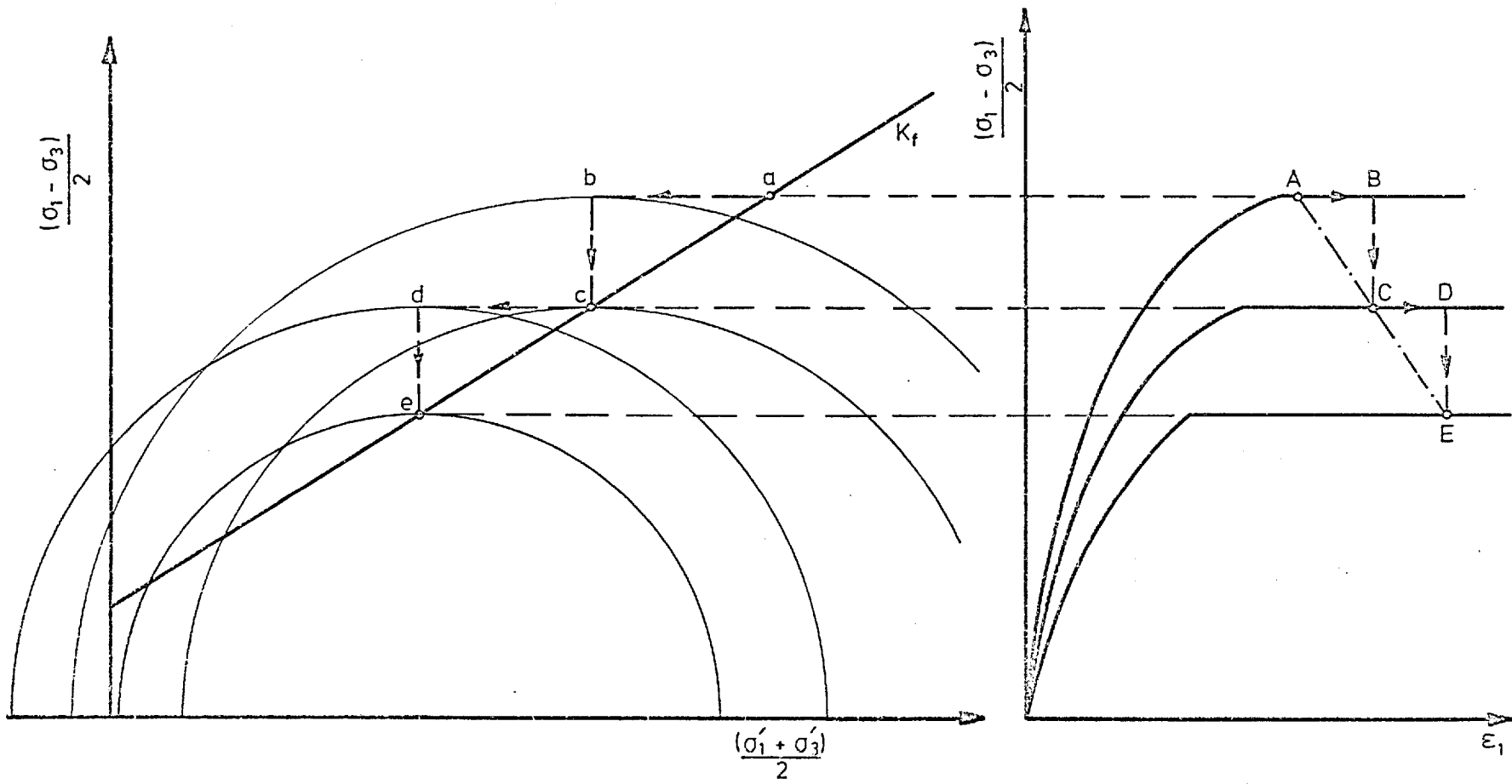
Fig. A.5   Idealised Strain-Softening Behaviour

REFERENCES

ACUM, W.E.A., and FOX, L. (1951). "Computation of load
stresses in a three-layer elastic system".
Geotechnique, Vol. 2, No. 4.

A.S.C.E. (1967). "Problems in design and construction of
earth and rockfill dams". Progress Report, Committee
on Earth and Rockfill Dams. Proc. A.S.C.E., Vol. 93,
SM3, pp 129-136.

AWOJOBI, A.O. (1974). "The invariance of Gibson's Law for
a stratum on a frictionless base". Geotechnique,
Vol. 24, No. 3, pp 359-366.

BARDEN, L. (1962). "Distribution of contact pressure under
foundations". Geotechnique. Vol. 12, No. 3.

BENSCOTER, S.V. (1944). "A symmetrically loaded base slab
on an elastic foundation". Transactions, A.S.C.E.,
Vol. 109, pp. 763-798.

BERTRAM, G.E. (1967). "Experience with seepage control
measures in earth and rockfill dams". Transactions
9th ICOLD Congress, Istanbul, Vol. 3.

BISHOP, A.W. (1952). "The stability of earth dams". Ph.D.
Thesis, University of London.

BISHOP, A.W. (1954). "The use of pore-pressure coefficients
in practice". Geotechnique, Vol. 4.

BISHOP, A.W. (1966a). "Soils and soft rocks as engineering
materials". Inaugural Lecture, Imperial College,
University of London.

BISHOP, A.W. (1966b). "The strength of soils as engineering materials". The Sixth Rankine Lecture. Geotechnique, Vol. 16, pp 89-130.

BISHOP, A.W. (1966c). "Discussion on Shek Pik Dam". Proc. I.C.E., Vol. 35 (Sept.).

BISHOP, A.W., and VAUGHAN, P.R. (1962). "Selset Reservoir". Design and performance of embankments. Proc. I.C.E., Vol. 21, pp 326-329.

BJERRUM, L. (1963). Discussion on "Interaction between structures and soils". Proc. European Conf. Soil Mech. and Found. Engg. (Wiesbaden), Vol. 2, pp 135-137.

BJERRUM, L. (1967). "Engineering geology of Norwegian normally-consolidated marine clays as related to settlements of buildings". 7th Rankine Lecture, Geotechnique, Vol. 17, pp 81-118.

BJERRUM, L. and EGGESTAD, A. (1963). "Interpretation of loading test on sand". Proc. European Conf. Soil Mech. and Found. Engg. (Wiesbaden), Vol. 1, pp 199-203.

BLACK, W.P.M. (1961). "The calculation of laboratory and in-situ values of California Bearing Ratio from bearing capacity data". Geotechnique, Vol. 11, pp 14-21.

BOND, D. (1961). "The influence of foundation size on settlement". Geotechnique, Vol. 11, No. 2, pp 121-143.

BOOKER, J.R. (1970). "Applications of theories of plasticity to cohesive frictional soils". Ph.D. Thesis, University of Sydney, Australia.

BOROWICKA, H. (1936). "Influence of rigidity of a circular
    foundation slab on the distribution of pressure
    over the contact surface". Proc. 1st I.C.S.M.F.E.,
    Vol. 2, pp 144-149.

BOROWICKA, H. (1938). "The distribution of pressure under
    a uniformly loaded elastic strip resting on elastic-
    isotropic ground". 2nd Congress, International Assoc.
    of Bridge and Structural Engineers, Final Report,
    Berlin.

BOSWELL, L.F. and SCOTT, C.R. (1975). "A flexible circular
    plate on a heterogeneous elastic half-space: influence
    coefficients for contact stress and settlement".
    Geotechnique, Vol. 25, No. 3, p 604.

BOUSSINESQ, M.J. (1885). "Application des potentiels, a
    l'etude de l'equilibre et du movement des solides
    elastiques". Gauthier-Villard, Paris.

BOWLES, J.E. (1975). "Spread footings" and "Combined and
    special footings". Foundation Engineering Handbook,
    Editors: Winterkorn, H.F. and Fang, H.Y. Van Nostrand
    Reinhold, pp 481-503, and pp 504-527.

BOZOZUK, M. and LEONARDS, G.A. (1972). "The Gloucester test
    fill". Proc. A.S.C.E. Specialty Conf. on Performance
    of Earth and Earth-supported Structures, Vol. 1,
    Part 1, pp 299-317.

BRINCH HANSEN, J. (1953). "Earth pressure calculation".
    Danish Technical Press, Copenhagen.

BRINCH HANSEN, J. (1961). "A general formula for bearing
    capacity". Danish Geotechnical Institute, Bulletin
    No. 11.

BRINCH HANSEN, J. (1963). "Discussion on hyperbolic stress-strain response: cohesive soils". Proc. A.S.C.E., J. S.M.F.D., Vol. 89, No. SM4, pp 242-243.

BRINCH HANSEN, J. (1970). "A revised and extended formula for bearing capacity". Danish Geotechnical Institute, Bulletin No. 28.

BROWN, P.T. (1969a). "Numerical analysis of uniformly loaded circular rafts on elastic layers of finite depth". Geotechnique, Vol. 19, No. 2, pp 301-306.

BROWN, P.T. (1969b). "Numerical analysis of uniformly loaded circular rafts on deep elastic foundations. Geotechnique, Vol. 19, No. 3, pp 399-404.

BROWN, P.T. and GIBSON, R.E. (1972). "Surface settlement of a deep elastic stratum whose modulus increases linearly with depth". Canadian Geotechnical Journal, Vol. 9, pp 467-476.

BUISMAN, A.S.K. (1935). "De weerstand van paalpunten in zand". De Ingenieur 50, pp Bt. 25-28, 31-35.

BUISMAN, A.S.K. (1936). "Results of long duration settlement tests". Proc. 1st I.C.S.M.F.E., Vol. 1, pp 103-106.

BURLAND, J.B. (1970). Discussion, Session A. Proc. Conf. on In-situ Investigations in Soils and Rocks. B.G.S., London, pp. 61-62.

BURLAND, J.B., SILLS, G.C. and GIBSON, R.E. (1973). "A field and theoretical study of the influence of non-homogeneity on settlement". Proc. 8th I.C.S.M.F.E., Moscow, Vol. 1, pp 39-46.

BURLAND, J.B. and WROTH, C.P. (1974). "Settlement of buildings and associated damage". Review Paper: Session V, Proc. Conf. on Settlement of Structures, Cambridge.

BURMISTER, D.M. (1943). "The theory of stresses and displacements in layer systems and application to design of airport runways". Highway Research Board, Vol. 23, pp 126-148.

BURMISTER, D.M. (1956). "Stress and displacement characteristics of a two-layer rigid base soil system: Influence diagrams and practical applications". Highway Research Board, Vol. 35, pp 773-814.

BURMISTER, D.M. (1958). "Evaluation of pavement systems of the WASHO road test layered system methods". Highway Research Board Bulletin, No. 177.

BURMISTER, D.M. (1967). "Applications of dimensional analyses in the evaluation of asphalt pavement performances". Paper for presentation at 5th Paving Conf., Albuquerque, New Mexico.

BUTLER, F.G. (1974). "Heavily over-consolidated clays". Proc. Conf. on Settlement of Structures, Cambridge. General Report and State-of-the-Art Review, Session 3.

CAQUOT, A. (1934). "Equilibre des massifs à frottement interne". Gauthier-Villard, Paris, pp 1-91.

CARLYLE, W.J. (1965). "Skek Pik Dam". Proc. I.C.E., Vol. 30 (March).

CARRIER, W.D. and CHRISTIAN, J.T. (1973). "Rigid circular plate resting on a non-homogeneous elastic half-space". Geotechnique, Vol. 23, No. 1, pp 67-84.

CASAGRANDE, A. and FADUM, R.E. (1942). "Application of soil

mechanics in designing building foundations".

Proc. A.S.C.E., Vol. 68, pp 1487-1520.

CHAE, Y.S., HALL, J.R. and RICHART, F.E. (1965). "Dynamic

pressure distribution beneath a vibrating footing".

Proc. 6th I.C.S.M.F.E., Vol. 2, pp 22-26.

CHEN, W.F. (1975). "Limit analysis and soil plasticity".

Elsevier Scientific Publishing Co.

CHEN, W.F. and DAVIDSON, H.L. (1973). "Bearing capacity

determination by limit analysis". Proc. A.S.C.E.,

J.S.M.F.D., Vol. 99, No. SM6, pp 433-449.

CHEN, W.F. and SCAWTHORN, C.R. (1970). "Limit analysis and

limit equilibrium solutions in soil mechanics".

Soils and Foundations. Vol. X, No. 3, pp 13-49.

CHRISTIAN, J.T. and CARRIER, W.D. (1978). "Janbu, Bjerrum

and Kjaernsli's chart reinterpreted". Canadian Geot.

J., Vol. 15, pp 123-128.

CLOUGH, R.W. and WOODWARD, R.J. (1967). "Analysis of

embankment stresses and deformations". Proc. A.S.C.E.,

J. S.M.F.D., Vol. 93, SM4, pp 529-549.

COOK, R.D. (1974). "Concepts and applications of finite

element analysis". John Wiley and Sons, Inc.

CORNFORTH, D.H. (1964). "Some experiments on the influence

of strain conditions on the strength of sand".

Geotechnique, Vol. 14, pp 143-167.

CUMMINGS, A.E. (1936). "Distribution of stresses under a

foundation". Transactions A.S.C.E., Vol. 101, pp

1072-1133.

D'APPOLONIA, D.J., D'APPOLONIA, E. and BRISSETTE, R.F. (1968). "Settlement of spread footings on sand". Proc. A.S.C.E., J. S.M.F.D., Vol. 94, SM3, pp 735-760.

D'APPOLONIA, D.J. and LAMBE, T.W. (1970). "Method of predicting initial settlement". Proc. A.S.C.E., J. S.M.F.D., Vol. 96, SM2, pp 523-544.

D'APPOLONIA, D.J., POULOS, H.G., and LADD, C.C. (1971) Initial settlement of structures on clay. Proc. A.S.C.E., SM and FDn., Vol. 97, SM10, p 1359.

DAVACHI, M.M. (1974). "Some problems in bearing capacity and settlement of shallow foundations". M.Sc. Report, Imperial College, University of London.

DAVIS, E.H. (1967). "A discussion of theories of plasticity and limit analysis in relation to the failure of soil masses". Proc. 5th Australian-New Zealand Conf. Soil Mech. and Fdn. Engng., pp 175-182.

DAVIS, E.H. and BOOKER, J.R. (1971). The bearing capacity of strip footings from the standpoint of plasticity theory". Proc. of the 1st Australian-New Zealand Conf. on Geomechanics. Vol.1,Melbourne, pp 276-282.

DAVIS, E.H. and BOOKER, J.R. (1973). "The effect of increasing strength with depth on the bearing capacity of clays". Geotechnique, Vol. 23, No. 4, pp 551-563.

DAVIS, E.H., and POULOS, H.G. (1963). "Triaxial testing and 3-dimensional settlement analysis". Proc. 4th Australian-New Zealand Conf. S.M. and F.E., Adelaide, pp 233-243.

DAVIS, E.H. and POULOS, H.G. (1968). "The use of elastic theory for settlement prediction under 3-dimensional conditions". Geotechnique, Vol. 18, No. 1, pp 67-91.

DAVIS, E.H. and POULOS, H.G. (1972). "Rate of settlement under 2- and 3-dimensional conditions". Geotechnique, Vol. 22, No. 1.

DAVIS, E.H., and TAYLOR, H. (1961). "The surface displacement of an elastic layer due to horizontal and vertical surface loading". Proc. 5th I.C.S.M.F.E., Vol. 1.

DE BEER, E.E. (1948). "Settlement records on bridges founded on sand". Proc. 2nd I.C.S.M.F.E., Rotterdam, Vol. 2, p. 111.

DE BEER, E.E. (1965a). "Bearing capacity and settlement of shallow foundations on sand". Symposium on Bearing Capacity and Settlement of Foundations, Duke Univ., pp 15-33.

DE BEER, E.E. (1965b). "The scale effect on the phenomenon of progressive rupture in cohesionless soils. Proc. 6th I.C.S.M.F.E., Vol. 2, pp 13-17.

DE BEER, E.E. (1970). "Experimental determination of the shape factors and the bearing capacity factors of sand". Geotechnique, Vol. 20, No. 4, pp 387-411.

DE BEER, E.E., and VESIC, A.S. (1958). "Etude expérimentale de la capacité portante du sable sous des fondations directes établies en surface". Annales des Traveaux Publics de Belgique 59, No. 3, pp 5-58.

DE JONG, J. and MORGENSTERN, N.R. (1971). "The influence of structural rigidity on the foundation loads of the CN Tower, Edmonton". Canadian Get. J. Vol. 8, No. 4, pp 527-537.

DESAI, C.S. (1974). "A consistent finite element technique for work-softening behaviour". Proc. of the Int. Conf. on Computational Methods in Nonlinear Mechanics, Austin, Tex., pp 969-978.

DESAI, C.S. (1977). "Deep foundations". Chapter 7, Numerical Methods in Geotechnical Engineering, ed. C.S. Desai and J.T. Christian, McGraw-Hill Book Co.

DESAI, C.S. and ABEL, J.F. (1972). "Introduction to the finite element method. A numerical method for engineering analysis". Van Nostrand Reinhold Company, London.

DIAS, J.L. (1967). "An isotropic frictional theory for a granular medium with and without cohesion". Ph.D. Thesis, Applied Mathematics, Brown University.

DRUCKER, D.C., PRAGER, W.,and GREENBERG, H.J. (1952). "Extended limit design theorems for continuous media". Quarterly of Applied Mathematics, Vol. 9, pp 381-389.

EGOROV, K.E., KUZMIN, P.G., and POPOV, B.P. (1957). "The observed settlements of buildings as compared with preliminary calculation". Proc. 4th I.C.S.M.F.E., Vol. 1, p 291.

EL-GHAMRAWY, M. (1978). Ph.D. Thesis, Imperial College, University of London, under preparation.

FOSTER, C.R. and FERGUS, S.M. (1951). "Stress distribution in a homogeneous soil". Highway Research Board, Research Report No. 12-F.

FRYDMAN, S. and ZEITLEN, J.G. (1969). "Some pseudo-elastic properties of granular media". Proc. 7th Int. Conf. SM and F Eng., Vol. 1, 1969, pp 135-141.

GARLANGER, J.E. (1972). "The consolidation of soils exhibiting creep under constant effective stress". Geotechnique, Vol. 22, No. 1, pp 71-78.

GIBSON, R.E. (1967). "Some results concerning displacements and stresses in a non-homogeneous elastic half-space." Geotechnique, Vol. 17, No. 1, pp 58-67.

GIBSON, R.E. (1968). "Correspondence: some results concerning displacements and stresses in a non-homogeneous elastic half-space". Geotechnique, Vol. 18, No. 2, pp 257-276.

GIBSON, R.E. (1969). "Correspondence: some results concerning displacements and stresses in a non-homogeneous elastic half-space". Geotechnique, Vol. 19, No. 1, pp 160-161.

GIBSON, R.E. (1974). "The analytical method in soil mechanics". 14th Rankine Lecture. Geotechnique, Vol. 24, No. 2, pp 115-140.

GIBSON, R.E. and SILLS, G.C. (1971). "Some results concerning the plane deformation of a non-homogeneous elastic half-space". Proc. Roscoe Memorial Conf. on Stress-strain behaviour of soils, pp 564-572.

GIRIJAVALLABHAN, C.V. and REESE, L.C. (1968). "Finite-element method for problems in soil mechanics". Proc. A.S.C.E., J. S.M.F.D., Vol. 94, SM2.

GIROUD, J.-P. (1972). "Settlement of rectangular foundation on soil layer". Proc., A.S.C.E., J.S.M.F.D., Vol. 98, No. SM1, pp 149-154.

GRANT, R., CHRISTIAN, J.T. and VANMARCKE, E.H. (1974).
"Differential settlement of buildings". Proc. A.S.C.E.,
Vol. 100, No. GT9, pp 973-991.

HAMZA, M.M. (1972). "Certain problems with nonlinear finite
elements. Part I: Acceleration techniques. Part II:
Studies on an earth dam". M.Sc. Thesis, University
of Wales, Swansea.

HAMZA, M.M. (1976). "The analysis of embankment dams by non-
linear finite element method". Ph.D. Thesis, Univ.
of London.

HANSEN, B. (1965). "A theory of plasticity for ideal friction-
less materials". Teknisk Forlag, Copenhagen.

HANSEN, B., and CHRISTENSEN, N.H. (1969). "Discussion on
theoretical bearing capacity of very shallow footings".
Proc. A.S.C.E., J. S.M.F.D., Vol. 95, No. SM6, pp
1568-1572.

HARR, M.E., DAVIDSON, J.L., HO, D., POMBO, L.E., RAMASWAMY,
S.V., and ROSNER, J.C. (1969). "Euler beams on two
parameter foundation models". Proc. A.S.C.E., J.S.M.F.D.,
Vol. 95, No. SM3, pp 933-948.

HENCKY, H. (1923). "Uber einige statisch bestimmte Falle
des Gleichgewichts in plastischen Körpern". Zeitschrift
angew. Math. und Mech. Vol. 3, pp 241-246.

HILL, R. (1949)."The plastic yielding of notched bars under
tension". Quarterly Journal of Mechanics and Applied
Mathematics, Vol. 2, pp 40-52.

HILL, R. (1950). "The mathematical theory of plasticity".
Oxford University Press.

HO, M.M.K. and BURWASH, W.J. (1968). "Vertical vibration of a rigid foundation resting on sand". Proc. Sym. on Vibration effects of earthquakes on soils and foundations. A.S.T.M., STP-450, pp 197-232.

HO, M.M.K. and LOPES, R. (1969). "Contact pressure of a rigid circular foundation". Proc. A.S.C.E., J. S.M.F.D., Vol. 95, SM3, pp 791-802.

HÖEG, K. (1972). "Finite element analysis of strain-softening clay. Proc. A.S.C.E, J. S.M.F.D., Vol. 98, No. SM1, pp 43-58.

HÖEG, K., CHRISTIAN, J.T. and WHITMAN, R.V. (1968). "Settlement of strip load on elastic-plastic soil". Proc. A.S.C.E., J. S.M.F.D., Vol. 94, SM2, pp 431-445.

HOOPER, J.A. (1974). "Analysis of a circular raft in adhesive contact with a thick elastic layer". Geotechnique, Vol. 24, No. 4, pp 561-580.

HOYAUX, B., and LADANYI, B. (1970)."Gravitational stress field around a tunnel in soft ground". Canadian Geot. J., Vol. 7, No. 1.

IRONS, B.M. and ZIENKIEWICZ, O.C. (1968). "The isoparametric finite element system - a new concept in finite element analysis". Proc. Conf. Recent Advances in Stress Analysis, Royal Aero. Soc.

JAMES, C.H.C., KRIZEK, R.J. and BAKER, W.H. (1969). "Bearing capacity of purely cohesive soils with a non-homogeneous strength distribution". Highway Research Record No. 282, pp 48-56.

JANBU, N. (1963)."Soil compressibility as determined by
oedometer and triaxial tests". Proc.1st European Conf.
on SM and F. Engng. Wiesbaden, Vol. 1, pp 19-25.

JANBU, N., BJERRUM, L., and KJAERNSLI, B. (1956). "Veiledning
ved Løsning av Fundamenteringsoppgaver". N.G.I.
Publication No. 16.

JONES, A. (1962). "Tables of stresses in 3-layer elastic
systems". Highway Research Board Bulletin, No. 342.

KENNARD, M.F., KNILL, J.L., and VAUGHAN, P.R. (1967). "The
geotechnical properties and behaviour of carboniferous
shale at the Balderhead Dam". Quarterly J. Eng.
Geology, Vol. 1, No. 1.

KENNARD, M.F., PENMAN, A.D.M., and VAUGHAN, P.R. (1967).
"Stress and strain measurements in the clay core
at Balderhead Dam". Trans. 9th ICOLD Congress, Vol.
3, Istanbul.

KÉRISEL, J. (1967). "Scaling laws in soil mechanics". Proc.
3rd Panamerican Conf. SMFE, Caracas, Vol. 3, pp
69-92.

KÉRISEL, J., and QUATRE, M. (1968). "Settlements under
foundations". Civ. Eng. and Pub. Wks. Review, May,
June.

KJAERNSLI, B., and TORBLAA, I. (1968). "Leekage through
horizontal cracks in the core of Hyttejuvet Dam".
Norwegian Geot. Institute. Pub. No. 80.

KLEIN, G.K., and DURAEV, A.E. (1971). "The effects of the
increase of modulus of deformation of the soil with
increasing depth for calculation of beams on a
continuous foundation". (in Russian), Gidrotekniskoie

Stroitelstro, June, pp 19-21.

KO, H.Y., and DAVIDSON, L.W. (1973). "Bearing capacity of

footings in plane strain". Proc. A.S.C.E., J. S.M.F.D.,

Vol. 99, SM1, pp 1-23.

KO, H.Y., and SCOTT, R.F. (1973). "Bearing capacity by

plasticity theory". Proc. A.S.C.E., J. S.M.F.D.,

Vol. 99, SM1, pp 25-43.

KRYNINE, D.P. (1938). "Pressures beneath a spread foundation".

Transactions, A.S.C.E., Vol. 103, pp 827-877.

KULHAWY, F.H., DUNCAN, J.M. and SEED, H.B. (1969). "Finite

element analysis of stresses and movements in embank-

ments during construction". Report No. TE-69-4 to

U.S. Army Engineers, Waterways Experiment Station.

Dept. of Civil Eng.,University of California, Berkeley.

KULHAWY, F.H., and GURTOWSKI, T.M. (1976). "Load transfer

and hydraulic fracturing in zoned dams". Proc. A.S.C.E.,

Vol. 102, No. GT9, pp 963-974.

LAING, J.M. (1971). "A finite element method for investi-

gating cracking in embankment dams". Ph.D. Thesis,

University of London.

LAMBE, T.W. (1964). "Methods of estimating settlement".

Proc. A.S.C.E., J. S.M.F.D., Vol. 90, SM5.

LAMBE, T.W. (1967). "Stress path method". Proc. A.S.C.E.,

J. S.M.F.D., Vol. 93, SM6.

LAMBE, T.W. (1973a). "Predictions in soil engineering".

13th Rankine Lecture. Geotechnique, Vol. 23, No. 2,

pp 149-202.

LAMBE, T.W. (1973b). "Soil parameters for predicting defor-
mations and stability". Proc. 8th I.C.S.M.F.E.,
Vol. 3, pp 3-25.

LEONARDS, G.A., and NARAIN, J. (1963). "Flexibility of clay
and cracking of earth dams". Proc. A.S.C.E., J. S.M.F.D.,
Vol. 89, No. SM2.

LUNDGREN, H., and MORTENSEN, K. (1953). "Determination by
the theory of plasticity of the bearing capacity of
continuous footings on sand". Proc. 3rd I.C.S.M.F.
E., Vol. I., pp 409-412.

MANDEL, J., and SALENCON, J. (1969). "Force portante d'un
sol sur une assise rigide". "The bearing capacity of
soils on a rock foundation". Proc. 7th I.C.S.M.F.E.,
Vol. 2, pp 157-164.

MARSAL, R.J. (1959). "Earth dams in Mexico". Proc. 1st
Panamerican Conf. on S.M.F.E., Vol. 3, Mexico.

MARSAL, R.J., and DE ARELLANO, L.R. (1967). "Performance of
El Infiernillo Dam". Proc. A.S.C.E., J. S.M.F.D.,
Vol. 93, No. SM4.

MEYERHOF, G.G. (1951). "The ultimate bearing capacity of
foundations". Geotechnique, Vol. 2, p. 302.

MEYERHOF, G.G. (1955). "Influence of roughness of base and
ground water conditions on the ultimate bearing
capacity of founcations". Geotechnique, Vol. 5, p 227.

MEYERHOF, G.G. (1965). "Shallow foundations". Proc. A.S.C.E.,
J. S.M.F.D., Vol. 91, SM2, pp 21-31.

MILOVIC, D.M., TOUZOT, G. and TOURNIER, J.P. (1970). "Stresses
and displacements in an elastic layer due to inclined

and eccentric load over a rigid strip". Geotechnique,
Vol. 20, No. 3, pp 231-152.

MINDLIN, R.D. (1936). "Forces at a point in the interior
of a semi-infinite solid". Physics, Vol. 7, No. 5,
pp 195-202.

MOGAMI, T. (1957). "Numerical tables for calculation of
stress components induced in a semi-infinite elastic
solid when a force is applied at a point in the
interior of the body". Kajima Construction Technical
Research Institute, Tokyo, Japan.

MOORHOUSE, D.C. (1972). "Shallow foundations". Proc.
Specialty Conf. on Performance of Earth and Earth-
supported Structures, A.S.C.E., Purdue Univ. Lafayette,
Indiana, Vol. 2, pp 71-109.

MORGAN, J.R. and SCALA, A.J. (1968). "Flexible pavement
behaviour and application of elastic theory - a review".
Proc. 4th Conf. Australian Road Research Board,
Melbourne, Vol. 4, part 2, p 1201.

MURFF,J.D. and MILLER, T.W. (1977). "Foundation stability
on Nonhomogeneous clays". Proc. A.S.C.E., Vol. 103,
No. GT10, pp 1083-1095.

NASCIMENTO, U. and SIMOES, A. (1957). "Relation between
CBR and modulus of strength". Proc. 4th I.C.S.M.F.E.,
Vol. 2, pp 166-168.

NAYAK, G.C. (1971). "Plasticity and large deformation
problems by the finite element method". Ph.D. Thesis,
University of Wales, Swansea.

NAYAK, G.C., and ZIENKIEWICZ, O.C. (1972). "Elasto-plastic
stress analysis. A generalisation for various con-
stitutive relations including strain-softening".
Int. J. for Num. Methods in Engng, Vol. 5, pp 113-135.

NAYLOR, D.J. (1974). "Stresses in nearly incompressible
materials by finite elements with applications to
the calculation of excess pore pressure". Int. Journ.
for Num. Meth. in Engng, Vol. 8, pp 443-460.

NEWMARK, N.M. (1942). "Influence charts for computation of
stresses in elastic foundations". Univ. of Illinois
Engineering Experiment Station, Bulletin No. 338,
pp 5-25.

NOBARI, E.S., and DUNCAN, J.M. (1972). "Effect of reservoir
filling on stresses and movements in earth and rock-
fill dams". U.S. Corps of Engineers, Report No. S-72-2.

NONVEILLER, E., and ANAGNOSTI, P. (1961). "Stresses and
deformations in cores of rockfill dams". Proc. 5th
I.C.S.M.F.E., Paris, Vol. 2, pp 673-680.

PARKES, E.W. (1956). "A comparison of the contact pressures
beneath rough and smooth rafts on an elastic medium".
Geotechnique, Vol. 6, No. 4, pp 183-189.

PATRICK, J.G. (1967). "Post-construction behaviour of Round
Butte Dam". Proc. ASCE, J. S.M.F.D., Vol. 93, No. SM4.

PEATTIE, K.R. (1962). "Stress and strain factors for 3-layer
elastic systems". Highway Research Board Bulletin,
No. 342.

PEATTIE, K.R. (1963). "A fundamental approach to the design
of flexible pavements". Proc. Int. Conf. on the

Structural Design of Asphalt Pavements, University of Michigan, pp 403-411.

PECK, R.B., and BAZARAA, A.R. (1969). Discussion: Settlement of spread footings on sand. Proc. A.S.C.E., Vol. 95, No. SM3.

PERLOFF, W.H. (1975). "Pressure distribution and settlement". Foundation Engineering Handbook, Winterkorn, H.F. and Fang, H.Y.,(eds.), Van Nostrand Reinhold, New York, pp 148-196.

POPE, R.J. (1967)."Evaluation of Cougar Dam Embankment performance". Proc. A.S.C.E., J. S.M.F.D., Vol. 93, No. SM4.

POULOS, H.G. (1967). "Stresses and displacements in an elastic layer underlain by a rough rigid base". Geotechnique, Vol. 17, pp 378-410.

POULOS, H.G. (1968). "The behaviour of a rigid circular plate resting on a finite elastic layer". Civil Eng. Trans. Instn. of Engrs., Aust., Vol. CE10, pp 213-219.

POULOS, H.G., and DAVIS, E.H. (1974). "Elastic solutions for soil and rock mechanics". John Wiley and Sons, Inc.

PRANDTL, L. (1920). "Uber die Härte plastischer Körper". Nachrichten von der Königlichen Gesellschaft der Wissenschaften zu Gottingen. Mathematisch - physikalische Klasse Berlin, p. 74-85.

PRÉVOST, J.-H., and HÖEG, K. (1975a). "Soil mechanics and plasticity analysis of strain softening". Geotechnique, Vol. 25, No. 2, pp 279-297.

PRÉVOST, J.-H., and HÖEG, K. (1975b). "Effective stress-strain-strength model for soils". Proc. A.S.C.E., Vol. 101, No. GT3, pp 259-278.

PRÉVOST, J.-H., and HÖEG, K. (1975c). "Analysis of pressure-meter in strain-softening soil". Proc. A.S.C.E., Vol. 101, No. GT8, pp 717-732.

RAYMOND, G.P. (1967). "The bearing capacity of large footings and embankments on clays". Geotechnique, Vol. 17, pp 1-10.

REISSNER, H. (1924). "Zum Erddruckproblem". Proc. 1st Int. Congress for Applied Mechanics, Delft, The Netherlands, pp 295-311.

REPORT OF THE INDEPENDENT PANEL ON FAILURE OF TETON DAM (1976). Report to U.S. Dept. of the Interior and State of Idaho. Idaho Falls, Idaho.

RODRIGUES, J.S. (1975). "The development and application of a finite element program for the solution of geo-technical problems". Ph.D. Thesis, University of Surrey.

ROSCOE, K.H., and BURLAND, J.B. (1968). "On the generalized stress-strain behaviour of wet clay". Engineering plasticity. Ed. J. Heyman and F.A. Lecku, Cambridge University Press. pp 535-609.

ROWE, P.W. (1968). "The influence of geological features of clay deposits on the design and performance of sand drains". I.C.E. Proc. Sup. Paper 70585, London.

ROWE, P.W. (1972). "The relevance of soil fabric to site investigation practice". The 12th Rankine Lecture, Geotechnique, Vol. 22, pp 195-300.

SADOWSKY, M. (1928). Z. Angew. Math. Mech., Vol. 8, p. 107.

SALENCON, J. (1974). "Bearing capacity of a footing on a $\phi = 0$ soil with linearly varying shear strength". Geotechnique, Vol. 24, No. 3, p 443.

SALENCON, J., FLORENTIN, P. and GABRIEL, Y. (1976)."Capacité portante globale d'une fondation sur un sol non-homogène". Geotechnique, Vol. 26, No. 2, p 351.

SCHIFFMAN, R.L. (1969). "The influence of adhesion on the stresses and displacements in an elastic half-space". Highway Research Record, No. 282, pp 17-24.

SCHIFFMAN, R.L. and GIBSON, R.E. (1964). "Consolidation of nonhomogeneous clay layers". Proc. A.S.C.E., J. SM and FD, Vol. 90, No. SM5, Sept. pp 1 - 30.

SCHMERTMANN, J.H. (1970). "Static cone to compute settlement over sand". Proc. A.S.C.E., J. S.M.F.D., Vol. 96, No. SM3.

SCHULTZE, E. (1961). "Distribution of stress beneath a rigid foundation". Proc. 5th I.C.S.M.F.E., Vol. 1, pp 807-813.

SCOTT, R.F. (1963). "Principles of soil mechanics". Addison-Wesley Publishing Company, Inc.

SHERARD, J.L., WOODWARD, R.J., GIZIENSKI, S.F., and CLEVENGER, W.A. (1963). "Earth and earth-rock dams". John Wiley and Sons, Inc.

SHIELD, R.T. (1954). "Stress and velocity fields in soil mechanics". Journal of Mathematics and Physics. Vol. 33, pp 144-156.

SIMONS, N.E. (1974). "Normally consolidated and lightly over-consolidated cohesive materials". Conf. on Settlement of Structures, Session 2, Cambridge, England.

SIMONS, N.E., and MENSIES, B.K. (1975). "A short course in foundation engineering". IPC Science and Technology Press.

SKEMPTON, A.W. (1948). "Vane tests in the alluvial plain of the River Forth near Grangemouth". Geotechnique, Vol. 1, No. 2, pp 111-124.

SKEMPTON, A.W. (1951). "The bearing capacity of clays". Building Research Congress, I.C.E. Div. 1, p 180.

SKEMPTON, A.W. (1954). "The pore-pressure coefficients A and B". Geotechnique, Vol. 4, pp 143-147.

SKEMPTON, A.W. (1957). "Discussion on the planning and design of the new Hong Kong airport". Proc. ICE, Vol. 7, pp 305-307.

SKEMPTON, A.W. and BJERRUM, L. (1957). "A contribution to the analysis of foundation on clay". Geotechnique, Vol. 7, No. 4, p 168.

SKEMPTON, A.W. and McDONALD, D.M. (1956). "The allowable settlement of buildings". Proc. ICE, Vol. 5, Part 3, p 727.

SMITH, I.M. (1976). "Aspects of the analysis of gravity offshore structures". Num. Meth. in Geomechanics, A.S.C.E., Vol. 2, pp 957-978, Blacksburg, Virginia.

SMITH, I.M. (1978). "Computer predictions in difficult soil conditions". Chapter 4 in Foundation Engineering in Difficult Ground, ed. F.G. Bell, Newnes-Butterworths, London.

SMOLTCZYK, H.U. (1967). "Stress computation in soil media". Proc. A.S.C.E., J. S.M.F.D., Vol. 93, No. SM2, pp 101-124.

SOKOLOVSKII, V.V. (1960). "Statics of soil media". Butterworth, London.

SOKOLOVSKII, V.V. (1965). "Statics of granular media". Pergamon Press Ltd., New York.

SOMMER, H. (1965). "A method for the calculation of settlements, contact pressures, and bending moments in a foundation including the influence of the flexural rigidity of the superstructure". Proc. 6th I.C.S.M.F.E., Montreal, Vol. 2, pp 197-201.

SOVINC, I. (1961). "Stresses and displacements in a limited layer of uniform thickness, resting on a rigid base, and subjected to an uniformly distributed flexible load of rectangular shape". Proc. 5th I.C.S.M.F.E., Vol. 1, pp 823-827.

SOVINC, I. (1969). "Displacements and inclinations of rigid footings resting on a limited elastic layer of uniform thickness". Proc. 7th I.C.S.M.F.E., Vol. 1, pp 385-389.

SOWERS, G.F. (1962). "Shallow foundations". Foundation Engineering, ed. G.A. Leonards, McGraw-Hill, New York.

SOWERS, G.F. (1975). "Analysis and design of lightly-loaded foundations". Proc. Conf. Analysis and Design in Geotechnical Engineering, A.S.C.E., June 9-12, Vol. 2, pp 49-78.

SQUIER, L.R. (1970). "Load transfer in earth and rockfill dams". Proc. A.S.C.E., J. S.M.F.D., Vol. 96, SM1, pp 213-233.

SUTHERLAND, H.B. (1974). "Granular materials". General
        report. Session 1, Proc. Conf. on Settlement of
        Structures, Cambridge, pp 473-499.

TAYLOR, D.W. (1948). Fundamentals of soil mechanics". John
        Wiley and Sons, New York.

TERZAGHI, K. (1925). "Erdbaumechanik auf Bodenphysika -
        lischer Grundlage". F. Deuticke, Vienna.

TERZAGHI, K. (1943). "Theoretical soil mechanics". John
        Wiley and Sons, Inc.

TERZAGHI, K. (1955). "Evaluation of coefficients of subgrade
        reaction". Geotechnique, Vol. 5, pp 297-326.

TERZAGHI, K., and PECK, R.B. (1948). "Soil mechanics in
        engineering practice". John Wiley and Sons, Inc.

TERZAGHI, K., and PECK, R.B. (1967). "Soil mechanics in
        engineering practice". 2nd Edition. Wiley International
        Edition. John Wiley and Sons, Inc., New York.

TIMOSHENKO, S.P. and GOODIER, J.N. (1951). "Theory of
        elasticity". 2nd ed. McGraw-Hill.

TIMOSHENKO, S.P. and GOODIER, J.N. (1970). "Theory of
        elasticity". 3rd ed. McGraw-Hill. International
        Student Edition.

TOMS, A.H. (1954). Discussion given at the Conf. on the
        North Sea Floods of 31 January/1 February 1953.
        The I.C.E., pp 103-105.

TRUSCOTT, E.G. (1977). "Behaviour of embankment dams".
        Ph.D. Thesis, Univesrity of London.

UESHITA, K., and MEYERHOF, G.G. (1967). "Deflection of
        multilayer soil systems". Proc. A.S.C.E., Vol. 93,
        No. SM5, pp 257-282.

VAUGHAN, P.R. (1965). "Field measurements in earth dams".
Ph.D. Thesis, University of London.

VAUGHAN, P.R. (1967). "Discussion on Question No 34 - The
behaviour and deterioration of dams". Transactions
9th ICOLC Congress, Vol. 6, p 434, Istanbul.

VAUGHAN, P.R. (1970). "Cracking of clay cores of dams".
Surveyor (London), Jan. 30, pp 32-34, and
Proc. Inst. Civil Eng., May, pp 115-117.

VAUGHAN, P.R. (1972). Discussion. Proc. 5th European Conf.
S.M.F.E., Madrid, Vol. 2, pp 72-75.

VAUGHAN, P.R. (1973). "M.Sc. Foundations course notes".
Imperial College, University of London.

VAUGHAN, P.R. (1974). "M.Sc. Embankment dams course notes".
Imperial College, University of London.

VAUGHAN, P.R. (1976a). "Stress changes in an element of
soil subject to an increase in pore pressure and a
very simple confining system. Unpublished.

VAUGHAN, P.R. (1976b). "Cracking of embankment dam cores
and the design of filters for their protection".
Lecture given in Madrid on 1 June 1976. To be pub-
lished in the Bulletin of: Sociedad Española de
Mechanica del Suelo y Cimentaciones.

VAUGHAN, P.R., DAVACHI, M.M., EL-GHAMRAWY, M.K., HAMZA, M.M.
and HIGHT, D.W. (1976). "Stability analysis of large
gravity structures". Proc. Conf. Behaviour of Off-shore
Structures, Trondheim, Vol. 1, pp 467-487.

VAUGHAN, P.R., KLUTH, D.J., LEONARD, M.W., and PRADOURA, H.H.M.
(1970). "Cracking and erosion of the rolled clay core

of Balderhead Dam and the remedial works adopted for its repair". Transactions 10th Congress Large Dams, Vol. 1, pp 73-93.

VESIĆ, A.S. (1961a). "Beams on elastic subgrade and Winkler's hypothesis". Proc. 5th I.C.S.M.F.E., Paris, pp 845-850.

VESIĆ, A.S. (1961b). "Bending of beams resting on isotropic elastic solid". Proc. A.S.C.E., J. E.M.D., Vol. 87, No. EM2, pp 35-53.

VESIĆ, A.S. (1963a). "Bearing capacity of deep foundations in sand". National Academy of Sciences, National Research Council, Highway Research Record, Vol. 39, pp 112-153.

VESIĆ, A.S. (1963b). "Theoretical studies of cratering mechanisms affecting the stability of cratered slopes". Final Report, Project No. A-655, Engineering Experiment Station, Georgia Institute of Technology, Atlanta, Georgia, pp 1-67.

VESIĆ, A.S. (1965). "Bearing capacity and settlement of foundations". Proc. Symposium on Bearing Capacity and Settlement of Foundations, Duke University, Durham.

VESIĆ, A.S. (1973). "Analysis of ultimate loads of shallow foundations". Proc. A.S.C.E., J. S.M.F.D., Vol. 99, No. SM1, pp 45-73.

VLASOV, V.Z., and LEONT'EV, U.N. (1966). "Beams, plates and shells on elastic foundations". (original in Russian), Translated under Israel Program for Scientific Translations, Jerusalem.

WESTERGAARD, H.M. (1938). "A problem of elasticity suggested by a problem in soil mechanics: soft material reinforced by numerous strong horizontal sheets". Stephen Timoshenko 60th Anniversary Volume, MacMillan and Co.

WINKLER, E. (1867). "Die Lehre von Elastizität und Festigkeit". Prague, pp 182-184.

YAMAGUCHI, H., KIMURA, T., and KONNO, H. (1968). "On the contact pressure distribution between rigid loads and an elastic solid underlain by a rigid boundary" Soils and Foundations, Vol. 8, No. 3, pp 46-62.

YONG, R.N.Y. (1960). "A study of settlement characteristics of model footings on silt". Proc. 1st Pan-American Conf. on S.M.F.E., Mexico, D.F., pp 492-513.

ZARETSKII, Yu., K. (1972). "Theory of soil consolidation". Israel Program for Scientific Translations.

ZARETSKII, Yu., K. and TSYTOVICH, N.A. (1965). "Consideration of heterogeneity and non-linear deformation of the base in the design of rigid foundations". Proc. 6th I.C.S.M.F.E., Montreal, Vol. 2.

ZEEVAERT, L. (1972). "Foundation engineering for difficult subsoil conditions". Van Nostrand Reinhold Co.

ZIENKIEWICZ, O.C. (1971). "The finite element method in engineering science". 2nd Edition, McGraw-Hill, London.